AD-A099 518 OREGON STATE UNIV CORVALLIS SCHOOL OF OCEANOGRAPHY F/G 8/10
COMPILATION OF REPRINTS NUMBER 57,(U)
JAN 81 R W SPINRAD, J R ZANEVELD, H PAK N00014-76-C-0067
UNCLASSIFIED REF-79-4 NL

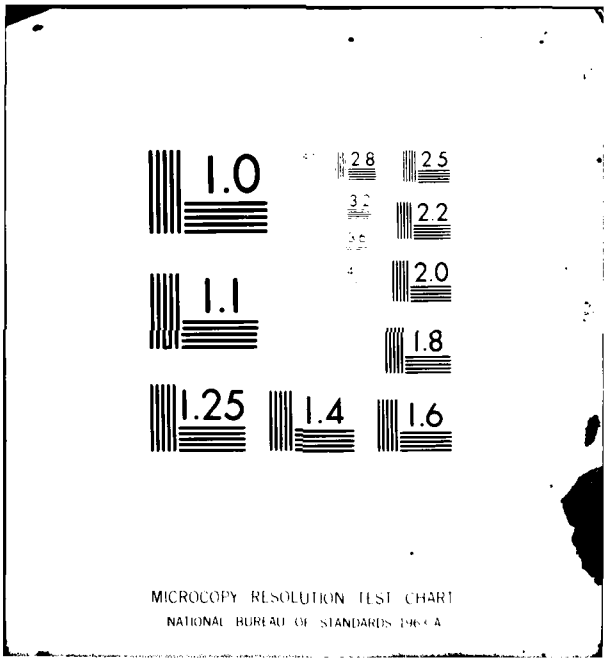
1.0
2.8
2.5
3.2
2.2
3.6
4
2.0
1.1
1.8
1.25
1.4
1.6
MICROCOPY RESOLUTION TEST CHART
NATIONAL BUREAU OF STANDARDS 1963 A

CONTENTS

FEEDING HABITS OF COD, CAPELIN, AND HERRING IN BALSFJORDEN, NORTHERN NORWAY, JULY-AUGUST 1978: THE IMPORTANCE OF EUPHAUSIIDS

W. G. Pearcy, C. C. E. Hopkins, S. Grønvik and R. A. Evans. Reprinted from Sarsia 64:269-277. 1979.

DIATOM TAPHOCOENOSES IN THE COASTAL UPWELLING AREA OFF WESTERN SOUTH AMERICA

Gretchen Schuette and Hans Schrader. Reprinted from Nova Hedwigia, Beiheft 64: 359-378. 1979.

OPTICAL AND PARTICULATE PROPERTIES AT OCEANIC FRONTS

J. Ronald V. Zaneveld and Hasong J. Pak. Reprinted from Journal of Geophysical Research 84(C12): 7781-7790. 1979.

OPTICAL PROPERTIES OF TURBIDITY STANDARDS

J. Ronald V. Zaneveld, Richard W. Spinrad, Robert Bartz. Reprinted from SPIE Vol. 208 - Ocean Optics VI: 159-168. 1979.

PRODUCTIVITY, SEDIMENTATION RATE, AND SEDIMENTARY ORGANIC MATTER IN THE OCEANS -- I. ORGANIC CARBON PRESERVATION.

P. J. Müller and E. Suess. Reprinted from Deep-Sea Research 26A: 1347-1362. 1979.

AN XBT DIGITAL RECORDING AND DISPLAY SYSTEM

Roderick Mesecar and James Wagner. Reprinted from OCEANS 1979 Conference Proceedings. Institute of Electrical and Electronic Engineers, Inc. San Diego, CA. 1979.

INTRODUCTION TO OCEAN OPTICS

Howard R. Gordon, Raymond C. Smith, and J. Ronald V. Zaneveld. Reprinted from SPIE Vol. 208 - Ocean Optics VI: 14-55. 1979.

Unclassified

SECURITY CLASSIFICATION OF THIS PAGE (When Data Entered)

REPORT DOCUMENTATION PAGE		READ INSTRUCTIONS BEFORE COMPLETING FORM
1. REPORT NUMBER: 79-4 ✓	2. GOVT ACCESSION NO.: AD-A099 528	3. RECIPIENT'S CATALOG NUMBER
4. TITLE (and Subtitle): IRRADIANCE AND BEAM TRANSMITTANCE MEASUREMENTS OFF THE WEST COAST OF THE AMERICAS		5. TYPE OF REPORT & PERIOD COVERED: Reprint
		6. PERFORMING ORG. REPORT NUMBER
7. AUTHOR(s): Richard W. Spinrad, J. Ronald V. Zaneveld, Hasong Pak		8. CONTRACT OR GRANT NUMBER(s): N00014-76-C-0067 ✓
9. PERFORMING ORGANIZATION NAME AND ADDRESS: School of Oceanography ✓, Oregon State University, Corvallis, OR 97330		10. PROGRAM ELEMENT, PROJECT, TASK AREA & WORK UNIT NUMBERS: NR 083-102
11. CONTROLLING OFFICE NAME AND ADDRESS: Office of Naval Research, Ocean Science & Technology Division, Arlington, VA 22217		12. REPORT DATE: January 20, 1979
		13. NUMBER OF PAGES: 4
14. MONITORING AGENCY NAME & ADDRESS (if different from Controlling Office)		15. SECURITY CLASS. (of this report): Unclassified
		15a. DECLASSIFICATION/DOWNGRADING SCHEDULE

16. DISTRIBUTION STATEMENT (of this Report)

Approved for public release; distribution unlimited

17. DISTRIBUTION STATEMENT (of the abstract entered in Block 20, if different from Report)

18. SUPPLEMENTARY NOTES

Reprint from Journal of Geophysical Research, Vol. 84, C1, January 20, 1979

19. KEY WORDS (Continue on reverse side if necessary and identify by block number)

20. ABSTRACT (Continue on reverse side if necessary and identify by block number)

Measurements of total irradiance versus depth and beam transmission versus depth were made at stations near shore along the west coast of the North and South American continents. The water types at each station were optically classified according to the system of Jerlov (1976), thus providing additional information for the description of the distribution of the world's ocean water types. In addition, the parameter k/c, where k is the irradiance attenuation coefficient and c is the beam attenuation coefficient, has been shown to be a useful parameter for determining the relative particle concentrations of

DD FORM 1 JAN 73 1473 EDITION OF 1 NOV 65 IS OBSOLETE
S/N 0102-014-6601

Unclassified

SECURITY CLASSIFICATION OF THIS PAGE (When Data Entered)

Unclassified

SECURITY CLASSIFICATION OF THIS PAGE (When Data Entered)

REPORT DOCUMENTATION PAGE		READ INSTRUCTIONS BEFORE COMPLETING FORM
1. REPORT NUMBER 79-5	2. GOVT ACCESSION NO.	3. RECIPIENT'S CATALOG NUMBER
4. TITLE (and Subtitle) NITROUS OXIDE PRODUCTION IN THE OCEAN		5. TYPE OF REPORT & PERIOD COVERED Reprint 6. PERFORMING ORG. REPORT NUMBER
7. AUTHOR(s) Yuval Cohen Louis I. Gordon		8. CONTRACT OR GRANT NUMBER(s) N00014-76-C-0067
9. PERFORMING ORGANIZATION NAME AND ADDRESS School of Oceanography Oregon State University Corvallis, OR 97330		10. PROGRAM ELEMENT, PROJECT, TASK AREA & WORK UNIT NUMBERS NR083-102
11. CONTROLLING OFFICE NAME AND ADDRESS Office of Naval Research Ocean Science & Technology Division Arlington, VA 22217		12. REPORT DATE 13. NUMBER OF PAGES
14. MONITORING AGENCY NAME & ADDRESS(if different from Controlling Office)		15. SECURITY CLASS. (of this report) Unclassified 15a. DECLASSIFICATION/DOWNGRADING SCHEDULE

16. DISTRIBUTION STATEMENT (of this Report)

Approved for public release; distribution unlimited

17. DISTRIBUTION STATEMENT (of the abstract entered in Block 20, if different from Report)

18. SUPPLEMENTARY NOTES

Reprinted from Journal of Geophysical Research, Vol. 84, No. C1, January 20, 1979.

19. KEY WORDS (Continue on reverse side if necessary and identify by block number)

20. ABSTRACT (Continue on reverse side if necessary and identify by block number)

Examination of vertical profiles of N_2O, oxygen, and nitrate from the Northeast and Northwest Atlantic, Northeast Pacific and eastern tropical North Pacific reveals a striking consistency in the relationships among them. With the exception of zones of active denitrification, N_2O is negatively correlated with oxygen and positively correlated with nitrate throughout the water column and it is, therefore, concluded that N_2O production in the ocean is associated with the oxidative regeneration of nitrate. In both the Atlantic and Pacific Oceans, the difference between the measured N_2O concentration and its

DD FORM 1 JAN 73 1473 EDITION OF 1 NOV 65 IS OBSOLETE
S/N 0102-014-6601

Unclassified
SECURITY CLASSIFICATION OF THIS PAGE (When Data Entered)

equilibrium solubility is linearly correlated with apparent oxygen utilization and from this relationship and the Redfield plankton decomposition model it is estimated that N_2O-nitrogen comprises about 0.1 to 0.4% of the nitrogen regenerated in the ocean. From the ratio of N_2O to nitrate production during nitrate regeneration and estimates of the overall regeneration of nitrate in the ocean, it is concluded that the total marine production of N_2O is in the range of 4 to 10 Tg-N yr^{-1}(6 to 16 Tg-N_2O yr^{-1}). This estimate is in good agreement with estimates of the N_2O loss to the atmosphere derived from N_2O measurements at the sea surface.

Unclassified

SECURITY CLASSIFICATION OF THIS PAGE (When Data Entered)

REPORT DOCUMENTATION PAGE		READ INSTRUCTIONS BEFORE COMPLETING FORM
1. REPORT NUMBER: 79-17	2. GOVT ACCESSION NO.	3. RECIPIENT'S CATALOG NUMBER
4. TITLE (and Subtitle): BIOLOGICAL PRODUCTION AND THE EXCHANGE OF OXYGEN AND CARBON DIOXIDE ACROSS THE SEA SURFACE IN STUART CHANNEL, BRITISH COLUMBIA		5. TYPE OF REPORT & PERIOD COVERED: Reprint 6. PERFORMING ORG. REPORT NUMBER
7. AUTHOR(s): Kenneth S. Johnson Ricardo M. Pytkowicz C. S. Wong		8. CONTRACT OR GRANT NUMBER(s): N00014-79-C-0004
9. PERFORMING ORGANIZATION NAME AND ADDRESS: School of Oceanography Oregon State University Corvallis, OR 97331		10. PROGRAM ELEMENT, PROJECT, TASK AREA & WORK UNIT NUMBERS: NR 083-102
11. CONTROLLING OFFICE NAME AND ADDRESS: Office of Naval Research Ocean Science & Technology Division Arlington, VA 22217		12. REPORT DATE: 1979 13. NUMBER OF PAGES: 9
14. MONITORING AGENCY NAME & ADDRESS (if different from Controlling Office)		15. SECURITY CLASS. (of this report): Unclassified 15a. DECLASSIFICATION/DOWNGRADING SCHEDULE

16. DISTRIBUTION STATEMENT (of this Report)

Approved for public release; distribution unlimited

17. DISTRIBUTION STATEMENT (of the abstract entered in Block 20, if different from Report)

18. SUPPLEMENTARY NOTES

Reprint from Limnol. Oceanogr., 24(3), pp. 474 to 482, 1979.

19. KEY WORDS (Continue on reverse side if necessary and identify by block number)

20. ABSTRACT (Continue on reverse side if necessary and identify by block number)

The rates at which concentrations of oxygen and carbon dioxide in Stuart Channel changed due to biological production and to exchange with the atmosphere were determined from measurements of the simultaneous changes in oxygen, pH, and titration alkalinity over a 15-day period in July 1976. Carbon dioxide was consumed by plankton at a rate of 10.8 μmol $CO_2 \cdot liter^{-1} \cdot d^{-1}$. CO_2 entered the surface layer by atmospheric exchange at a rate of 0.49 μmol $CO_2 \cdot liter^{-1} \cdot d^{-1}$. The piston velocity was calculated to be 2.2×10^{-3} $cm \cdot s^{-1}$. Oxygen was produced at

DD FORM 1 JAN 73 1473 EDITION OF 1 NOV 65 IS OBSOLETE
S/N 0102-014-6601

Unclassified

SECURITY CLASSIFICATION OF THIS PAGE (When Data Entered)

a rate of 14.1 μmol $O_2 \cdot liter^{-1} \cdot d^{-1}$, due to photosynthetic activity. The rate of oxygen loss to the atmosphere was 9.8 μmol $O_2 \cdot liter^{-1} \cdot d^{-1}$. The piston velocity was 1.6×10^{-3} $cm \cdot s^{-1}$.

Unclassified

SECURITY CLASSIFICATION OF THIS PAGE (When Data Entered)

REPORT DOCUMENTATION PAGE	READ INSTRUCTIONS BEFORE COMPLETING FORM
1. REPORT NUMBER: 79-18	2. GOVT ACCESSION NO. / 3. RECIPIENT'S CATALOG NUMBER
4. TITLE (and Subtitle): ACOUSTICAL ESTIMATION OF ZOOPLANKTON POPULATIONS	5. TYPE OF REPORT & PERIOD COVERED: Reprint
	6. PERFORMING ORG. REPORT NUMBER
7. AUTHOR(s): Charles F. Greenlaw	8. CONTRACT OR GRANT NUMBER(s)
9. PERFORMING ORGANIZATION NAME AND ADDRESS: School of Oceanography, Oregon State University, Corvallis, Oregon 97331	10. PROGRAM ELEMENT, PROJECT, TASK AREA & WORK UNIT NUMBERS
11. CONTROLLING OFFICE NAME AND ADDRESS: Office of Naval Research, Ocean Science & Technology Division, Arlington, Virginia 22217	12. REPORT DATE: 1979 / 13. NUMBER OF PAGES
14. MONITORING AGENCY NAME & ADDRESS (if different from Controlling Office)	15. SECURITY CLASS. (of this report): Unclassified / 15a. DECLASSIFICATION/DOWNGRADING SCHEDULE

16. DISTRIBUTION STATEMENT (of this Report)

Approved for public release; distribution unlimited

17. DISTRIBUTION STATEMENT (of the abstract entered in Block 20, if different from Report)

18. SUPPLEMENTARY NOTES

Reprint from Limnol. Oceanogr. 24(2), p. 226-242, 1979.

19. KEY WORDS (Continue on reverse side if necessary and identify by block number)

20. ABSTRACT (Continue on reverse side if necessary and identify by block number)

Acoustical estimates of zooplankton abundance can be made rigorously if the scattering behavior as a function of size and frequency for the zooplankters is known. Measurements of scattering at a single frequency can be used to estimate abundance if the mean zooplankter size is known. Measurements at two frequencies can be used to estimate the dominant size as well as abundance if a single size zooplankter dominates the acoustical scattering. Measurements at several frequencies can be used to estimate size distributions and (cont.)

DD FORM 1 JAN 73 1473 EDITION OF 1 NOV 65 IS OBSOLETE S/N 0102-014-5601

Unclassified

SECURITY CLASSIFICATION OF THIS PAGE (When Data Entered)

abundances. In a field experiment, acoustical scattering was measured at three frequencies for zooplankton layers composed largely of euphausiids (for which an approximate scattering model is known). These data are analyzed by each method and estimates of numerical abundance given.

Unclassified

SECURITY CLASSIFICATION OF THIS PAGE (When Data Entered)

REPORT DOCUMENTATION PAGE	READ INSTRUCTIONS BEFORE COMPLETING FORM
1 REPORT NUMBER: 79-19	2 GOVT ACCESSION NO. / 3 RECIPIENT'S CATALOG NUMBER
4 TITLE (and Subtitle): MID-OCEAN OBSERVATIONS OF ATMOSPHERIC RADIATION	5 TYPE OF REPORT & PERIOD COVERED: Reprint
	6 PERFORMING ORG. REPORT NUMBER
7 AUTHOR(s): James J. Simpson Clayton A. Paulson	8 CONTRACT OR GRANT NUMBER(s): N00014-76-C-0067
9 PERFORMING ORGANIZATION NAME AND ADDRESS: School of Oceanography Oregon State University Corvallis, Oregon 97331	10 PROGRAM ELEMENT, PROJECT, TASK AREA & WORK UNIT NUMBERS: NR 083-102
11 CONTROLLING OFFICE NAME AND ADDRESS: Office of Naval Research Ocean Science & Technology Division Arlington, Virginia 22217	12 REPORT DATE: 1979 13 NUMBER OF PAGES: 16
14 MONITORING AGENCY NAME & ADDRESS(if different from Controlling Office)	15 SECURITY CLASS. (of this report): Unclassified 15a DECLASSIFICATION/DOWNGRADING SCHEDULE

16 DISTRIBUTION STATEMENT (of this Report)

Approved for public release; distribution unlimited

17 DISTRIBUTION STATEMENT (of the abstract entered in Block 20, if different from Report)

18 SUPPLEMENTARY NOTES

Reprinted from the Quarterly Journal of the Royal Meteorological Society 105 (444), pp. 487-502, 1979.

19 KEY WORDS (Continue on reverse side if necessary and identify by block number)

20 ABSTRACT (Continue on reverse side if necessary and identify by block number)

Mid-ocean (35°N 155°W) observations of the various components of radiative flux were made from the R/P FLIP during the period 2 through 13 February 1974. Cloud cover ranged from clear skies to overcast, and water vapour pressure varied between 9 and 18 mb, with sea surface temperature near 15.0°C.

The net longwave radiative fluxes reported here were obtained: (1) by taking the difference between simultaneous measurements of net all-wave and net solar fluxes; and (2) by direct measurements with a net longwave radiometer

DD FORM 1 JAN 73 1473 EDITION OF 1 NOV 65 IS OBSOLETE S/N 0102-014-6601

Unclassified

SECURITY CLASSIFICATION OF THIS PAGE (When Data Entered)

designed by G. W. Paltridge. When observations during rain and fog are excluded, the difference between night-time 15-minute averages by the two methods is generally less than $1 mWcm^{-2}$. During day-time, indirect measurements are often larger than direct by about $5 mWcm^{-2}$; from internal evidence we prefer the direct values.

The albedo of the sea surface was calculated from simultaneous measurements of downward and upward solar fluxes. The observations were analysed to represent albedo as a function of solar altitude and atmospheric transmittance, following the work of R. E. Payne; our results suggest that Payne's smoothed representation is suitable for use over the open ocean. Albedo was observed to decrease with increasing wind speed for clear skies with solar altitude between 15 and 30 degrees but no variation was discernible at higher solar altitudes.

Empirical formulae for calculating both shortwave and net longwave components of the radiative flux were compared with measurements. A formula due to F. E. Lumb for determining the incident solar flux given solar altitude, cloud amount and cloud type, consistently yields good agreement with the measurements, within about 1 $mWcm^{-2}$. Daily averages of net longwave flux calculated from several empirical formulae using a linear correction for clouds are within $2 mWcm^{-2}$ of the observations reported in this paper. Since daily radiation balance values were measured to only 5 $mWcm^{-2}$, the limitations of the best current empirical formulae are evident.

Unclassified

SECURITY CLASSIFICATION OF THIS PAGE (When Data Entered)

REPORT DOCUMENTATION PAGE	READ INSTRUCTIONS BEFORE COMPLETING FORM
1 REPORT NUMBER: 79-20	2 GOVT ACCESSION NO. / 3 RECIPIENT'S CATALOG NUMBER
4 TITLE (and Subtitle): MINERAL PHASES FORMED IN ANOXIC SEDIMENTS BY MICROBIAL DECOMPOSITION OF ORGANIC MATTER	5 TYPE OF REPORT & PERIOD COVERED: Peprint / 6 PERFORMING ORG. REPORT NUMBER
7 AUTHOR(s): Erwin Suess	8 CONTRACT OR GRANT NUMBER(s): N00014-76-C-0067
9 PERFORMING ORGANIZATION NAME AND ADDRESS: School of Oceanography, Oregon State University, Corvallis, Oregon 97331	10 PROGRAM ELEMENT, PROJECT, TASK AREA & WORK UNIT NUMBERS
11 CONTROLLING OFFICE NAME AND ADDRESS: Office of Naval Research, Ocean Science & Technology Division, Arlington, Virginia 22217	12 REPORT DATE: 1979 / 13 NUMBER OF PAGES: 13
14 MONITORING AGENCY NAME & ADDRESS(if different from Controlling Office)	15 SECURITY CLASS (of this report): Unclassified / 15a DECLASSIFICATION DOWNGRADING SCHEDULE

16 DISTRIBUTION STATEMENT (of this Report)

Approved for public release; distribution unlimited

17 DISTRIBUTION STATEMENT (of the abstract entered in Block 20, if different from Report)

18 SUPPLEMENTARY NOTES

Reprinted from Geochimica et Cosmochimica Acta 43, pp. 339-352, 1979.

19 KEY WORDS (Continue on reverse side if necessary and identify by block number)

20 ABSTRACT (Continue on reverse side if necessary and identify by block number)

Microbial decomposition of organic matter in recent sediments of the Landsort Deep - an anoxic basin of the central Baltic Sea - resulted in the formation of a characteristic assemblage of authigenic mineral precipitates of carbonates, sulfides, phosphates, and amorphous silica. The dominant cystalline phases are a mixed Mn-carbonate [$(Mn_{0.85}Ca_{0.10}Mg_{0.05})CO_3$], Mn-sulfide [MnS] and Fe-carbonate [$FeCO_3$]. Amorphous Fe-sulfide [FeS], Mn-phosphate [$Mn_3(PO_4)_2$] and a mixed Fe-Ca-phosphate [$(Fe_{0.86}Ca_{0.14})_3(PO_4)_2$]

DD FORM 1 JAN 73 1473 EDITION OF 1 NOV 65 IS OBSOLETE S/N 0102-014-6601

Unclassified

SECURITY CLASSIFICATION OF THIS PAGE (When Data Entered)

were identified by their chemical compositions only. The variability in composition of these solid phases and their mode of occurrence as a co-existing assemblage constrains the conditions and solution composition from which they precipitated. Estimates of activities for dissolved Fe, Mn, PO_4, CO_3 and S in equilibrium with such an assemblage are close to those found in recent anoxic interstitial water-sediment systems. It is important to have detailed knowledge of the composition and stability conditions of these solid precipitates in order to refine stoichiometric models of interstitial nutrient regeneration in anoxic sediments.

Unclassified

SECURITY CLASSIFICATION OF THIS PAGE (When Data Entered)

REPORT DOCUMENTATION PAGE	READ INSTRUCTIONS BEFORE COMPLETING FORM
1. REPORT NUMBER: 79-21	2. GOVT ACCESSION NO. / 3. RECIPIENT'S CATALOG NUMBER
4. TITLE (and Subtitle): COMPARISON OF THE FEEDING HABITS OF MIGRATORY AND NON-MIGRATORY STENOBRACHIUS LEUCOPSARUS (MYCTOPHIDAE)	5. TYPE OF REPORT & PERIOD COVERED: Reprint 6. PERFORMING ORG. REPORT NUMBER
7. AUTHOR(s): W. G. Pearcy, H. V. Lorz, W. Peterson	8. CONTRACT OR GRANT NUMBER(s): N00014-67-A-0369-0007
9. PERFORMING ORGANIZATION NAME AND ADDRESS: School of Oceanography, Oregon State University, Corvallis, Oregon 97331	10. PROGRAM ELEMENT, PROJECT, TASK AREA & WORK UNIT NUMBERS: NR 083-102
11. CONTROLLING OFFICE NAME AND ADDRESS: Office of Naval Research, Ocean Science & Technology Division, Arlington, Virginia 22217	12. REPORT DATE: 1979 13. NUMBER OF PAGES: 8
14. MONITORING AGENCY NAME & ADDRESS(if different from Controlling Office)	15. SECURITY CLASS. (of this report): Unclassified 15a. DECLASSIFICATION/DOWNGRADING SCHEDULE

16. DISTRIBUTION STATEMENT (of this Report)

Approved for public release; distribution unlimited

17. DISTRIBUTION STATEMENT (of the abstract entered in Block 20, if different from Report)

18. SUPPLEMENTARY NOTES

Reprinted from Marine Biology 51, p. 1-8, 1979.

19. KEY WORDS (Continue on reverse side if necessary and identify by block number)

20. ABSTRACT (Continue on reverse side if necessary and identify by block number)

Stenobrachius leucopsarus, the most abundant species of myctophid fishes off Oregon, USA, has a bimodal distribution at night, with a peak of abundance in the upper 100 m composed of diel vertical migrants, and another peak at 300 to 500 m composed of fish that did not migrate the night they were caught. We compared the feeding habits of these two groups of fish in an attempt to learn if deep fish migrated to surface waters. Low similarity of diets, differences in the rank order of common prey, and similar states of stomach

DD FORM 1 JAN 73 1473 EDITION OF 1 NOV 65 IS OBSOLETE S/N 0102-014-6601

Unclassified

SECURITY CLASSIFICATION OF THIS PAGE (When Data Entered)

fullness and digestion of prey suggest that fish captured in deep water at night probably did not feed exclusively in shallow water on previous nights. They probably fed in deep water. The similarity in food habits between deep and shallow fish is most readily explained by daytime feeding by fish in deep water and by broad vertical distributions of prey.

Unclassified

SECURITY CLASSIFICATION OF THIS PAGE (When Data Entered)

REPORT DOCUMENTATION PAGE	READ INSTRUCTIONS BEFORE COMPLETING FORM
1. REPORT NUMBER: 79-22	2. GOVT ACCESSION NO. / 3. RECIPIENT'S CATALOG NUMBER
4. TITLE (and subtitle): OBSERVATIONS OF UPPER OCEAN TEMPERATURE AND SALINITY STRUCTURE DURING THE POLE EXPERIMENT	5. TYPE OF REPORT & PERIOD COVERED: Reprint 6. PERFORMING ORG. REPORT NUMBER
7. AUTHOR(s): James J. Simpson Clayton A. Paulson	8. CONTRACT OR GRANT NUMBER(s): N0014-76-C-0067
9. PERFORMING ORGANIZATION NAME AND ADDRESS: School of Oceanography Oregon State University Corvallis, Oregon 97331	10. PROGRAM ELEMENT, PROJECT, TASK AREA & WORK UNIT NUMBERS: NR 083-102
11. CONTROLLING OFFICE NAME AND ADDRESS: Office of Naval Research Ocean Science & Technology Division Arlington, Virginia 22217	12. REPORT DATE: 1979 13. NUMBER OF PAGES: 16
14. MONITORING AGENCY NAME & ADDRESS(if different from Controlling Office)	15. SECURITY CLASS. (of this report): Unclassified 15a. DECLASSIFICATION/DOWNGRADING SCHEDULE

16. DISTRIBUTION STATEMENT (of this Report)

Approved for public release; distribution unlimited

17. DISTRIBUTION STATEMENT (of the abstract entered in Block 20, if different from Report)

18. SUPPLEMENTARY NOTES

Reprinted from Journal of Physical Oceanography 9 (5): pgs. 869-884, 1979.

19. KEY WORDS (Continue on reverse side if necessary and identify by block number)

20. ABSTRACT (Continue on reverse side if necessary and identify by block number)

Mid-ocean observations (35°N, 155°W) of temperature and salinity were made from R/P FLIP during the period 28 January-14 February 1974 as part of the NORPAX POLE Experiment.

Autocorrelations for the time series of depth of several σ_t surfaces confirm the presence of a semi-diurnal internal tide whose amplitude is about 10 m. The period of 12.7 h determined from the autocorrelation analysis is not statistically significantly different from the period of the M2 semidiurnal

DD FORM 1 JAN 73 1473 EDITION OF 1 NOV 65 IS OBSOLETE S/N 0102-014-6601

Unclassified

SECURITY CLASSIFICATION OF THIS PAGE (When Data Entered)

tide (12.4 h). The coherence between pairs of time series of the depth of the σ_t surfaces is high, ranging from 0.97 to 0.91 at the frequency of the peak in the spectrum corresponding to the semi-diurnal tide. The coherence between a given σ_t surface and deeper lying surfaces decreases slowly with the mean separation between surfaces. The vertical coherence scale suggests that most of the energy of the semi-diurnal internal tide is in the low-order modes. The data show that the phase difference between surfaces increases with the mean separation between surfaces at the approximate rate of $+35^{\circ}$ $(100\ m)^{-1}$. Estimates of the vertical and horizontal wavelengths of the observed semi-diurnal internal tide are 1 km and 35 km, respectively.

One-dimensional mixed-layer deepening models fail to predict the mixed-layer depths and temperatures observed during POLE. Horizontal advection, as evidenced from the salinity maximum frequently occurring at the bottom of the mixed layer and other near-surface changes in salinity and temperature not associated with local surface forcing, are responsible for the failure. During the one period in which the one-dimensional models may be applicable a value of the mixing energy flux coefficient m = 0.0017 was obtained.

Unclassified

SECURITY CLASSIFICATION OF THIS PAGE (When Data Entered)

REPORT DOCUMENTATION PAGE	READ INSTRUCTIONS BEFORE COMPLETING FORM
1. REPORT NUMBER: 79-23	2. GOVT ACCESSION NO. / 3. RECIPIENT'S CATALOG NUMBER
4. TITLE (and Subtitle): MESOPELAGIC FISHES OF THE BERING SEA AND ADJACENT NORTHERN NORTH PACIFIC OCEAN	5. TYPE OF REPORT & PERIOD COVERED: Reprint 6. PERFORMING ORG. REPORT NUMBER
7. AUTHOR(s): William G. Pearcy, Takahisa Nemoto, Muneo Okiyama	8. CONTRACT OR GRANT NUMBER(s): N00014-76-C-0067
9. PERFORMING ORGANIZATION NAME AND ADDRESS: School of Oceanography, Oregon State University, Corvallis, Oregon 97331	10. PROGRAM ELEMENT, PROJECT, TASK AREA & WORK UNIT NUMBERS: NR 083-102
11. CONTROLLING OFFICE NAME AND ADDRESS: Office of Naval Research, Ocean Science & Technology Division, Arlington, Virginia 22217	12. REPORT DATE: 1979 13. NUMBER OF PAGES: 9
14. MONITORING AGENCY NAME & ADDRESS (if different from Controlling Office)	15. SECURITY CLASS. (of this report): Unclassified 15a. DECLASSIFICATION DOWNGRADING SCHEDULE

16. DISTRIBUTION STATEMENT (of this Report)

Approved for public release; distribution unlimited

17. DISTRIBUTION STATEMENT (of the abstract entered in Block 20, if different from Report)

18. SUPPLEMENTARY NOTES

Reprinted from the Journal of the Oceanographic Society of Japan 35 (3-4): pgs. 127-135, 1979.

19. KEY WORDS (Continue on reverse side if necessary and identify by block number)

20. ABSTRACT (Continue on reverse side if necessary and identify by block number)

Fourteen midwater trawl collections to depths of 450 m to 1.400 m were taken at eleven stations in the Bering Sea and adjoining regions of the northern North Pacific by the R/V HAKUHO MARU during the summer of 1975. A total of 29 kinds of fishes were identified. Mesopelagic fishes of the families Myctophidae, Gonostomatidae and Bathylagidae predominated in the catches, contributing 14 species (94%) of the fishes caught.

Seventeen species of fishes were caught in the Bering Sea, and all of these are known from nearby areas. The mesopelagic fish fauna of the ... (cont.)

DD FORM 1 JAN 73 1473 EDITION OF 1 NOV 65 IS OBSOLETE S/N 0102-014-6601

Unclassified

SECURITY CLASSIFICATION OF THIS PAGE (When Data Entered)

Bering Sea is similar to that in adjoining regions of the northern North Pacific Ocean: endemic species are rare or absent.

Stenobrachius nannochir was usually the most common mesopelagic fish in our catches. Stenobrachius leucopsarus is a diel vertical migrant that is usually the dominant mesopelagic fish in modified Subarctic waters of the northeastern Pacific. The change in dominance from S. nannochir in the western Bering Sea to S. leucopsarus in the eastern Bering Sea is related to differences in oceanographic conditions.

Unclassified

SECURITY CLASSIFICATION OF THIS PAGE (When Data Entered)

REPORT DOCUMENTATION PAGE	READ INSTRUCTIONS BEFORE COMPLETING FORM
1 REPORT NUMBER: 79-24	2 GOVT ACCESSION NO. / 3 RECIPIENT'S CATALOG NUMBER
4 TITLE (and Subtitle): FEEDING HABITS OF COD, CAPELIN, AND HERRING IN BALSFJORDEN, NORTHERN NORWAY, JULY-AUGUST 1978: THE IMPORTANCE OF EUPHAUSIIDS	5 TYPE OF REPORT & PERIOD COVERED: Reprint / 6 PERFORMING ORG. REPORT NUMBER
7 AUTHOR(s): W. G. Pearcy, C. C. E. Hopkins, S. Grønvik and R. A. Evans	8 CONTRACT OR GRANT NUMBER(s): N00014-76-C-0067
9 PERFORMING ORGANIZATION NAME AND ADDRESS: School of Oceanography, Oregon State University, Corvallis, Oregon 97331	10 PROGRAM ELEMENT, PROJECT, TASK AREA & WORK UNIT NUMBERS: NR 083-102
11 CONTROLLING OFFICE NAME AND ADDRESS: Office of Naval Research, Ocean Science & Technology Division, Arlington, Virginia 22217	12 REPORT DATE / 13 NUMBER OF PAGES
14 MONITORING AGENCY NAME & ADDRESS (If different from Controlling Office)	15 SECURITY CLASS. (of this report): Unclassified / 15a DECLASSIFICATION/DOWNGRADING SCHEDULE

16 DISTRIBUTION STATEMENT (of this Report)

Approved for public release; distribution unlimited

17 DISTRIBUTION STATEMENT (of the abstract entered in Block 20, if different from Report)

18 SUPPLEMENTARY NOTES

Reprinted from Sarsia 64: 269-277, 1979.

19 KEY WORDS (Continue on reverse side if necessary and identify by block number)

20 ABSTRACT (Continue on reverse side if necessary and identify by block number)

Midwater and bottom trawls were used at two stations (120 and 180 m depth) in Balsfjorden during the summer of 1978 to study the feeding of fishes on euphausiids, one of the major causes of 120 kHz sound scattering. The principal food of cod consisted of capelin (Mallotus villosus), euphausiids (Thysanoessa raschii, T. inermis, and Meganyctiphanes norvegica), and shrimp (Pandalus borealis).

At the 120 m station, herring and small cod fed mainly on euphausiids.

DD FORM 1 JAN 73 1473 EDITION OF 1 NOV 65 IS OBSOLETE S/N 0102-014-6601

Unclassified

SECURITY CLASSIFICATION OF THIS PAGE (When Data Entered)

Because of diel vertical migrations, euphausiids are presumably close to the bottom during the day at this depth, and hence very susceptible to predation by both pelagic and benthic fishes. During the darkest period of the 24-hr day cod caught in midwater (50-70 m depth) had appreciable quantities of fresh euphausiids in their stomachs.

At the 180 m station euphausiids were relatively unimportant in the food of cod caught in bottom trawls but were numerous in cod caught in midwater trawls at depths of the 120 kHz sound scattering layer. The scattering layer did not impinge on the bottom at this station. It migrated from depths of about 150 m by day into the upper 100 m at night; both capelin and cod were associated with the layer. Although copepods were the most numerous type of prey in capelin stomachs from the 180 m station, euphausiids predominated volumetrically.

Unclassified

SECURITY CLASSIFICATION OF THIS PAGE (When Data Entered)

REPORT DOCUMENTATION PAGE	READ INSTRUCTIONS BEFORE COMPLETING FORM
1 REPORT NUMBER: 79-25	2 GOVT ACCESSION NO. / 3 RECIPIENT'S CATALOG NUMBER
4 TITLE (and Subtitle): DIATOM TAPHOCOENOSES IN THE COASTAL UPWELLING AREA OFF WESTERN SOUTH AMERICA	5 TYPE OF REPORT & PERIOD COVERED: Reprint
	6 PERFORMING ORG. REPORT NUMBER
7 AUTHOR(s): Gretchen Schuette, Hans Schrader	8 CONTRACT OR GRANT NUMBER(s): N00014-76-0067
9 PERFORMING ORGANIZATION NAME AND ADDRESS: School of Oceanography, Oregon State University, Corvallis, Oregon 97331	10 PROGRAM ELEMENT, PROJECT, TASK AREA & WORK UNIT NUMBERS
11 CONTROLLING OFFICE NAME AND ADDRESS: Office of Naval Research, Ocean Science & Technology Division, Arlington, Virginia 22217	12 REPORT DATE: 1979 / 13 NUMBER OF PAGES: 20
14 MONITORING AGENCY NAME & ADDRESS(if different from Controlling Office)	15 SECURITY CLASS. (of this report): Unclassified / 15a DECLASSIFICATION/DOWNGRADING SCHEDULE

16. DISTRIBUTION STATEMENT (of this Report)

Approved for public release; distribution unlimited

17. DISTRIBUTION STATEMENT (of the abstract entered in Block 20, if different from Report)

18 SUPPLEMENTARY NOTES

:: Reprinted from Nova Hedwigia, Beiheft 64: 359-378, 1979.

19. KEY WORDS (Continue on reverse side if necessary and identify by block number)

20. ABSTRACT (Continue on reverse side if necessary and identify by block number)

Diatom floral analysis of 116 sediment surface samples obtained off Peru reveals a boundary in the sediments between coastal upwelling influenced sediments and sediments outside the highly productive realm. Sinuous patterns of relative abundance for meroplanktic species (Actinocyclus octonarius, Actinoptychus senarius, and Cyclotella striata/stylorum) may preserve the meander-like patterns of surface water parameters off Peru. The occurrence of loci of high abundance of diatom valves per gram of dry (cont.)

DD FORM 1 JAN 73 1473 EDITION OF 1 NOV 65 IS OBSOLETE S/N 0102-014-6601

Unclassified

SECURITY CLASSIFICATION OF THIS PAGE (When Data Entered)

sediment, and the limited occurrence of Skeletonema costatum and of a species of the genus Delphineis are additional pieces of evidence that upwelled tongues of cold water have a correspondingly patchy sediment signal.

Unclassified

SECURITY CLASSIFICATION OF THIS PAGE (When Data Entered)

REPORT DOCUMENTATION PAGE		READ INSTRUCTIONS BEFORE COMPLETING FORM
1 REPORT NUMBER: 79-26	2 GOVT ACCESSION NO	3 RECIPIENT'S CATALOG NUMBER
4 TITLE (and Subtitle): OPTICAL AND PARTICULATE PROPERTIES AT OCEANIC FRONTS		5 TYPE OF REPORT & PERIOD COVERED: Reprint
		6 PERFORMING ORG. REPORT NUMBER
7 AUTHOR(s): J. Ronald V. Zaneveld, Hasong J. Pak		8 CONTRACT OR GRANT NUMBER(s): N00014-76-C-0067
9 PERFORMING ORGANIZATION NAME AND ADDRESS: School of Oceanography, Oregon State University, Corvallis, Oregon 97331		10 PROGRAM ELEMENT, PROJECT, TASK AREA & WORK UNIT NUMBERS: NR 083-102
11 CONTROLLING OFFICE NAME AND ADDRESS: Office of Naval Research, Ocean Science & Technology Division, Arlington, Virginia 22217		12 REPORT DATE: 1979
		13 NUMBER OF PAGES: 10
14 MONITORING AGENCY NAME & ADDRESS(if different from Controlling Office)		15 SECURITY CLASS. (of this report): Unclassified
		15a DECLASSIFICATION/DOWNGRADING SCHEDULE

16 DISTRIBUTION STATEMENT (of this Report)

Approved for public release; distribution unlimited

17 DISTRIBUTION STATEMENT (of the abstract entered in Block 20, if different from Report)

18 SUPPLEMENTARY NOTES

Reprinted from Journal of Geophysical Research 84 (C12): 7781-7790, 1979.

19 KEY WORDS (Continue on reverse side if necessary and identify by block number)

20 ABSTRACT (Continue on reverse side if necessary and identify by block number)

Distributional patterns of optical and particulate properties at oceanic fronts follow general patterns. These patterns are examined by means of three examples: the front associated with the Columbia River plume in winter, the upwelling front off the Oregon coast during the summer, and the front in the eastern equatorial Pacific. It is shown that the optical and particulate matter distributions at oceanic fronts are the result of three major processes: (1) advection of inorganic matter into the frontal (cont.)

DD FORM 1 JAN 73 1473 EDITION OF 1 NOV 65 IS OBSOLETE
S/N 0102-014-6601

Unclassified
SECURITY CLASSIFICATION OF THIS PAGE (When Data Entered)

zone, (2) advection of biological materials into the front, and (3) generation of particulate matter by biological processes in the front itself.

Unclassified

SECURITY CLASSIFICATION OF THIS PAGE (When Data Entered)

REPORT DOCUMENTATION PAGE		READ INSTRUCTIONS BEFORE COMPLETING FORM
1. REPORT NUMBER: 79-27	2. GOVT ACCESSION NO.	3. RECIPIENT'S CATALOG NUMBER
4. TITLE (and Subtitle): OPTICAL PROPERTIES OF TURBIDITY STANDARDS		5. TYPE OF REPORT & PERIOD COVERED: Reprint
		6. PERFORMING ORG. REPORT NUMBER
7. AUTHOR(s): J. Ronald V. Zaneveld, Richard W. Spinrad, Robert Bartz		8. CONTRACT OR GRANT NUMBER(s): N00014-76-C-0067
9. PERFORMING ORGANIZATION NAME AND ADDRESS: School of Oceanography, Oregon State University, Corvallis, Oregon 97331		10. PROGRAM ELEMENT, PROJECT, TASK AREA & WORK UNIT NUMBERS: NR 083-102
11. CONTROLLING OFFICE NAME AND ADDRESS: Office of Naval Research, Ocean Science & Technology Division, Arlington, Virginia 22217		12. REPORT DATE: 1980
		13. NUMBER OF PAGES: 10
14. MONITORING AGENCY NAME & ADDRESS (if different from Controlling Office)		15. SECURITY CLASS. (of this report): Unclassified
		15a. DECLASSIFICATION/DOWNGRADING SCHEDULE

16. DISTRIBUTION STATEMENT (of this Report)

Approved for public release; distribution unlimited

17. DISTRIBUTION STATEMENT (of the abstract entered in Block 20, if different from Report)

18. SUPPLEMENTARY NOTES

Reprinted from SPIE 208 - Ocean Optics VI (1979): 159-168.

19. KEY WORDS (Continue on reverse side if necessary and identify by block number)

20. ABSTRACT (Continue on reverse side if necessary and identify by block number)

Measurements of light scattering and light attenuation were made for suspensions of formazine and diatomaceous earth. Light scattering was measured for light of wavelength 632.8 nm at angles from 0.1° to 1.0° and for light of wavelengths 400, 500, 550, 600, 650, and 700 nm at 45 . Light attenuation was measured over a 25 cm pathlength for light of 660 nm. These measurements were made for suspensions which varied from 0 to 40 Jackson Turbidity Units of formazine and 0 to 40 mg/l of diatomaceous (cont.)

DD FORM 1 JAN 73 1473 EDITION OF 1 NOV 65 IS OBSOLETE
S/N 0102-014-6601

Unclassified

SECURITY CLASSIFICATION OF THIS PAGE (When Data Entered)

earth. The results indicate the necessity for multiple optical measurements for determinations of turbidity of water. In addition, the tables and curves presented may be used in the calibration of light scattering meters and transmissometers which are used for turbidity studies.

Unclassified

SECURITY CLASSIFICATION OF THIS PAGE (When Data Entered)

REPORT DOCUMENTATION PAGE		READ INSTRUCTIONS BEFORE COMPLETING FORM
1. REPORT NUMBER: 79-28	2. GOVT ACCESSION NO.	3. RECIPIENT'S CATALOG NUMBER
4. TITLE (and Subtitle): PRODUCTIVITY, SEDIMENTATION RATE, AND SEDIMENTARY ORGANIC MATTER IN THE OCEANS -- I. ORGANIC CARBON PRESERVATION		5. TYPE OF REPORT & PERIOD COVERED: Reprint 6. PERFORMING ORG. REPORT NUMBER
7. AUTHOR(s): P. J. Muller, E. Suess		8. CONTRACT OR GRANT NUMBER(s): N00014-76-C-0067
9. PERFORMING ORGANIZATION NAME AND ADDRESS: School of Oceanography, Oregon State University, Corvallis, Oregon 97331		10. PROGRAM ELEMENT, PROJECT, TASK AREA & WORK UNIT NUMBERS: NR 083-102
11. CONTROLLING OFFICE NAME AND ADDRESS: Office of Naval Research, Ocean Science & Technology Division, Arlington, Virginia 22217		12. REPORT DATE: 1979 13. NUMBER OF PAGES: 16
14. MONITORING AGENCY NAME & ADDRESS (if different from Controlling Office)		15. SECURITY CLASS. (of this report): Unclassified 15a. DECLASSIFICATION/DOWNGRADING SCHEDULE

16. DISTRIBUTION STATEMENT (of this Report)

Approved for public release; distribution unlimited

17. DISTRIBUTION STATEMENT (of the abstract entered in Block 20, if different from Report)

18. SUPPLEMENTARY NOTES

Reprinted from Deep-Sea Research 26A: 1347-1362, 1979.

19. KEY WORDS (Continue on reverse side if necessary and identify by block number)

20. ABSTRACT (Continue on reverse side if necessary and identify by block number)

Comparison of rates of accumulation of organic carbon in surface marine sediments from the central North Pacific, the continental margins off northwest Africa, northwest and southwest America, the Argentine Basin, and the western Baltic Sea with primary production rates suggests that the fraction of primary produced organic carbon preserved in the sediments is universally related to the bulk sedimentation rate. Accordingly, less than 0.01% of the primary production becomes fossilized in slowly accumulating pelagic

DD FORM 1 JAN 73 1473 EDITION OF 1 NOV 65 IS OBSOLETE
S/N 0102-014-6601

Unclassified

SECURITY CLASSIFICATION OF THIS PAGE (When Data Entered)

sediments [(2 to 6 mm (1000 y)$^{-1}$] of the Central Pacific, 0.1 to 2% in moderately rapidly accumulating [2 to 13 cm (1000 y)$^{-1}$] hemipelagic sediments off northwest Africa, northwest America (Oregon) and southeast America (Argentina), and 11 to 18% in rapidly accumulating [66 to 140 cm (1000 y)$^{-1}$] hemipelagic sediments off southwest America (Peru) and in the Baltic Sea.

The empirical expression:

$$\% \text{ Org-C} = \frac{0.0030 \cdot R \cdot S^{0.30}}{P_s(1-\emptyset)}$$

implies that the sedimentary organic carbon content (% Org-C) doubles with each 10-fold increase in sedimentation rate (S), assuming that other factors remain constant; i.e., primary production (R), porosity (Ø) and sediment density (P_s). This expression also predicts the sedimentary organic carbon content from the primary production rate, sedimentation rate, dry density of solids, and their porosity; it may be used to estimate paleoproductivity as well. Applying this relationship to a sediment core from the continental rise off northwest Africa (Spanish Sahara) suggests that productivity there during interglacial oxygen isotope stages 1 and 5 was about the same as today but was higher by a factor of 2 to 3 during glacial stages 2, 3, and 6.

Unclassified

SECURITY CLASSIFICATION OF THIS PAGE (When Data Entered)

REPORT DOCUMENTATION PAGE		READ INSTRUCTIONS BEFORE COMPLETING FORM
1. REPORT NUMBER 79-29	2. GOVT ACCESSION NO.	3. RECIPIENT'S CATALOG NUMBER
4. TITLE (and Subtitle) AN XBT DIGITAL RECORDING AND DISPLAY SYSTEM		5. TYPE OF REPORT & PERIOD COVERED Reprint
		6. PERFORMING ORG. REPORT NUMBER
7. AUTHOR(s) Roderick Mesecar James Wagner		8. CONTRACT OR GRANT NUMBER(s) N00014-79-C-0004
9. PERFORMING ORGANIZATION NAME AND ADDRESS School of Oceanography Oregon State University Corvallis, Oregon 97331		10. PROGRAM ELEMENT, PROJECT, TASK AREA & WORK UNIT NUMBERS
11. CONTROLLING OFFICE NAME AND ADDRESS Office of Naval Research Ocean Science & Technology Division Arlington, Virginia 22217		12. REPORT DATE 1979 13. NUMBER OF PAGES 4
14. MONITORING AGENCY NAME & ADDRESS(if different from Controlling Office)		15. SECURITY CLASS. (of this report) Unclassified 15a. DECLASSIFICATION/DOWNGRADING SCHEDULE

16. DISTRIBUTION STATEMENT (of this Report)

Approved for public release; distribution unlimited

17. DISTRIBUTION STATEMENT (of the abstract entered in Block 20, if different from Report)

18. SUPPLEMENTARY NOTES

Reprinted from OCEANS 1979 Conference Proceedings, Inst. of Electrical and Electronic Engineers, Inc., Sept. 1979.

19. KEY WORDS (Continue on reverse side if necessary and identify by block number)

20. ABSTRACT (Continue on reverse side if necessary and identify by block number)

Thousands of expendable bathy-thermographs (XBTs) are used annually for ocean monitoring. This paper briefly describes the application of a microprocessor-based computer to encode signals directly from the XBTs, in a digital format for dissemination, and to prepare a bathy-message for radio transmission.

Reference is also made to the development activity for other sensors to be used as expendable probes.

DD FORM 1 JAN 73 1473 EDITION OF 1 NOV 65 IS OBSOLETE
S/N 0102-014-6601

Unclassified
SECURITY CLASSIFICATION OF THIS PAGE (When Data Entered)

Unclassified

SECURITY CLASSIFICATION OF THIS PAGE (When Data Entered)

REPORT DOCUMENTATION PAGE		READ INSTRUCTIONS BEFORE COMPLETING FORM
1. REPORT NUMBER 79-30	2. GOVT ACCESSION NO.	3. RECIPIENT'S CATALOG NUMBER
4. TITLE (and Subtitle) INTRODUCTION TO OCEAN OPTICS		5. TYPE OF REPORT & PERIOD COVERED Reprint 6. PERFORMING ORG. REPORT NUMBER
7. AUTHOR(s) Howard R. Gordon Raymond C. Smith J. Ronald V. Zaneveld		8. CONTRACT OR GRANT NUMBER(s) N00014-76-0067
9. PERFORMING ORGANIZATION NAME AND ADDRESS School of Oceanography Oregon State University Corvallis, Oregon 97331		10. PROGRAM ELEMENT, PROJECT, TASK AREA & WORK UNIT NUMBERS NR083-102
11. CONTROLLING OFFICE NAME AND ADDRESS Office of Naval Research Ocean Science & Technology Division Arlington, Virginia 22217		12. REPORT DATE 1979 13. NUMBER OF PAGES 41
14. MONITORING AGENCY NAME & ADDRESS(if different from Controlling Office)		15. SECURITY CLASS. (of this report) Unclassified 15a. DECLASSIFICATION/DOWNGRADING SCHEDULE

16. DISTRIBUTION STATEMENT (of this Report)

Approved for public release; distribution unlimited

17. DISTRIBUTION STATEMENT (of the abstract entered in Block 20, if different from Report)

18. SUPPLEMENTARY NOTES

Reprinted from SPIE, vol. 208, Ocean Optics VI (1979), pgs. 14-55.

19. KEY WORDS (Continue on reverse side if necessary and identify by block number)

20. ABSTRACT (Continue on reverse side if necessary and identify by block number)

In this introductory survey of optical oceanography we first present the fundamental inherent and apparent optical properties of natural waters. Relationships between these inherent and apparent optical properties, as related through the radiative transfer equation, are then presented. Following the first three theoretical sections brief discussions describing the application of ocean optics to geophysics, biological oceanography, and ocean remote sensing are then presented.

DD FORM 1 JAN 73 1473 EDITION OF 1 NOV 65 IS OBSOLETE
S/N 0102-014-6601

Unclassified

SECURITY CLASSIFICATION OF THIS PAGE (When Data Entered)

Irradiance and Beam Transmittance Measurements off the West Coast of the Americas

RICHARD W. SPINRAD, J. RONALD V. ZANEVELD, AND HASONG PAK

School of Oceanography, Oregon State University, Corvallis, Oregon 97331

Measurements of total irradiance versus depth and beam transmission versus depth were made at stations near shore along the west coast of the North and South American continents. The water types at each station were optically classified according to the system of Jerlov (1976), thus providing additional information for the description of the distribution of the world's ocean water types. In addition, the parameter k/c, where k is the irradiance attenuation coefficient and c is the beam attenuation coefficient, has been shown to be a useful parameter for determining the relative particle concentrations of ocean water.

INTRODUCTION

Optical classification of ocean water is an important means of distinguishing water types. *Jerlov* [1951] presented a method of classification according to spectral transmittance of downward irradiance at high solar altitude. Downward irradiance is defined as the radiant flux on an infinitesimal element of the upper face (0°–180°) of a horizontal surface containing the point being considered, divided by the area of that element [*Jerlov*, 1976]. *Jerlov*'s [1951] classification defined three different oceanic water types and five coastal water types, but further experimentation [*Jerlov*, 1964; *Aas*, 1967, 1969; *Matsuike*, 1967, 1973; *Matsuike and Sasaki*, 1968; *Højerslev*, 1973, 1974*a*, *b*; *Matsuike and Kishino*, 1973; *Shimura and Ichimura*, 1973; *Morel and Caloumenos*, 1974; *Rutkovskaya and Khaiemskiy*, 1974] has shown that the world's ocean waters may better be classified by 10 different curves of irradiance transmittance versus depth (Figure 1 shows the approximate curves of irradiance versus depth for each of the water types from *Jerlov* [1976]). Unfortunately, measurements of irradiance penetration are lacking in many areas of the world.

In this experiment, irradiance penetration measurements were made in conjunction with measurements of the water transmissivity. These measurements yield a parameter which, when used with the irradiance attenuation coefficient, can define water types even more clearly than the irradiance attenuation coefficient alone. The more parameters used to identify water types, the more accurately the water type can be described. It is shown in this paper that the method of water type identification by irradiance penetration measurements alone may yield untrue conclusions about the similarities in particle content or yellow matter content of the two water masses. That is, two water masses may have nearly identical values of an irradiance attenuation coefficient (thereby classifying them as the same water type, optically, according to *Jerlov* [1976]) but may in fact have very different profiles of light transmission versus depth. An explanation for this discrepancy is presented.

EXPERIMENTAL PROCEDURE AND RESULTS

Measurements with the irradiance meter and transmissivity meter were taken once a day at 1200 hours local time approximately 250 miles apart from Newport, Oregon, to Chimbote, Peru (Figure 2). Observations were made to depths of approximately 75 m. At two stations (8 and 9), equipment malfunctions prevented measurements from being taken.

The irradiance meter used had a flat opal glass diffuser as a cosine collector and contained a signal log amplifier to provide an output signal between ±4 V dc. The spectral response of the irradiance meter is shown in Figure 3. The transmissivity meter consisted essentially of a light-emitting diode (wavelength = 650 nm), collimating lenses, and a photodiode. The optical path length of the meter was 0.25 m.

The irradiance meter indicated values of the logarithm of the irradiance versus depth. From this information the value of the irradiance attenuation coefficient k could be calculated as follows [*Jerlov*, 1976]:

$$k = \frac{d(\log E)}{dz} \simeq \frac{\Delta(\log E)}{\Delta z}$$

where E is the measured irradiance and z is the depth below the ocean surface. Variations in solar elevation due to changes in latitude were considered in the calculation of k.

The transmissivity meter indicated the ratio of the radiant flux transmitted through 0.25 m of seawater to the incident radiant flux. The total attenuation coefficient c can be obtained from the measured transmissivity as follows [*Jerlov*, 1976]:

$$T = e^{-cr}$$

where T is the percent transmission, c is the total attenuation coefficient, and r is the geometrical path length of the meter.

In this experiment, r = 0.25 m; therefore

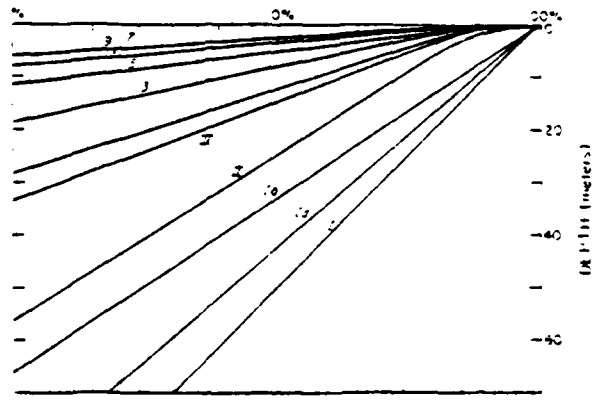

Fig. 1. Irradiance transmittance versus depth for 10 water types.

Paper number 8C0944.

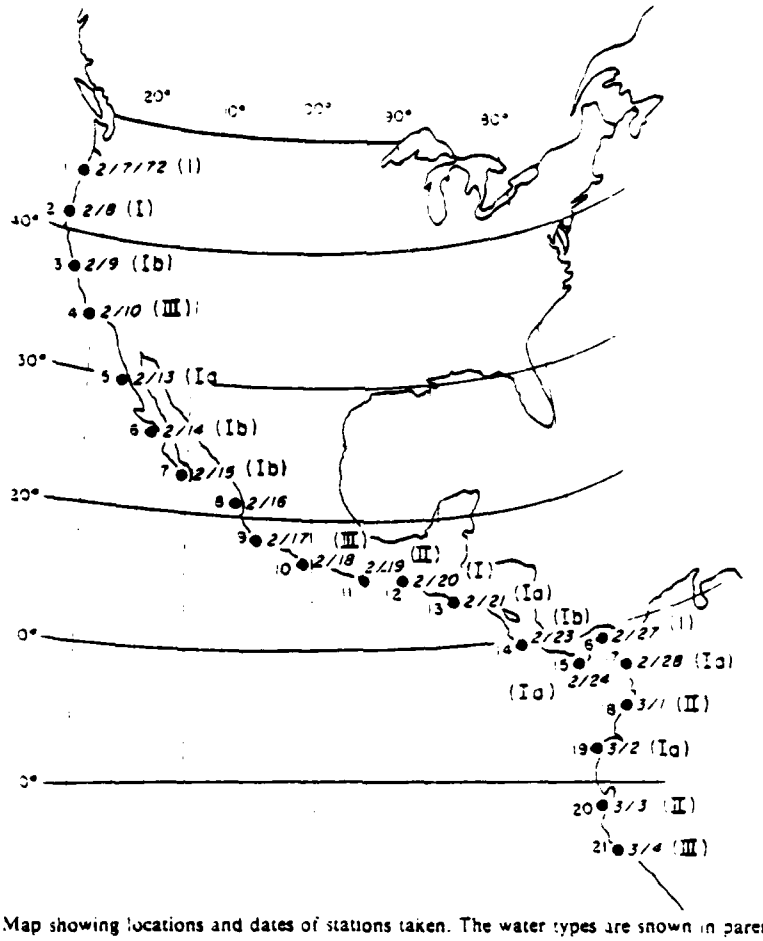

Fig. 2. Map showing locations and dates of stations taken. The water types are shown in parentheses.

$$T = e^{-0.2kc}$$

or

$$c = -4 \ln T$$

The high degree of accuracy obtained from the c meter is attributed to the precise collimation of the main beam and the small solid angle of detection [see *Bartz et al.*, 1978].

In Table 1 the measured values of k, T, and c and the quantity k/c are shown for each of the stations. Variations in transmissivity with depth indicated that for a given decrease in transmission (corresponding to an increase in c) the irradiance attenuation coefficient k increased proportionally. Therefore, neglecting slight variations (less than 5%), the values of k/c were quite constant with depth below the 3 or 4 m of surface

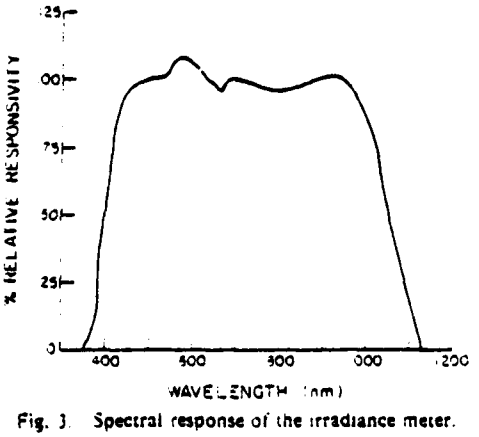

Fig. 3. Spectral response of the irradiance meter.

TABLE 1. Irradiance and Transmissivity Results From All Stations

Station	k, m^{-1}	Percent Transmission	c, m^{-1}	k/c
1	0.063	81.0	0.843	7.5 × 10^{-2}
2	0.021	92.0	0.794	2.64 × 10^{-2}
3	0.031	88.5	0.489	6.37 × 10^{-2}
4	0.055	85.5	0.627	8.78 × 10^{-2}
5	0.022	92.9	0.750	2.98 × 10^{-2}
6	0.029	85.5	0.628	4.66 × 10^{-2}
7	0.032	83.0	0.745	4.34 × 10^{-2}
10	0.053	82.5	0.770	6.89 × 10^{-2}
11	0.039	82.5	0.770	5.07 × 10^{-2}
12	0.013	84.0	0.697	1.92 × 10^{-2}
13	0.024	82.0	0.794	3.02 × 10^{-2}
14	0.029	57.3	2.23	1.32 × 10^{-2}
15	0.023	21.0	6.24	3.37 × 10^{-2}
16	0.068	50.8	2.713	2.52 × 10^{-2}
17	0.023	62.0	1.91	1.21 × 10^{-2}
18	0.034	83.5	0.721	4.73 × 10^{-2}
19	0.027	51.3	2.63	1.02 × 10^{-2}
20	0.043	77.3	1.03	4.19 × 10^{-2}
21	0.052	71.3	1.35	3.83 × 10^{-2}

TABLE 2. Classification of Water Types by Irradiance Attenuation Coefficient k

Water Type [*Jerlov*, 1976]	k, m^{-1}	Stations of This Water Type
I	0.016	2, 12
Ia	0.025	5, 13, 15, 17, 19
Ib	0.030	3, 6, 7, 14
II	0.035	1, 20, 18
III	0.055	4, 10, 21
	0.068	11, 16
3	0.095	
5	0.154	
7	0.223	
9	0.282	

water. Table 2 shows the values of k used to define water types optically [*Jerlov*, 1976]. This table also shows the classification of the water types from this experiment as identified solely by the irradiance attenuation coefficient k.

In Figure 4 the values of k for each station have been plotted against the values of c for the same station. Constant values of k/c are shown in the figure, and the values of k for various water types are shown along the abscissa.

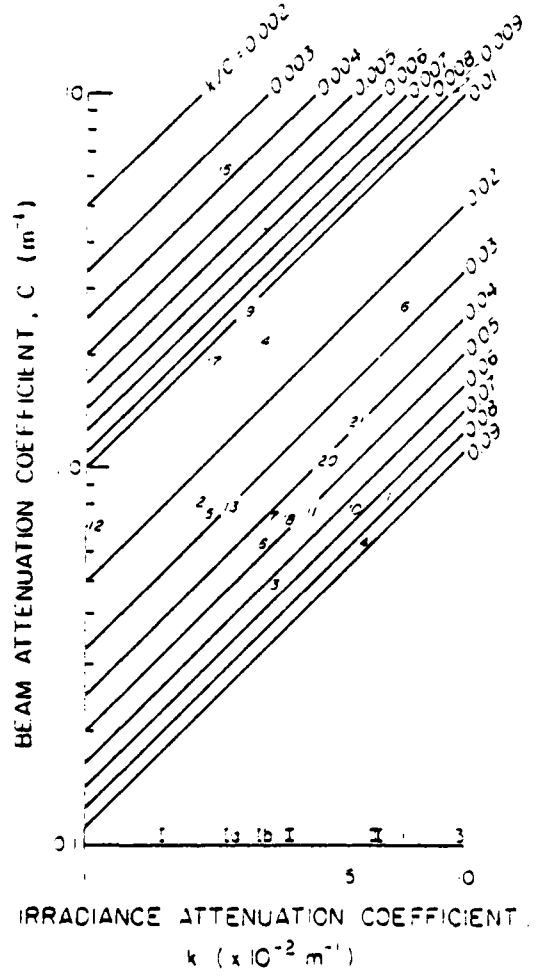

Fig. 4. Irradiance attenuation coefficient and beam attenuation coefficient measured at each station. Numbers correspond to station numbers.

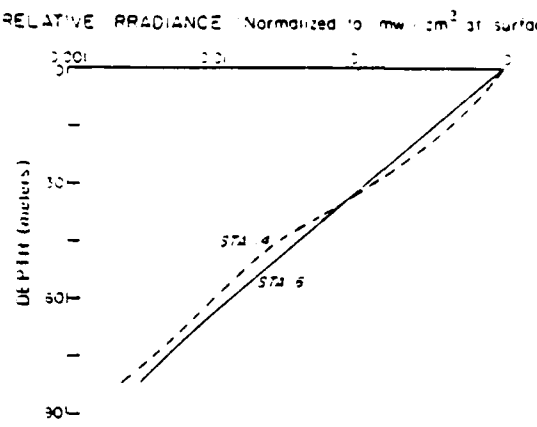

Fig. 5. Irradiance profiles with depth at stations 6 and 14.

OBSERVATIONS AND CONCLUSIONS

As Table 1 shows, a given water column may have a similar or identical value of k as another water column, but the value of c may be quite different. This is also seen in Figures 5 and 6, which show typical profiles of irradiance and transmissivity at stations 6 and 14. An important factor to consider is that c, in this experiment, was measured at a single wavelength of light (650 nm), whereas k was measured for the range of wavelengths from approximately 400 nm to 1000 nm. The fact that the value of c at 650 nm may be different for two water columns having identical values of k is an indication that the types of material in the two samples may differ significantly. The existence of yellow matter in the seawater could not be detected by the transmissivity meter alone, since the absorption of light by yellow matter is negligible for light of wavelength 650 nm [*Jerlov*, 1976]. However, particulate light attenuation at that wavelength is quite significant [*Burt*, 1958]. At the shorter wavelengths of light, both particulate matter and yellow substance contribute significantly to light attenuation.

The parameter k/c is a useful indication of relative amounts of particulate matter and yellow substance in seawater. The higher the value of k/c is, the more yellow matter or the less particulate content there is in the sample. The value of k for wavelengths of 400–1000 nm may be the same for a particle-laden sample as for a sample of water containing much yellow matter. The two samples would be quite different in nature and so should be classified as such. The use of a transmissivity

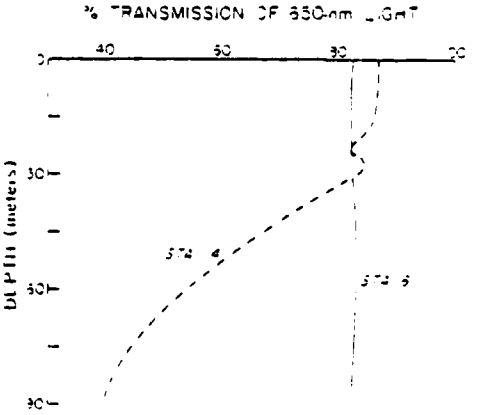

Fig. 6. Transmissivity profiles with depth at stations 6 and 14.

meter in conjunction with an irradiance meter allows such a classification. For example, stations 1, 3, 4, and 10 all have high values of k/c. The hypothesis that this represents large amounts of yellow matter may be justified by the fact that each of these stations is near a large river or city (possible sources of yellow matter). Station 1 is near the mouth of the Columbia River; station 3 is near the mouths of the Sacramento and American rivers at San Francisco; station 4 is offshore of Los Angeles, and station 10 is near the mouth of the Rio Balsas, one of the largest rivers on the west coast of Mexico. Conversely, the stations with the lowest values of k/c are in the region of the Gulf of Panama, an area which contains very few rivers and which may act as a depository for particulate matter being transported by the Equatorial Countercurrent.

The results of this experiment, as shown in Figure 4, indicate the use of the parameters k and c as water type identifiers. Unfortunately, these were the only oceanographic measurements taken at these stations, so correlations between the values of k/c and other hydrographic, chemical, or biological measurements are unobtainable. It would appear, however, that the values of k and k/c together provide useful parameters for water type identification. The measurement of k alone gives an indication of solar energy penetration into the sea: a measurement useful for mixed layer studies and biological analysis. The measurement of k/c indicates the type of material suspended or dissolved in the water.

The implications of this experiment are twofold. First, *Jerlov*'s [1976] chart of water types has been expanded to include measurements off the west coast of North, Central, and South America. Second, the use of the parameter k/c together with the parameter k has been shown to be of value in the identification of ocean water types according to material suspended or dissolved within the water.

Acknowledgments. The authors wish to thank Robert Bartz for his work in the development and fabrication of the combined irradiance and transmissivity meter and the crew of the R. V. *Cayuse* for their assistance and cooperation during the cruise. We also wish to thank Pam Wegner for typing the manuscript. Support from the Office of Naval Research through contract N000014-76-C-0067 under project NR 083-102 is gratefully acknowledged.

REFERENCES

Aas, E., The natural history of the Hardangerfjord, 9, Irradiance in Hardangerfjorden, *Univ. Oslo Inst. Geofys. Rep.*, *46*, 59–78, 1967.

Aas, E., On submarine irradiance measurements, *Univ. Copenhagen Inst. Phys. Oceanogr. Rep.*, *6*, 45 pp., 1969.

Bartz, R., J. R. V. Zaneveld, and H. Pak, A transmissometer for profiling and moored observations in water, *Proc. Simp. Soc. Phot. Opt. Eng. 22nd.*, *160*, 1978.

Burt, W. V., Selective transmission of light in tropical Pacific waters, *Deep Sea Res.*, *5*, 51–61, 1958.

Højerslev, N. K., Inherent and apparent optical properties of the western Mediterranean and the Hardangerfjord, *Univ. Copennagen Inst. Phys. Oceanogr. Rep.*, *21*, 70 pp., 1973.

Højerslev, N. K., Inherent and apparent optical properties of the Baltic, *Univ. Copennagen, Inst. Phys. Oceanogr. Rep.*, *23*, 70 pp., 1974a.

Højerslev, N. K., Daylight measurements for photosynthetic studies in the western Mediterranean, *Univ. Copennagen Inst. Phys. Oceanogr. Rep.*, *26*, 38 pp., 1974b.

Jerlov, N. G., Optical studies of ocean water, *Rep. Swed. Deep-Sea Exped.*, *3*, 73–97, 1951.

Jerlov, N. G., Optical classification of ocean water, in *Physical Aspects of Light in the Sea*, pp. 45–49, University of Hawaii Press, Honolulu, 1964.

Jerlov, N. G., *Marine Optics*, 231 pp., Elsevier, New York, 1976.

Matsuike, K., Study on the optical characteristics of the waters in the three oceans, I, Optical structure of the Kurosmio (Japan Current) from lat. 20°S to lat. 31°N along the meridian of 142°E, *J. Tokyo Univ. Fish.*, *53*, 31–40, 1967.

Matsuike, K., A study on optical nature in oceanic waters, *Mer.*, *11*–44, 1973.

Matsuike, K., and M. Kishino, Measurement of insolation and submarine light, Preliminary report of the Hakuho Maru cruise KH-7[illegible] 3 (IBP cruise), June 8–July 29, 1971, pp. 27–42, Ocean Res. Inst., Univ. of Tokyo, Tokyo, 1973.

Matsuike, K., and Y. Sasaki, The optical characteristics of the water in the three oceans, II, Optical structure of the Antarctic Ocean from lat. 45°S to lat. 70°S and from the meridian of 132°E to 149°W, including the Ross Sea, *J. Tokyo Univ. Fish.*, *54*, 57–74, 1968.

Morel, A., and L. Caloumenos, Variabilite de la repartition spectrale de l'energie photosynthetique, *Tethys*, *6*, 93–104, 1974.

Rutkovskaya, V. A., and E. N. Khalemskii, Calculating the depths of penetration of solar energy in sea water (with the Pacific as an example), *Oceanology*, *14*, 398–404, 1974.

Shimura, S., and S. Ichimura, Selective transmission of light in the ocean waters and its relation to phytoplankton photosynthesis, *J. Oceanogr. Soc. Jap.*, *29*, 257–266, 1973.

(Received June 2, 1978;
revised August 28, 1978;
accepted September 5, 1978.)

Nitrous Oxide Production in the Ocean

YUVAL COHEN

Environmental Protection Service, Ministry of the Interior, Jerusalem, Israel 91060

LOUIS I. GORDON

School of Oceanography, Oregon State University, Corvallis, Oregon 97331

Examination of vertical profiles of N_2O, oxygen, and nitrate from the Northeast and Northwest Atlantic, Northeast Pacific and eastern tropical North Pacific reveals a striking consistency in the relationships among them. With the exception of zones of active denitrification, N_2O is negatively correlated with oxygen and positively correlated with nitrate throughout the water column and it is, therefore, concluded that N_2O production in the ocean is associated with the oxidative regeneration of nitrate. In both the Atlantic and Pacific Oceans, the difference between the measured N_2O concentration and its equilibrium solubility is linearly correlated with apparent oxygen utilization and from this relationship and the Redfield plankton decomposition model it is estimated that N_2O-nitrogen comprises about 0.1 to 0.4% of the nitrogen regenerated in the ocean. From the ratio of N_2O to nitrate production during nitrate regeneration and estimates of the overall regeneration of nitrate in the ocean, it is concluded that the total marine production of N_2O is in the range of 4 to 10 Tg-N yr^{-1} (6 to 16 Tg-N_2O yr^{-1}). This estimate is in good agreement with estimates of the N_2O loss to the atmosphere derived from N_2O measurements at the sea surface.

INTRODUCTION

Interest in the sources and sinks of atmospheric nitrous oxide (N_2O), arising from the realization that N_2O catalyzes ozone reduction in the stratosphere [*Crutzen*, 1970], has stimulated a lively debate on the role of the ocean in the global N_2O cycle. However, only one aspect of the marine N_2O cycle, namely the net N_2O flux across the ocean-atmosphere interface, is relevant to the ozone depletion problem, hence in this connection the ocean has been treated as a simple system which acts either as a net source [*Hahn and Junge*, 1977; *Liu et al.*, 1977] or as a net sink [*McElroy et al.*, 1976] for atmospheric N_2O.

Basically, two approaches, often yielding conflicting results, have been used to calculate the N_2O exchange between the ocean and the atmosphere. The first involves extrapolating to global scale fluxes calculated from the results of N_2O measurements at the sea surface combined with models for gas exchange [*Hahn*, 1974*a*; *Hahn and Junge*, 1977; *Liss and Slater*, 1974]. The second approach is based on the assumption that as in soils, N_2O production in seawater arises primarily from denitrification and that therefore it can be evaluated from estimates of marine denitrification multiplied by some numerical value for the N_2O yield in the process [*McElroy et al.*, 1977; *Council for Agricultural Science and Technology*, 1976]. The recent studies of *Cohen and Gordon* [1978] and *Cohen* [1978], however, clearly demonstrated that unlike the situation commonly encountered in soils, denitrification in the marine environment results in N_2O consumption rather than production, and, therefore, the second approach is invalid.

From N_2O and oxygen measurements in the North Atlantic and from the results of assays in natural seawater incubated with ammonia and various organic substrates, *Yoshinari* [1973] concluded that N_2O production in seawater arises primarily from nitrification. This conclusion was later supported by the N_2O, oxygen and nutrients data of *Cohen and Gordon* [1978] from the eastern tropical North Pacific. *Bremner and Blackmer* [1978] have recently demonstrated the release of N_2O from soils during aerobic nitrification. If this applies to the ocean as a whole then it should be possible to estimate the marine production of N_2O from information on the recycling of nitrate within the ocean.

This paper presents an examination of N_2O, oxygen, and nitrate data from the Atlantic and Pacific Oceans in an attempt to establish the relationships among these variables and to estimate the overall production of N_2O in the ocean.

DATA

N_2O data from the Northeast Atlantic (NEA) are from *Hahn* [1974*a*, 1975] and oxygen data are from *Roether et al.* [1974]. In these reports only graphic presentations of the water column data are given. Surface N_2O concentrations in the North Atlantic are listed in *Hahn* [1974*a*]. His N_2O measurements were made at sea by thermal conductivity gas chromatography (GC) with a precision of about 5%. The accuracy of these N_2O measurements will be discussed later.

N_2O and oxygen data from the Northwest Atlantic (NWA) and the Caribbean are from *Yoshinari* [1973, appendix]. N_2O samples were analyzed on shore by helium ionization GC about one month after collection. The precision of measurement was about 3.5% and the estimated accuracy about 5%. Since neither *Hahn* [1974*a*, 1975] nor *Yoshinari* [1973] measured nitrate, some Geosecs North Atlantic nitrate data [*Bainbridge*, 1975] was used here.

N_2O, oxygen and nitrate data from the eastern tropical North Pacific (ETNP) are from *Cohen et al.* [1977] and *Cohen and Gordon* [1978]; N_2O data from the Northeast Pacific (NEP) is first reported here and the oxygen and nitrate data are from *Murray et al.* [1977]. The N_2O measurements were made by electron capture GC [*Cohen*, 1977] with a precision of about 2% and estimated accuracy of 3%.

The solubility coefficients of N_2O in seawater were calculated by fitting *Weiss*' [1970] equation, which expresses the Bunsen solubility coefficient of a gas as a function of temperature and salinity, to the data of *Markham and Kobe* [1941] for the solubility of N_2O in aqueous sodium chloride solutions. *Junge et al.* [1971] estimated that the Bunsen coefficients so obtained are accurate to about ±7% but R. F. Weiss (personal communication, 1977) estimates their accuracy to be better

Paper number 8C1031
0148-0227/79/013C-1031$01.00

than 3%. *Weiss'* [1970] oxygen solubility coefficients were used to calculate oxygen saturation.

RESULTS

In almost all the marine environments where N_2O measurements have been made its distribution appears to be inversely correlated with that of dissolved oxygen (*Junge et al.*, 1971; *Hahn*, 1974a, 1975; *Yoshinari*, 1973, 1976; *Cohen*, 1978, 1977). Exceptions to this pattern have been found only in oxygen deficient environments where oxygen-based respiration was not the major biological respiratory mechanism [Cohen, 1978, 1977]. As an illustration of these relationships, typical vertical profiles of N_2O, oxygen, and nitrate from the North Atlantic, NEP and ETNP are shown in Figure 1. In both the North Atlantic and the NEP the N_2O profiles are essentially mirror images of the oxygen profiles with maximal N_2O concentrations in the oxygen minimum. In the ETNP N_2O is inversely correlated with oxygen throughout the water column except for the oxygen deficient layer at ca. 150 to 700 m where consumption of N_2O by denitrification results in minima in the N_2O profiles [*Cohen and Gordon*, 1978]. The profiles from the ETNP shown in Figure 1 are examples of maximal (station 12) and minimal (station 9) denitrification as reflected by the intensity of the N_2O and nitrate minima.

Among the environments considered here, the lower the oxygen concentration at the depth corresponding to the N_2O maximum, the higher the N_2O concentration at the N_2O maximum (Table 1). This appears to be the case also when N_2O and oxygen saturations rather than absolute concentrations are considered. For each environment the N_2O saturation value in Table 1 is relative to the ambient atmospheric N_2O concentration. While the different atmospheric N_2O concentrations listed in Table 1 most probably reflect both real variations in N_2O and systematic calibration errors among the analytical procedures used, the differences in the N_2O saturation values among the various environments are considered real since in each case the same method was used for the N_2O measurements in air and water.

From the foregoing, it appears that N_2O concentrations (or saturations) progressively increase with decreasing oxygen concentrations (or saturations) throughout the Northern Hemisphere. This is reminiscent of the relationships between oxygen and the nutrient elements which are regenerated at the expense of oxygen, and as shown in Figure 1, the vertical distribution of N_2O closely resembles that of nitrate except in the uppermost nitrate-depleted part of the water column.

The N_2O-oxygen relationships differ in the NWA, NEP, and ETNP above and below the oxygen minimum. This is illustrated for selected representative stations in Figure 2. For a given oxygen concentration N_2O levels in the NWA are higher below the oxygen minimum than above it while the reverse is true for the NEP and the ETNP. The variations in the N_2O-O_2 slopes may arise from regional variations in the rates of N_2O production and oxygen consumption and also from mixing of different water masses containing different initial concentrations of N_2O and oxygen.

Similar to the definition of 'apparent oxygen utilization' (AOU) by *Redfield et al.* [1963]:

$$AOU = O_{2(g,sl)}^{\text{saturation}} - O_2^{\text{measured}} \quad (1)$$

'apparent N_2O production' (ΔN_2O) was defined by *Yoshinari* [1973] as:

$$\Delta N_2O = N_2O^{\text{measured}} - N_2O_{(g,sl)}^{\text{saturation}} \quad (2)$$

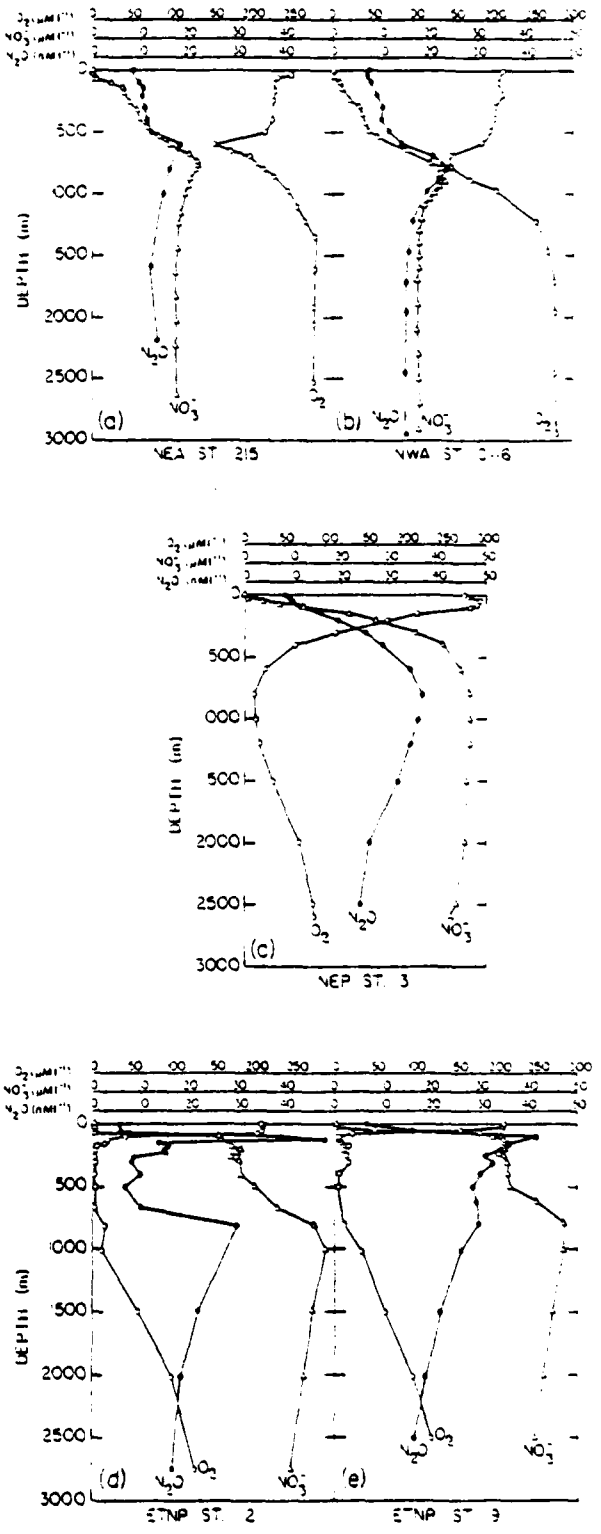

Fig. 1. Vertical profiles of N_2O, oxygen and nitrate from (a, b) the North Atlantic, (c) Northeast Pacific, and (d, e) Eastern Tropical North Pacific. (a) 'Meteor' cruise 21, station 215 [*Hahn*, 1975; *Roether et al.*, 1974]. Nitrate data from Geosecs station 27 [*Bainbridge*, 1975]. (b) Station C-16 [*Yoshinari*, 1973]. Nitrate data from Geosecs station 29 [*Bainbridge*, 1975]. (c) T. G. Thompson cruise TT-121, station 3. (d, e) 'Wecoma' cruise Wetoc 77-1, stations (d) 12 and (e) 9 [*Cohen et al.*, 1977].

TABLE 1. Mean N_2O and Oxygen Concentrations and Percent N_2O and Oxygen Saturations at the N_2O Maxima in Some Marine Environments

Location	N_2O Concentration, nmol l^{-1}	Oxygen Concentration, μmol l^{-1}	N_2O Saturation, %	Oxygen Saturation, %	Atmospheric N_2O Concentration ppbv
Northeastern Atlantic[a]	16.8 ± 1.8(3)	173 ± 19(3)	172 ± 19	82 ± 2	273
Northwestern Atlantic[b]	21.4 ± 1.7(12)	154 ± 10(8)	190 ± 18	53 ± 4	325
Caribbean[c]	27.9 ± 0.9(7)	130 ± 3	240 ± 11		328
Northeastern Pacific[d]	36.9(1)	12(1)	321	4	278
Eastern Tropical North Pacific[e]	39.5 ± 4.5(9)	11 ± 3(8)	497 ± 55	4 ± 3	287

Percent N_2O saturations are relative to the Atmospheric N_2O concentrations listed in column 6. Number in parentheses is number of stations.

[a] Average values for stations 213, 214, 215, 'Meteor' cruise 23, *Hann* [1975]. Both N_2O and oxygen data are from graphical presentations in the original reports.

Average values for stations C-7, C-11, C-16, C-20, *Yoshinari* [1973, appendix].

[c] Average values from *Yoshinari* [1973, appendix]. Only an average value for the oxygen concentration in the oxygen minimum of the Caribbean is given.

[d] Station 3, 'T. G. Thompson' cruise TT-121.

[e] Average values for station 3-12, 'Wecoma' cruise Weloc-77-I [*Cohen et al.*, 1977]. The relatively large standard deviation of the oxygen measurements reflects the inaccuracy of the Winkler procedure at very low oxygen concentrations.

Thus, $\Delta N_2O/AOU$ is the ratio of N_2O production to oxygen consumption. *Yoshinari* [1973] found a linear relationship between ΔN_2O and AOU in the NWA. The relationships between ΔN_2O and AOU at Yoshinari's four stations from the NWA, one station from the NEP and ten stations from the ETNP are shown in Figure 3. (In the ETNP only samples containing more than 10 μmol O_2 l^{-1} were considered since at lower O_2 concentration the effects of denitrification are dominant [*Cohen and Gordon*, 1978].)

A comparison of Figures 2 and 3, noting that both employ the same scales reveals that in the NWA the two slopes, above and below the oxygen minimum, on the N_2O-O_2 diagram have merged into one on the ΔN_2O-AOU diagram. The deep samples (ca. >1400 m), however, do not fall on this trajectory but cluster around ca. 50 μmol AOU l^{-1}. In the Pacific, on the other hand, the separation between the samples from above and below the oxygen minimum is greater on the ΔN_2O-AOU diagram than on the N_2O-O_2 diagram.

Results of linear regressions of ΔN_2O versus AOU for all the groups of points in Figure 3 are listed in Table 2 and the corresponding regression lines are plotted in Figure 3. As can be seen from the high correlation coefficients for the regressions, a linear function adequately describes the relationships between ΔN_2O and AOU in the Pacific also, provided that samples from above and below the oxygen minimum are grouped separately. (The regression coefficients in Table 2 for Yoshinari's data from the NWA are slightly different than those he obtained for the same data, probably because of small differences in the calculations of the N_2O solubility coefficients.)

The ratios of N_2O production to oxygen consumption ($\Delta N_2O/AOU$ on a molar basis), referred to here as the 'N_2O oxidative ratios,' for the different groups of samples in Figure 3 vary from $7.6 \cdot 10^{-3}$ to $2.18 \cdot 10^{-2}$ (Table 2). The N_2O oxidative ratios for the 0 to 1000 m depth range in the NWA and for the 0 to 800 m depth range in the NEP are quite similar and both are about half the oxidative ratio in shallow waters of the ETNP. The regression lines for these three suites of samples have near zero intercepts. The N_2O oxidative ratios in deep waters of the NEP and the ETNP are higher than those found in shallower waters and the corresponding regression lines have large negative intercepts.

Because ΔN_2O was found to be a linear function of AOU and since nitrate regeneration is also linearly related to oxygen consumption [*Redfield et al.*, 1963] it is possible to calculate the ratio of N_2O production to nitrate production. According to the *Redfield et al.* [1963] plankton decomposition model:

$$(CH_2O)_{106}(NH_3)_{16}H_3PO_4 + 138O_2 = 106CO_2 + 122H_2O + 16HNO_3 + H_3PO_4 \quad (3)$$

16 moles of nitrate are formed at the expense of 138 moles of oxygen. Extensive tests of the model in various areas of the ocean [*Alvarez-Borrego et al.*, 1975] showed that it is consistent with field data. Thus, the ratio of N_2O to nitrate production is $(\Delta N_2O/AOU) \cdot (138/16)$. Values of this ratio for the environments considered in Figure 3, where N_2O formation is expressed as a percentage of the nitrate formation on a μg atom-N basis vary from 0.13 to 0.37% (Table 3).

Discussion

The Relationship Between Oxygen Consumption and N_2O Production in the Ocean

Examination of vertical profiles of N_2O, oxygen, and nitrate from the Atlantic and Pacific Oceans reveals a striking con-

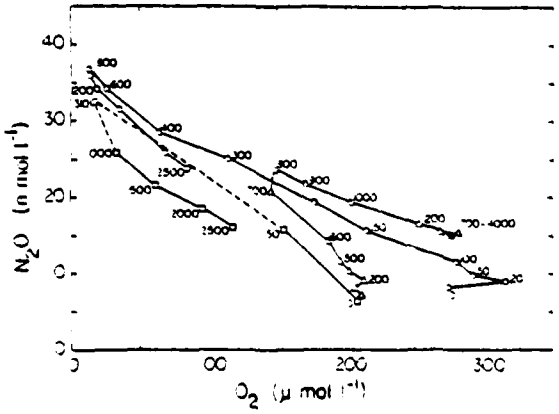

Fig. 2. N_2O-oxygen relationships for stations in the Northwest Atlantic (triangles, *Yoshinari* [1973], station C-16), Northeast Pacific (circles, station 3), and Eastern Tropical North Pacific (squares, *Cohen et al.* [1977], station 9). The dotted line covers the region where samples contained less than 10 μM O_2.

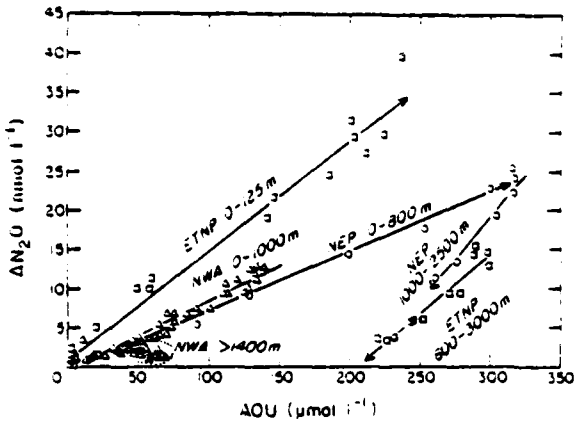

Fig. 3. ΔN_2O-AOU relationships for four stations from the Northwest Atlantic [*Yoshinari*, 1973, stations C-7, C-11, C-16, C-20], one station from the Northeast Pacific (station 3), and ten stations from the Eastern Tropical North Pacific (only samples containing more than 17 μM O_2 l^{-1}) [*Cohen et al.*, 1977, stations 2–12). (*a*) Northwest Atlantic 0–1000 m. (*b*) Northeast Pacific 0–800 m. (*c*) Eastern Tropical North Pacific 0–125 m. (*d*) Northeast Pacific 1000–2500 m. (*e*) Eastern Tropical North Pacific 600–3000 m. The dotted line encircles the Northwest Atlantic samples from depths greater than 1400 m. Arrowheads indicate increasing depth.

sistency in the relationships among them. N_2O is positively correlated with nitrate and negatively correlated with oxygen throughout the water column in both oceans except where denitrification occurs in the ETNP. Like nitrate production, N_2O production was found to be linearly related to oxygen consumption in all the marine environments studied (Figure 3) and this supports the conclusions of *Yoshinari* [1973] and *Cohen and Gordon* [1978] that N_2O production in the ocean primarily arises from nitrification, the process whereby nitrate is regenerated.

The overall variation in the ratios of N_2O production to oxygen consumption, and hence to nitrate production, among the environments investigated is rather small (less than a factor of 3, Table 2). However, the differences in these ratios for waters deeper and shallower than ca. 300 to 1000 m in both the Atlantic and Pacific are significant. We do not fully understand these differences, but a possible clue can be derived from examination of the temperature and salinity distributions of the NWA, NEP and ETNP (Figure 4). In the NWA and NEP, variations in the ΔN_2O to AOU ratios (Figure 3) occur at approximately the same depths where singularities appear on the temperature-salinity diagrams. These singularities indicate the transition from the locally formed central water masses to the deep water masses of northern and southern origins [*Sverdrup et al.*, 1942]. The situation is more complicated in the ETNP because there, the two regression lines in Figure 3 represent waters separated by the oxygen deficient zone where ΔN_2O is not linearly related to AOU. The water below ca. 600 m in the ETNP is comprised of a mixture of Intermediate Water (characterized by a salinity minimum) and Deep Pacific Water. In both the Atlantic and Pacific, the nonlinearity of the upper part of the θ-S diagrams apparently does not affect the ΔN_2O to AOU ratios. It is thus possible that variations in the ΔN_2O to AOU ratios reflect different characteristics, with respect to N_2O formation, of the relatively warm, central water masses and the cold, deep water masses. The abundance of nitrifying microorganisms, the fraction of these which contribute to N_2O formation and the availability and composition of the oxidizable organic matter might be some of the distinctive properties of water masses of different origins. The limited data base of this work does not permit a detailed discussion of this hypothesis and clearly, measurements of N_2O, oxygen and nutrients in the southern and northern source regions of the deep waters of the ocean are required for this purpose.

Estimates of N_2O Production in the Ocean and Its Escape to the Atmosphere

Given the relative constancy of the N_2O oxidative ratios and assuming that the N_2O-nitrate relationships established here are representative of the whole ocean, an attempt can be made to estimate the rate of N_2O production in the ocean. A model for the marine nitrogen cycle, taken from the global model of *Liu et al.* [1977], is shown in Figure 5. The reader is referred to the original paper for details on the estimation of the various numerical values but some relevant points will be mentioned here. The large nitrogen reservoir in marine sediments was neglected because the transfer rates between this reservoir and the others were considered to be very small; the values for nitrogen input into the ocean are independent estimates but the output value for marine denitrification is a forced value based on a steady state assumption; similarly, the nitrogen mineralization rate is a forced value determined from independent estimates of the rate of nitrogen assimilation in the ocean. Taking the 2000 Tg-N yr^{-1} (1 Tg = 10^{12}g) mineralization rate as a maximal estimate of the oxidative production of nitrate in the ocean and an average value of 0.2% for the ΔN_2O to ΔNO_3^- ratio in the process (Table 3), the total oceanic N_2O production rate would be 4 Tg-N yr^{-1} or 6.3 Tg-N_2O yr^{-1}. Because of all the values in Figure 5 the estimated N_2O production rate depends only upon the nitrogen mineralization rate, it is important to note that a somewhat independent estimate of this rate by *McElroy et al.* [1976], 1500 Tg-N yr^{-1}, is quite similar to that of *Liu et al.* [1977].

Assuming a steady state N_2O distribution, N_2O production must be balanced by N_2O loss from the ocean. The only known oceanic sinks for N_2O are its escape to the atmosphere at the air-sea interface and its biochemical consumption in oxygen deficient and anoxic waters [*Cohen*, 1978, 1977]. Since the magnitude of the latter sink is at the present time unknown and its areal extent limited it will be neglected for the moment

TABLE 2. Regression Equations of ΔN_2O (nmol l^{-1}) on AOU (μmol l^{-1}) for Some Marine Environments

Location	Depth Range, m	Regression Equation	r	n
Northwestern Atlantic	100–2500	$\Delta N_2O = -0.437 + (0.089 \pm 0.003)AOU$	0.972	36
Northeastern Pacific	0–800	$\Delta N_2O = -0.928 + (0.076 \pm 0.003)AOU$	0.993	8
	100–2500	$\Delta N_2O = -46.248 + (0.218 \pm 0.026)AOU$	0.988	5
Eastern Tropical North Pacific*	0–125	$\Delta N_2O = 0.909 + (0.140 \pm 0.004)AOU$	0.986	
	600–3000	$\Delta N_2O = -31.330 + (0.152 \pm 0.013)AOU$	0.957	14

*Only samples with O_2 > 17 μmol l^{-1}.

TABLE 3. N_2O Production in Some Marine Environments Expressed as a Percentage of Nitrate Production on a μg atom-N Basis

Environment	$\Delta N_2O/\Delta NO_3^-$, %
North Atlantic	
0–1000 m	0.15
Northeast Pacific	
0–800 m	0.13
1000–2500 m	0.37
Eastern Tropical North Pacific	
0–125 m	0.24
700–3000 m	0.26

and the estimated N_2O production rate given here will be compared to available data on the rate of N_2O loss to the atmosphere. The procedure will be to calculate an average oceanic surface supersaturation of N_2O required to produce an N_2O flux into the atmosphere of 4 Tg-N yr^{-1} and to compare this calculated value with the results of N_2O measurements at the sea surface.

According to the 'stagnant film' model [*Bolin*, 1960], the rate limiting step in gas exchange across the air-sea interface is molecular diffusion through a laminar layer. The gas flux (F) across the interface is:

$$F = \frac{D}{Z} \cdot \Delta \qquad (4)$$

where D is the gas molecular diffusion coefficient, Z is the thickness of the laminar layer and Δ is the difference between the measured concentration of the gas at the base of the laminar layer and its equilibrium solubility. Taking 18°C as the average surface temperature of the ocean [*Bialek*, 1966, p. 54] a N_2O molecular diffusion coefficient of $2 \cdot 10^{-5}$ cm^2 s^{-1} at this temperature (interpolated from the values given in *Broecker and Peng* [1974]), a Z value of $50 \cdot 10^{-4}$ cm [*Broecker and Peng*, 1974], a flux of 6.3 Tg-N_2O yr^{-1} ($4.5 \cdot 10^{12}$ nmol N_2O s^{-1}), and multiplying the right hand side of (4) by the total area of the ocean ($361 \cdot 10^{18}$ cm^2), a Δ value of 0.32 nmol N_2O l^{-1} is obtained. Taking an average atmospheric N_2O concentration of 290 ppbv, the N_2O equilibrium solubility at 18°C and 35‰ salinity would be 7.29 nmol l^{-1}. Combining this value with the above result for Δ, the surface water of the ocean would on the average be 105% supersaturated with N_2O. It is important to note that this calculation is relatively insensitive to changes in the atmospheric N_2O concentration. Taking the lowest (250 ppbv) and highest (328 ppbv) atmospheric N_2O concentrations listed in Table 1 instead of 290 ppbv would change the final result for the average oceanic surface supersaturation by less than 1%.

The above results will now be compared to the results of direct N_2O measurements at the sea surface. Table 4 includes all the presently available surface N_2O measurements with the exception of one data set, that of *Rasmussen et al.* [1976], from the Eastern Pacific. The data of *Rasmussen et al.* [1976] is not included because of the large scatter in the N_2O saturation values, especially south of the equator. For example, their surface N_2O saturation values at 5.7 and 7.6°S were 105 and 280%, respectively (see also *Cohen and Gordon* [1977, Figure 6]). The other data sets in Table 4 were grouped with respect to latitude and replicate observations at one location were averaged. With the exception of the data from the 'Meteor' cruise 16 which will be discussed in detail below, surface N_2O saturations in both the Atlantic and Pacific Oceans are quite low with an average value of 109%. This average supersaturation is higher than the 105% calculated above but in light of the uncertainties involved in the calculations both results are compatible. Considering the range of the $\Delta N_2O/\Delta NO_3^-$ values in Table 3, an uncertainty of a factor of 2 is quite reasonable for the flux calculated from the N_2O-nitrate relationships. Taking 8 rather than 4 Tg-N yr^{-1} for the flux value in (4) would yield an average surface N_2O supersaturation of 109%.

Other estimates of the N_2O exchange across the ocean-atmosphere interface can be examined in terms of (4) and Table 4. Maximal estimates are those of *Hahn* [1974*a*, 1975] and *Hahn and Junge* [1977] who concluded that the ocean is a net source for atmospheric N_2O with a magnitude of 16 to 160 Tg-N yr^{-1} and a most likely value of 45 Tg-N yr^{-1} (170 Tg-N_2O yr^{-1}), and a minimal estimate is that of *McElroy et al.* [1976] who argued that the ocean is a net sink for atmospheric N_2O with a magnitude of 40 Tg-N yr^{-1} (63 Tg-N_2O yr^{-1}).

Hahn's [1974*a*, 1975] and *Hahn and Junge*'s [1977] estimates of the oceanic N_2O flux were obtained by extrapolating to a global scale the results of N_2O measurements in surface and shallow waters of the North Atlantic made during the 'Meteor' cruises in 1969 to 1971 (Table 4). On the basis of that data, *Hahn* [1974*a*] concluded that 'our measurements yield an average N_2O saturation of 180% for the North Atlantic surface water.' Apparently, as was pointed out by *McElroy et al.* [1976], this conclusion was heavily weighted by the few measurements from the 1969 cruise. Of these measurements, one (293% saturation) was not a surface sample and of the surface samples only one was more than 180% supersaturated with N_2O. Furthermore, the analytical method for the seawater N_2O measurements employed in 1969 was much less precise than that used in 1970 and 1971, and it is also significant that *Yoshinari*'s [1973] data from the Northwest Atlantic reveals surface N_2O supersaturations much lower than those found by Hahn at approximately the same latitudes in the Northeast Atlantic in 1969. Inserting *Hahn and Junge*'s [1977] most likely value for the oceanic N_2O flux into the atmosphere (170 Tg-N_2O yr^{-1}, derived from (4) with $Z = 50 \cdot 10^{-4}$ cm) into (4) without changing the numerical values of the other parameters used above would yield an average 150% N_2O supersaturation for the whole surface of the ocean. Table 4, however, shows that with the exception of the results from the 'Meteor' cruise in 1969, not a single surface sample, from anywhere in the ocean, was more than 135% supersaturated with N_2O.

The conclusion of *McElroy et al.* [1976] that the ocean is a net sink for atmospheric N_2O is also inconsistant with the data in Table 4. Inserting their flux estimate of −63 Tg-N_2O yr^{-1} into (4) yields an average oceanic N_2O saturation of 56%, a value not supported by any field data. It should be mentioned that, in part, McElroy et al.'s conclusions were based on

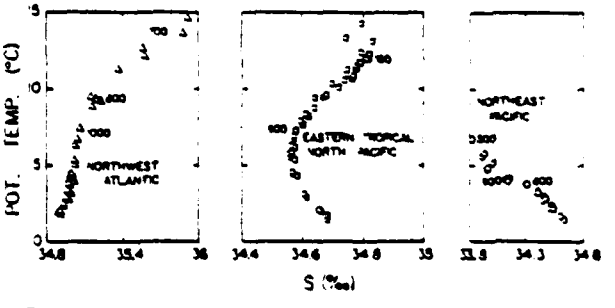

Fig. 4. Potential temperature-salinity diagrams for (*a*) the Northwest Atlantic [*Yoshinari*, 1973], (*b*) Eastern Tropical North Pacific [*Cohen et al.*, 1977], and (*c*) Northeast Pacific [*Murray et al.*, 1977].

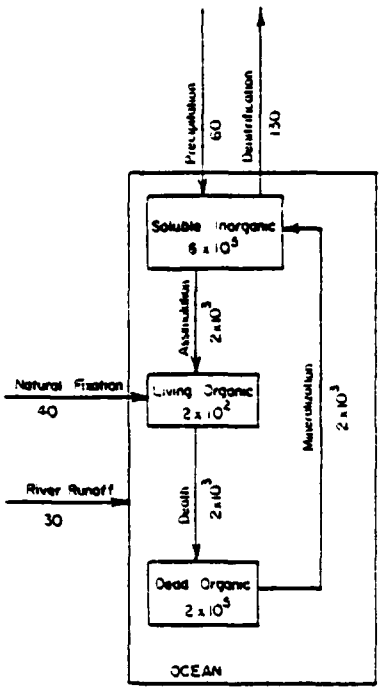

Fig. 5. The marine nitrogen cycle (part of Figure 2 of *Liu et al.* [1977]). *Units are in* Tg-N (1 Tg = 10^{12} g) *for reservoir contents or* Tg-N per year for transfer rates.

combining their own interpretation of *Hahn*'s [1974a] data with earlier N_2O measurements by *Craig and Gordon* [1963]. However, the data of Craig and Gordon were composites of N_2O samples from various geographic locations and depths which in light of Figure 1 cannot be considered representative of surface data.

CONCLUSIONS

Neither *Hahn*'s [1974a] and *Hahn and Junge*'s [1977] nor *McElroy et al.*'s [1976] estimates of the N_2O exchange between the ocean and the atmosphere are supported by the presently available surface N_2O data. On the other hand, the estimate presented here of an oceanic source of atmospheric N_2O with a magnitude of less than 10 Tg-N yr^{-1} (16 Tg-N_2O yr^{-1}) which was derived from information on the cycling of nitrogen within the ocean is in good agreement with the results of N_2O measurements in surface waters. In spite of this agreement it should be clear that the analysis presented here is far from being a complete N_2O budget for the ocean. First, N_2O data from the Pacific Ocean are very limited and no data are available for the Indian and Southern Oceans. Data from the Southern Ocean are especially important because they provide insight into the N_2O-oxygen-nitrate relationships at the time the bulk of the ocean's deep waters are formed. Second, if *Hahn*'s [1975] proposition that N_2O might be formed as a byproduct of nitrate assimilation by phytoplankton is true, an additional N_2O source, which was not accounted for in the present analysis, might exist in the euphotic zone. Although the data of *Cohen and Gordon* [1978] from the ETNP and N_2O profiles from different seasons in the Northwest Atlantic [*Yoshinari*, 1973] indicate that if this source exists its contribution is rather small, the possibility has to be investigated. Third, the quantitative significance of denitrification sites in the ocean as sinks for N_2O needs to be evaluated. Oxygen deficient and truly anoxic waters comprise only a small fraction of the total volume of the ocean but these are the primary marine sinks for combined nitrogen [*Codispoti*, 1973]. Fourth, it is possible that in the present analysis the overall rate of

TABLE 4. Surface N_2O Saturation in the Ocean

Cruise, Date	Location	Number of Samples[a]	Mean N_2O Saturation, %	Range of N_2O Saturation, %	Number of Samples with N_2O Saturation, >120%	Reference, Atmospheric N_2O Concentration
'Meteor' cruise 16 April 1969	0.6°N, 32°W	1	232		1	*Hahn* [1974a, Table 2], 250 ppbv
	10.3°N, 32°W	1	293[b]		1	
	25.6°N, 30°W	1	175		1	
	36.6°N, 30°W	1	157		1	
	59.9°N, 30°W	1	125		1	
'Meteor' cruise 20b June 1970	62.0°–65.1°N, 8.2°–19.3°W	18	113	104–135	3	250 ppbv
'Meteor' cruise 23c June 1971	38.5°–48.5°N, 11.5°–43.0°W	7	124	120–130	6	270 ppbv
Feb.–Oct. 1972	34.7°–42.3°N, 61.4°–74.6°W	6	102	93–114	0	
Feb.–March 1972	27.4°–32.7°N, 69.5°–79.4°W	3	110	100–126	1	*Yoshinari* [1973, Appendix A], 328 ppbv
Feb.–March 1972	11.3°–18.6°N, 60.2°–74.6°W	10	113	109–123	2	
'T.G. Thompson' cruise TT121, July 1977	46.8°N, 126.8°W	1	105		0	this work, 278 ppbv
'Wecoma' cruise Wefoc 77-1 Jan. 1977	34.2°N, 120.2°W	1	105		0	
	28.0°N, 116.0°W	1	100		0	*Cohen et al.* [1977], 287 ppbv
	3.7°–19.8°N,[c] 105.9°–112.0°W	9	111	96–124	1	
		56 (total)[d]	109 (mean)[d]		13 (total)[d]	

[a]Replicate measurements at one location were averaged and counted here as one sample.
[b]Sample taken at a depth of 25 m.
[c]These stations were grouped because all are within the oxygen deficient zone of the ETNP [*Cohen and Gordon*, 1978].
[d]Excluding the 'Meteor' cruise 16 data.

marine nitrification was overestimated. This rate was taken as equal to the nitrogen mineralization rate which in turn was estimated from the rate of nitrogen assimilation in the ocean (Figure 5). Because part of the nitrogen assimilated by plants is in the form of ammonia released by the biota and formed from the degradation of organic nitrogen compounds, the present estimate of nitrification and accordingly the estimate of N_2O production are probably maximal.

Acknowledgments. We thank J. W. Murray of the University of Washington for the opportunity to participate in the TT-121 cruise of R. V. T. G. Thompson. Our research was supported by the Office of Naval Research through contract N00014-76-C-0067 under project NR083-102.

REFERENCES

Alvarez-Borrego, S. D., D. Guthrie, C. H. Culberson, and P. K. Park, Test of Redfield's model for oxygen-nutrient relationships using regression analysis, *Limnol. Oceanogr., 20*, 795–805, 1975.

Bainbridge, A. E., Geosecs Atlantic final hydrographic data report, Geosecs Operations Group/National Science Foundation, Washington, D. C., 1975.

Bialek, E. L., Handbook of oceanographic tables, *Spec. Publ. SP-68*, U.S. Naval Oceanogr. Office, Washington, D. C., 1966.

Bolin, B., On the exchange of CO_2 between the atmosphere and the sea, *Tellus, 12*, 274–281, 1960.

Bremner, J. M., and A. M. Blackmer, Nitrous oxide: Emission from soils during nitrification of fertilizer nitrogen, *Science, 199*, 295–296, 1978.

Broecker, W. S., and T. H. Peng, Gas exchange rates between air and sea, *Tellus, 26*, 21–35, 1974.

Codispoti, L. A., Denitrification in the eastern tropical North Pacific Ocean, Ph.D. thesis, Univ. of Wash., Seattle, 1973.

Cohen, Y., Shipboard measurement of dissolved nitrous oxide in seawater by electron capture gas chromatography, *Anal. Chem., 49*, 1238–1240, 1977.

Cohen, Y., Consumption of dissolved nitrous oxide in an anoxic basin, Saanich Inlet, B. C., *Nature, 272*, 235–237, 1978.

Cohen, Y., and L. I. Gordon, Nitrous oxide in the oxygen minimum of the eastern tropical North Pacific: Evidence for its consumption during denitrification and possible mechanisms for its production, *Deep Sea Res., 25*, 509–524, 1978.

Cohen, Y., M. D. Lilley, and L. I. Gordon, Hydrographic and chemical observations in the eastern tropical North Pacific Ocean—January 1977, *Ref. 78-5*, School of Oceanogr., Ore. State Univ., Corvallis, 1978.

Council for Agricultural Science and Technology, Effects of increased nitrogen fixation on stratospheric ozone, *Rep. 53*, Dep. of Agron., Iowa State Univ., Ames, 1976.

Craig, H., and L. I. Gordon, Nitrous oxide in the ocean and marine atmosphere, *Geochim. Cosmochim. Acta, 27*, 949–955, 1963.

Crutzen, P. J., The influence of nitrogen oxides on the atmospheric ozone content, *Quart. J. Roy. Meteorol. Soc., 96*, 320–326, 1970.

Hahn, J., The North Atlantic Ocean as a source of atmospheric N_2O, *Tellus, 26*, 160–168, 1974a.

Hahn, J., Nitrous oxide in air and seawater over the Atlantic Ocean, in *The Changing Chemistry of the Oceans*, edited by D. Dyrssen and D. Jagner, pp. 53–69, John Wiley, New York, 1974b.

Hahn, J., N_2O measurements in the Northeast Atlantic Ocean, *Meteor Forschungsergebnisse, Reihe A, 16*, 1–14, 1975.

Hahn, J., and C. Junge, Atmospheric nitrous oxide: A critical review, *Naturforsch., 32a*, 190–214, 1977.

Junge, C., and J. Hahn, N_2O measurements in the North Atlantic, *J. Geophys. Res., 76*, 3143–3146, 1971.

Junge, C., B. Bucknolt, K. Schutz, and R. Beck, N_2O measurements in air and in seawater over the Atlantic, *Meteor Forschungsergebnisse, Reihe B, 5*, 1–11, 1971.

Liss, P. S., and P. B. Slater, Flux of gases across the air-sea interface, *Nature, 246*, 181–184, 1974.

Liu, S. C., R. J. Cicerone, and T. M. Donahue, Sources and sinks of atmospheric N_2O and the possible ozone reduction due to industrial fixed nitrogen fertilizers, *Tellus, 29*, 251–263, 1977.

Markham, A. E., and K. A. Kobe, Solubility of carbon dioxide and nitrous oxide in salt solution, *J. Amer. Chem. Soc., 63*, 449–454, 1941.

McElroy, M. B., J. W. Elkins, S. C. Wofsy, and Y. L. Yung, Sources and sinks for atmospheric N_2O, *Rev. Geophys. Space Phys., 14*(2), 143–150, 1976.

McElroy, M. B., S. C. Wofsy, and Y. L. Yung, The nitrogen cycle: Perturbations due to man and their impact on atmospheric N_2O and O_3, *Phil. Trans. Roy. Soc. London, Ser. B, 277*, 159–181, 1977.

Murray, J. W., B. Spell, and G. Friederick, Hydrographic and nutrient data from the Cascadia Basin (July 1977), *Spec. Rep. 81*, Dep. of Oceanogr., Univ. of Wash., Seattle, 1977.

Rasmussen, R. A., D. Pierotti, J. Kresnec, and B. Halter, Report on the cruise of the Alpha Helix Research Vessel, March 5 to 20, 1976, National Science Foundation grant OCE-75-04688 A03, 1976.

Redfield, A. C., B. H. Ketchum, and F. A. Richards, The influence of organisms on the composition of sea water, in *The Sea*, vol. 2, edited by M. N. Hill, pp. 26–77, Interscience, New York, 1963.

Roether, W., J. M. Gieskes, and W. Husseis, Hydrography of a transatlantic section from Portugal to the Newfoundland Basin, *Meteor Forschungsergebnisse, Reihe A, 14*, 13–32, 1974.

Sverdrup, H. U., M. W. Johnson, and R. H. Fleming, *The Oceans*, Prentice-Hall, Englewood Cliffs, N.J., 1942.

Weiss, R. F., The solubility of nitrogen, oxygen and argon in water and seawater, *Deep Sea Res., 17*, 721–735, 1970.

Yoshinari, T., Nitrous oxide in the sea, *Ph.D. Thesis*, Dalhousie Univ., Halifax, N.S., 1973.

Yoshinari, T., Nitrous oxide in the sea, *Mar. Chem., 4*, 189–202, 1976.

(Received March 31, 1978;
revised August 28, 1978;
accepted September 5, 1978.)

Limnol. Oceanogr., 24(3), 1979, 474–482

Biological production and the exchange of oxygen and carbon dioxide across the sea surface in Stuart Channel, British Columbia[1]

Kenneth S. Johnson[2] *and Ricardo M. Pytkowicz*
School of Oceanography, Oregon State University, Corvallis 97331

C. S. Wong
Ocean Chemistry Division, Institute of Ocean Sciences,
Sidney, British Columbia V8L 4B2

Abstract

The rates at which concentrations of oxygen and carbon dioxide in Stuart Channel changed due to biological production and to exchange with the atmosphere were determined from measurements of the simultaneous changes in oxygen, pH, and titration alkalinity over a 15-day period in July 1976. Carbon dioxide was consumed by plankton at a rate of 10.3 μmol CO_2 liter^{-1}·d^{-1}. CO_2 entered the surface layer by atmospheric exchange at a rate of 0.49 μmol CO_2 liter^{-1}·d^{-1}. The piston velocity was calculated to be 2.2×10^{-3} cm·s^{-1}. Oxygen was produced at a rate of 14.1 μmol O_2 liter^{-1}·d^{-1}, due to photosynthetic activity. The rate of oxygen loss to the atmosphere was 9.8 μmol O_2 liter^{-1}·d^{-1}. The piston velocity was 1.6×10^{-3} cm·s^{-1}.

The cycles of CO_2 and O_2 from the atmosphere to the surface layer of the ocean and within the surface layer are of great interest, particularly because of the role that the ocean may play as a sink for anthropogenic CO_2. Some of the major fluxes in these cycles are the production and consumption of O_2 and CO_2 by biological activity and the exchange of these gases from the atmosphere to the ocean. We present here a short term study of these fluxes.

The exchange of O_2 across the air–sea interface and the net amount of biological production were determined in the Gulf of Maine by Redfield (1948) from considerations of the simultaneous changes in O_2 and PO_4 concentrations with time in the water column. A similar study was made by Pytkowicz (1964) off the Oregon coast. More recent studies of gas exchange have tended to emphasize CO_2 because of the concern over the fate of anthropogenic CO_2. The difference in the ^{14}C activity of the ocean and the atmosphere has been used to determine the rate of CO_2 exchange (Park and Hood 1963; Broecker and Peng 1974). The results of these measurements provide information only about the rate of gas exchange and not biological uptake. Other studies on gas exchange have been summarized by Kester (1975) and Skirrow (1975).

Methods used to estimate primary production in seawater have been summarized by Strickland (1965). Primary production is typically measured in a water sample isolated in a container, which may introduce systematic errors. Few measurements of production have been based on determinations of in situ changes in chemical properties. Smith (1973) calculated the rate of biological uptake of CO_2 on a coral reef from changes in the total inorganic carbon content (TCO_2) of ocean water as it flowed across the reef. Atmospheric exchange was ignored because Smith estimated it to be <10% of the total change. A later study showed that atmospheric CO_2 exchange could be important in areas of lower productivity (Smith and Pesret 1974).

Our study of the cycles of O_2 and CO_2 in the surface layer of Stuart Channel is

[1] This research was supported in part by the Oceanography Section of the National Science Foundation and by the Office of Naval Research.
[2] Present address: Mar. Sci. Inst., Univ. Calif., Santa Barbara 93106.

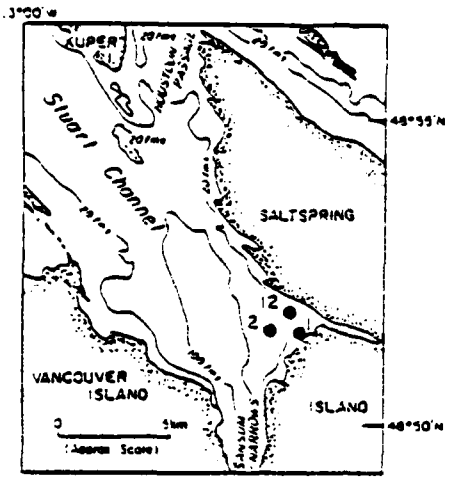

Fig. 1. Sampling stations in Stuart Channel. Data shown in Fig. 2 obtained at station 12.

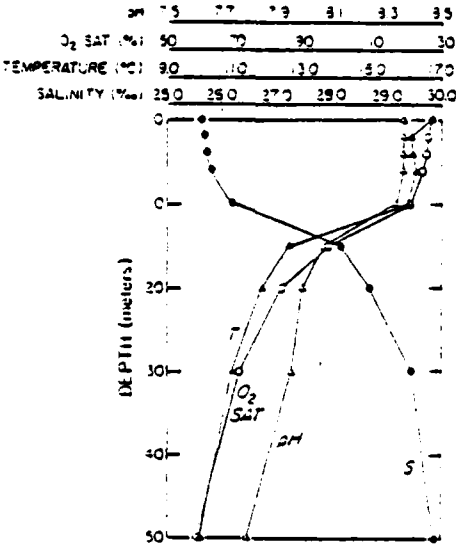

Fig. 2. Hydrographic data obtained at station 12 in Stuart Channel on 19 July 1962. Data from Waldichuk et al. (1968*b*). Location of station shown in Fig. 1.

based on observed changes in the in situ concentrations of O_2 and CO_2 with time.

C. A. Curtis and D. Plath assisted in gathering field data. Y. Cohen and C. T. Chen made valuable suggestions.

Hydrographic conditions in Stuart Channel

Our study was made from 5–22 July 1976 in Stuart Channel (Canadian Gulf Islands about 45 km north of Victoria, B.C.; Fig. 1). The distribution of chemical properties in the channel was studied extensively from 1954–1965 (Waldichuk et al. 1968*b*). During summer months the channel is strongly stratified in both temperature and salinity. The conditions in July 1962 at a station within 0.5 km of our sampling site (Fig. 2) show a well mixed surface layer between 8 and 10 m deep. Below the surface layer there is a strong gradient in all properties that inhibits any mixing between the deep water and the surface layer. Horizontal gradients within the channel are small; for example, salinity variations across the channel and along the central axis are usually <1.0‰ at a constant depth in the surface layer (Waldichuk et al. 1968*b*).

The low salinity of the surface layer of the adjacent Strait of Georgia is maintained by runoff from the Fraser River, which has a high rate of flow during summer (Waldichuk 1964; Takahashi et al. 1977). However, in Saanich Inlet, about 20 km to the south, the surface water shows an occasional increase in salinity of several parts per thousand which has been attributed to upwelling (Takahashi et al. 1977 and references cited therein). Here we show that a similar phenomenon probably occurs in Stuart Channel.

Theory

The change in the oxygen concentration of seawater over some period of time can be expressed as

$$\Delta O_2 = \Delta O_2^a - \Delta O_2^b \qquad (1)$$

where superscript *a* indicates the change due to invasion or evasion of gas from or to the atmosphere and superscript *b* refers to changes due to biological processes (Redfield 1948). Changes due to mixing are considered below.

The change in the TCO_2 concentration over a period of time can be expressed as

$$\Delta TCO_2 = \Delta TCO_2^a - \Delta TCO_2^b + \Delta TCO_2^c \quad (2)$$

where superscripts a and b have the same meaning as in Eq. 1 and superscript c refers to the change due to dissolution or precipitation of carbonate minerals (Smith 1973). Although we are primarily concerned with the cycle of CO_2 in surface waters, the total inorganic carbon concentration is used in Eq. 2 because CO_2 participates in a number of rapid equilibrium reactions with HCO_3^- and CO_3^{2-}.

The quantities on the left-hand sides of Eq. 1 and 2 can be found directly from the difference in two measurements of the O_2 or TCO_2 concentration of seawater. In order to resolve these total changes into the individual components on the right-hand sides of Eq. 1 and 2 we need additional equations to relate ΔTCO_2^a to ΔO_2^a, ΔTCO_2^b to ΔO_2^b and ΔTCO_2^c to the change in titration alkalinity and ΔTCO_2^b.

We can relate ΔTCO_2^b to ΔO_2^b in the following manner. The average chemical composition of marine plankton has been determined to be $(CH_2O)_{106}(NH_3)_{16}H_3PO_4$ (Redfield et al. 1963). The production and decomposition of particulate organic matter, therefore, proceeds according to the formula

$$(CH_2O)_{106}(NH_3)_{16}H_3PO_4 + 138O_2 \underset{\text{production}}{\overset{\text{decomposition}}{\rightleftharpoons}} 106CO_2 + 16HNO_3 + H_3PO_4 + 122H_2O. \quad (3)$$

This scheme of production and decomposition has been verified by several workers. Specifically, it has been shown that the changes in TCO_2 and O_2 due to biological processes can be modeled by the equation

$$\Delta O_2^b/\Delta TCO_2^b = -138/106 = -1.30 \quad (4)$$

when the concentrations of both species are expressed in units of moles per liter (Culberson and Pytkowicz 1970).

ΔTCO_2^a and ΔO_2^a can be related to each other by means of the stagnant film model of gas exchange. In this model the flux of a gas across the air–sea interface is given by

$$\text{Flux}(\mu\text{mol}\cdot\text{cm}^{-2}\cdot\text{s}^{-1}) = D(C^* - C)/z \quad (5)$$

where D is the molecular diffusion coefficient of the gas, z is the thickness of the surface film, and C^* and C are the equilibrium and bulk concentrations in the well mixed surface layer (Bolin 1960). ΔO_2^a and ΔTCO_2^a are related to the flux by

$$\Delta O_2^a = \int_{t_1}^{t_2} [D_{O_2}(O_2^* - O_2)/zh]\,dt \quad (6)$$

and

$$\Delta TCO_2^a = \int_{t_1}^{t_2} [D_{CO_2}(CO_2^* - CO_2)/zh]\,dt \quad (7)$$

where h is the depth of the surface mixed layer and t is time. In this equation the concentration of molecular CO_2 actually $CO_2 + H_2CO_3$ is used rather than TCO_2.

The molecular diffusion coefficients of CO_2 and O_2 tabulated by Broecker and Peng (1974) are related by the equation

$$D_{O_2} = 1.26D_{CO_2} \quad (8)$$

over the temperature range (14°–17°C) that we encountered in Stuart Channel.

The molecular diffusion coefficient of CO_2 may be effectively increased by two factors. Chemical reaction of CO_2 in the laminar surface film will enhance the rate of diffusion. This effect is negligible for surface films <100 μ thick (Bolin 1960). We found from our measurements that the surface film was 66 μ thick, and we have therefore ignored chemical enhancement of CO_2 diffusion. The presence of the enzyme carbonic anhydrase will also increase the rate of CO_2 exchange (Berger and Libby 1969). We have no way to evaluate this effect, and our results will have to be considered as a lower limit on the possible rate of CO_2 exchange.

If the quantities in the integrals of Eq. 6 and 7 vary linearly over short periods

time, and further, if the changes in O_2 and CO_2 are greater than those of z, h, and the diffusion coefficients, then we can rewrite these equations as

$$\Delta O_2'' = D_{O_2}[(O_2'' - O_2)_{t_1} - (O_2'' - O_2)_{t_2}]\Delta t/2zh \quad (9)$$

and

$$\Delta TCO_2'' = D_{CO_2}[(CO_2'' - CO_2)_{t_1} - (CO_2'' - CO_2)_{t_2}]\Delta t/2zh. \quad (10)$$

The equation relating $\Delta O_2''$ to $\Delta TCO_2''$ can now be found from Eq. 8, 9, and 10:

$$\Delta O_2''/\Delta TCO_2'' = 1.26\frac{[(O_2'' - O_2)_{t_1} - (O_2'' - O_2)_{t_2}]}{[(CO_2'' - CO_2)_{t_1} - (CO_2'' - CO_2)_{t_2}]} = Q. \quad (11)$$

The change in TCO_2 due to precipitation or dissolution of carbonate minerals can be obtained from the measured change in the titration alkalinity and $\Delta TCO_2''$:

$$\Delta TCO_2'' = 0.5[\Delta TA - (17/106)\Delta TCO_2''] \quad (12)$$

where ΔTA is the change in titration alkalinity. The first term on the right-hand side of Eq. 12 arises simply because the removal of carbonate ions from seawater causes a change in TA that is twice as large as $\Delta TCO_2''$ (Skirrow 1975). The decomposition of biomass by reaction 3 results in the release of 16 molecules of nitric acid and one of phosphoric acid for every 106 molecules of CO_2 (Brewer et al. 1975), and the acid released will neutralize a portion of the titration alkalinity. The second term on the right-hand side is therefore present to correct ΔTA for that portion of it which was neutralized by acid released during decomposition or generated during production.

Equations 1, 2, 4, 11, and 12 can be used to solve for each of the terms of the right-hand sides of Eq. 1 and 2. For example, rearranging these equations yields

$$\Delta O_2'' = \frac{[\Delta TCO_2 - 0.5\Delta TA - (1.08/1.30)\Delta O_2]}{[1.Q - 1.08/1.30)]} \quad (13)$$

where Q is defined in Eq. 11. All of the quantities in this equation can be obtained from field measurements of O_2, pH, TA, temperature, and salinity. A time series of these measurements will thus allow the amount of primary production and exchange of O_2 and CO_2 with the atmosphere to be calculated.

Method

Water samples were obtained at station 1, on the end of a 60-m-long pier (Fig. 1). Additional samples were taken 1 km offshore (station 2) to check horizontal variability. All samples were taken at a depth of about 0.5 m.

Oxygen was determined by the Carpenter (1965) modification of the Winkler method. The precision (1 SD) of replicate analyses by this method was estimated to be ±0.6%. pH was measured with a Beckman pH meter having a display precise to ±0.01 pH. Replicate determinations had a standard deviation of ±0.015 pH. We measured titration alkalinity by the method of Culberson et al. (1970), using the Beckman pH meter; the accuracy of the meter limited precision to ±0.8%. Temperature was measured in situ to the nearest 0.1°C. Salinity was measured with an inductive salinometer. All analyses were done within 1 h of sampling except for the salinity measurements.

The TCO_2 and CO_2 concentrations were calculated from the pH and TA data using the apparent equilibrium constants of Mehrbach et al. (1973) for the carbonate system and the equation of Edmond and Gieskes (1970) for the borate system. The concentrations of CO_2'' and O_2'' were calculated using the Bunsen coefficients given by Weiss (1970, 1974).

Results

The data for salinity and TCO_2 from 5–22 July 1976 and O_2 from 7–22 July at station 1 are shown in Fig. 3. O_2 data before 7 July are not available. The salinity shows a maximum (~26.8‰) over the period from 9–16 July. This is similar to the changes found by Takahashi et al. (1977)

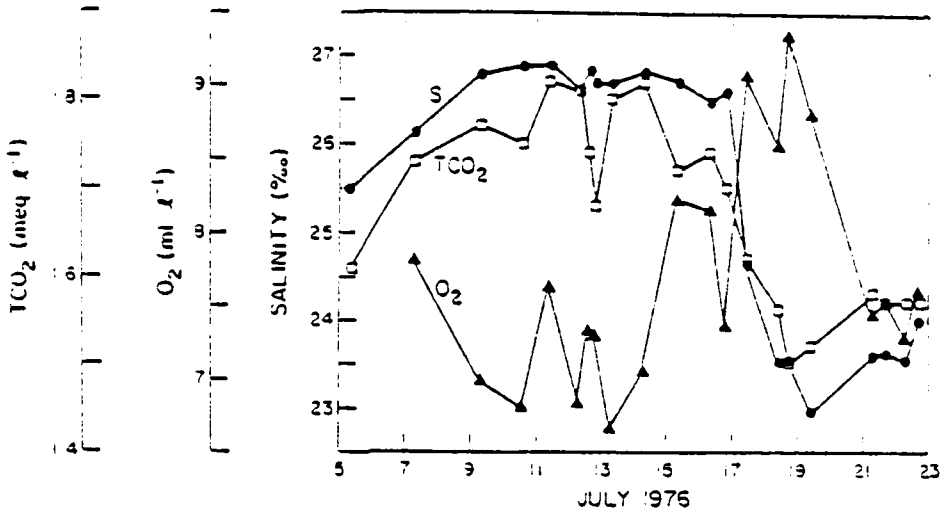

Fig. 3. Surface salinity (●), O_2 (▲), and TCO_2 (■) concentrations at station 1, July 1976.

in nearby Saanich Inlet and is probably the result of upwelling of deep water. Since the mixing of upwelled deep water and surface water causes conservative changes in O_2 and TCO_2 that obscure the nonconservative changes in which we are interested, all of the data were normalized to a constant salinity of 26.8‰. The normalization procedure, discussed below, takes into account the effect of the TA, TCO_2, and O_2 concentrations of the freshwater.

We have assumed, as discussed earlier, that the low salinity of the surface water in Stuart Channel is maintained by runoff from the Fraser River. The TA and TCO_2 of the Fraser River are about 0.75 meq·liter^{-1} during summer, although variations are large (Waldichuk et al. 1968*a*). The salinity is zero and the oxygen concentration is within a few percent of equilibrium with the atmosphere. The data were therefore normalized with the following equations:

$$TA^* = [TA - (S/26.8 - 1)0.75] \cdot 26.8/S, \quad (14)$$

$$TCO_2^* = [TCO_2 - (S/26.8 - 1)0.75] \cdot 26.8/S, \quad (15)$$

and

$$O_2^* = [O_2 - (S/26.8 - 1)O_2^*] \cdot 26.8/S. \quad (16)$$

O_2^* is the equilibrium concentration of O_2 in freshwater having the same temperature as the seawater in which the measurements were made. The second term in each equation removes the contribution of the river water to each quantity.

The normalized values TA^*, TCO_2^*, and O_2^* have been substituted into Eq. 13 to calculate the change in O_2 concentration due to atmospheric exchange between each pair of measurements. The value of Q in Eq. 13 was calculated from Eq. 11 by using the actual concentrations of O_2 and CO_2 measured in the water column, as the gas exchange was determined by in situ conditions and not the normalized values. The quantities ΔO_2^*, ΔTCO_2^*, $\Delta TCO_2^{\prime}$, and $\Delta TCO_2^{\prime\prime}$ were then calculated for each successive pair of observations. The total changes in each component of Eq. 1 and 2 since 7 July were obtained by summing all the changes between successive observations. When we henceforth refer to any

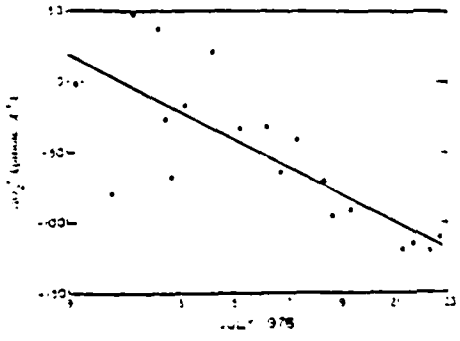

Fig. 4. Total change of O_2' relative to 7 July 1976 plotted against time. Solid line is regression equation fit to data.

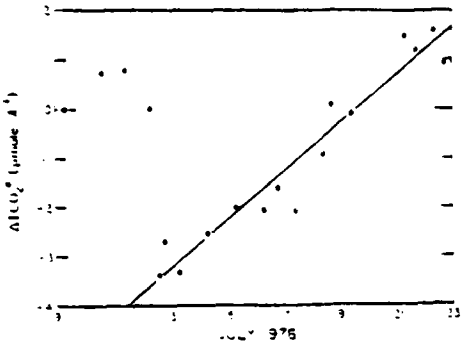

Fig. 5. As Fig. 4, for TCO_2'. First four data points have been excluded from regression for reasons discussed in text.

quantity ΔX, now we will mean the total change in that quantity relative to 7 July.

The values of $\Delta O_2'$, $\Delta O_2'$, $\Delta TCO_2'$ and $\Delta TCO_2'$ are plotted against the date in July in Figs. 4 through 7. Clear systematic trends in all of these plots indicate that there have been systematic increases in the amount of particulate organic carbon (POC) in Stuart Channel and that there have been net fluxes of CO_2 and O_2 across the air–sea interface.

Linear regression equations were fit to the data to quantify their trends (Table 1). The slopes of each equation give the rate of change in each quantity. The data for ΔTCO_2 are independent of time, indicating that there was no detectable precipitation or solution of $CaCO_3$.

The data from station 2 were indistinguishable from the data obtained at the shore station. We have, therefore, assumed that the data from station 1 are representative of concentrations in the channel.

Discussion

Biological production and seasonal heating are the master variables controlling the cycling of O_2 and CO_2 in the surface layer of the ocean. The production and consumption of O_2 and CO_2 by the phytoplankton generate the gradients that drive the exchange of these gases between the ocean and the atmosphere. Large temperature changes during spring and fall will change the equilibrium solubility of O_2 and CO_2 and also cause exchange of these gases between the at-

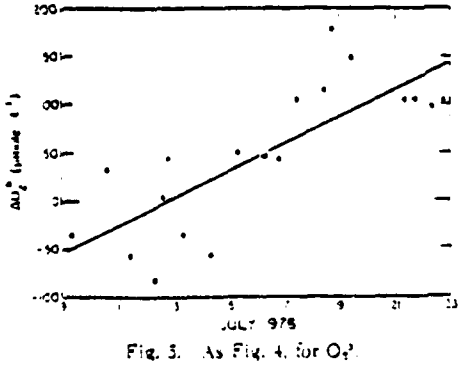

Fig. 6. As Fig. 4, for O_2'.

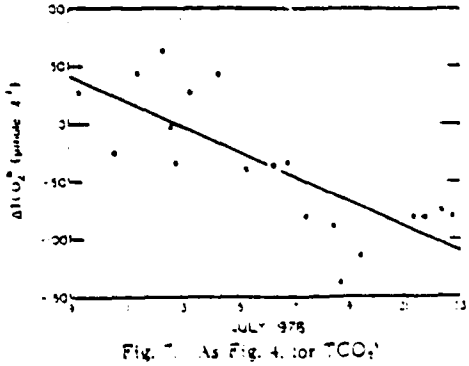

Fig. 7. As Fig. 4, for TCO_2'.

Table 1. Linear regression equations fit to data. All equations of form $\Delta Y = A + Bt$, where t is decimal date in July and Y and A are in μmol liter^{-1} and B is in μmol liter^{-1} d^{-1}. Errors in A and B are 1 SD. R^2 is coefficient of determination.

Y	A	B	R^2
O_2'	.07 ± 32	−9.6 ± 1.9	0.61
O_2'	−150 ± 45	14.1 ± 2.7	0.61
TCO_2'	−9.6 ± 0.7	0.49 ± 0.04	0.93
TCO_2'	1.38 ± 24	−10.8 ± 2.1	0.61
TCO_2'	2.3 ± 17	0.14 ± 1.0	0.00

mosphere and the sea. However, during our study the temperature changed, in general, <3°C and heating of the surface waters therefore played a minor role. Thus, the magnitudes and even the signs of the changes in O_2 and CO_2 due to exchange depended primarily on the net amount of primary production.

The amount of primary production is, in turn, dependent on the nutrient concentrations and light intensity. The factor most likely to limit biological production during summer is nutrient availability. In Saanich Inlet, periodic blooms of phytoplankton occur during summer (Takahashi et al. 1977), induced by upwelling of deep water high in nutrients.

The sharp increase in salinity at the beginning of our study implies an upwelling event which was probably the cause of a similar phytoplankton bloom in Stuart Channel. The surface water was initially supersaturated with CO_2, indicating either that consumption of particulate organic matter had been exceeding production before the input of nutrients or that a temperature increase in the surface water had lowered the equilibrium solubility of CO_2. However, the surface waters became undersaturated in CO_2 on the third day after the salinity increase. Evidently, primary production had increased in response to the elevated nutrient concentrations caused by the upwelling. During the initial period in which CO_2 was supersaturated, the flux of CO_2 was from the ocean to the atmosphere (Fig. 6). However, after the increase in biological production the CO_2 became undersaturated and the flux of CO_2 across the sea surface was reversed. We have, therefore, excluded the first four points, obtained when the water was supersaturated, from the regression of the total change in ΔTCO_2' against time. There was no analogous reversal in the direction of the O_2 flux because of its very high level of supersaturation.

Although we would perhaps be justified in excluding the first four data points from the other regression equations we have not done so. No significant change in the slopes is found if these points are excluded, but the coefficient of determination R^2 increases slightly.

The regression lines through the plots of ΔO_2' and ΔTCO_2' versus time have slopes of 14.1 ± 2.7 μmol O_2 liter^{-1} d^{-1} and −10.8 ± 2.1 μmol TCO_2 liter^{-1} d^{-1} (Table 1). These slopes correspond to the rates at which O_2 was produced and TCO_2 was removed in Stuart Channel due to biological activity during the period of our study. The rate of change of TCO_2 is equal to the net primary production minus any CO_2 regenerated in the surface layer by zooplankton grazing or microbial decomposition of organic matter.

ΔO_2' and ΔTCO_2' would ordinarily be expected to follow some exponential growth curve; however, over the period we have studied, the linear fit to the data is adequate, within the precision of the measurements. The scatter about the line is primarily due to analytical error and patchiness, but there will certainly be some effect of diurnal variations in primary production, changes in light intensity due to variations in cloud cover, and changing nutrient concentrations and plankton population size.

The rate of change in TCO_2 due to biological uptake that we found compares well with other measurements made near this area. Takahashi et al. (1977) measured the amount of carbon in phytoplankton cells in Saanich Inlet as a function of time; we calculated from their data an increase of 16.4 μmol C liter^{-1} d^{-1} during the bloom they label No. 3 (July 1973). This change in POC corresponds to a biological uptake rate of −16.4 μmol

TCO_2 liter^{-1}·d^{-1}—a result close to ours. Measurements of primary production by the ^{14}C method in Saanich Inlet also yield results that support our conclusions (Fulton et al. 1969).

The slope of $\Delta TCO_2'$ versus time determined from the regression equation in Table 1 is 0.49 ± 0.04 μmol TCO_2 liter^{-1}·d^{-1}. If the depth of the mixed layer (h) is 10 ± 2 m, then the flux of CO_2 gas across the sea surface is 0.49 ± 0.14 μmol O_2 cm^{-2}·d^{-1}. (The increased error reflects the uncertainty in h.) The average difference between the concentration of O_2 in the surface layer which would have been at equilibrium with the atmosphere and the actual concentration was 13 μmol CO_2 liter^{-1}, assuming an atmospheric CO_2 partial pressure of 3.30 × 10^{-4} atm. This quantity can be combined with the flux to find the piston velocity (e) for the exchange of CO_2 (e_{CO_2}) in Stuart Channel:

$$e_{CO_2} = D_{CO_2}/z = 2.2 \times 10^{-3}\ \text{cm·s}^{-1} \quad (17)$$

The average value found by Broecker and Peng (1974) for the world ocean is 1.7 × 10^{-3} cm·s^{-1}. A value identical with ours was obtained during summer near Barbados (Broecker and Peng 1971).

The average thickness of the laminar surface film in Stuart Channel was 66 μm. Broecker and Peng (1971) found z = 63 μm in summer by means of radon measurements in the Atlantic. A diffusion coefficient of 1.45 × 10^{-5} cm^2·s^{-1} was used to calculate our value (Broecker and Peng 1974).

We calculated the flux of O_2 across the sea surface to be −9.8 ± 1.9 μmol O_2 cm^{-2}·d^{-1} using the results in Table 1 and h = 10 m. The average difference between the equilibrium concentration and the in situ concentration of O_2 in the surface layer was −79 μmol O_2 liter^{-1}. These values yield a piston velocity for O_2 of 1.6 × 10^{-3} cm·s^{-1}. Redfield (1948) found a piston velocity of 4 × 10^{-3} cm·s^{-1} during summer in the Gulf of Maine; Pytkowicz (1964) found e_{O_2} = 3 × 10^{-3} cm·s^{-1} off the coast of Oregon. These values are in good agreement considering the different conditions in the various study areas.

Our results confirm the assumption of Smith (1973) that changes in the TCO_2 content of the ocean on a daily basis are primarily due to biological production in areas of high productivity. The average value of $\Delta TCO_2'$ was only 4.5% of ΔTCO_2^0. This is not the case for O_2, however. The magnitude of the average daily change in $\Delta O_2'$ was 70% of that of ΔO_2^0. The flux of O_2 from the ocean to the atmosphere was important in maintaining the observed O_2 concentrations on a daily basis in Stuart Channel.

As we noted earlier, there was no detectable $CaCO_3$ precipitation in Stuart Channel during our study. Examination of the calcium carbonate budget measured by Smith (1972) off the California coast indicates that a maximum limit on the net $CaCO_3$ removal rate would be −1.1 μmol TCO_2 liter^{-1}·d^{-1}, assuming that all $CaCO_3$ is removed from the 10-m-thick surface layer. The uncertainty in our results is of the same order of magnitude.

Although it was not possible to assess accurately the rate at which $CaCO_3$ was being deposited in the sediments, an improvement of an order of magnitude in the precision of the measurement of titration alkalinity would allow a much more accurate determination of the $CaCO_3$ removal rate from the surface layer of the ocean. Most of this improvement can be achieved by simply using a pH meter more accurate than ours (Johnson et al. 1977).

References

BERGER, R., AND W. F. LIBBY. 1969. Equilibration of atmospheric carbon dioxide with sea water: Possible enzymatic control. Science 164: 1395–1397.

BOLIN, B. 1960. On the exchange of carbon dioxide between the atmosphere and the sea. Tellus 12: 274.

BREWER, P. G., C. T. WONG, M. P. BACON AND D. W. SPENCER. 1975. An oceanic calcium problem? Earth Planet. Sci. Lett. 26: 81–87.

BROECKER, W. S., AND T. H. PENG. 1971. The vertical distribution of radon in the Bomex area. Earth Planet. Sci. Lett. 11: 99–108.

——— AND ——— 1974. Gas exchange rates between air and sea. Tellus 26: 19–35.

CARPENTER, J. H. 1965. The Chesapeake Bay Institute technique for the Winkler dissolved oxygen method. Limnol. Oceanogr. 10: 141–143.

CULBERSON, C., AND R. M. PYTKOWICZ. 1970. Oxygen-total carbon dioxide correlation in the eastern Pacific Ocean. J. Oceanogr. Soc. Jpn. 26: 95–100.

——— ——— AND J. E. HAWLEY. 1970. Seawater alkalinity determination by the pH method. J. Mar. Res. 28: 15–21.

EDMOND, J. M., AND J. M. GIESKES. 1970. On the calculation of the degree of saturation of seawater with respect to calcium carbonate under in situ conditions. Geochim. Cosmochim. Acta 34: 1261–1291.

FULTON, J. D., O. D. KENNEDY, H. SEKI, AND K. STEPHENS. 1969. Biological, chemical, and physical observations in Saanich Inlet, Vancouver Island British Columbia, 1968. Fish. Res. Bd. Can. Manuscr. Rep. Ser. 1018. 2 v.

JOHNSON, K. S., R. VOLL, C. A. CURTIS, AND R. M. PYTKOWICZ. 1977. A critical examination of the NBS pH scale and the determination of titration alkalinity. Deep-Sea Res. 24: 915–926.

KESTER, D. R. 1975. Dissolved gases other than CO_2, p. 497–556. *In* J. P. Riley and G. Skirrow [eds.], Chemical oceanography, v. 1, 2nd ed. Academic.

MEHRBACH, C., C. H. CULBERSON, J. E. HAWLEY, AND R. M. PYTKOWICZ. 1973. Measurement of the apparent dissociation constants of carbonic acid in seawater at atmospheric pressure. Limnol. Oceanogr. 18: 897–907.

PARK, K., AND D. W. HOOD. 1963. Radiometric field measurement of CO_2 exchange from the atmosphere to the sea. Limnol. Oceanogr. 8: 287–289.

PYTKOWICZ, R. M. 1964. Oxygen exchange rates off the Oregon coast. Deep-Sea Res. 11: 381–389.

REDFIELD, A. C. 1948. The exchange of oxygen across the sea surface. J. Mar. Res. 7: 347–361.

———, B. H. KETCHUM, AND F. A. RICHARDS. 1963. The influence of organisms on the composition of sea-water, p. 26–77. *In* M. N. Hill [ed.], The sea, v. 2. Interscience.

SKIRROW, G. 1975. The dissolved gases—carbon dioxide, p. 1–192. *In* J. P. Riley and G. Skirrow [eds.], Chemical oceanography, v. 2, 2nd ed. Academic.

SMITH, S. V. 1972. Production of calcium carbonate on the mainland shelf of southern California. Limnol. Oceanogr. 17: 28–41.

——— 1973. Carbon dioxide dynamics: A record of organic carbon production, respiration, and calcification in the Eniwetok reef flat community. Limnol. Oceanogr. 18: 106–120.

——— AND F. PESRET. 1974. Processes of carbon dioxide flux in the Fanning Island lagoon. Pac. Sci. 28: 225–245.

STRICKLAND, J. D. 1965. Production of organic matter in the primary stages of the marine food chain, p. 477–610. *In* J. P. Riley and G. Skirrow [eds.], Chemical oceanography, v. 1. Academic.

TAKAHASHI, M., D. L. SEIBERT, AND W. H. THOMAS. 1977. Occasional blooms of phytoplankton during summer in Saanich Inlet, B.C., Canada. Deep-Sea Res. 24: 773–780.

WALDICHUK, M. 1964. Dispersion of kraft-mill effluent from a submarine diffuser in Stuart Channel, British Columbia. J. Fish. Res. Bd. Can. 21: 1259–1316.

——— J. R. MARKERT, AND J. H. MEIKLE. 1968a. Fraser River Estuary, Burrard Inlet, Howe Sound and Malaspina Strait physical and oceanographic data, 1957–1966. Fish. Res. Bd. Can. Manuscr. Rep. Ser. 939. 2 v.

———, J. H. MEIKLE, AND J. R. MARKERT. 1968b. Physical and chemical oceanographic data from the east coast of Vancouver Island, 1965–1966. Fish. Res. Bd. Can. Manuscr. Rep. Ser. 959. 2 v.

WEISS, R. F. 1970. The solubility of nitrogen, oxygen and argon in water and seawater. Deep-Sea Res. 17: 721–735.

——— 1974. Carbon dioxide in water and seawater: The solubility of a non-ideal gas. Mar. Chem. 2: 203–215.

Submitted: 20 September 1978
Accepted: 28 November 1978

Limnol. Oceanogr., 24(2), 1979, 226–242

Acoustical estimation of zooplankton populations[1]

Charles F. Greenlaw[2]
School of Oceanography, Oregon State University, Corvallis 97331

Abstract

Acoustical estimates of zooplankton abundance can be made rigorously if the scattering behavior as a function of size and frequency for the zooplankters is known. Measurements of scattering at a single frequency can be used to estimate abundance if the mean zooplankter size is known. Measurements at two frequencies can be used to estimate the dominant size as well as abundance if a single size zooplankter dominates the acoustical scattering. Measurements at several frequencies can be used to estimate size distributions and abundances. In a field experiment, acoustical scattering was measured at three frequencies for zooplankton layers composed largely of euphausiids (for which an approximate scattering model is known). These data are analyzed by each method and estimates of numerical abundance given.

Estimates of zooplankton abundances are routinely obtained by counting subsamples of specimens caught with nets or pumps. The process is tedious and time consuming, although it can provide detailed descriptions of species and developmental stages, and results are not generally available for several months after the original collection. Moreover, conventional sampling methods suffer from many well known problems, including problems with the sampling devices themselves, such as avoidance and clogging in nets, and problems associated with the nature of sequential samples. Some of the latter concerns have been reviewed by Kelley (1976), particularly the effects of discrete sampling at spatial and temporal intervals larger than the scales of variability of the zooplankton populations.

It has been possible for many years to ameliorate some of the problems of discrete sampling by using echosounders to direct the sampling at a particular station. Echograms have been used to estimate large-scale horizontal extents (Barraclough et al. 1969) and small-scale vertical extents (Northcote 1964; McNaught 1968) of zooplankton and to determine depths at which to take conventional samples of the organisms. The virtues of echosounder records are the speed of areal coverage and the real-time data presentation of the echogram. The drawbacks are many, including the difficulty of interpreting the echogram and the frequent inability to distinguish even broad classes of organisms. Many echosounders are poorly suited for detecting zooplankton. Perhaps the most significant drawback, from a biological standpoint, is that acoustical sampling yields no specimens of the organisms.

Despite these disadvantages, the speed of acoustical sampling and the potential for obtaining high-resolution, synoptic data over large areas has encouraged research into methods for getting quantitative estimates of zooplankton populations from acoustical measurements. McNaught (1968, 1969) discussed methods for estimating biomass of freshwater zooplankton from echograms by an empirical calibration process. Assuming a particular acoustical scattering model applied to cladocerans, copepods, and mysids, he also showed that echosounders were "size-selective" samplers according to their operating frequency. Developing this idea, he proposed a multifrequency echosounder to estimate biomass in several size ranges and used such a device to estimate biomass in Lake Ontario (McNaught et al. 1975). The reported acoustical estimates of biomass were one or two orders of magnitude above historical measures, but these discrepancies may partially be due to calibration errors (McNaught pers. comm.).

[1] Supported by the Office of Naval Research.
[2] Present address: Tracor, Inc., 6500 ... Lane, Austin, Texas 78721.

Since this empirical conversion from acoustical measurements to biomass relies on regression relationships between acoustical data and biomass from simultaneous net samples, the acoustical estimates contain all of the errors and biases of the net data. In principle, the acoustical estimates can be no better than equivalent net samples; in practice, the acoustical estimates are probably much less accurate. In addition, empirical calibrations from one particular population of zooplankton probably do not apply to other populations where the size and species distributions are different.

Recent work has produced a more rigorous approach to quantitative acoustical sampling. Greenlaw (1977) measured scattering strengths of individual, preserved zooplankters over a range of frequencies. A simple scattering model (Johnson 1977*a*) was a good approximation for euphausiids and sergestid shrimp (but not for copepods, which exhibited a distinctive scattering behavior). Johnson (1977*b*) developed a least-squares method for estimating abundances and size distributions of scatterers (for which a scattering model is known) from acoustical measurements at several frequencies and applied this to measurements of the deep scattering layer.

Recently I was able to collect acoustical scattering data at three frequencies on a zooplankton layer known to consist largely of euphausiids. These data and the euphausiid scattering model have been used to produce estimates of abundances and size distributions as functions of depth. Only two sets of data, day and night records for a single station, are presented here. These records were chosen because they were made on the same day at the same station, whereas the remaining records came from widely separated stations, or longer time intervals, or both. There are few confirmatory data on the abundance estimates, so these results must be considered preliminary. The agreement between acoustical estimates and the available net data is quite good however, especially for the small number of frequencies used.

The basic least-squares-estimation computer program was written by R. K. Johnson. D. Standley produced the three-dimensional plots. Sizes of euphausiids were measured by W. G. Pearcy and L. Marx. I thank J. L. Laroche for comments during the preparation of this manuscript.

Volume scattering

The estimation methods I used are based on quantitative measurements of volume scattering strength. This measure is defined by

$$S_v = 10 \log(I_s/I_i)$$

where I_s is the scattered intensity from a unit volume containing scatterers, measured at 1 m from the volume, I_i is the intensity incident on the volume, and S_v is the volume scattering strength in decibels (dB). S_v is obtained from measured echo voltages at the echosounder receiver by use of the sonar equation (Urick 1975). This equation has corrections for acoustical calibrations of the echosounder and the directional characteristics of the transducer, and it accounts for the range-dependent losses due to spreading and absorption.

A measure related to S_v is the volume backscattering cross-section, σ_v. This is a linear measure of relative scattered intensity for a unit volume and can be found from S_v by

$$S_v = 10 \log(\sigma_v/4\pi).$$

The units of σ_v are m^2. The fundamental assumption of volume scattering is that the total scattered intensity from a volume containing a random distribution of scatterers is, on average, equal to the sum of the scattered intensities from each individual. The relative scattered intensity from an individual can be expressed as a backscattering cross-section, σ; thus the volume backscattering cross-section of a particular unit volume is, on average, equal to the sum of the individual backscattering cross-sections of the scatterers contained in that unit volume.

Scattering model

Greenlaw (1977) found that the scattering behavior of individual, preserved euphausiids and sergestid shrimp was well approximated by a fluid sphere scattering model (Johnson 1977*a*) for dorsal, ventral, and side aspects. Scattering strengths at anterior aspect were significantly lower and it was suggested that a more complex model would have to be developed to account for this directional scattering response. I assume here that the Johnson model is accurate for euphausiids and treat the effect of directionality as a source of error.

The scattering model is a simplified version of a fluid sphere model developed by Anderson (1950). It has four parameters: a, the radius of the sphere; g, the ratio of the density of the sphere to the density of the surrounding medium; h, the ratio of sound speeds; and f, the frequency of the incident sound field. The equation is (Johnson 1977*a*; Greenlaw 1977; typographical errors in these references are corrected here)

$$\sigma/\pi a^2 = \left[4\left(\frac{1-gh^2}{3gh^2} - \frac{1-g}{1-2g}\right)^2\right] \left[\frac{2(ka)^4}{2+3(ka)^4}\right] \quad (1)$$

where σ is the acoustical backscattering cross-section and k is the wave number, $k = 2\pi f/c$ (c is the speed of sound in the medium).

This scattering model is a function of both frequency and scatterer radius. The functional dependence of backscattering cross-section on each of these variables separately is different, as is evident in Fig. 1. The upper curves in the figure show the variation of σ with frequency for two sizes of euphausiid, the lower curves display the behavior of σ with radius for two choices of frequency. In both cases, the density and sound speed contrasts are assumed to be $g = 1.044$ and $h = 1.010$. The regression relation between euphausiid total length, L (mm), and radius (Greenlaw 1977)

$$a = 0.095 - 0.134L \quad (2)$$

is used in the upper curves.

The upper curves of Fig. 1 show the effect of frequency on σ for euphausiids 7 and 22 mm long. Clearly, the larger euphausiid is the stronger scatterer; however the shape of the scattering curve for each size is constant. Changing the value of the scatterer radius moves the curve in both level and frequency, but the shape is invariant. Moreover, this curve has distinct regions (in frequency) where the functional relation between σ and frequency is approximately constant. At low frequencies (the Rayleigh region) the backscattering cross-section is proportional to the fourth power of frequency, whereas at high frequencies (the geometric-optics region) σ is essentially constant. At intermediate frequencies (the resonance region) the backscattering cross-section is a constantly varying function of frequency. The location of these regions in frequency depends on the scatterer radius, but the regions exist for all choices of radius.

The lower curves of Fig. 1 illustrate the size dependence of σ for two choices of echosounder frequency, 100 and 200 kHz. Again, larger euphausiids are stronger scatterers; for them the scattering strength is essentially independent of frequency (radii >3 or 4 mm). The ratio of the scattering strengths at the two frequencies increases as the size decreases, however. This behavior suggests that the frequency dependence of the scattering could be used to discriminate sizes of the scatterers—at least for scatterers below some particular threshold radius. It is not obvious from the figure, but a lower size threshold exists also. At very high frequencies, the ratio of scattering strengths for different radii is equal to the square of the ratio of the radii. This is the region in the lower panel where the two curves merge. At very low frequencies, the ratio of the scattering strengths is proportional to the sixth power of the ratio of the radii. In both regions, ratios are independent of frequency. In the frequency span

where the resonance regions for the sizes involved overlap, however, the ratio of scattering strengths is a function of both the sizes and the frequencies and *it is this region which a multifrequency echosounder can exploit.*

The curves in the lower panel of Fig. 1 demonstrate the size selectivity of an echosounder according to the operating frequency that was suggested by McNaught (1968). For a given threshold of detectable scattering strength, the use of a higher frequency will allow detection of smaller scatterers. For example, at a detection threshold corresponding to $\sigma \geq 10^{-9}$m², a 100-kHz echosounder would be "sensitive" to scatterers larger than about 2 mm in radius but a 200-kHz echosounder would be equally "sensitive" to scatterers as small as 1 mm. In general, detection of very small scatterers requires very high frequencies.

The backscattering cross-sections predicted for euphausiids are extremely small, even at high frequencies. The predicted value of σ of a 22-mm euphausiid at 100 kHz is about 10^{-7} m² whereas the backscattering cross-section for a nonswimbladder fish of the same size, in dorsal aspect, is about $2.6 \cdot 10^{-5}$ m at the same frequency (Love 1977). The scattered intensity from this small fish is about 260 times that from a single euphausiid. Equivalently, the volume scattering from a region containing one 22-mm fish is equal to the volume scattering from the same size region containing about 260 euphausiids of the same length. Since the scattered intensities from fishes are much larger than those from euphausiids, detection and estimation of euphausiids in the presence of fish may be difficult.

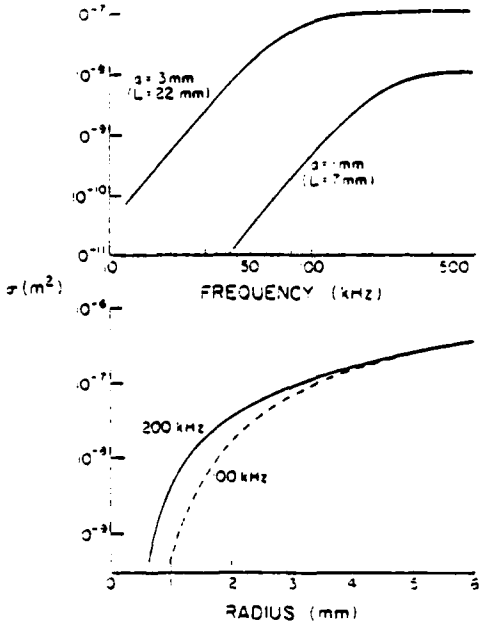

Fig. 1. Predicted backscattering cross-sections for a euphausiid vs. frequency for two sizes of euphausiid (upper) and vs. size of euphausiid for two frequencies (lower). Parameters g and h are estimated median in situ values.

Estimation methods

The strength of the volume scattering produced by a population of zooplankters is a function of the concentration of the zooplankters, the distribution of sizes, and the echosounder frequency. The size distribution and frequency affect the scattering strength predictably if the scattering model for the zooplankter is known and the scattering strength is directly proportional to concentration. We can use these relationships in several ways to obtain estimates of the population abundance. The three estimation methods described below differ in the number of frequencies at which measurements are required, but each assumes that the scattering model for the zooplankter is known. The methods are general in the sense that any scattering model (with a distinctive resonance region) can be assumed. For purposes of illustration, I will use the euphausiid scattering model.

Single-frequency methods—We assume that a single size class dominates the acoustical scattering and that this size is known (a_0). Since the volume backscattering cross-section is assumed equal, on average, to the sum of the individual

backscattering cross-sections, we have the relation

$$\langle \sigma_v(f, z) \rangle \approx N(z)\sigma(f, a_0) \quad (3)$$

for measurements at frequency f and depth z, where $N(z)$ is numerical abundance·m^{-3}. The symbol $\langle \bullet \rangle$ is used to denote mean-square average values. Given measurements of $\langle \sigma_v \rangle$ and estimates for σ, Eq. 3 can be solved for the numerical abundance profile, $N(z)$. In principle, measurements at any frequency can be used to estimate $N(z)$.

The assumption of a single size class is quite restrictive. Under certain circumstances, however, this single-frequency estimation method can be extended to populations of many sizes. Suppose the size distribution of a population is known (e.g. from net samples) and it can be assumed that this size distribution is representative of the population over the entire area of acoustical measurements. If F_i is the fraction of zooplankters of size a_i, then we can write the analogous equation to Eq. 3

$$\langle \sigma_v(f, z) \rangle \approx N(z) \sum_i F_i \sigma(f, a_i).$$

The frequency is constant and the size distribution is known, so the summation can be evaluated by using the fractional abundances and the scattering model to obtain an effective backscattering cross-section, $\bar{\sigma}(f, \bar{a})$. The numerical abundances can be calculated from

$$\langle \sigma_v(f, z) \rangle \approx N(z)\bar{\sigma}(f, \bar{a}). \quad (4)$$

If scattering model 1 is applicable, we can explicitly write $\bar{\sigma}$ as

$$\bar{\sigma}(f, \bar{a}) = K \sum_i F_i \frac{2(ka_i)^4}{2 + 3(ka_i)^4} a_i^2 \quad (5)$$

where K includes the constant terms of Eq. 1. We see that $\bar{\sigma}$ is proportional to a weighted sum of the geometric cross-sectional areas. For high frequencies and nearly normal size distributions, the weighted sum in Eq. 4 will approach the square of the mean radius.

Two-frequency method—We assume that a single size class dominates the acoustical scattering but that the size is not known or may vary from place to place. If the scattering model for the zooplankters is known, we may be able to estimate the dominant size and numerical abundance for measurements at two properly chosen frequencies.

Consider measurements of σ_v at the frequencies f_{Hi} and f_{Lo}. If we form the ratio of the volume backscattering cross-sections, substitute scattering model 1, and solve for the radius, the result is

$$a^4 = \frac{2}{3} \frac{r^4 - R}{\left(\frac{2\pi}{c} f_{Hi}\right)^4 (R - 1)} \quad (6)$$

where $r = f_{Hi}/f_{Lo}$ and $R = \sigma_v(f_{Hi})/\sigma_v(f_{Lo})$. This expression can be put in nondimensional form by defining the geometric mean frequency, $\bar{f}$, and rearranging to obtain

$$(ka)^4 = \frac{2}{3} \frac{r^4 - R}{r^2(R - 1)} \quad (7)$$

where $\bar{k} = 2\pi\bar{f}/c$. In this form the right-hand side is a function of the ratio of measured backscattering cross-sections alone, with the frequency ratio a constant parameter. Since only real values of $\bar{k}a$ are allowed, the range of plausible values for R is bounded by $1 < R < r^4$. The maximum expected value of R occurs for the smallest scatterer sizes (Rayleigh region) and the measured ratio approaches 1 for large scatterers (geometric-optics region). In the intermediate (resonance) region, the magnitude of the measured ratio for a given $\bar{k}a$ is intermediate between the bounds but, clearly, will be larger for increasing choices of the frequency ratio.

Curves of $\bar{k}a$ versus the backscattering cross-section ratio are shown in Fig. 2 for three choices of the frequency ratio $r = 2^{1/2}$, $3^{1/2}$, and $4^{1/2}$. Two features deserve emphasis: first, the sensitivity of the measurements to small changes in size (through $\bar{k}a$) increases as the frequency

ratio increases and the trend of the curves suggests use of the largest possible frequency ratio for better resolution of size. It should be noted, though, that the larger intensity ratios are produced mostly by low absolute intensities at f_{ω}. Hence the precision of the estimate of R decreases as r increases. Noise considerations will probably limit r to values <2 or 3. Second, only a limited range of $\bar{k}a$ can be resolved by these measurements. This range depends on r, but is about $0.4 \leq \bar{k}a \leq 1$. Thus the mean of the frequencies must be carefully chosen according to the sizes expected. Estimates of sizes larger or smaller than this range will be subject to large errors, depending on the precision of the measurements.

Once an estimate of the dominant size is obtained, the measurements of σ_v at each frequency can be used to estimate abundances from Eq. 3. If we consider that the ratio of measured values is used to estimate the radius, then an appropriate estimate of abundance might be the geometric mean of the two single-frequency estimates.

Multifrequency method—This requires the minimum number of assumptions about the population—it is only necessary that a scattering model with a distinct resonance region apply to the zooplankters. Suppose the size distribution of the scatterers can be adequately represented by m size classes, a_i. At a given depth, the average abundance of scatterers of size a_i is N_i (per m^3). If we measure volume backscattering cross-sections at n frequencies, the following equations apply

$$\begin{aligned}
\sigma_v(f_1) &= N_1\sigma(f_1, a_1) + N_2\sigma(f_1, a_2) \\
&\quad + \cdots + N_m\sigma(f_1, a_m) \\
\sigma_v(f_2) &= N_1\sigma(f_2, a_1) + N_2\sigma(f_2, a_2) \\
&\quad + \cdots + N_m\sigma(f_2, a_m) \\
&\vdots \qquad\qquad \vdots \\
\sigma_v(f_n) &= N_1\sigma(f_n, a_1) + N_2\sigma(f_n, a_2) \\
&\quad + \cdots + N_m\sigma(f_n, a_m) \qquad (8)
\end{aligned}$$

where $\sigma(f_j, a_i)$ is the backscattering cross-section at frequency f_j for an individual

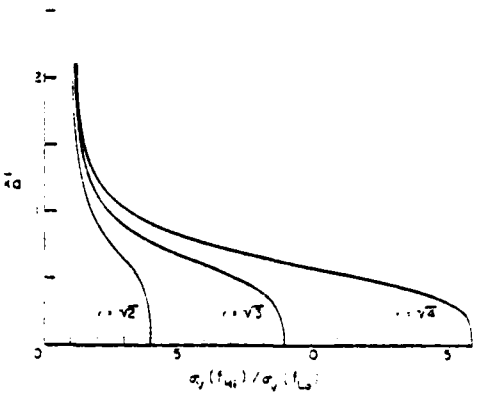

Fig. 2. Relation between mean nondimensional frequency ($\bar{k}a$) and ratio of measured volume backscattering cross-sections at two frequencies for three choices of ratio of frequencies, r. Curves are independent of density and sound speed contrasts.

of size a_i, obtained from the scattering model. These equations form a linear set with constant coefficients of $\sigma(f_j, a_i)$, measured values $\sigma_v(f_j)$, and unknowns N_i. In matrix form

$$B = SN$$

where B is the vector with elements $\sigma_v(f_j)$, S is the $n \times m$ scattering model matrix with elements $\sigma(f_j, a_i)$, and N is the vector of unknown abundances N_i. In general, the number of frequencies is not necessarily equal to the number of size classes.

Equation 8 can be solved by least-squares estimation methods. It is necessary to constrain N_i to nonnegative values in order that physically justifiable results are obtained, but this does not substantially complicate the solutions. An algorithm (NNLS) for solving the nonnegative least-squares problem has been given by Lawson and Hanson (1974), who also discussed general optimization methods for the under- and overdetermined cases. A similar algorithm has been applied to scattering from swimbladder fishes by Johnson (1977*b*). The Lawson and Hansen algorithm is computationally superior to the constrained steepest-descent method used by John-

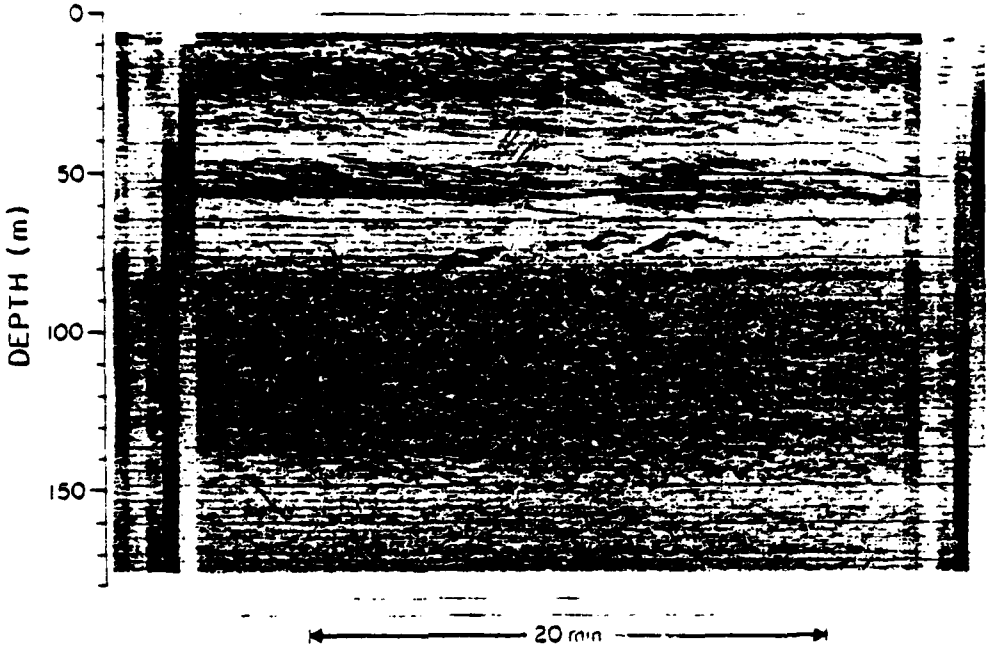

Fig. 3. Echogram showing typical daytime scattering structure in Saanich Inlet, August 1977. Echosounder frequency, 79 kHz. Depth scale corrected for transducer depth.

son (R. K. Johnson pers. comm.). I used a version of the NNLS algorithm here.

This estimation method is not limited to the use of a single scattering model. In principle, any number of models can be incorporated in Eq. 8 by adding terms of the form $N_i\sigma(f_j, a_i)$ for each additional scattering model. The ability of the algorithm to separate scatterers into several classes of scatterer types will depend largely on how different the scattering models are. The inclusion of a scattering model for fish probably will not reduce the effects of this interference to any useful extent, however, if the scattering contributed by the fish greatly exceeds that of the zooplankton.

Experimental results

Data collection—Scattering from zooplankton was measured during a research cruise in August 1977 to Saanich Inlet, a small fjord on the southeastern end of Vancouver Island. The inlet proper is about 18 km long and 7 km wide at the widest; its central portion is >200 m deep and its mouth is partially blocked by a sill at 75-m depth. Because of the sill, an oxygen-depleted zone is created in the deep waters which tends to compress the natural vertical range of the biota (Herlinveaux 1962; Bary 1966*b*). The deep water oxygen is apparently renewed by periodic flushing over the sill, probably annually in late summer or early fall (Anderson and Devol 1973).

Saanich Inlet has an unusually abundant population of euphausiids, principally *E. pacifica*. In the daytime the euphausiids are found in a deep layer (80–130 m, typically) together with amphipods, chaetognaths, and copepods. A significant fraction of this deep layer migrates to the surface at night. Day or

night, the euphausiid abundances are one or two orders of magnitude greater than typical open ocean concentrations (Bary 1966*a*; Pieper 1971). Larger fishes caught in the inlet include hake, dogfish, herring, and salmon; smaller fish such as myctophids and juveniles of many species are sometimes found within the zooplankton layer during the daytime and always at the surface at night. A typical echogram (Fig. 3) illustrates the main features of the daytime scattering structure. The deep layer extending from 80–130 m contains most of the euphausiid population. The layer is not uniform with depth and appears to change with time (or space—the ship was drifting during these recordings) into a multilayer structure. Echoes from fish lace the deep layer in this record; their presence varied considerably from day to day and at different stations. The occasional "blob" above the layer is caused by a large fish or fishes. The thin layer at 50 m could contain zooplankton, or fish, or both. The dark, horizontal trace in this layer is an echo from a sampling device in use while these records were being made. The scattering from the surface to about 35 m is mostly resolvable as individuals and thus is probably small fish. The frequency was not especially high—79 kHz.

Acoustical scattering strength profiles were measured at irregular intervals from 13–19 August whenever the ship was on station in the central basin. The data were collected with a computer-controlled research echosounder capable of selecting a sequence of transducers and the proper drive frequencies and amplitudes for each, triggering a certain number of pings, and digitizing and (mean-square) averaging the envelopes of the received echoes. A modified echogram recorder (Ross) was used to generate transmit triggers to the computer and to record echograms. The transducers were mounted on a frame, with the major response axes aligned vertically downward in the echosounder configuration, suspended over the side at about 3-m depth while collecting data. Data at several frequencies from 27 to 426 kHz were collected at most stations but, for various reasons, only the data at 79, 103, and 169 kHz are considered reliable enough to present here.

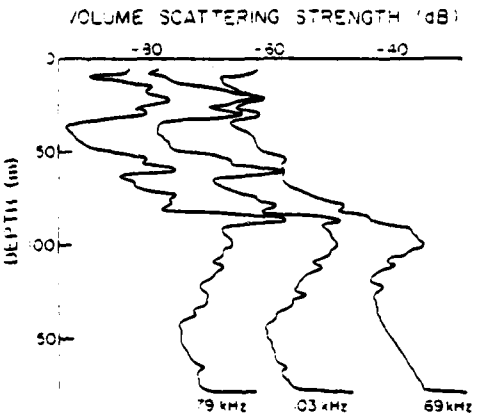

Fig. 4. Depth profiles of volume scattering strength, S_v, at three frequencies for a daytime station (1615 PDT) at Saanich Inlet. Profile at 103 kHz has been offset −10 dB and profile at 169 kHz by −20 dB, for clarity.

Typical profiles of daytime volume scattering strength are shown in Fig. 4. The deep layer is evident at about 80–130 m for all three frequencies, although there is a bump at 85 m present only at the lower two. The echogram recorded while these data were being taken shows that a fish or small school of fish drifted through the insonified area during the lower frequency measurements and was gone when the 169-kHz data were recorded. Similarly, the structure at 55 m appears to be a fish or fish school passing through the insonified area. The scattering strengths peak at about 95–100 m and fall off above and below this.

Net tows in the zooplankton layer were made on three different days with a 1-m² multiple plankton sampler, but these tows were not taken for the purpose of comparison with the acoustical data. Two net tows were made through the station where most of the acoustical data were obtained, but on days when no acoustical stations could be made. The remainder

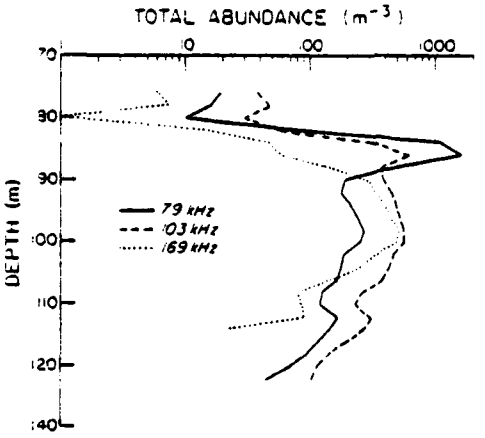

Fig. 5. Single-frequency acoustical estimates of numerical abundance in deep zooplankton layer, assuming all scatterers are euphausiids 15 mm long (a = 2.1 mm). Estimates at three frequencies presented separately. Median values of g and h used to estimate scattering cross-sections.

of the net tows began or ended at the principal acoustical station, thus the deep nets were fished up to 5 km away from the acoustical station. Moreover, echograms recorded at stations up- and down-bay from the principal acoustical station generally showed a different vertical structure—the deep layer beginning at different depths and sometimes having two or three nearly distinct layers. This spatial variation may have been compounded by temporal influences as well, for CDT data taken throughout the cruise suggest that flushing may have been occurring during this period. Therefore, I have made no serious attempt to compare the acoustical estimates of abundances with the net samples.

Live zooplankton from several net hauls were kept in chilled seawater for measurements of density and sound speed. Density and sound speed in situ were obtained from CDT casts. The measurements on live euphausiids yielded mean values for the density and sound speed contrasts of $g = 1.044$ and $h = 1.010$. The bounds for all measurements were $1.037 \leq g \leq 1.052$ and $1.000 \leq h \leq 1.020$. Measurement methods have been described elsewhere (Greenlaw 1977). It is assumed that these estimates are independent of temperature, salinity, and pressure over the ranges involved.

Acoustical estimates—A subsample of 50 euphausiids from a net tow at 85 m taken at the acoustical station was measured; mean length was 15 mm. If we assume that the mean size is a reasonable approximation to the effective size, then the single-frequency method can be used to produce numerical abundance estimates for each of the scattering strength profiles of Fig. 4. The mean radius for a length of 15 mm is, from Eq. 2, $a \approx 2.1$ mm. We assume mean values for g and h and use Eq. 1 to calculate backscattering cross-sections for the mean individual at each frequency. The estimates of numerical abundance are obtained from Eq. 3.

Profiles of estimated abundance at each frequency are plotted in Fig. 5. Only the main layer is shown, as it is the major concentration during the daytime. The numerical estimates are in reasonable agreement over the main portion of the layer. The lower frequency estimates are about a factor of two less than the estimates at 103 kHz but have essentially the same shape. The estimate at 169 kHz agrees with the data at 103 kHz at the peak of the layer, but appears to have a different shape. The peak at 86 m at 79 kHz and 103 kHz is the interference from fish, which obscures comparisons of shape at the upper edge of the layer. The lower edge of the layer is sharper at 169 kHz than at the lower frequencies; this is probably an artifact due to the lower signal-to-noise ratio at this frequency compared to the other data. All of these estimates are plausible.

The size distribution of the euphausiids was estimated from measurements on 100 euphausiids from the same net tow (*see Fig. 8*) and used to calculate effective backscattering cross-sections at the three frequencies from Eq. 5; estimates of numerical abundance were obtained from Eq. 4. These estimates were nearly identical with those shown in Fig.

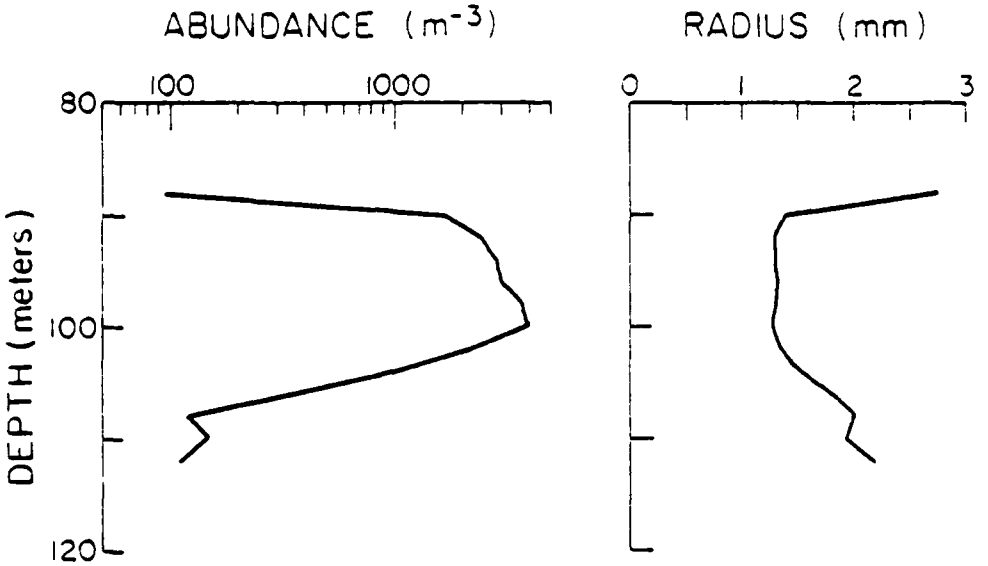

Fig. 6. Two-frequency acoustical estimates of dominant-scatterer radius and abundance in daytime deep layer obtained from volume scattering measurements at 79 and 169 kHz. Abundances are geometric mean of single-frequency estimates at each frequency calculated using estimated radius.

3. Apparently, for this distribution and these frequencies, mean size is a good estimate for effective size. This may prove true in practice for most measurements on euphausiids.

Estimates of numerical abundance and dominant size were made using the two-frequency method, but with poor results. Figure 6 shows the estimates obtained from the data at 169 kHz and 79 kHz (r = 2.14). The abundance estimate, in this case the geometric mean of the two estimates obtained, is about six times the single-frequency estimates. Over the peak of the layer, the estimated radius is only 1.2 mm (length about 8 mm). Since the single-frequency estimates are consistent with one another and with the estimate of the effective radius equal to about 2.1 mm, these two-frequency estimates cannot be considered accurate. The main cause of the discrepancies probably is the distribution of sizes in the population. No one size actually dominates the scattering (although an effective size can be used to replace the distribution for abundance calculations at a single frequency) and the differences in scattering at the two frequencies is "smeared" by this size distribution. In addition, the calculated value of $\bar{k}a$ is 1.0 for this frequency pair, which is at the limit of resolution for this method. The other possible frequency pairs are less desirable, one yielding r = 1.30 and the other $\bar{k}a$ = 1.2. Hence none of the available frequency pairs are particularly satisfactory for two-frequency estimates of size and abundance for this population.

Least-squares estimation of the size abundances was conducted for seven radii classes, a = 0.5, 1, . . . , 3.5 mm at all three frequencies. The range of sizes was determined in part by the measured size distribution of the euphausiids. Fewer radii classes degraded resolution of the size distribution; more radii classes did not improve the resolution noticeably. The choice of seven radii classes for data taken at only three frequencies ensures that the least-squares problem is highly underdetermined. Qualitatively, we would

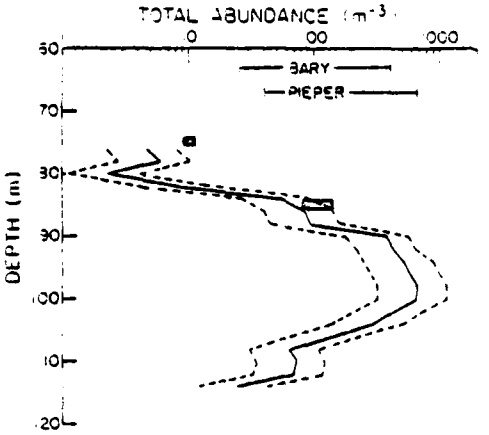

Fig. 7 Acoustical estimates of total numerical abundance in deep zooplankton layer obtained from least-squares estimation algorithm using all three frequencies. Solid curve is estimated profile using median values for g and h; dashed curves are abundances for extreme combinations of measured ranges of g and h. Abundance estimates from nets fished near this station on other days shown as hatched boxes. Historical estimates of peak abundances from Bary (1966a) and Pieper (1971) shown as bars.

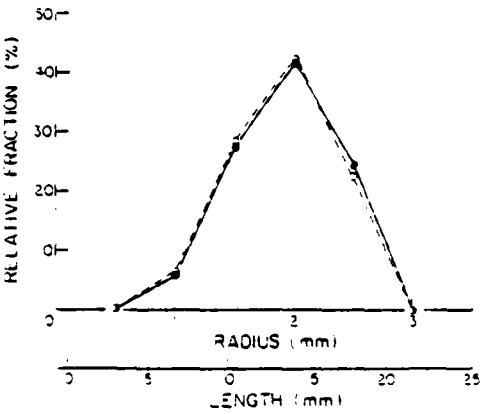

Fig. 8. Comparison of acoustically estimated scatterer size distribution (solid) and measured distribution of euphausiid lengths (dashed) from a net sample. Acoustical estimate is an average (92–102 m) over peak of daytime layer. Net haul made at 80-m depth over a 4.5-km path about 3 h after acoustical measurements.

expect the solutions to be "mushy" in the sense that many solutions exist that are not significantly better or worse than others according to particular measures. The solutions chosen in this analysis are those for which the euclidean norm of the vector N and the residual norm, $\| B - AN \|$, are jointly minimum (Johnson pers. comm.).

The solid curve in Fig. 7 is a numerical abundance profile for the daytime layer data of Fig. 4 obtained from the least-squares algorithm. The abundances plotted are the sums of the abundances in each size class at a particular depth. Median values of the density and sound speed contrasts were used in the scattering matrix; the range of numerical estimates corresponding to the total range of measured values for g and h are also shown.

The shape of the abundance profile is nearly identical to the single-frequency estimate at 169 kHz (Fig. 5) and the numerical estimates are similar. The interference from fish appears here as a small bump in the profile at 86 m. Abundance estimates from the two net tows taken at the acoustical stations (but on different days) are shown at the appropriate depths. These data compare well with the acoustical estimates, but since they do not include the main portion of the zooplankton layer, are insufficient to verify the analysis. Also shown are the ranges of the abundance estimates obtained by Bary (1966a) and Pieper 1971) for net tows in the densest part of this scattering layer with the "catcher," a small mouth opening, high speed, opening-closing net. The acoustical estimates are in reasonable agreement with these historical catch data.

Figure 8 shows the percentage size distribution of the acoustical estimates and the measured size distribution of 100 euphausiids collected in a net haul. The acoustical data are an average over the middle of the layer, 92–102 m. The net sample was obtained about 2 km from the acoustical station at a depth of 80 m. At the time of the tow (1900 PDT), this depth put the net into the upper portion of the layer. The agreement between the

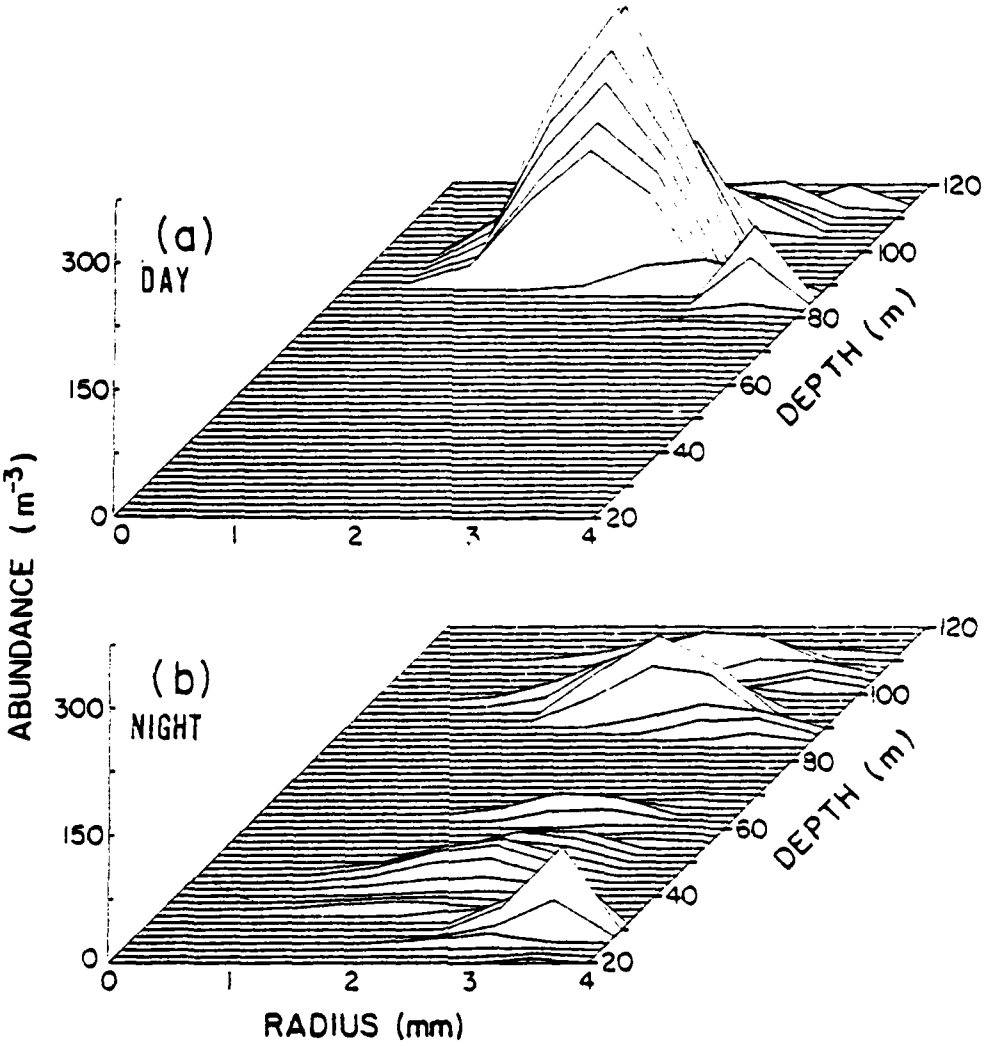

Fig. 9. Acoustically estimated size abundance profiles for 20–120-m depth range. Data shown are (a) day (1615 PDT) and (b) night (2110 PDT) at same station in Saanich Inlet. Daytime data correspond to scattering profiles of Fig. 5. Artificial zeroes have been added at 0.0- and 4.0-mm radius to enhance readability.

distributions is remarkable. If we assume that the distribution of sizes of the euphausiids is less variable over horizontal distances than the numerical abundances, then the comparison in Fig. 8 is strong evidence for the efficacy of the acoustical sampling. The good agreement between the size distributions implies that, for these data at least, euphausiids are the dominant causes of the acoustical scattering.

The size abundance estimates for the daytime layer are presented in three-dimensional form in Fig. 9a and a similar plot of the nighttime scattering at the same station in Fig. 9b. The depth range

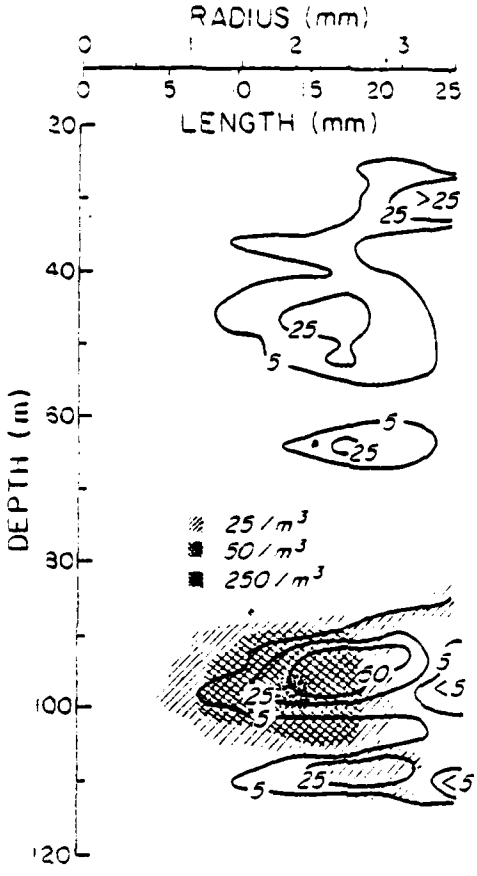

Fig. 10. Numerical abundance contours No. m^{-3} vs. size and depth for data of Fig. 9. Daytime contours shown as hatched regions; night contours as solid lines.

is 20–120 m in both. These are also about the limits of valid data. The lower depth is approximately the point where no signals were seen above the noise level. At the gain settings necessary to obtain useful echo levels from the deep layer, the receiver often clipped signals in the first 20 m, especially at night; thus data above 20 m are unreliable. Radii classes at 0 and 4 mm are shown.

In the three-dimensional perspective, the daytime layer appears dense and thin, with a definite size distribution structure. Larger scatterers appear above and below the layer. The size distribution peak is at 2.0 mm (14.2-mm length) throughout the layer. At night the profile changes dramatically. There is a residual layer or perhaps two layers at the location of the daytime layer, but it is composed of mostly larger scatterers. The overall impression is of significantly fewer scatterers in the night data for the depth range 20–120 m.

The size/depth resolution of the acoustical estimates can be exploited to allow presentation of the data in forms suited to particular analyses. Numerical total abundance profiles and the three-dimensional size/abundance plots are two examples. Another is the contour size/abundance plot of Fig. 10. This representation, which superimposes the daytime and nighttime data, emphasizes population density maxima, or "cores," in depth and size. For example, the nighttime residual layer is clearly a dual layer in this figure, the upper with a core at 94 m and the lower with a core at 108 m. Assuming that these data are from the same population as the daytime data, we can draw conclusions about the vertical migration response of the population as a function of size.

It is apparent from the contour plot that the residual night layers are composed of size classes that were present in similar or higher concentration at the same depths in the daytime, and there is no reason to suppose that any significant vertical excursions were required to create the dual layer structure. The cores of the residual layers consist of larger individuals, 14–22 mm long, although in lower concentrations than are present during the day. The midwater layers have cores of 17-mm (62-m layer) and 12–20-mm (46-m layer) euphausiids at concentrations comparable to the deeper residual layers. Thus the larger euphausiids (>10 mm long) seem to distribute into several minidistributions throughout the water column at night. The smaller organisms (<10 mm long) disappear almost entirely from the 20–120-m depth

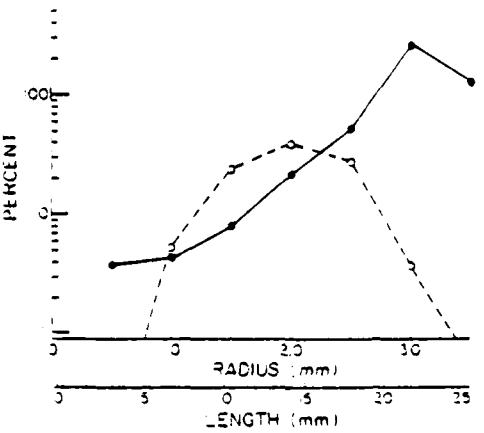

Fig. 11. Number of scatterers of each size remaining in 20–120-m depth range at night, expressed as fraction of daytime abundances in same depth range (solid curve). Total percentage size distribution for daytime estimates shown as dashed curve. Note that estimates of apparent "recruitment" in larger size classes are based on a small fraction of total number of scatterers.

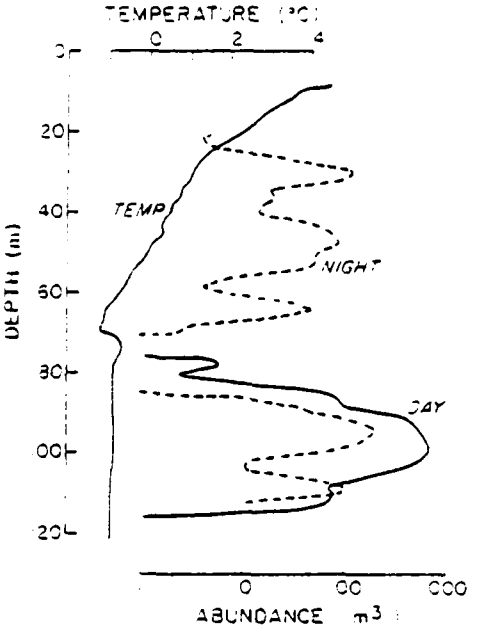

Fig. 12. Day and night total numerical abundance profiles compared to temperature profile. Hiatus in abundance is associated with temperature inversion at about 76 m for both distributions.

region, presumably having migrated to the region above 20 m.

The apparent migration can be quantified by using the acoustical estimates. Figure 11 presents the fractions of scatterers remaining in the 20–120-m range at night for each size class. The fractions were calculated by dividing the total number of scatterers in each size class over the 20–120-m depth interval for the night data by the corresponding estimate for the day data. Estimates in the larger two sizes that seemed obviously to be caused by fish were deleted. The results are an estimate of the fraction of scatterers in each size class that apparently has remained in the 20–120-m depth interval. Also on the figure is the percentage size distribution of all scatterers (excluding "fish") for the 20–120-m day data. The fraction-remaining curve shows a pronounced trend for larger fractions of smaller organisms to migrate out of the 20–120-m depth region. Again, assuming these data are from the same population and neglecting any potential horizontal advection). Virtually all of the smallest ($L \leq 10$ mm) organisms are absent from the night data. About three-fourths of the medium-size (15 mm) and half of the larger (20 mm) euphausiids have apparently migrated into surface waters. The increase in the largest size classes at night may be an estimation error or may be caused by fishes migrating downward or horizontally. It should be noted that these classes contain only a small fraction of the scatterers.

This description of vertical migration has assumed that the numerical estimates for the night data are as accurate as those for the day data. This may not be the case, however. I noted in discussing the scattering model that the scattering strengths of euphausiids at anterior or posterior aspects are lower than at dorsal aspect. I have assumed that the average orientation of euphausiids is horizontal so that

dorsal aspect scattering strengths are appropriate) for these analyses. Sameoto and Paulowich (1977, pers. comm.) have examined euphausiid orientations from photographs taken by a camera towed in the Gulf of St. Lawrence. The orientations observed were distributed over all angles but the mean value for daytime records was nearly 0° (horizontal, dorsal up); at night, however, a significant number of animals were oriented almost head-up, and the change from horizontal to near-vertical orientations seemed to take several hours. If the average orientation at night is inclined toward the vertical, then the volume scattering strengths will be less than for the same distributions of animals with horizontal orientations. In addition, the amount of reduction at a fixed frequency is dependent on the lengths of the euphausiids and is greater for the smaller ones (Greenlaw 1977). An overall decrease in scattering strength due to an orientation change at night would result in underestimating actual abundance. The greater reduction in scattering strengths for the smaller euphausiids would result in relatively larger estimation errors for smaller animals. Thus both the overall abundances and size distributions can be affected by changes in orientation from the horizontal.

The comparisons given here show both a reduction in total abundances and a proportionately greater reduction of the smaller euphausiids at night. These effects could be due to differential vertical migration into the surface waters or to changes in the average orientation of the organisms at night. If orientation is the sole difference, rough calculations with a conjectured aspect-dependent model (Greenlaw 1977) show that an average orientation of about 45° would be needed to account for the discrepancy in total abundances. More likely a combination of differential vertical migration and (possibly depth-dependent) orientation have produced the effects observed, but the data are insufficient to resolve this question.

One of the principal advantages of an acoustical sampler over conventional sampling methods is the essentially continuous nature of the data. If the numerical estimates are correct, then the depth resolution of an echosounder cannot be approached by any practicable sampling plan. Such resolution could be useful in studies such as investigating relationships between distributional patterns and physical-chemical properties of the habitat. As an example, in Fig. 12 the numerical abundance estimates for day and night are compared with a temperature profile from the same station (following night). There is a striking association between the hiatus of the abundance profiles (which are assumed to be about the limiting or "steady state" distributions for day and night) and the temperature inversion at 76 m. Most likely the temperature inversion indicates an intrusion of water over the sill of the inlet, in which case this depth zone would be a region of relatively high velocity shear and it is reasonable that zooplankton might avoid it. Resolution of this phenomenon by conventional means would be extraordinarily difficult.

Remarks

These data cannot be considered conclusive proof that acoustical sampling methods are precise estimators of zooplankton abundances. The suggestion is quite strong, however, that this is indeed the case under certain circumstances. The abundances of euphausiids estimated acoustically in Saanich Inlet are in reasonable agreement with historical estimates for net tows. The high abundances suggest that the data were taken at or near a seasonal peak in standing stocks, which is also in accord with historical data (Pieper 1971). The most impressive evidence is the remarkable correlation between acoustical and net-tow estimates of size distributions, which is much too good to be fortuitous.

These methods rely on a scattering model as a basis for the estimates and thus are limited in application to zoo-

plankters for which there is a scattering model. At present this restricts the use to euphausiids (and, perhaps, only during the daytime where orientation can be presumed horizontal). However, scattering models can be developed and verified by laboratory measurements for other common zooplankters. The degree of approximation inherent in a model does set a limit on the accuracy of estimates made using it, but this limit can be reduced by refining the models. Use of an applicable scattering model is preferable to empirical methods for several reasons. The principal drawback of empirical relations between scattering strengths and common biological measures of abundance is that neither number of scatterers nor biomass is a fundamental acoustical quantity. At very low frequencies, where all scatterers can be considered as Rayleigh scatterers, the backscattering cross-sections are proportional to radius to the sixth power or volume squared. At very high frequencies, the backscattering cross-sections are proportional to radius squared or to the cross-sectional area. Because the volume backscattering cross-section is composed of a *sum* of terms in volume squared or cross-sectional area, we cannot take its square root or raise it to the $^3/_2$ power and obtain a quantity proportional to volumes. Similarly, the expression used for the single-frequency estimates of a population of mixed sizes (Eq. 5) shows that the number of organisms is not a fundamental quantity if the size distribution of the population changes.

Single-frequency estimates are the easiest to obtain and may well suffice for most applications. In principle any echosounder can be used to measure volume scattering strengths, but in practice careful consideration must be given to choice of operating frequency. Detection ranges of echosounders tend to decrease dramatically as the operating frequency is increased, principally because of the increase in absorption at high frequencies. The volume scattering strength of a population of euphausiids will increase rapidly with frequency up to a point (about where $ka = 1$ for the mean size scatterers) and then increase much more slowly as the increments of scattering strength for the smallest scatterers becomes less for each increase in frequency. The change in volume scattering strength for a change in the abundance of the smallest scatterers will always be less than the change in volume scattering strength for an equal change in the abundance of larger scatterers. This is true at all frequencies and imposes a minimum detectable abundance change on the measurements. If measurements are made at a sufficiently high frequency so that $ka \approx 1$ for the smallest scatterer, however, the increment in volume scattering strength for a change in the abundance of the smallest scatterers is maximized and the best possible resolution obtained. As an example, suppose that the smallest euphausiid we expect to find in significant numbers is 6 mm long. The corresponding radius is 0.9 mm and the minimum frequency for which $ka \approx 1$ is $f = 265$ kHz. There are echosounders with operating frequencies in this range, but probably results would be adequate with an echosounder operating at the more common frequency, 200 kHz.

Two-frequency estimates of size and abundance were very different from the single- and multifrequency measurements for this particular population. Probably this method would not produce satisfactory results with any population that includes a variety of sizes. There may be circumstances when a population is dominated by a single size class, however, and this method could be useful in estimating that size.

The multifrequency estimates are clearly the most elegant results of acoustical sampling. These data were obtained with the absolute minimum number of frequencies and certainly better solutions would be possible with measurements at more frequencies. There are no rules for choosing the optimum number of frequencies but there are guidelines for choosing the range of frequencies.

Ideally, we would like to have our estimate be sensitive to changes in the abundance of the smallest and largest size classes by a single scatterer. Since the increment in volume backscattering cross-section for the smaller size will be less than that for the larger size irrespective of frequency, we cannot expect to achieve this sort of resolution. That is, acoustical estimation will always be less sensitive to changes in the abundance of the smaller sizes. In addition, ambient noise and measurement uncertainties will make it unlikely that we can achieve sensitivity to a change of only a single large scatterer. As a practical alternative, we can choose the upper and lower frequencies on the basis of resolution independent of the other scatterers and recognize that estimating smaller sizes is inherently less accurate than estimating larger sizes.

If the smallest size class only were present, we would expect optimal solutions of abundance if the highest measurement frequency were chosen so that the measurements were near the upper range of the resonance region for these scatterers. Thus we would want $ka \approx 1$ at the highest frequency for the smallest size class. Similarly, if only the largest size class were present, we would choose the lowest frequency so that measurements at this frequency were at the lower end of the resonance region, or $ka \approx 0.7$. These are conservative guides and could be relaxed considerably. If we apply these limits, the range of maximum sensitivity for the measurements presented here is about $1.4 \leq a \leq 2.1$ mm.

References

ANDERSON, J. J., AND A. H. DEVOL. 1973. Deep water renewal in Saanich Inlet, an intermittently anoxic basin. Estuarine Coastal Mar. Sci. 1: 1–10.

ANDERSON, V. C. 1950. Sound scattering from a fluid sphere. J. Acoust. Soc. Am. 22: 426–431.

BARRACLOUGH, W. E., R. J. LEBRASSEUR, AND O. D. KENNEDY. 1969. Shallow scattering layer in the subarctic Pacific Ocean; detection by high frequency echosounder. Science 166: 611–613.

BARY, B. MCK. 1966*a*. Backscattering at 12 kc/s in relation to biomass and numbers of zooplanktonic organisms in Saanich Inlet, British Columbia. Deep-Sea Res. 13: 655–666.

——— 1966*b*. Qualitative observations of scattering of 12 kc/s sound in Saanich Inlet, British Columbia. Deep-Sea Res. 13: 667–677.

GREENLAW, C. F. 1977. Backscattering spectra of preserved zooplankton. J. Acoust. Soc. Am. 62: 44–52.

HERLINVEAUX, R. H. 1962. Oceanography of Saanich Inlet in Vancouver Island, British Columbia. J. Fish. Res. Bd. Can. 19: 1–37.

JOHNSON, R. K. 1977*a*. Sound scattering from a fluid sphere revisited. J. Acoust. Soc. Am. 61: 375–377.

——— 1977*b*. Acoustic estimation of scattering-layer composition. J. Acoust. Soc. Am. 61: 1636–1639.

KELLEY, J. C. 1976. Sampling the sea, p. 361–387. *In* D. H. Cushing and J. J. Walsh [eds.], The ecology of the seas. Saunders.

LAWSON, C. L., AND R. J. HANSON. 1974. Solving least squares problems. Prentice-Hall.

LOVE, R. H. 1977. Target strength of an individual fish at any aspect. J. Acoust. Soc. Am. 62: 1397–1403.

MCNAUGHT, D. C. 1968. Acoustical determination of zooplankton distributions. Proc. 11th Conf. Great Lakes Res. 1968: 76–84.

——— 1969. Developments in acoustic plankton sampling. Proc. 12th Conf. Great Lakes Res. 1969: 61–68.

———, M. BUZZARD, AND S. LEVINE. 1975. Zooplankton production in Lake Ontario as influenced by environmental perturbations. U.S. EPA Rep. EPA-660/3-75-021, p. 40–63.

NORTHCOTE, T. G. 1964. Use of a high-frequency echosounder to record distribution and migration of *Chaoborus* larvae. Limnol. Oceanogr. 9: 87–91.

PIEPER, R. C. 1971. A study of the relationship between zooplankton and high-frequency scattering of underwater sound. Ph.D. thesis, Univ. British Columbia. 72 p.

SAMEOTO, D. D., AND S. PAULOWICH. 1977. The use of 120 kHz sonar in zooplankton studies. Oceans '77 Conf. Rec. (IEEE/MTS), v. 2, p. 39A1–39A6.

URICK, R. J. 1975. Principles of underwater sound. McGraw-Hill.

Submitted: 4 May 1978
Accepted: 21 September 1978

(*From the* QUARTERLY JOURNAL OF THE ROYAL METEOROLOGICAL SOCIETY, Vol. 105, No. 444, April 1979)

Quart. J. R. Met. Soc. (1979), **105**, pp. 487–502

551.521.1:551.521.2

Mid-ocean observations of atmospheric radiation

By JAMES J. SIMPSON and CLAYTON A. PAULSON

School of Oceanography, Oregon State University, Corvallis, Oregon 97331

(Received 8 February 1978; revised 1 August 1978)

SUMMARY

Mid-ocean (35°N 155°W) observations of the various components of radiative flux were made from the R/P FLIP during the period 2 through 13 February 1974. Cloud cover ranged from clear skies to overcast, and water vapour pressure varied between 9 and 18 mb, with sea surface temperature near 15·0°C.

The net longwave radiative fluxes reported here were obtained: (1) by taking the difference between simultaneous measurements of net all-wave and net solar fluxes; and (2) by direct measurements with a net longwave radiometer designed by G. W. Paltridge. When observations during rain and fog are excluded, the difference between night-time 15-minute averages by the two methods is generally less than 1 mW cm^{-2}. During day-time, indirect measurements are often larger than direct by about 5 mW cm^{-2}; from internal evidence we prefer the direct values.

The albedo of the sea surface was calculated from simultaneous measurements of downward and upward solar fluxes. The observations were analysed to represent albedo as a function of solar altitude and atmospheric transmittance, following the work of R. E. Payne; our results suggest that Payne's smoothed representation is suitable for use over the open ocean. Albedo was observed to decrease with increasing wind speed for clear skies with solar altitude between 15 and 30 degrees but no variation was discernible at higher solar altitudes.

Empirical formulae for calculating both shortwave and net longwave components of the radiative flux were compared with measurements. A formula due to F. E. Lumb for determining the incident solar flux given solar altitude, cloud amount and cloud type, consistently yields good agreement with the measurements, within about 1 mW cm^{-2}. Daily averages of net longwave flux calculated from several empirical formulae using a linear correction for clouds are within 2 mW cm^{-2} of the observations reported in this paper. Since daily radiation balance values were measured as only 5 mW cm^{-2}, the limitations of the best current empirical formulae are evident.

1. INTRODUCTION

The ability to determine accurately the exchange of heat between atmosphere and ocean is important in several scientific and practical applications, including: (1) investigation of atmospheric and oceanic circulation; (2) weather forecasting; (3) investigation of thermal modifications in the lower atmosphere and upper ocean; and (4) investigation of the dynamics of climate. The objectives of this paper are to describe observations of radiation over the mid-Pacific and to compare the observations with suggested parameterizations of radiative fluxes at the surface.

The heat flux budget at the air–sea interface can be expressed

$$Q_T = (1-\alpha)Q_S - Q_B + Q_{BC} - Q_L - Q_{SE}, \qquad (1)$$

where Q_T is the total heat flux into the ocean, Q_S the incident solar flux, α the sea surface albedo, Q_B the longwave flux emitted from the sea surface, Q_{BC} the longwave flux emitted from the atmosphere, and Q_L and Q_{SE} the latent and sensible heat fluxes from the sea surface to the atmosphere. The net longwave flux, Q_{BN}, may be introduced in Eq. (1) to replace $Q_{BC} - Q_B$, and the net all-wave flux, $Q_N = (1-\alpha)Q_S + Q_{BN}$, may be introduced to replace all the radiative terms. Typically, the sensible heat flux is an order of magnitude less than the latent heat flux, which is of the same order as the net longwave flux.

Few radiative flux measurements have been made at sea. Lumb (1964), Payne (1972), Reed (1977) and Tabata (1964) have analysed observations of shortwave radiation. Char-

neil (1967) reported observations of longwave radiation near Hawaii. Reed and Halpern (1975) reported both shortwave and net longwave observations off the Oregon coast.

2. Instrumentation

A description of the instrumentation used is given in Table 1.

Measurements of the net longwave flux are usually obtained by subtracting simultaneous measurements of the net all-wave flux, Q_N, and the net solar flux, $(1-\alpha)Q_S$. The accuracy of such measurements can be low during day-time because the net longwave flux is frequently an order of magnitude less than the differenced quantities. Net longwave fluxes reported here were also measured directly with a radiometer manufactured by Middleton Instruments and calibrated by CSIRO (Paltridge 1969). The instrument consists of a standard Funk net radiometer converted to a net longwave radiometer by surrounding the radiometer with a black polythene sphere to filter shortwave radiation. The filter is rotated by an electric motor to eliminate effects of differential heating of the filter by absorption of solar radiation. The transmittance of the filter is zero below a wavelength of 2·5 μm and increases to about 40% at 25 μm, modified by absorption bands at 6·5 and 14 μm. Paltridge calculated that the effect of the variability of the transmittance of the filter on the measurements will be about $\pm 5\%$ for the blackbody temperature of the earth's surface varying by ± 20 degC about 10°C.

3. Observations

Measurements of the incident solar, reflected solar, net all-wave and net longwave radiative fluxes were made from the R/P FLIP (floating instrument platform: Bronson and Glosten 1968) during the period 2 to 14 February 1974 as a part of the POLE experiment, a component of the North Pacific experiment NORPAX. The sea surface temperature was also observed using a radiation thermometer. The R/P FLIP occupied a station approximately 800 miles north of the Hawaiian Island chain under free drift conditions. Its position ranged between 35°09′ and 34°56′N, 155°05′ and 155°25′W.

The R/P FLIP provides an ideal platform from which to make measurements of radiative fluxes because of the stability induced by having about 90 m of her length submerged (as a large spar buoy). Hence, errors due to variable sensor orientation, as occur on conventional ships in response to surface waves and swell, are largely eliminated. Vertical motions of FLIP were about 10 cm, and pitch and roll amplitudes were about 2°. The radiometers were located as shown schematically in Fig. 1, to minimize shadowing by the hull and the main boom.

The signal from each instrument was transmitted by shielded cable to the platform laboratory, amplified and recorded in stripchart form by use of a multi-point potentio-

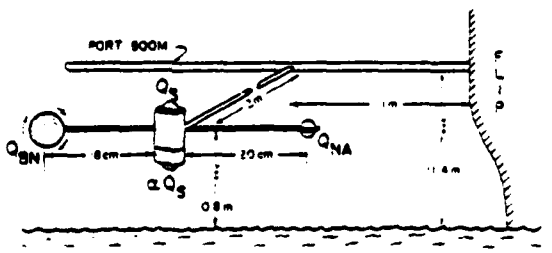

Figure 1. Schematic diagram showing location of instruments used to measure net longwave radiation, Q_{SN}, incoming and upward solar radiation, Q_S and αQ_S respectively, and net all-wave radiation, Q_N.

TABLE 1. SUMMARY OF INSTRUMENTATION

Device	Manufacturer	Physical parameter	Spectral response (μm)	Sensitivity (mV/mW cm^{-2})	Accuracy (%)	Time response (s)
Pyranometer	Eppley (8–48)	Incident flux, Q_s	0·2·5	0·109	2–3	15–20
Pyranometer	Eppley (8–48)	Reflected flux, αQ_s	0·2·5	0·112	2–3	15–20
Net radiometer with black polythene sphere	Middleton Co.	Net longwave flux, Q_{lN}	> 2·5	0·045	7·5	15–20
Net radiometer	Swissteco Pty Ltd.	Net all-wave flux, Q_N	0·3–60	0·459	2·5	15–20

TABLE 2. MEAN DAILY VALUES OF RADIATIVE FLUXES AND METEOROLOGICAL VARIABLES

Date (Feb. 1974)	Incident solar (mW cm^{-2})	Upward solar (mW cm^{-2})	Net all-wave (mW cm^{-2})	Net long (mW cm^{-2})	Day-time cloud cover (fraction)	24-hour cloud cover (fraction)	Sea surface temperature (°C)	Air temperature (°C)	Vapour pressure (mb)
3	7·8	0·4	5·3	2·8	0·9	1·0	14·6	14·6	13·8
4	9·2	0·7	7·1	1·0	1·0	1·0	14·8	14·8	16·7
5	10·0	0·7	6·6	- 2·3	0·6	0·8	14·9	15·6	17·2
6	12·5	1·1	5·3	4·2	0·2	0·3	14·8	14·8	13·7
7	16·9	1·6	7·8	7·6	0·2	0·2	14·7	13·2	9·3
8	14·8	1·0	6·3	6·8	0·4	0·4	14·7	14·3	11·5
9	7·0	0·5	3·5	- 2·8	0·9	0·9	14·7	13·9	15·5
10	6·5	0·4	4·4	0·6	1·0	1·0	14·8	14·6	15·6
11	8·8	0·6	5·8	1·5	1·0	1·0	14·8	14·2	14·2
12	9·0	0·6	4·8	4·3	0·9	0·9	14·7	15·2	15·4
13	10·3	0·7	5·5	2·3	0·9	0·7	14·6	15·7	15·9

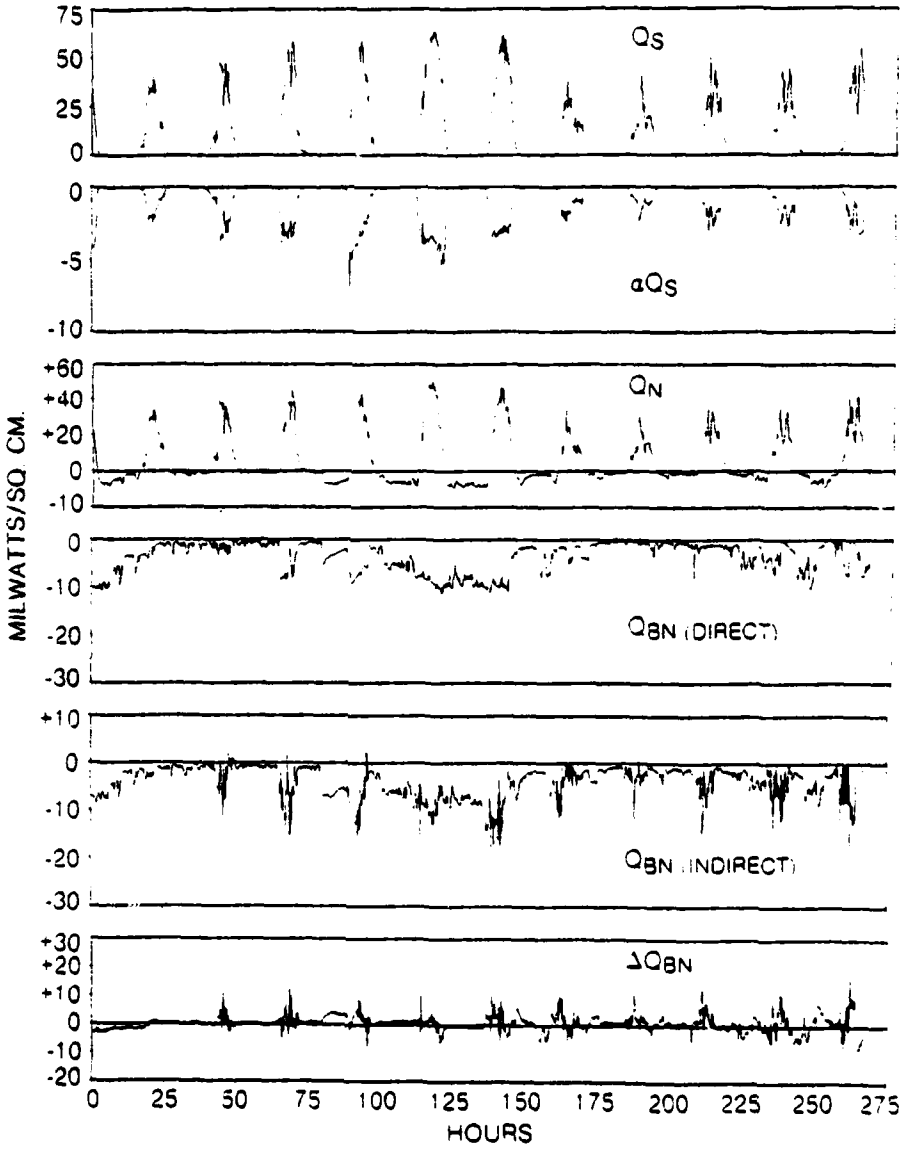

Figure 2. Time series of 15-minute averages of the various radiative components. Q_s is incident solar radiation; αQ_s, upward solar radiation; Q_N, net all-wave radiation; Q_{BN}, net longwave radiation; and ΔQ_{BN}, Q_{BN}(direct) minus Q_{BN}(indirect). The time of start is 0135 GMT on 3 February 1974.

metric recorder. A sampling rate of 5 to 10 samples per minute per channel was maintained throughout the experiment.

A digital representation of the data was obtained using a chart digitizer. The records were merged to obtain a continuous time series of the measured variables for the experimental period. Occasional errors caused by radio interference were removed from the records by interpolation. Less than 1% of the data was affected by such interference. From

the resulting time series, sequential averages over 1 and 15 minutes were constructed. The time series of 15-minute averages for the entire experimental period are shown in Fig. 2.

A summary of the daily mean radiative fluxes and other meteorological data is provided in Table 2. The mean cloud cover estimates of Table 2 are time-weighted averages of the fraction of estimated cloud cover. Averages are given for both day-time (sunrise to sunset) and 24-hour periods. Stratus and cirrus clouds were the dominant types observed. Cirrus clouds were neglected in estimating cloud amount if blue sky could be seen through the clouds: Quinn and Burt (1968) have shown that such clouds have an insignificant effect on attenuating solar radiation. A maximum mean daily solar flux of $16{\cdot}9\,\mathrm{mW\,cm^{-2}}$ was observed on a day having nearly clear skies ($C = 0{\cdot}2$ where C is fractional cloud cover), while the minimum mean daily value of $6{\cdot}5\,\mathrm{mW\,cm^{-2}}$ corresponded to completely overcast skies.

4. Net longwave flux

Two independent measurements of net longwave flux were made during the POLE experiment. A direct measurement was obtained by use of the net longwave radiometer described above. Indirect measurements were made by differencing measurements of the net all-wave radiative flux, Q_N and the net solar flux, $(1-\alpha)Q_S$. Values of the fluxes obtained by the two methods are referred to as direct and indirect measurements.

Records of the 15-minute averages of the directly measured net longwave fluxes are plotted in Fig. 2 together with a record of the difference between direct and indirect measurements. The daily mean direct fluxes and atmospheric conditions are given in Table 2. Several features are immediately evident in Fig. 2. The mean difference over the entire observational period between night-time direct and indirect measurements is only 2% of the mean of either, showing good agreement in the absence of solar radiation. There is, however, disagreement between direct and indirect 15-minute averages on several nights. This disagreement is believed to be due to fog, mist and rain. Both radiometers give erroneous readings under these conditions because of wetting of the exterior surfaces. The second, third, fifth and sixth nights of observations were without fog, mist or rain and the difference between direct and indirect measurements on those nights is within $\pm 1\,\mathrm{mW\,cm^{-2}}$.

Day-time comparisons of direct and indirect measurements of net longwave radiation (Fig. 2) show that indirect measurements are, on average, 30% larger than direct measurements. Indirect measurements also exhibit a degree of variability during the day which is absent at night and is therefore thought spurious. The lack of agreement between direct and indirect measurements during the day can best be accounted for as the error resulting from taking the difference of two large measurements, both of which are subject to experimental error. At midday, the incident solar and net all-wave radiative fluxes are about an order of magnitude larger than the net longwave flux. Given an error in each measurement of $\pm 5\%$, we expect the error of the difference to be as large as the difference itself, about $\pm 5\,\mathrm{mW\,cm^{-2}}$. Referring to Fig. 2, the difference between direct and indirect measurements lies between $\pm 5\,\mathrm{mW\,cm^{-2}}$ more than 90% of the time. The tendency for indirect measurements to exceed direct measurements during the day suggests that calibrations of the pyranometers and net all-wave radiometers are in disagreement for shortwave radiation: unfortunately, we were unable to test this in the laboratory.

Because of this possibility, direct measurements of net longwave radiation are almost certainly more reliable than the indirect measurements. The direct measurements show that the net longwave flux from the sea surface is on average greater during the day than at night. This result is consistent with generally less cloud cover during the day, as reported by Dorman *et al.* (1974) from an analysis of observations at Ocean Station 'N' (30°N 140°W).

TABLE 3. ALBEDO VALUES AVERAGED OVER 2° INTERVALS OF SOLAR ALTITUDE AND 0·1 INTERVALS OF ATMOSPHERIC TRANSMITTANCE, T. THE NUMBERS IN PARENTHESIS ARE THE NUMBER OF RAW ALBEDO VALUES USED TO OBTAIN THE AVERAGE. AN ASTERISK INDICATES THAT THE DIFFERENCE BETWEEN THE VALUES SHOWN AND SMOOTHED VALUES GIVEN BY PAYNE (1972) IS ≤0·01

	Solar altitude (°)																						
T	0	2	4	6	8	10	12	14	16	18	20	22	24	26	28	30	32	34	36	38	40	42
0·05		0·054* (2)	0·394 (1)	0·083 (2)	0·069* (2)	0·083 (1)	0·052 (2)	0·019 (1)		0·020 (2)	0·005 (1)	0·009 (1)	0·055* (2)	0·071* (2)								
0·15		0·122 (8)	0·090 (6)	0·060 (11)	0·051 (7)	0·062* (9)	0·056* (5)	0·060* (1)	0·060* (7)	0·067* (3)	0·057* (4)	0·064* (4)	0·065* (4)	0·056* (2)	0·058* (4)	0·058* (2)	0·058* (1)	0·062* (2)	0·064* (5)	0·065* (2)	0·061* (5)	0·061* (2)
0·25		0·050 (5)	0·072 (2)	0·042 (1)	0·064 (4)	0·068 (2)	0·074* (4)	0·079 (6)	0·056 (2)	0·072* (5)	0·057 (3)	0·061* (7)	0·065* (6)	0·059* (7)	0·060* (3)	0·062* (5)	0·061* (4)	0·060* (3)	0·063* (4)	0·061* (4)	0·061* (11)	0·058* (3)
0·35			0·229* (3)		0·206 (1)	0·064 (1)		0·078 (3)	0·079 (5)	0·069 (2)	0·080* (3)	0·078* (2)	0·070* (3)	0·060 (2)	0·062* (5)	0·061* (5)	0·061* (6)	0·060* (3)	0·060* (7)	0·060* (6)	0·060* (7)	0·058* (1)
0·45		0·157 (1)					0·208 (1)			0·102 (1)	0·096 (1)	0·108* (1)	0·070 (1)	0·085* (2)	0·072* (2)	0·070* (3)	0·062* (4)	0·064* (5)	0·063* (6)	0·061* (15)	0·061* (8)	0·060* (1)
0·55			0·361 (1)		0·332* (4)	0·267* (3)	0·225 (3)	0·138 (1)	0·225 (3)	0·120 (1)		0·084 (1)	0·100* (2)	0·089* (4)	0·082* (3)	0·081* (3)	0·066 (2)	0·069* (4)	0·068* (3)	0·065* (12)	0·057* (3)	0·060* (1)
0·65			0·165 (1)	0·197 (1)		0·400 (1)	0·363 (1)	0·181 (1)	0·150 (3)	0·155* (4)	0·136* (6)	0·130 (2)	0·107* (2)	0·107* (1)	0·088* (4)	0·079* (4)	0·072* (4)	0·065* (5)	0·062* (8)	0·058* (10)	0·055* (8)	
0·75												0·118* (1)		0·090* (1)		0·081* (1)	0·077* (4)	0·067* (3)	0·063* (1)	0·060* (5)	0·054* (3)	
0·85																						

5. ALBEDO

The albedo of the sea surface is defined as the ratio of the upward to the downward solar flux immediately above the air–sea interface. Two sources contribute to the upward component: emergent irradiance due to back-scattered light from below the sea surface; and irradiance reflected from the sea surface. Payne (1972) concludes, on the basis of observations in Buzzards Bay and the Sargasso Sea, that the ratio of emergent to downward flux is about 0·005. Ivanoff (1977) states that the ratio has a maximum of 0·02 for very clear water but in general is less than 0·005.

Payne analysed observations to represent the albedo, x, as a function of the solar altitude, θ, and the atmospheric transmittance, Γ, which was included to allow for the dependence of x on the radiance distribution from the sky. Atmospheric transmittance is defined as the ratio of downward irradiance with an atmosphere to that without an atmosphere, i.e.

$$\Gamma = Q_S r^2 / S \sin\theta , \qquad (2)$$

where S is the solar constant, taken as 135 mW cm^{-2}, and r is the ratio of actual to mean earth–sun separation. For the case of no atmosphere ($\Gamma = 1{\cdot}0$), the incident flux is dependent only upon the altitude of the sun and the sun–earth distance. Increased atmosphere and cloud cover result in enhanced absorption, reflection and scattering of the incoming solar flux. The overall effect is to produce a more nearly uniform radiance distribution, thus reducing the dependence of albedo on solar altitude. In the limit of heavy overcast ($\Gamma \leqslant 0{\cdot}1$), a nearly isotropic radiance distribution results. The use of transmittance to parameterize albedo may be questionable at low sun angles because Γ may increase without limit (finite sky radiation) as θ approaches zero.

Payne's observations were taken from a fixed platform in a bay off the coast of Massachusetts. Observations were made from 25 May to 28 September during which time the solar altitude ranged to 72° and the mean wind speed was about 3·7 m s^{-1}. The transmittance ranged from near zero to about 0·75. Payne fitted smooth curves to the albedo as a function of transmittance for observations in intervals of 2° of solar altitude. He extrapolated the curves to regions of solar altitude and transmittance in which there were no observations. In carrying out the extrapolation, he imposed a boundary condition on the value and the slope of the curve of albedo *vs.* transmittance for transmittance equal to unity. The slope was assumed equal to zero, and the albedo was derived from reflectances calculated from a theory due to Saunders (1967). It was assumed that the ratio of downward irradiance to that emerging from the sea was 0·005 and that the surface roughness corresponded to a wind speed of 3·7 m s^{-1}.

The observations reported here were analysed similarly to those of Payne. Values of albedo were calculated from 15-minute averages of incident and reflected fluxes. Corresponding values for solar altitude and atmospheric transmittance were also computed. The resulting data were sorted into 2° intervals of solar altitude and averaged over intervals of 0·1 in transmission coefficient. The resultant values of mean albedo, as well as the number of values used to obtain each mean, are shown in Table 3. This table may be compared with a similar table of smoothed observations given by Payne.

Observations of albedo for particular ranges of atmospheric transmittance are shown in Fig. 3 as a function of solar altitude. The scatter of the data for low solar altitudes occurs because the cosine response of the radiometers is poor for solar altitudes less than 5° and because of generally increasing uncertainty in the measurements as the magnitude of the irradiance decreases. Very small variation of albedo with solar altitude is observed in Fig. 3(a), suggesting, as one might expect, that for overcast conditions ($\Gamma \leqslant 0{\cdot}33$) albedo has a

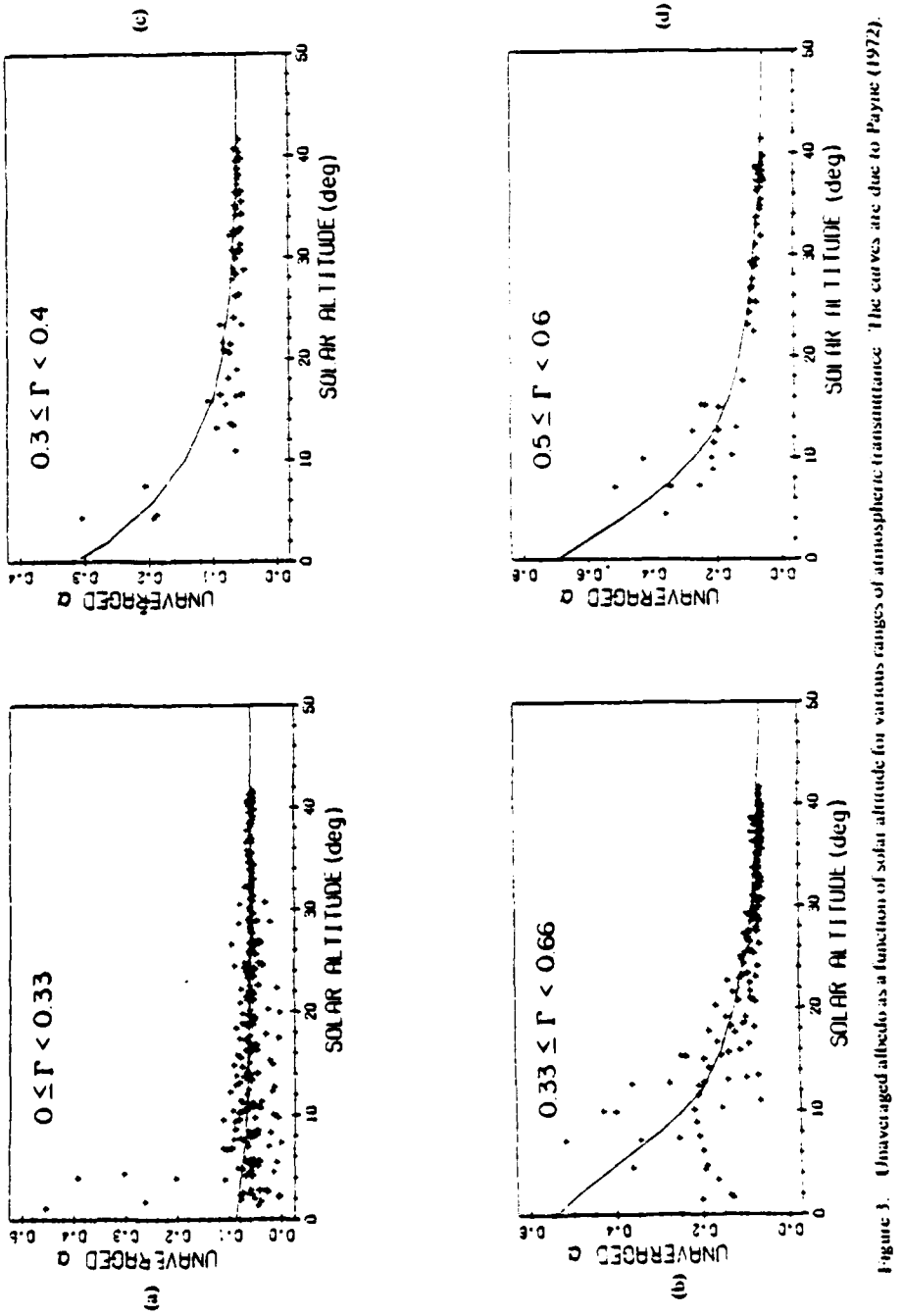

Figure 3. Unaveraged albedo as a function of solar altitude for various ranges of atmospheric transmittance. The curves are due to Payne (1972).

negligible dependence on solar altitude. The observations agree well with Payne's suggested curve. The mean albedo for observations shown in Fig. 3(a) is 0·066 ± ·004, where the uncertainty is ± one standard deviation. For the range of atmospheric transmittance most nearly approaching an isotropic radiance distribution ($\Gamma \leqslant 0{\cdot}1$) the mean albedo is 0·060 ± ·01, which is in excellent agreement with Payne's value of 0·061 ± ·005. In Fig. 3(b), albedo is shown as a function of solar altitude for intermediate transmittance ($0{\cdot}33 \leqslant \Gamma \leqslant 0{\cdot}66$). Figs. 3(c) and 3(d) provide finer resolution with respect to atmospheric transmittance. The results are generally consistent with Payne's smoothed curves.

Representative plots of albedo as a function of atmospheric transmission for a given range of solar altitude are shown in Fig. 4. The scatter in the data is seen to be largest for the range of low solar altitudes ($\theta < 15°$) as previously explained. Some of the scatter may be caused by variations in solar altitude within each range. For the high altitude range, $30° < \theta < 45°$, the scatter is significantly reduced and the curve suggested by Payne is supported.

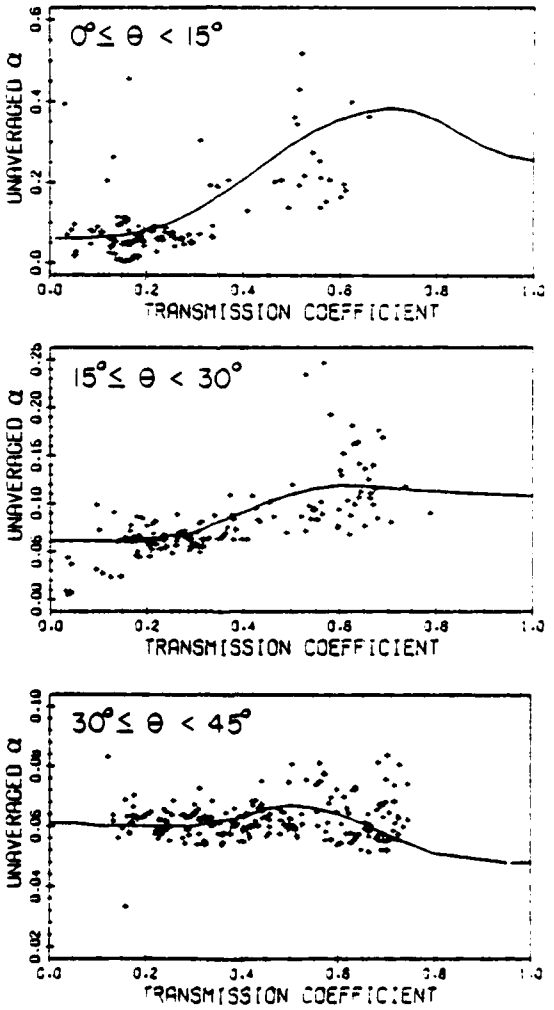

Figure 4. Unaveraged albedo as a function of atmospheric transmittance for various ranges of solar altitude.

The percentage differences between our observations of albedo and Payne's curves, averaged over 2° intervals of solar altitude and over all values of transmittance, are plotted in Fig. 5 as a function of solar altitude. For increasing solar altitude, the difference decreases from about -6% at $\theta = 20°$ to -2% at 40°. This systematic difference is within the specified accuracy of the pyranometers (Table 1). The differences are larger and more variable for solar altitudes less than 20°, reflecting the greater uncertainty in measurements at low solar altitudes as well as uncertainties caused by increased effects of variable surface roughness and radiance distribution of the sky. Payne shows that uncertainty in the measurements of albedo increases rapidly for solar altitude below 20°. Even though our observations of albedo are systematically lower than Payne's, we conclude that the differences are within the combined experimental uncertainty of both sets of observations.

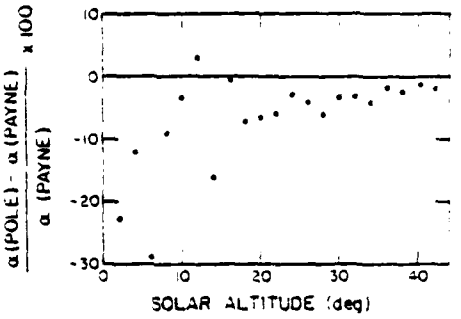

Figure 5. The average deviation of observed values of albedo from Payne's (1972) curves as a function of solar altitude.

The effect of sea surface roughness on albedo was investigated by sorting the observations with $\Gamma > 0{\cdot}6$ according to solar altitude and wind speed. The analysis was limited to large values of transmittance because the effect of roughness on albedo is expected to be largest under clear skies. The values of albedo were sorted by 15° intervals of solar altitude and normalized by the mean albedo for the given range of solar altitude. Mean values were then obtained by averaging over $2\,m\,s^{-1}$ bands and were plotted as a function of wind speed. Insufficient data at low solar altitudes precludes discussion for the range $\theta < 15°$. No discernible dependence on sea surface roughness was evident in the large scatter associated with the high altitude range, $30° \leqslant \theta \leqslant 45°$. Values in the intermediate range, $15° \leqslant \theta \leqslant 30°$, are shown in Fig. 6. The data qualitatively support decreasing albedo with increasing wind speed as observed by Payne, and also as calculated by Payne based on a theory due to Saunders (1967). The slope of the line in Fig. 6 corresponds to Payne's observations and theoretical calculations for clear skies with $17° \leqslant \theta \leqslant 25°$. The theory predicts that the effects of variable sea surface roughness will be negligible for solar altitudes greater than 30°.

The average day-time albedo shows the expected correlation with cloud cover. The seven days of high mean cloud cover ($0{\cdot}9 \leqslant C \leqslant 1{\cdot}0$) have an average albedo of 0·064. This value corresponds well with Payne's value of 0·061 corresponding to a nearly isotropic radiance distribution. For relatively cloudless periods, higher mean albedo is found: 0·09 for both 6 and 7 February, computed from daily average values of incident and upward solar flux when the average cloud cover was 0·2. Such augmented mean values are due to the large albedo with low sun under clear skies. A climatological estimate of albedo, 0·08 (Payne), for the month of February at 35°N in the Atlantic agrees with the mean value for the experimental period, $0{\cdot}07 \pm 0{\cdot}01$.

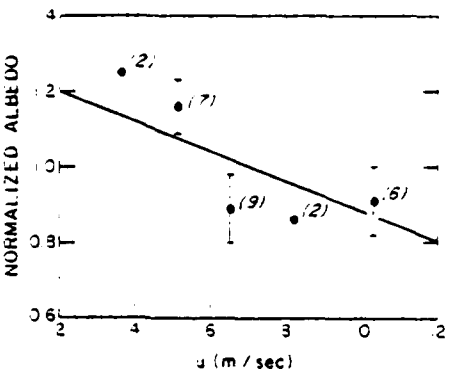

Figure 6. Normalized albedo *v.* wind speed for transmission coefficient greater than 0·6 and solar altitude between 15° and 30°. Numbers in parentheses are the number of values averaged to obtain each point. Vertical bars represent the standard error. The line has the slope calculated by Payne (1972) from a theory due to Saunders (1967).

In summary, the observed variation of albedo with solar altitude and transmittance is in good agreement with near-shore observations reported by Payne. Apart from experimental error, the scatter of the observations about Payne's smoothed curves can be ascribed to various causes:

(1) Part of the scatter in Figs. 3 and 4 is caused by a true variation of albedo within the given ranges of transmittance and solar altitude.

(2) Variability in surface roughness associated with varying winds can cause scatter at low values of solar altitude ($\theta < 30°$). Mean winds during the POLE experiment were 6 m s^{-1} compared with 3·7 m s^{-1} for the observations reported by Payne.

(3) The distribution of radiation from the sky cannot be unambiguously characterized by the transmittance. For example, consider two cases having the same intermediate value of transmittance, say 0·3, one in which the solar radiation is attenuated by intermittent, dense clouds and the other in which there is a uniform, thin layer of cloud. The albedo for these two cases would probably be different, as can be deduced from Payne's curves of albedo *v.* transmittance, which are nonlinear between conditions of heavy overcast ($\Gamma = 0$) and clear skies ($\Gamma > 0{\cdot}6$)

(4) There may be disagreement at high values of transmittance where Payne's smoothed curves are influenced by the imposed boundary conditions at $\Gamma = 1{\cdot}0$. As discussed above, these boundary conditions are derived theoretically and lack observational support.

6. Parameterizations

(a) *Shortwave flux*

Numerous empirical relations have been advanced to predict the attenuation of solar radiation by clouds. Relations suggested by several authors are given in Table 4. In this table, Q_0 represents the insolation under clear skies and is calculated from the formula due to Seckel and Beaudry (1973) (see also Reed 1977). Seckel and Beaudry's formula is based on data in the Smithsonian Meteorological Tables, using an atmospheric transmission coefficient of 0·7. Reed compared several formulae for estimating clear-sky insolation with coastal and oceanic observations and concluded that the relations due to Seckel and Beaudry (1973) and Lumb (1964) were the most reliable. The parameter C in Table 4 is the fractional cloud cover and ϕ is the noon solar altitude. The relation due to Wyrtki (1965)

TABLE 4. COMPARISON OF OBSERVATIONS OF INCIDENT SOLAR RADIATION WITH PREDICTIONS OF EMPIRICAL FORMULAE

Reference	Formula	Overestimate of 11-day mean predictions (%)	Mean square difference, observation–prediction (mW^2cm^{-4})
Houghton (1954)	$Q_0(1{\cdot}28-1{\cdot}03C)$	−10	10·3
Kimball (1928)	$Q_0(1-0{\cdot}71C)$	−18	5·4
Lumb (1964)	$135(a-bs)s$	0	0·7
Reed (1977)	$Q_0(1-0{\cdot}62C-0{\cdot}0019\phi)$	5	2·8
Wyrtki (1965)	$Q_0(1-0{\cdot}38C-0{\cdot}38C^2)$	−17	8·2

is an adaptation of a previous relationship suggested by Budyko (1956) and Berland (1960). The coefficients 0·38 are valid for latitudes less than 60°. In the relation due to Lumb, a and b are empirical constants dependent on cloud amount and type. The parameter s is the mean of the solar altitudes at the beginning and end of the hour over which the insolation is calculated.

The empirical formulae shown in Table 4 were compared with observations by computing predictions of the mean daily insolation and comparing these predictions with the observations tabulated in Table 2. Excepting Lumb's formula, all the computations were made using the averaged day-time cloud cover tabulated in Table 2. Predictions using Lumb's formula were made for each hour of the day and then averaged to obtain a daily prediction. Predictions were averaged over the 11-day period and compared with the average of the observations over the same period. The percentage differences between averaged observations and predictions are tabulated in Table 4 together with the mean square of the differences between daily predictions and observations. The formulae due to Reed (1977) and Lumb (1964) are in closest agreement with observations. All the remaining formulae tend to underestimate the observed insolation. Plots of the predictions due to Reed and Lumb are shown in Fig. 7. The agreement between Lumb's formula and observations is remarkably good, suggesting that daily predictions can be made with an accuracy of 1 mW cm^{-2}. The greater accuracy of Lumb's formula is undoubtedly because both cloud amount and cloud type are incorporated into the prediction. Lumb's formula was derived from weather ship observations in the North Atlantic (52°30'N 20°W); the present comparison suggests it may have validity over extensive areas of the ocean. If estimates of cloud type are not available, Reed's formula is preferable. Reed's formula is based on an extensive set of coastal and oceanic observations.

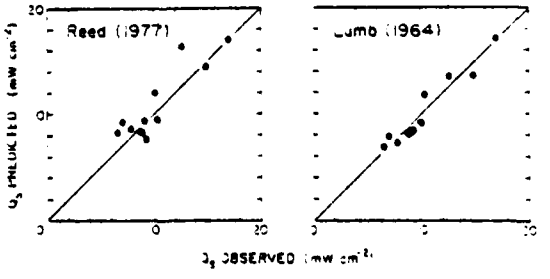

Figure 7. Daily observations of average insolation v. estimates from formulae due to Reed (1977) and Lumb (1964).

TABLE 5. FORMULAE FOR CALCULATING NET LONGWAVE RADIATION UNDER CLEAR SKIES

Author	Formula
Anderson (1952)	$\varepsilon\sigma(T_s^4 - T_a^4(0.74 - 0.0049e_a))$
M. E. and T. G. Berliand (Budyko 1956)	$\varepsilon\sigma T_s^4(0.39 - 0.05e_a^{\frac{1}{2}}) - 4\varepsilon\sigma T_s^3(T_s - T_a)$
Brunt (1932); M. E. and T. G. Berliand (Budyko 1974)	$\varepsilon\sigma T_s^4(0.39 - 0.05e_a^{\frac{1}{2}})$
Efimova (Budyko 1974)	$\varepsilon\sigma T_s^4(0.254 - 0.00495e_a)$
Swinbank (1963)	$\varepsilon\sigma T_s^4(1 - 9.35 \times 10^{-6} T_s^2)$

(b) *Net longwave flux*

Several formulae used to calculate net longwave radiative transfer between the earth's surface and the atmosphere under clear skies are given in Table 5, in which ε is the emissivity of the surface (taken as 0·97 after Anderson (1952)), σ the Stefan–Boltzman constant, T_s surface temperature, e_a atmospheric vapour pressure in mb, and T_a air temperature. The formula due to Brunt (1932) has coefficients suggested by M. E. and T. G. Berliand (Budyko 1974). The formula due to M. E. and T. G. Berliand (Budyko 1974) is similar to Brunt's formula, the difference being an additional term dependent on the sea–air temperature difference. The formulae due to Anderson (1952) and Efimova (Budyko 1974) become nearly identical if one assumes $T_a = T_s$. Swinbank's (1963) formula is the only one independent of vapour pressure. Most of the formulae in Table 5 were derived from observations over land. Anderson's formula, however, was derived exclusively from observations over a lake. Swinbank's formula was based primarily on observations over land, but included observations over the Indian Ocean. Reed (1976) concluded that Efimova's formula gave predictions in good agreement with observations under clear skies over the ocean.

The formulae in Table 5 were compared with observations during the POLE experiment. Observations during clear skies are tabulated in Table 6 together with predictions of the empirical formulae. The 'weighted average' is weighted by the duration of individual observations. All the formulae underestimate the observations, although the significance is not large because of the scatter. Efimova's formula most strongly disagrees with the observations, by 15% on average, although the standard deviation about the mean is a minimum. Swinbank's formula agrees in the mean, but it yields the largest standard deviation. The weighted mean of estimates by Berliand's formula also agrees with the mean of the observations.

TABLE 6. OBSERVATIONS AND ESTIMATES OF NET LONGWAVE RADIATION UNDER CLEAR SKIES

Date of start Feb. 1974	Time of start (local)	Duration (h)	T_s (°C)	T_a (°C)	e_a (mb)	Q_{BN} observed (mW cm^{-2})	Overestimate (%) Brunt	Berliand	Anderson	Efimova	Swinbank
2	1530	6·0	14·6	14·6	13·4	9·9	−21	−21	−26	−28	−14
5	0830	2·5	14·9	15·6	17·2	7·9	−12	−17	−19	−19	8
6	0830	6·5	14·8	15·5	15·7	7·0	4	−2	−6	−5	22
7	0700	13·5	14·7	13·1	9·0	8·4	3	10	0	−10	−3
7	2200	17·5	14·7	13·4	10·6	9·2	−7	1	−9	−17	−8
12	2230	1·0	14·6	14·3	13·4	10·0	−22	−21	−26	−29	−15
						Average:	−9	−8	−14	−18	−2
						Weighted average:	−5	−1	−9	−15	−2
						Standard deviation:	10	12	10	9	13
						Weighted standard deviation:	9	10	9	7	11

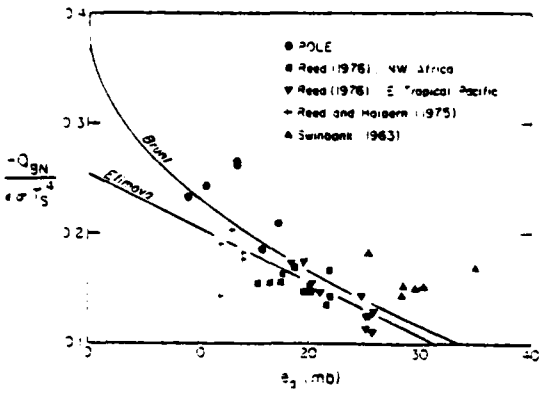

Figure 8. Normalized net longwave radiation, as a function of vapour pressure. The curves are defined in Table 5.

For further comparison between observation and prediction of net longwave radiation under clear skies, we have plotted in Fig. 8 several sets of non-dimensional fluxes as functions of vapour pressure. Values of surface temperature and upward longwave flux from Swinbank's (1963) observations were obtained by adding 0·5 degC to observed values of air temperature to obtain T_s and then computing the upward flux from $\varepsilon\sigma T_s^4$. An air–sea temperature difference of 0·5 degC is typical of tropical latitudes (see, e.g., Paulson *et al.* 1972). There is disagreement between the observations. The three sets reported by Reed (1976) and Reed and Halpern (1975) are consistent with each other and agree with Efimova's formula as reported by Reed (1976). Both the POLE observations over the mid-Pacific and Swinbank's observations over the Indian Ocean are systematically higher for given values of vapour pressure than the remaining observations.

It is not surprising that there is systematic disagreement between various sets of observations of net longwave radiative flux and predictions of empirical formulae. Observations of net longwave radiation are difficult to make at sea, particularly from a conventional ship (Hinzpeter (1970)) and may have errors larger than the incident solar flux. Disagreement between observations may also be ascribed to the approximation made in all the empirical formulae that net longwave flux depends at most on surface temperature and near-surface atmospheric temperature and humidity. The net longwave flux under clear skies clearly depends also on the temperature and humidity distribution throughout the lower atmosphere. This dependence is illustrated by observations reported by Reed (1975) showing the effect of thermal inversions on the net longwave flux over the sea.

In the presence of clouds, a correction must be applied to clear-sky predictions of net longwave radiation. Linear correction factors with various coefficients were applied to predictions by each of the formulae given in Table 5. It was found that a factor of $1-0{\cdot}8\,C$ yielded predictions in approximate average agreement with observations. A plot of predicted daily values *vs.* observations is shown in Fig. 9 for Anderson's formula. Similar comparisons using the formulae of Brunt and of Berliand, with the same cloud factor, are equally satisfactory. It appears that daily values of net longwave radiation can be predicted with an accuracy of 2 mW cm^{-2}. A cloud factor of $1-0{\cdot}8\,C$ may be compared with Reed's (1976) suggestion of $1-0{\cdot}9\,C$ for middle and high latitudes and $1-0{\cdot}7\,C$ for the tropics. Laevastu (1967) suggested factors dependent on cloud type as follows: (1) stratocumulus, $1-0{\cdot}9\,C$; (2) altostratus, $1-0{\cdot}6\,C$, and (3) cirrus, $1-0{\cdot}25\,C$.

On the basis of the POLE observations, the formulae due to Brunt, M. E. and T. G.

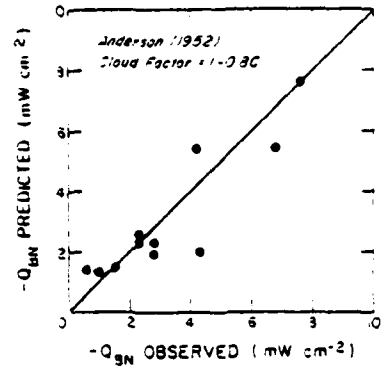

Figure 9. Daily averaged observations of net longwave radiation *v.* estimates based on Anderson's (1952) formula multiplied by a linear cloud factor.

Berliand, and Anderson are equally acceptable. The formula due to Efimova systematically underpredicted radiation under clear skies, while Swinbank's formula gave large scatter. Reed (1976), however, finds Efimova's formula in good agreement with three sets of observations. Additional observations are required to improve confidence in predictions of net longwave radiation from routine measurements.

ACKNOWLEDGMENTS

This research was supported by the Office of Naval Research through contract N00014–76–C–0067 under project NR 083–102. The cooperation of the officers and crew of the R/P FLIP, the use of oceanic observations of longwave radiation made available by R. K. Reed and the assistance of A. Lillich in the analysis is gratefully acknowledged. Some of the computations were carried out at the computer facility of the National Center for Atmospheric Research which is sponsored by the National Science Foundation.

REFERENCES

Anderson, E. R. 1952 Energy budget studies, *U.S. Geol. Survey Circ.*, 229, 71–119.

Berliand, T. G. 1960 Metodika klimatologishcheskikh radiatsii (Method of climatological calculation of global radiation), *Meteorol. i Gidrol.*, 6, 9–12.

Bronson, E. D. and Glosten, E. R. 1968 Floating instrument platform. *Tech. Rept.*, Marine Physical Laboratory, San Diego, Calif.

Brunt, D. 1932 Notes on radiation in the atmosphere, *Quart. J. R. Met. Soc.*, 58, 389–420.

Budyko, M. I. 1956 *The heat balance of the earth's surface* (English translation by N. A. Stepanova, Gidrometeorologicheskoe, Leningrad, U.S. Weather Bur., Washington, D.C., 1958).

1974 *Climate and life*, Academic Press, New York.

Charnell, R. L. 1967 Long-wave radiation near the Hawaiian Islands, *J. Geophys. Res.*, 72, 489–495

Dorman, C. E., Paulson, C. A. and Quinn, W. H. 1974 An analysis of 20 years of meteorological and oceanographic data from ocean station N, *J. Phys. Oceanog.*, 4, 645–653.

Hinzpeter, H. 1979 Atmospheric radiation in *Instruments and methods in air-interaction*, L. Hasse, R. Davis and F. Dobson, editors (to be published).

Houghton, H. G. 1954 On the annual heat balance of the northern hemisphere, *J. Met.*, 11, 1–9.

Ivanoff, A.	1977	Oceanic absorption of solar energy, in *Modelling and prediction of the upper layers of the ocean*, E. B. Kraus, editor, Pergamon Press, Oxford, 47–71.
Kimball, H. H.	1928	Amount of solar radiation that reaches the surface of the earth on the land and on the sea, and methods by which it is measured, *Mon. Weath. Rev.*, **56**, 393–398.
Laevastu, T.	1967	Cloud factor in long-wave radiation formulae, *J. Geophys. Res.*, **72**, 4277.
Lumb, F. E.	1964	The influence of cloud on hourly amounts of total radiation at the sea surface, *Quart. J. R. Met. Soc.*, **90**, 43–56.
Paltridge, G. W.	1969	A net long-wave radiometer, *Ibid.*, **95**, 635–638.
Paulson, C. A., Leavitt, E. and Fleagle, R. G.	1972	Air–sea transfer of momentum, heat and water determined from profiles during BOMEX, *J. Phys. Oceanog.*, **2**, 487–497.
Payne, R. E.	1972	Albedo of the sea surface, *J. Atmos. Sci.*, **29**, 959–970.
Quinn, W. H. and Burt, W. V.	1968	Incoming solar radiation over the tropical Pacific, *Nature*, **217**, 149–150.
Reed, R. K.	1975	Variations in oceanic net long-wave radiation caused by atmospheric thermal structure, *J. Geophys. Res.*, **80**, 3819–3820.
	1976	An estimation of net long-wave radiation from the oceans, *Ibid.*, **81**, 5793–5794.
	1977	On estimating insolation over the ocean, *J. Phys. Oceanog.*, **7**, 482–485.
Reed, R. K. and Halpern, D.	1975	Insolation and net long-wave radiation off the Oregon coast, *J. Geophys. Res.*, **80**, 839–844.
Saunders, P. M.	1967	Shadowing on the ocean and the existence of the horizon, *Ibid.*, **72**, 4643–4649.
Seckel, G. R. and Beaudry, F. H.	1973	The radiation from sun and sky over the North Pacific Ocean (abstract), *Trans. Amer. Geophys. Union*, **54**, 1114.
Swinbank, W. C.	1963	Long-wave radiation from clear skies, *Quart. J. R. Met. Soc.*, **89**, 339–348.
Tabata, S.	1964	Insolation in relation to cloud amount and sun's altitude, *Studies in Oceanography*, K. Yoshida ed., University of Tokyo, Tokyo 202–210.
Wyrtki, K.	1965	The average annual heat balance of the North Pacific Ocean and its relation to ocean circulation, *J. Geophys. Res.*, **70**, 4547–4559.

Geochimica et Cosmochimica Acta Vol. 43, pp. 339 to 352
© Pergamon Press Ltd. 1979 Printed in Great Britain

0016-7037/79/0301-0339$02.00/0

Mineral phases formed in anoxic sediments by microbial decomposition of organic matter

ERWIN SUESS
School of Oceanography, Oregon State University, Corvallis, OR 97331, U.S.A.

(*Received* 16 *May* 1978; *accepted in revised form* 2 *November* 1978)

Abstract—Microbial decomposition of organic matter in recent sediments of the Landsort Deep—an anoxic basin of the central Baltic Sea—resulted in the formation of a characteristic assemblage of authigenic mineral precipitates of carbonates, sulfides, phosphates and amorphous silica. The dominant crystalline phases are a mixed Mn-carbonate [$(Mn_{0.85}Ca_{0.10}Mg_{0.05})CO_3$], Mn-sulfide [MnS] and Fe-carbonate [$FeCO_3$]. Amorphous Fe-sulfide [FeS], Mn-phosphate [$Mn_3(PO_4)_2$] and a mixed Fe-Ca-phosphate [$(Fe_{0.86}Ca_{0.14})_3(PO_4)_2$] were identified by their chemical compositions only. The variability in composition of these solid phases and their mode of occurrence as a co-existing assemblage constrains the conditions and solution composition from which they precipitated. Estimates of activities for dissolved Fe, Mn, PO_4, CO_3 and S in equilibrium with such an assemblage are close to those found in recent anoxic interstitial water–sediment systems. It is important to have detailed knowledge of the composition and stability conditions of these solid precipitates in order to refine stoichiometric models of interstitial nutrient regeneration in anoxic sediments.

INTRODUCTION

THE STOICHIOMETRY of interstitial nutrient regeneration from decomposition of sedimentary organic matter has increasingly taken into account that secondary dissolution, sorption and precipitation reactions actually control the dissolved metabolites and oxidants instead of decomposition reactions based solely on microbial sulfate-, nitrate- and carbonate-reduction models (BALZER, 1978; MURRAY *et al.*, 1978; WHITICAR, 1978; ALLER, 1977; BENDER *et al.*, 1977; BERNER, 1977; HARTMANN *et al.*, 1976; SUESS, 1976a; SHOLKOVITZ, 1973; a.o.).

In environments of slow sedimentation stoichiometric decomposition reactions can be used in a limited way to model nutrient regeneration provided: (1) the actual carbon:nitrogen:phosphorus elemental ratios of the *decomposing organic matter* are known, (2) preferential stripping of phosphorus and nitrogen relative to carbon remains insignificant, and (3) metabolites simply accumulate in the interstitial solutions. In environments of rapid sediment accumulation, however, and those with high rates of input of organic matter, interstitial metabolite concentrations exceed solubilities of certain inorganic equilibria resulting in the formation of authigenic minerals and thus preferential removal of one or several of the dissolved constituents (MARTENS *et al.*, to be published; MURRAY *et al.*, 1978; EMERSON, 1976; SUESS, 1976b; BRICKER and TROUP, 1975; BERNER, 1972; HARTMANN *et al.*, 1973; a.o.). Another mechanism for removal of metabolites is ion-exchange as recently shown for dissolved NH_4^+ in clay-rich anoxic sediments (SUESS and MÜLLER, in prep.).

The wealth of pore water chemical analyses available for the evaluation of such secondary interstitial equilibration reactions is hardly matched by the dearth of information on sedimentary solid phases actually formed as a result of microbial decomposition of organic matter, the iron sulfides and some Mn-Fe-phosphates being here the notable exceptions (EMERSON, 1976; TESSENOW, 1975, 1974; BERNER, 1972; HALLBERG, 1974, 1968). This communication describes the chemical composition, X-ray diffraction results and isotopic characteristics of Fe- and Mn-Ca-carbonates and Mn-sulfides, and of amorphous silica and Mn-Fe-phosphate phases from organic-rich anoxic sediments of the Landsort Deep, north-central Baltic Sea. The solids are believed to be products of bacterial metabolism, their apparent solubilities in seawater await investigation to be used in stoichiometric modelling. The note further illustrates the mode of occurrence, morphology and surface textures of these authigenic precipitates and stresses the usefulness of such *remineralization assemblages* in recognizing terrestrially-influenced marginal sea environments in the ancient sedimentary record and in characterizing interstitial water chemistry at the time of formation.

METHODS

Four types of sediment analyses in various combinations were used to elicit the total solid phase composition of the major portions of distinct laminae of inorganic chemical precipitates found in the sediments of the Landsort Deep:

(1) *Acid-leach* treatment of bulk samples was used to remove and separate from the sediment all mineralization products, i.e. carbonate and phosphate phases. It was later found that manganese sulfide was also readily soluble in diluted HCl. Desalted, ground and dried sediment samples ranging in weight from 500–1000 mg were acidified with 15 ml of 10 vol% HCl at room temperature for ~10 hr. The suspensions were filtered through 0.45 μm membrane filters and repeatedly washed with double-distilled water. The final leach volume was adjusted to 50 ml and aliquo-

priate dilutions used for standard atomic absorption spectroscopy of Mn, Fe, Ca and Mg contents (FÖRSTNER and MÜLLER, 1975; HERMANN, 1975), and soluble PO_4 was determined using the ammonium-molybdic acid method.

In addition sulfur was measured on separate sample splits by automatic titration of SO_3 with potassium-iodate and starch–iodide indicator after oxydative combustion in the LECO-induction furnace; the precision of this procedure was $\pm 0.005\%$ S. Carbonate-CO_2 was measured on separate sample splits by i.r.-absorption of CO_2 evolved by phosphoric acid treatment with a precision of $\pm 0.1\%$ CO_2 (HARTMANN *et al.*, 1976). All results are listed in Table 1.

(2) *Bulk chemical analyses* of indurated, crust-like laminae with a minimum of adjacent sediment were thought to yield compositions of relatively pure mineralization products from microbial decomposition of organic matter. Two types of indurated crust-like laminae were isolated, cleaned of any adherent sediment, repeatedly soaked in double-distilled water and air-dryed. One type was a whitish manganese carbonate crust supported by an amorphous silica framework (Figs. 2, 3b,c) and the other consisted of a number of reddish-brown lense-shaped manganese sulfide concretions (Figs. 2, 4a,b). Four separate pieces each of crust and concretion material, ranging in weights from 14 to 75 mg were analyzed and the results are listed in Tables 4 and 6, respectively.

Mn-carbonate–silica crust. Two pieces of crust (Crust A and B) were first ignited at 800°C without pre-treatment in a muffle furnace for 3 hr and then the oxide residues analyzed for Ca, Mn, Fe and SiO_2 by standard techniques. Two other crust (C and D) were ignited after HCl-treatment and SiO_2 determined on the residue (HERMANN, 1975).

Mn-sulfide concretions. Pre-weighed portions of material were dissolved in 10 vol% HCl in a N_2-atmosphere and the evolving H_2S swept into a reservoir of pre-calibrated iodine solution. The amount of sulfur was calculated to a precision of $\pm 0.2\%$ S from the iodine reduced to iodide. The excess iodine, not consumed in the oxidation of S^{2-} was backtitrated with Na-thiosulfate (JANDER and WENDT, 1958). The remaining HCl extract—purged of H_2S—was used to determine the Mn, Ca and Fe contents. Carbonate-CO_2 was determined on only two of the four concretions (C and D) by passing the evolved gas through acidified iodine solution and on to the i.r.-analyzer as described under (1). The instrument response was calibrated with CO_2 evolved from known amounts of reagent grade calcite which was also passed through an acidified iodine trap.

Since Mn-sulfide is unstable under atmospheric con-

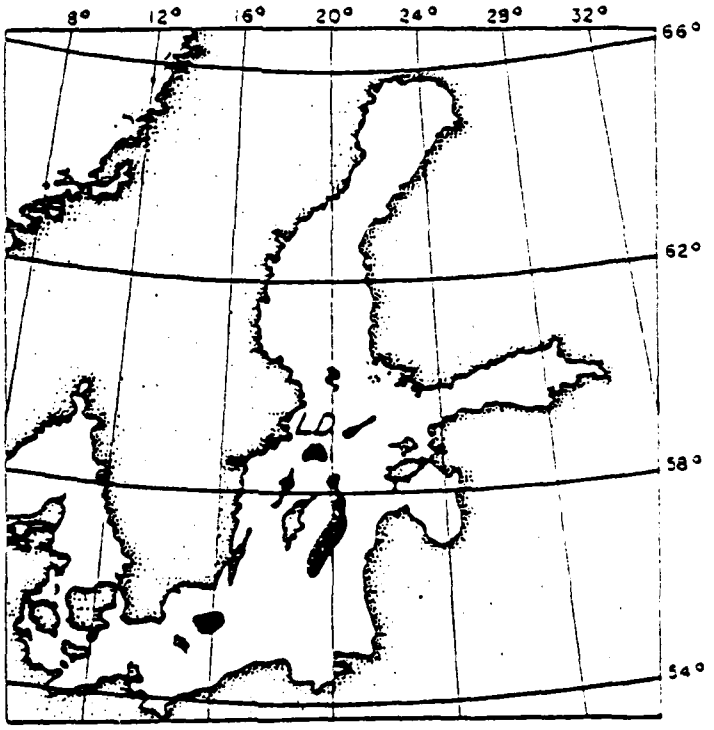

Fig. 1. Baltic Sea; the maximum extent of anoxic bottom water conditions in 1969 according to GRASSHOFF (1975) is shown by the black areas; the Landsort Deep (*LD*; 460 m) is the deepest of these basins.

Fig. 2. Radiograph of laminated sediments from the Landsort Deep; the layers are chemical precipitates from microbial decomposition of organic matter; scale in cm.

Fig. 3. Mixed Mn-carbonate concretions (b,c) within a structural frame of amorphous silica (a,b) from laminated sediments of Landsort Deep; scales = 10 μm. Scanning electron micrographs. V. Reimann, Geol.-Pläontol. Inst., University of Kiel.

Fig. 4. Euhedral MnS crystals from laminated sediment of Landsort Deep; scales = 50 μm. Scanning electron micrographs. V. Reimann.

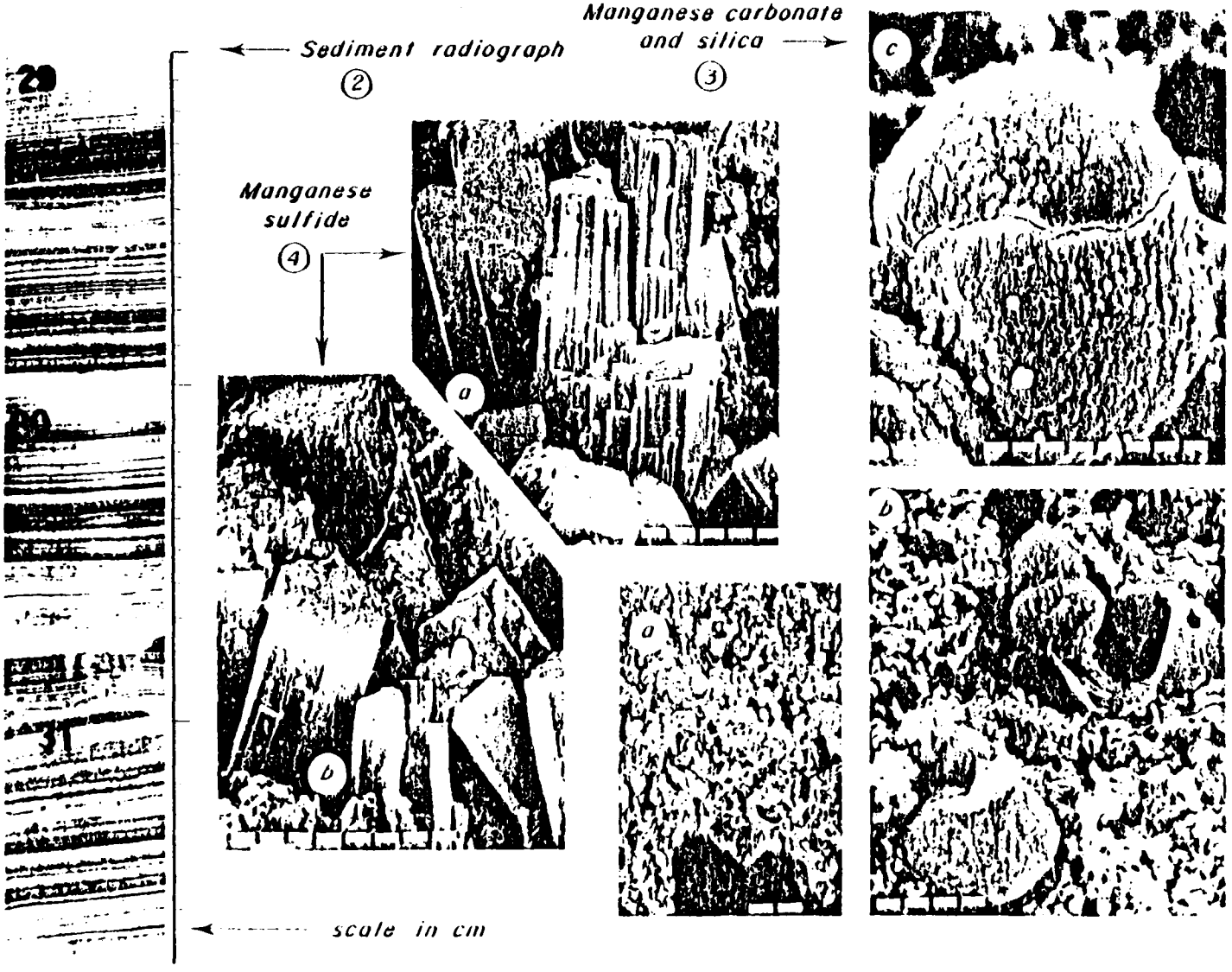
Sediment radiograph
(2)
Manganese carbonate
and silica
(3)
Manganese
sulfide
(4)
a
b
c
a
b
scale in cm

Figs. 2, 3 and 4

ditions, certain concretions had begun to oxidize from the surface inward. The degree of alteration is seen in the difference between Mn and S found in concretions A, B and C. The difference is thought to be due to oxygen and a correction applied assuming MnO_2 as the alteration product. An alteration product in the form of Mn-oxide was later confirmed by simultaneous microprobe analyses for Mn, S and O across the cut surface of a MnS-concretion (Fig. 7).

(3) *X-ray diffraction and microprobe analyses and scanning electronmicroscopy* of hand-picked portions of these laminae were used to support results of bulk chemical analyses. Standard procedures for X-ray diffraction analyses were followed using random powder mounts prepared in aluminum sample holders and scanned at rates of 1.4° 2θ/min under Ni-filtered Cu-K_α radiation. Quartz, present in traces in most samples, and metallic aluminium served as internal standards to check the d-spacings for the carbonate and sulfide phases reported in Tables 2a and 5.

(4) *Fractional leach* treatment of bulk sediments with gradually increasing H^+-ion concentration was used to remove selectively and in sequence carbonate, phosphate and sulfide phases in order to study the individual solid phase compositions—particularly that of phosphates for which no X-ray diffraction pattern was obtained.

For the fractional leach treatment ≈ 100 mg of ground sediment were packed in a 0.5 cm o.d. chromatographic column with a very fine sintered glass disc at the bottom. Dead-space was packed with glass-wool and a reservoir of 25 ml capacity attached to the top of the column. About 15 ml double distilled water were passed through the column at a rate of <0.5 ml/min, and the eludant solution collected in two 5 ml fractions. The remaining 5 ml in the reservoir were mixed with 10 ml of glacial acetic acid and elution continued. After collecting two more fractions the remaining diluted acetic acid was replaced by concentrated acetic acid and three additional fractions collected. Then the procedure was repeated using first diluted and eventually conc. HCl and four more fractions collected. All 11 fractions were separately analyzed for their dissolved Mn, Ca, Fe, Ca and PO_4-contents as was done for the HCl-leach treatment; see (1). The compositions of the individual leach fractions are illustrated in Fig. 3 and the results listed in Table * for Sediment A with the fractions grouped into acetic acid and hydrochloric acid extracts.

AUTHIGENIC CONSTITUENTS IN SEDIMENTS OF THE BALTIC SEA

Metabolic production of CO_2 in oxic environments, particularly in the oceanic water column, forces the carbonate equilibrium towards undersaturation with respect to solid phases leading to dissolution of carbonate minerals (SKIRROW, 1975; KROOPNICK, 1974; a.o.). In the anoxic environments, however, generation of CO_2 leads to increased supersaturation. This is ascribed mainly to the pH-buffering effect by proteolytic formation of hydrogen sulfide, other weak acids and possibly H^+-ion exchange (SUESS, 1976b; GIESKES, 1974; BEN-YAAKOV, 1973; BERNER *et al.*, 1970).

These reactions in the anoxic environment are responsible for the excellent preservation of calcareous microfossils under conditions of SO_4-reduction (BERGER and SOUTAR, 1970) and the authigenic formation of carbonate minerals. One such example is the mixed Mn-Ca-carbonates found in the Baltic Sea basins (DEBYSER, 1961; MANHEIM, 1961; HARTMANN, 1964; VARENTSOV, 1975). Manganese as the major cation—rather than calcium or iron—seems to be characteristic of terrestrially-dominated organic matter input to the Baltic Sea. Predominantly of humic composition, this organic matter supplies upon microbial oxidation large quantities of dissolved manganese to react with the metabolites carbonate, sulfide and phosphate (MANHEIM, 1961; GRIPENBERG, 1934; a.o.).

A sediment core from the Landsort Deep, the deepest of a series of anoxic basins of the Baltic Sea (Fig. 1), contains a sequence of finely laminated sediments (Fig. 2) (SUESS, 1976b; DEBYSER, 1961). The laminations are due to distinct layers of inorganic chemical precipitates of Mn-carbonates, phosphates, silica and sulfides rather than to the annual varves commonly found in Baltic Sea deposits (NILSSON, 1970; KOLP, 1966; MASICKA, 1963; IGNATIUS, 1958; SAURAMO, 1958). The bulk chemical composition of acid leachable portions from eleven of these layers and their total carbonate and sulfur contents are shown in Table 1 and Fig. 5. It is clear from the analytical results that carbonate, containing dominantly Mn, is the most abundant phase. However, regression analyses between various combinations of cations and anions show that the closest cor-

Table 1. Composition of acid-soluble fraction of eleven layers of authigenic precipitates from Landsort Deep sediments; concentrations are in μmol/100 mg and the Σ of ions are in μequiv. 100 mg of dry sediment

Mn^{2+}	Ca^{2+}	ΣFe^{*}	Mg^{2+}	CO_3^{2-}	PO_4^{3-}	S_{total}	S^{2-***}	Σ cation	Σ anion**
109	9.8	31	15.4	155	5.1	60	1	331	445
284	18.3	54	19.4	327	15.3	93	25	751	887
400	22.2	33	25.4	477	22.5	91	-15	962	1173
197	5.9	46	13.8	171	9.3	91	7	525	553
145	2.5	40	12.9	111	12.8	93	40	400	506
262	5.6	55	15.5	230	23.9	106	72	677	744
437	19.2	45	20.8	380	15.2	147	119	1044	1100
100	27.5	47	19.6	407	11.1	37	-12	790	827
554	28.2	37	21.5	516	13.3	237	126	1282	1345
138	13.3	51	16.4	179	6.3	59	49	477	498
125	20.3	58	20.1	346	13.3	92	58	847	915

* $Fe_{total} = Fe^{2+}$

** calculated S^{2-} = Σ cation equiv. − $(CO_3)^{2-}$ equiv. − PO_4^{3-} equiv.

*** $S_{total} = S^{2-}$

relation is obtained between the sum of all cations and the sum of all anions (Fig. 6) rather than between specific cations and anions corresponding to defined compounds.

	Regression analysis between constituents	
(a)	$y = 1.15x - 2.09$ (See Fig. 6)	
	x = Σcations	$r^2 = 0.97$
	y = Σanions assuming S^{2-}	
(b)	$y = 1.018x - 5.42$	
	x = Σcations	$r^2 = 0.95$
	y = Σanions assuming S^-	
(c)	$y = 0.0885x - 7.83$	
	x = Σcations	$r^2 = 0.90$
	$y = \Sigma CO_3^{2-} + PO_4^{3-}$	
(d)	$y = 0.890x - 54.17$	
	x = Σcations	$r^2 = 0.88$
	$y = CO_3^{2-}$	
(e)	$y = 0.940x + 28.95$	
	$x = Mn^{2+}$	$r^2 = 0.86$
	$y = CO_3^{2-}$	

The slight excess in the sum of anions—assuming total sulfur = S^{2-}—is due to the fact that Σcations represent the acid-soluble fraction only and that sulfur represents the total fraction including acid-insoluble S^0 and S^- of the sediment. Accordingly, the actual acid-soluble sulfur fraction is S^{2-} = Σcations − (CO_3^{2-} + PO_4^{3-}). These results are listed in Table 1, column 9 (S^{2-} calculated).

The acid-leach results further indicate that no or insignificant amounts of Mn- and Fe-oxides were present—which generally cause large cation excess—and that an assemblage of carbonates, sulfides and phosphates of varying solid solution compositions is present and the task at hand is to partition the constituents among these co-existing phases.

Carbonates and amorphous silica

Several laminae of the core section consisted of indurated crusts and could be physically isolated for X-ray diffraction and chemical analysis. X-ray diffraction data of the carbonate-rich crusts (Table 2a) reveal the presence of two carbonate mineral phases, one with unit cell dimensions slightly larger than those of pure $MnCO_3$ (rhodochrosite) but considerably smaller than those of $CaCO_3$ (calcite) (GOLDSMITH and GRAF, 1960, 1958), and the other with d-spacings characteristic of $FeCO_3$ (siderite).

Detailed chemical analysis (Table 2b) of hand-picked portions of 'pure' crust material by fractional leaching in diluted acetic acid and hydrochloric acid

Table 2a. X-ray diffraction analysis of carbonate crusts from Landsort Deep sediments; d-spacings in ångström

Manganese carbonate concretions	Relative intensities	Calcite $CaCO_3$	Rhodochrosite $MnCO_3$	Siderite $FeCO_3$	hkl
3.69	20	3.86	3.86	[illegible]	110
2.873	100	3.035	2.84	[illegible]	104
2.407	30	2.495	2.39	2.43*	113
2.19	50	2.285	2.172	2.13**	202
2.035	40	2.095	2.00	1.961	024
1.843	20	1.927	1.829	[illegible]	214
1.784	80	1.913	[illegible]	[illegible]	018
1.546	15	1.587	1.533	1.525	122
1.466	10	1.525	1.452	[illegible]	214
1.436	3	1.518	1.423	[illegible]	028
1.390	5	1.440	1.379	[illegible]	330

Reflections observed for siderite: weak, strong, n.f. = not found. *,** = interference with aluminum and quartz, respectively.

Table 2b. Composition of acid-soluble fraction of carbonate and amorphous silica crusts from Landsort Deep sediments; concentrations in μmol/100 mg of dry sediment

	MnO	CaO	FeO	MgO	P_2O_5	CO_2
Crust A*						
Acetic acid extract	111.7	20.5	3.2	4.8	1.1	n.d.
HCl-extract of residue	1.5	3.8	10.1	1.2	2.2	n.d.
Combined extracts	113.2	21.2	13.3	5.8	3.3	142.0**
Crust B*						
Total HCl-extract	141.3	8.7	14.3	5.3	1.40	142.2
Crust D*						
Total HCl-extract	88.4	4.8	12.3	4.2	1.55	111.3

* Same samples as in Table 4

** $(CO_2)_A = (CO_2, P_2O_5)_{extract\,C,D} - (P_2O_5)_A$.

Table 3. Ranges of stable carbon isotope composition for inorganic and organic carbon species in Baltic Sea water, organisms and sediments; expressed in $\delta^{13}C$ relative to SMOW and PDB, respectively

	Seawater	Benthic organisms and sediments	
	CO_2	Organic carbon	Carbonate carbon
Western Baltic	+1 to +1	+1 to +1	+1 to +1
Central Baltic	+1 to +2	+1 to +1	+1
Sediments			
east. Baltic		+1 to +1	+1 to +1
Landsort Deep		+1 to +1	+1 to +1

Data compiled from ERLENKEUSER *et al.* (1975) ERLENKEUSER and WILLKOMM (1975) and SUESS and ERLENKEUSER (1975).

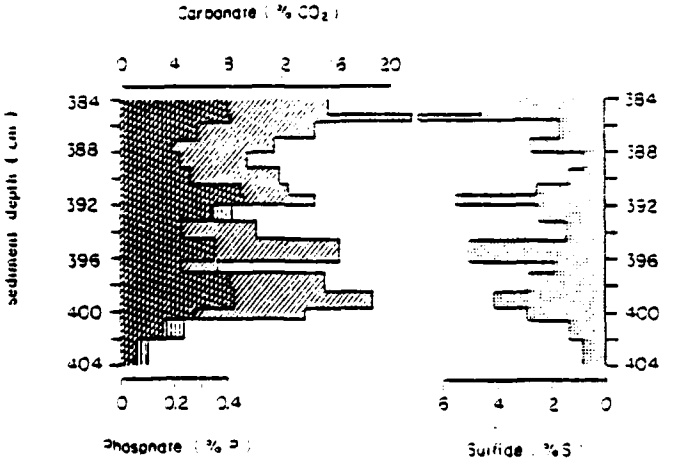

Fig. 5. Depth distribution of carbonates, sulfides and phosphates in section of laminated core; scales in wt% of dry sediment.

confirmed the X-ray diffraction analysis in that a mixed Mn-Ca-Mg-carbonate mineral phase was present and revealed in addition that Fe is contained in a separate mineral phase.

Evidence for $FeCO_3$ and $(MnCaMg)CO_3$ as separate phases from chemical evidence is seen in the fact that the total soluble cation contents of Crusts C and D are perfectly balanced by their total anions: i.e. Crust C cations = 298 meq/100 mg and anions = 295 meq/100 mg. Crust D cations = 225 meq/100 mg and anions = 229 meq/100 mg and that Fe is contained exclusively in the HCl-extract as indicated by Crust A. Furthermore, the CO_3/PO_4 equivalent ratios for Crusts C and D ranged between 42 and 43, assuming the same for Crust A yields a CO_2 content of 142 mmol/100 mg. This amount of CO_2 exceeds the equivalent sum of Mn + Ca + Mg-PO_4 in the acetic acid extract: i.e. 284 meq/CO_3^{2-} and 270 meq cations. The excess of 14 meq CO_3^{2-} 100 mg, however, cannot be accounted for by the equivalent sum of cations in the HCl-extract unless soluble Fe is included thus substantiating the presence of $FeCO_3$. Since Fe was not extracted by diluted acetic acid but was extracted by HCL $FeCO_3$ must be separate from the $(MnCaMg)CO_3$ phase.

The mixed carbonate phase has the approximate composition: $(Mn_{0.85}Ca_{0.10}Mg_{0.05})CO_3$ as will be shown later by a normative calculation of all phases found in the laminated sediments. Isotopic analysis of the mixed Mn-carbonates showed quite a strong depletion in ^{13}C with values of $\delta^{13}C = -13‰$. This isotopic ratio further attests to the biogenic origin of the Mn-carbonate phase. Table 3 summarizes stable C-isotope ratios for water, biogenic carbonates and organic matter for the Baltic Sea environment suggesting that about 50% of the carbonate might have originated from organic matter and the remainder from inorganic bicarbonate of the Baltic Sea bottom water to account for the observed $\delta^{13}C$ values (SUESS, 1976b; ERLENKEUSER *et al.*, 1975). ROBERTS and WHELAN (1975) and HATHAWAY and DEGENS (1969) also report finds of isotopically light carbonates as the result of microbially produced CO_2.

One dominant mode of occurrence of the mixed Mn-carbonates from the Landsort Deep sediments is in spherical micro-concretions throughout a structural frame of amorphous silica as illustrated in Figs. 3b,c. The concretions ranged in size from 5–25 μm in diameter; in most cases they formed clusters of coalescing spheres. Their surface texture

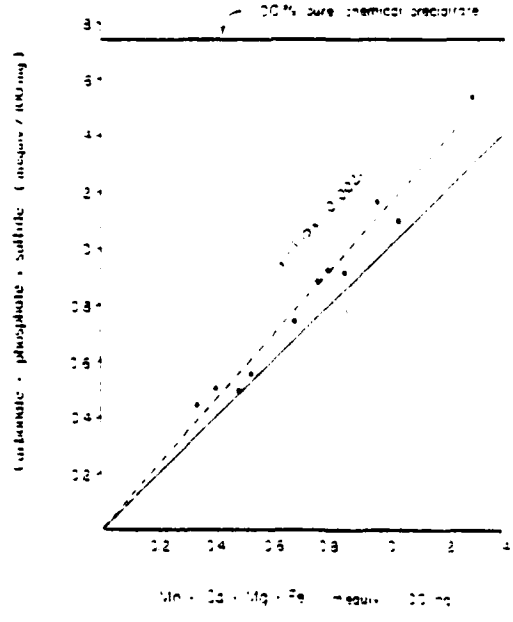

Fig. 6. The sum of HCl-soluble cations and combined equivalent sum of carbonate-, phosphate-, and sulfide anions of eleven selected layers from laminated core section.

Table 4. Composition of carbonate and amorphous silica crusts from Landsort Deep sediments: these samples are free of sulfur and sulfides; concentrations in wt%

	Crust A	Crust B	Crust C	Crust D
weight loss after HCl-leach	--	--	28.1	32.1
ignition at 800°C	21.8	27.4	11.5	7.2
SiO_2	74.5	68.9	58.1	59.7
			100.1	100.1
MnO_2	9.4	7.5		
CaO	2.3	1.3		
MgO	n.d.	n.d.		
Fe_2O_3	n.d.	1.3		
P_2O_5	n.d.	n.d.		
	98.0	99.8		

appeared quite like that of calcified bacterial colonies variously reported from anoxic environments and certain microbiological experiments (MORITA *et al.*, 1975; SUESS and FÜTTERER, 1972; OPPENHEIMER, 1961; LALOU, 1957).

The structural frame of amorphous silica (Fig. 3a) had no recognizable biogenic features, had a spongy appearance providing pore space for the formation of the mixed Mn-carbonate phases, and was restricted to single friable layers of < 1 mm in thickness throughout the core section. X-ray diffraction and chemical analyses (Table 4) confirmed that no other phase was present within the layer and that it consisted of 95% of SiO_2 and of 5% of H_2O expelled at 300°C. I believe that the amorphous silica layers are chemical precipitates of remobilized biogenic silica in close connection with decomposition of organic matter and thus constitute part of a characteristic remineralization assemblage along with the carbonates, phosphates and sulfides. From extensive studies by others of dissolved interstitial water nutrient constituents and silica dissolution experiments it appears that silica is remobilized at constant proportions relative to the other remineralization constituents, so as to indicate simultaneous dissolution of biogenous siliceous tests and oxidation of organic matter (MURRAY *et al.*, 1978; STEIN, 1977; SUESS, 1976b). In the absence of silica uptake by degraded clay minerals or flux to the overlying bottom waters, this excess of dissolved biogenous silica may well precipitate as a precursor for incipient chert formation.

Mn-*sulfide*

High dissolved Mn^{++} concentrations in anoxic bottom waters and pore waters (up to 3.10^{-5} M) are typical for Baltic Sea basins (BALZER, 1978; DIAFARI, 1976). Upon mineralization of sedimentary organic matter by SO_4-reduction, the H_2S produced as a metabolite may therefore precipitate MnS in this environment, rather than Fe-sulfides as is usually the case under anoxic marine conditions. ALLER (1977) and BALZER (1978) have compared ion concentration products of the appropriate dissolved species with solubility products of various phases of manganese sulfides and carbonates. They concluded that the interstitial waters of Long Island Sound and Baltic Sea sediments, respectively, are in equilibrium with respect to such phases and that precipitation of MnS may well exert some influence on the dissolved interstitial water species of these environments. BARON and DEBYSER (1957) and DEBYSER (1961) first discovered sedimentary MnS in the anoxic deposits of the Baltic Sea. MnS as the cubic mineral alabandite is otherwise only known from hydrothermal deposits (PALACHE *et al.*, 1952) and corresponds in its crystal structure to one of two synthetic high-temperature MnS-modifications described by SCHNAASE (1933). The sedimentary MnS-phase, however, found by BARON and DEBYSER (1957), and described here, has a hexagonal crystal structure (Table 5) and corresponds to SCHNAASE's (1933) low temperature MnS precipitate, a modification which he called β-MnS (wurtzite). In the newer terminology as used by ASTM, Schnaase's β-MnS (wurtzite) is identical to the γ-MnS modification. It is clear from the work of Baron and Debyser and the findings reported here that γ-MnS, a manganese sulfide of hexagonal crystal structure, is the first—and so far only—occurrence of a distinct sedimentary manganese sulfide mineral of authigenic nature (GLASBY, 1977; CALVERT and PRICE, 1977).

Its dominant modes of occurrence are in single crystals or clusters of euhedral crystals (Figs. 4a,b)

Table 5. X-ray diffraction analysis of manganese sulfide concretions from Landsort Deep sediments: d-spacings in ångström

MnS Concretion Landsort Deep	Relative Intensities	Baron & Debyser, 1957	γ-MnS Hexagonal Schnaase, 1933	hkil
3.44	100	3.43	3.45	1010
3.21	60	3.21	3.24	0002
3.038	40	3.03	3.06	1011
2.355	10	2.352	2.36	1012
1.992	50	1.992	1.99	1120
1.830	20	1.82	1.83	1013
1.721	5	1.725	1.72	2020
1.695	20	1.69	1.7	1122
1.561	5	1.566	1.57	2021
1.337	5	1.32	1.32	2022
n.d.	--	1.45	1.45	1300
1.342	5	1.344	1.35	2023
1.302	5	n.d.	1.30	2130
1.274	5	n.d.	1.28	2131
1.205	5	1.204	1.21	2132, 1015

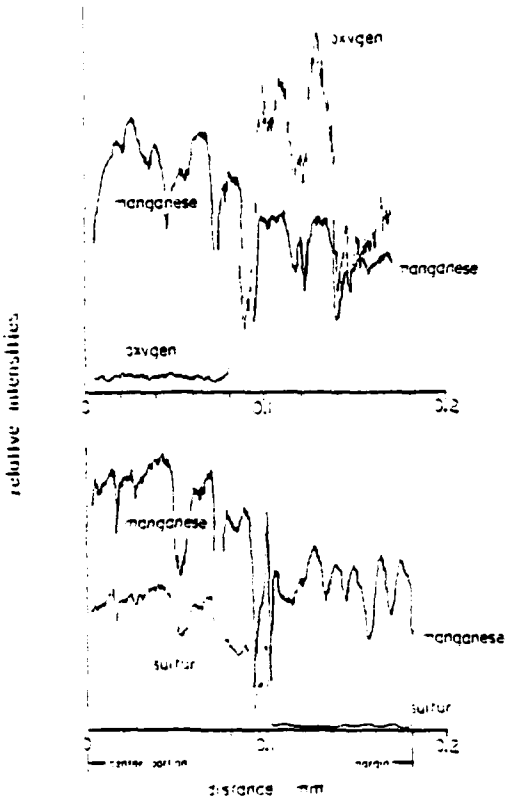

Fig. 7. Microprobe line scans of Mn-K_α, O-K_α, and S-K_α intensities across the cut surface of a MnS-concretion; the center portion shows pure MnS whereas oxidation products due to laboratory handling, most likely MnO_2, cover the surface (see also chem. analyses in Table 6). Microprobe analysis: D. Ackermann, Min-Petrogr. Inst., University of Kiel.

and in dense lenses resembling boudinage structures. The accurate chemical composition is difficult to determine owing to the apparent instability of MnS at laboratory conditions and to its ubiquitous association with other Mn-mineral phases. A microprobe linescan from the margin to the center of a lense-shaped concretion shows the association of Mn with oxygen in the outer portion, assumed to be due to MnO_2 by oxidation during laboratory handling, and of Mn and sulfur in the center portion (Fig. 7). This is also reflected in the bulk chemical analyses of four concretions detailed in Table 6. The excess of Mn, not bound by sulfur, is assumed to be present in the alteration product MnO_2. The wt%, of oxygen thus calculated adds to almost 100% of the total weight of the samples, particularly so with Concretion B. Furthermore, Concretion D required almost no oxygen correction because its soluble portion consisted to >98% of MnS and had presumably undergone negligible alteration. The insoluble fractions are clay impurities; none of the trace constituents Ca or Fe are believed to be in the MnS-structure but are probably leached from the clay and carbonate impurities. It is very likely that authigenic MnS-formation (γ-MnS) is indicative of terrestrially dominated, marine environments undergoing extensive mineralization of humic organic matter by microbial SO_4-reduction.

Phosphates

The solid products of remineralization of organic phosphorous are more difficult to identify than those just discussed. BALZER (1978), MURRAY *et al.* (1978), ALLER (1977), EMERSON (1976) and BRICKER and TROUP (1975) have shown from equilibrium considerations of interstitial water data that remineralization of organic matter in Fe-dominated sediments tends to produce Fe-carbonates and Fe-phosphates. Bricker and Troup present rather tenuous evidence from X-ray diffraction analysis that vivianite is actually present as an authigenic phase in Chesapeake Bay sediments. It appears from their findings that vivianite is extremely unstable and its X-ray diffraction pattern disappears within minutes after exposing the sample to atmospheric oxygen. This is contrary to other reports of Fe^{II}-phosphates in sediments and in experimental precipitates which show well crystallized vivianite to be quite stable (TESSENOW, 1975; ROSENQUIST, 1970; GULBRANDSEN, 1969). Yet the phosphorus-rich samples retrieved from the Landsort Deep contained no recognizable crystalline phosphate phases although total PO_4 contents were as high as 10 wt%. Table 7 shows the acid-leachable composition of three splits from one sediment sample high

Table 6. Bulk composition of manganese sulfide concretions from Landsort Deep sediments; concentrations in wt%(a) and mol%(b)

	Concr. A		Concr. B		Concr. C		Concr. D	
	a	b	a	b	a	b	a	b
Manganese	53.2	0.969	55.7	1.014	50.5	0.919	53.9	0.981
Sulfur	16.2	0.504	17.8	0.420	14.6	0.457	20.9	0.364
Difference		0.465		0.584		0.462		0.017*
Difference as Oxygen	14.9	0.930	18.7	1.168	14.8	0.924	0.5	0.034
Calcium	0.1	--	0.1	--	0.1	--	0.4	--
Iron	0.8	--	0.8	--	0.8	--	0.5	--
Carbonate	n.d.	--	n.d.	--	1.9	--	0.6	--
Insoluble	12.4	--	12.1	--	11.3	--	7.5	--
	98.6		99.2		95.6		94.5	

* Minimal oxygen correction for HCl-soluble portion because this sample is the least affected by laboratory alteration (>98% MnS).

Table 7. Composition of leachable fractions of bulk sediments containing mixed carbonates and phosphates: concentrations in μmol/100 mg of dry sediment

	MnO	CaO	FeO	MgO	P_2O_5	CO_2*
Sediment A						
Acetic acid extract	125.2	31.4	13.9	7.4	15.9	93.8
HCl-extract of residue	20.1	5.9	19.2	24.7	12.2	94.8
Combined extract	145.3	37.3	33.2	32.1	27.9	112.2
Sediment B						
Total HCl-extract	144.2	24.7	37.3	7.5	28.2	(112.2)
Sediment C						
Total HCl-extract	144.7	2.5	38.8	12.9	32.8	(112.2)

* All three samples are homogenized splits. CO_2 was determined on a fourth split and is assumed to be the same for samples A–C. samples B and C were extracted with dil. HCl, whereas A was subjected to fractional leach (Fig. 3).

in mixed carbonates, sulfides and soluble phosphates from the anoxic deposits of the Landsort Deep. X-ray diffraction analysis confirmed the presence of $(MnCaMg)CO_3$ and MnS as encountered in the crusts and concretions, respectively. It is evident from the leachable constituents that in addition to these phases also Mn-Fe-phosphates were present in the sediments.

To further detail the composition of the X-ray amorphous phosphate phase(s) a fractional leach with increasing H^+-ion concentrations and continuous monitoring of the eluded fractions was performed. The rather complex elution pattern (Fig. 3) indicates that:

(1) the Mn-Ca-Mg-carbonate phase—described earlier—is leached first (A) along with an

(2) unknown phosphate compound (I);

(3) the trailing of the Fe-maximum (B) attests to the separate Fe-carbonate phase being dissolved at slightly different pH-conditions just as encountered in the fractional leaches of crusts.

The following complex elution pattern results from:

(4) the dissolution of Mn-sulfide (C)—as described for the concretions;

(5) a second unknown phosphate compound (II); and

(6) finally the increased mobility of Fe and Mg (D) at very low pH-values signaling the destruction of aluminosilicates.

The dissolution of the mixed carbonate phase (A) was accompanied by vigorous evolution of CO_2 upon addition of acetic acid, whereas subsequent dissolution of Mn-sulfide (C) by dil. HCl was clearly recognized by the evolution of H_2S. To judge from the shoulders of the Fe- and Ca-peaks near (C) it is quite likely that these two cations are contained in the second unknown phosphate compound (II).

This qualitative interpretation of the elution pattern is in agreement with the results of the sequential dissolution of the mixed carbonate crusts discussed earlier (Table 2b) in that Fe-release is close with but clearly separate from Mn-Ca-Mg-release and thus argues strongly in favor of a separate Fe-phase. The

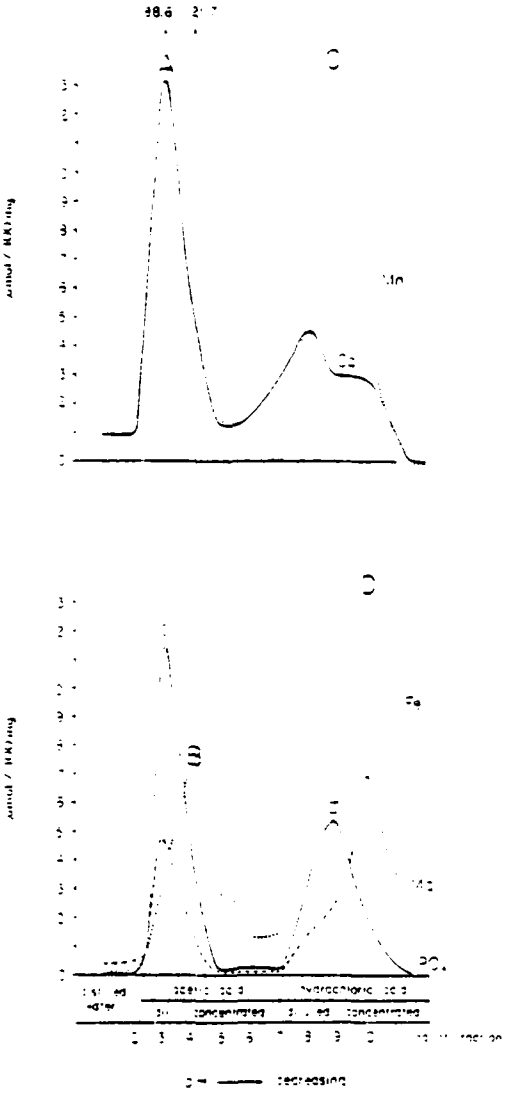

Fig. 3. Sequential leach pattern of soluble cations and phosphates from bulk sample of laminated sediments. eleven fractions were collected and separately analyzed while the leach solution gradually changed from distilled water to diluted to concentrated acetic acid and further to diluted and concentrated hydrochloric acid. The sum of the leached constituents is listed in Table 7. Sediment A, elution peaks A, B, C, D are explained in the text as well as phosphate elution peaks I and II.

combined HCl-extracts of the carbonate crusts further showed that the

$$\Sigma\text{cation-equiv.} - PO_4\text{-equiv.} = CO_3\text{-equiv.},$$

thus indicating that Fe soluble in concentrated acetic acid is contained in $FeCO_3$.

The amount of $CaCO_3$ in the mixed carbonate phase varies between 3 and 24%, and thus appears to be the only source of uncertainty in evaluating the composition and amounts of all phases present

Table 3. Balance of acid-leachable sediment constituents contained in solid phases as mineralization products.

	Mn	Ca	Fe	Mg	PO_4	CO_2	S	Products
Initial leach composition								
Acetic acid, 1 h, and conc.	1.5	21	14	8	1.6	134	0	--
HCl-leach, diluted	30	0	26	0	2.2	0	40	--
Step I								
Remove all acetic-acid-	1.5	21	0	8	1.6	120	0	14 $FeCO_3$
soluble as iron carbonate	30	0	26	0	2.2	0	40	--
Step II								
Remove all CO_2 as	24	0	0	0	1.6	0	0	120 $Mn_{0.8}Ca_{0.4}Mg_{0.8}CO_3$
mixed carbonate	30	0	26	0	2.2	0	40	--
Step III								
Remove all acetic acid solu-	0	0	0	0	0	0	0	8 $Mn_3(PO_4)_2$
ble PO_4 and remaining Mn	30	0	26	0	2.2	0	40	--
Step IV								
Remove all HCl-soluble Mn	0	0	0	0	0	0	0	--
and some Fe as sulfides	0	0	26	0	2.2	0	0	13 FeS_2 + 30 MnS
Step V								
Remove all remaining ions	0	0	0	0	0	0	0	--
as a mixed orthophosphate	0	0	0	0	0	0	0	3 $Fe_{1.6}Ca_{1.4}(PO_4)_2$

TOTAL PHASE COMPOSITION AND IMPLICATIONS ON SOLUTION CHARACTERISTICS

In order to elucidate the composition of the unknown phosphate phases all fractional leach results from carbonate crusts as well as sediment splits are here combined to provide the basis for a quasi-normative calculation of the unknown phases. Accordingly, these results, where the partitioning of ions between acetic acid soluble and hydrochloric acid soluble phases is crucial, are idealized to conform to the following constraints (Table 3):

(1) Σsoluble cations = Σsoluble anions: this requires a quantity of soluble S^{2-} of 40 μmol/100 mg of sediment (Table 1);

(2) Σacetic acid soluble cations − acetic acid soluble phosphate = Σcarbonate ions: this difference amounts to 134 μmol CO_2/100 mg sediment (Table 2b);

(3) The amount of acetic acid-soluble Ca is fixed at 21 μmol/100 mg sediment, this being the maximum quantity encountered from all analyses (Sediment A, Table 7);

(4) All Fe soluble in concentrated acetic acid is contained in $FeCO_3$; this is supported by the continuous elution pattern (Fig. 3) and by results of Tables 2b and 7; this quantity amounts to 14 μmol/100 mg sediment;

(5) Mn-sulfide is a pure phase with no isomorphic substitution and is soluble only in dil. HCl, thus all HCl-soluble Mn is contained in MnS, this amount is here 30 μmol/100 mg sediment (Table 3); and

(6) Mg and Fe released from breakdown of aluminosilicates can be estimated from the elution peaks at low pH values (Fig. 3); for Fe this amount is 14 μmol/100 mg and for Mg is 7 μmol/100 mg; this then explains the differences in Fe and Mg soluble in concentrated and diluted HCl, respectively (Table 7, Sediment A vs Sediment B, C).

Within these constraints it is possible to calculate the compositions and contents of each phase of the remineralization assemblage as detailed in Table 3. Added to the phases thus calculated should be an amount of amorphous silica of as high as 300 μmol/100 mg to complete the assemblage. This quantity however, seems highly variable and is only vaguely related to the phosphates, sulfides and carbonates.

It was intended to draw attention to the compositional variability of authigenic phases actually formed during decomposition of sedimentary organic matter in order to refine equilibrium models currently in use describing interstitial nutrient regeneration. In the following considerations it will be emphasized how valuable it would be to have thermodynamic quantities or at least accurate *apparent solubilities* in seawater for these phases since they so closely control the interstitial water composition. Assuming the phases to be co-existent, i.e. to be in equilibrium with the interstitial solution composition, the following set of conditions must all be met:

$$(Mn)^3(PO_4)^2 = K_1^*;\ K_1^* = 10^{-23.2}$$

TESSENOW (1974) (1)

$$(Fe)(CO_3) = K_2^*;\ K_2^* = 10^{-9.9}$$

MURRAY *et al.* (1978) (2)

$$(Mn^{2+})(CO_3) = K_3^*;\ \text{see (12)} \quad (3)$$

$$(Fe)(S) = K_4^*;\ K_4^* = 10^{-15.7}$$

BERNER (1967) (4)

$$(Mn)(S) = K_5^*;\ K_5^* = 10^{-14.9}$$

ALLER (1977) (5)

$$(Fe^{2+})^3(PO_4)^2 = K_6^*;\ \text{see (12)} \quad (6)$$

$$a(OH)\,a(H) = K_{AP}^* = 10^{-14.00} \quad (7)$$

$$(PO_4) = \frac{\Sigma\text{phosphate}}{1 + \dfrac{a_H}{K_{PO_4}^*} + \dfrac{a_H^2}{K_{HPO_4}^* K_{PO_4}^*} + \dfrac{a_H^3}{K_{H_2PO_4}^* K_{HPO_4}^* K_{PO_4}^*}} \quad (8)$$

AD-A099 518 OREGON STATE UNIV CORVALLIS SCHOOL OF OCEANOGRAPHY F/G 8/10
COMPILATION OF REPRINTS NUMBER 57,(U)
JAN 81 R W SPINRAD, J R ZANEVELD, H PAK N00014-76-C-0067
UNCLASSIFIED REF-79-4 NL

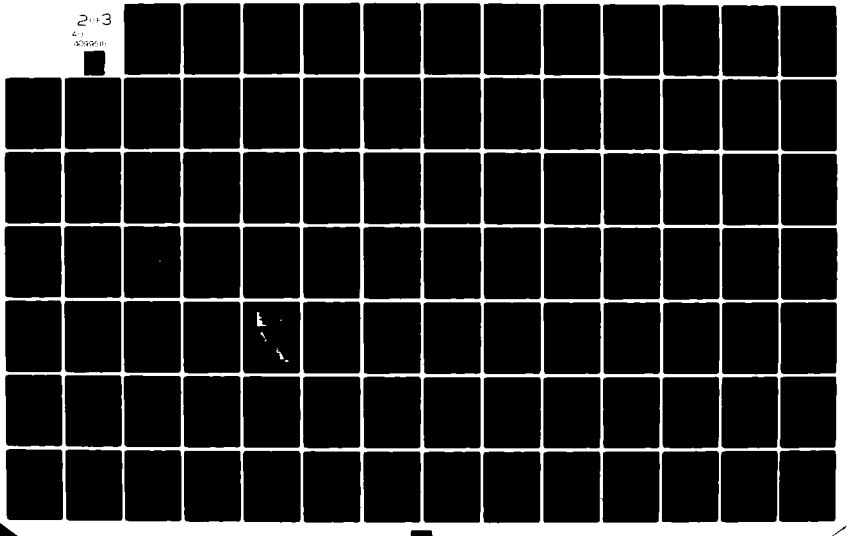

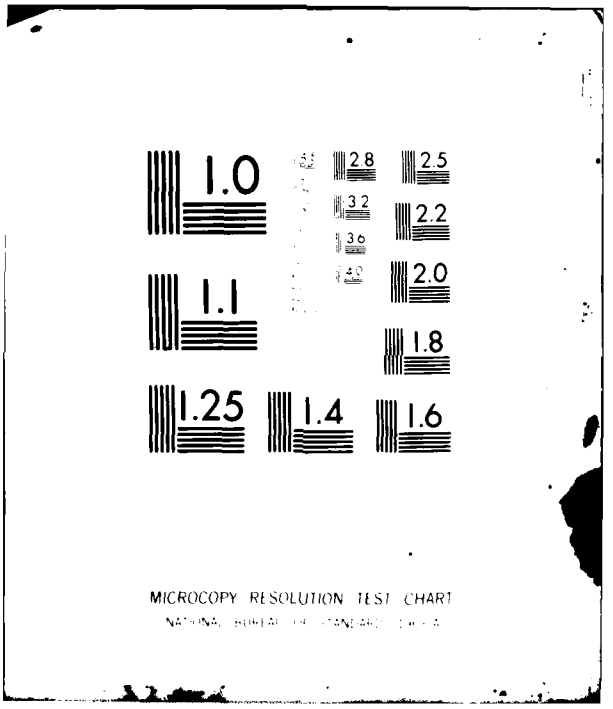
1.0
2.8
2.5
3.2
2.2
3.6
4.0
2.0
1.1
1.8
1.25
1.4
1.6
MICROCOPY RESOLUTION TEST CHART

$$(CO_3) = C.A. \cdot \frac{K'_{CO_3} a_H}{1 - 2K'_{CO_3} a_H} \quad (9)$$

$$(S) = \Sigma H_2S \frac{K'_1 \cdot K'_{HS}}{a_H^2 - (K'_{HS} \cdot a_H)} \quad (10)$$

K' = apparent solubility products
K^0 = thermodynamic solubility product
* = Ca-substitution
( ) = concentrations, mole/l
a( ) = activities

where:

(a) K'_1 to K'_9 are the apparent solubility products of the co-existing mineral phases in seawater:

(b) K'_3 and K'_8 both refer to the apparent solubility products of phases with mixed activities of components of a solid solution: i.e. $(Mn_{0.30}Ca_{0.15}Mg_{0.05})CO_3$ and $(Fe_{0.86}Ca_{0.14})_3(PO_4)_2$ respectively;

(c) none of these K'-values is accurately known;

(d) Σphosphate = total dissolved phosphate and $K'_{H_3PO_4}$, K'_{HPO_4}, K'_{PO_4} are the apparent dissociation constants of phosphoric acid in seawater; according to ATLAS (1975) for 33‰ S and 10°C:

$$K'_{H_3PO_4} = 1.95 \cdot 10^{-2}$$
$$K'_{HPO_4} = 7.82 \cdot 10^{-7}$$
$$K'_{PO_4} = 1.00 \cdot 10^{-9};$$

(e) C.A. = carbonate alkalinity and K'_{HCO_3} and K'_{CO_3} are the apparent dissociation constants of carbonic acid in seawater; according to MEHRBACH *et al.* (1973) for 35‰ S and 25°C:

$$K'_{HCO_3} = 1.07 \cdot 10^{-6}$$
$$K'_{CO_3} = 7.94 \cdot 10^{-10}; \text{ and}$$

(f) ΣH_2S = total dissolved hydrogen sulfide and K'_{HS} and K'_1 the apparent dissociation constants of hydrogen sulfide in seawater; according to SKOPTINSEV (1957) as cited in BALZER (1978):

$$pK'_{HS} = 7.04 - 0.4 \cdot \mu^{1/2}$$
$$pK'_1 = 14.92 - 1.2 \cdot \mu^{1/2}$$
$$\mu = \text{ionic strength.}$$

Simultaneous analytical solution of the above system of equations is difficult because they are not completely independent of each other, nor is a sufficient number of constants accurately known, yet a numerical estimation of ion activities by fixing one of the five unknown constituents and utilizing the thermodynamic solubilities as shown for eqns. (1), (2), (4) and (5) yields a set of activities for all dissolved constituents which quite closely resemble those encountered in natural interstitial water systems. In the case of the Landsort Deep sediments interstitial total dissolved Fe was determined by DEBYSER (1961) and found to be $(Fe_T) = 10^{-4.02}$ moles/l for the core section enriched in chemical precipitates. With the recent activity coefficient estimates for dissolved Fe^{++} by MURRAY *et al.* (1979), the following activities are obtained for the above multiple equilibrium system:

$$(Fe_T) \cdot \gamma_{Fe^{++}} =$$
$$a(Fe) = 10^{-4.02} \cdot 10^{-1.52} = 10^{-5.54}$$
$$a(S) = 10^{-10.14} \text{ from eqn. (4)}$$
$$a(CO_3) = 10^{-4.36} \text{ from eqn. (2)}$$
$$a(Mn) = 10^{-4.62} \text{ from eqn. (5) and } a(S)$$
$$a(PO_4) = 10^{-8.05} \text{ from eqn. (1) and } a(Mn). \quad (11)$$

Furthermore, re-substituting these activities into eqns. (3) and (6) yields thermodynamic end-member activity products for the mixed carbonate and phosphate phases:

$$a(Mn^*)a(CO_3) = 10^{-9.99} = K'^0_3$$
$$a(Fe^*)^3 a(PO_4)^2 = 10^{-33.92} = K'^0_8 \quad (12)$$

* Ca-substitution.

In the case of the mixed Mn-Ca-Mg-carbonate the ion activity product is higher than that of pure Mn-carbonate and in the case of the mixed Fe-Ca-phosphate it is lower than that of pure $Fe_3(PO_4)_2$. Both trends are expected when considering the degree of Ca-substitution and the solubility products of the respective pure Ca-phases (TESSENOW, 1974; ROBERSON, 1966; GARRELS and CHRIST, 1965). If these intermediate solubility products are confirmed experimentally it would have far-reaching implications in that the solution composition in such a system could control the mixed solid composition rather than the other way around.

In the particular case of the Landsort Deep the authigenic phases constitute such a large percentage of the sediment that they can hardly be considered precipitates of a limited amount of pore water solutes in a quasi-closed system but rather as having formed under continuous supply of dissolved solutes. A similar view was recently expressed by COOKE (1977) in a different connection by explaining the varying $MgCO_3$-composition of calcite surfaces in response to experimentally imposed Mg-concentration changes in the reacting seawater solution. In the interstitial water–solid sediment system the composition of the precipitated mixed phases then may be looked upon as accommodating a certain solution composition rather than controlling it.

Acknowledgements—Initial work for this research was begun at the University of Kiel and was later expanded at Oregon State University under support from the Office of Naval Research grant N00014-76-C-0067 to study remineralization processes of sedimentary organic matter. At both institutions I owe thanks to colleagues and technical assistants: in particular I wish to thank M. HARTMANN (Kiel) and P. MÜLLER (Kiel) for fruitful discussions and G. DAVIS (Corvallis), H. MÖLLER (Kiel) and C. UNGERER (Corvallis) for valuable assistance.

REFERENCES

ALLER R. C. (1977) The influence of macrobenthos on chemical diagenesis in marine sediments. Unpublished Ph.D. dissertation, Yale University, New Haven, CN.

ATLAS E. L. (1976) Phosphate equilibria in seawater and interstitial waters. Ph.D. dissertation, Oregon State University, Corvallis.

Balzer W. (1978) Untersuchungen über Abbau organischer Materie und Nährstoff-Freisetzung am Boden der Kieler Bucht beim Übergang vom oxischen zum anoxischen Milieu. Ph.D. dissertation, Kiel University.

Baron G. and Debyser J. (1957) Sur la presence dans des vases organiques de la mer Baltique de sulfure manganeux β-hexagonal. *C.R. Acad. Sci. Francais* **245**, 1148–1150.

Bender M. L., Fanning K. A., Froelich P. N., Heath G. R. and Maynard V. (1977) Interstitial nitrate profiles and oxidation of sedimentary organic matter in the eastern Equatorial Atlantic. *Science* **198**, 605–608.

Ben-Yaakov S. (1973) pH buffering of pore water of recent anoxic marine sediments. *Limnol. Oceanogr.* **18**, 86–94.

Berger W. H. and Soutar A. (1970) Preservation of plankton shells in an anaerobic basin off California. *Geol. Soc. Am., Bull.* **81**, 275–282.

Berner R. A. (1967) Thermodynamic stability of sedimentary iron sulfides. *Am. J. Science* **265**, 773–785.

Berner R. A. (1972) *Sulfate reduction, pyrite formation, and the oceanic sulfur budget.* In *The Changing Chemistry of the Oceans* (eds. D. Dyrssen and D. Jagner), pp. 347–361. Nobel Symposium 20. Almqvist and Wiksell, Stockholm.

Berner R. A. (1977) Stoichiometric models for nutrient regeneration in anoxic sediments. *Limnol. Oceanogr.* **22**, 781–786.

Berner R. A., Scott M. R. and Thomlinson C. (1970) Carbonate alkalinity in the pore waters of anoxic marine sediments. *Limnol. Oceanogr.* **15**, 544–549.

Bricker O. P., III and Troup B. N. (1975) Sediment–water exchange in Chesapeake Bay. In *Estuarine Research* (ed. L. E. Cronin), Vol. 1, pp. 3–27. Academic Press.

Calvert S. E. and Price N. B. (1977) Shallow water, continental margin and lacustrine nodules: distribution and geochemistry. In *Marine Manganese Deposits* (ed. G. P. Glasby), pp. 45–86. Elsevier.

Cooke R. C. (1977) Factors regulating the composition, change and stability of phases in the calcite–seawater system. *Mar. Chem.* **5**, 75–92.

Debyser J. (1961) Contribution à l'étude geochimique des vases marine. These soutenue devant la Faculte des Sciences de Paris le 6 avril 1959. *Inst. Francais du Petrole, Ref.*, 6005, 1–249. Edit. Technip., Paris.

Djafari D. (1976) Mangan-Eisenakkumulate in der Kieler Bucht. Ph.D. Dissertation, University of Kiel.

Emerson S. (1976) Early diagenesis in anaerobic lake sediments: chemical equilibria in interstitial waters. *Geochim. Cosmochim. Acta* **40**, 925–934.

Erlenkeuser H., Metzner H. and Willkomm H. (1975) University of Kiel radiocarbon measurements—VIII. *Radiocarbon* **17**, 276–300.

Erlenkeuser H. and Willkomm H. (1973) University of Kiel radiocarbon measurements—VII. *Radiocarbon* **15**, 113–126.

Förstner U. and Müller G. (1974) *Schwermetalle in Flüssen und Seen.* Springer.

Garrels R. M. and Christ Ch. L. (1965) *Solution, Minerals and Equilibria.* Harper & Row.

Gieskes J. M. (1974) The alkalinity–total carbon dioxide system in sea-water. In *The Sea* (ed. E. D. Goldberg), *Marine Chemistry*, Vol. 5, pp. 123–151.

Glasby G. P. (ed.) (1977) *Marine Manganese Deposits.* Elsevier.

Goldsmith J. R. and Graf D. L. (1958) Relation between lattice constants and composition of the Ca–Mg-carbonates. *Am. Mineralogist* **43**, 84–101.

Goldsmith J. R. and Graf D. L. (1960) Subsolidus relations in the system $CaCO_3$–$MgCO_3$–$MnCO_3$. *J. Geol.* **68**, 324–335.

Grasshoff K. (1975) The hydrochemistry of landlocked basins and fjords. In *Chemical Oceanography* (eds. J. P. Riley and G. Skirrow), Vol. 2, pp. 456–598. Academic Press.

Gripenberg S. (1934) A study of the sediments of the North Baltic and adjoining seas. *Fennia* **60**, 1–231.

Gulbrandsen R. A. (1969) Physical and chemical factors in the formation of marine apatite. *Econ. Geol.* **64**, 356–383.

Hallberg R. O. (1968) Some factors of significance in the formation of sedimentary metal sulphides. *Stockholm Contrib. Geol.* **15**, 39–66.

Hallberg R. O. (1974) Metal distribution along a profile of an intertidal area. *Est. Coastal Mar. Sci.* **2**, 153–170.

Hartmann M. (1964) Zur Geochemie von Mangan und Eisen in der Ostsee. *Meyniana* **14**, 3–20.

Hartmann M., Müller P., Suess E. and van der Weijden C. H. (1973) Oxidation of organic matter in recent marine sediments. "*Meteor*" *Forschungsergeb. Reihe C* **12**, 74–86.

Hartmann M., Müller P., Suess E. and van der Weijden C. H. (1976) Chemistry of Late Quaternary sediments and their interstitial waters from the NW African continental margin. "*Meteor*" *Forschungsergeb. Reihe C*, **24**, 1–67.

Hathaway J. C. and Degens E. T. (1969) Methane derived marine carbonates of Pleistocene age. *Science* **165**, 690–692.

Hermann A. G. (1975) *Praktikum der Gesteinsanalyse.* Springer.

Ignatius H. (1958) On the rate of sedimentation in the Baltic Sea. *Extr. C. R. Soc. Geol. Finl.* **30**, 135–145.

Jander G. and Wendt H. (1958) *Einführung in das anorganisch-chemische Praktikum.* Hirzel.

Kroopnick P. (1974) The dissolved O_2–CO_2–^{13}C system in the eastern equatorial Pacific. *Deep-Sea Res.* **21**, 211–227.

Kolp O. (1966) Rezente Fazies der westlichen und südlichen Ostsee. *Peterm. Geograph. Mitt.* **110**, 1–16.

Lalou C. (1957) Studies on bacterial precipitation of carbonates in seawater. *J. Sediment. Petrol.* **27**, 190–195.

Manheim F. T. (1961) A geochemical profile in the Baltic Sea. *Geochim. Cosmochim. Acta* **25**, 52–70.

Martens C. S., Berner R. A. and Rosenfeld J. (to be published) Interstitial water chemistry of Long Island Sound sediments—II. Nutrient regeneration and phosphate removal. To be published in *Limnol. Oceanogr.*

Masicka H. (1963) Essai de definition stratigraphique ainsi que l'âge de la carotte prelevee de la Baie Gdansk. *Baltica* **21**, 51–70.

Mehrbach C., Culberson C. H., Hawley J. E. and Pytkowicz R. M. (1973) *Measurement of the apparent dissociation constants of carbonic acid in seawater at atmospheric pressure.* *Limnol. Oceanogr.* **18**, 897–907.

Morita R. Y., Cuff C. and Patrick J. (1975) Anaerobic microbial precipation of calcite: a preliminary study. *Am. Soc. Microbiol., Annual Meeting*, 1975 (Abstract).

Murray J. W., Grundmanis V. and Smethie W. M., Jr. (1978) Interstitial water chemistry in sediments of Saanich Inlet. *Geochim. Cosmochim. Acta* **42**, 1011–1026.

Nilsson E. (1970) On the Late-Quaternary history of southern Sweden and the Baltic Basin. *Baltica* **4**, 11–32.

Oppenheimer C. H. (1961) Note on the formation of spherical aragonitic bodies in the presence of bacteria from the Bahama Bank. *Geochim. Cosmochim. Acta* **23**, 295–299.

Palache Ch., Berman H. and Frondel C. (1952) *The System of Mineralogy of J. D. Dana and E. S. Dana*, Vol. 1, pp. 207–208. Wiley.

Roberson C. E. (1966) Solubility implication of apatite in sea water. *U.S. Geol. Survey, Prof. Pap.* **550**, 173–185.

Roberts H. H. and Whelan T., III (1975) Methane-derived carbonate cements in barrier and beach sands of a subtropical delta complex. *Geochim. Cosmochim. Acta* **39**, 1085–1089.

ROSENQUIST I. TH. (1970) Formation of vivianite in Holocene clay sediments. *Lithos* 3, 327–334.

SALRAMO M. (1958) Die Geschichte der Ostsee. *Ann. Acad. Sci. Fennicae, Ser. A. III. Geolog.-Geograph.* 51, 6–522.

SCHNAASE H. (1933) Kristallstruktur der Manganosulfide und ihrer Mischkristalle mit Zinksulfid und Cadmiumsulfid. *Z. Phys. Chemie Abt. B.* 20, 89–117.

SHOLKOVITZ E. (1973) Interstitial water chemistry of Santa Barbara Basin sediments. *Geochim. Cosmochim. Acta* 37, 2043–2073.

SKIRROW G. (1975) The dissolved gases—carbon dioxide. In *Chemical Oceanography* (eds. J. P. Riley and G. Skirrow), Vol. 2, pp. 1–192. Academic Press.

STEIN C. L. (1977) Dissolution of diatoms and diagenesis in siliceous sediments. Ph.D. Thesis, Harvard University.

SUESS E. (1976a) Nutrients near the depositional interface. In *The Benthic Boundary Layer* (ed. I. N. McCave), pp. 57–79. Plenum.

SUESS E. (1976b) Porenlösungen mariner Sedimente—Ihre chemisches Zusammensetzung als Ausdruck frühdiagenetischer Vorgänge. Habilitationsschrift, Universität Kiel.

SUESS E. and ERLENKEUSER H. (1975) Anthropogenic metal and carbon input in Baltic Sea sedimentary basins. In *Geoscientific Studies and the Potential of the Natural Environment* (ed. M. Brüderlin), pp. 203–214. Deutsche UNESCO Kommission, Köln.

SUESS E. and FÜTTERER D. (1972) Aragonitic oolids: experimental precipitation from seawater in the presence of humic acid. *Sedimentology* 19, 129–139.

SUESS E. and MULLER P. (submitted) Interaction between K and NH_4 in marine pore solutions and sediments. Submitted to *Geochim. Cosmochim. Acta*.

TESSENOW U. (1974) Lösungs-, Diffusions- und Sorptionsprozesse in der Oberschicht von Seesedimenten—IV. Reaktionsmechanismen und Gleichgewichte im System Eisen–Mangan–Phosphat im Hinblick auf die Vivianitakkumulation im Ursee. *Arch. Hydrobiol. Suppl.* 47, 1–79.

TESSENOW U. (1975) Lösungs-, Diffusions- und Sorptionsprozesse in der Oberschicht von Seesedimenten—II. Rezente Akkumulation von Eisen(II)phosphate (Vivianit) im Sediment eines meromiktischen Moorses (Ursee, Hochschwarzwald) durch postsedimentäre Verlagerung. *Arch. Hydrobiol. Suppl.* 47, 143–189.

VARENTSOV I. M. (1975) Geochemical aspects of formation of iron-manganese ores in recent shelf seas. In *Problems of Lithology and Geochemistry of Sedimentary Rocks and Ores* (Strakhov Anniversary Volume) (ed. A. V. Peive), pp. 150–165. Nauka, Moskau.

WHITICAR M. J. (1978) Relationship of interstitial gases and fluids during early diagenesis in some marine sediments. Ph.D. Dissertation, University of Kiel.

Marine Biology 51, 1-8 (1979)

MARINE BIOLOGY

Comparison of the Feeding Habits of Migratory and Non-Migratory *Stenobrachius leucopsarus* (Myctophidae)

W.G. Pearcy, H.V. Lorz and W. Peterson

School of Oceanography, Oregon State University; Corvallis, Oregon, USA

Abstract

Stenobrachius leucopsarus, the most abundant species of myctophid fishes off Oregon, USA, has a bimodal distribution at night, with a peak of abundance in the upper 100 m composed of diel vertical migrants, and another peak at 300 to 500 m composed of fish that did not migrate the night they were caught. We compared the feeding habits of these two groups of fish in an attempt to learn if deep fish migrated to surface waters. Low similarity of diets, differences in the rank order of common prey, and similar states of stomach fullness and digestion of prey suggest that fish captured in deep water at night probably did not feed exclusively in shallow water on previous nights. They probably fed in deep water. The similarity in food habits between deep and shallow fish is most readily explained by daytime feeding by fish in deep water and by broad vertical distributions of prey.

Introduction

Many species of oceanic micronekton undertake diel vertical migrations; other species are non-migratory (Baird, 1971; Badcock and Merrett, 1976; Pearcy *et al.*, 1977). Based on observations from submersibles, Barham (1971), Clarke (1971), and Pickwell *et al.* (1971) suggested that not all migratory organisms perform vertical migrations every diel period. They noted the occurrence of myctophid fishes, euphausiids, and physonect siphonophores at daytime depths during the night or after the main scattering layer had migrated upward during the evening. Migratory and non-migratory portions of a population have also been revealed from midwater trawling studies. Tucker (1951), Paxton (1967) and Clarke (1973) found that substantial numbers of some species of myctophids (lanternfishes) may remain at daytime depths during the night and do not migrate toward the surface. This paper concerns such a myctophid, *Stenobrachius leucopsarus*.

Stenobrachius leucopsarus is predominant in the mesopelagic fish community of the upper 200 m at night off Oregon (Pearcy, 1964, 1971, 1977). In an earlier study, Pearcy and Mesecar (1971) found large numbers of *S. leucopsarus* at night from depths of 0 to 100 m and 350 to 420 m. Small *S. leucopsarus* are known to have gas-filled swimbladders (Capen, 1967; Butler and Pearcy, 1972) and are suspected to be a major contributor to the 12 kHz scattering layers common at these depths off Oregon, and to biological sound scattering in oceanic waters of the entire northeastern Pacific Ocean.

Migratory and non-migratory fractions of the *Stenobrachius leucopsarus* population were clearly revealed by a recent comparison of day and night vertical distributions obtained from quantitative, opening-closing midwater collections off Oregon (Pearcy *et al.*, 1977). Two maxima were obvious in the vertical distributions at night: one in the upper 100 m, the other near the daytime peak of abundance at 300 to 500 m. The number of fish was about equal in these two depth strata. Initially, we suspected this dual behavior to be related to ontogenetic differences in vertical distributions such as those found by Clarke (1973) and Badcock and Merrett (1976). However, a broad size range of *S. leucopsarus* occurred in both shallow and deep water at night during all seasons, and the size-frequency distributions within these two depth zones were not statistically different, a finding that is relevant to this paper. Also, the lack of size differences among migratory and

0025-3162/79/0051/0001/$01.60

non-migratory fish is an argument against the idea that large *S. leucopsarus*, which lack the physiological constraints imposed by gas-filled swimbladders, are more extensive vertical migrants than the small fish with gas-filled swimbladders (see Butler and Pearcy, 1972).

We propose two hypothetical types of behavior to explain the observed, non-migratory distributions of *Stenobrachius leucopsarus*: (1) The fish found in deep water at night (non-migrants) infrequently or never undertake diel vertical migrations; or (2) These fish actually migrate, but not every night. The fish caught at depth have merely "taken the night off" from their upward excursions. Perhaps individuals migrate to the surface waters to feed every other night, and remain at depth in a lethargic state (Barham, 1971; Clarke, 1971) for a day or more. They may not respond to the normal sensory cues to migrate if they are satiated (Zusser, 1958).

In this paper we examine the food habits of the migratory and non-migratory portions of the *Stenobrachius leucopsarus* population in an attempt to test these alternative hypotheses. If fish feed only at the surface at night, prey organisms should be very similar for fish caught at shallow and deep depths, but stomach fullness and stage of digestion should be markedly different. On the other hand, if the fish found at depth during the night rarely migrate, they must feed at depth and the species composition of their food should differ from that found in migratory fish which presumably feed in surface waters. Although food habits of *S. leucopsarus* have been investigated (Paxton, 1967; Collard, 1970; Cailliet, 1972; Tyler and Pearcy, 1975) this aspect of the feeding ecology has not been studied for any lanternfish.

Materials and Methods

Stenobrachius leucopsarus were collected with an Isaacs-Kidd midwater trawl equipped with a 1 m^2 multiple plankton sampler with 5 codend nets (Pearcy *et al.*, 1977). Collections were made at approximately 120 km off Newport, Oregon (44° 40'N; 125°35'W) in September 1972, November 1972, June 1973, and September 1974. The fish were fixed in 10% formalin at sea and stored in 35% isopropanol in the laboratory. Fish examined for this study were collected at random hours of the night (30 min after sunset to 30 min before sunrise). Food habits of fish from depths of 0 to 100 m (shallow) and 300 to 700 m (deep) were compared from 36 collections. Shallow nets fished about 30 min, deep nets about 1 h. A total of 696 *S. leucopsarus* were examined, 534 from 0 to 100 m and 162 from 300 to 700 m. Standard lengths (SL) ranged from 30 to 85 mm.

Individual fish were measured, stomachs removed and stomach fullness determined on a scale of 0 to 3 where: 0 = empty; 1 = partly full, rugae not distended; 2 = full stomach, rugae partially distended; 3 = very full stomach, no apparent rugae, stomach very distended (Tyler and Pearcy, 1975). The contents were flushed into a syracuse dish, examined, labeled, and stored in vials. Stages of digestion of food were categorized on a scale of 1 to 3 where: 1 = organisms well digested; 2 = organisms partly digested; 3 = organisms well preserved, fresh. When possible, individual food items were identified to species. The total lengths of copepods and amphipods and the carapace lengths of euphausiids were measured when possible. Data on food habits are expressed as: frequency of occurrence of a taxon based on all fish examined including those with empty stomachs, and average number of individual prey items per fish calculated for all fish with food in their stomachs.

Swimbladders were examined under a dissecting binocular microscope for morphological differences.

Results

Swimbladder Structure

Swimbladders were examined to determine if differences existed in the percentage of thin-walled (presumably gas-filled) swimbladders in *Stenobrachius leucopsarus* captured at depths of 0 to 100 m and 300 to 700 m at night. According to Butler and Pearcy (1972), who described the structure of *S. leucopsarus* swimbladders, gas-filled swimbladders have thin walls, whereas swimbladders that lack gas inclusions are fat-invested, reduced and thick-walled. Our results in Table 1 agree with those of Butler and Pearcy in that most small *S. leucopsarus* had thin-walled swimbladders, and most large fish had thick-walled swimbladders. Although Butler and Pearcy found no gas in *S. leucopsarus* larger than 40 mm, 9 fish of 40 to 49 mm were found with thin-walled or transitional swimbladders in the present study, suggesting that they may have contained gas. In any case, no large differences were obvious: fish with thin-walled swimbladders occurred at both depths in about the same proportions.

Stomach Fullness and Stage of Digestion

Our data indicate no major differences in stomach fullness of shallow and deep fish (Fig. 1). Most fish at both depth intervals had food in their stomachs except for small fish (<40 mm) in deep water.

The stage of digestion of food items in deep fish indicates that the percent of fresh food increased with increasing size (Fig. 1). The trend was inverse in shallow fish: percent of fresh food decreased with increasing size. For fish >70 mm, a larger proportion of deep than shallow fish contained fresh food.

Thus, small fish (<40 mm) in deep water at night usually had a small quantity of well-digested food in their stomachs, whereas small fish caught at shallow depths usually had full stomachs of relatively fresh food. (Fish <40 mm represented 48% of the catch at 0 to 100 m and 30% at 300 to 700 m). Large fish from both depths differed little in stomach fullness and stage of digestion. Most deep fish ≥40 mm had nearly full stomachs of fresh food.

Food Composition

The percentage that each major prey taxa comprised of the total number of prey organisms and the frequency of occurrence of major prey taxa are shown in Fig. 2 for fish of different sizes from 0 to 100 m and 300 to 700 m. Several differences are apparent. Based on number of prey organisms, copepods were the dominant prey taxa in deep fish. Copepods were also the most numerous prey for fish <60 mm in shallow water, but euphausiids predominated for fish >60 mm. Therefore, large fish from shallow water fed mainly on euphausiids, whereas large fish from deep water and small fish from both depths fed mainly on copepods. Trends based on frequency of occurrence also show differences in the feeding habits of shallow and deep fish. Euphausiids occurred more frequently than copepods in surface-caught fish, while the opposite trend generally obtained for fish from deep water (Fig. 2).

The average number of food items per fish (Table 2A) reflects these basic trends in food composition. An average of only 1 or 2 prey were found in fish from shallow water and in small fish from deep water. Small fish usually contained a few copepods; big fish often contained one large euphausiid. Large fish from deep water, on the other hand, often had many food organisms in their stomachs. These were mainly copepods.

Table 1. *Stenobrachius leucopsarus*. Percent comparison of thin-walled and thick-walled swimbladders by length intervals from 455 myctophids captured in the two depth zones

	Length (mm)						
	20–29	30–39	40–49	50–59	60–69	70–79	80–89
0–100 m							
thin	93	68	16[a]	0	0	0	0
thick	7	32	84	100	100	100	100
300–700 m							
thin	87	54	0	0	0	0	0
thick	13	46	100	100	100	100	100

[a]Nine of these were transitional between thin- and thick-walled.

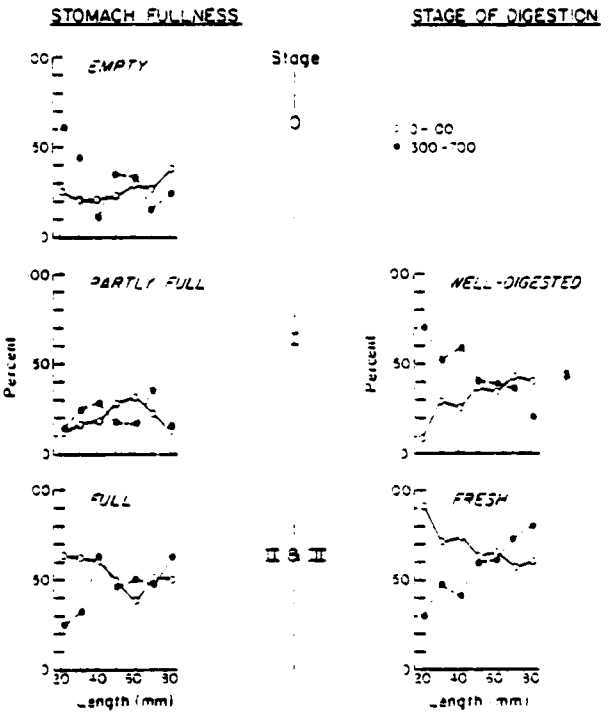

Fig. 1. *Stenobrachius leucopsarus*. Comparison of stomach fullness and stage of digestion of food items for 10 mm length-groups from 0 to 100 m and 300 to 700 m depths

Hence, variation in number of prey with size of fish depended on prey composition, which in turn was related to depth of capture.

Because fresh food is the best indication of the kind of prey consumed at the depth of capture of the fish, we noted the percentages of the two major taxa of fresh food from shallow and deep fish in Table 2B. Shallow fish of all length groups contained a high percentage of euphausiids, while deep fish had a high percentage of copepods.

A list of prey items identified from the stomachs of *Stenobrachius leucopsarus*

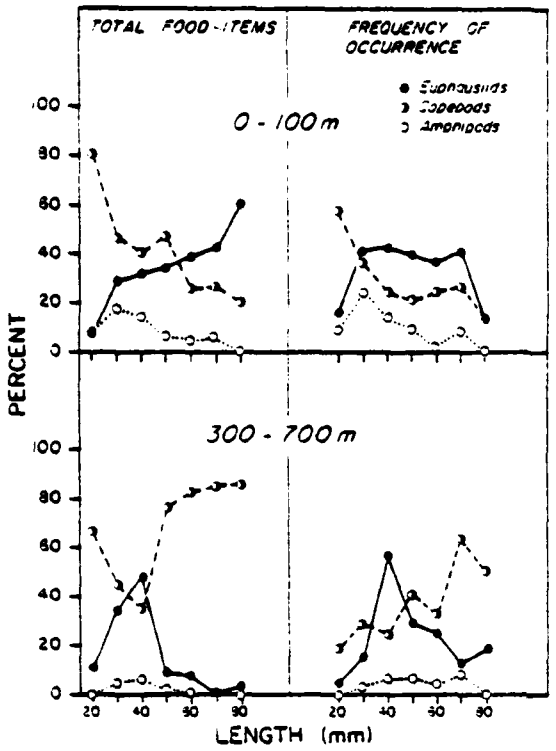

Fig. 2. *Stenobrachius leucopsarus*. Percent that each prey taxa comprised of total number of prey organisms and frequency of occurrence of major prey taxa in stomachs of different sizes (abscissa) of myctophids from 0 to 100 m and 300 to 700 m depths

Table 2. *Stenobrachius leucopsarus*. A) Average number of food items per fish stomach that contained food, and B) percentage of fresh (Stage 1) copepods and euphausiids, from stomachs of fish from 0 to 100 m and 300 to 700 m, September and November, 1972. n: Number of fish examined; nd: no data

	Length (mm)						
	20–29	30–39	40–49	50–59	60–69	70–79	80–89
A) Average no. of food items							
0–100 m	2.3	1.9	1.7	1.7	2.0	1.6	1.0
300–700 m	9.8	1.1	1.4	3.8	4.0	13.8	12.8
(B) Percentage of fresh prey							
0–100 m							
Copepods	nd	18	12	15	20	29	nd
Euphausiids	50	71	80	75	61	71	100
n	3	21	17	16	23	3	1
300–700 m							
Copepods	nd	50	67	76	94	72	67
Euphausiids	nd	50	33	4	6	nd	nd
n		2	3	9	7	6	7

Table 3. Taxa identified from stomachs of *Stenobrachius leucopsarus*

Copepods	Euphausiids
Calanus spp.	*Euphausia pacifica*
Calanus plumchrus	*Nematoscelis difficilis*
Calanus cristatus	*Thysanoessa* spp.
Calanus tenuicornis	Euphausiacea
Calanus pacificus	Amphipods
Calanus marshallae	*Parathemisto pacifica*
Eucalanus spp.	*Phronima* spp.
Eucalanus bungii	*Primno abyssalis*
Paracalanus parvus	Amphipoda
Pseudocalanus spp.	Decapods
Aetideidae	*Sergestes similis*
Aetideus pacificus	Mysids
Chiridius spp.	*Boreomysis rostrata*
Gaetanus spp.	Mysidacea
Gaidius spp.	Ostracoda
Euchirella spp.	Fish
Chirundina streetsi	*Stenobrachius leucopsarus*
Pareuchaeta spp.	*Tarletonbeania crenularis*
Scottocalanus spp.	Miscellaneous
Scaphocalanus spp.	Chaetognaths
Scolecithricidae	Fish scales
Metridiidae	Unidentified eggs
Metridia pacifica	Gastropods
Metridia lucens	Tintinnids
Pleuromamma spp.	
Lucicutia spp.	
Heterorhabdus spp.	
Candacia spp.	
Candacia columbiae	
Acartia longiremis	
Dichona similis	
Oncaea spp.	
Aegisthus mucronatus	

Table 4. *Stenobrachius leucopsarus*. Rank order of the 10 most common prey in diets of myctophids from 0 to 100 m and 300 to 700 m based on average number of prey per fish and frequency of occurrence

0–100 m	300–700 m
Based on number of prey per fish	
Euphausia pacifica	*Eucalanus bungii*
Euphausiacea	*Calanus* spp.
Parathemisto pacifica	*Calanus plumchrus*
Metridia pacifica	Ostracoda
Pareuchaeta spp.	Metridiidae
Calanus cristatus	*Pareuchaeta* spp.
Calanus plumchrus	Euphausiacea
Fish scales	*Euphausia pacifica*
Candacia columbiae	Fish scales
Eucalanus bungii	*Calanus marshallae*
Based on frequency of occurrence	
Euphausia pacifica	*Calanus plumchrus*
Euphausiacea	*Pareuchaeta* spp.
Parathemisto pacifica	Euphausiacea
Metridia pacifica	Ostracoda
Pareuchaeta spp.	*Eucalanus bungii*
Calanus cristatus	Metridiidae
Calanus plumchrus	*Euphausia pacifica*
Fish scales	*Calanus* spp.
Heterorhabdus spp.	*Heterorhabdus* spp.
Eucalanus bungii	Fish scales

(Table 3) indicates that more species of copepods than any other group were consumed.

The 10 most common prey taxa are ranked in Table 4 for fish from 0 to 100 m and 300 to 700 m to compare the rank order of frequency of occurrence and average number of prey between the two depths. Many of the prey taxa were common to both depths, indicating similarity in the occurrence of prey in deep and shallow fish. However, the rank orders of prey are different; some prey were common in the diets of fish from only one depth.

On the basis of average number of prey, the amphipod *Parathemisto pacifica*, and the copepods *Metridia pacifica*, *Calanus*

cristatus, and *Candacia columbiae* were common prey of deep fish. *C. columbiae* and *Euchirella* spp. (not listed in Table 4) were found only in the diet of shallow fish. Euphausiids ranked within the top 10 prey for both depths but were the most abundant food taxa only for fish from 0 to 100 m, where they ranked first and second in importance. Because euphausiids are among the largest prey, they clearly predominated the diet of shallow fish on a volume or weight basis. *Eucalanus bungii*, *Calanus* spp., *Calanus plumchrus* and ostracods replaced euphausiids and *P. pacifica* as the predominant prey in deep-water fish. Ostracods and *Calanus marshallae* were only common in fish from 300 to 700 m.

On the basis of frequency of occurrence, euphausiids and *Parathemisto pacifica* again were most common in shallow fish. *P. pacifica* ranked within the top 10 prey taxa only in fish from 0 to 100 m. Ostracods were again listed as prey only for fish caught from 300 to 700 m. *Calanus plumchrus*, *Eucalanus bungii* and *Paraeuchaeta* spp. were the most frequently occurring food in fish from deep water.

Percent similarity (the sum of the percentages of individual taxa common to the diet of both groups of fish) was calculated to determine the similarity of food composition between shallow and deep fish. The percent similarity was 40% based on number of prey items. In addition, Spearman rank correlation coefficients were calculated among those food taxa that occurred in 5% or more of deep or shallow fish for each of the 4 cruises and for all cruises combined. Rank correlation coefficients ranged from 0.07 to 0.30 for comparisons of frequency of occurrence or mean number of prey, either for all sizes combined, for fish <40 mm or for fish >40 mm SL. All coefficients are non-significant ($P > 0.2$), indicating that although deep and shallow fish fed on many of the same taxa, abundant or frequently occurring prey were usually different, even for fish of one size category.

Data on the vertical distribution and migration of prey species can conceivably provide important clues to the time and depth of feeding. Unfortunately, detailed information for the eastern North Pacific Ocean is lacking for most prey species. Several of the taxa listed in Table 3 have vertical distributions that correspond to the depth of capture of the fish. For example, *Parathemisto pacifica*, an important prey only for shallow fish, is reported to have a maximum abundance near the surface (Lorz and Pearcy, 1975; Marlowe and Miller, 1975). Ostracods, important prey only for deep fish, are thought to reside primarily in deep water (B. Frost, personal communication) or subsurface waters (Marlowe and Miller, 1975).

Only Stage V *Calanus plumchrus* were found in *Stenobrachius leucopsarus* stomachs. This copepod was consumed mainly by deep fish in the winter. It has been found in greatest abundance in surface waters during the summer months (Peterson and Anderson, 1966; Jawed, 1973; Marlowe and Miller, 1975) and migrates into deep water during the winter (Sekiguchi, 1975). *C. cristatus*, which also demonstrates seasonal migrations from shallow waters in the spring and summer to deep waters in the winter (Sekiguchi, 1975), was found only in fish caught in shallow waters during June.

Several species have vertical distributions which did not correspond with our data on depth of capture of fish. *Eucalanus bungii*, important prey for deep fish, has its greatest abundance in subarctic waters within the upper 100 m both day and night according to Marlowe and Miller (1975). *Candacia columbiae* was found only in shallow fish, but is thought to migrate in limited numbers above 100 m (Cameron, 1957; Peterson and Anderson, 1966; Marlowe and Miller, 1975).

Other prey species, such as *Metridia pacifica* and *Euphausia pacifica* undertake diel vertical migrations into the upper 100 m at night (Brinton, 1967; Marlowe and Miller, 1975). These species were more common as prey for shallow than for deep fish, but could be consumed by fish from both depths. Many of the prey also have broad vertical distributions, extending hundreds of meters (Marlowe and Miller, 1975), and therefore may be available as prey in either shallow or deep water.

Discussion

Our data indicate that *Stenobrachius leucopsarus* captured at depths of 0 to 100 m and 300 to 700 m fed on many of the same taxa, but the similarity of diets was only 40% and the rank order of prey taxa based on both frequency of occurrence and abundances were different. Moreover, some common prey taxa were found only in fish from one depth of capture. Evidence from stomach fullness and stage of digestion of stomach items also suggests that large fish from both depth strata had often fed just prior to capture. Small fish generally had small amounts of well-digested food in deep water and full stomachs of fresh food in shallow water. Small fish from both depths also

ate mostly copepods. Although these trends suggest that small fish may feed primarily in surface waters at night, the species composition of their prey was different. Therefore, most indications, although none are unequivocal, lead in combination to the conclusion that the fish residing in deep water by night fed at depth, rather than exclusively near the surface at night.

The food habits of *Diaphus theta*, another common lanternfish off Oregon, are similar to those of *Stenobrachius leucopsarus* from 0 to 100 m. Of the prey listed in Table 4, euphausiids, *Euphausia pacifica* and *Metridia pacifica* also ranked as the three most frequently occurring prey of *D. theta* off Oregon, whereas *Calanus plumchrus* and *Pareuchaeta* spp., prey occurring frequently in deep *S. leucopsarus*, were not common in the diet of *D. theta* (see Tyler and Pearcy, 1975). *D. theta* is a diel migrator with no residual mode of individuals remaining in deep water at night (Pearcy *et al.*, 1977). The similarities in the diet of migratory *S. leucopsarus* and *D. theta*, therefore, suggest that both species feed at night on common epipelagic prey. The differences between deep *S. leucopsarus* and *D. theta* reinforce our suggestions that deep *S. leucopsarus* do not feed primarily in near-surface waters.

Feeding periodicity, rates of digestion and the vertical distribution of prey species are important considerations in resolving when and where feeding occurred. Hopkins and Baird (1977) reviewed the papers on diel feeding periodicity of mesopelagic fishes. They reported that distinct feeding cycles are present in many strong migrators which ascend into epipelagic waters at night. These migrators, including 7 species of myctophids, are principally nocturnal predators. Only two species of myctophids were listed as acyclic feeders. Tyler and Pearcy (1975) examined the evidence for feeding periodicity of *Stenobrachius leucopsarus* by examining fish caught mainly in the upper 200 m at night and deeper waters by day. More full stomachs occurred in the night and morning (20.00 to 13.25 hrs) than in the afternoon (12.30 to 20.40 hrs). A larger percentage of empty stomachs were found in the afternoon, but full stomachs and empty stomachs were found throughout the diel period. This suggests that migratory *S. leucopsarus* feed principally at night, but some fish caught at depth, which probably included a mixture of migratory and non-migratory fish, fed during the day.

Another explanation for the occurrence of full stomachs and fresh food items in deep *Stenobrachius leucopsarus* caught at night (this study) and during the day (Tyler and Pearcy, 1975) could be a slow rate of digestion and evacuation of stomach contents. Although rates of digestion have not been measured directly for any mesopelagic fish, Baird *et al.* (1975) found that the myctophid *Diaphus taaningi* contained many prey items in the first half of the night while those taken prior to evening ascent were "essentially empty". Significant digestion occurred at night after feeding in surface waters, where temperatures were 20°C or higher. Consequently, fishes with pronounced feeding cycles probably clear their digestive tracts daily (Hopkins and Baird, 1977). Rates of digestion of *S. leucopsarus* in surface waters that are rarely over 16°C, and in deep waters that are 4° to 7°C, are probably slower than those suggested by Baird *et al.* (1975), however. Lethargic fish in deep water may have reduced metabolic and digestive rates. Nevertheless, prey eaten by day in deep water and later found intact in fish caught in the upper 100 m at night could account for some or all of the similarities between deep and shallow fish in this study. To explain similarities in the diet by feeding of both groups in surface waters would require the less likely condition that prey consumed at the surface are digested very little in fish that remain in deep water throughout the day and part of the following night when they were captured.

The adaptive significance of the bimodal nocturnal distribution of this lanternfish is unknown. Marlowe and Miller (1975) found similar distributions for some oceanic zooplankton and speculated that they may be related to McLaren's (1963) hypothesis, which proposes an advantage to actively feeding above the thermocline and assimilating food in deep, cooler waters. This implies diel migrations of animals between the two depth modes. In the case of *Stenobrachius leucopsarus*, however, bimodal distributions were obvious during November and February, when the thermocline was weakly developed (Pearcy *et al.*, 1977) and the "energy bonus" would theoretically be small because of minimal temperature differences between daytime and nighttime depths.

Barham (1971) observed that about one-half the number of myctophids (largely *Stenobrachius leucopsarus*) seen below 100 m during a night submersible dive off San Diego were immobile and vertically oriented. He speculated that such myctophids may maintain a "state of suspended activity" with little or no

diel vertical migration for prolonged periods of time and that this behavior may allow them to conserve energy and remain inconspicuous to predators. As pointed out by Barham, lethargy is associated with myctophids which have a high lipid content, such as *S. leucopsarus* (Nevenzel et al., 1969; Butler and Pearcy, 1972; Childress and Nygaard, 1973). The energy conserved by lethargic, non-migratory behavior may facilitate storage of large quantities of calories, as lipids, which in turn is related to the approximate neutral buoyancy of this species.

Acknowledgements. This research was supported by the Office of Naval Research (Contract N000-14-67-A-0369-0007) under Project Nr. 083-102. We thank C.B. Miller for reviewing the manuscript.

Literature Cited

Badcock, J. and N.R. Merrett: Midwater fishes in the eastern north Atlantic - I. Vertical distribution and associated biology in 30°N, 23°W, with developmental notes on certain myctophids. Prog. Oceanogr. *7*, 3-58 (1976)

Baird, R.C.: The systematics, distribution and zoogeography of the marine hatchet fishes (family Sternoptychidae). Bull. Mus. comp. Zool. Harv. *142*, 1-128 (1971)

-, T.L. Hopkins and D.F. Wilson: Diet and feeding chronology of *Diaphus taaningi* (Myctophidae) in the Cariaco Trench. Copeia *1975*(2), 356-365 (1975)

Barham, E.G.: Deep-sea fishes: lethargy and vertical orientation. *In:* Proceedings of an International Symposium on Biological Sound Scattering in the Ocean, pp 100-118. Ed. by G.B. Farquhar. Washington, D.C.: Maury Center for Ocean Science 1971

Brinton, E.: Vertical migrations and avoidance capability of euphausiids in the California Current. Limnol. Oceanogr. *12*, 451-483 (1967)

Butler, J.L. and W.G. Pearcy: Swimbladder morphology and specific gravity of myctophids off Oregon. J. Fish. Res. Bd Can. *29*, 1145-1150 (1972)

Cailliet, G.M.: The study of feeding habits of two marine fishes in relation to plankton ecology. Trans. Am. microsc. Soc. *91*, 88-89 (1972)

Cameron, F.E.: Some factors influencing the distribution of pelagic copepods in the Queen Charlotte Island area. J. Fish. Res. Bd Can. *14*, 165-202 (1957)

Capen, R.L.: Swimbladder morphology of some mesopelagic fishes in relation to sound scattering. Res. Rep. U.S. Navy Electron. Lab., S Diego, Calif. *1447*, 1-29 (1967)

Childress, J.J. and M.H. Nygaard: The chemical composition of midwater fishes as a function of depth of occurrence off southern California. Deep-Sea Res. *20*, 1093-1109 (1973)

Clarke, W.D.: Comparison of different investigative techniques for studying the deep scattering layers. *In:* Proceedings of an International Symposium on Biological Sound Scattering in the Ocean, pp 550-562. Ed. by G.B. Farquhar. Washington, D.C.: Maury Center for Ocean Science 1971

Clarke, T.A.: Some aspects of the ecology of lanternfishes (Myctophidae) in the Pacific Ocean near Hawaii. Fish. Bull. U.S. *71*, 401-433 (1973)

Collard, S.B.: Forage of some eastern Pacific midwater fishes. Copeia *1970*(2), 348-354 (1970)

Hopkins, T.L. and R.C. Baird: Aspects of the feeding ecology of oceanic midwater fishes. *In:* Oceanic sound scattering prediction, pp 325-360. Ed. by N.R. Anderson and B.J. Zahuranec. New York: Marine Science Series, Plenum Press 1977

Jawed, M.: Numerical abundance of dominant copepods from the Northeast Pacific Ocean: Columbia River effluent area, 1963. Tech. Rep. Dep. Oceanogr. Wash. *286*, 1-106 (1973)

Lorz, H.V. and W.G. Pearcy: Distribution of hyperiid amphipods off the Oregon coast. J. Fish. Res. Bd Can. *32*, 1442-1449 (1975)

Marlowe, C.J. and C.B. Miller: Patterns of vertical distribution and migrations of zooplankton at Ocean Station "P." Limnol. Oceanogr. *20*, 824-844 (1975)

McLaren, I.A.: Effects of temperature on growth of zooplankton, and the adaptive value of vertical migration. J. Fish. Res. Bd Can. *20*, 685-727 (1963)

Nevenzel, J.C., W. Rodegker, J.S. Robinson and M. Kayama: The lipids of some lanternfishes (family Myctophidae). Comp. Biochem. Physiol. *31*, 25-36 (1969)

Paxton, J.R.: Biological notes on southern California lanternfishes (family Myctophidae). Calif. Fish Game *53*, 214-217 (1967)

Pearcy, W.G.: Some distributional features of mesopelagic fishes off Oregon. J. mar. Res. *22*, 83-102 (1964)

- Distribution and ecology of oceanic animals off Oregon. *In:* The Columbia River Estuary and adjacent ocean waters, pp 357-377. Ed. by A.T. Pruter and D.L. Alverson. Washington, D.C.: University of Washington Press 1971

- Variations in abundance of sound scattering animals off Oregon. *In:* Oceanic sound scattering prediction. pp 647-666. Ed. by N.R. Anderson and B.J. Zahuranec. New York: Marine Science Series, Plenum Press 1977

-, E.E. Krygier, R. Mesecar and F. Ramsey: Vertical distribution and migration of oceanic micronekton off Oregon. Deep-Sea Res. *24*, 223-245 (1977)

- and R.S. Mesecar: Scattering layers and vertical distribution of oceanic animals off Oregon. *In:* Proceedings of an International Symposium on Biological Sound Scattering in the Ocean, pp 381-394. Ed. by G.B. Farquhar. Washington, D.C.: Maury Center for Ocean Science 1971

Peterson, W.K. and G.C. Anderson: Net zooplankton data from the Northeast Pacific Ocean: Columbia River effluent area, 1961, 1962. Tech. Rep. Dep. Oceanogr. Univ. Wash. 160, 1-225 (1966)

Pickwell, G.V., R.J. Want, E.G. Barham, W.E. Batzler and I.E. Davies: Biological acoustic scattering off southern California, Baja California, and Guadalupe Island. In: Proceedings of an International Symposium on Biological Sound Scattering in the Ocean, pp 490-502. Ed. by G.B. Farquhar. Washington, D.C.: Maury Center for Ocean Science 1971

Sekiguchi, H.: Seasonal and ontogenetic vertical migrations in some common copepods in the northern region of the North Pacific. Bull. Fac. Fish. Mie Univ. 2, 29-38 (1975)

Tucker, G.H.: Relation of fishes and other organisms to the scattering of underwater sound. J. mar. Res. 10, 215-238 (1951)

Tyler, H.R. and W.G. Pearcy: The feeding habits of three species of lanternfishes (family Myctophidae) off Oregon, USA. Mar. Biol. 32, 7-11 (1975)

Tusser, S.G.: A study of the causes of diurnal vertical migrations in fishes. Trudy Soveshch. Ikhtiol. Kom. 9, 115-120 (1958). Translation by U.S. Fish and Wildlife Service, Biology Laboratory, Boothbay Harbor, Maine 1959, USA)

Dr. W.G. Pearcy
School of Oceanography
Oregon State University
Corvallis, Oregon 97331
USA

Date of final manuscript acceptance: October 27, 1978. Communicated by M.R. Tripp, Newark

Reprinted from JOURNAL OF PHYSICAL OCEANOGRAPHY, Vol. 9, No. 5, September 1979
American Meteorological Society
Printed in U. S. A.

Observations of Upper Ocean Temperature and Salinity Structure During the POLE Experiment

JAMES J. SIMPSON[1] AND CLAYTON A. PAULSON

School of Oceanography, Oregon State University, Corvallis 97331

(Manuscript received 4 September 1978, in final form 19 March 1979)

ABSTRACT

Mid-ocean observations (35°N, 155°W) of temperature and salinity were made from *R/P Flip* during the period 28 January–14 February 1974 as part of the NORPAX POLE Experiment.

Autocorrelations for the time series of depth of several σ_t surfaces confirm the presence of a semi-diurnal internal tide whose amplitude is about 10 m. The period of 12.7 h determined from the autocorrelation analysis is not statistically significantly different from the period of the M2 semidiurnal tide (12.4 h). The coherence between pairs of time series of the depth of the σ_t surfaces is high, ranging from 0.97 to 0.91 at the frequency of the peak in the spectrum corresponding to the semi-diurnal tide. The coherence between a given σ_t surface and deeper lying surfaces decreases slowly with the mean separation between surfaces. The vertical coherence scale suggests that most of the energy of the semi-diurnal internal tide is in the low-order modes. The data show that the phase difference between surfaces increases with the mean separation between surfaces at the approximate rate of $\sim 35° (100\ m)^{-1}$. Estimates of the vertical and horizontal wavelengths of the observed semi-diurnal internal tide are 1 km and 35 km, respectively.

One-dimensional mixed-layer deepening models fail to predict the mixed-layer depths and temperatures observed during POLE. Horizontal advection, as evidenced from the salinity maximum frequently occurring at the bottom of the mixed layer and other near-surface changes in salinity and temperature not associated with local surface forcing, are responsible for the failure. During the one period in which the one-dimensional models may be applicable a value of the mixing energy flux coefficient $m = 0.0017$ was obtained.

1. Introduction

Temporal variations in upper ocean temperature and salinity structure are caused by the exchange of energy, momentum and mass across the air-sea interface and by advection. To better understand upper ocean processes and evaluate existing parameterizations of such processes, the POLE Experiment, a component of the North Pacific Experiment (NORPAX) was conducted during the period 28 January–14 February 1974.

The experimental site (near 35°N, 155°W) is shown in Fig. 1. The North Pacific Current dominates the general circulation of this region. The observational area lies in the transition zone between the trade winds to the south and the westerlies to the north. Large-scale changes in the curl and divergence of the wind stress and in the exchange of heat and mass occur in such a region. Superimposed on this flow are several other features which complicate the hydrodynamics of the region. The subtropical front is known to meander, in the mean, between 31° and 33°N (Roden, 1974). Observations (Roden, 1970, 1972) suggest that in winter the horizontal temperature and salinity gradients contribute approximately equally to the density gradient, while in summer the temperature gradient weakens. The horizontal salinity gradient appears to remain about the same throughout the year. The region of the trade winds northeast of the Hawaiian Island Chain has upward fluxes of latent heat in excess of 9.8 mW cm^{-2} over a 24 h period. This leads to the formation of a high-salinity Subtropical Water Mass which contrasts markedly with the less saline eastern Pacific Central Water characteristically found north of 35°N. This saline subtropical water can penetrate to depths as great as 200 m (Reid, 1965; Seckel, 1968).

The purpose of this paper is to report observations of temperature and salinity obtained during a 15-day period of intensive sampling from *R/P Flip* as part of the NORPAX POLE Experiment and to interpret these observations in terms of physical processes, both local and advective, which might explain the observed structure.

2. Observations

Vertical profiles of temperature and salinity were taken from *R/P Flip*, (Floating Instrument Platform (Bronson and Glosten, 1968)) throughout

[1] Present affiliation: Scripps Institution of Oceanography, La Jolla, CA 92093.

0022-3670/79/050869-16$00.00

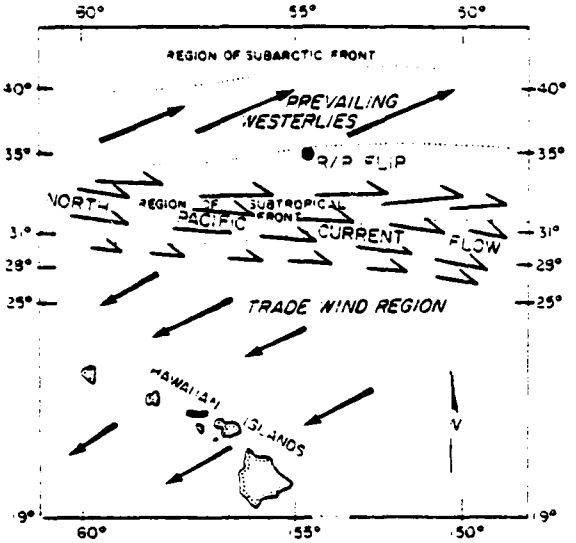

FIG. 1. The POLE Experiment was conducted in the central North Pacific approximately 300 miles north of the Hawaiian Islands. *R.P Flip* occupied a station centered around 35°N, 155°W. The region is hydrographically complex.

the period 30 January–14 February 1974, approximately 300 mi north of the Hawaiian Island Chain under free drift conditions. *Flip* is a large manned spar buoy with approximately 90 m of its 130 m length submerged, resulting in a high degree of stability. Typical heave amplitudes were about 10 cm, while pitch and roll amplitudes were usually less than 2°. The position of *Flip* ranged from 35°39′ to 34°36′N and from 155°05′ to 155°25′W. Profiling was concentrated in the surface layer and thermocline. The maximum depth reached was 325 m. On average, eight profiles were measured per day. On occasion, more intensive sampling was maintained.

In addition to profiles of temperature and salinity, measurements of atmospheric radiation (Simpson and Paulson, 1979a) and oceanic irradiance (Paulson and Simpson, 1977) were made. Sea surface temperature was measured with a Barnes Engineering Company PRT-5 radiation thermometer (Simpson and Paulson, 1979b). Standard cup anemometers were used to measure wind speed. Dry- and wet-bulb temperatures were measured approximately hourly by use of a ventilated psychrometer. Bucket temperatures were recorded at the same time. Estimates of wind stress and latent and sensible heat flux were obtained by use of the standard bulk formula. The exchange coefficient used was 1.4×10^{-3}. Hourly values of observed and derived quantities are shown in Fig. 2. These values were obtained by interpolating between observations using a cubic spline.

Direct measurements of the latent and sensible heat flux, using the eddy correlation technique, were made (Friehe and Schmitt, 1976). The variability of the near-surface currents was observed with a vertically profiling current meter system and with drogues (Davis *et al.*, 1978).

3. Instrumentation

A Bissett-Berman Model 9040 Salinity/Temperature/Depth (STD) Measuring System was used as the profiling device. Temperature is determined with a platinum resistance thermometer having a time constant of 0.35 s, according to the manufacturer. Salinity is determined from simultaneous measurements of conductivity, temperature and depth. The time response of the conductivity probe is 10 ms. Unfortunately, conductivity is not the recorded variable. Rather, the instrument internally compensates for the effects of temperature and pressure and gives a direct estimate of salinity. Accuracies for depth, temperature and salinity are 1 m, 0.01°C and 0.03‰, with corresponding resolutions of 0.2 m, 0.005°C and 0.01‰. Data were recorded in digital form with a sampling rate of 5 Hz.

Temperature was standardized against a Mueller platinum resistance bridge. Salinity was standardized with reference to surface samples taken during each profile. A Bisset-Berman Model 6230 inductive salinometer was used to determine the salinity of the surface samples. This device can accurately resolve salinity to within 0.003‰.

A correction was applied to the depth signal to eliminate the effect of ambient atmospheric pressure. Corrections due to platform motion were unnecessary, as the amplitude of *Flip*'s vertical oscillations is typically 10 cm.

Spectral analysis of GATE B-scale data, taken with Bisset-Berman Model 9040 STD's, suggests that a large percentage of the variance associated with the pressure signal is contributed at frequencies >0.67 Hz. This variance is thought to be internal system noise (Elliot, 1975). The GATE results suggest that a low-pass filter is required to attenuate signals above 0.67 Hz. A two-stage running mean filter, designed by Holland (1968), was used.

Differences in the time constants of the temperature and salinity sensors introduce errors in the observed values of temperature and salinity. To correct the temperature signal for the thermal inertia of the sensor, a local temperature gradient was calculated from a 12-point, noncentered, linear regression. The center of the regression is 0.3 s ahead of the point to be corrected. The corrected temperature T_c is then given in terms of the uncorrected temperature T_u, i.e.,

$$T_c = T_u + \gamma \frac{\Delta T_u}{\Delta t}, \qquad (3.1)$$

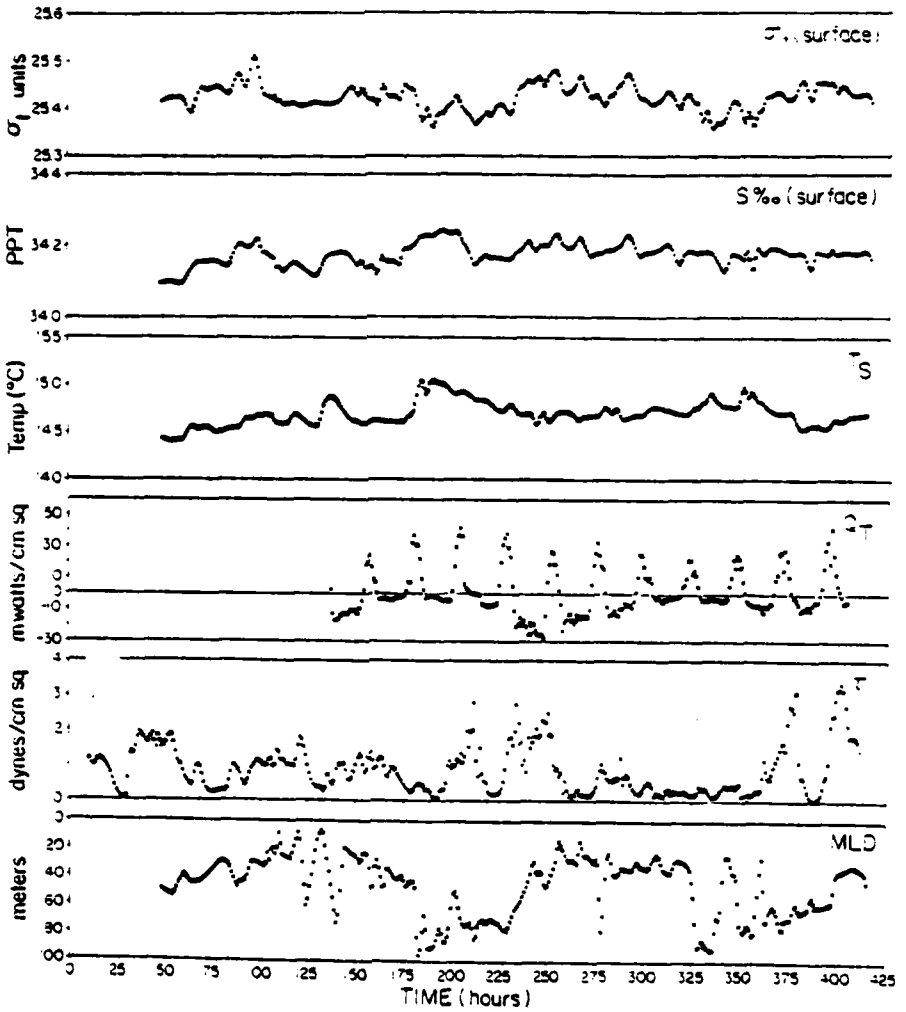

FIG. 2. Hourly values of the surface σ_t, surface salinity, sea surface temperature, total heat flux at the surface Q_T, wind stress τ, and the mixed-layer depth MLD. Hourly values were obtained by interpolating between observations using a cubic spline. The origin of the abcissa is 1000 GMT 28 January 1974.

where γ is the response time of the temperature sensor.

The salinity correction is based on a relation (Mosetti, 1967) between the conductivity C and the measured temperature and salinity T_m and S_m:

$$C = (\Gamma + \mu T_m^k) S_m^h, \tag{3.2}$$

where $\Gamma = 1.17013$, $\mu = 0.03299$, $k = 1.05257$ and $h = 1.10807$. As this relation is assumed to hold for both corrected and measured values, the correction factor assumed the form

$$\lambda = \left(\frac{\Gamma + \mu T_m^k}{\Gamma + \mu T_c^k} \right)^{-h}. \tag{3.3}$$

The corrected salinity S_c, specified in terms of the observed salinity S_m, then assumes the form

$$S_c = S_m[(\lambda - 1)\xi - 1]. \tag{3.4}$$

This relation reduces to the correction used by Elliot (1975) for the case $\xi = 1$. The factor ξ is introduced to minimize the cumulative magnitude of the inversions in the density profiles determined from the corrected profiles of temperature and salinity. Observations of density inversions are most likely introduced by erroneous salinity measurements made in the presence of sharp temperature gradients. Occasionally, turbulence in the water may cause real density inversions which can persist only for brief periods. The corrected salinity was low-pass filtered, in a manner analogous to pressure. Numerous numerical experiments indicated that the observed density inversions were minimized with $\xi = 6$. The resulting triplets T_c,

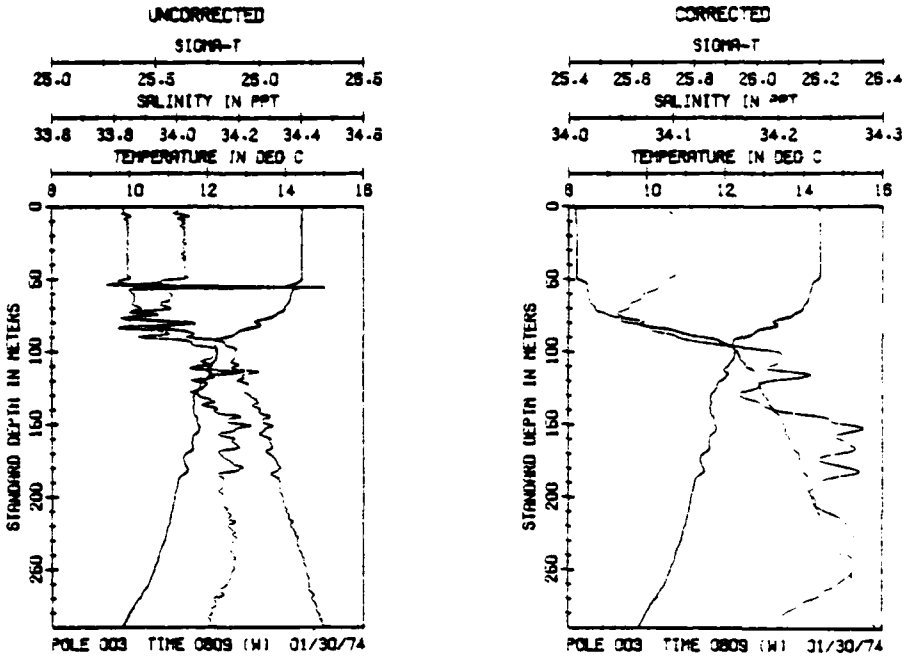

FIG. 3. Examples of uncorrected and corrected temperature, salinity and density profiles for a typical hydrocast. Corrections were made for the difference in the time response of the conductivity and temperature sensors.

$S_c D$) were averaged over 1 m intervals, and standard depth values computed by interpolation from the averaged data sets. The σ_t profiles were computed using a series expansion in terms of the corrected temperature and salinity (Fofonoff and Tabata, 1958; Sweers, 1971). In Fig. 3 uncorrected and corrected profiles of temperature, salinity and σ_t are shown for a typical observation. A data report summarizing all the STD observations has been prepared (Simpson and Paulson, 1977).

4. Surface conditions

a. Surface wind stress

The observational period was characterized by low wind speeds. The wind stress, calculated from the bulk formulas with a drag coefficient of 1.4×10^{-3}, has a mean value of 0.66 dyn cm^{-2} (10 dyn cm^{-2} = 1 Pa). For one 3-day period the wind stress is considerably less than 0.5 dyn cm^{-2}. From Fig. 2 it is evident that only two periods of relatively high winds occurred during the experiment: one near the center of the experiment with a maximum wind stress of 2.7 dyn cm^{-2} and the other at the end of the experiment with a maximum wind stress of 3.3 dyn cm^{-2}.

b. Surface heat flux

The net all-wave and longwave radiative fluxes were measured with a Swissteco Pty. Ltd. MS-1 net radiometer and a Middleton Instruments net longwave radiometer, respectively. The net all-wave radiative flux includes radiation in the bandwidth 0.3–60.0 μm. The net solar flux was measured with Eppley radiometers. The latent and sensible heat fluxes were determined from standard meteorological observations, using the bulk formulas and a drag coefficient of 1.4×10^{-3}. The total heat flux Q_T was computed from these observations. The sea surface temperature was constructed by extrapolating the 1 m temperature values, measured with the STD, to the surface. Hourly values (shown in Fig. 2) of these surface variables were obtained by interpolating between observations with a cubic spline.

The net all-wave flux dominated the surface heat balance for most of the experiment. However, midway through the experiment enhanced surface cooling occurred. An increase in wind speed during this period resulted in a large latent heat transfer. The sensible heat flux never exceeded ± 2.0 mW cm^{-2} (1 mW cm^{-2} = 10 W m^{-2}) and typically was less than ± 1.0 mW cm^{-2}. Friehe and Schmitt (1974) computed average values of the latent and sensible heat fluxes for the 17 days of observations. They found that the sensible heat flux was two orders of magnitude less than the latent heat flux for this period. They report an average Bowen ratio of 0.013, substantially less than the commonly used value of 0.1.

TABLE 1. Daily heat flux budgets for the POLE experiment computed symmetrically about local solar noon. All units are in mW cm^{-2} and represent average values over a 24 h period. Heat gain by the ocean is assumed positive.

Date February 1974	Total heat flux	Radiative heat flux	Turbulent heat flux
3	−1.1	5.1	−6.2
4	6.3	7.0	−0.7
5	6.1	6.7	−0.6
6	−0.5	5.1	−5.6
7	−8.9	7.6	−16.5
8	−2.3	6.3	−8.6
9	2.2	4.0	−1.8
10	3.3	4.4	−1.1
11	2.4	5.7	−3.3
12	2.3	4.5	−2.2

A daily heat budget is given in Table 1. Heat gain by the ocean is taken positive. Daily flux values were calculated as a centered average about local solar noon (time zone W).[2] These results indicated that the ocean gained heat for six days, was in near-thermal equilibrium with the atmosphere for two days, and lost heat for two days. These results, coupled with the observed low wind stress, indicate that upper ocean dynamics might have been dominated by net surface heating for a part of the experiment.

[2] W time = GMT − 10 h.

c. *Mass and buoyancy flux*

Only one period of intense precipitation occurred during the experiment. Overall, evaporation and precipitation were in near equilibrium, with precipitation exceeding evaporation by 23 mg cm^{-2}.

At the surface the buoyancy flux M_0 is determined by air-sea transfer (Dorrestein, 1979)

$$M_0 = g\rho^{-1}[\beta Q_T c_p^{-1} + \kappa S(R - E) - \beta \Delta T R], \quad (4.1)$$

where g is the acceleration due to gravity, ρ the density of seawater, β the thermal coefficient of expansion for seawater, Q_T the total heat flux at the surface, c_p the specific heat of seawater at constant pressure, κ the saline coefficient of contraction, S the surface salinity, E and R are the evaporation and precipitation rates, respectively, and ΔT is the difference in temperature between the precipitated water and the surface water. Mass gain by the ocean is positive. Hourly values of the surface temperature, salinity and density are shown in Fig. 2. These time series show the expected diurnal variation associated with daytime heating and nighttime cooling. Overall, the mass flux at the interface had little influence on the buoyancy flux, except possibly during one brief period of precipitation which occurred near midnight on 5 February

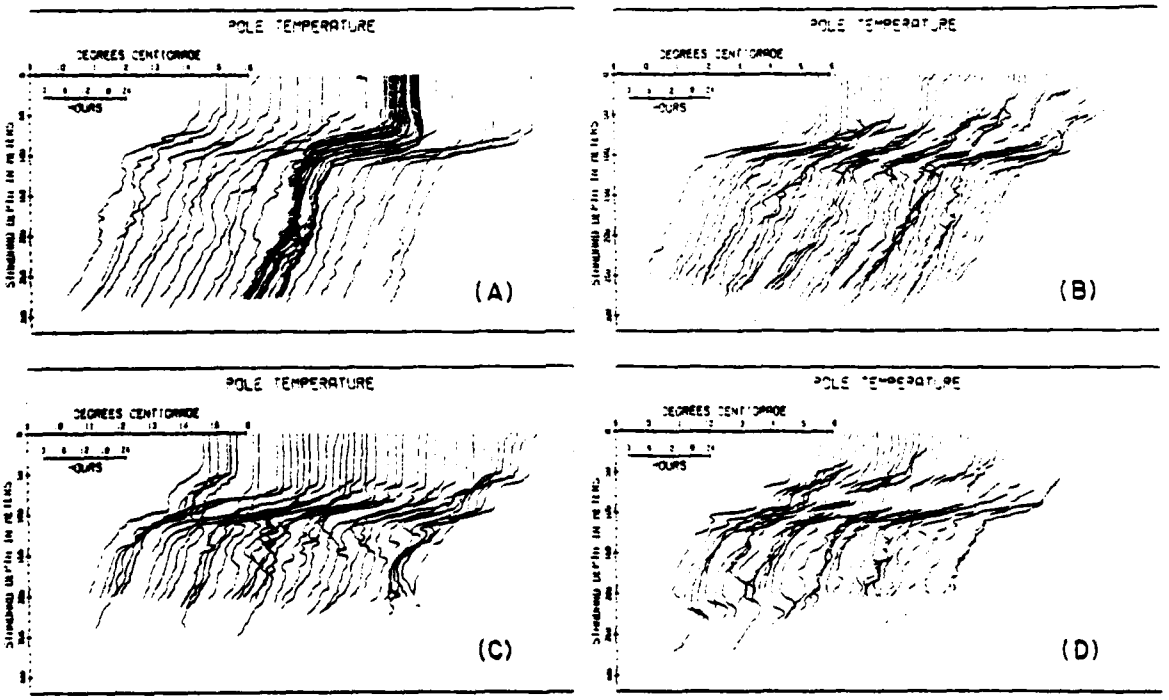

FIG. 4. Profiles of temperature taken during the experimental period. The spacing between adjacent profiles is proportional to the time difference between hydrocasts.

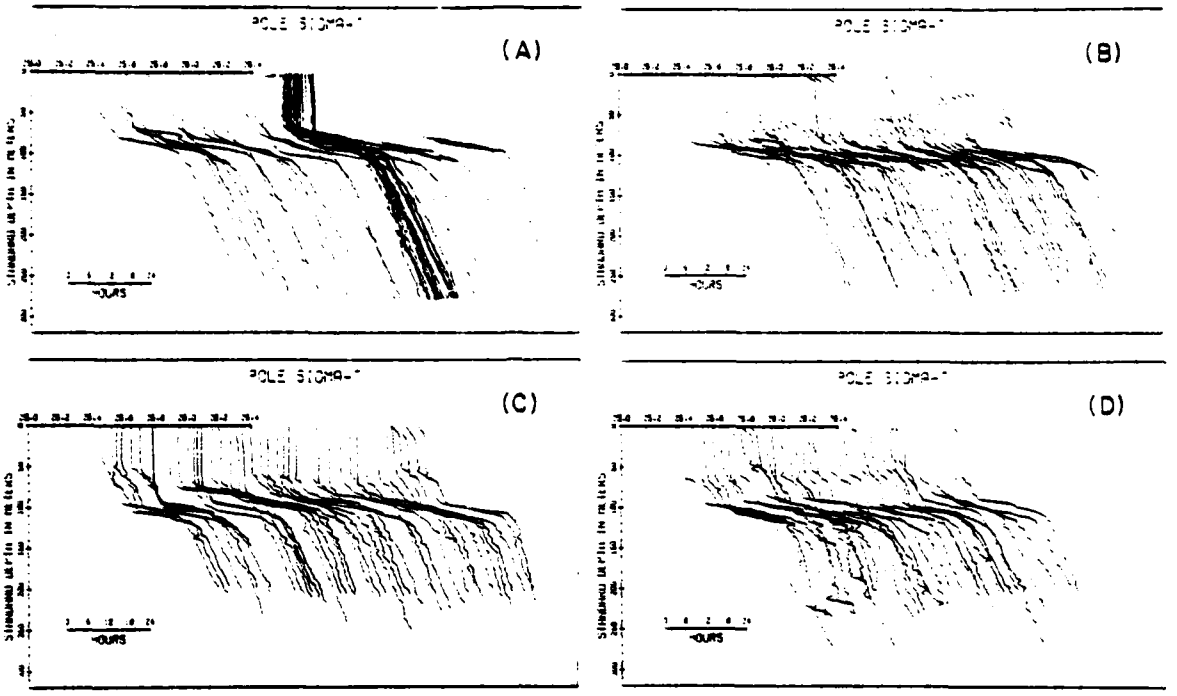

FIG. 5. Profiles of σ_t taken during the experimental period. The spacing between adjacent profiles is proportional to the time difference between hydrocasts.

(Simpson, 1977). The net heat flux at the surface dominated the buoyancy flux throughout the experiment.

5. The surface layer

Profiles of temperature and σ_t for the entire experiment are shown in Figs. 4 and 5, respectively. The spacing between adjacent profiles is proportional to the time interval between measurements. The seasonal thermocline is at a depth of ~100 m. However, for large periods of time the layer above the seasonal thermocline is far from well mixed. Temperature inversions are frequently seen at the base of the mixed layer. These inversions are compensated by observed salinity maxima so that the density profile is stable. Steplike structure and multiple isothermal layers frequently form in the surface layer during periods of low winds and net heat gain at the surface. During subsequent, though brief, periods of high winds these features are eroded quickly. Comparison of the temperature and σ_t profiles indicates that the density structure was determined principally by temperature.

The well-mixed layer usually consists of the upper 10 to 100 m of the ocean, is characterized by nearly uniform density structure, and responds directly to atmospheric forcing for time scales greater than an hour. The mixed-layer depth, shown in Fig. 2, is defined as the shallowest depth at which the density is not more than 0.02 σ_t units less than the density at a depth of 5 m. Diurnal variations in mixed-layer depth resulting from local surface processes are evident. The low wind speeds and positive total heat fluxes, which characterized the POLE Experiment, favored the formation of warm shallow surface layers of nearly uniform density, shown in Fig. 4. Such features persisted until periods of sustained high winds occurred, whereupon the depth of the mixed layer was reestablished between 50 and 60 m.

The only significant departures from this pattern occurred midway into and at the end of the experiment. The period 6–8 February is marked by intermittently high wind stress (frequently >2.5 dyn cm^{-2}) and enhanced evaporative and net longwave heat fluxes. These processes combined to produce the period of sustained deepening shown. Initially, high wind stress ($\tau = 2.9$ dyn cm^{-2}) resulted in a period of rapid deepening during the 15 h interval beginning 200 h after the initiation of observations. A subsequent quiescent period ($\tau \leq 0.5$ dyn cm^{-2}) allowed for the quick reestablishment of a warm, light surface layer. During the interval 230–270 h into the experiment, sustained winds again occurred ($\tau > 2.0$ dyn cm^{-2}) and the rapid and sustained deepening shown in Fig. 2 followed.

Contours of σ_t for the observational period are shown in Fig. 6. The scale at the base of the figure

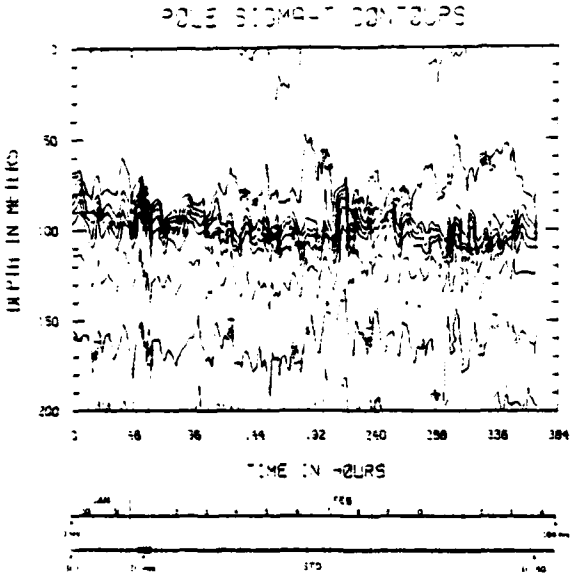

FIG. 6. The isopycnal distribution observed during POLE. The contour interval is 0.1 σ_t units. The σ_t surfaces show strong semi-diurnal variation in vertical amplitude about their mean position.

indicates the time at which a given STD profile was made. Convergence of the isopycnals between 50 and 80 m occurs during periods of high winds. The isotherms behave in a similar fashion. This feature is absent in the isohaline contours (Simpson, 1977), suggesting that the temporal variations in the density structure of the upper 100 m are due primarily to thermal processes.

During periods of calm winds, a warm surface layer, corresponding to the 25.4 isopycnal, formed rapidly. Thus, for part of the observational period the ocean gained heat due to surface processes, acting on diurnal time scales or longer, and intermittently took on some of the characteristics of a summertime well-mixed layer. These observations are consistent with those of Barnett (1976), who found that the total heat content down to a depth of 300 m along a 170°W section at approximately 30°N was slightly greater in February than in January.

6. The subsurface layer

Time series of depth for selected σ_t surfaces occurring at a depth below 60 m are shown in Fig. 7. All the time series show a strong semi-diurnal variation in vertical amplitude about their mean position. These time series correspond to σ_t surfaces of 25.6, 25.9, 26.0 and 26.1 and occur at mean depths of 92.1, 106.3, 124.7 and 163.2 m, respectively. The first four central moments for each time series are given in Table 2. The upper three σ_t surfaces all have a positive skewness ranging from 0.43 (σ_t = 25.6) to 0.33 (σ_t = 26.0). Only the deepest surface (σ_t = 26.1) has a slightly negative skewness, $s = -0.04$. The positive skewness of these records suggests they are similar to surface gravity waves.

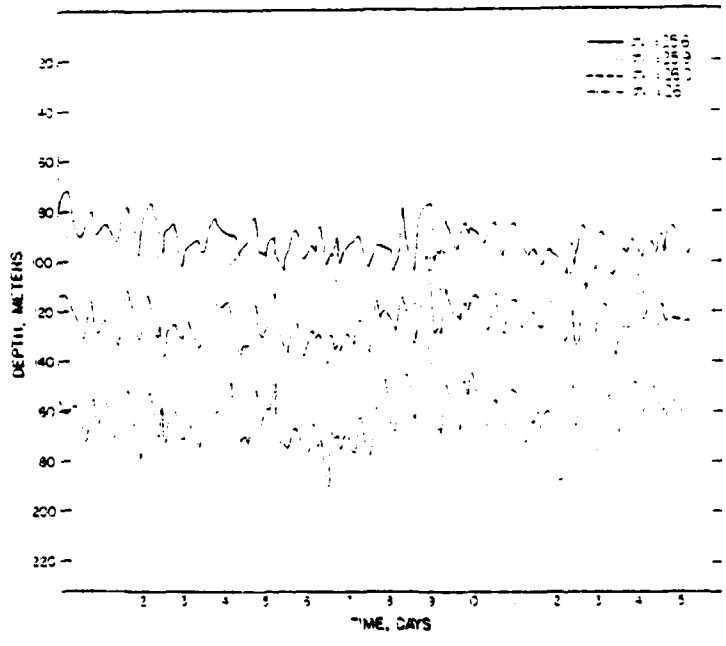

FIG. 7. Time series of depth of four σ_t surfaces occurring below 60 m. The time series correspond to the 25.6, 25.9, 26.0 and 26.1 σ_t surfaces at mean depths of 92.1, 106.3, 124.7 and 163.2 m, respectively.

TABLE 2. Statistical parameters for the σ_t surfaces shown in Fig. 7. The skewness S and kurtosis K are normalized by σ^3 and σ^4, respectively, where σ is the standard deviation.

σ_t	Mean depth (m)	Standard deviation (m)	S	K
25.6	92.1	6.9	.43	2.97
25.9	106.8	6.6	.46	3.05
26.0	124.7	6.9	.33	3.35
26.1	163.2	9.4	−.04	3.39

The kurtosis is close to 3 for all of the records suggesting the variations in amplitude of a given surface are nearly normally distributed. However, the kurtosis increases with depth, reaching a maximum value of 3.39 (σ_t = 26.1). This suggests that progressively deeper surfaces are less well-approximated by a normal distribution.

The autocorrelation function of a signal $u(t)$ having zero mean is

$$\Phi(\tau') = \frac{\overline{u(t)u(t')}}{\overline{u^2}}, \qquad (6.1)$$

where the time difference $\tau' = t' - t$. It provides a measure of the time interval over which $u(t)$ is correlated with itself. Autocorrelations for the four σ_t surfaces are shown in Fig. 8. The unit of lag is 14.36 min, and the length of the series is 15.5 days. Several features are evident from these autocorrelations. The autocorrelation function, characteristic of turbulent processes, is well damped, may become slightly negative after a few lags and then rapidly approaches zero. This insures that the integral scale for the turbulent process is small. By contrast, the autocorrelation function for each of the σ_t surfaces in Fig. 7 shows an oscillatory behavior, remaining highly coherent for a period of 2 days or longer. The oscillatory pattern shown in Fig. 8 has a period of 12.7 h. This period is not statistically significantly different from the semidiurnal M2 tidal period of 12.4 h (Defant, 1961). This suggests the presence of a semi-diurnal internal tide.

A frequency spectrum for each of the four σ_t surfaces is shown in Fig. 9. Most of the variance occurs at periods corresponding to the semidiurnal period or longer. Considerable energy occurs at the inertial period: for a latitude of 35° the inertial period T_p corresponds to 20.8 h. For periods less than the semidiurnal period, the spectrum falls off rapidly.

Phase and coherence spectral estimates were calculated for the various combinations of σ_t surfaces. These spectra are shown in Figs. 10 and 11, respectively. The values of the coherence and phase at the frequency corresponding to the peak in the coherence spectrum for each pair are given in Table 3. The peak in the coherence spectrum corresponds to a period of 11.5 h, close to the M2 semi-diurnal tidal period. The length of the time series prevents finer spectral resolution of the frequency scale. The coherence among all pairs is high, ranging from a maximum value of 0.97 for both the 25.6–25.9 and 25.9–26.0 pairs to a low of 0.91 for the 25.6–26.0 pair. The coherence between pairs of σ_t surfaces is shown as a function of the mean separation between surfaces in Fig. 12.

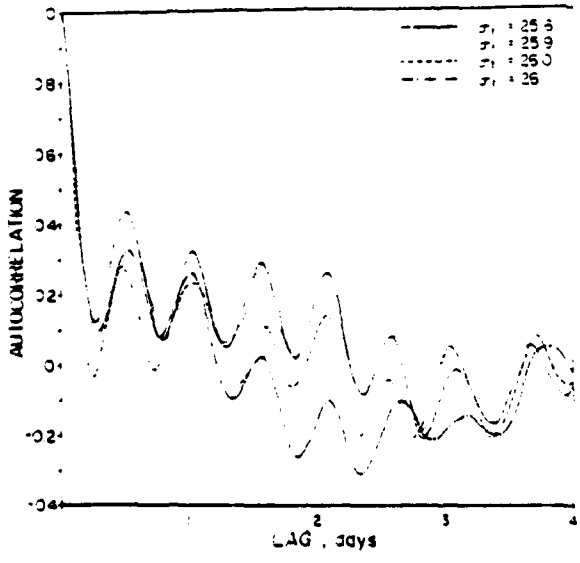

FIG. 8. Autocorrelation functions for the σ_t surfaces observed during POLE. The unit of lag is 14.36 min and the length of the series is 15.5 days. The period of the oscillation is 12.68 h, close to that of the semi-diurnal M2 tide, 12.42 h.

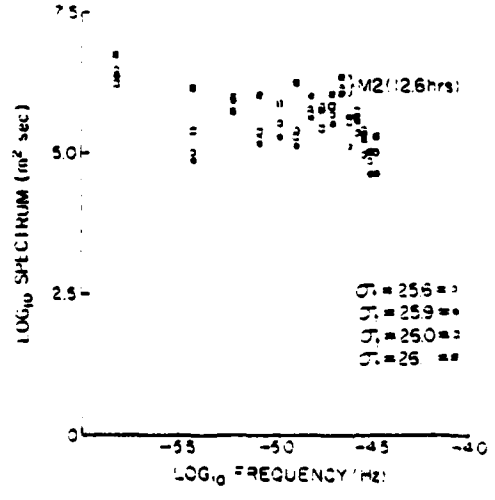

FIG. 9. Individual spectra for the four σ_t surfaces. The semi-diurnal spectral peak occurs at 12.6 h. For periods below the semi-diurnal, the spectra fall off rapidly.

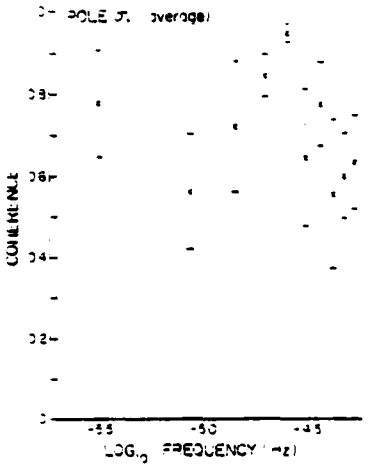

FIG. 10. Average coherence spectrum for the various combinations of σ_t surfaces. The error estimate is one standard deviation of the four band-averaged coherence spectra about the mean. A high coherence ($0.91 \leq COH \leq 0.97$) at the peak in the spectrum occurs for all pairs.

The coherence between a given σ_t surface and deeper-lying surfaces decreases slowly with the mean separation between surfaces. An estimate of the vertical wavelength λ_z of the semi-diurnal internal tide can be calculated from the coherence vs mean separation data by fitting the data to different types of curves. A parabolic least-squares fit of coherence as a function of mean separation between σ_t surfaces, forced through the point (0,1.0) suggests that an approximate length scale at which the coherence falls to zero is 170 m. Since this zero crossing corresponds to one-fourth the vertical wavelength, the estimate of λ_z obtained from the parabolic fit is 0.7 km. The uncertainty in this length scale is high. Data at depths >200 m were not routinely taken, hence the shape of the curve of the coherence vs mean separation is uncertain. The assumed parabolic dependence may be unrealistic. The same data fit to a cosine curve forced through the point (0,1.0) has a zero crossing at 180 m corresponding to a quarter-wavelength. This fit suggests that an estimate of the vertical wavelength is $\lambda_z \approx 0.7$ km, which is the same as the previous estimate. Parabolic and cosine fits without forcing the curves through the point (0,1.0) yielded estimates of $\lambda_z = 0.9$ and 1.2 km, respectively. For the calculations that follow a value of $\lambda_z \approx 1$ km is assumed. The vertical wavelength is approximately equal to one-third the total depth, implying third-order modal dynamics dominate the signal.

TABLE 3. Coherence and phase estimators for the σ_t surfaces shown in Fig. 7. Values correspond to the frequency at the peak in the coherence spectrum, 11.5° h.

σ_{t1}/σ_{t2}	Mean separation (m)	Coherence	Phase
25.6/25.9	16.8	0.97	−8
25.6/26.0	32.6	0.95	−3
25.6/26.1	71.1	0.91	−25
25.9/26.0	17.9	0.97	−11
25.9/26.1	56.4	0.93	−33
26.0/26.1	38.5	0.93	−22

The phase estimators between different σ_t surfaces, corresponding to the frequency of the peak in the coherence spectrum, are shown in Fig. 13 as a function of the mean separation between surfaces. The figure suggests that for a given σ_t surface, deeper lying surfaces lag the given surface by an amount dependent on the mean separation between surfaces. The only exception is the 25.6–25.9 pair for which the 25.9 surface leads the 25.6 surface by 8°. The data suggests that the phase difference increases with separation at the approximate rate of −35° (100 m)$^{-1}$. This value yields an estimate of the vertical wavelength $\lambda_z = 1.2$ km which is consistent with our previous estimate. Deeper lying surfaces lagging shallower surfaces is consistent with upward energy propagation (e.g., Turner, 1973).

The dispersion relation for an internal wave under the assumption of a linear density gradient and the Boussinesq approximation (Turner, 1973) is

$$\omega = N\left(\frac{k^2}{k^2 + m^2}\right)^{1/2}. \qquad (6.2)$$

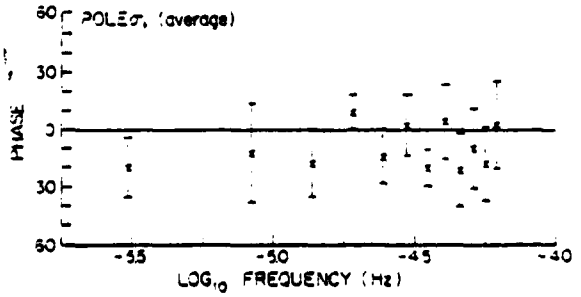

FIG. 11. Average phase spectrum for the various combinations of surfaces. The error estimate is one standard deviation of the four band-averaged phase spectra about the mean.

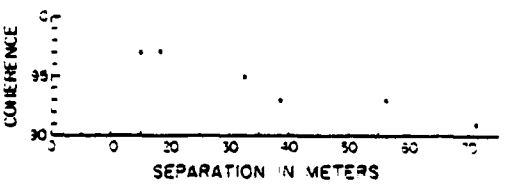

FIG. 12. Coherence as a function of mean separation between σ_t surfaces. An estimate of the vertical wavelength from the coherence vs depth data is $\lambda_z \approx 1$ km.

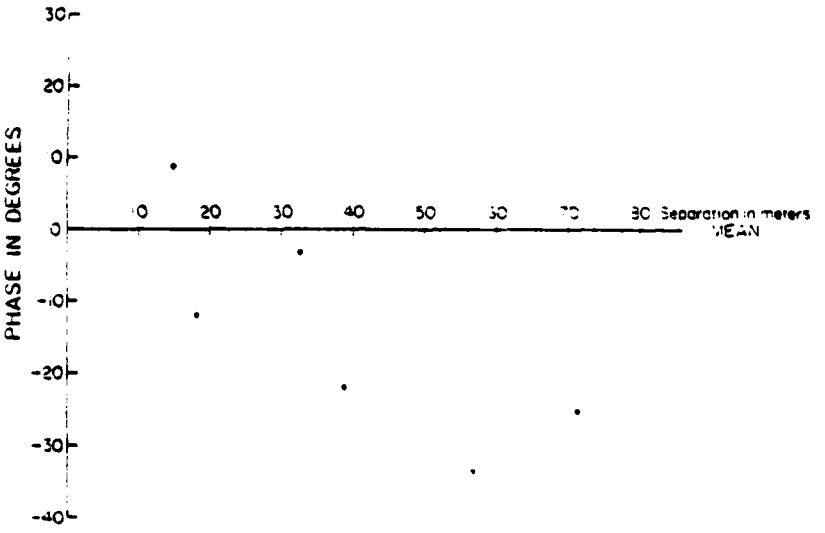

FIG. 13. The phase estimator at the frequency corresponding to the peak in the coherence spectrum as a function of the mean separation between σ_t surfaces. The data suggest that the phase difference between surfaces increases with the mean separation between surfaces at the approximate rate of -3° (100 m)$^{-1}$.

where ω is the wave frequency, N the buoyancy frequency and k and m are the vertical and horizontal wavenumbers, respectively. The buoyancy frequency was determined from the observed density using the relation

$$N = \frac{g}{\bar{\rho}} \left| \frac{\partial \rho}{\partial z} \right|^{1/2}. \tag{6.3}$$

where g is the acceleration due to gravity, $\bar{\rho}$ the mean density and $\partial\rho/\partial z$ the observed vertical gradient of density. The buoyancy frequency at a depth of 145 m was calculated from the mean depths of the $\sigma_t = 26.0$ and $\sigma_t = 26.1$ surfaces. The mean separation between these surfaces is $\Delta z = 38.5$ m and the density difference is $\Delta\rho = 0.1 \times 10^{-3}$ g cm^{-3}. Thus, the buoyancy frequency is 2.9 cycles h^{-1}. The buoyancy frequency is the upper limit of frequency for which internal wave motions can exist in a stratified fluid. For low-frequency motions $k^2 \ll m^2$ and the dispersion relation simplifies. With $\omega = 1/12$ cph, $N = 3$ cph and $m = 1$ km^{-1} an estimate of the horizontal wavelength is $\lambda_h \approx 36$ km. For $N = 2.5$ cph, the horizontal wavelength is $\lambda_h \approx 30$ km. In making these estimates of the horizontal wavelength a value of the buoyancy frequency at shallow depth (145 m) was used since STD casts were not taken routinely at great depths. The buoyancy frequency may be smaller further down, say at 500 m, and a deeper value of N may be more appropriate since the vertical wavelength $\lambda_v \approx 1$ km. In the dispersion relation [Eq. (6.2)] effects of rotation were neglected. However, such effects would decrease the estimate of λ_h by no more than 20%.

Observations of the semi-diurnal internal tide in the central Pacific (42°N, 158°W) have been reported by Barnett and Bernstein (1975). Their observations suggest that the vertical displacement of isotherms is between 5 and 10 m, in good agreement with the presently reported results. The validity of Barnett and Bernstein's use of isotherms as a tracer of vertical water movement is degraded by the presence of weak temperature gradients and temperature inversions which frequently occurred in their data at the 100 m level. If one ignores the data at the 100 m level, the coherence between the 75 and 150 m levels is 0.84 and between the 50 and 150 m levels is 0.76 with phase shifts of $-4°$ and $-13°$, respectively. These values of coherence, while smaller than those presently reported, are in good qualitative agreement with our observations. The coherence between isotherms might be expected to be less than that between isopycnals because density is a better tracer of water motion than is temperature. The phase estimates of Barnett and Bernstein agree in sign and approximate magnitude with the observations reported here. Both sets of observations suggest that deeper-lying surfaces lag a given surface by an amount dependent on the mean separation between surfaces. This result is consistent with an interpretation of upward propagation of energy.

One may make an estimate of the horizontal wavelength of the semi-diurnal internal tide based on the phase difference between the moorings reported in Barnett and Bernstein (1975). They observed a coherence of 0.7 and a phase difference of 57° between temperature signals measured from two moorings

5.2 km apart. If one assumes that the wave crests were oriented perpendicular to the line between moorings, an estimate of the horizontal wavelength $\lambda_h = 33$ km is obtained $[(360/57) \times 5.2]$. If, however, the wave crests were oriented at some angle θ to the line between moorings, the estimate of λ_h would be reduced. If it is assumed that waves from any direction are equally probable, then the estimate of 33 km must be multiplied by the absolute magnitude of $\sin\theta$ averaged over the interval $[0, \pi/2]$. Under this assumption $\lambda_h = 21$ km. These estimates are in fair agreement with values of λ_h determined from our measurements and Eq. (6.2). Barnett and Bernstein found no significant coherence between moorings separated by distances of 50 km or more. This result is consistent with all the estimates of λ_h reported in this work and supports third-order modal dominance of the observed internal tide. There were no moorings for separation distances in the range 5.2–50 km.

Hendry (1977) has reported an analysis of the semi-diurnal tide based on observations in the North Atlantic during the Mid-Ocean Dynamics Experiment. He finds that the first baroclinic mode is dominant in the internal semi-diurnal tide. The calculated and observed horizontal wavelengths corresponding to the first mode are 160 km. The internal tide appears to be generated near the Blake Escarpment 700 km from the observational area. Our results and those of Barnett and Bernstein (1975) appear to be inconsistent with Hendry's. However, given the uniqueness of the Blake Escarpment, the generation and characteristics of internal tides observed in the central North Pacific may be quite different from those observed by Hendry.

Additional reports of open ocean measurements of the internal tide are comparatively rare in the literature (Wunsch, 1975). The amplitude of the semi-diurnal internal tide observed during POLE is about 10 m. This value agrees well with similar observations off the California continental shelf (Lee, 1961; Reid, 1956; Summers and Emery, 1963). Mid-Atlantic observations (Seiwell, 1942) show much smaller semi-diurnal internal wave amplitudes, as small as 2.2 m. Observations by Weston and Reay (1969) made during southwest approaches to Britain have amplitudes 5–6 m higher than those presently reported. More observations are required before an adequate description of the semi-diurnal internal tide can be made.

7. Comparison with theory

The local response of the well-mixed layer to a transient wind stress is discussed theoretically by Pollard *et al.* (1973). The PRT model predicts that, after one-half pendulum day, deepening is arrested at a depth h_{max} given by

$$h_{max} \approx \frac{2^{3/4} U_*}{(Nf)^{1/2}}, \tag{7.1}$$

where U_* is the friction velocity, f the Coriolis parameter and N the buoyancy frequency of the stably stratified fluid below the well-mixed layer, not including the step in stratification at the base. The mixed-layer depths observed during POLE are typically two to three times greater than those predicted by the PRT model. This suggests that entrainment at the base of the mixed layer, due to the shear of the mean flow, was insignificant during the POLE Experiment. This result is consistent with velocity measurements made during the experiment (Davis *et al.*, 1978). They found that, at frequencies below 0.05 Hz, the currents at all levels above 135 m were highly coherent, nearly parallel and of similar magnitude. The velocity measurements imply little shear available to erode the base of the mixed layer as required by the PRT model.

Niiler (1975) suggests that for steady, positive, surface heating and wind stress, deepening is arrested at a depth

$$h_{max} \approx 2m_0 \left(\frac{\tau_0}{\rho_0}\right)^{3/2} \rho_0 c_p \beta g Q_0, \tag{7.2}$$

where Q_0 is the surface heat flux, c_p the specific heat of sea water, β the thermal coefficient of expansion of sea water and g the acceleration due to gravity. The constant m_0 is related to the Kraus-turner constant m through the relation $m = (c_{10}\rho_a/\rho_0)^{1/2} m_0$, where c_{10} is the drag coefficient at 10 m, ρ_a and ρ_0 are the densities of air and water, respectively. For values of Q_0 greater than a few mW cm^{-2}, the predicted values of h_{max}, with $m = 0.0012$, underestimate the observed mixed-layer depths by about a factor of 2. This implies the assumed value of m is too small by a similar factor.

The theory of the seasonal thermocline advanced by Kraus and Turner (1967) assumes that the turbulent energy available for mixing is some constant fraction m of the downward transfer of energy from the local wind field. Through entrainment, this energy is used to raise the potential energy of the water column. Since the salinity did not contribute significantly to the observed density structure during POLE, the potential energy may be calculated by the method of Turner (1969). A mixing event 370 h into the experiment was chosen since it was least likely to be affected by horizontal advection. Analysis for this event yields a value of $m = 0.0017$, in fair agreement with the value $m = 0.0012$ observed by Denman (1973a,b).

Considerable disagreement exists in the reported values of m. Perhaps m is not a constant but rather a function of local oceanic conditions. The possibility of high-energy inertial oscillations in the

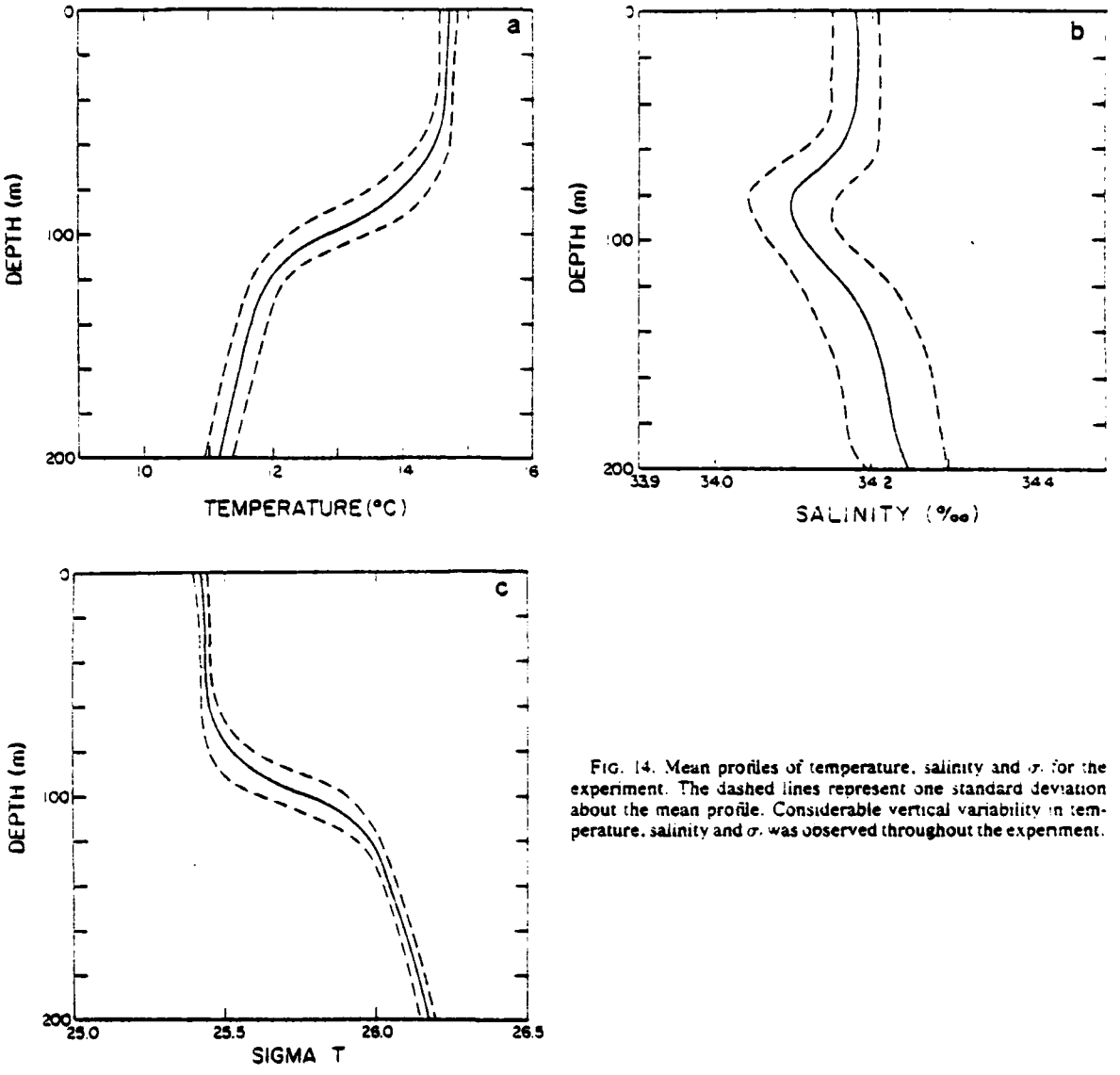

FIG. 14. Mean profiles of temperature, salinity and σ_t for the experiment. The dashed lines represent one standard deviation about the mean profile. Considerable vertical variability in temperature, salinity and σ_t was observed throughout the experiment.

mixed layer at the time of observations reported by Turner (1969) may partially explain the order-of-magnitude discrepancy in the reported values of m.

8. Advection

Mean profiles of temperature, salinity and σ_t, based on all the STD casts taken during the experiment, are shown in Fig. 14. Departures from the mean, calculated as one standard deviation from the mean, are represented by the dashed lines in the figure. The data suggest that considerable variation occurred in the vertical distribution of temperature, salinity and density observed during the experiment. A mean T-S diagram for the upper 200 m, together with standard deviation, is shown in Fig. 15. Several features are immediately evident from these figures. The high temperature and salinity of the surface waters are representative of the Eastern North Pacific Central Water characteristically found near 35°N. This water mass must be distinguished from the larger Western North Pacific Central Water mass. (Sverdrup *et al.*, 1942). The shallow salinity minimum in the figure is characteristic of the eastern North Pacific (Reid, 1973; Kenyon, 1978) and extends southward to the equator. This salinity minimum should be distinguished from the minimum associated with North Pacific Intermediate Water which occurs at greater depths. This Intermediate Water is present below the

central water masses all over the North Pacific. Below the Intermediate Water, the salinity increases regularly. Here Pacific Common Water is found.

Individual hydrocasts taken throughout the experiment are shown in Fig. 16. They show the frequent presence of salinity-compensated temperature inversions at the base of the upper layer and suggest that horizontal advection, variable with depth, is relevant to a complete understanding of the observed structure. The salinity maxima shown in the figure can be associated with the Subtropical Water Mass formed in the trade winds region northeast of the Hawaiian Island Chain where the flux of latent heat typically exceeds 9.8 mW cm^{-2} over a 24 h period (Wyrtki, 1965). The intermittent lateral interleaving of this water mass is characteristic of observations made during the POLE Experiment and may partially explain the failure of one-dimensional mixed-layer deepening theories to properly model the observed mixed-layer depths and surface temperatures.

An estimate of the horizontal temperature gradient can be made from the vertically integrated conservation of heat equation

$$\frac{\partial H}{\partial t} + \nabla\cdot(UH) - \nabla\cdot(\nabla AH) = Q, \qquad (8.1)$$

where $\partial H/\partial t$ is the local rate of change of heat content H, $\nabla\cdot(UH)$ is the horizontal divergence of the heat flux, due to advective processes associated with ocean current U, $\nabla\cdot(\nabla AH)$ is the divergence of heat flux, both horizontal and vertical, associated with mixing processes, characterized by an Austauch coefficient A, and Q is the total heat flux due to turbulent and radiative transfer processes at the air-sea interface.

Vertical motions at the base of the vertically integrated layer are neglected. Mixing processes of the form $\nabla\cdot(\nabla AH)$ may reasonably be neglected for time scales of a few hours. The air-sea heat exchange processes were measured directly and the local change in heat content was calculated from the observed temperature profiles. The second term in Eq. (8.1) was calculated as the residual of the remaining terms. Current meter observations (Davis *et al.*, 1978) suggest typical velocities past *Flip* (i.e., relative currents) are of the order 1 to 10 cm s^{-1}. These results lead to temperature gradients of the order ±0.1 to ±0.01°C km^{-1}.

Errors associated with the total surface heat flux are about ±10%. The vertically integrated changes in heat content are within the stated accuracies of the observed temperature profiles (±5%). The most serious error in the estimate of the horizontal temperature gradient may be the neglect of vertical advection at the base of the vertically integrated layer. These errors, coupled with errors in the current meter observations, suggest that the above estimate of horizontal temperature gradient is accurate only to within an order of magnitude.

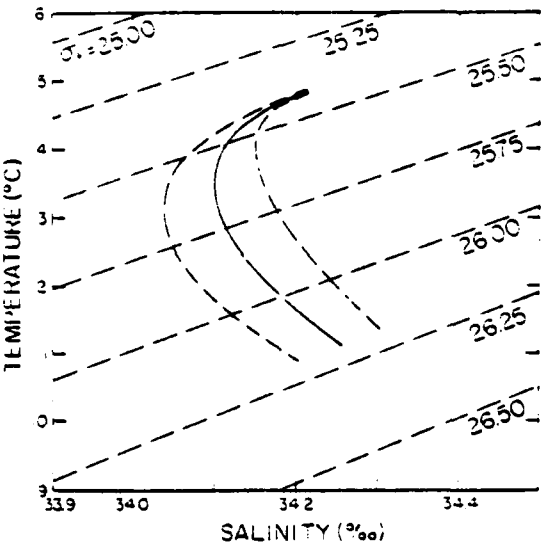

FIG. 15. A mean *T-S* diagram, constructed from all the profiles. The dashed line represents one standard deviation about the mean. The eastern North Pacific Central Water is evidenced by the high temperatures and salinities of the surface layer. The shallow salinity minimum is characteristic of the eastern North Pacific and should be distinguished from the salinity minimum associated with North Pacific Intermediate Water which occurs at greater depth.

Our estimates of horizontal temperature gradients can be compared with the analysis of XBT, AXBT and STD observations during POLE by Barnett *et al.* (1977). They found that the average near-surface (0–50 m) horizontal temperature gradient over a region 400 km in diameter was 0.005 °C km^{-1}. Superimposed on the mean field were fluctuations having a standard deviation of 0.4 °C about the mean. Approximately half of the variability was associated with horizontal scales of less than 50 km. Taking 0.2°C (25 km)$^{-1}$ = 0.008°C km^{-1} we obtain an estimate of the characteristic temperature gradient associated with small-scale variability. When this gradient is added to the mean gradient, the estimate of local gradients falls within the range we estimated from our observations.

9. Conclusion

Analysis of 15 days of intensive STD profiling from *R/P Flip* as part of the NORPAX POLE Experiment yields the following results:

1) Autocorrelations for the time series of depth of several σ_t surfaces confirm the presence of a semi-diurnal internal tide in the observed records.

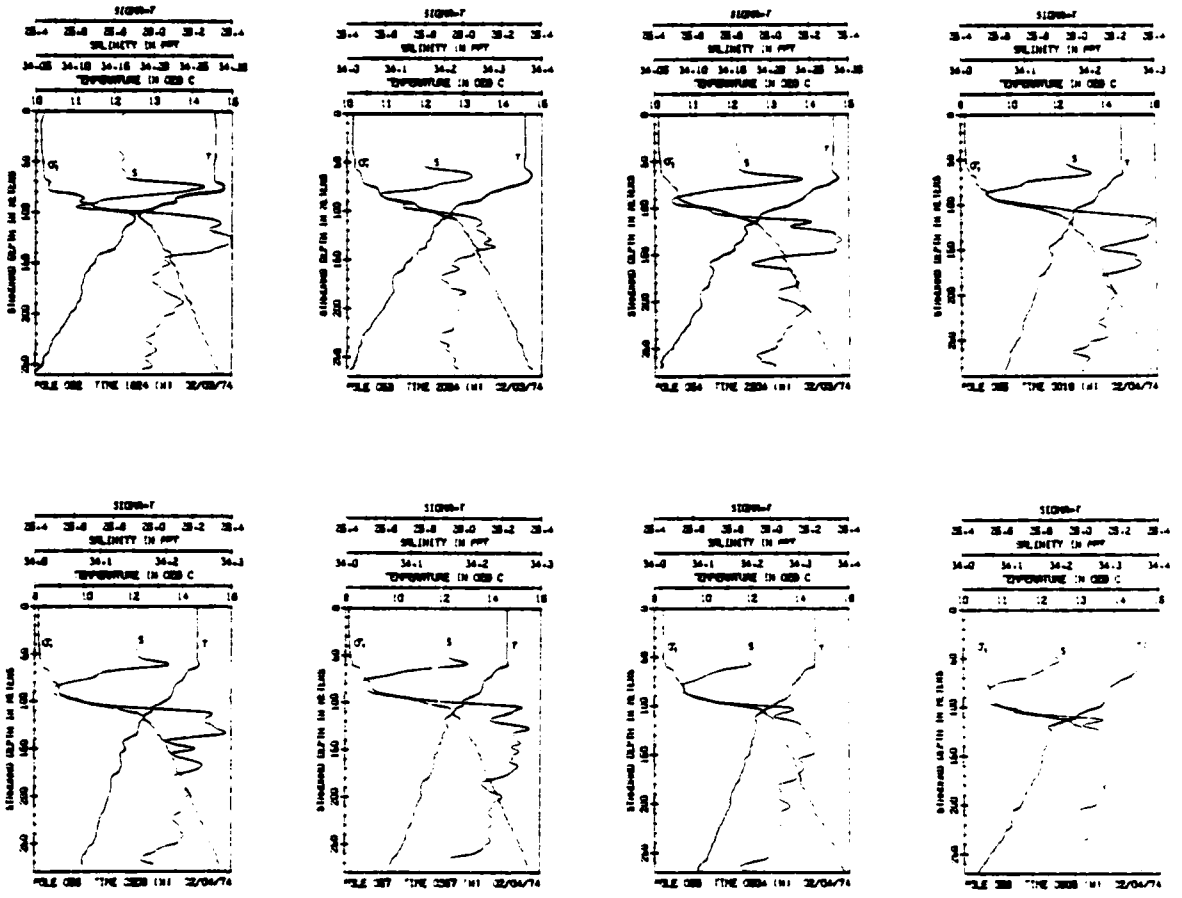

FIG. 16. Individual profiles of temperature, salinity and σ_t taken during the experiment. The salinity maxima frequently occurring at depth suggests horizontal advection of the Subtropical Water mass formed in the evaporative basin northeast of Hawaii.

The period of 12.7 h determined from the autocorrelation analysis is not statistically significantly different from the 12.4 h period of the M2 semi-diurnal tide.

2) The amplitude of the semi-diurnal internal tide is about 10 m and agrees with other observations in the Pacific.

3) The coherence between all pairs of time series of the depth of σ_t surfaces is high, ranging from 0.97 to 0.91. The peak in the coherence spectrum corresponds to a period of 11.6 h, close to the M2 semi-diurnal tidal period. Energy from the semi-diurnal tide is smeared into the next highest frequency band. The limited length of the records prevents finer spectral resolution in the frequency domain.

4) The coherence between a given σ_t surface and deeper lying surfaces decreases slowly with the mean separation between surface. An estimate of the vertical wavelength λ_z of the semi-diurnal internal tide obtained from the coherence vs mean separation data is 1 km.

5) The vertical coherence scale suggests that most of the energy of the semi-diurnal tide is in the third-order modes.

6) For a given σ_t surface, deeper-lying surfaces lag the given surface in time by an amount dependent on the mean separation between surfaces. The data suggest that the phase difference increases with separation at the approximate rate of $-35°\,(100\text{ m})^{-1}$. Deeper lying surfaces lagging shallower surfaces is consistent with the suggestion that energy is being propagated vertically upward. An estimate of the vertical wavelength λ_z from the phase data is 1.2 km.

7) An estimate of the horizontal wavelength of the semi-diurnal internal tide calculated from the measured buoyancy frequency and the dispersion relation for internal waves under the assumptions of a linear density gradient and the Boussinesq approximation is $30 \leq \lambda_h \leq 35$ km. Affects of rotation were neglected but can effect the estimate by no more than 20%.

8) The observations of the semi-diurnal internal tide presently reported are consistent with those re-

ported by Barnett and Bernstein (1975) based on temperature observations made from moorings in the central North Pacific. Our results and those of Barnett and Bernstein (1975) appear to be inconsistent with those of Hendry (1977).

9) One-dimensional mixed-layer deepening models failed to predict the mixed-layer depths and temperatures observed during POLE. Horizontal advection, as evidenced from the salinity maximum frequently occurring at the bottom of the mixed layer and other near-surface changes in salinity and temperature unassociated with local surface forcing, are responsible for the failure.

10) For the one mixing event in which the possible effects of horizontal advection could be ignored, a value of the mixing energy-flux coefficient $m = 0.0017$ was obtained. This is in fair agreement with the value of 0.0012 reported by Denman.

11) Estimates of the local temperature gradient calculated as the residual in the conservation of heat equation from measurements of the surface heat flux and vertical temperature structure are within the range $0.1-0.01°C\ km^{-1}$. These values are consistent with similar estimates made by Barnett *et al.* (1977) using XBT, ABXT and STD observations.

Acknowledgments. This research was supported by the Office of Naval Research through Contract N0014-76-C-0067 under project NR 083-102. The cooperation of the officers and crew of the *R/P Flip* and the assistance of Alan Lillich in the analysis is gratefully acknowledged. Some of the computations were carried out at the computer facility of the National Center for Atmospheric Research which is sponsored by the National Science Foundation. The authors wish to thank Dr. R. A. de Szoeke for his helpful comments during the preparation of the manuscript. The constructive suggestions of the two anonymous reviewers and the typing skills of Sue Watt, Ruth Ebey and Ruth Hill are gratefully acknowledged. The MLRG graphics department, under the direction of Fred Crowe, prepared the figures.

REFERENCES

Barnett, T. P., 1976: Large scale variation of the temperature field in the North Pacific Ocean. *Naval Res. Rev.*, March, 36–51.

——, and R. L. Bernstein, 1975: Horizontal scales of midocean internal tides. *J. Geophys. Res.*, **80**, 1962–1964.

——, R. A. Knox and R. A. Weller, 1977: Space/time structure of the near-surface temperature field during the NORPAX POLE Experiment. *J. Phys. Oceanogr.*, **7**, 572–579.

Bronson, E. D., and E. R. Glosten, 1968: Floating instrument platform. Scripps Inst. Oceanogr., Univ. Calif., Mar. Phys. Lab. Tech. Rep., SIO Ref. 62-64, 23 pp.

Davis, R., T. P. Barnett and C. S. Cox, 1978: Variability of near-surface currents observed during the POLE Experiment. *J. Phys. Oceanogr.*, **8**, 290–301.

Defant, A., 1961: *Physical Oceanography*, Vols. 1 and 2. Pergamon Press, 729 pp., 598 pp.

Denman, K. L., 1973a: A time-dependent model of the upper ocean. *J. Phys. Oceanogr.*, **3**, 173–184.

——, 1973b: Energy changes associated with wind mixing in the upper ocean. *Fish. Res. Bd. Can. Tech. Rep.*, No. 380, 15 pp.

Dorrestein, R., 1979: On the vertical buoyancy flux below the sea surface as induced by atmospheric factors. *J. Phys. Oceanogr.*, **9**, 229–231.

Elliot, G. W., 1975: Automatic processing system for oceanographic data from U.S. B-scale ships in GATE. *STD Conference and Proceedings*, Plessey Environmental Systems, 163–175.

Fofonoff, N. P., and S. Tabata, 1958: Program for oceanographic computations and data processing on the electronic digital computer ALWAC III-E. DP-1 oceanographic station data program. *Fish. Res. Bd. Can. Ms. Rep. Ser.* (Oceanographic and Limnological), No. 25, 33 pp.

Fnehe, C. A., and K. F. Schmitt, 1974: Estimates of surface heat fluxes during POLE. *NORPAX Highlights*, 2, 8–9.

——, 1976: Parameterization of air-sea interface fluxes of sensible heat and moisture by bulk aerodynamic formulas. *J. Phys. Oceanogr.*, **6**, 801–809.

Hendry, R. M., 1977: Observations of the semi-diurnal internal tide in the western North Atlantic Ocean. *Phil. Trans. Roy. Soc. London*, **A286**, 1–24.

Holland, J. Z., 1968: An application of some statistical techniques to study eddy structure. U.S. Atomic Energy Commission, Div. Tech. Inform., Tech. Rep. No. TID-24585, 340–350.

Kenyon, K. E., 1978: The shallow salinity minimum of the eastern North Pacific in winter. *J. Phys. Oceanogr.*, **8**, 1061–1069.

Kraus, E. B., and J. S. Turner, 1967: A one-dimensional model of the seasonal thermocline—II. The general theory and its consequences. *Tellus*, **19**, 98–106.

Lee, O. S., 1961: Observations of internal waves in shallow water. *Limnol. Oceanogr.*, **6**, 312–321.

Mosetti, F., 1967: A new formula for the connection of seawater conductivity with salinity and temperature. *Boll. Geofis. Teor. Appl.*, **8**, 213–217.

Niiler, P. P., 1975: Deepening of the wind-mixed layer. *J. Mar. Res.*, **33**, 405–427.

Paulson, C. A., and J. J. Simpson, 1977: Irradiance measurements in the upper ocean. *J. Phys. Oceanogr.*, **7**, 952–956.

Pollard, R. T., P. B. Rhines and R. O. R. Y. Thompson, 1973: The deepening of the wind mixed layer. *Geophys. Fluid Dyn.*, **3**, 381–404.

Reid, J. L., 1956: Observations of internal tides in October. *Trans. Amer. Geophys. Union*, **37**, 278–289.

——, 1965: Intermediate waters of the Pacific Ocean. *Johns Hopkins Oceanogr. Stud.*, **2**, 85 pp.

——, 1973: The shallow salinity minimum of the Pacific Ocean. *Deep-Sea Res.*, **20**, 51–68.

Roden, G. I., 1970: Aspects of the mid-Pacific transition zone. *J. Geophys. Res.*, **75**, 1097–1109.

——, 1972: Temperature and salinity fronts at the boundaries of the subarctic-subtropical transition zone in the western Pacific. *J. Geophys. Res.*, **77**, 7155–7187.

——, 1974: Thermohaline structure, fronts and sea-air energy exchange of the trade wind region east of Hawaii. *J. Phys. Oceanogr.*, **4**, 168–182.

Seckel, G., 1968: A time sequence oceanographic investigation in the North Pacific trade wind zone. *Trans. Amer. Geophys. Union*, **49**, 377–386.

Sewell, H. R., 1942: An analysis of vertical oscillations in the southern North Atlantic. *Proc. Amer. Phil. Soc.*, **85**, 136–158.

Simpson, J. J., 1977: Small scale temperature structure of the upper ocean. Ph.D. dissertation, Oregon State University, 148 pp.

——, and C. A. Paulson, 1977: Mixed layer observations during the NORPAX POLE Experiment: A data report. Oregon State Univ., Data Rep. 66, Ref. 77-6, 167 p.

——, and ——, 1979a: Mid-ocean observations of atmospheric radiation. *Quart. J. Roy. Meteor. Soc.*, 105, 487–502.

——, and ——, 1979b: The spectrum of sea surface temperature. *J. Phys. Oceanogr.* (to be submitted).

Sverdrup, H. U., M. W. Johnson and R. H. Fleming, 1942: *The Oceans: Their Physics, Chemistry, and General Biology*. Prentice-Hall, 1087 pp.

Summers, H. J., and K. O. Emery, 1963: Internal waves of tidal period of Southern California. *J. Geophys. Res.*, 68, 827–839.

Sweers, H. E., 1971: A comparison of methods used to calculate sigma-*t*, specific volume anomaly and dynamic height. *Mar. Tech. Soc. J.*, 5, 7–26.

Turner, J. S., 1969: A note on wind mixing at the seasonal thermocline. *Deep-Sea Res.*, 16, 297–300.

——, 1973: *Buoyancy Effects in Fluids*. Cambridge University Press, 367 pp.

Weston, D. E., and W. W. Reay, 1969: Tidal period internal waves in a tidal stream. *Deep-Sea Res.*, 16, 473–478.

Wunsch, C., 1975: Internal tides in the Ocean. *Rev. Geophys. Space Phys.*, 13, 167–180.

Wyrtki, K., 1965: The average annual heat balance of the North Pacific Ocean and its relation to ocean circulation. *J. Geophys. Res.*, 70, 4547–4559.

Mesopelagic Fishes of the Bering Sea and Adjacent Northern North Pacific Ocean

William G. PEARCY, Takahisa NEMOTO and Muneo OKIYAMA

Reprinted from the *Journal of the Oceanographical Society of Japan* Vol. 35, Nos. 3-4

September 1979

Journal of the Oceanographical Society of Japan
Vol. 35, pp. 127 to 135, 1979

Mesopelagic Fishes of the Bering Sea and Adjacent Northern North Pacific Ocean*

William G. PEARCY**, Takahisa NEMOTO*** and Muneo OKIYAMA***

Abstract: Fourteen midwater trawl collections to depths of 450 m to 1,400 m were taken at eleven stations in the Bering Sea and adjoining regions of the northern North Pacific by the R/V Hakuho Maru during the summer of 1975. A total of 29 kinds of fishes were identified. Mesopelagic fishes of the families Myctophidae, Gonostomatidae and Bathylagidae predominated in the catches, contributing 14 species (94%) of the fishes caught.

Seventeen species of fishes were caught in the Bering Sea, and all of these are known from nearby areas. The mesopelagic fish fauna of the Bering Sea is similar to that in adjoining regions of the northern North Pacific Ocean: endemic species are rare or absent.

Stenobrachius nannochir was usually the most common mesopelagic fish in our catches. *Stenobrachius leucopsarus* is a diel vertical migrant that is usually the dominant mesopelagic fish in modified Subarctic waters of the northeastern Pacific. The change in dominance from *S. nannochir* in the western Bering Sea to *S. leucopsarus* in the eastern Bering Sea is related to differences in oceanographic conditions.

1. Introduction

The mesopelagic fishes of the northern North Pacific have been studied by Soviet, Japanese and American scientists (RASS, 1955; PARIN, 1961; KAWAGUCHI, 1973; WISNER, 1976; and others). FEDOROV (1973a, b) presented a detailed account of the ichthyofauna of the Bering Sea. To our knowledge, however, this is the first paper on the relative and actual abundance of the oceanic deep-sea fishes from this region. Preliminary comparisons of the mesopelagic fish fauna of the Bering Sea with adjoining regions of the North Pacific Ocean are also made.

2. Method and stations

Fishes were collected from the R/V Hakuho Maru (Cruise KH-75-4) with a 3-m Isaacs-Kidd Midwater Trawl (IKMT) towed obliquely from the surface to a maximum depth of 450 to 720 m (shallow tows) or to a maximum depth of 960 to 1,400 m (deep tows) at fourteen stations (Fig. 1). A tow was also made over the continental shelf (Stn. 12) to 45 m, but no fish was collected. A TSK Depth-Distance Recorder, which provided estimates of the distance and water volume sampled, indicated that depths within the sampling interval were sampled about equally. Tows were made between June 28 and August 11, 1975. All tows were made during daylight (or twilight) except for the shallow tow at Stn. 3 (see Table 1).

The fourteen tows in which fishes were collected were from eleven different stations which represented the following regions: Kurile-Kamchatka area to the Komandorskii (Commander) Islands, the western and the eastern portions of the Bering Sea along 57°N, the Gulf of Alaska, and the western Subarctic Pacific (see Fig. 1).

3. Results

A total of 29 different species of fishes were identified from the fourteen IKMT tows (Table 2). The families represented by the most species were Myctophidae (six species), Gonostomatidae (four species) and Bathylagidae (four species). These three families comprised 94% of the total number of fishes collected. Myctophids were by far the most numerous (72% of the numbers), followed by bathylagids (13%) and gonostomatids (9%).

Myctophids of the genus *Stenobrachius* numerically dominated the fish catches: *S.*

* Received Aug. 8, 1978, revised Apr. 5 and accepted Aug. 14, 1979.
** School of Oceanography, Oregon State University, Corvallis, Oregon 97331, USA
*** Ocean Research Institute, University of Tokyo

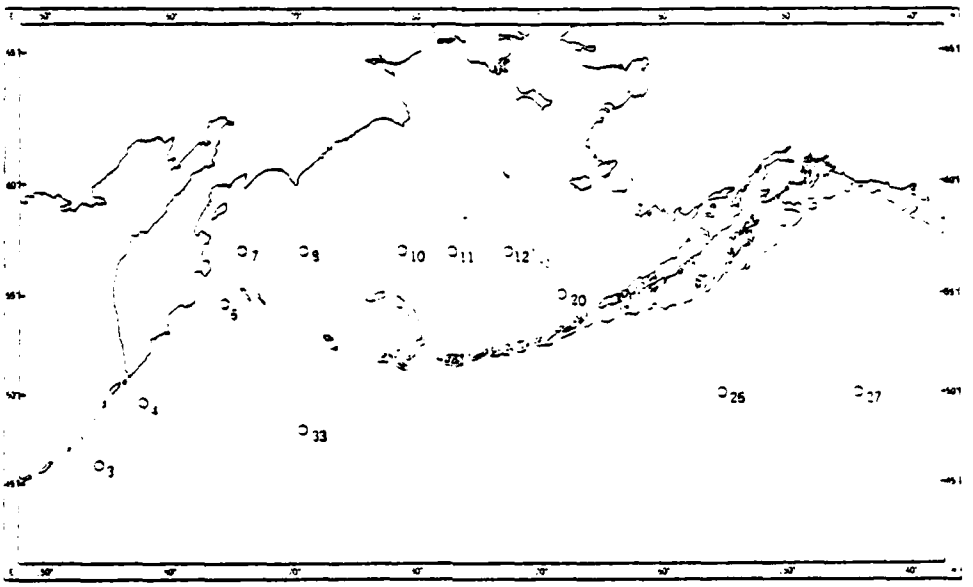

Fig. 1. Sampling position of Isaacs-Kidd Midwater Trawl in the Bering Sea on the Hakuho Maru Cruise KH-75-4 in 1975.

Table 1. Summary of Isaacs-Kidd Midwater Trawls on the Hakuno Maru Cruise KH-75-4.

Station	Location Mid Point		Date	Time	Wire Out (m)	Maximum Depth of tow (m)
	Latitude	Longitude				
3	46°30.6′N	154°26.7′E	June 28	0145-0319	2,000	640
3	46°56.1′N	154°41.3′E	,, 28	0333-0710	4,000	1,400
4	49°37.0′N	157°29.6′E	,, 29	0740-0930	2,000	700
6	54°34.4′N	164°37.6′E	July 1	1830-2000	2,000	600
7	57°10.8′N	169°04.3′E	,, 2	1610-1730	2,000	520
7	57°24.5′N	167°12.0′E	,, 2	1742-2353	4,000	1,400
8	57°00.4′N	170°58.4′E	,, 5	0903-1043	2,000	570
10	57°02.3′N	179°08.6′E	,, 7	1255-1420	2,000	520
11	57°07.3′N	176°55.7′W	,, 7	1328-2125	3,000	960
11	57°03.9′N	176°57.0′W	,, 7	2120-2222	1,500	450
12	57°01.1′N	172°27.3′W	,, 9	1002-1017	150	45
20	55°02.6′N	168°06.0′W	,, 13	1733-1911	2,000	630
26	49°57.5′N	155°02.0′W	,, 18	1945-2113	2,000	720
27	50°00.3′N	144°33.1′W	,, 20	0647-0816	2,000	590
33	47°56.5′N	170°58.9′E	Aug. 11	2025-2150	2,000	1,000

nannochir and *S. leucopsarus* comprised respectively 40 % and 29 % of all the individuals captured (Table 2). Next in importance were *Leuroglossus schmidti* (10 %) and *Cyclothone atraria* (8 %). These four species made up 87 % of the catch.

Stenobrachius nannochir and *S. leucopsarus* occurred at all stations and in every tow. One of these two species was the most numerous species in eleven tows, and the two species ranked first and second in abundance in eight collections. *Stenobrachius nannochir* was more common than *S. leucopsarus* in all samples except in the eastern Bering Sea (Stns. 10 and 20) and in the western Subarctic Region (Stn. 33, deep). Where *S. nannochir* was the most abundant species, it composed 25 to 65 % of the catch; where it was not dominant, *S. leucopsarus* comprised 25 to 34 % of the numbers of fish caught and was usually the most numer-

Table 2. Total numbers of each species of fish caught and catches at each station on the Hakuho Maru Cruise KH-75-4.
(Depth given for each station is maximum depth of tow; L: Larva(e) only)

Species	Total number caught	Western N. Pac.	Kuriles-Kamchatka				Bering Sea							Gulf of Alaska	
							Western		Eastern						
		Stn. 33 1,000 m	Stn. 3 640 m	Stn. 3 1,400 m	Stn. 4 700 m	Stn. 6 600 m	Stn. 7 520 m	Stn. 7 1,400 m	Stn. 8 570 m	Stn. 10 520 m	Stn. 11 450 m	Stn. 11 960 m	Stn. 20 630 m	Stn. 26 720 m	Stn. 27 590 m
Protomyctophum thompsoni	25	1			5	2								6	11
Stenobrachius leucopsarus	342	9	7	1	2	8	19	6	24	38	95	25	64	11	33
Stenobrachius nannochir	478	7	13	53	60	38	36	42	30	17	11	39	40	25	67
Stenobrachius sp. ?	2													2	
Lampanyctus jordani	1													1	
Lampanyctus regalis	1							1							
Diaphus theta	12	9												2	1
Cyclothone pallida	2						1							1	
Cyclothone pseudopallida	3		2				1								
Cyclothone atraria	96	7		33	2			50				4			
Gonostoma gracile	1					1									
Chauliodus macouni	25		1		3	3	3	2		5				3	5
Tactostoma macropus	1													1	
Bathylagus pacificus	26	1		5	5	4	2	3	1			4	1		
Bathylagus milleri	7		1	1	1						1			2	1
Bathylagus ochotensis	3		2												1
Leuroglossus schmidti	120		25	4	11	8	10	5	3	18	4	3	28	1	
Nansenia candida	1														1
Macropinna microstoma	2				1										1
Benthalbella dentata	2													1	1
Melamphaes lugubris	2			1	1										
Poromitra crassiceps	1	1													
Scopeloberyx sp.	2	1		1											
Nectoliparis pelagicus	9									6	1		2		
Malacocottus sp.	2				1		1								
Hemilepidotus sp.	4		2	2											
Coryphaenoides sp.	3					2	1								
L. *Theragra chalcogramma*	15									3		2	10		
L. *Atheresthes evermanni*	1						1								
L. *Kemnaridtius hippoglossoides*	1										1				
L. Undentified larvae	2								1						1
Total	1,192														

ous fish.

In the more numerous shallow tows, the average abundance (Σ numbers / Σ estimated volumes of water filtered) of *S. nannochir* was 0.62 individuals / 1,000 m³ (range 0.24 to 1.35), and for *S. leucopsarus* was 0.36 individuals / 1,000 m³ (range 0.03 to 2.28). The relative abundance of *S. nannochir* was highest at the western stations (Stns. 4 and 6) near Kamchatka and in the Gulf of Alaska (Stns. 26 and 27), and was lowest in the Bering Sea. The values decreased from 0.55 to 0.26/1,000 m³ along the four stations (Stns. 7, 3, 10, 11) transect from west to east across the Bering Sea at a latitude of 57°N.

Leuroglossus schmidti (juveniles and larvae) was found at all stations except Stns. 27 and 33, those stations in the Gulf of Alaska and the western North Pacific farthest from land. Largest numbers per 1,000 m³ were caught in the Bering Sea and near Kamchatka.

Seventeen of the total of 29 species of fishes were caught in the Bering Sea. All 17 were also caught from other regions sampled on this cruise, except for five species (*Lampanyctus regalis*, *Nectoliparis pelagicus*, *Theragra chalcogramma*, *Atheresthes evermanni*, and *Reinhardtius hippoglossoides*) which are known from other areas of the northern North Pacific (see Tables 2 and 3). Two species are reported for the first time (to our knowledge) from the Bering Sea: *Cyclothone pallida** and *Cyclothone pseudopallida*. Two of the species caught in regions other than the Bering Sea have not previously been reported from the Bering Sea by other researchers: *Nansenia candida* and *Scopeloberyx* sp.

The major difference between the species composition of our deep and shallow tows was attributable to the larger numbers of *Cyclothone atraria* in deep tows (94) than in shallow tows (2). The average size of *S. nannochir* was also larger in deep than shallow tows.

4. Discussion

There is no evidence for a unique, endemic mesopelagic fish fauna in the Bering Sea (Table 3). All the species caught in our study in the Bering Sea are known to occur in other regions of the North Pacific. None of the 35 species of mesopelagic-bathypelagic fishes listed by FEDOROV (1973a) from the Bering Sea is a local endemic. Most are widespread in the northern part of the North Pacific. Some are most common in the eastern North Pacific, others in the western North Pacific.

The number of species of oceanic deep-sea fishes listed by FEDOROV (1973a) for the Bering Sea is almost as many as that listed by PARIN (1961) for the northern North Pacific, suggesting that the species diversity of mesopelagic fishes may not be reduced in the high-latitude Bering Sea basin. Some of the species found in the Bering Sea (e.g., *P. thompsoni*, *D. theta*, *T. macropus*) may be expatriates, however, and may not be part of reproductively viable populations. We have little information on this subject.

The predominance of *S. nannochir* in most of our samples suggests that it may be the most common species of *Stenobrachius*, and the most common mesopelagic fish, in the northern North Pacific. PARIN (1961) and KAWAGUCHI (pers. comm.) also found that *S. nannochir* was more abundant than *S. leucopsarus* in samples in the northwestern Pacific. PEARCY (unpublished) caught more *S. nannochir* than *S. leucopsarus* in oblique IKMT tows to depths of 500 m or below whereas *S. leucopsarus* was most numerous in tows to 200 m at night in the vicinity of the Gulf of Alaska and Alaskan Peninsula. Off Oregon, *S. leucopsarus* is the most numerous mesopelagic fish, both in the 0–1,000 m water column or in the upper 200 m at night (PEARCY, 1964, 1977; PEARCY *et al.*, 1977).

Thus *S. nannochir* appears to be more common than *S. leucopsarus* in the northern North Pacific within the upper 1,000 m, but it apparently does not migrate into epipelagic waters at night as does *S. leucopsarus*. These differences in vertical distributions and diel migrations may be the best explanation for the lack of *S. nannochir* in Aron's (1960) shallow IKMT samples, and for the predominance of *S. leucopsarus* over *S. nannochir* reported by PARIN (1961) in the northern Northeast Pacific.

Many small (25–45 mm standard length) *S. nannochir* were caught during our cruise, but only large specimens are known from Transi-

* RASS (1955) lists "*C. pallida* (?)" for the Bering Sea, but MUKHACHEVA (1964, 1967) does not list it for the Bering Sea.

Table 3. Known occurrence of each species of fish caught from this and other studies for four regions of the northern North Pacific: Western North Pacific (W. N. Pac.), Kurile-Kamchatka area (K.-K.), Bering Sea (B.S.), and Gulf of Alaska (G.A.). 1: WISNER 1976), 2: PARIN 1961), 3: RASS 1955), 4: MAKUSHOK (1970), 5: ARON (1962), 6: KULIKOVA 1960), 7: FEDOROV (1973a, b), 8: MUKHACHEVA (1964), 9: KAWAGUCHI (1973), 10: HART (1973), 11: RASS and KASHKINA 1967), 12: JOHNSON (1974) 13: EBELING (1962), 14: SHMIDT 1950), 15: BEKKER 1967), 16: UENO (1971). (– indicates species caught in this study; L: Larva(e) only)

Species	W. N. Pac.	K.-K.	B. S.	G. A.
Protomyctophum thompsoni	1, 2 –	1, 3, 4 –	3, 5, 7, 15	1, 2, 5 –
Stenobrachius leucopsarus	1, 2, 6 –	1, 3, 4, 6 –	3, 6, 7 –	1, 2, 3, 6 –
Stenobrachius nannochir	1, 2, 6 –	1, 2, 4, 6 –	2, 3, 6, 7 –	1, 2, 3 –
Stenobrachius sp.				–
Lampanyctus jordani	1, 2, 6	1, 3, 4, 6	1, 3, 6, 7	1 –
Lampanyctus regalis	2	1, 3, 4, 6, 16	7 –	1, 2, 3
Diaphus theta	2 –	4	7	1, 2, 5 –
Cyclothone pallida	2	3, 4, 16	–	2 –
Cyclothone pseudopallida	8	4, 8 –	–	
Cyclothone atraria	8 –	3, 4, 8 –	3, 7, 8 –	3, 8
Gonostoma gracile	2, 9	2, 4, 9 –	7	
Chauliodus macouni	2	3, 4, 10, 16 –	3, 7, 10 –	2, 3, 5, 10 –
Tactostoma macropus	2	3, 4, 16	7	2, 3, 5, 10 –
Bathylagus pacificus	2, 6, 11 –	3, 4, 11, 16 –	3, 7, 10, 11 –	2, 3, 10, 11
Bathylagus milleri	2, 11	3, 4, 11, 16 –	3, 7, 11 –	2, 3, 11 –
Bathylagus ochotensis	11	4, 11 –	7 –	–
Leuroglossus schmidti	2	3, 4, 16 –	3, 7, 10 –	2, 3, 10 –
Nansenia candida				10 –
Macropinna microstoma	2	3, 10, 16 –	7, 16	2, 3, 10 –
Benthalbeila dentata	12	4	7, 16	2, 12 –
Melamphaes lugubris	13	4, 13 –	7	5, 13
Poromitra crassiceps	+	3, 4, 16 –	7	10
Scopeloberyx sp.	+	4 –		
Nectoliparis pelagicus		4, 7, 10, 14	7, 10, 14 –	5, 10
Malacocottus sp.		4, 14, 16 –	14 –	10
Hemilepidotus sp.		4, 10, 14, 16 –	10, 14	10
Coryphaenoides sp.		3, 4, 10, 16 –	3, 10 –	3, 10
L *Theragra chalcogramma*		10, 14	10, 14 –	10, 14
L *Atheresthes evermanni*		14, 16	7, 14 –	
L *Reinhardtius hippoglossoides*		10, 14, 16	10, 14 –	10
L Unidentified larvae			–	

tional-modified Subarctic waters in the northeastern Pacific (PEARCY, unpublished). This indicates a reproductive population of *S. nannochir* in the northern North Pacific. Some small *S. leucopsarus* were also caught on our cruise; but young animals predominate in the catches off Oregon where all age-groups are present (PEARCY *et al.*, 1977; SMOKER and PEARCY, 1970).

Therefore we conclude that *S. nannochir* is basically a lower mesopelagic species adapted to the oceanographic conditions of the northern North Pacific. *Stenobrachius leucopsarus*, on the other hand, is a diel vertical migrant that is most abundant in modified Subarctic waters of the northeastern Pacific. In the genus *Stenobrachius*, only *S. nannochir* is found in the cold Sea of Okhotsk (KAWAGUCHI, pers. comm.) which is covered with ice in the winter. The distribution of *S. nannochir* therefore indicates that it is better adapted to cold temperatures than *S. leucopsarus*.

Stenobrachius nannochir was the most abundant lanternfish at the two western stations, but *S. leucopsarus* was most abundant at the two eastern stations along 57°N in the Bering Sea (Table 2 and Fig. 1). This change in predominance of these two *Stenobrachius* species across the Bering Sea may also be correlated with oceanographic differences. The main inflow into the Bering Sea is between the Commander and the Near Islands where surface waters are typical of the Subarctic Pacific (FAVORITE, 1974; HUGHES *et al.*, 1974). A southerly flow of cold water along the Kamchatka Peninsula produces a general counterclockwise gyre of cold water in the western Bering Sea (TAKENOUTI and OHTANI, 1974). The water in the deep portion of the central or eastern Bering Sea is modified by upwelling of water associated with counterclockwise flow and surface divergence. This water has a deeper upper mixed layer, lower salinity gradient in the thermocline, and a warmer dichothermal and mesothermal layer than the western Bering Sea (see TAKENOUTI and OHTANI, 1974). A gyre of relatively warm water is also indicated in the deep water of the eastern Bering Sea (TAKENOUTI and OHTANI, 1974).

Oceanographic measurements on the Hakuho Maru Cruise indicate that the temperature and salinity in the western Bering Sea were similar to those of the Subarctic region south of the Aleutian Islands, having a strong seasonal thermocline, and cold water of about −0.5°C at 50 m. A tongue of this cold water of less than 1.0°C extended eastward at about 200 m depth from Stns. 7 and 8, but did not protrude as far east as Stn. 11 (Fig. 2). The temperature minimum of the dichothermal layer was weakly developed in the eastern vs. the western Bering Sea. Isohalines domed toward the surface in the central area, and salinity values decreased markedly along the eastern and western margins of the Bering Sea (HATTORI, 1977). Thus the eastern Bering Sea was less stratified and was warmer than the western Bering Sea in the summer (see also FAVORITE, 1974) and may be a more favorable environment for *S. leucopsarus* in this region.

Acknowledgement

The authors appreciate the generous assistance and helpful discussions with Dr. K. KAWAGUCHI. Mr. D. STEIN made helpful comments on the manuscript. The first author is grateful to the Ocean Research Institute and the Japan Society for the Promotion of Science for inviting him to Japan as a visiting professor at the Ocean Research Institute, University of Tokyo, and to the U. S. Office of Naval Research (Contract N00014-76-C-0067 under Project NR083-102) for partial support of this research.

References

ARON, W. (1960): The distribution of animals in the Eastern North Pacific and its relationship to physical and chemical conditions. Dept. of Oceanography, Univ. of Washington, Tech. Rep., (63), 65 pp. and appendix.

ARON, W. (1962): The distribution of animals in the Eastern North Pacific and its relationship to physical and chemical conditions. J. Fish. Res. Bd. Canada, 19, 271-314.

BEKKER, V. E. 1967): Lanternfishes fam. Myctophidae). *In*, The Pacific Ocean. The Biology of the Pacific Ocean. Book III. ed. by V. G. KORT, pp. 174-197. (U. S. Naval Oceanogr. Office Translation 528).

EBELING, A. W. (1962): Melamphaidae I. Systematics and zoogeography of the species in the bathypelagic fish genus *Melamphaes* Gunther. Dana Rep., 58, 1-139.

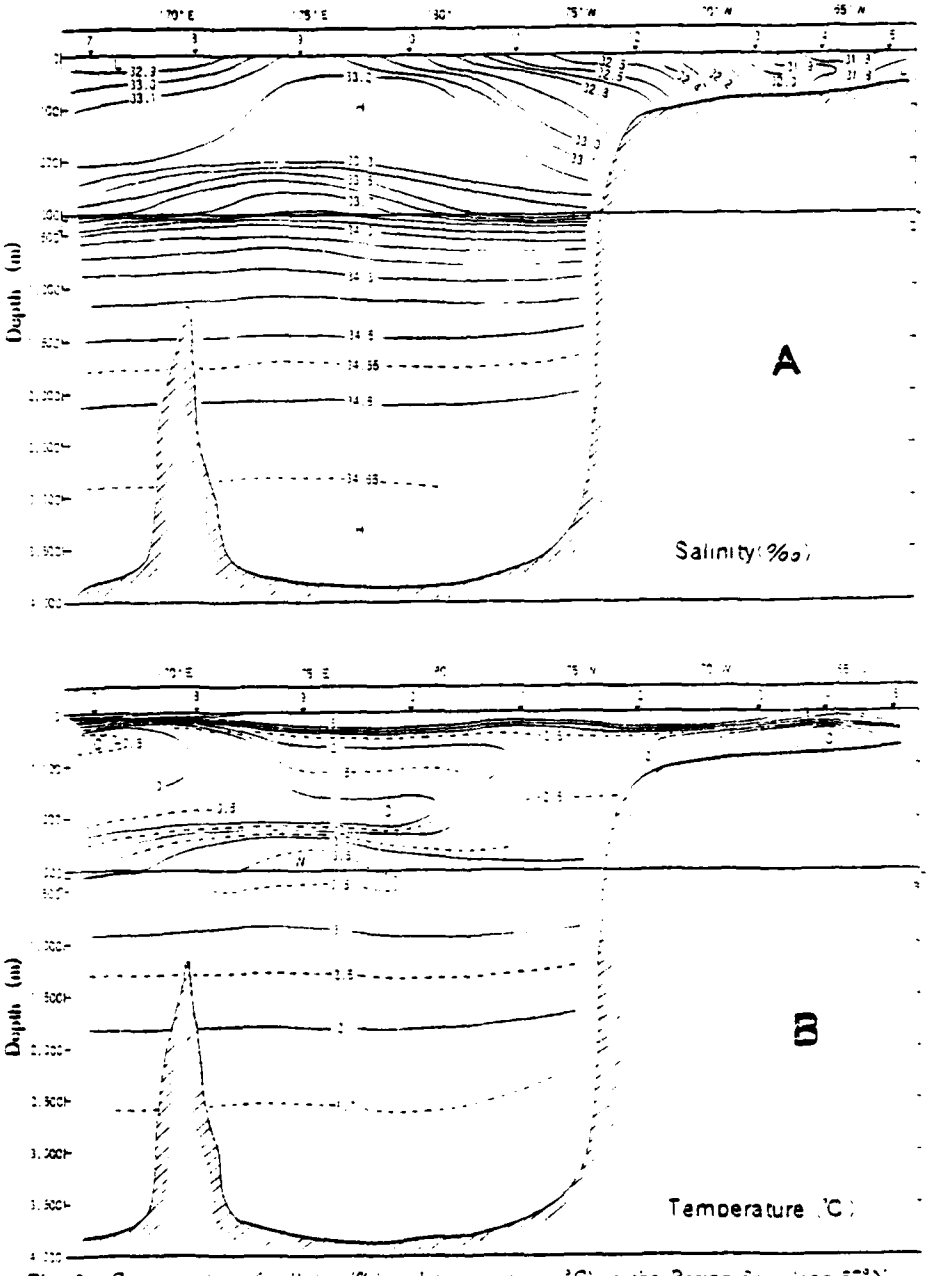

Fig. 2. Cross section of salinity (‰) and temperature (°C) in the Bering Sea along 57°N.

FAVORITE, R. (1974): Flow into the Bering Sea through Aleutian Island passes. *In*, Oceanography of the Bering Sea. ed. by D. W. HOOD and E. J. KELLEY, Univ. Alaska, Fairbanks, pp. 3-37.

FEDOROV, V. V. (1973a): Ichthyofauna of the continental slope of the Bering Sea and some aspects of its origin and formation. Izv. Tikhookean. Nauchno-issled. Inst. Rybn. Khoz. Okeanogr., 87, 3-41. (Transl. Series No. 3345, Fish. Mar. Serv. Canada).

FEDOROV, V. V. (1973b): A list of Bering Sea fish. Izv. Tikhookean. Nauchno-issled. Inst. Rybn. Khoz. Okeanogr., 87, 42-71. (Transl. Series No. 3271, Fish. Mar. Serv. Canada).

HART, J. L. (1973): Pacific Fishes of Canada. Fish Res. Bd. Canada. Bull., 180, 740 pp.

HATTORI, A. (editor) (1977): Hydrographic characteristics of studied sea areas. Prelim. Rep. Hakuho Maru Cruise KH-75-4. Ocean Res. Inst. Univ. Tokyo, 87 pp.

HUGHES, F. W., L. K. COACHMAN and K. AAGAARD. (1974): Circulation, transport and water exchange in the western Bering Sea. *In*, Oceanography of the Bering Sea. ed. by D. W. HOOD and E. J. KELLEY, Univ. Alaska, Fairbanks, pp. 59-98.

JOHNSON, R. K. (1974): A revision of the Alepisauroid family Scopelarchidae (Pisces, Myctophiformes). Fieldiana (zool.), 66, 1-249.

KAWAGUCHI, K. (1973): Biology of *Gonostoma gracile* Günther (Gonostomatidae) II. Geographical and vertical distribution. J. Oceanogr. Soc. Japan, 29, 27-34.

KULIKOVA, E. B. (1960): The lampanyctids (genus *Lampanyctus*) of the Fareastern seas and of the northwestern part of the Pacific Ocean. Trudy Inst. Okeanol. Akad. Nauk SSSR, 31, 166-204.

MAKUSHOK, V. M. (1970): Data on fishes collected in the area of the Kurile-Kamchatka Trench on the 39th cruise of the R/V «Vityaz» in the summer of 1966. Trudy Inst. Okeanol. Akad. Nauk SSSR, 86, 513-535.

MUKHACHEVA, V. A. (1964): On the genus *Cyclothone* (Gonostomatidae, Pisces) of the Pacific Ocean. Trudy Inst. Okeanol. Akad. Nauk SSSR, 73, 98-146.

MUKHACHEVA, V. A. (1967): Bristle mouth (genus *Cyclothone*, fam. Gonostomatidae). *In*, The Pacific Ocean. The Biology of the Pacific Ocean. Book III. ed. by V. G. KORT, pp. 198-220. U. S. Naval Oceanogr. Office Translation 523).

PARIN, N. V. (1961): The distribution of deep-sea fishes in the upper bathypelagic layer of the Subarctic Waters of the Northern Pacific Ocean. Trudy Inst. Okeanol. Akad. Nauk SSSR, 45, 259-278.

PEARCY, W. G. (1964): Some distributional features of mesopelagic fishes off Oregon. J. Mar. Res., 22, 83-102.

PEARCY, W. G. (1977): Variations in abundance of sound scattering animals off Oregon. *In*, Oceanic Sound Scattering. ed. by N. R. ANDERSON and B. J. ZAHURANEC, Plenum Press, New York, pp. 647-666.

PEARCY, W. G., E. E. KRYGIER, R. MESECAR, and R. RAMSEY. (1977): Vertical distribution and migration of oceanic micronekton off Oregon. Deep-Sea Res., 24, 223-245.

RASS, T. S. (1955): Deep-Sea fishes of the Kurile-Kamchatka Trench. Trudy Inst. Okeanol. Akad. Nauk SSSR, 12, 328-339.

RASS, T. S. and A. A. KASHKINA (1967): Bathypelagic fishes of the Northern Pacific (Pisces, Bathylagidae). Trudy Inst. Okeanol. Akad. Nauk SSSR, 84, 209-221.

SHMIDT, P. Yu. (1950): Fishes of the Sea of Okhotsk. Izdatel'stuo Akad. Nauk SSSR, 392 pp. (Trans. Israel Prog. Sci. Trans. 1965).

SMOKER, W. and W. G. PEARCY (1970): Growth and reproduction of the lanternfish *Stenobrachius leucopsarus*. J. Fish. Res. Bd. Canada, 27, 1265-1275.

TAKENOUTI, A. Y. and K. OHTANI (1974): Currents and water masses in the Bering Sea: A review of Japanese work. *In*, Oceanography of the Bering Sea. ed. by D. W. HOOD and E. J. KELLEY, Univ. Alaska, Fairbanks, pp. 39-57.

UENO, T. (1971): List of the marine fishes from the waters of Hokkaido and its adjacent regions. Sci. Rep. Hokkaido Fish. Experimental Station, 13, 61-102.

WISNER, R. L. (1976): The taxonomy and distribution of lanternfishes (fam. Myctophidae) of the Eastern Pacific Ocean. Navy Ocean Res. and Develop. Activity Rep., No. 3, 229 pp.

ベーリング海および隣接する北部北太平洋における中深層魚類

W. G. PEARCY*, 堤本敬久**, 中山宗雄**

要旨：1975年夏のベーリング海および隣接する北部北太平洋における白鳳丸航海中，11観測点において14回の中層トロール採集が 450 m から 1,500 m に達する深度について行われた．採集された魚類については29種が同定された．中深層魚類としてはハダカイワシ科 (Myctophidae)，ヨコエソ科 (Gonostomatidae)，およびソコイワシ科 (Bathylagidae) に属する種類が卓越し，14種（個体数の 94%）を占めた．ベーリング海においては17種が出現したが，これらの種類は全て隣接海域からも報告されており，この縁海の中深層魚類相は隣接する北部北太平洋のそれと類似し，固有種は稀かまたはこれを欠いているものと考えられた．ハダカイワシ科の1種 *Stenobrachius nannochir* は最も普通に採集試料中に出現した．同じく優占して出現した同属種 *Stenobrachius leucopsarus* は通常日周期鉛直移動を行なう種で，北東太平洋の亜寒帯域における中深層魚類の優占種として知られるものである．前者がベーリング海西部において卓越し，後者が東部ベーリング海域において卓越した理由は海況の違いに基づくものと推定された．

* オレゴン州立大学海洋学部
School of Oceanography, Oregon State University, Corvallis, Oregon 97331, U.S.A.
** 東京大学海洋研究所
〒164 東京都中野区南台 1-15-1

FEEDING HABITS OF COD, CAPELIN, AND HERRING IN BALSFJORDEN, NORTHERN NORWAY, JULY–AUGUST 1978: THE IMPORTANCE OF EUPHAUSIIDS

W.G. Pearcy, C.C.E. Hopkins, S. Grønvik & R.A. Evans

SARSIA

Pearcy, W.G., C.C.E. Hopkins, S. Grønvik, & R.A. Evans 1979 12-21. Feeding habits of cod, capelin, and herring in Balsfjorden, northern Norway, July–August 1978: The importance of euphausiids. *Sarsia* 64:269–277. Bergen. ISSN 0036–4827.

Midwater and bottom trawls were used at two stations (120 and 180 m depth) in Balsfjorden during the summer of 1978 to study the feeding of fishes on euphausiids, one of the major causes of 120 kHz sound scattering. The principal food of cod consisted of capelin (*Mallotus villosus*), euphausiids (*Thysanoessa raschii*, *T. inermis*, and *Meganyctiphanes norvegica*), and shrimp (*Pandalus borealis*).

At the 120 m station, herring and small cod fed mainly on euphausiids. Because of diel vertical migrations, euphausiids are presumably close to the bottom during the day at this depth, and hence very susceptible to predation by both pelagic and benthic fishes. During the darkest period of the 24-hr day cod caught in midwater (50–70 m depth) had appreciable quantities of fresh euphausiids in their stomachs.

At the 180 m station euphausiids were relatively unimportant in the food of cod caught in bottom trawls but were numerous in cod caught in midwater trawls at depths of the 120 kHz sound scattering layer. The scattering layer did not impinge on the bottom at this station. It migrated from depths of about 150 m by day into the upper 100 m at night; both capelin and cod were associated with the layer. Although copepods were the most numerous type of prey in capelin stomachs from the 180 m station, euphausiids predominated volumetrically.

W.G. Pearcy, School of Oceanography, Oregon State University, Corvallis, Oregon 97 331 U.S.A. — C.C.E. Hopkins, S. Grønvik, and R.A. Evans, Institute of Biology and Geology, University of Tromsø, N-9001 Tromsø, Norway.

INTRODUCTION

Biological sound scattering layers (SSL's) are a common feature of oceanic regions (Farquhar 1971) as well as of some neritic areas, including fjords of northern Norway. In Balsfjorden, Hopkins & al. 1978) found high concentrations of euphausiids or krill, calanoid copepods, and chaetognaths at the same depths as dense 120 kHz SSL's. Scattering at this frequency has been associated with euphausiids by Kinzer (1971), Sameoto (1976), and Greenlaw (1979). Diel vertical migrations of animals, like euphausiids, may result in large concentrations of biomass near the sea floor during the day (Hopkins & Gulliksen 1978) where they are vulnerable to predation by benthic fishes during daylight periods (Isaacs & Schwartzlose 1965).

The objective of this study was to sample animals with large pelagic and benthic trawls, often at depths of the 120 kHz sound scattering, to learn more about the predation of krill by fishes and the role of SSL organisms in the food web of Balsfjorden. Of the two benthic stations sampled, one was shallower and the other deeper than the daylight depth level of the SSL's. The importance of euphausiids in the food web of commercially important fishes should be evaluated before development of intensive krill fisheries in an area.

MATERIAL AND METHODS

Collections with a bottom shrimp trawl and/or a midwater trawl were made on three cruises in Balsfjorden from F/F *Johan Ruud* or *Ottar* on 13 July, 1–2, and 25–26 August 1978. The first two cruises sampled near Tennes (69°17′ N, 19°23′ E), where the bottom depth was about 120 m. The last cruise sampled near Svartnes (69°21′ N, 19°06′ E), where the bottom was 180–190 m.

The shrimp trawl had a footrope of 18 m and 4 cm (stretch) mesh in the body and codend. The pelagic trawl had an 18 × 8 m mouth opening and mesh that graded from 10 cm to 1 cm in the codend. The pelagic trawl was used with a sonic pinger (Simrad Trawl Eye) which was used to monitor depth of the net while fishing. All tows were 30 to 60 minutes in duration.

Simrad EK 120 and or EK 38 kHz echosounders were used to measure biological sound scattering on the *Johan Ruud* cruises, but unfortunately the 120 kHz echosounder was not operative on the 1–2 August cruise.

The species composition of the trawl catches was noted and the rank order of abundance of the common species was estimated based on visual estimates of volumes. Fishes were measured (total length) and stomachs of cod and herring were removed and preserved in 10–20 % formalin and seawater at sea. Stomachs of similar-sized specimens of one species of fish were preserved in the same bottle. A total of 170 cod and 65 herring stomachs were removed and examined.

In the laboratory, stomachs were opened, fullness was noted on a scale of 0 (empty) to + (full), and the degree of digestion of food was noted on a scale of 1 (fresh) to 3 (well-digested). The number and types of organisms in each stomach were recorded. In the case of well-digested animals, numbers were estimated from the least digestible parts such as euphausiid eyes and fish vertebral columns. After all stomachs for a size group of fish were examined, wet weights of fishes, euphausiids, shrimp, and miscellaneous animal taxa from the stomach contents were obtained to the nearest 0.1 g. Food organisms found loose in the jar were included in these weights.

Capelin were preserved whole in 10 % formalin at sea and stomachs were removed in the laboratory. A total of 154 capelin were examined. Numbers and kinds of food organisms were noted but because of the small amount of stomach content wet weights were not taken.

RESULTS

The presence of fishes and motile crustaceans in the shrimps and midwater trawl collections, along with the rank order of abundance of the most common species, are shown in Table 1. The total number of species caught at the two stations was low.

Catches

120 m station. *Pandalus borealis* comprised the bulk of the bottom shrimp trawl catches at the 120 m station, averaging about 20 to 30 kg per half-hour tow, followed by cod *Gadus morhua*, long rough dab *Hippoglossoides platessoides* or capelin *Mallotus villosus*. Many herring *Clupea harengus* were caught in one shrimp trawl tow 1 August, 1650–1720 h. In the midwater trawl at this station only cod or capelin were caught. About 250 kg of capelin were caught in the day-time tow to 50–65 m, and about 100 kg of cod were caught in the night-time midwater trawl at this depth. These were the largest catches of fish in this study.

180 m station. At the 180 m station, capelin comprised the largest portion of all shrimp

Table 1. The species of crustaceans and fishes caught in shrimp- and midwater-trawl tows at the 120 m and 180 m station. Numbers indicate the rank order of abundance of the four species comprising the largest volume in the catches, and the presence (—) of other species.

	120 m					180 m							
	Shrimp trawl			Midwater		Shrimp trawl				Midwater trawl			
Day – month and hours of the tow	13 July 1130 1230	1 Aug. 1650 1720	1 Aug. 2320 2350	1 Aug. 1900 1930 50–65 m	2 Aug. 0000 0030 50–65 m	25 Aug. 1715 1745	26 Aug. 0400 0430	26 Aug. 0740 0810	26 Aug. 1400 1500	25 Aug. 1602 1634 150 m	26 Aug. 0157 0240 55–100 m	26 Aug. 0616 0703 150 m	26 Aug. 1300 1400 150 m
Pandalus borealis	1	1	1	—	—	2	2	3	2	—	—	—	—
Meganyctiphanes norvegica and *Thysanoessa*	—	—	—	—	—	—	—	—	—	3	1	1	1
Gadus morhua	3	3	2	2	1	+	+	2	+	2	+	2	3
Trisopterus esmarkii	—	—	—	—	—	—	—	—	—	—	—	—	—
Clupea harengus	—	2	+	—	—	—	—	—	—	—	—	—	—
Mallotus villosus	+	—	3	1	2	1	1	1	1	1	2	3	2
Ammodytes marinus	—	—	—	—	—	—	—	—	—	—	3	+	—
Lumpenus lampretaeformis	—	—	—	—	—	—	—	—	—	—	—	—	—
Leptoclinus maculatus	—	—	—	—	—	—	—	—	—	—	—	—	—
Lycodes vahli	—	—	—	—	—	—	—	—	—	—	—	—	—
Agonus cataphractus	—	—	—	—	—	—	—	—	—	—	—	—	—
Hippoglossoides platessoides	2	+	+	—	—	3	3	+	3	—	—	—	—
Raja radiata	—	—	—	—	—	—	—	—	—	—	—	—	—

trawl catches, followed usually by shrimp, long rough dab, and cod. Capelin were also common in midwater trawl catches, all of which were towed at depths of 120 kHz scattering layers. Euphausiids *Meganyctiphanes norvegica* and *Thysanoessa* spp. however were the most abundant animals in three of the four midwater tows. Since most of these euphausiids would not be retained by the coarse 4 cm mesh, these catches represent only a fraction of those entering the net. Cod was the second to fourth most common species. Small cod were rare at this station. Sand eel, *Ammodytes marinus*, was common in the night and early morning tows.

Feeding habits of cod

The kinds of animals found in cod stomachs from all collections are listed in Table 2. Because of the limited number of fish examined and the restricted geographic and seasonal coverage, the number of prey species is low compared to other studies (e.g. RAE 1967; A. Klementsen unpubl. data for Balsfjorden).

Fish, krill, and shrimp were the most important foods for cod at both stations during the study period (Tables 3 and 4).

120 m station — shrimp trawl. A clear trend was apparent in the type of food consumed by different sizes of cod caught in the shrimp trawl collections at 120 m. Small cod (< 25 cm total length) mainly ate krill (73–94 % of the wet weight of stomach contents). Euphausiids were *Thysanoessa inermis* and *T. raschii* in about equal proportions. They were 14 to 25 mm long (total length). All small cod had krill in their stomachs. Numbers averaged 23–26 per cod stomach during the day and 8 at 'night' (2320–2350 h), suggesting that krill are more available to small cod near the bottom during periods of high light intensity. The number of stomachs examined was low, however, and slow rates of digestion (DAAN 1973) may confound these diel trends.

Amphipods (mainly *Parathemisto abyssorum* and *Halirages fulvocinctus*) were found in 38 % of the stomachs of small cod. All stomachs that contained amphipods also contained euphausiids. Polychaetes were present in only 5 of 43 small cod indicating that these fish fed predominantly on vertically migrating pelagic or hyperbenthic animals.

Table 2. Food items identified from cod stomachs.

Fishes
- *Mailotus villosus*
- *Ammodytes marinus*
- *Leptoclinus maculatus*
- *Hippoglossoides platessoides*
- *Leptogonus decagonus*

Shrimps, hermit crabs
- *Pandalus borealis*
- *Sabinea septemcarinatus*
- *Pagurus bernhardus*

Euphausiids, mysids
- *Thysanoessa inermis*
- *Thysanoessa raschii*
- *Meganyctiphanes norvegica*
- Mysidacea

Amphipods
- *Parathemisto abyssorum*
- *Hyperoche medusarum*
- *Monoculoides packardi*
- *Rhachotropis macropus*
- *Arrhis phyllonyx*
- *Halirages fulvocinctus*
- *Ischyrocerus anguipes*
- Lysianassidae sp.

Cumaceans
- *Diastylis* spp.

Asteroid
- *Cienodiscus crispatus*

Polychaetes
- *Nephtys* sp.
- *Harmothoe imbricata*
- *Lumbrineris* sp.

Pelecypod — unidentified
Gastropod — unidentified

Large cod (27–72 cm) ate mainly shrimp *Pandalus borealis* or capelin. The cod caught around midnight had mostly capelin in their stomachs. These capelin were in advanced stages of digestion and were probably eaten earlier in the day. It is therefore unlikely that these capelin were eaten by cod in the net (i.e. net feeding).

Most of the *P. borealis* in the cod stomachs, on the other hand, appeared to be fresh and undigested, raising suspicions that they may have been consumed after both cod and shrimp were concentrated in the net. A. Klementsen (pers. comm.), who also found that shrimp were the most important food for large cod in this area of Balsfjorden, observed no correlation between the trawl catch of *P. borealis* and their

Table 3. Food of the cod at the 120 m station in Balsfjorden on a percentage weight basis for stomachs with food. The three most common species caught in each trawl collection by volume are also given, where Sh = shrimp, Dab = long rough dab, Her = herring, Cap = capelin, and Euph = euphausiids. > means more abundant than. n = number of cod stomachs.

Date, time (h) Common species	n	Length range of cod cm	Percent — wet weight Euph.	Fish	Shrimp	Misc.
Shrimp trawl						
13 Aug. 1130–1230 Sh > Dab > Cod	22	14–19	94	0	3	3
	13	20–25	82	5	10	3
	11	27–37	13	26	61	2
	4	38–48	2	42	56	0
1 Aug. 1650–1720 Sh > Her > Cod	4	20–25	73	0	22	6
	3	27–33	41	42	17	0
	2	46–70	30	0	20	0
1 Aug. 2320–2350 Sh > Cod > Cap	4	17–21	77	0	5	19
	11	41–53	<1	97	2	0
	11	58–72	<1	80	19	0
Midwater trawl						
1 Aug. 1930–2000 (Cap > Cod) 50–65 m	8	54–70	<1	100	0	0
2 Aug. 0000–0030 (Cod > Cap) 50–65 m	9	32–40	7	93	0	0
	10	40–46	7	91	2	0
	10	55–66	17	83	0	0

numbers in cod caught in the same tows. In some instances, cod had shrimp in their stomachs but no shrimp were caught in the net. Therefore comsumption of shrimp may not be an artifact of net feeding but simply a result of slow digestion rates.

120 m station — midwater trawl. The two midwater trawl tows at this station were made at the same depth, 50–65 m, at 1930 h and 2400 h to observe possible diel differences in catch and in food habits that may be associated with vertical migrations. The 38 kHz echograms showed fish-type echoes at this depth during the 1930–2000 tow; these were probably capelin as large numbers (~250 kg) of this species were caught. The few cod caught in this tow had almost exclusively capelin in their stomachs (averaging 21 capelin per stomach), some quite fresh indicative of recent feeding.

During the 2400–0030 h midwater trawl a few fish-type echoes were present at the 50–65 m towing depth but most of them had ascended into the upper 30 m. Only a few capelin were caught in this tow but large numbers of cod (~100 kg) were captured. The differences between these two tows suggest ascent of both capelin and cod into upper waters when irradiance was minimal. These cod contained partially digested capelin in their stomachs which comprised 83–93 % of the weight of their stomach contents. Interestingly, krill were also important (7–17 %) of the wet weight and the average numbers per stomach were 2, 17, and 54, for 34–40, 40–50, and 55–66 cm cod respectively. Most of these krill were undigested and had probably just been consumed. The diel difference in the amount of cod caught and their feeding habits in midwater appeared to be related to the vertical migration of euphausiids.

Differences between the importance of *P. borealis* in the feeding habits of cod caught in the shrimp and midwater trawls are discussed later. Another difference between catches of the two types of nets was the absence of small cod in midwater catches. Small cod apparently did not migrate off the bottom as much as large cod (see BRUNEL 1965, 1972) perhaps a behavior that reduces their vulnerability to predation by large cod (DAAN 1973; O.M. Smedstad unpubl.).

180 m station — shrimp trawl. Capelin was by far the most important food for cod caught near the bottom in the shrimp trawl at this station (Table 4). Because only two cod

Table 4. Food of cod at the 180 m station in Balsfjorden on a percentage weight basis from stomachs containing food. The three most common animals by volume in the catches are also given, where Cap = capelin, Sh = shrimp, Dab = long rough dab, Ammo = sand eel, and Eupn = euphausiids. > means more abundant than. n = number of cod stomachs.

Date time h Common species	n	Length range of cod cm	Percent — wet weight Eupn.	Fish	Shrimp	Misc.
Shrimp trawl						
25 Aug. 1715–1745 Cap > Sh > Dab	4	50–70	2	91	7	<1
26 Aug. 0400–0450 Cap > Sh > Dab	5	59–67	3	82	10	5
	3	39–49	10	87	3	<1
26 Aug. 0740–0810 Cap > Sh > Cod	5	21–65	<1	96	4	0
26 Aug. 1400–1500 Cap > Sh > Dab	5	46–62	6	82	12	0
Midwater trawl — in 120 kHz SSL						
25 Aug. 1602–1634 Cap > Eupn > Cod						
150 m	4	67–73	39	60	2	0
	3	50–60	26	74	0	0
	2	27–41	94	3	0	3
26 Aug. 0157–0240 Cap > Eupn > Ammo						
55–100 m	4	68–74	4	96	1	0
	7	51–61	56	40	3	1
26 Aug. 0616–0703 Cap > Eupn > Ammo						
150 m	3	44–58	24	71	5	0
26 Aug. 1309–1400 Eupn > Cap > Cod						
150 m	3	39–74	44	47	9	0

smaller than 30 cm were caught, the diets of small and large cod could not be compared. Shrimp were less important at this station than at the 120 m station. Although krill occurred frequently they never constituted more than 10 % of the total weight of stomach contents of any group of cod caught in the shrimp trawl.

Diel differences in diet were not evident. Most capelin from cod stomachs were partially digested, indicating that they had not been eaten while in the net.

180 m station — midwater trawl. Capelin was also the predominant prey of cod caught in regions of midwater sound scattering that were sampled with the midwater trawl during all tows (Table 4). Euphausiids, however, were also important and comprised from 4 to 94 % of the stomach contents of these pelagic-caught cod. Both *M. norvegica* and *Thysanoessa* spp. were common. The number of krill eaten by these cod was large, averaging 29 to 146 krill per stomach for all but the smallest cod (27–41 cm) where it averaged 3.3.

An example of the 120 kHz echograms shows that the scattering layer was at about 150 m during the day and between 50 and 100 m at night (Fig. 1). These were the depths that were sampled with the midwater trawl.

Feeding habits of herring

120 m station — shrimp trawl. The stomachs of 49 herring 23–31 cm were examined from the shrimp trawl catches at the 120 m station. Nearly all of these herring had stomachs full of euphausiids. *Thysanoessa inermis* and *T. raschii* comprised 94 % of the stomach contents by weight. They were relatively fresh and undigested. Copepods were also present (percentages based on numbers of copepods were: Stage IV and V, *Metridia longa* 91 %, *Pseudocalanus* spp. 3 %, and unidentified 6 %). Amphipods *Parathemisto abyssorum* and post-larval *P. borealis* were sometimes present. These results are a further indication that euphausiids were concentrated near the bottom where they were preyed upon by herring and small cod.

180 m station — midwater trawl. Sixteen herring (15–18 cm) were also examined from a midwater trawl catch at 160 m at the 180 m station. Copepods were found in all but one of the stomachs and many stomachs contained hundreds of individuals. Of the copepods identified, 90 % were *M. longa*, 5 % *Pseudocalanus* spp., and 5 % unidentified. Euphausiids and euphausiid eyes were found in six herring. In this collection, copepods, and not euphausiids, were the major food of herring.

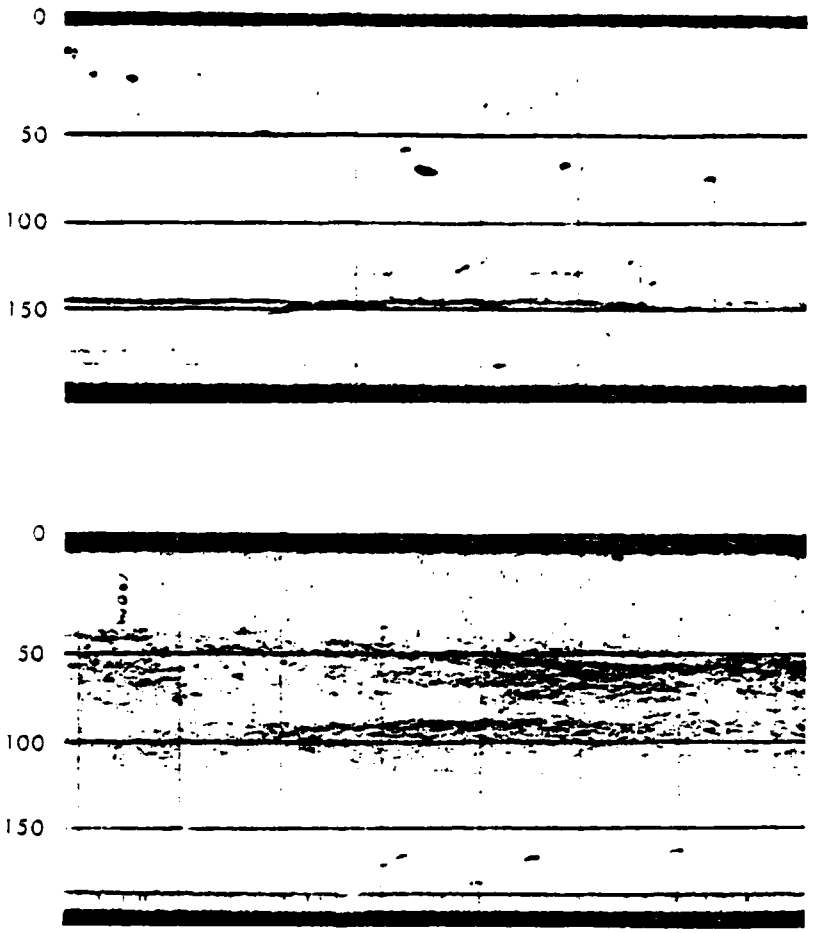

Fig. 1. 120 kHz echograms at the 180 m station in Balsfjorden. Upper: During midwater trawl at 150 m, 25 Aug. 1978, 1602–1634 h. Lower: During midwater trawl at 55–100 m, 26 Aug. 1978, 0157–0240 h.

Feeding habits of capelin

120 m station — midwater trawl. The 44 capelin examined from the midwater trawl at the 120 m station at depths of 50–65 m, 1930–2000 h, all had stomachs that were less than one-half full. Many stomachs were empty. The food items that were identified consisted mainly of a few copepods per stomach (91 % *Pseudocalanus elongatus*, 5 % *Calanus finmarchicus*, and 4 % *Metridia longa*) or more rarely a few chaetognaths or mysids. Euphausiids were not found.

180 m station — midwater trawl and shrimp trawl. In contrast to the 120 m station, the 110 capelin 10–15 cm TL examined from both the midwater trawl in the vicinity of the SSL at 55–150 m and the bottom trawls at the 180 m station, had larger amounts of food in their stomachs. *Thysanoessa* spp. were the main food (Table 5) on a volumetric basis. The average number of euphausiids from stomachs that contained krill was 1.3 animals in capelin caught in both bottom and midwater trawls. One capelin contained eight krill. Cope-

Table 5. Occurrence of euphausiids Eupn. and copepods Cop. from the stomachs of capelin captured in shrimp and midwater trawls at the 180 m station.

Time of tow	Frequency of empty stomachs	Frequency of occurrence Euph.	Cop.	Average number Euph. stomach
Shrimp trawl				
1715–1745	6/10	4/4	0/4	1.0
0400–0450	9/20	7/11	4/11	1.0
0740–0810	3/17	11/14	4/14	1.5
1400–1500	5/14	6/9	4/9	1.3
Midwater trawl				
1602–1632	10/17	4/7	3/7	0.9
0157–0240	9/14	2/5	4/5	0.8
0616–0703	3/7	2/4	3/4	0.5
1309–1400	3/11	8/8	1/8	2.0

pods were common prey in about one-third of these capelin, and although they were much more numerous than euphausiids, on the average, they never comprised the bulk of the contents for fish in a trawl collection. Over 95 % of the identified copepods were *Metridia longa*. A few *Pseudocalanus elongatus* and one *Podon* were identified.

DISCUSSION

Although euphausiids and pelagic animals are not important food for cod in the North Sea (RAE 1967; DAAN 1973; ARNTZ, 1974), they are known to be very important in more northern seas. WIBORG (1948, 1949) reported that krill, mainly *T. inermis*, was the most important food for 0, I, and II-group cod on trawling grounds in northern Norway and fjords of northern Norway, including Balsfjorden. *Thysanoessa inermis* was also important cod food off Bear Island and Spitsbergen, especially during the spring and summer (BROWN & CHENG 1946) and in the Barents Sea (BROTSKY 1931 as cited by BROWN & CHENG). SIDORENKO (1962) found that cod fed extensively on euphausiids in waters off western Greenland, and ZADULSKAIA & SMIRNOV (1939) reported that krill and hyperiid amphipods were of greatest importance for cod in the Barents Sea. ZATSEPIN & PETROVA (1939) noted a pronounced seasonal cycle in the feeding of cod from the southern Barents Sea: krill were the most important food in summer months and capelin, herring, and polar cod were most important at other times of the year. In more recent years, capelin and shrimp were reported to be the most important food for cod in the Barents Sea (O. M. Smedstad unpubl.). BRUNEL 1965 found that herring, capelin, and euphausiids *Thysanoessa* and *Meganyctiphanes* in that order, were the most important pelagic prey for cod from the Gulf of St. Lawrence.

Few studies have been made on the feeding habits of capelin and herring from northern regions. Capelin are known to prey on surface swarms of *Thysaonessa raschii* in the Barents Sea, and according to PROKHOROV 1965) euphausiids compose most of the weight of the stomach contents of capelin in this region, followed by copepods and amphipods.

In this study, euphausiids were important prey for the three commercially important fishes that predominated the catches: cod, capelin, and herring. Euphausiids were the main food of small cod and herring at the 120 m station. During the daytime, euphausiids presumably are near the bottom at this depth and hence were particularly susceptible to capture by bottom or near-bottom fishes. At the 180 m station, 120 kHz sound scattering layers and associated euphausiids did not impinge on the bottom (Fig. 1), but resided at about 150 m during the day. At this station, few euphausiids were caught in bottom compared to midwater trawls and cod captured in bottom trawls had not fed as heavily on euphausiids as midwater-caught cod. Apparently at this deeper station, euphausiids were far enough above the bottom to escape intense predation by bottom-dwelling cod. Thus interactions of diel migrants, such as euphausiids, with benthic and midwater fishes may be an important mechanism for transfer of energy in marine food webs (ISAACS & SCHWARTZLOSE 1965).

Several observations suggest two different feeding behaviors for cod in Balsfjorden: pelagic feeders and benthic feeders. Large cod caught in bottom tows at 120 m ate substantial amounts of shrimp. Cod caught in midwater at night, on the other hand, had eaten mainly capelin and only 3 small *Pandalus*. This suggests that these midwater cod had not recently fed on the bottom and had been preying almost exclusively on pelagic animals, mostly capelin and euphausiids.

At the 180 m station, cod caught on the bottom during day and night periods had few euphausiids in their stomachs. Conversely, cod caught in midwater contained large numbers of euphausiids during either day or night periods.

These differences in feeding habits suggest that some cod were primarily benthic and had not migrated far off the sea floor to feed and others were predominantly pelagic and preyed on vertically migrating capelin and krill.

Several *Leptoclinus maculatus* were found in cod caught in midwater at the 120 m station but this fish, normally considered to be benthic, was also caught in midwater trawls (Table 1), so it cannot be used as an indicator of benthic feeding. Similarly, small *P. borealis* were found in a few of cod caught in midwater at night at both stations, but small shrimp were also caught in night-time midwater trawls, so their presence in cod stomachs does not necessarily represent benthic feeding. *Ammodytes* were also found in both cod stomachs and midwater trawl catches from night-time tows.

BRUNEL (1965, 1972) reviewed the evidence for vertical migrations, the pelagic existence of cod and possible causal mechanisms for migratory behavior. In his study in the Gulf of St. Lawrence, he distinguished two types of vertical migrations: a type bringing cod into midwater at night and near the bottom during the day and a 'residual' type when cod reside in midwater during the day. These conclusions were based on echograms, catches of cod in bottom trawls and gill nets, food habits of cod, and the abundance of their main prey. He thought that the cod were attracted to midwater during the day by visual stimuli of pelagic prey swarming during the period of maximum daylight from May to mid-July. TROUT (1957) and TEMPLEMAN & FLEMING (1962) also recognized that cod may live in midwater for extended periods, or migrate vertically and reside close to the bottom during the day. We suggest that cod exhibit both types of behavior in Balsfjorden during the summer.

ACKNOWLEDGEMENTS

The first author is grateful to the University of Tromsø for financial supports as a visiting researcher in Norway and to the Office of Naval Research for support through Contract N00014-76-C-0067 under Project NR 083-102. We all thank the crews of the R.V *Johan Ruud* and *Ottar* for their splendid cooperation and patience. Eivind Oug for identification of some benthic animals. Wim Vader for identification of amphipods, and A.G. Carey, Jr. for comments on the manuscript.

REFERENCES

ARNTZ, W.E. 1974. Die Nahrung juveniler Dorsche *Gadus morhua* L. in der Kieler Bucht. — *Ber. dt. wiss. Komm. Meeresforsch.* 23: 97–129.

BROWN, W.W. & C. CHENG 1946. Investigations into the food of the cod *Gadus callarias* L. off Bear Island, and the cod and haddock *G. aeglefinus* L. off Iceland and the Murman coast. — *Hull. Bull. mar. Ecol.* 3(18): 35–71.

BRUNEL, P. 1965. Food as a factor or indicator of vertical migrations of cod in the western Gulf of St. Lawrence. — *Int. Comm. Northwest Atlantic Fish. Spec. Publ.* 6: 439–448.

— 1972. The Gaspe cod ecosystem in the Gulf of St. Lawrence. III. The daily and seasonal vertical migrations of cod *Gadus morhua* in 1960–62. — *Naturaliste Can.* 99: 287–357.

DAAN, N. 1973. A quantitative analysis of the food intake of North Sea cod, *Gadus morhua*. — *Neth. J. Sea Res.* 6: 479–517.

FARQUHAR, G.B. ed. 1971. *Proceedings of an international symposium on biological sound scattering in the ocean.* — Maury Center for Ocean Science, Washington, D.C. 629 pp.

GREENLAW, C.F. 1979. Acoustical estimation of zooplankton populations. — *Limnol. Oceanogr.* 24: 226–242.

HOPKINS, C.C.E. & B. GULLIKSEN. 1978. Diurnal vertical migration and zooplankton–epibenthos relationships in a north Norwegian fjord. — Pp. 271–280 in: MCLUSKY, D.S. & A. BERRY eds., *Physiology and behaviour of marine organisms. Proc. 12th European Symp. Mar. Biol.* Pergamon Press, Oxford.

HOPKINS, C.C.E., S. FALK-PETERSON, K. TANDE & H.C. EILERTSEN. 1978. A preliminary study of zooplankton sound scattering layers in Balsfjorden, structure, energetics, and migrations. — *Sarsia* 63: 255–264.

ISAACS, J.D. & R.A. SCHWARTZLOSE 1965. Migrant sound scatterers: interaction with the sea floor. — *Science, N.Y.* 150: 1810–1813.

KINZER, J. 1971. On the contribution of euphausiids and other plankton organisms to deep scattering layers in the eastern north Atlantic. — Pp. 476–489 in: FARQUHAR, G.B. ed. *Proc. int. Symp. Biol. Sound Scattering in the Ocean.* Maury Center for Ocean Science, Washington, D.C.

PROKHOROV, V.S. 1965. Ecology of the Barents Sea capelin *Mallotus villosus* Muller and prospects for commercial utilization. — *Trudy polyarn. nauchnoissled. Inst. Morsk. ryb. Khoz. Okeanogr.* 19: 1–70. Fish Res. Bd. Can. Transl. Ser. No. 813, 1967.

RAE, B.B. 1967. The food of cod in the North Sea and west of Scotland grounds. — *Mar. Res., Dept. Agric. Fish. Scotland* 1: 1–68.

SAMEOTO, D.D. 1976. Distribution of sound scattering layers caused by euphausiids and their relation to chlorophyll *a* concentrations in the Gulf of St. Lawrence. — *J. Fish. Res. Bd Can.* 33: 681–687.

SIDORENKO, L.N. 1962. Feeding of cod in western Greenland Waters. — Pp. 249–255 in: MART, Y.Y. ed., *Issledovaniya nauchno-issled. Inst. Morsk. ryb. Khoz. Okeanogr. Soviet Fisheries Investigations*

in the Northwest Atlantic. Israel Progr. Sci. Transl. 1963.

TEMPLEMAN, W. & A.M. FLEMING. 1962. Cod tagging in the Newfoundland area during 1947 and 1948. — *J. Fish. Res. Bd. Can.* 19:445–487.

TROUT, G.C. 1957. The Bear Island cod: migrations and movements. — *Fishery Invest., Lond., Ser. 2,* 21:1–31.

WIBORG, K.F. 1948. Some observations on the food of cod *Gadus callarias* L., of the 0–II group from deep water and the littoral zone in northern Norway and from deep water at Spitzbergen. *Fisk.Dir. Skr., Ser. Havundersøkelser* 9(4):1–19.

– 1949. The food of cod *Gadus callarias* L. of the 0–II group from deep water in some fjords of northern Norway. — *Fisk.Dir. Skr., Ser. Havundersøkelser* 9(8):1–27.

ZADULSKAIA, E.S. & K.S. SMIRNOV. 1939. Diurnal patterns of feeding of cod on the fishing grounds of the Barents Sea. — *Trudy Vsesoyuzn. nauchno-issled. Inst. morsk. ryb. Khoz. Okeanogr.* 4:321–338. Fish. Res. Bd. Can. Transl. Ser. No. 483.

ZATSEPIN, V.I. and N.S. PETROVA. 1939. The food of commercial stocks of cod in the southern part of the Barents Sea. — *Trudy polyarn. nauchno-issled. Inst. Morsk. ryb. Khoz. Okeanogr.* 5:1–171. Fish Res. Bd. Can. Transl. Ser. No. 498, 1964.

Received 13 March 1979.

Nova Hedwigia · Beiheft 64 · 1979

Diatom Taphocoenoses in the Coastal Upwelling Area off Western South America

by

Gretchen Schuette and Hans Schrader

School of Oceanography, Oregon State University, Corvallis, OR 97331, U.S.A.

With 13 figures

Abstract: Diatom floral analysis of 116 sediment surface samples obtained off Peru reveals a boundary in the sediments between coastal upwelling influenced sediments and sediments outside the highly productive realm. Sinuous patterns of relative abundance for meroplanktic species (*Actinocyclus octonarius*, *Actinoptychus senarius*, and *Cyclotella striata/stylorum*) may preserve the meander-like patterns of surface water parameters off Peru. The occurrence of loci of high abundance of diatom valves per gram of dry sediment, and the limited occurrence of *Skeletonema costatum* and of a species of the genus *Delphineis* are additional pieces of evidence that upwelled tongues of cold water have a correspondingly patchy sediment signal.

Introduction

The diatom fraction of 116 sediment surface samples collected off western South America was studied in order to identify on the Peru continental margin the sediment record of coastal upwelling. The purpose was to differentiate sediments containing this record from those not influenced by the high rates of primary production associated with coastal upwelling (Ryther 1969).

Diatoms dominate the phytoplankton communities in coastal upwelling regions (Blasco 1971, Margalef 1973, Hart & Currie 1960, Berger 1976), and the preservation and abundance of their valves in hemipelagic sediments along the western coasts of continents has been documented (Calvert 1966, Calvert and Price 1971, Zhuse 1972). This study analyzes the distinct patterns of diatom distribution found in recent sediments preserving evidence of recurrent coastal upwelling off Peru.

The coastal upwelling process is described by Smith (1978). He estimates that the response to wind events off Peru occurs within 50 km from shore, with a depth of origin around 70 meters subsurface for the water found at the surface after favorable winds. A poleward undercurrent dominates the shelf with mean currents in a direction opposite to the mean wind, except in a shallow surface layer. The curvature of the midshelf bathymetry and of the shelf break are thought to influence the alongshore flow, its variability, and the magnitude of upwelling (SCOR Wg 36 1976). Maeda & Kishimoto (1970) have found upwelling centers to be present consistently at 5°, 11° and 15° S over a 17 year period, but further observational studies are needed to describe and locate the physical process of upwelling and to delineate its effect on plant and animal populations. This sediment study provides a testimony to the persistence of upwelling at certain locations.

Materials and Methods

Samples were taken from the uppermost sediments retrieved at the coring stations listed in Table I. The numbers in the first column will be used in the rest of this paper when referring to stations (see also Fig. 1). The ship and year of the cruise are registered in the OSU core numbers: e.g., W77- indicates the 1977 cruise of RV Wecoma; Y71-, the 1971 cruise of RV Yaquina; FD75-, the 1975 cruise of RV Francis Drake.

Those cores collected by the Reineck box (RB), the Kasten (K), the free fall (FF), and the gravity (G or MG) corers appeared to successfully retrieve the surface layer of sediments. The uppermost sediments may have been lost in the recovery of some of the piston (P) cores.

The uppermost few centimeters (in some cases, only the first one cm; at most, the first 20 cm) of the Wecoma cores were placed in plastic bags when the cores were first opened aboard the ship. Samples were later taken from these bags of composite surface sediments. Thus, the nearshore samples, which may have been deposited at rates of about 66-140 cm/1000 years (see Discussion), represent from about 7 to 300 years of deposition.

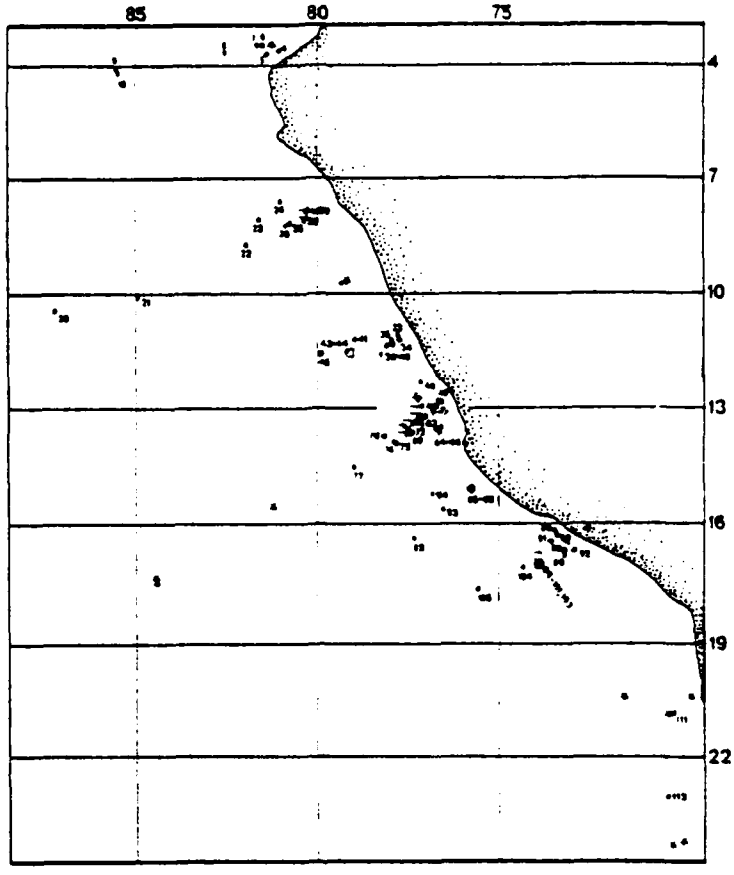

Fig. 1. Station locations, some stations are not numbered. □, stations not included in data analysis because of evidence of reworking of older floras; *, barren samples.

Samples were taken from bags as described above, or from the top sediments of cores stored in the OSU Core Repository. The procedure was to fill a bulk density ring of ca. 1.5 cm diameter (1 cm high) by pushing it into the soft sediments. Piston cores and gravity cores are split in half lengthwise for storage, and the tube samplers were pushed into the middle of the top of a core-half at a right angle to the long axis of the core-half, thus sampling the top 1.5 cm of the core. Downcore samples from W7706-64 were taken in the same way at selected depths in the core.

All samples were oven dried for 24 hours at 60° C in the sampling tubes and then extracted into the beakers used for the acid cleaning procedure. The dry weight of each sample was in a range from 0.5-2.0 grams.

Slide preparation followed the procedure outlined in Schrader (1974) and Schrader & Gersonde (1978) with the following exceptions: 1) Slides were made for all samples from a 50 ml dilution of the acid resistant residue remaining after cleaning and fractional sedimentation to remove the clay fraction. Automatic pipets were used for this subsampling. 25 µl were placed on slides for surface sediment samples; 50 µl for downcore samples. 2) Coverglasses were allowed to air dry.

The microscopical investigations were done on a Leitz-Orthoplan-Orthomat microscope using high power and high resolution apochromatic oil immersion objectives. Counts were made using the highest available magnification (Objective Apo oil 100×, n.A. 1.32. Ocular: Periplan GW 10× M) with counting procedures standardized in our lab after Schrader & Gersonde (1978). Each slide was counted in traverses randomly laid over the middle of the coverglass. About 300 valves were counted per slide, although, in some stations from the oceanic plate or outside the productive coastal region, limited preservation of diatoms in the sediments prohibited reaching this figure.

Observations

Numbers of diatom valves per gram of dry original sediment were calculated as described in Schrader & Gersonde (1978) and these values are listed in Table I. Barren and almost barren surface samples are indicated in this table by a zero value.

Approximately 110 different marine planktic and benthic species were identified. Some species represented reworked or exposed Pleistocene/Pliocene/Miocene floras. Some species were displaced freshwater diatoms. These occurred in greatest abundance (still less than 1% of the total assemblage) at sites 91, 94, 95, 99 and 104. Core tops with displaced shallow water marine benthics and with reworked older material are indicated in Table I.

Sixty-three species or species group categories were adopted for systematic counting and the relative abundance values in these categories were determined at 91 stations. From these 91 stations, 9 stations outside the coastal regime were eliminated from further analysis (stations 11-19), and 7 stations (27, 42, 58, 61, 70, 71, and 102) were eliminated because of evidence of reworking of older floras. The data from the following stations were combined because of proximity of the stations: 6+7, 9+10, 33+34, 35+36, 37+38, 39+40, 43+44, 48+49, 50+51, 54+56+57, 64+65+66, 69+72, 85+86+87+88, 89+90, 93+94, 95-101+103.

The original 63 species categories were altered in the following manner. Some species were left out of further data reduction because they are very rare in the samples (*Coscinodiscus A., C. asteromphalus, Lithodesmium undulatum, Thalassiosira gravida, Pseudotriceratium punctatum*), or because they are displaced benthics (*Triceratium alternans* and the category "marine benthics"), or because they represent reworked floras (i.e., *Cussia lancettula*). Some species were combined because similarity of morphology prevented consistent distinctions between species during routine counting procedures, i.e., *Actinocyclus curvatulus/Coscinodiscus rothii; Thallasiothrix mediterranea/T. longissima; Thalassiosira eccentrica/T. symmetrica/T. punctifera/T. spinosa;* and all *Chaetoceros* resting spores. To decrease the number of variables, species of similar distribution in our data set were combined as follows:

— *Cyclotella striata* + *Cyclotella stylorum*

— *Asteromphalus* group + *A.* #1 + *A.* #2

— *Coscinodiscus africanus* + *C. tabularis*

— *Coscinodiscus nodulifer* + *C. radiatus*

— *Coscinodiscus obscurus* + *C. perforatus*

— *Stephanopyxis palmeriana* + *S. turris*

— *Thalassiosira* A + *Thalassiosira* B

— *Thalassiothrix* spp. + *T. mediterranea/T. longissima* + *T. frauenfeldii*

Further analysis then was based on the resulting 43 taxonomic categories. The matrix of 49 stations and 42 "species" (Table II) was the basis for a Q-mode (Fortran IV program CABFAC, Klovan &

Imbrie 1971, Imbrie & Kipp 1971) analysis of data. R-mode analysis (SPSS Subprogram FACTOR, PA2, Varimax Orthogonal Rotation) of the same data set (but without stations 111 and 113) was also accomplished.

Discussion

Interpretation of our data allows conclusions regarding the location of recurrent coastal upwelling off Peru and regarding the identification of species and species groups characteristic of sediments influenced by coastal upwelling. Preliminary data analysis supported the hypothesis that upwelling influenced sediments may be recognized and separated from adjacent regimes by the diatom composition of sediments. A factor analysis of species counts in 35 categories from 70 stations was undertaken to verify a sediment signal of the coastal upwelling process. This analysis produced 3 factors accounting for 93% of the variance in the data set and the factor loadings did generate interpretable distribution patterns for these factors.

Factor 1, accounting for 63% of the variance (Fig. 2), has high loadings in all continental margin stations. It is dominated by the resting spores of *Chaetoceros*. Factor 2, accounting for 20% of the variance (Fig. 3), has high loadings in the oceanic plate stations. It is dominated by *Coscinodiscus nodulifer*. It is not unexpected that 83% of the variance in our data set rests on the large differences between oceanic and coastal phytoplankton assemblages since Q mode analysis compares abundant species. Factor 3, accounting for 10% of the variance (Fig. 4), has highest loadings at stations 22, 27, 30, 40, 54, and 61, and is characterized by *Cyclotella striata/stylorum*. This factor did resolve distinct regions of importance for an assemblage which may be characteristic of coastal upwelling.

Fig. 2. Factor 1. Contours in this figure and Figs 3, 4, 7-12 were drawn, in those places where there was poor sample control, so as to conform to the concept of a sinuous seaward boundary for upwelling influenced sediments. This concept is strongly supported in areas of good control. Fig. 3. Factor 2. Fig. 4. Factor 3.

2

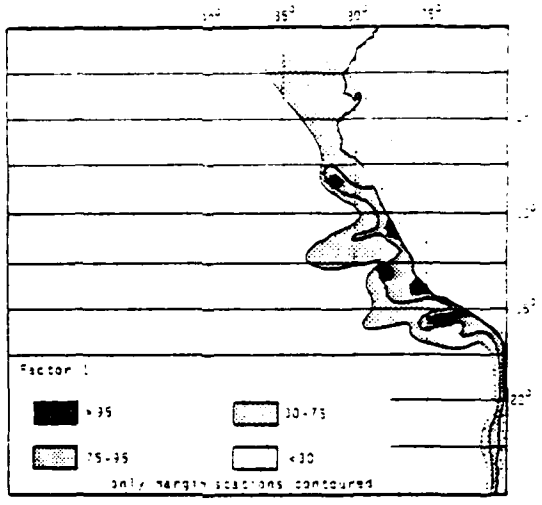
Factor 1
>.95
.90-.75
.75-.95
<.90
only margin stations contoured

3

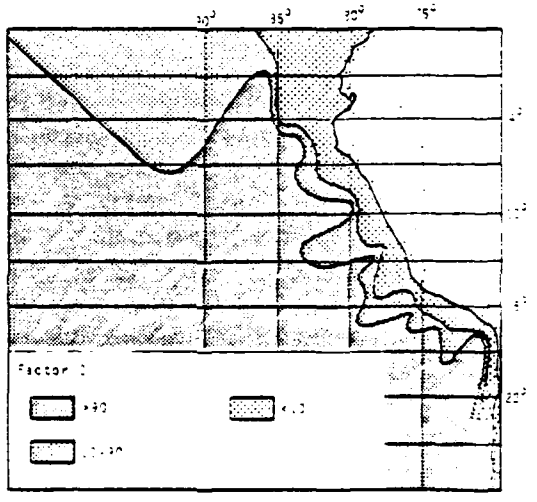
Factor 2

4

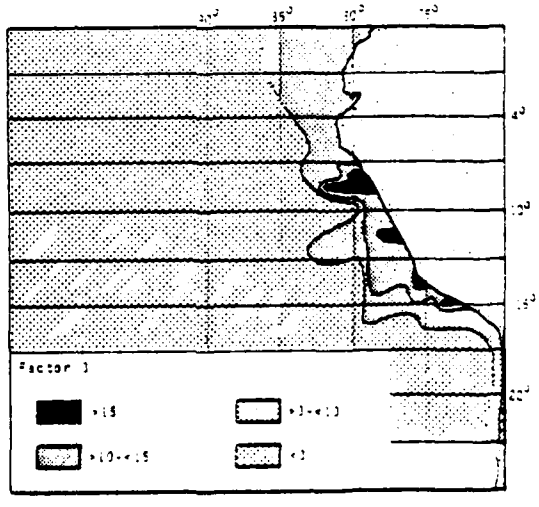
Factor 3

Meroplanktic Species

Cyclotella striata/stylorum, along with two other relatively abundant species, *Actinocyclus octonarius* and *Actinoptychus senarius*, are meroplanktic species, i.e., organisms which either produce a resting spore or possess a sedentary stage or dormant phase in their life cycle (Smayda 1958). Meroplanktic species are cosmopolitan in middle and low latitudes and occur in turbulent near-shore waters. Apparently none of the meroplanktic species abundant in sediments off Peru dominates phytoplankton assemblages in the surface waters (Strickland et al. 1969). But heavy silicification of the valves of these diatoms enhances their preservation, and the high supply of all diatoms to deposits underlying areas of high fertility and productivity accounts for the presence and abundance of meroplanktic species in these sediments.

When the abundance of the meroplanktic group of species (relative to all diatom species) is plotted in a depth-shore distance profile, the restriction of this component to a particular depth and shore-distance range becomes apparent (Fig. 5). Highest relative abundance occurs between 20 and 60 nautical miles from shore and in water depth of less than 2500 meters. *Chaetoceros* resting spores, which we have seen are also important in sediments underlying the near-shore productive region, have their peak in abundance further offshore and thus at greater water depths (Fig. 6). Formation of *Chaetoceros* resting spores may occur during a *Chaetoceros*-dominated stage of succession when nutrients are nearly exhausted in the euphotic zone (Guillard & Kilham 1977). Thus, the offshore distribution pattern for these spores may be interpreted to reflect the seaward edge of nutrient-replete surface waters.

Zhuse (1972) recorded *Chaetoceros* spore dominance on the shelf off Callao. She also found that diatom assemblages consisted of large "neritic" species at some of her coastal stations. She characterized

Fig. 5. Distribution of relative abundance of the meroplanktic species group (*Actinocyclus octonarius* – *Actinoptychus senarius* – *A. splendens* – *Cyclotella striata/stylorum*). Sample stations were plotted according to their water depth and distance perpendicular to the coastline. Fig. 6. Distribution of relative abundance of the *Chaetoceros* resting spores. Sample stations plotted as in Fig. 5. Fig. 7. Occurrence of *Delphineis*.

5

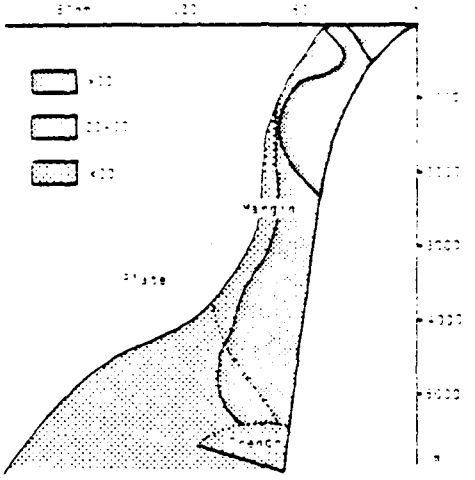

6

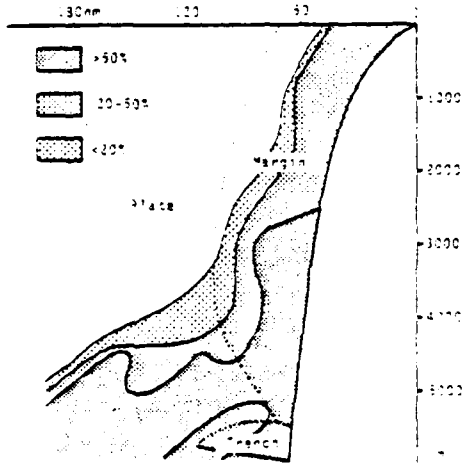

7

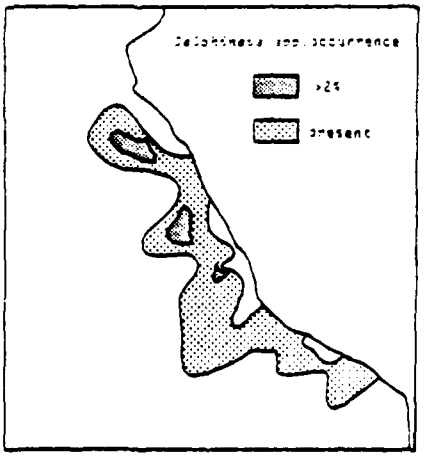

the distribution of her moderately-warm water — subtropical diatom complex, which consists chiefly of "neritic" species, as corresponding with the area of the cold Peru-Chile current. The extension of this complex away from the coast in the latitude of Callao (12° S) concurs in general with the high relative abundance of our meroplanktic complex at stations 39, 40, 54, 55, 57, 59-61, 63-65 and 69-71.

Diatom Abundance

The circulation within a coastal upwelling regime accounts for its anomalous character compared to adjacent regimes. The familiar profile or circulation (Hart & Currie 1960) includes wind induced offshore transport of surface water and compensating upwelling of nutrient rich deeper waters. This circumstance provides for high fertility and high primary productivity in a near-shore zone and concomitant preservation of siliceous microfossils in sediments underlying this zone. There is a boundary, then, between the productive coastal upwelling region where nutrients upwell to the euphotic layer and the less productive oceanic realm where light energy is separated from deep nutrient reserves. This boundary is documented by our surface sediment data.

Our calculations of abundance of diatoms per gram of dry sediment reveal a sinuous boundary of the coastal upwelling region of high abundance with the oceanic realm, and discrete loci of highest abundance within a definite latitudinal range. Five clusters of high values occur at these stations: (1) 23, 24, 26; (2) 33, 34; (3) 42, 43, 44; (4) 48, 58, 61, 62, 63, 66, 68, 69, 70, 71, 72, 73, 74; (5) 91, 99, 102. Four areas are offset from the coastline suggesting offshore centers of upwelling influence, in addition, perhaps, to the near-shore region of high abundance evident at about 12° S. The inner shelf region is not well represented in the sample net; this study is predominantly of midshelf of oceanic plate sediments. Other inner shelf deposits were not sampled.

Available accumulation rates are in permissive agreement with the coarse distinction between diatom-rich sediments within the upwelling region and oceanic diatom-poor sediments. Pb 210 dating of the uppermost part of the cores from stations 34 and 65 gives sedimenta-

tion rates of 140 cm/1000 years and 66 cm/1000 years respectively. Accumulation rates calculated for these cores [dry bulk density (salt corrected) × sedimentation rate × number of diatoms/g] are 7.4 and 0.3 million diatoms/cm^2/year. On the other hand, accumulation rates for oceanic plate sediments range from zero to about 0.05 million diatoms/cm^2/year.

Zhuse (1972) also established the existence of a region of highly siliceous facies in a restricted area near Peru, and her figure of 20-50 million valves/gram of sediment on the shelf and trench near Callao is in general agreement with our data (her data did not include the area south of Pisco between 13 1/2° and 19° S). She also remarked that the quantitative distribution of diatoms in the surface layer of sediments is "highly uneven". Variations are indeed great in sediments at the coastal stations. Our data, as was stated above, could not be encompassed by simple contours parallel to the coast.

Occurrence of *Delphineis*

The distribution of one species of the genus *Delphineis* matches in its occurrence offshore areas of highest diatom abundance per gram (Fig. 7). Areas of greatest relative abundance (greater than 2%) are centered at station 23 and at station 60 matching the two major centers of diatom valve abundance, near 8° S, and between 13 and 14° S. *Delphineis* is present in greater than 1% relative abundance at stations 95 and 99, in the center of high abundance of diatoms per gram around 17° S. It is relatively abundant (1.4-3.3%) near station 42 where diatom abundance was also greater than 30 million valves/gram.

Delphineis is of particular interest as it may be a specific indicator of coastal upwelling. We have found that it occurs only in active coastal upwelling regions of the present and in deposits representing locations affected by very productive coastal surface waters of the past. The taxonomy of this genus is currently under revision. Simonsen (1974) described a form from the Indian Ocean as *Rhaphoneis surirelloides*, some specimens of which we feel belong into the genus *Delphineis* as defined by Andrews (1977). A similar form described by Fryxell & Miller (1978) from the west coast of South Africa as *Fragilaria karstenii* probably also belongs to this genus. In addition, *Rhaphoneis*

ischaboensis, found by Zhuse (1972) in sediments off Peru, and described by Mertz (1966) from the Pisco Formation, has strong affinities for *Delphineis*.

Relative Abundance Data

The relative abundance data for all 43 species categories (Table II) were examined in order to identify species, or groups of species, characteristic of coastal upwelling. The patterns produced by these basic data may also be used to characterize sediments underlying a coastal upwelling regime and to describe the geographic limits of influence of the coastal upwelling phenomenon on surface sediments. The sinuous pattern of sedimentation of important diatom species and species groups, and the localized high abundances of species and groups distinguishes this region.

Important species with highest abundance outside the coastal region between 7° and 18° S include: *Coscinodiscus nodulifer*, *Pseudoeunotia doliolus*, and *Thalassionema nitzschioides* v. *parva*. The category *Coscinodiscus nodulifer* + *C. radiatus* is present in greater than 20% at all stations west of 84° W with a high value of 61.1% at station 21. But it also has high abundance (greater than 15%) at these stations: 8, 22, 25, 35–36, 45, 55, 74, 76, 77; and occurs in all samples examined. As Zhuse suggested (1972), the distribution of a complex of diatoms associated with the "tropical" region may be illustrated by the distribution of *Coscinodiscus nodulifer*. The eastern boundary of this complex must be characterized, however, as approching and receding from the coast as it outlines the areas of upwelling influence mentioned above (Fig. 8).

Pseudoeunotia doliolus occurs in greater than 5% at almost all stations on the oceanic plate, but it also occurs in greater than 5% at stations 77, 82, and 84. *Thalassionema nitzschioides* v. *parva* occurs on the margin in greater than 5% at stations 4, 6–7, 8, 45, 64–65–

Figs 8-12. Relative abundances of *Coscinodiscus nofulifer/C. radiatus*, *Cycloteila striata/stylorum*, *Actinocyclus octonarius*, *Actinoptychus senarius*, and the *Thalassiosira eccentrica* group. — Fig. 13. Shannon-Wiener diversity values showing a displacement offshore of highest values.

8

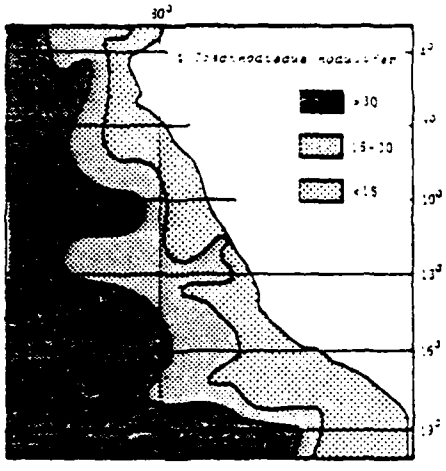

9

10

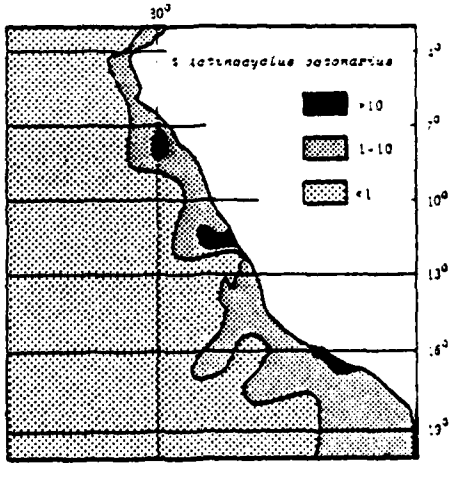

11

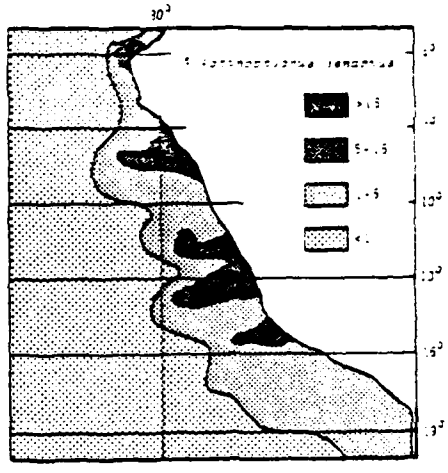

12

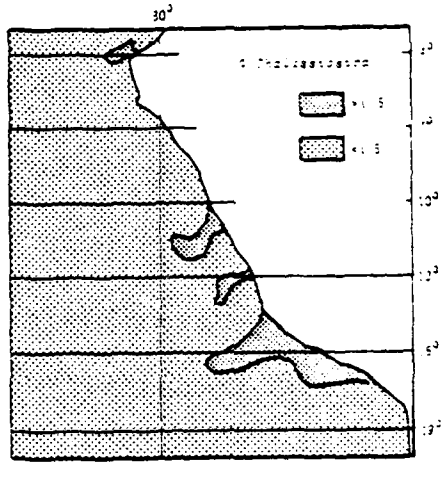

13

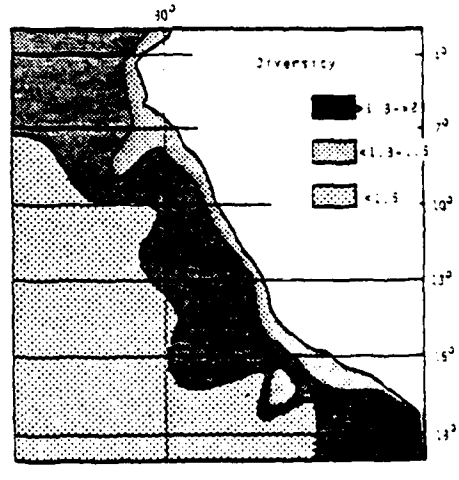

66, and 83. Other species identified as characteristic of tropical oceanic waters which are present in lesser percentages include *Thalassiosira oestrupii. Roperia tesselata.* and *Rhizosolenia bergonii.*

Important species east of 84° W include *Chaetoceros* resting spores. *Cyclotella striata/stylorum. Actinocyclus octonarius. Actinoptychus senarius. Thalassionema nitzschioides.* and the *Thalassiosira eccentrica* group.

Chaetoceros spores reach 75-85% of the entire population at our southernmost stations, 111 and 113, which is in agreement with Zhuse's (1972) data from off Antofagasta (23-24° S). However, we also found high percentages (greater than 50%) at stations 4, 23, 24, 33+34, 42, 48+49, and 62, as well as in 8 stations in the region not covered by the Russian survey: 74, 75, 85-88, 91, 93−94, 95-101+103, 104, and 105. In fact there are only 9 margin stations with values less than 30% *Chaetoceros* resting spores: 22, 25, 28, 30, 37−38, 39+40, 60, 82, and 92.

Cyclotella striata/stylorum has a maximum abundance of 35% at station 22, greater than 20% at 28 and 15-20% at 25, 26, 30 and 55. It is present at all margin stations and is greater than 5% at 32 stations (Fig. 9).

Actinocyclus octonarius occurs in greater than 10% relative abundance at 6 stations with a maximum of 30.8% at stations 89+90. High abundances occur in the following additional stations: 28, 30, 37+38, 39+40, and 92 (Fig. 10).

Actinoptychus senarius occurs (with a maximum of 25.5% at station 60) in greater than 5% at 23 stations but in greater than 10% at only 9 stations: 5, 25, 28, 35+36, 46, 50+51, 55, 59, and 60 (Fig. 11).

The *Thalassiosira eccentrica* group occurs in 1-5% at many nearshore stations between 11 and 18° S (Fig. 12). Station 60 shows an especially high percentage of 26.5%.

Thalassionema nitzschioides occurs in margin samples at greater than 10% at 24 stations. This category includes all forms of this species as described by various authors (Heiden & Kolbe 1927, Hustedt 1959, Van Heurck 1880, Frenguelli 1949, Hasle & de Mendiola 1967, Hasle 1960, Kolbe 1954, 1955, 1957, and Mertz 1966) except the variety *parva.*

Factor Analysis of Samples in the Coastal Region

Q-mode factor analysis was applied to reveal the major patterns of variation within the coastal upwelling region itself. 98% of the total variance in the diatom taphocoenoses was accounted for by five factors. The species which were major contributors to these 5 factors are the *Chaetoceros* resting spore group already mentioned, *Coscinodiscus nodulifer/C. radiatus* characteristic of oceanic waters, and four other species: *Actinocyclus octonarius, Cyclotella striata/stylorum, Actinoptychus senarius,* and the *Thalassiosira eccentrica* species group (see Table III for the calculated factor scores showing the contributions of these species and groups to the five factors). The Varimax Factor matrix in Table IV indicates the importance of each factor at each site and the distribution of these factor loadings supports the major conclusions with regard to the character of the upwelling influenced region.

The sediments influenced by upwelling do indeed have a diatom flora which is distinct from that of sediments associated with adjacent oceanographic regimes. 69% of the variance in the data is located in two factors which define this distinction. The boundaries of the nearshore productivity region coincide with the area of highest loadings for Factor 1 in which the *Chaetoceros* resting spore group is dominant. The highest loadings for Factor 2 reflect the incursions of a more oceanic assemblage.

The characterization of the upwelling regime as producing tongue-like patterns of sedimentation for almost all diatom species and species groups found in sediments is also supported in this analysis. The loadings of those factors dominated by meroplanktic species illustrate the discontinuous nature of the upwelling signal in the sediments. That is, our findings are in permissive agreement with a concept in which high primary production as a result of coastal upwelling occurs in relatively stable plumes or areas of upwelling (SCOR Wg 36 1973, 1974, 1976). Our work can be considered along with other observations and efforts in modelling upwelling ecosystems which have modified the more conventional view of upwelling as a continuous band of nutrient- and phytoplankton-rich water parallel to the coast.

The Q-mode factor analysis satisfied our interest in the relationships among the samples. Interest in species associations or assem-

blages required R-mode analysis in which even the rarely encountered species would receive equal consideration along with the abundant forms that dominated the cross-products matrix analysis of CABFAC. 28 R-mode factors were necessary to account for 90% of the variance. This is not unexpected considering the patchy distribution of many species (see Fig. 13 for a map of the Shannon/Wiener diversity values for our samples). 66.5% of the variance, however, could be explained by 10 factors (Tables V and VI). Many of these factors pointed to a variety of distribution patterns within the two major realms recognized in the first two factors of the Q-mode analysis: Five factors (explaining together 60.0% of the variance explained by the 10 factors) are interpreted as describing relationships between oceanic diatom complexes and elements of the predominantly meroplanktic upwelling assemblages.

Some of these factors deserve special mention. The assemblage most characteristic of oceanic waters, and accounting for 25% of the variance explained by the 10 factors, included: *Coscinodiscus nodulifer/C. radiatus, Nitzschia marina, Pseudoeunotia doliolus, Rhizosolenia bergonii,* and *Thalassionema nitzschioides* v. *parva.* Important to negative loadings in this factor were *Chaetoceros* resting spores. Another factor explaining 14.4%, collected *Actinoptychus senarius, Stephanopyxis palmeriana/S. turris* and *Thallasiosira* species, including the *Thalassiosira eccentrica* group and *T. oestrupii. Actinoptychus curvatulus/Coscinodiscus rothii,* members of the genus *Asteromphalus, Coscinodiscus africanus/C. tabularis* form an assemblage which has a pattern of distribution which, loosely, is inverse to that of *Actinocyclus octonarius. Cyclotella striata/stylorum* and *Coscinodiscus obscurus/C. perforatus* are important in a distribution pattern occurring mainly north of 13° S.

The distribution of the *Delphineis* species was also highlighted in one factor (Factor 10, accounting for 5% of the variance explained by the 10 factors) in which this species dominated the factor loadings. It is significant that this relatively rare species helps account for a portion of the variance, from an objective statistical viewpoint as well as from our more subjective view.

Of special interest was a factor (Factor 7) accounting for 6.5% of the variance explained by the 10 factors. The highest factor loadings

define an area coinciding with offshore regions of high abundance of diatoms in the sediments. *Skeletonema costatum*, a dissolution sensitive species, is important in this factor. Its occurrence in the sediments (Table II) corresponds to the area of the highest factor loadings, and its presence in sediments below even 3000 meters water depth is a reflection of the abundant supply which enhances diatom preservation over this narrow region. *Skeletonema costatum* is, then, another indicator species for coastal upwelling off Peru as it also points to the influence of high productivity induced by coastal upwelling.

In summary, we have established a base line for coastal upwelling off Peru which can be described by: (1) the sinuous pattern of relative abundance of individual species and species groups, and of species collected by factor analysis to describe the variation between samples, and (2) the occurrence of discrete centers of upwelling influence, marked by high abundances of some indicator species, including the "endemic" *Delphineis* species. Areas of upwelling influence occur off Peru at about 8°, 13-14°, and about 17° S.

Comparison of our surface base line with surface samples from another upwelling area will help verify a common response of biogenous components to coastal upwelling in other geographic areas. Historical variation in the location and intensity of upwelling may be determinable by downcore studies of the fluctuation in the abundance of diatoms and in the relative abundance of species groups that we have shown to testify to the influence of coastal upwelling. Preliminary analysis of downcore samples from one core (W7706-64) within the coastal upwelling influenced region strongly suggests that historical variation in the abundance of the oceanic versus the meroplanktic component is of significance. The parallel occurrence of *Delphineis* supports an interpretation of hemipelagic and pelagic intervals based on sediment color change. Further analysis of downcore samples from this and other stations within the upwelling region will establish the persistence of the phenomenon over time and the reoccurrence of parameters that we have shown to be evidence of the influence of coastal upwelling.

Acknowledgements

This study which is part of an integrated study on "Patterns and Processes of Continental Margin Sedimentation off Peru" conducted by the Marine Geology Group of the School of Oceanography, Oregon State University, Corvallis, was supported by Office of Naval Research Grant N00014-76-0067 and National Science Foundation Grant OCE 77-20624. We thank George Andrews, Paul Loubere, David Nelson, and Erwin Suess for their constructive review of parts of the manuscript and Dave DeMaster for the absolute dating of surface sediments from cores #34 and #65.

Tables

Because of their size the tables could not be included in this publication. These may be obtained by writing to School of Oceanography, Oregon State University, Corvalis, OR 97331, and requesting Data Report No. 73, Oregon State University, School of Oceanography, Reference No. 79-8. — The tables: Table I. List of sediment surface samples. — Table II. Relative abundance of 43 species at 49 stations. — Table III. Varimax Factor Matrix (Q-Mode). — Table IV. Varimax Factor Score Matrix (Q-Mode). — Table V. Rotated Factor Matrix (R-Mode). — Table VI. Factor Score Matrix (R-Mode).

References

ANDREWS, G.W. (1977) - Morphology and stratigraphic significance of Delphineis, a new marine diatom genus. Nova Hedwigia, Beih. 54, 243-260.

BERGER, W.H. (1976) - Biogenous deep sea sediments: production, preservation and interpretation. In: Chemical Oceanography (J.P. Riley and R. Chester, eds.), 5, 265-388. London: Academic Press.

BLASCO, D. (1971) - Composicion y distribucion del fitoplankton en la region del afloramiento de las costas perunas. Investigacion Pesquera 35, 01-112.

CALVERT, S.E. (1966) - Accumulation of diatomaceous silica in the sediments of the Gulf of California. Geol. Soc. Amer. Bull. 77, 569-596.

CALVERT, S.E. & N.B. PRICE (1971) - Recent sediments of the South-West African shelf. ICSU/SCOR, Working Party 31, Symp. Cambridge, 1970. Inst. of Geol. Sc., Rep. No. 70/16, 175-185.

FRENGUELLI, J. (1949) - Diatomeas fosiles de los yacimientos chilenos de Tiltil y Mejillones. Darwiniana 9(1), 97-157.

FRYXELL, G.A. & W.J. MILLER III (1978) - Chain-forming diatoms: Three araphid species. Bacillaria 1, 113-136.

GUILLARD, R.L. & P. KILHAM (1977) - The ecology of marine planktic diatoms. In: The Biology of Diatoms (D. Werner, ed.). Bot. Monogr. 13, 372-469.

HART, T.J. & R.J. CURRIE (1960) - The Benguela Current. Discovery Rept. 31, 123-298.

HASLE, G.R. (1960) - Phytoplankton and ciliate species from the tropical Pacific. Skrifter Utgitt av Det Norske Videnskaps-Akademi i Oslo, I. Mat.-Naturv. Klasse 1960(2), 5-50.

HASLE, G.R. & B.R. DE MENDIOLA (1967) - The fine structure of some Thalassionema and Thalassiothrix species. Phycologia 6(2/3), 107-125.

HEIDEN, H. & R.W. KOLBE (1927) - Die marinen Diatomeen der Deutschen Südpolar-Expedition 1901-1903. Deutsche Südpolar-Expedition VIII. Botanik, 450-745.

HUSTEDT, F. (1959) - Die Kieselalgen Deutschlands, Österreichs und der Schweiz. Band 7 of Rabenhorst, G.L., Kryptogamenflora - Teil 2, 845 pp. Leipzig: Akademische Verlagsgesellschaft.

IMBRIE, J. & N.G. KIPP (1971) - New method for quantitative paleo-climatology: Application to a late Pleistocene Caribbean core. In: The Late Cenozoic Glacial Ages (K. Turekian, ed.), 71-181. New Haven: Yale University Press.

KLOVAN, J.E. & J. IMBRIE (1971) - An algorithm and Fortran IV program for large scale Q mode factor analysis. J. Int. Assoc. Mathem. Geol. 3(1), 61-77.

KOLBE, R.W. (1954) - Diatoms from Equatorial Pacific cores. In: Reports of the Swedish Deep-Sea Expedion, vol VI, 3-49.

KOLBE, R.W. (1955) - Diatoms from Equatorial Atlantic cores. In: Reports of the Swedish Deep-Sea Expedition, vol. VII, 151-184.

KOLBE, R.W. (1957) - Diatoms from Equatorial Indian Ocean cores. In: Reports of the Swedish Deep-Sea Expedition, vol. IX, 3-50.

MAEDA, S. & R. KISHIMOTA (1970) - Upwelling off the coast of Peru. J. Oc. Soc. Jap. 26, 300-309.

MARGALEFF, R. (1973) - Fitoplankton marino de la region de affloramiento del NW de Africa. Res. Exp. Cient. B/0 Cornide 2, 65-94.

MERTZ, D. (1966) - Mikropaläontologische und sedimentologische Untersuchung der Pisco-Formation Südperus. Palaeontographica Abt. B, 118(1-3), 1-51.

RYTHER, J.H. (1969) - Photosynthesis and fish production in the sea. Science 166, 72-76.

SCHRADER, H.-J. (1974) - Proposal for a standardized method of cleaning diatom bearing deep-sea and land-exposed marine sediments. Nova Hedwigia, Beih. 45, 403-409.

SCHRADER, H.-J. & R. GERSONDE (1978) - Diatoms and silicoflagellates. Utrecht Micropaleo. Bull. 17, 129-176.

SCOR Wg 36 (1973) - SCOR Wg 36 Coastal upwelling processes. Report 1st meeting, Corvallis, Oregon. Proc. of the Scientific Committee on Oceanic Research 9, 25-33.

SCOR Wg 36 (1974) - SCOR Wg 36 Coastal Upwelling Processes. Report 2nd Meeting, Kiel FRG. Proc. of the Scientific Committee on Oceanic Research 10, 120-128.

SCOR Wg 36 (1976) - SCOR Wg 36 Coastal Upwelling Processes, Report 3rd Meeting, Banyuls-sur-Mer, France. Proc. of the Scientific Committee on Oceanic Research 11, 30-36.

SIMONSEN, R. (1974) - The diatom plankton of the Indian Ocean Expedition of RV "Meteor" 1964-1965. "Meteor" Forschungsergebnisse, Reihe D, 19, 1-107.

SMAYDA, T.J. (1958) - Biogeographical studies of marine phytoplankton. Oikos 9, 158-191.

SMITH, R.L. (1978) - Physical oceanography of coastal upwelling regions. A comparison: Northwest Africa, Oregon, and Peru. Symposium on the Canary Current: Upwelling and Living Resources. No. 4, 10 pp.

STRICKLAND, J.D.H., R.W. EPPLEY & B.R. DE MENDIOLA (1969) - Phytoplankton populations, nutrients and photosynthesis in Peruvian coastal waters. Bot. Inst. Mar. Peru. 2, 4-45.

VAN HEURCK, H. (1880-1885) - Synopsis des Diatomées de Belgique. Anvers: 235 pp.

ZHUSE, A.P. (1972) - Diatoms in the surface sediment layer of the Chilean-Peruvian region of the Pacific Ocean. Okeanologiia 12(5), 831-841. Moscow (in Russian).

Optical and Particulate Properties at Oceanic Fronts

J. RONALD V. ZANEVELD AND HASONG J. PAK

School of Oceanography, Oregon State University, Corvallis, Oregon 97331

Distributional patterns of optical and particulate properties at oceanic fronts follow general patterns. These patterns are examined by means of three examples: the front associated with the Columbia River plume in winter, the upwelling front off the Oregon coast during the summer, and the front in the eastern equatorial Pacific. It is shown that the optical and particulate matter distributions at oceanic fronts are the result of three major processes: (1) advection of inorganic matter into the frontal zone, (2) advection of biological materials into the front, and (3) generation of particulate matter by biological processes in the front itself.

INTRODUCTION

The distribution of optical and particulate properties of oceanic fronts is influenced by the dynamics at the front both directly by means of advection and mixing of particulate matter and indirectly by means of biological processes in the special environment of the front. There are many types of fronts. Of the six types listed by *Bowman* [1978] we will here present optical and particle distributions of three types: (1) a front at the boundary of a riverine plume, the Columbia River plume in winter, (2) a coastal upwelling front, and (3) a front of planetary scale, the equatorial front in the east equatorial Pacific.

Since a front is the boundary between two water masses with different temperature, density or other characteristics, one can also expect different optical characteristics as the biological environments on either side of the front are probably dissimilar. Since the water masses have a different origin and history, the inorganic component of the suspended matter can be expected to differ as well.

The light scattering characteristics of a water mass depend largely upon the nature of the suspended materials, since the scattering due to water itself is usually small compared to that due to suspensoids. The light absorption characteristics of a water mass are due to water itself, dissolved salts, and the so-called 'yellow matter' (humic acids, by-products of organic decay). Attenuation is the sum of light scattering and absorption. For oceanic waters, light scattering is the more variable parameter. In the visible region of the spectrum attenuation is due to absorption and scattering by particulate matter, absorption by yellow matter and attenuation due to 'pure' seawater. Absorption by yellow matter is strongly wavelength dependent, in the visible region decreasing exponentially with increasing wavelength. One can closely approximate the attenuation due to particles only by measuring the attenuation coefficient at a wavelength larger than 600 nm, where yellow matter absorption is very low, and subtracting the attenuation due to water.

The directional properties of the scattering are described by the volume scattering function, $\beta(\theta)$.

The volume scattering function is defined by

$$\beta(\theta) = \frac{dI(\theta)}{E\,dv} \quad m^{-1}\ sr^{-1}$$

where $dI(\theta)$ is the radiant intensity of scattered light emanating from the volume element dv when it is illuminated by an irradiance E. The total scattering coefficient b is then given by

$$b = 2\pi \int_0^{\pi} \beta(\theta) \sin\theta\, d\theta \quad m^{-1}$$

If we then denote the absorption coefficient by a (m^{-1}), we may set

$$c = (m^{-1})\ a + b \quad m^{-1}$$

where c is the attenuation coefficient. The light scattering properties of suspended matter are related to other properties of the suspensoids in a complicated manner. For a given sample, the light scattering depends on the concentration, size distribution, index of refraction distribution, and shape distribution of the suspended matter. In confined areas, the latter three parameters are often nearly constant, so that the particulate light scattering and attenuation can be considered to be proportional to the particulate matter concentration. For a review of the optical properties of seawater, see *Jerlov* [1976].

Particulate matter concentration can be described as a weight concentration if the samples are obtained by filtration and weighing, or as a volume concentration if a resistive pulse (such as Coulter) counter is used. The slope of the particle size distribution can be used as an indicator of the average size of the particles. In order to do so one must assume a mathematical model for the size distribution. The most commonly employed one is the Junge or hyperbolic distribution given by

$$g(D) = ND^{-C}$$

where $g(D)$ is the number of particles with diameters larger than D um, N is the number of particles larger than 1 um in diameter, and C is the slope of the size distribution. C is inversely related to the mean size of the particles. A measure of the index of refraction of suspended particles can be obtained by using the method of *Zaneveld and Pak* [1973], or *Zaneveld et al.* [1974].

Particulate matter parameters and hence optical parameters in the ocean are nonconservative. The concentration and composition of suspended matter in a water mass change constantly due to settling, biological activities, flocculation, and chemical reactions. These processes do take time however, so that within scales of tens of kilometers and days, particulate matter parameters tend to behave conservatively

Paper number 9C1179.
0148-0227/79/009C-1179$01.00

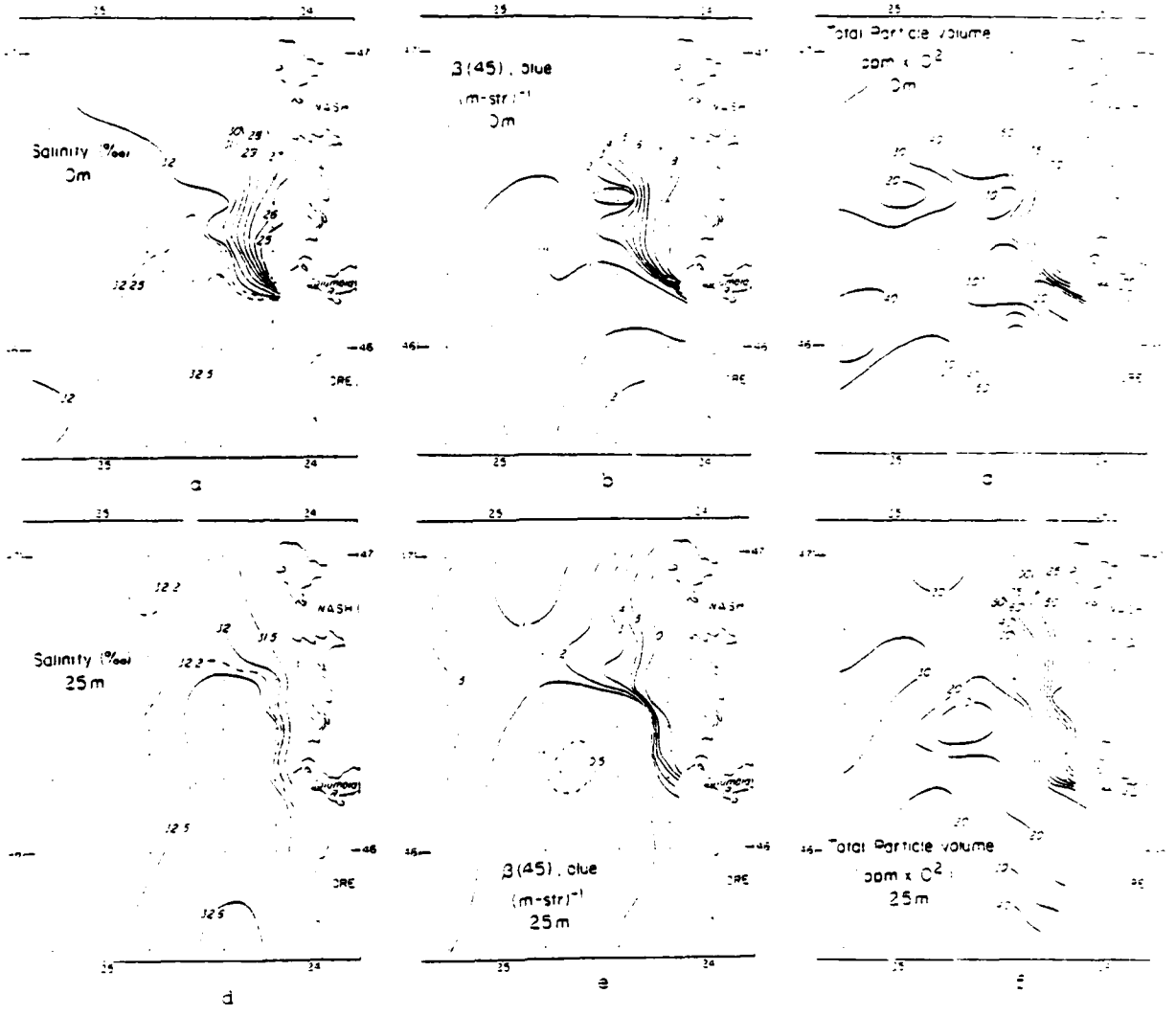

Fig. 1. Salinity, light scattering at 45°, and total particle volume at 0- and 25-m depth off the Oregon-Washington coast during November 1973.

Large gradients of temperature, salinity, and density are generally accompanied by large gradients in particle and optical properties, as the hydrographic differences constitute different biological climates. The inorganic particle component is also likely to be different due to the different histories of the water masses.

A number of researchers have published data from regions where fronts are common (for example, *Gibbs* [1974], Amazon River outflow; *Kullenberg* [1974], West African upwelling region). *Zaneveld et al.* [1969] have reported an observation of optical properties at a front obtained by towing a beam transmissometer across the front. *Pak and Zaneveld* [1974], have used optical properties to study frontogenesis in the eastern Pacific Ocean.

First, we will consider a front during a period when biological activity is minimal, so that the only nonconservative feature of the particle dynamics is settling. Such a front occurs at the edge of the Columbia River plume in the winter. Fronts associated with large biological activities display more complicated optical and particle parameter distributions than the front associated with the Columbia River plume in winter. Such biologically active fronts occur at those locations where a large density gradient is accompanied by a nutrient gradient. In this paper, we will discuss two such fronts. The first is a front associated with coastal upwelling off the Oregon coast. The second is the equatorial front found in the eastern Pacific.

THE COLUMBIA RIVER PLUME FRONT

Figures 1*a*-1*f* show distributions of three parameters associated with the Columbia River front. In the winter and fall (these data were taken during November 1973) the nearshore current is toward the north. The fresh and particle rich river water forms a strong salinity and optical front near the river mouth (Figures 1*a*, 1*b*, and 1*c*). The optical properties, for example light scattering at 45°, $\beta(45°)$, at the surface shows the offshore boundary of the plume to be virtually identical to that defined by the salinity distribution at the surface. The total particle volume shows a similar distribution. The river water mixes with the ocean water as it travels north, and hence the front is weakened. The optical and particle fronts at the

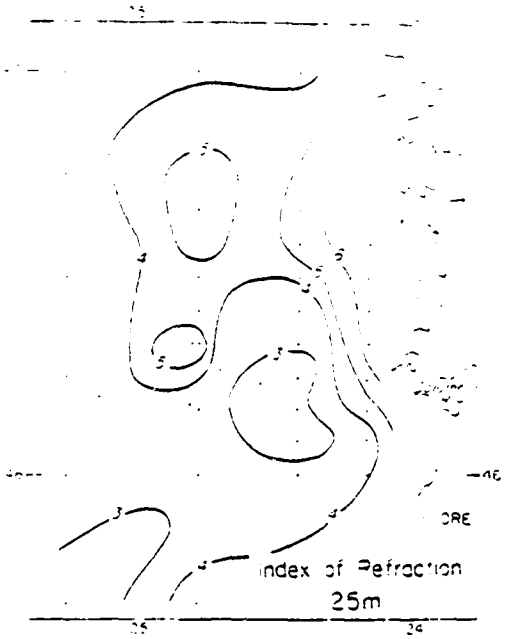

Fig. 2. Index of refraction of suspended particulate matter relative to water in the same region as Figure 1. The parameter plotted is (relative index of refraction − 1) × 100.

surface do not weaken more rapidly than the salinity front, nor is there any evidence of settling as there is no apparent north-south gradient of light scattering or particle volume inside of the river plume. Over a distance of some 90 km along the plume the optical and particle properties at the surface thus behave in a conservative manner.

The subsurface front (Figures 1*d*, 1*e*, and 1*f*) presents different features. At 25-m depth the salinity (and hence density) front is much weaker than at the surface, whereas the optical and particle fronts are stronger than at the surface. The much less dense river water tends to stay at the surface, whereas a fraction of the particulate matter tends to settle. This sorting of particles must occur already in the river mouth itself, as no further evidence of settling (reduction of particle concentration in a poleward direction along the axis of the river plume) is present. In addition, bottom nepheloid layers could contribute to the particle concentration at 25-m depth since the water depth in this region is approximately 25–30 m. The weather and water conditions do not vary a great deal meridionally in the area of study, so that the bottom nepheloid layer in this region does not vary to a large extent within the plume (about 90 km along the Washington coast). Thus the high particle concentration under the Columbia River plume shown at the 25-m level may partly be drawn from river-borne particles and partly from the bottom nepheloid layer generated by winter storm activity. For a further discussion on the formation of bottom nepheloid layers along the Oregon coast, see *Pak and Zaneveld* [1977].

The index of refraction of suspended particles were calculated using the method of *Zaneveld and Pak* [1973] (Figure 2). The number plotted is (relative index of refraction − 1) × 100. It is seen that an index of refraction gradient exists at the front. The high index of refraction material in the plume is probably suspended matter of terrigenous origin. The offshore waters with a higher proportion of biological material, have a lower index of refraction.

COASTAL UPWELLING FRONT

Stevenson et al. [1974] and *Mooers et al.* [1976] describe a circulation near the front. Shoreward of the front the flow consists of onshore flow over most of the water column, with fast offshore flow in a shallow surface layer. At the front the fast offshore flow meets the lighter water mass and flows under it offshore. Offshore of the front, another upwelling cell circulating in the same sense is found. A simpler model of zonal circulation is presented by *Huyer* [1976]. In that case only one cell is present and the front is a surface divergence. It is possible that both types of circulation exist, the one cell during the height of an upwelling event, and the two cell during relaxation. Little direct evidence for the onshore-off-shore flow regime exists, and the optical data can be particularly useful in such a case [*Pak et al.*, 1970; *Kitchen et al.*, 1978].

We will examine here the data from a cruise during August of 1974 off the Oregon coast. The wind was weak and variable (2–5 m/s) during the cruise, but in the preceding week upwelling favorable winds have been present. Some aspects of these data are discussed in *Kitchen et al.* [1978].

Figure 3 shows the light transmission at 660 nm, the log log slope of the cumulative size distribution and the temperature for three consecutive transects taken at 45°N latitude from 0 to 20 km offshore. The three consecutive transects were taken in less than 48 hours, so they show the temporal variations in the zonal flow regime. In all three transects strong surface optical (and hence particle concentration) fronts occur at 5–12 km offshore. Only in the third transect is there evidence of a temperature front at the same location. At all transects a strong thermocline is present as well as a particle maximum (indicated by a transmission minimum) that, between 5 and 15 km offshore, is located 2.5 m beneath the bottom of the surface mixed layer, coinciding with the thermocline. Figure 4 shows vertical profiles of σ_t and particle volume calculated from transmission values. The maximum particle concentration occurs at the surface inshore of the front and at about 5-m depth offshore of the front. It should further be noted that the optical surface front is associated with a large horizontal gradient in the slope of the particle size distribution. Since small slopes in particle size distributions imply a relative abundance of large particles and vice versa, it is seen that the particles shoreward of the front are on the average much larger than those seaward of the front. This is further demonstrated by the particle size distributions themselves (Figure 5). Clearly, two types of size distributions are present: (1) inshore of the front (at 3.7 km offshore) at 1-m depth, the concentration of large particles is two orders of magnitude larger than offshore of the front, (2) at 5-m depth the front is not quite as sharp, but an order of magnitude separates the large particle concentration at 7.4 and 11.1 km offshore.

Nutrient and chlorophyll *a* data taken at the same time as the data in Figure 3*d* show that there is a large overlap in the region of high chlorophyll concentration near the coast and the region of low slopes of the cumulative size distribution.

Zooplankton biomass determinations were made three days prior to the data displayed on Figure 3*a*. The time difference is large in a region of high variability, but it was noted that the zooplankton biomass is highest in regions of high chlorophyll

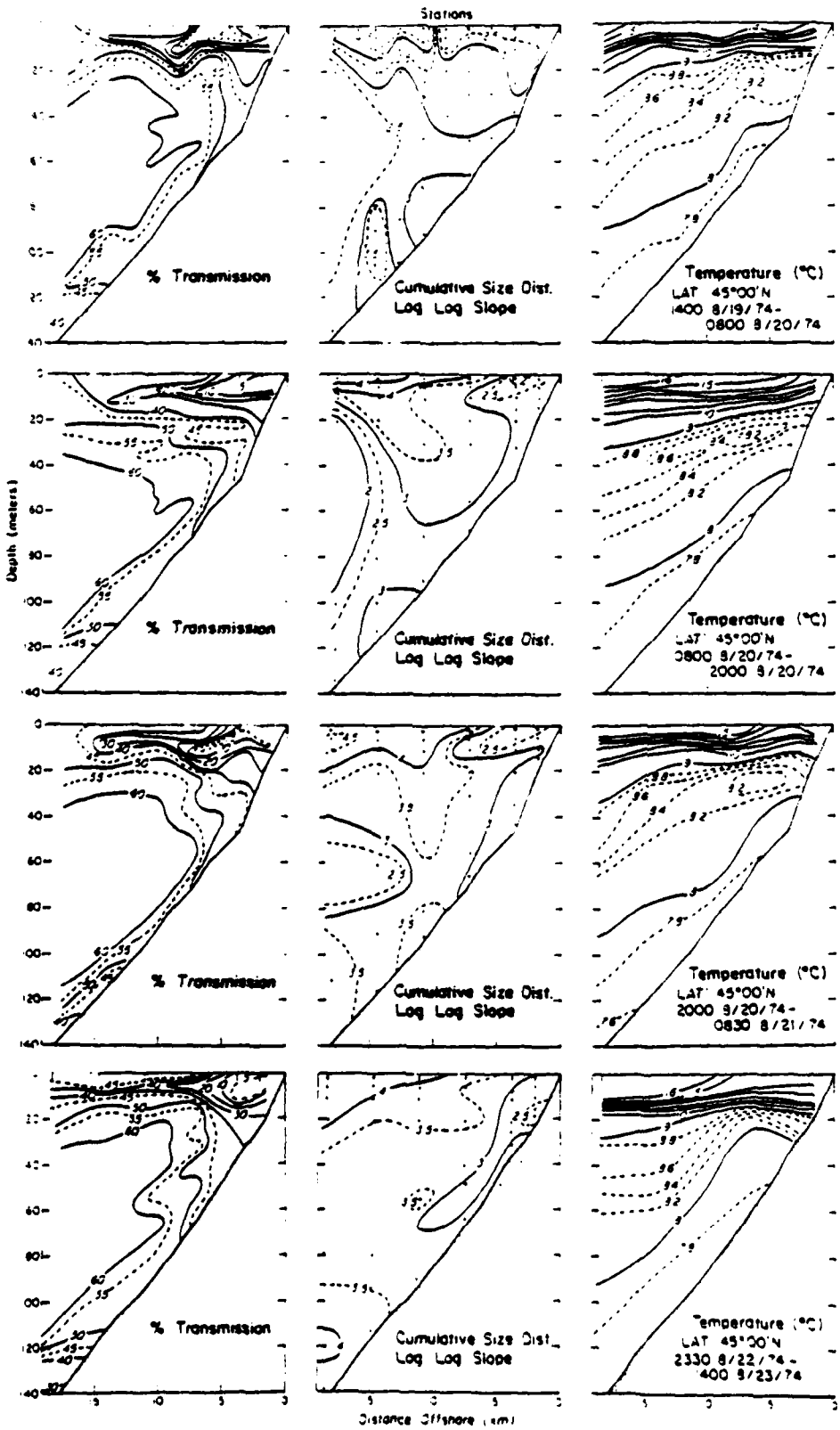

Fig. 3. Transmission, log-log slopes of the particle size histograms and temperature of four consecutive transects at 45°00'N latitude off the Oregon coast.

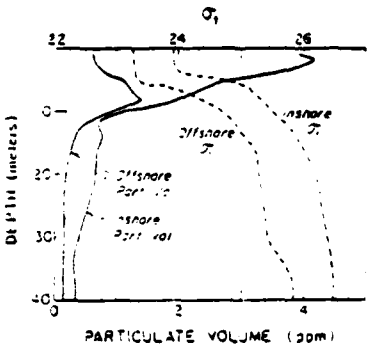

Fig. 4. Vertical profiles of particulate volume (computed from light transmission values) and density for typical stations inshore and offshore of the particle front.

and particle concentration. The offshore near-surface water had 2 orders of magnitude less zooplankton biomass than the near-shore near-surface water.

It is generally assumed [*Mooers et al.*, 1978] that upwelling introduces nutrient rich water into the euphotic zone near-shore, permitting rapid growth of phytoplankton. The size distributions (Figure 5) shows that these inshore plankton consist of a relatively large number of larger plankton (log-log slopes are less than 3.0). Offshore of the front the surface waters are poorer in nutrients and contain few particles. Thus the particle distribution supports the phytoplankton growth conditions across the front. At the thermocline there is still enough light to permit growth, and nutrients are also present although in small quantity. These nutrients reach the thermocline by means of upward diffusion from the nutrient rich deep water. The thermocline is a stable environment in which particle residence times can be large and in which nutrients and sunlight are available. Hence a vertical particle maximum is present at the thermocline offshore of the front. An important result is the distinctly different size distributions inshore and offshore of the front. While the numbers of small particles on either side of the front are of the same order of magnitude, the number of large particles differ by two orders of magnitude. Abundance of the layer particle inshore of the front is consistent with favorable grow conditions for phytoplankton, which owes to nutrient supply associated with upwelling. Thus the front separates distinct biological environments which are manifested in optical and particle characteristics.

EQUATORIAL FRONT

The front of the eastern equatorial Pacific has been described by *Wyrtki* [1966], *Wooster* [1969], *Stevenson et al.* [1970], and *Pak and Zaneveld* [1974]. The front is a permanent, shallow feature confined to the upper 100 m. The location varies seasonally. The front is probably related to upwelling in the equatorial undercurrent (Cromwell Current). Near the Galapagos Islands the front is approximately oriented in a zonal direction.

The equatorial front is similar to the upwelling front off Oregon in that a colder, nutrient rich water mass is adjacent to a warmer, nutrient poor water mass (Figures 6*a*–6*d*). The resultant distribution of optical properties is dissimilar to that off Oregon (Figure 7*a*). Whereas in the coastal upwelling front the maximum light scattering and minimum transmission occurred in the cold, nutrient rich water, in the equatorial front region, the light scattering maximum appears to occur on the nutrient rich side of the frontal zone itself. This observation is supported by the particle concentration data (Figure 7*b*). A comparison between the two frontal regions should not be carried too far as the scales are completely different, the equatorial frontal zone being tens of kilometers wide. A study of the particle size distributions shows a weak indication of a band of larger average particle size at the front.

DISCUSSION AND CONCLUSIONS

If we define an oceanic front as the boundary between two water masses, then this front will in nearly all cases also be a boundary of optical and particulate matter properties. Different water masses are influenced by different sources of inorganic materials. Most importantly, since the hydrographic and chemical properties of two water masses must be different, their oceanic climates must be different as well. As a result, the flora and fauna in each water mass should also be different.

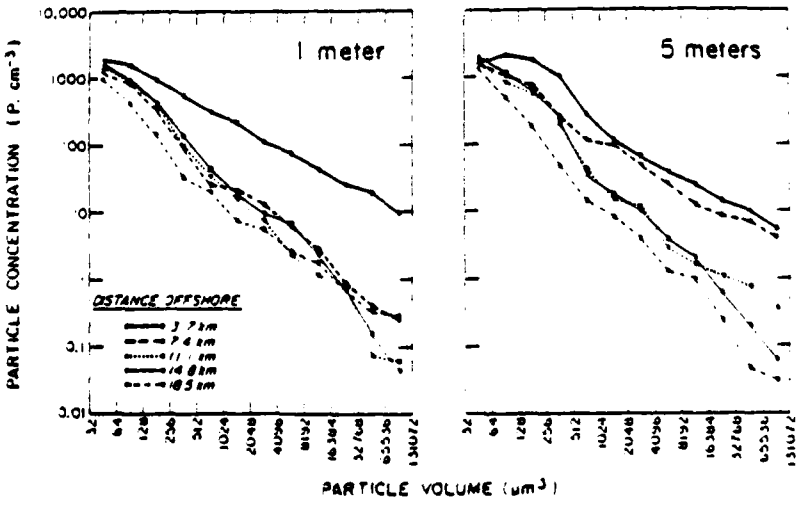

Fig. 5. Particle size histograms for samples taken from 1- and 5-m depths at varying distances from shore at 45°00'N latitude from 2000 PDT on August 20, 1974 to 0830 PDT on August 21, 1974.

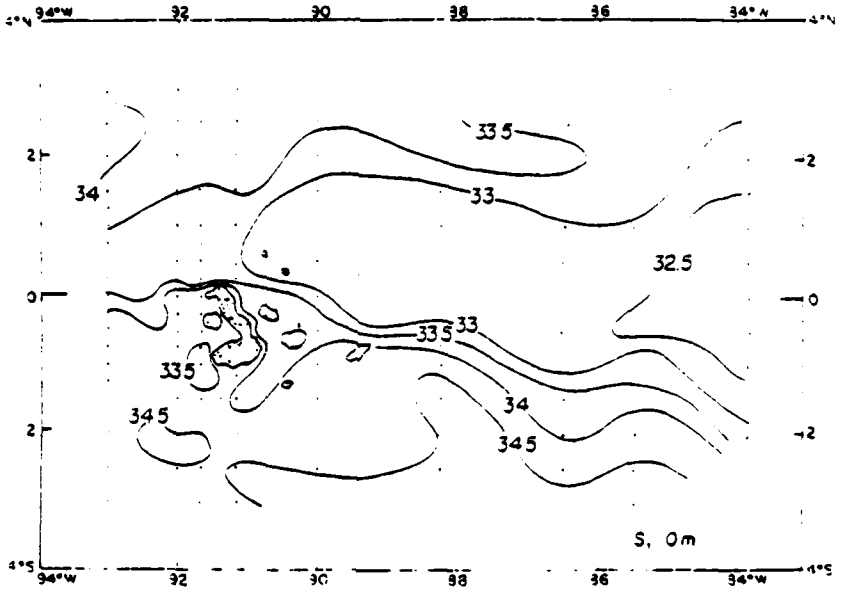

Fig. 6a

Fig. 6. Horizontal distributions of T(°C), S(‰), σ_t, and nitrate ($\mu g\ l^{-1}$) in the sea surface.

A small change in the dissolved chemicals (nutrients) can have a large effect on the biological nature of a water mass. Small chemical or hydrographic differences can thus lead to large differences in optical and particulate matter properties. In such a case, optical properties would be extremely useful for the study of fronts.

The frontal zone itself can provide a unique biological environment. In a boundary zone between a nutrient rich cold and a nutrient poor warm water mass, the water may still be warm enough and also contain enough nutrients for a plankton species from the warm water mass to bloom. In such a case the front is marked by optical and particle properties that differ from the two adjacent water masses.

Interestingly, none of the data presented here shows any direct effect of settling. Figure 1c shows a particle and scattering maximum near the bottom, but this maximum does not increase to the north. Furthermore, particle size data show that the average size of the particles in this near-bottom maximum is smaller than in the surface particle maximum. Their index of refraction, however, is larger. This seems to indicate that smaller but optically more dense (and hence probably also possessing a higher specific gravity) particles settle out almost

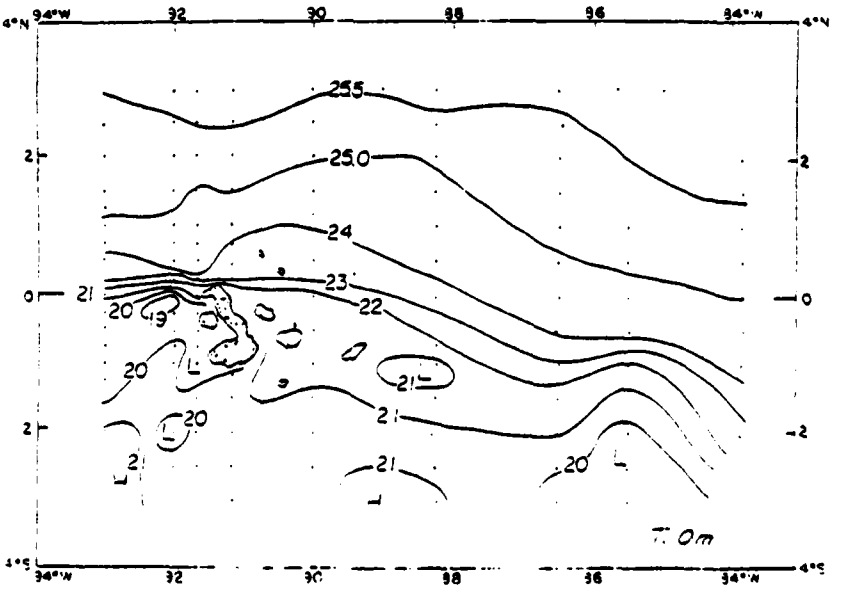

Fig. 6b

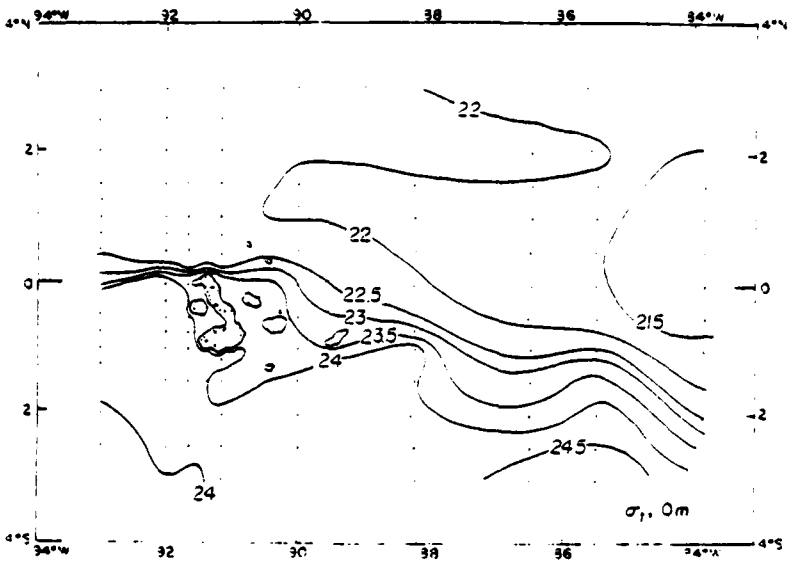

Fig. 6c

immediately. The optically less dense, but larger particles stay at the surface. In the time required to carry the particles some 90 km to the north (on the order of several days) no significant settling from the surface layer can be detected, nor do any blooms occur. The distribution of optical properties at the Columbia River front is thus governed by northward advection. The zonal gradients of light scattering and particle concentration at the western edge of the plume become smaller due to diffusion as the materials in the plume are transported to the north. At 25-m depth the optical gradients at the front are larger than the hydrographic ones as much of the particulate load of the river flows out near the bottom, whereas the less dense river water stays near the surface. As mentioned before these particles may also be related to a bottom nepheloid layer. The contribution of bottom erosion to the plume is small as the offshore boundary of the particle rich water is well defined and the outer boundary of the bottom nepheloid layer is usually not sharply defined [*Pak and Zaneveld*, 1977].

The zonal gradients at the optical front are determined by lateral mixing as the current carries the riverine particles northward. Biological events and settling do not appear to have much influence except in the vicinity of the river mouth.

It is of interest to speculate whether the observed distributions in the coastal upwelling regime tend to support the single- or two-celled zonal circulation models. In the absence of meridional variations the observations do not support the single-cell model as there would be no source for the clear surface water offshore of the front. The double-cell model might apply if the clear surface water offshore of the front constitutes a cell. It is much more likely that the observed distribu-

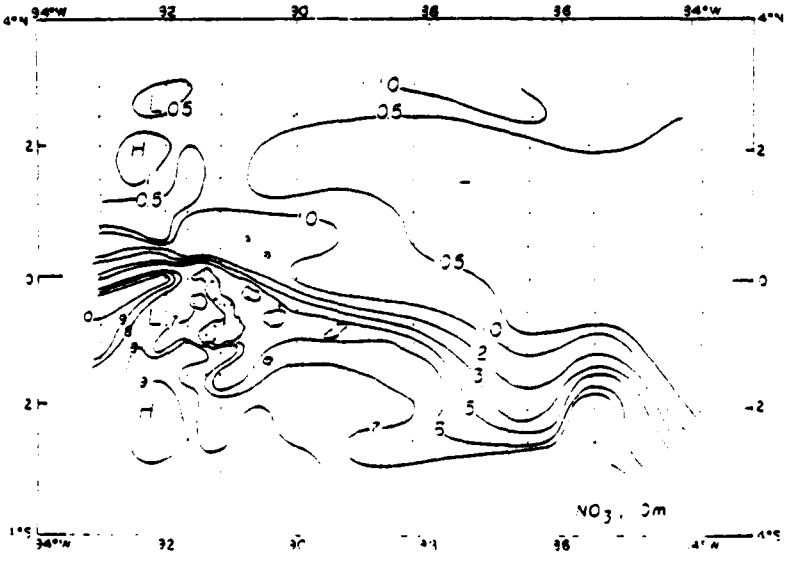

Fig. 6d

Fig. 7a

Fig. 7. Horizontal distribution of total volume concentration of suspended particles, volume scattering function at 45°, $\beta(45°)$, and A, one of the parameters in the exponential particle size distribution Ve^{-Ar}, in the sea surface.

tions are not the result of the one- or two-cell circulation models but of the circulation during and after an upwelling event [*Halpern*, 1976].

During an upwelling event rapid near-surface offshore flow is present while nutrients are brought to the surface. This results in high productivity with the maximum concomitant with the equator surface jet (L. Small, personal communication). During relaxation of the upwelling event the biomass maximum moves inshore. Since our observations were made during weak winds following strong northwest winds, it is likely that the observations represent the distribution of particulate matter and optics during relaxation of an upwelling event. Our observations would then support *Halpern*'s [1976] interpretation of an upwelling event and subsequent relaxation and the associated biological processes as described by L. Small (personal communication). The optical front is thus the outer boundary of the shoreward transported biomass produced earlier during an upwelling event.

The tongue of turbid water at the thermocline offshore of the front (depth is about 10 m from 5 to 15 km offshore, see Figure 3) is of considerable interest, as the data contradict earlier interpretations of such features. One usually assumes that such a tongue of turbid water indicates advection of the turbid water along an isopycnal or settling of particles from the surface layer and subsequent trapping at the maximum density gradient. The optics and temperature data would tend to sup-

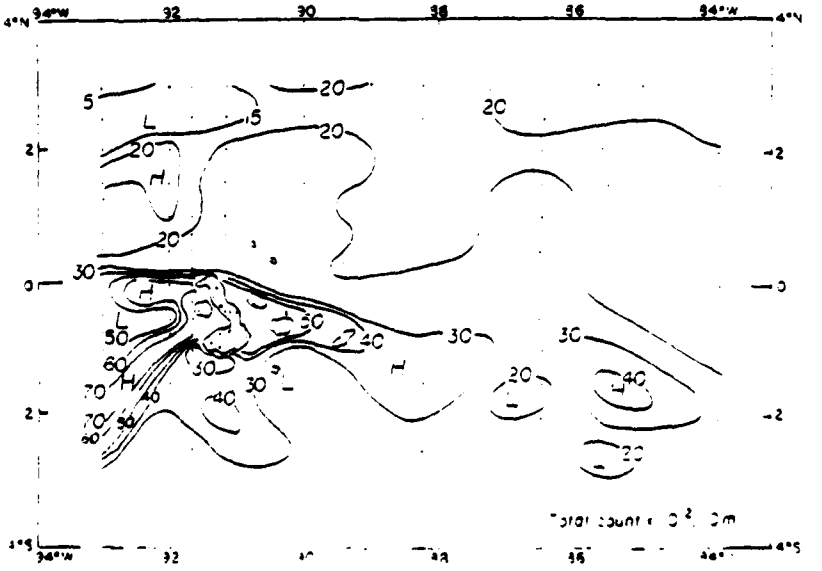

Fig. 7b

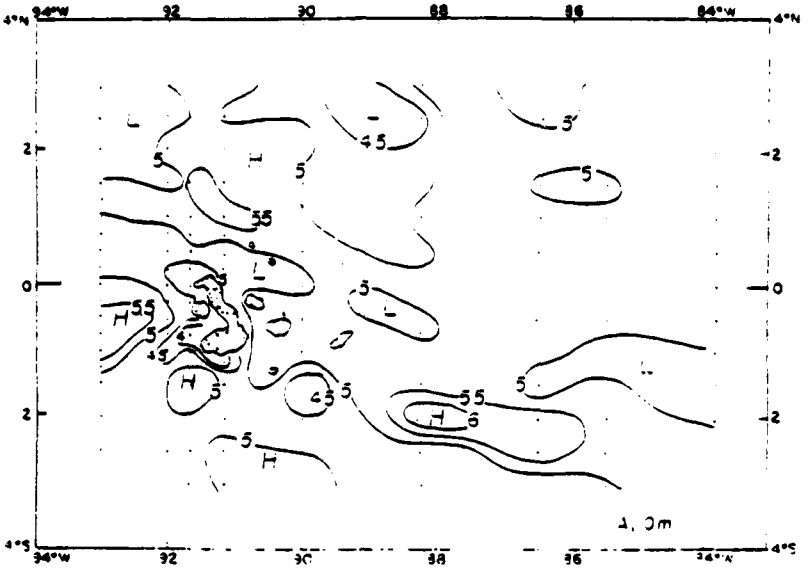

Fig. 7c

port that contention. The particle size distribution data (Figure 5) shows, however, that the particle maximum in the thermocline offshore is different from that inshore of the front. This does not imply that advection at the depth of the thermocline is nonexistent. Since the nature of the particles is different at either side of the front simple advection cannot explain the maximum. It is possible that advection exists but that the phytoplankton are consumed by zooplankton at the same rate as the advection. In a sense the thermocline is a vertical front, separating cold nutrient rich water and warm nutrient poor water. Such a situation can give rise to an optical 'amplification' of the boundary, by means of phytoplankton growth. In this case, as the boundary is horizontal, sufficient sunlight must penetrate also. The maximum is probably not the result of settling of particles into a density gradient, as the westward current is strong enough to transport the particles out of the region before the nearly neutrally buoyant phytoplankton can settle to the thermocline.

The strong vertical density gradient is a region of large stability and hence minimal vertical mixing. The particles generated in that region by a biological process will not rapidly disperse by vertical mixing, so that the weak mixing of the thermocline does contribute to the vertical particle maximum.

The particle maximum at about 10-m depth (the top of the thermocline) is due to growth of phytoplankton in the upper thermocline region where sufficient daylight penetrates and where sufficient nutrients are available via upward diffusion. The population can maintain itself as vertical mixing is a minimum. *Halpern* [1976] shows that the rapid offshore flow during an upwelling event occurs down to about 15 m. The offshore extent of the particle maximum at the thermocline is thus only weakly influenced by the upwelling event in contrast with the inshore surface maximum.

A feature similar to the thermocline particle maximum can be observed in the equatorial front. Since the front is several tens of kilometers wide in this case, the residence time is long enough to permit particle concentrations in the front of two to three times those outside of the frontal zone. The particles in the front tend to be larger than those outside (Figure 7c). It is likely that the particle volume maximum near the Galapagos Islands is related to terrigenous particles introduced by current interaction with the islands (for a discussion of the interaction of the current structure of the Galapagos Islands, see *Pak and Zaneveld* [1973]).

It can be concluded that the optical and particulate matter distributions at ocean fronts are the result of three major processes: (1) advection of inorganic matter, terrigenous in origin to the front; (2) advection of biological materials (plankton and detritus) to the front; and (3) generation of particulate matter by biological processes in the front itself.

Acknowledgments. This research was supported by the Office of Naval Research through contract N00014-76-C-0067 under project NR 083-102 and by the Department of Energy, Division of Biological and Biomedical Sciences under contract EY-76-S-06-2227, task agreement 29.

REFERENCES

Bowman, M. J., Proceedings, in *Oceanic Fronts in Coastal Processes*, edited by M. J. Bowman and W. E. Esaias, Springer, New York, 1978.

Gibbs, R. J., Principles of studying suspended materials in water, in *Suspended Solids in Water*, edited by R. J. Gibbs, pp. 3–16, Plenum, New York, 1974.

Halpern, D., Structure of a coastal upwelling event observed off Oregon during July 1973, *Deep Sea Res.*, *23*, 495–508, 1976.

Huyer, A., A comparison of upwelling events in two locations: Oregon and Northwest Africa, *J. Mar. Res.*, *34*(4), 531–546, 1976.

Jerlov, N. G., *Marine Optics*, 231 pp., Elsevier, New York, 1976.

Kitchen, J. C., J. R. V. Zaneveld, and H. Pak, The vertical structure and size distributions of suspended particles off Oregon during the upwelling season, *Deep Sea Res.*, *25*, 453–468, 1978.

Kullenburg, G., The distribution of particulate matter in a Northwest African coastal upwelling area, in *Suspended Solids in Water*, edited by R. J. Gibbs, pp. 195–202, Plenum, New York, 1974.

Mooers, C. N. K., C. A. Collins, and R. L. Smith, The dynamic structure of the frontal zone in the coastal upwelling region off Oregon, *J. Phys. Oceanogr.*, *6*, 3–21, 1976.

Mooers, C. N. K., C. N. Flagg, and W. C. Boicourt, Prograde and retrograde fronts, in *Oceanic Fronts in Coastal Processes*, edited by M. J. Bowman and W. E. Esaias, Springer, New York, 1978.

Pak, H., and J. R. V Zaneveld, The Cromwell Current on the east side of the Galapagos Islands, *J. Geophys. Res.*, *78*(33), 7845–7859, 1973.

Pak, H., and J. R. V. Zaneveld, Equatorial front in the Eastern Tropical Pacific, *J. Phys. Oceanogr.*, *4*(4), 570–578, 1974.

Pak, H., and J. R. V Zaneveld, Bottom nepheloid layers and bottom mixed layers observed on the continental shelf off Oregon, *J. Geophys. Res.*, *82*(27), 3921–3931, 1977.

Pak, H., G. F. Beardsley, Jr., and R. L. Smith, An optical and hydrographic study of a temperature inversion off Oregon during upwelling, *J. Geophys. Res.*, *75*, 629–636, 1970.

Stevenson, M. R., G. G. Oscar, and J. Santoro De Ycaza, *Marine Atlas of the Pacific Coastal Waters of South America*, University of California Press, Berkeley, 1970.

Stevenson, M. R., R. W. Garvine, and B. Wyatt, Lagrangian measurements in a coastal upwelling zone off Oregon, *J. Phys. Oceanogr.*, *4*, 321–336, 1974.

Wooster, W. S., Equatorial front between Peru and Galapagos, *Deep Sea Res.*, *16*, 407–419, 1969.

Wyrtki, K., Oceanography of the eastern equatorial Pacific Ocean, in *Annual Reviews of Oceanography and Marine Biology*, vol. 4, pp. 33–68, Annual Reviews, Inc., Palo Alto, Calif., 1966.

Zaneveld, J. R. V., and H. Pak, Method for the determination of the index of refraction of particles suspended in the ocean, *J. Opt. Soc. Amer.*, *63*, 321–324, 1973.

Zaneveld, J. R. V., M. Andrade, and G. F. Beardsley, Measurements of optical properties at an oceanic front observed near the Galapagos Islands, *J. Geophys. Res.*, *74*(23), 5540–5541, 1969.

Zaneveld, J. R. V., D. Roach, and H. Pak, The determination of the index of refraction distribution of oceanic particulates, *J. Geophys. Res.*, *79*(27), 4091–4095, 1974.

(Received April 26, 1978;
revised July 12, 1979;
accepted July 16, 1979.)

Reprinted from SPIE Vol. 208—Ocean Optics VI

Optical properties of turbidity standards

J. Ronald V. Zaneveld, Richard W. Spinrad, Robert Bartz
School of Oceanography, Oregon State University
Corvallis, Oregon 97331

Abstract

Measurements of light scattering and light attenuation were made for suspensions of formazin and diatomaceous earth. Light scattering was measured for light of wavelength 632.8 nm at angles from 0.1° to 1.0° and for light of wavelengths 400, 500, 550, 600, 650, and 700 nm at 45°. Light attenuation was measured over a 25 cm pathlength for light of 660 nm. These measurements were made for suspensions which varied from 0 to 40 Jackson Turbidity Units of formazin and 0 to 40 mg/l of diatomaceous earth. The results indicate the necessity for multiple optical measurements for determinations of turbidity of water. In addition the tables and curves presented may be used in the calibration of light scattering meters and transmissometers which are used for turbidity studies.

Introduction

Emphasis on the monitoring of environmental parameters had led to the need for a better method of quantifying the turbidity of water. Certain standards have been used in the past as indicators of turbidity. Specifically, formazin and diatomaceous earth are the most common substances used for turbidity calibrations[1,2]. These substances are used because of the availability, ease of preparation and reproducibility of calibration results. In the research described herein transmission measurements were made with light of wavelength 660 nm in various concentrations of formazin in water and diatomaceous earth in water. In addition, volume scattering functions were measured at near-forward angles and at 45° for both substances in various concentrations. The scattering measurements were made with light of wavelength 632.8 nm for the near-forward measurements and 650 nm for the 45° measurements. In addition measurements were made of the volume scattering function at 45° for wavelengths of 400, 450, 500, 600, 650, and 700 nm for both substances. Particle size analyses were made using a Coulter Counter.

The optical properties described above are inherent properties which do not change with changes in the radiance distribution[3]. Within a water sample light may be attenuated by absorption and/or scattering. The attenuation coefficient, c, therefore represents the ratio of the radiant flux lost from a beam of infinitesimal width to the incident flux and divided by the thickness of the layer of the medium through which the beam is passing. Also,

$$c = a + b$$

where a is the absorption coefficient and b is the scattering coefficient, each defined similarly to c but representing only absorption or scattering, respectively. The units of a, b and c are m^{-1}. The fraction of light transmitted through a pathlength r (in meters, is related to c as follows:

$$T = e^{-cr}$$

The volume scattering function, $\beta(\theta)$, is defined as the radiant intensity (watts/steradians) from a volume element (m^3) in a given direction, (θ) per unit of irradiance (watts/m^2) and per unit volume:

$$\beta(\theta) = \frac{dI(\theta)}{E\,dV}$$

where $I(\theta)$ = radiant intensity scattered at angle θ relative to the main beam

E = irradiance

V = volume

In addition, Austin[4] has shown that

$$\beta(\theta) = \frac{P_\theta}{P_o}\,\frac{1}{2\pi}$$

where P_0 is the power of light incident on the sample volume; P_θ is the power leaving the volume at angle θ from the main beam; L is the length of the volume along the direction of propagation of unscattered light; and Ω is the solid angle into which the light is scattered.

The volume scattering function, $\beta(\theta)$, and the scattering coefficient, b, are related as follows:

$$b = 2\pi \int_0^\pi \beta(\theta) \sin\theta d\theta$$

Measurements of T, c, b for forward angle scattering, and $\beta(45°)$ were made in the research described herein.

The measurements of transmission and scattering were made in order to quantify the optical properties of turbidity standards. The need for such a quantification was emphasized by Austin[4] and Freeman[5]. By accurately determining the optical properties of turbidity standards intercalibration of optical equipment can be simplified and standardized. The results of this work supply an easily reproducible calibration procedure for light transmission and light scattering measurements. After calibrating a transmissometer or a light scattering meter using a formazin or diatomaceous earth suspension as was done in this research a water sample may be tested for transmission or light scattering. The results can then be compared to a concentration of formazin or diatomaceous earth that gives the same transmission or light scattering value. In this way all water samples could be compared to universal standards of transmission and scattering. No single measurement is sufficient to identify any water mass. Gibbs[7] and Austin[4] stress the importance of using many types of optical measurements to identify a water mass. Water masses containing different types of particles may have nearly identical transmission properties[8]. For this reason, various scattering and transmission measurements were made on the turbidity standards used in this work.

Experimental Procedure

The measurements of light transmission were made with a 25 cm pathlength beam transmissometer as described by Bartz, et al.[6]. It operates at a wavelength of 660 nm. Consequently, effects of yellow matter (or dissolved humic acids and by-produces of biological activity) in the water will not be seen in the data obtained since the attenuation of 660 nm light by yellow matter is negligible[3]. The attenuation detected by the beam transmissometer is due only to absorption and scattering of light by particles in the water and the water itself. The use of a 1/4 m pathlength permits measurements of transmission of light in samples having very high attenuation coefficients. Concentrations of formazin were mixed using the method as described in Standard Methods for the Examination of Water and Wastewater[1]. The concentrations used for the transmission and 45° scattering measurements were 0, 0.25, 0.5, 0.75, 1.0, 1.5, 2, 3, 6, 12, 24, and 40 Jackson Turbidity Units (JTU).

A concentration of 400 JTU was obtained by mixing 5 ml of a 1% (by weight) hydrazine sulfate solution with 5 ml of a 10% (by weight) solution of hexamethylenetetramine and 90 ml distilled water. Different concentrations (i.e., JTU's) were obtained by diluting the 400 JTU sample with distilled water. The diatomaceous earth was mixed to obtain identical concentrations based on the fact that Jackson Turbidity Units are equivalent to parts per million silica (diatomaceous earth)[2]. Replicate measurements of attenuation and scattering were made for each concentration of each substance. To test the reproducibility of the results two separate batches of both the formazin and diatomaceous earth suspensions were used for the experiment.

Measurements of light scattering were taken at the same time as the transmission determinations. Light scattered at 45° was measured using a Brice-Phoenix light scattering photometer[3]. Measurements were made for light of wavelength 650 nm for each concentration of formazin and diatomaceous earth. In addition, light scattering measurements were made at 400, 450, 500, 550, 600, 650, and 700 nm for an arbitrary concentration of each of the two substances. This was done to determine the qualitative variation of the volume scattering function with wavelength for the formazin and diatomaceous earth.

Using the narrow angle scattering meter and method as described by Spinrad, et al.[3] measurements of the volume scattering function at angles between 0.1° and 1.0° were made for a number of concentrations of the formazin and diatomaceous earth suspensions. Specifically, near-forward angle volume scattering functions were determined for formazin concentrations of 0.5, 1, 2, 3, 5 and 12 JTU and for diatomaceous earth concentrations corresponding to 0.5, 1, 2, 3 and 12 JTU. These concentrations were used since they provided the best signal-to-noise ratio in the output of the narrow angle scattering meter. Lower concentrations produce very little scattered light and higher concentrations reduce the main beam reference light to an extremely low value. Measurements of the near-forward volume scattering function are important for correcting errors in transmission determinations which are

caused by forward scattered light.

Results and Discussion

The results of the transmission experiment are shown in Table I and Figure 1 for both the formazin and the diatomaceous earth. The transmission, T, as measured, is converted into a beam attenuation coefficient, c, as follows:

$$T = e^{-cr}$$

where r = optical pathlength (0.25 m in this case)

c = attenuation coefficient (in units of m^{-1})

therefore $c = -4 \ln T$.

TABLE I

Jackson Turbidity Units	$c - c_{water}$ (m^{-1}) Mean	Corrected for Forward Scatter	Standard Deviation	$\beta(45°) - \beta(45°)_{water}$ (m^{-1} $ster^{-1}$) Mean	Standard Deviation
Diatomaceous Earth					
0	0		0	0	0
.25	.1040		.0194	.00519	.00052
.5	.1967	.3258	.0199	.00724	.00180
.75	.2820		.0068	.01411	.00209
1	.3692	.9263	.0208	.01949	.00030
1.5	.5598		.0363	.03020	.00316
2	.7062	1.564	.0026	.03910	.01172
3	1.063	3.064	.0248	.06480	.00967
6	2.131		.0219	.11097	.01624
12	4.289	8.348	.0976	.24367	.05036
24	8.355		.1527	.42947	.00325
40	13.32		.3889	1.0855	.12780
Formazin					
0	0		0	0	0
.25	.1121		.0048	.00972	.00051
.5	.2203	.2626	.0007	.01811	.00111
.75	.3289		.0053	.02323	.00123
1	.4340	.5070	.0092	.03660	.00077
1.5	.6485		.0099	.05464	.00092
2	.8681	1.019	.0158	.07208	.00204
3	1.2973	1.745	.0230	.10688	.00459
6	2.5950	3.398	.0386	.20920	.01116
12	5.2340	6.154	.0915	.48616	.01389
24	10.2533		.1172	1.07529	.02899
40	16.4300		.1735	2.04907	.07750

The term c_w represents the beam attenuation coefficient of clean water (0 JTU or 0 $\frac{mg}{l}$ of silica). Since we are interested only in the optical properties of the formazin and the diatomaceous earth c_w is subtracted from the value of c as obtained from the transmission data.

The beam transmissometer has an acceptance half-angle of 1.35° in water. This means that any light that is scattered within 1.35° of the main beam will be detected by the instrument and will be deemed to be unattenuated light. To correct for this narrow angle scattering results are used as follows:

The total scattered light within an angle, α, from the main beam is given by

$$b_f = 2\pi \int_0^{\alpha} \beta(\vartheta) \sin\vartheta d\vartheta$$

where $\beta(\vartheta)$ is the volume scattering function and is approximately constant in the near-forward region[3].

Therefore,

$$b_f = 2\pi\beta(\vartheta) \int_0^{\alpha} \sin\vartheta d\vartheta$$

$$= 2\pi\beta(\vartheta) (1 - \cos\alpha) .$$

The transmission, as measured will include this scattered light.

So,

$$T_{measured} = e^{-(c + b_f)}$$

and

$$T_{theoretical} = e^{-c}$$

Therefore,

$$T_{theoretical} = T_{measured} e^{-b_f}$$

or

$$\exp(-c_t r) = \exp(-c_m r) \exp(-2\pi\beta(\vartheta) (1 - \cos\alpha))$$

where c_t and c_m are the theoretical and measured attenuation coefficients, respectively.

For $r = 0.25$ m, this yields,

$$c_t = c_m - 8\pi\beta(\vartheta) (1 - \cos\alpha)$$

In Table I c_m is listed as $(c - c_w)$ and c_t is listed as $(c - c_w)$ corrected for forward scatter. The results as shown in Figure 1 demonstrate the obvious differences in transmission vs. concentration between formazin and diatomaceous earth. Corrected beam attenuation coefficient values are consistently higher for the diatomaceous earth. That is, a concentration (in terms of JTU's) of diatomaceous earth will transmit less light than the same concentration of formazin since the amount of forward scattered light is different for each. The slope of the formazin curve changes less than the slope of the curve for diatomaceous earth when corrections for forward scattering are made. This is due to the fact that the diatomaceous earth suspension has a larger mean particle size than the formazin. Large particles scatter much more light at near-forward angles than do smaller particles. This is shown by the mean values of the near-forward angle volume scattering functions in Table II. Mean particle diameters are 1.55 μm for the formazin and 8.75 μm for the diatomaceous earth. The scattering at near-forward angles is consistently higher for the diatomaceous earth samples.

TABLE II

JTU or $\frac{mg}{l}$ Silica	Mean Near-Forward Volume Scattering Function (m^{-1} $ster^{-1}$)	
	Diatomaceous Earth	Formazin
0.5	18.51	6.067
1.0	79.86	10.47
2.0	122.9	21.61
3.0	286.9	54.1
5.0	--	115.1
12.0	633.5	231.9

Figure 2 shows the variation of scattering at 45° (650 nm) with concentration of each suspension. The scattering values of pure water (0 JTU or 0 $\frac{mg}{l}$ silica) have been subtracted to yield only the particulate scattering. Scattering values of the formazin are always higher than those of diatomaceous earth at 45° whereas the size distribution determined the different curves of near-forward scattering the relative indices of refraction (to water) could be more important in determining the different slopes of the volume scattering functions at 45°. From Figure 2 it would seem that the index of refraction of the formazin is higher than that of the diatomaceous earth. Generally, a size distribution of a single material will scatter more at 45° the higher its index of refraction is[11,12]. For near-forward angle scattering particle size is generally more important than index of refraction in determining the volume scattering function. Using a method as described by Woodward[13] it is found that multiple light scattering would not be experimentally detectable (at least 10% higher than single scattering values) until the concentration is approximately 40 JTU or 40 $\frac{mg}{l}$. This is apparent in Figure 2 as the linearity of the curves disappears at some concentration between 24 JTU and 40 JTU.

The qualitative variation of light scattered at 45° with wavelength for formazin and diatomaceous earth is shown in Table III and Figures 3 and 4. Arbitrary concentrations (of approximately 1.0 to 3.0 JTU) of each suspension were used to determine the wavelength dependence of scattering for each substance. The results indicate a λ^{-1} dependence of scattering for both the formazin and the diatomaceous earth. This clearly shows that neither of the two samples is colloidal since a colloid would be a Rayleigh scatterer with a λ^{-4} scattering dependence. Both formazin and diatomaceous earth are suspensions in which the scattering by particles larger than the wavelength predominates. Morel[15] has shown the λ^{-1} dependence for scattering by particle suspensions.

TABLE III

Spectral Scattering of Formazin

λ nm	$\beta(45)$ $m^{-1}ster^{-1}$
400	0.06370
450	0.04365
500	0.03297
550	0.02858
600	0.02447
650	0.02203
700	0.01637

Spectral Scattering of Diatomaceous Earth

λ nm	$\beta(45)$ $m^{-1}ster^{-1}$
400	0.20602
450	0.16038
500	0.12755
550	0.11160
600	0.09658
650	0.07542
700	0.05649

Conclusions

The use of JTU's as indicators of turbidity has been questioned[2,4,5,14]. Callaway, et al.[3] have demonstrated that water samples having identical particle concentrations may display very different light attenuation coefficients. This has been demonstrated here for two commonly used turbidity references. Obviously, the use of the Jackson Turbidity Unit is inadequate to define the optical properties of a particular water mass. The JTU can, however, be accurately used as an indicator of a particle concentration.

The tables and curves presented in this paper supply information that allows the calibration of beam transmissometers (at 660 nm) and light scattering photometers (at 650 nm) using common, well-tested turbidity standards. The characteristics of the particular instruments (such as acceptance angles) must be known to make use of the information contained herein.

It is important to emphasize that the results obtained here show very clearly that no single optical measurement is sufficient to define a water mass. Measurements of transmission alone or scattering alone do not define turbidity. The single concept of turbidity is best replaced by a matrix of parameters including transmission and scattering (both near-forward and at large angles).

Acknowledgments

The authors would like to thank David W. Menzies for his assistance in the laboratory during this experiment. We are also grateful to Pam Wegner for typing the manuscript. This research has been supported by the Office of Naval Research, contract N00014-76-C-0067 under project NR083-102 and the Department of Energy, contract No. EY 76-S-06-2227, Task Agreement No. 29.

Literature Cited

1. American Public Health Association, American Water Works Association, Water Pollution Control Federation, Standard Methods for the Examination of Water and Wastewater, 13th ed., pp. 349-356, American Public Health Association, Wash., D.C. (1971).

2. Pickering, R. J., U. S. Geological Survey Open-File Report 76-153, pp. 1-7 (1976).

3. Jerlov, N. G., Marine Optics, pp. 1-10, Elsevier Pub. Co., New York (1976).

4. Austin, R. in Proceedings NOIC Turbidity Workshop, pp. 45-74, National Oceanographic Instrumentation Center, Wash., D.C. (1974).

5. Freeman, D. H., in Proceedings NOIC Turbidity Workshop, pp. 143-152, National Oceanographic Instrumentation Center, Wash., D.C. (1974).

6. Bartz, R., J. R. V. Zaneveld and H. Pak, in Proceedings of the Society of Photo-Optical Instrumentation Engineers, v. 160, pp. 102-108, Society of Photo-Optical Instrumentation Engineers, Bellingham, WA (1978).

7. Gibbs, R. J., in Proceedings NOIC Turbidity Workshop, pp. 17-22, National Oceanographic Instrumentation Center, Wash., D.C. (1974).

8. Callaway, R. J., A. M. Teeter, D. W. Browne, and G. R. Ditsworth, in Proceedings of the Symposium American Museum of Natural History, pp. 199-211, ed. by M. Grant Gross, New York (1975).

9. Pak, H., The Columbia River as a source of marine light scattering particles, Ph.D. Thesis, Oregon State University, 119 p., 1970.

10. Spinrad, R. W., J. R. V. Zaneveld, and H. Pak, Applied Optics, v. 17, pp. 1125-1130 (1978).

11. Morel, A., Indicatrices de diffusion calculees par la theorie de mie pour les systemes polydisperses, en vue de l'application aux particules marines, pub. by Centre de recherches Oceanographiques, Villefrancne-sur-mer, France (1973).

12. Shifrin, K., and I. Salganik, Tables of Light Scattering, v. 5, Leningrad, Russia (1973).

13. Woodward, D. H., J. Opt. Soc. Amer., v. 54, pp. 1325-1331 (1964).

14. Booth, R., in Proceedings NOIC Turbidity Workshop, pp. 101-106. National Oceanographic Instrumentation Center, Wash., D.C. (1974).

15. Morel, A., in AGARD Lecture Series no. 61 on Optics of the Sea, pp. 3.1-3.76, North Atlantic Treaty Organization Advisory Group for Aerospace Research and Development, Langley Field, Virginia, 1973.

Figure Captions

Fig. 1. Beam attenuation coefficient, c, versus particle concentration (in JTU for the formazin and $\frac{mg}{\ell}$ for the diatomaceous earth). Plots are for formazin corrected for forward scattered light (.....), diatomaceous earth corrected for forward scattered light (-.-.-.), formazin uncorrected (----) and diatomaceous earth uncorrected (——).

Fig. 2 Volume scattering function at 45°, β(45), versus particle concentration (in JTU for the formazin and $\frac{mg}{\ell}$ for the diatomaceous earth) for formazin (----) and diatomaceous earth (——).

Fig. 3. Volume scattering function at 45°, β(45), versus wavelength, λ, of incident light for formazin sample. Line corresponds to $\beta(45) = 38\ \lambda^{-4} - 0.0401$.

Fig. 4. Volume scattering function at 45°, β(45), versus wavelength, λ, of incident light for diatomaceous earth sample. Line corresponds to $\beta(45) = 132.86\ \lambda^{-4} - 0.1272$.

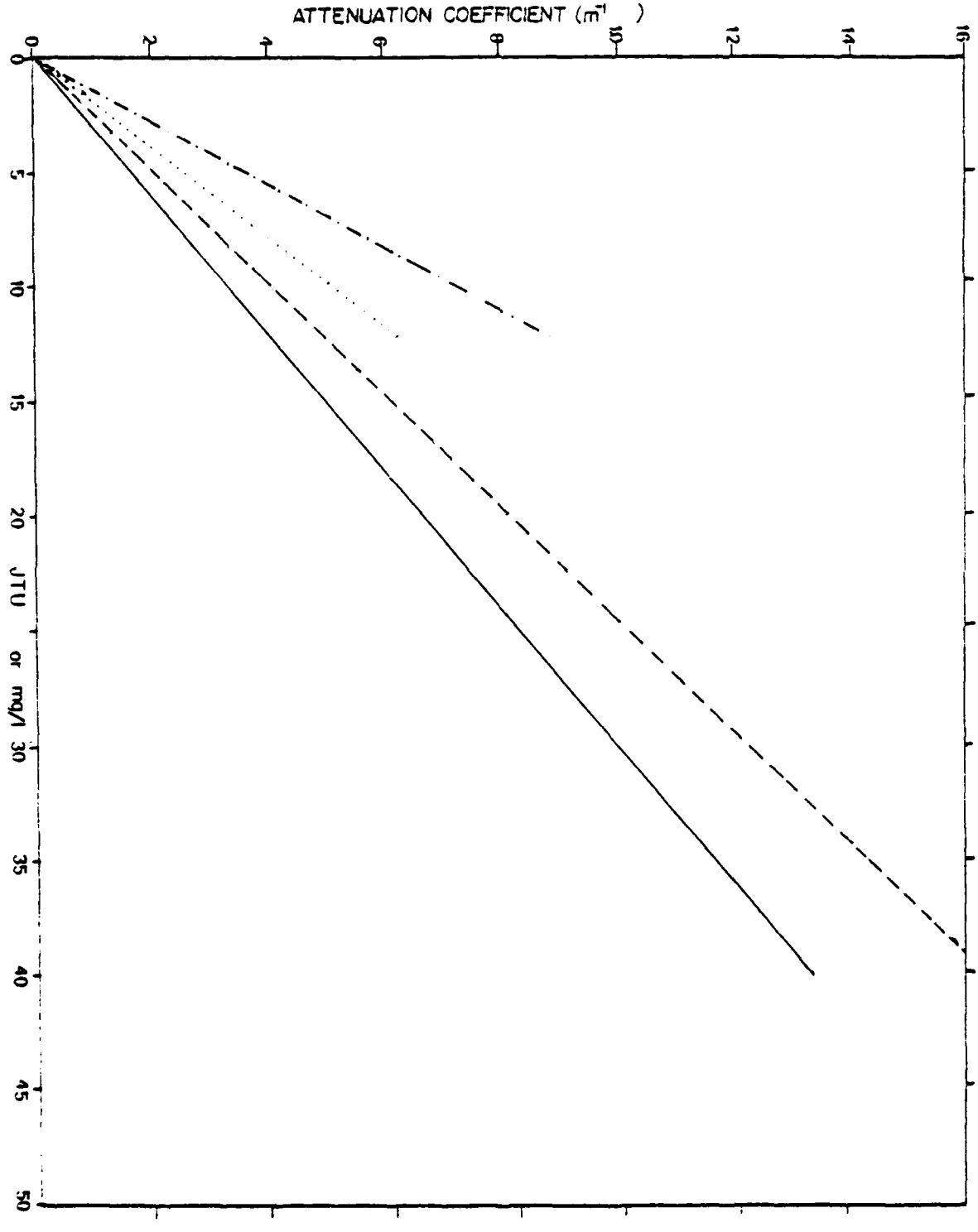
ATTENUATION COEFFICIENT (m⁻¹)
0
2
4
6
8
10
12
14
16
0
5
10
15
20
25
30
35
40
45
50
JTU or mg/l

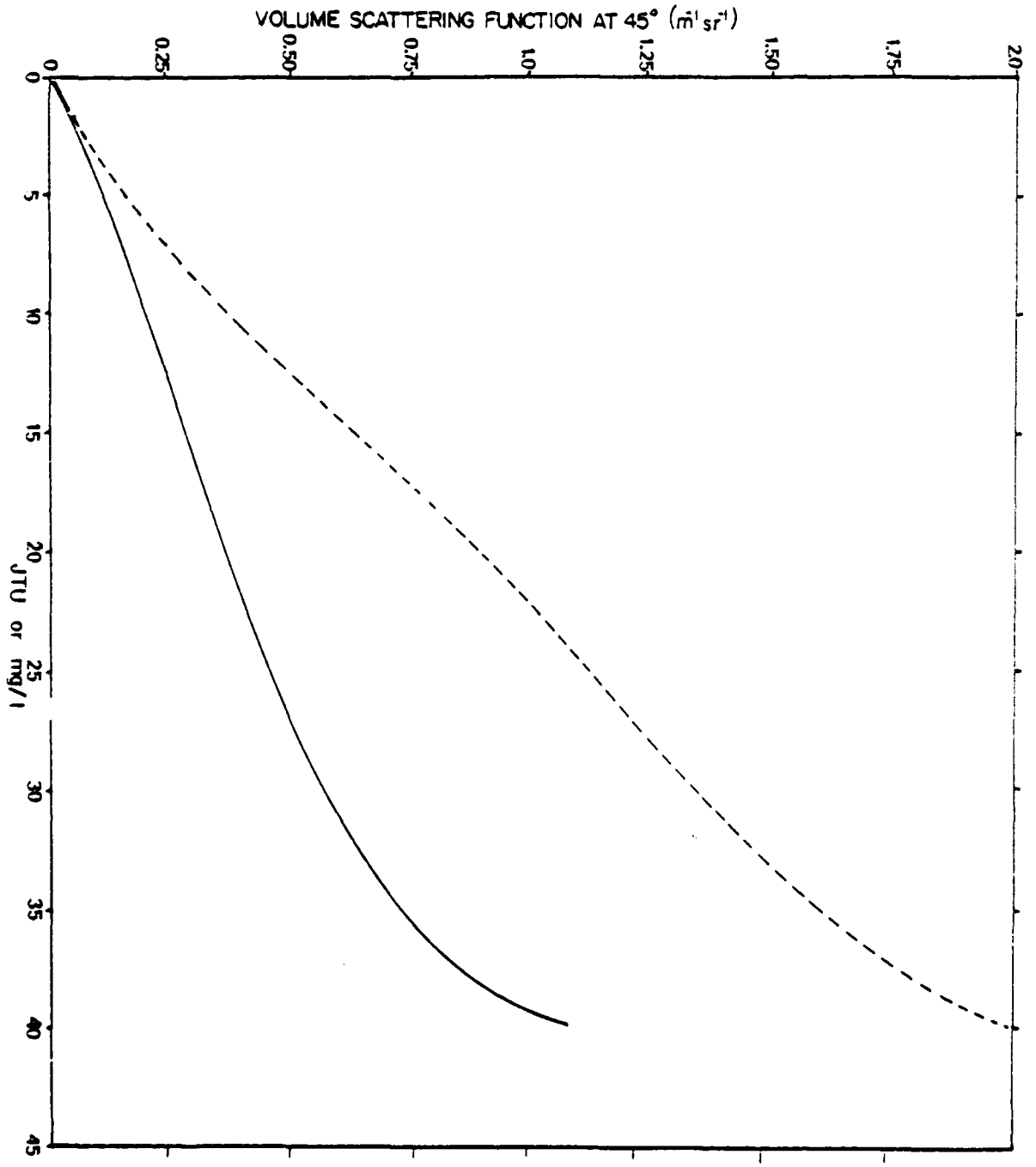
VOLUME SCATTERING FUNCTION AT 45° (m⁻¹sr⁻¹)
0
0.25
0.50
0.75
1.0
1.25
1.50
1.75
2.0
0
5
10
15
20
25
30
35
40
45
JTU or mg/l

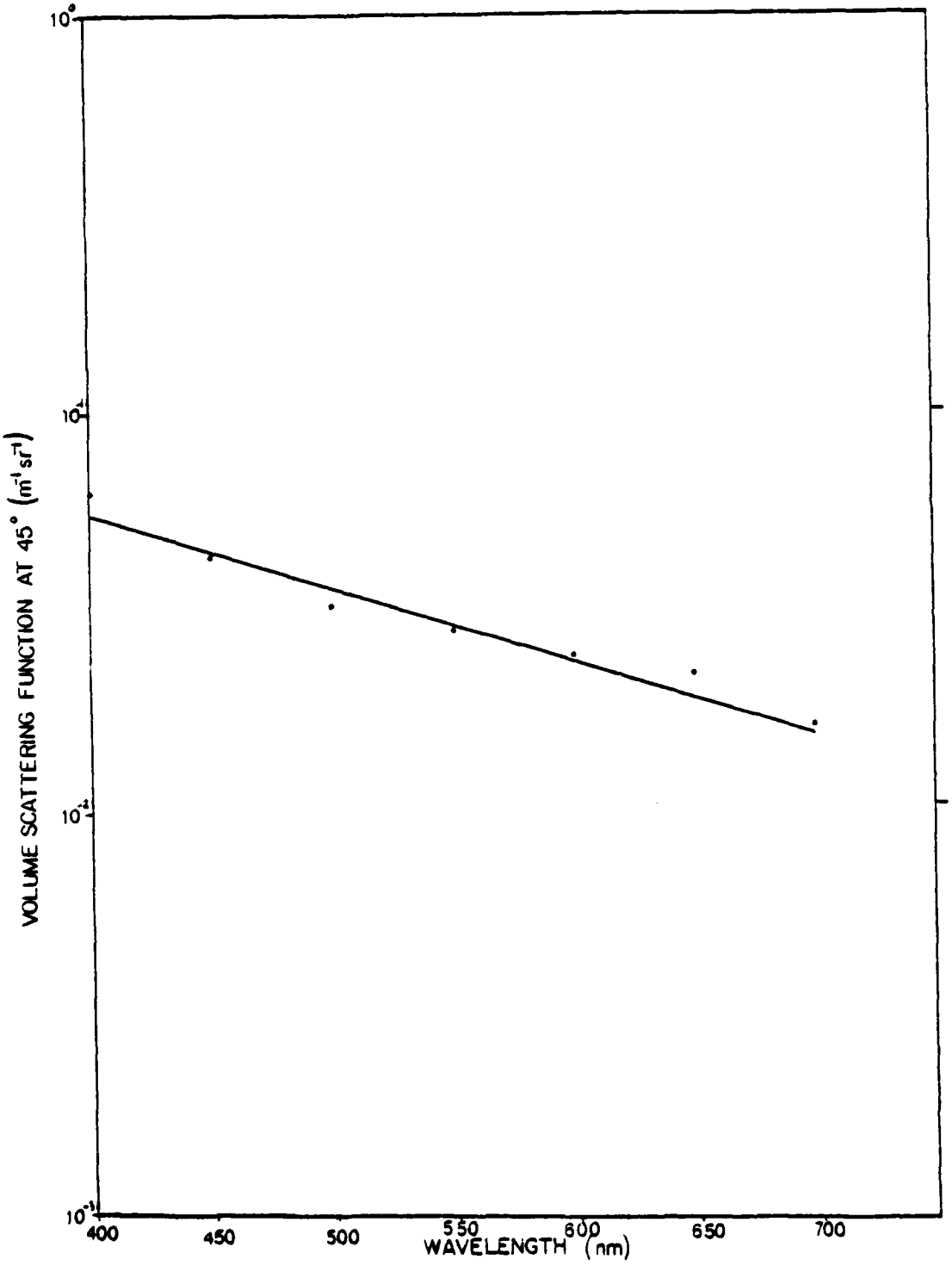
VOLUME SCATTERING FUNCTION AT 45° (m⁻¹sr⁻¹)
10⁰
10⁻¹
10⁻²
10⁻³
400
450
500
550
600
650
700
WAVELENGTH (nm)

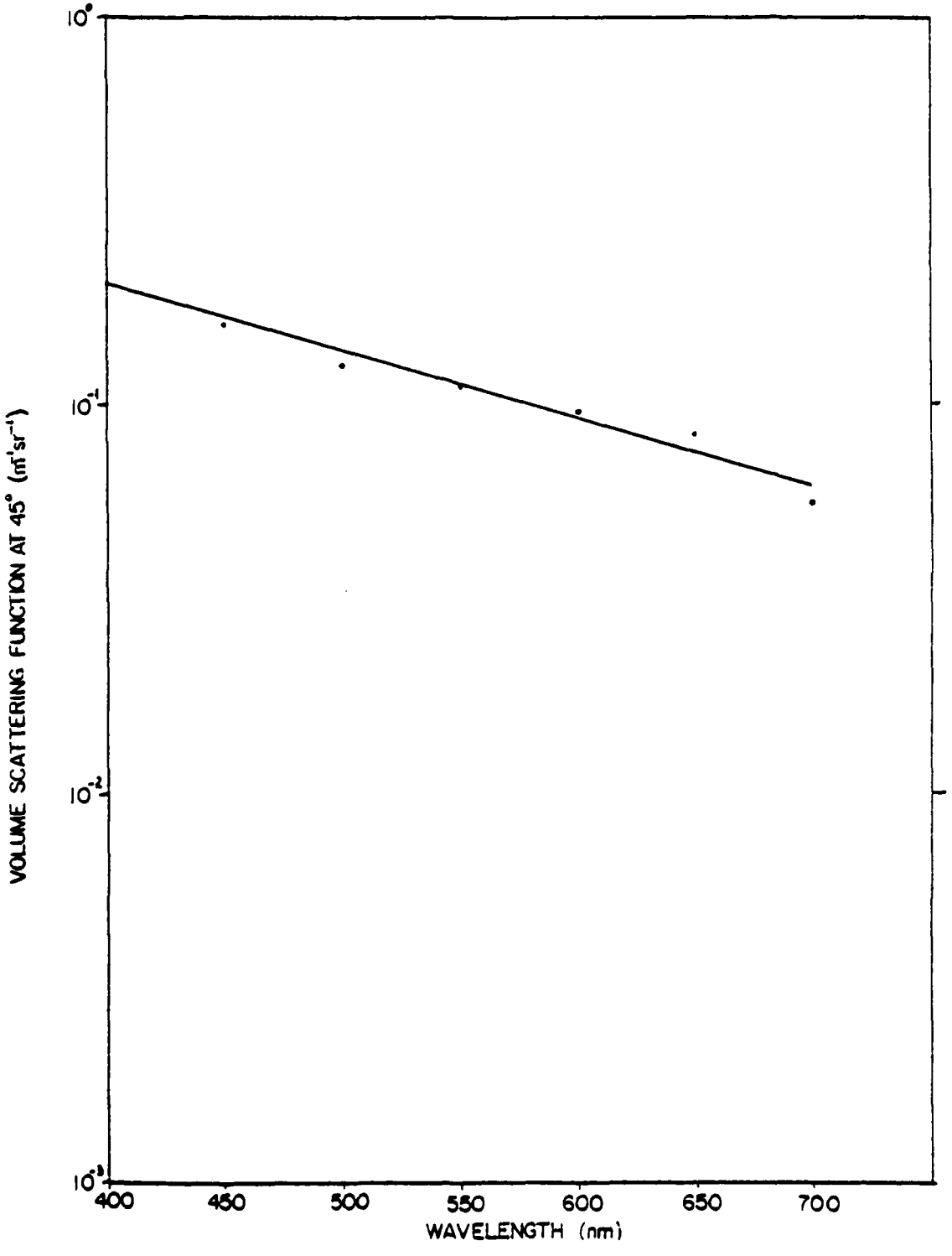
VOLUME SCATTERING FUNCTION AT 45° (m⁻¹sr⁻¹)
10°
10⁻¹
10⁻²
10⁻³
400
450
500
550
600
650
700
WAVELENGTH (nm)

Deep-Sea Research, Vol. 26A, pp. 1347 to 1362
Pergamon Press Ltd 1979. Printed in Great Britain

0011-7471/79/1201-1347 $02.00/0

Productivity, sedimentation rate, and sedimentary organic matter in the oceans—I. Organic carbon preservation

P. J. MÜLLER* and E. SUESS†

(*Received* 7 *November* 1978; *in revised form* 27 *June* 1979; *accepted* 31 *July* 1979)

Abstract—Comparison of rates of accumulation of organic carbon in surface marine sediments from the central North Pacific, the continental margins off northwest Africa, northwest and southwest America, the Argentine Basin, and the western Baltic Sea with primary production rates suggests that the fraction of primary produced organic carbon preserved in the sediments is universally related to the bulk sedimentation rate. Accordingly, less than 0.01% of the primary production becomes fossilized in slowly accumulating pelagic sediments [2 to 6 mm (1000 y)$^{-1}$] of the Central Pacific, 0.1 to 2% in moderately rapidly accumulating [2 to 13 cm (1000 y)$^{-1}$] hemipelagic sediments off northwest Africa, northwest America (Oregon) and southeast America (Argentina), and 11 to 18% in rapidly accumulating [66 to 140 cm (1000 y)$^{-1}$] hemipelagic sediments off southwest America (Peru) and in the Baltic Sea.

The empirical expression:

$$\% \text{ Org-C} = \frac{0.0030 \cdot R \cdot S^{0.50}}{\rho_s(1-\Phi)}$$

implies that the sedimentary organic carbon content (% Org-C) doubles with each 10-fold increase in sedimentation rate (S), assuming that other factors remain constant; i.e., primary production (R), porosity (Φ) and sediment density (ρ_s). This expression also predicts the sedimentary organic carbon content from the primary production rate, sedimentation rate, dry density of solids, and their porosity; it may be used to estimate paleoproductivity as well. Applying this relationship to a sediment core from the continental rise off northwest Africa (Spanish Sahara) suggests that productivity there during interglacial oxygen isotope stages 1 and 5 was about the same as today but was higher by a factor of 2 to 3 during glacial stages 2, 3, and 6.

INTRODUCTION

IT IS A characteristic feature of many hemipelagic sediments, accumulating fast enough to resolve the last glacial and interglacial periods, that glacial sections contain considerably more organic matter than interglacial sections. Such a distribution has been described for sediments from the northwest African continental margin (MÜLLER, 1975a, b; HARTMANN, MÜLLER, SUESS and VAN DER WEIJDEN, 1976), the Argentine Basin (STEVENSON and CHENG, 1972) and apparently is true also for South Indian continental slope sediments (MARCHIG, 1972), as shown by HARTMANN *et al.* (1976).

As an example, Fig. 1(a) shows organic carbon fluctuations in a sediment core from the northwest African continental margin at a water depth of 2575 m. The oxygen isotope stratigraphy (Fig. 1d) for the core is that determined by SHACKLETON (1977) (see also THIEDE, 1977; SUESS, THIEDE and MÜLLER, 1978). Accordingly it penetrates the past 140,000-year record and shows low organic matter contents in sediments deposited during

* Geologisch-Paläontologisches Institut der Universität Kiel, Olshausenstr. 40-60, D-2300 Kiel, F.R.G.
† School of Oceanography, Oregon State University, Corvallis, OR 97331, U.S.A.

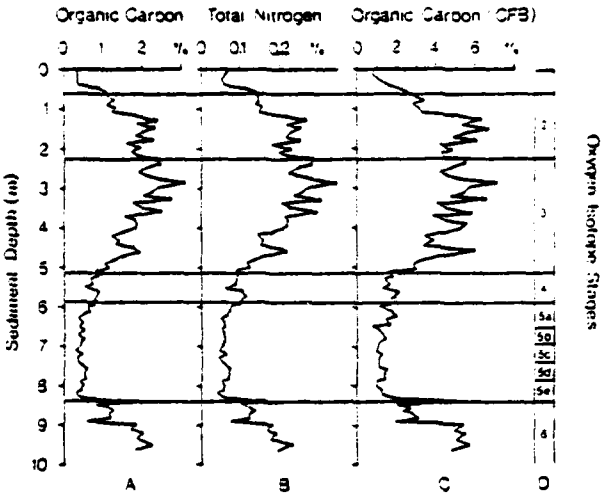

Fig. 1. Organic carbon and total nitrogen distribution in core 12392-1 from the continental rise off Spanish Sahara, after SUESS *et al.*, 1978 (for station data see Table 1); oxygen isotope stratigraphy from SHACKLETON (1977); CFB = Carbonate free basis.

interglacial stages 1 and 5 but higher concentrations (by factors of 3 to 7) in sediments deposited during glacial stages 2, 3 and 6.

The variations of major constituents in this core, i.e., calcium carbonate and to a lesser extent quartz (SUESS *et al.*, 1978), which act as dilutents of organic matter, are not large enough to account for the cyclic organic matter distribution. Therefore, the relative organic carbon fluctuations remain the same when calculated on a carbonate-free basis (Fig. 1c). Similarly, variations in grain size composition (CHAMLEY, DIESTER-HAASS and LANGE, 1977) are smaller than the organic matter fluctuations, thus excluding a textural control. There is also no evidence that a significant fraction of the organic matter in the core is of non-marine origin (DEBYSER, PELET and DASTILLUNG, 1977) so that quite likely the cyclic organic matter distribution reflects changing primary production rates during glacial and interglacial times (with the exception of the relatively cold and brief oxygen isotope stage 4 where no increase in organic carbon contents was noted).

It is a general feature of such cores with cyclic organic matter distributions that organic rich sections coincide with increased bulk sedimentation rates (STEVENSON and CHENG, 1972; HARTMANN *et al.*, 1976): rapid sedimentation enhances the preservation of organic matter. TOTH and LERMAN (1977) and BERNER (1978) showed that the first-order reaction rate constants for reduction of interstitial sulfate and production of interstitial ammonia and phosphate are proportional to the second power of the sedimentation rate, suggesting that increasing sedimentation rates favor the preservation of labile organic substances. HEATH, MOORE and DAUPHIN (1977) found that the organic carbon accumulation rates in marine sediments are proportional to the 1.4th power of the bulk sediment accumulation rate points to the same phenomenon.

Hence the question is raised as to whether the higher organic matter contents in glacial sections of core 12392 (Fig. 1a, b) and similar cores are due to better preservation or higher

input of organic matter (cf. HARTMANN *et al.*, 1976). The purpose of the present study is to find a quantitative relationship between primary production rates as reflected by organic matter input to sediments, sedimentation rates, and sedimentary organic carbon contents as an answer to the above question.

DATA SOURCES

This study is based on 26 analyses of surface sediments from Pacific Ocean, Atlantic Ocean, and Baltic Sea regions covering a wide range of sedimentary organic carbon contents, sedimentation rates, and primary production rates of the surface waters. The regions selected are thought to meet a basic requirement in that the major fraction of accumulating organic matter is of marine origin and thus reflects primary productivity. The regions are the Central Pacific Ocean southeast of Hawaii, the continental slopes off northwest Africa (Spanish Sahara), northwest America (Oregon), southwest America (Peru), the Argentine Basin, and the Eckernförder Bay of the western Baltic Sea (Fig. 2).

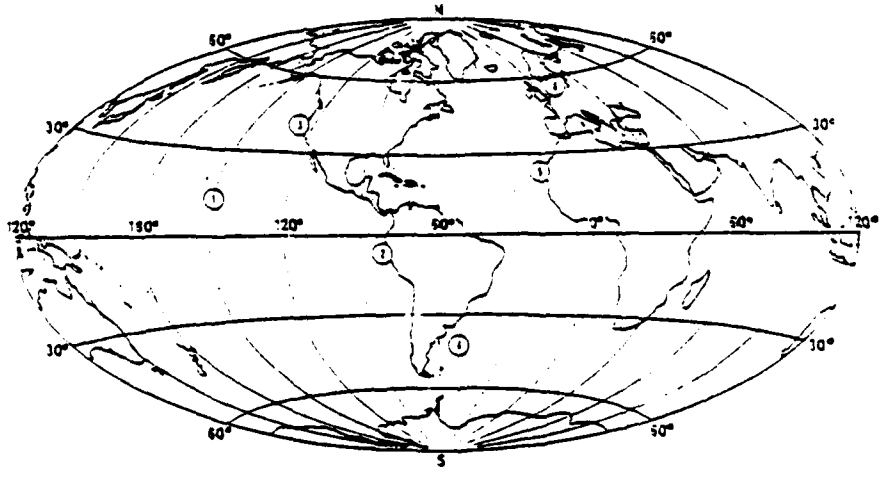

Fig. 2. Principal areas of investigation (for station data see Table 1).

Geographic positions and water depths of all core locations are listed in Table 1. Organic carbon contents, sedimentation rates, and primary production rates were selected from the publications listed in Table 2 after careful scrutiny of the various methods used in generating the data.

Assumptions were made with respect to the dry density of solids and porosity of the sediments because in most cases only water contents were available as direct measurements. The mean dry density of 14 Holocene sediment samples off northwest Africa is 2.71 g cm^{-3} with a standard deviation of 0.04 (after KÖGLER, University of Kiel, unpublished data). This value was used in calculations for all northwest African sediments. A slightly lower value (2.6 g cm^{-3}) was assumed for the carbonate-poor Argentine Basin and Baltic Sea sediments. Porosities of the above sediments were then calculated using the

Table 1. Geographic positions and water depths of surface sediments and core 12392-1 used in this study. Central Pacific station numbers correspond to original shipboard designations V405-4-104, V405-4-493, V408-1-13, V408-1-19, V408-1-36, V405-1-41 and V408-1-58 as used in the reference cited

Region	Station	Latitude	Longitude	Water depth (m)	Reference
Northwest Africa	12392-1	25°10'N	16°51'W	2575	SEIBOLD, 1972
..	12310-3	23°30'N	18°43'W	3076	..
..	12327-4	23°08'N	17°44'W	2037	..
..	12328-4	21°09'N	18°34'W	2798	..
..	12329-4	19°22'N	19°56'W	3315	..
..	12336-1	16°14'N	20°26'W	3645	..
..	12337-4	15°58'N	18°07'W	3085	..
..	12347-1	15°50'N	17°51'W	2710	..
..	12345-4	15°29'N	17°22'W	966	..
..	12344-3	15°26'N	17°21'W	711	..
..	13209-2	12°29'N	20°03'W	4713	SEIBOLD and HINZ, 1976
Argentine Basin	V-15-141	45°44'S	50°45'W	5934	STEVENSON and CHENG, 1972
..	V-15-142	44°54'S	51°32'W	5885	..
West Baltic	13947	54°32'N	10°04'E	28	WHITICAR, 1978
..	13939	54°32'N	10°04'E	28	..
..	12897	54°31'N	10°02'E	28	..
Central North Pacific	10127-2	13°42'N	151°39'W	5686	SCHULTZE-WESTRUM, 1973; BEIERSDORF *et al.*, 1974
..	10132-1	6°13'N	148°57'W	5004	..
..	10140-1	9°15'N	148°45'W	5144	..
..	10141-1	9°07'N	148°47'W	5189	..
..	10145-1	4°00'N	144°49'W	4599	..
..	10147-1	3°50'N	145°02'W	4619	..
..	10175-1	9°19'N	146°01'W	5164	..
Peru Margin	7706-39	11°15'S	77°57'W	186	This study
..	7706-36	13°37'S	76°51'W	370	..
Oregon Margin	7610-8	44°36'N	126°20'W	2060	..

expression by BERNER (1971):

$$\Phi = \frac{W p_s}{W p_s + (1 - W) p_w} \quad (1)$$

where W = % H_2O (wet wt)/100; p_s = dry density of solid sediment material (g cm^{-3}); p_w = density of interstitial water, taken to be 1.025 g cm^{-3}.

Porosities listed in brackets in Table 3 were estimated by comparison with sediments from the same region and similar lithologies because water contents for these samples were not available.

The dry density and porosity values for the Central Pacific sediments were taken from HARTMANN, KÖGLER and MÜLLER (1978), and those for Peru and Oregon margin sediments were calculated from wet bulk densities and water contents determined by KELLER (Oregon State University) and kindly made available for this study. The very low dry densities of the Peru margin samples are due to their extremely high organic contents (Table 3).

ORGANIC CARBON ACCUMULATION RATES

The organic carbon contents of the sediments ranged from 0.2 to 0.4% (dry wt) in the Central Pacific to up to 21% off Peru and co-vary to some extent with the sedimentation rates (Fig. 3A) (see also HEATH *et al.*, 1977). Comparison with primary production rates

Table 2. Sources for data on organic carbon contents, sedimentation rates, and primary production rates

Region	Organic carbon	Sedimentation rate	Primary production rate
Northwest Africa	MOLLER, 1975a, b	DIESTER-HAASS *et al.*, 1973; PFLAUMANN, 1975; THIEDE, 1977; SUESS *et al.*, 1978, Biostratigraphy, Oxygen isotope stratigraphy, ^{14}C-dating	SCHEMAINDA *et al.*, 1975
Baltic Sea	WHITICAR, 1978	ERLENKEUSER *et al.*, 1974 ^{14}C-dating	BODUNGEN, 1975
Argentine Basin	STEVENSON and CHENG, 1972	STEVENSON and CHENG, 1972 Biostratigraphy	MENZEL, 1974*
Central Pacific	MOLLER, 1977; MOLLER and MANGINI, 1979	MANGINI and SONNTAG, 1977 MOLLER and MANGINI, 1979 ^{230}Th and ^{231}Pa	MENZEL, 1974 VAN ANDEL *et al.*, 1975
Peru Margin	This study	DEMASTER, 1979 ^{210}Pb and ^{14}C-dating	GUILLEN *et al.*, 1973
Oregon Margin	This study	DUNCAN *et al.*, 1970 Biostratigraphy, ^{14}C dating	SMALL *et al.*, 1972 ANDERSON, 1964

* Average rate for coastal (non-upwelling) regions

Table 3. Analytical data as taken from the references listed in Table 2 and used in calculating organic carbon accumulation rates (equation 2) in units of mass area^{-1} time^{-1} and as per cent of primary production (R). See text for explanation of other symbols. Porosities in (ϕ) were estimated from comparison with similar northwest African surface sediments. A dry density of solids of 2.6 g cm^{-3} was assumed in the case of the carbonate-poor Argentine Basin and Baltic Sea sediments

Station	Depth (cm)	C (%)	ρ_s (g/cm^3)	Φ (vol %/100)	S (cm/1000 y)	R (gC m^{-2} y^{-1})	Org. Carbon Acc. Rate (gC m^{-2} y^{-1})	(% of R)
12392-1	2–10	0.35	2.71	0.64	4.7	75	0.160	0.21
12340-3	0–2	0.34	2.71	(0.76)	2.5	90	0.055	0.06
12327-4	0–1	1.34	2.71	0.85	6.0	130	0.327	0.25
12328-4	0–1	1.66	2.71	(0.79)	12.7	250	1.20	0.48
12329-4	0–2	0.61	2.71	0.77	2.0	90	0.076	0.085
12336-1	0–2	0.44	2.71	0.75	2.2	75	0.066	0.085
12337-4	0–2	1.46	2.71	(0.79)	4.0	160	0.332	0.21
12347-1	0–1	2.34	2.71	0.79	9.1	175	1.21	0.69
12345-4	0–1	3.67	2.71	(0.79)	7.3	210	1.53	0.73
12344-3	0–2	2.59	2.71	(0.79)	7.3	210	1.08	0.51
13209-2	0–10	0.51	2.71	(0.79)	2.0	70	0.058	0.085
V-15-141	0–1	0.72	(2.60)	0.63	3.3	100	0.229	0.23
V-15-142	0–2	0.92	(2.60)	0.63	3.8	100	0.336	0.34
11947	0–20	4.91	(2.60)	0.85	140	160	26.8	17
13939	0–20	5.16	(2.60)	0.85	140	160	28.2	18
12897	0–20	4.87	(2.60)	0.84	140	160	28.4	18
10127-2	0–2	0.28	2.65	0.86	0.19	50	0.0020	0.0039
10132-1	0–4	0.22	2.65	0.80	0.58	50	0.0068	0.014
10140-1	0–2	0.33	2.49	0.85	0.41	50	0.0051	0.010
10141-1	0–2	0.31	2.49	0.85	0.36	50	0.0042	0.0083
10145-1	0–2	0.21	2.65	0.80	0.32	100	0.0036	0.0036
10147-1	0–2	0.23	2.65	0.80	0.43	100	0.0052	0.0052
10175-1	0–2	0.40	2.48	0.84	0.23	50	0.0037	0.0073
7706-39	0–3	12.5	1.89	0.88	140	330	39.7	12
7706-36	0–3	21.2	1.93	0.86	66	330	37.8	12
7610-8	0–1	1.50	2.42	0.88	10	100	0.436	0.40

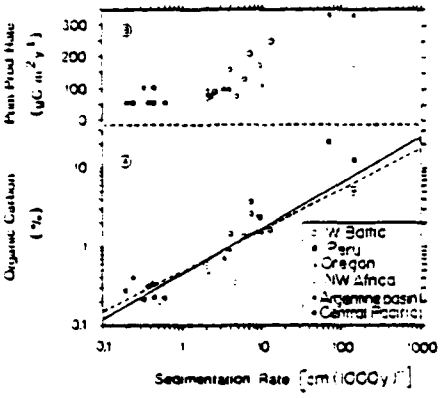

Fig. 3 Organic carbon contents of surface sediments versus sedimentation rates (A); scattering is in part due to the concomitant increase in primary production rates (B). The solid regression line ($Y = 0.46X^{0.37}$, $n = 26$, $r = 0.90$) suggests a 2-fold increase of organic carbon with each 4-fold increase of the sedimentation rate (see text for restrictions). The dashed line represents equation (4) taking $\rho_s = 2.58$ and $\phi = 0.80$ (mean values from Table 3).

(Fig. 3B) suggests that the scatter in Fig. 3(A) is in part due to the different productivities in the regions studied, but "dilution" of organic matter by varying amounts of calcium carbonate and quartz may be equally important.

Organic carbon concentrations were transformed to organic carbon accumulation rates using equation (2) (see also: MURRAY, GRUNDMANIS and SMETHIE, 1978) to compensate for "dilution" effects and more importantly to make the values comparable to primary production rates:

$$C_A = \frac{C \cdot S}{10} \rho_s (1 - \phi) \tag{2}$$

where C_A = organic carbon accumulation rate (g C m^{-2} y^{-1}); C = organic carbon content (% dry wt); S = sedimentation rate [cm(1000 y)$^{-1}$]; ρ_s = dry sediment density (g dry sediment per cm^3 dry sediment); and ϕ = porosity (volume of water per volume of bulk wet sediment).

Organic carbon accumulation rates are listed in Table 3 and plotted against the sedimentation rates in Fig. 4. They are lowest in the slowly accumulating pelagic sediments of the Central Pacific and about four orders of magnitude higher in the rapidly deposited sediments of the Baltic Sea and the upper continental slope of the Peruvian margin. Off northwest Africa and northwest America and in the Argentine Basin, organic carbon accumulation rates are between both extremes. The two Black Sea sediments included in Fig. 4 (arrows) were not considered in calculating the regression line and will be discussed separately.

The regression equation obtained from the log-log plot in Fig. 4 is:

$$C_A = 0.0246\, S^{1.523}, \tag{3}$$

where C_A and S are the organic carbon accumulation rate and sedimentation rate as defined above.

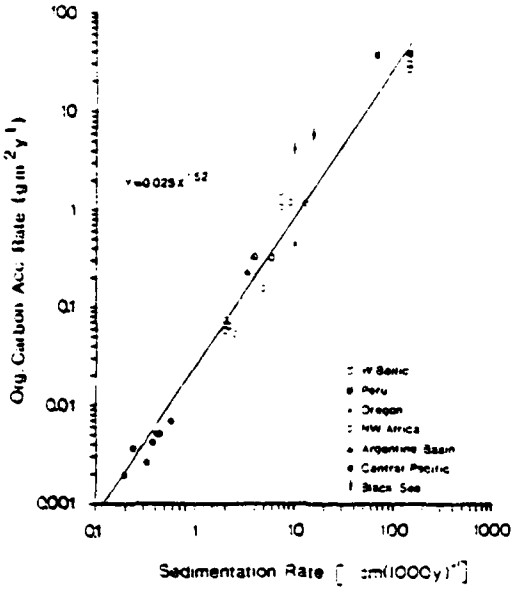

Fig. 4. Organic carbon accumulation rates (Y) as a function of sedimentation rates (X) (number of samples: $n = 26$; correlation coefficient: $r = 0.986$). Two samples from the Black Sea are shown for comparison (arrows) but are not included in regression analysis (see text).

We should like to point out that in Fig. 4 C_A and S are partially dependent variables [see equation (2)] such that a correlation exists *a priori* between them. However, this leads only to fortuitous findings if the C-org contents remain constant. This is not the case in our data set, therefore we find it legitimate to use this functionality to derive equations (5) and (6). The exponent of the sedimentation rate in equation (3) is in good agreement with the value of 1.4 calculated by HEATH *et al.* (1977) for 50 marine sediments (10 were the same as in this study) using g cm^{-2} (1000 y)$^{-1}$ as units for the sedimentation rate. Accordingly the *organic carbon accumulation rate* in marine sediments should approximately double with each 1.6-fold increase of the sedimentation rate.

Substituting equation (2) for the organic carbon accumulation rate (C_A) in equation (3) and solving for the organic carbon content (C) we obtain equation (4) which predicts the sedimentary organic carbon content from sedimentation rate (S), dry density (ρ_s), and porosity (Φ):

$$C = \frac{0.246 \cdot S^{0.52}}{\rho_s(1-\Phi)}. \tag{4}$$

Equation (4) suggests that the sedimentary *organic carbon content* increases by a factor of 2 with each 4-fold increase of the sedimentation rate as illustrated in Fig. 3. However, this is obtained from a relationship not considering productivity changes, which to some extent parallel the changes of sedimentation rates (Fig. 3) and thus probably overestimates the degree of preservation by increasing sedimentation rates. To compensate for this effect organic carbon accumulation rates were normalized to the primary production rate, i.e.,

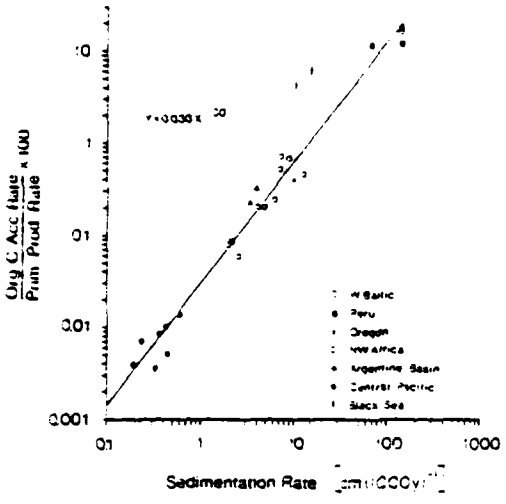

Fig. 5. Organic carbon accumulation rates normalized to primary production rates (expressed as %) as a function of sedimentation rates ($n = 26$; $r = 0.992$). Two samples from the Black Sea (arrows) are shown for comparison only and are not included in the regression analysis (see text).

expressed as % of primary production (Table 3) and again plotted versus the sedimentation rates (Fig. 5). The resulting regression equation is:

$$\frac{C_A}{R} \cdot 100 = 0.030 \cdot S^{0.30}, \tag{5}$$

where C_A, R, and S are the organic carbon accumulation rate, primary production rate, and sedimentation rate [same units as defined for equation (2)].

Again substituting equation (2) for the organic carbon accumulation rate in equation (5) and solving for the organic carbon content we obtain equation (6), which also is graphically displayed in Fig. 6:

$$C = \frac{0.0030 \cdot R \cdot S^{0.30}}{\rho_s(1-\Phi)}. \tag{6}$$

Equation (6) predicts the sedimentary organic carbon content (C) from the annual average primary production rate (R), sedimentation rate (S), dry density (ρ_s), and porosity (Φ) to within a factor of 2, as illustrated in Fig. 7. Moreover, it shows that the organic content of a sediment doubles with a 10-fold increase in the sedimentation rate, assuming other factors remain constant. We feel that this is a reasonable estimate of the effect that sedimentation rate has on the preservation of accumulating organic matter.

Consequently, in slowly accumulating pelagic sediments with $< 1\%$ organic carbon contents as in the Central Pacific, only about 0.01% of primary produced organic carbon is preserved (Table 3, Fig. 5), a figure already estimated by BRUYEVICH (1963). On the other hand, 10 to 20% of the primary produced organic carbon is preserved in sediments accumulating as rapidly as in the Peruvian margin and Baltic Sea deposits studied here. In regions with moderately rapid sedimentation rates (i.e., a few centimeters to a few

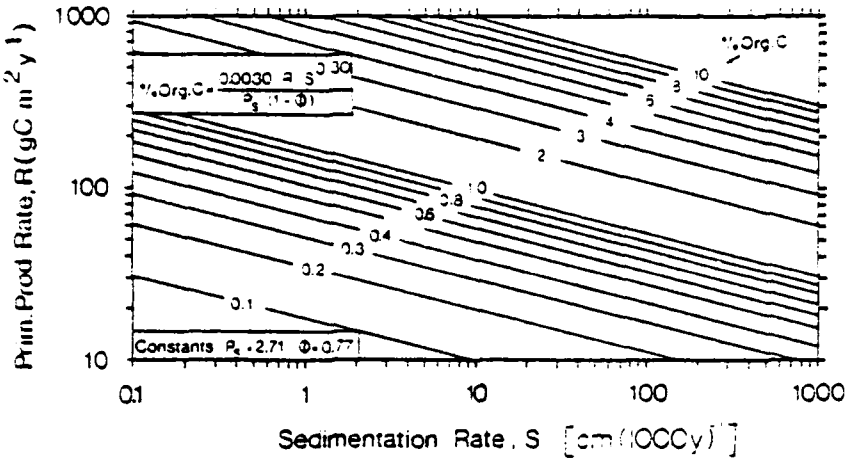

Fig. 6. Illustration of the dependence of sedimentary organic carbon contents on primary production rates (R) and sedimentation rates (S) at constant dry density of solids (ρ_s) and porosity (Φ). The constants assumed are average values for northwest African sediments listed in Table 3. At a constant primary production rate the organic carbon content approximately doubles with each 10-fold increase in the sedimentation rate.

decimeters each 1000 y; e.g., off northwest Africa, on the Oregon margin, and in the Argentine Basin) the respective percentages of preserved organic carbon range between 0.1 and 1% of the amounts produced.

The finding that the sedimentation rate largely determines the fraction of primarily produced organic carbon that eventually becomes fossilized in sediments also suggests that most of the organic material escaping the photic zone is remineralized at the sea bottom rather than during settling through the water column. This is mainly a consequence of the different residence times of particles in the water column and at the sea bottom. For example, particle settling times through a 5000-m deep water column are in the order of weeks, months or years, depending on particle size and shape and also on currents (e.g.,

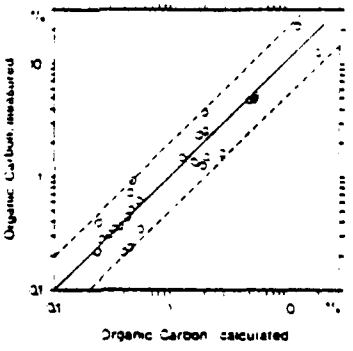

Fig. 7. Measured organic carbon contents of surface sediments and values calculated from equation (6), using the data listed in Table 3. The values agree within a factor of 2, as shown by the dotted lines.

AD-A099 518 OREGON STATE UNIV CORVALLIS SCHOOL OF OCEANOGRAPHY F/G 8/10
COMPILATION OF REPRINTS NUMBER 57,(U)
JAN 81 R W SPINRAD, J R ZANEVELD, H PAK N00014-76-C-0067
UNCLASSIFIED REF-79-4 NL

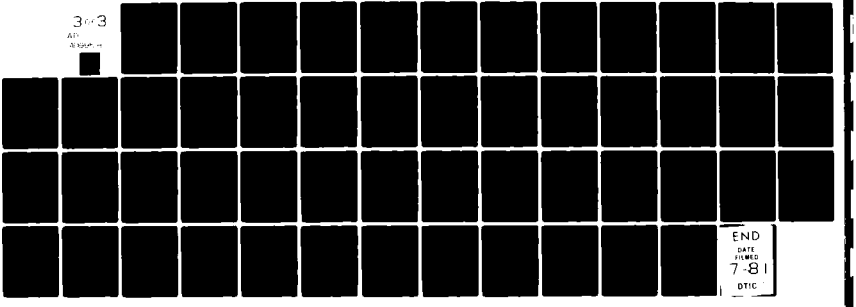

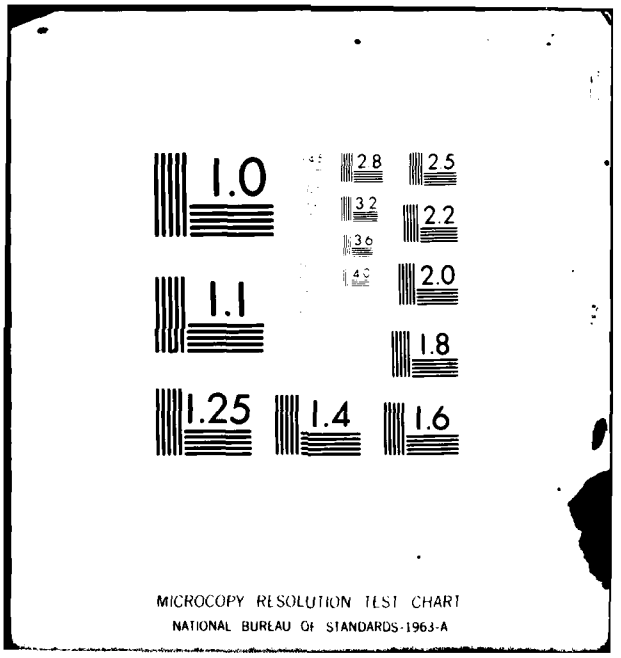
1.0
2.8
2.5
3.2
2.2
3.6
4.0
2.0
1.1
1.8
1.25
1.4
1.6
MICROCOPY RESOLUTION TEST CHART
NATIONAL BUREAU OF STANDARDS-1963-A

LERMAN, LAL and DACEY, 1975; MCCAVE, 1975; BERGER, 1976; HONJO, 1977; CALVET, 1978); however, particles remain at or close to the sediment-water interface for hundreds or thousands of years depending on the sedimentation rate, bioturbation, and resuspension by bottom currents.

The relationships described here are based on sediments deposited under more or less oxygenated seawater (see also DOW, 1978). Only at the Baltic Sea and Peruvian margin stations can the oxygen of bottom waters be entirely depleted, and then only seasonally. Sediments accumulating under permanently anoxic bottom waters, e.g., modern Black Sea sediments, may exhibit similar relationships, but the fraction of primary produced organic carbon that becomes fossilized is much higher than under oxic bottom water conditions and may reflect an unknown fraction of terrestrially derived organic matter. Relevant data and discussions on preservation of organic matter as a function of oxygen content of the water column are in DEUSER (1971), DEGENS (1974), HIRST (1974), ROSS and DEGENS (1974) and DEMAISON and MOORE (1979). The organic carbon preserved in Black Sea sediments is equivalent to 4 to 6% of the primary production (DEUSER, 1971) and thus higher by a factor of 5 to 6 than predicted from Fig. 5. This may reflect a slower rate of degradation of organic matter in euxinic environments. However, Black Sea surface sediments appear to be dominated by terrigenous organic matter, as shown by SIMONEIT (1978) on the basis of solvent-soluble markers and by PETERS, SWEENEY and KAPLAN (1978) on the basis of stable carbon and nitrogen isotopes. Hence, the deviation of the two Black Sea samples from the regression line in Figs 4 and 5 may reflect a higher terrestrial organic matter input relative to marine sources rather than slower degradation.

ESTIMATION OF PALEO-PRODUCTIVITY

The relationships described here enable us to test whether the cyclic organic carbon distribution found in sediment cores off Spanish Sahara (HARTMANN *et al.*, 1976) reflects temporal changes in productivity or differences in degree of preservation as a result of varying sedimentation rates.

The following discussion concerning such a test is based on data from core 12392-1 from the continental rise off Spanish Sahara. The organic carbon and nitrogen distributions are shown in Fig. 1(a), (b), the oxygen isotope stratigraphy has been studied in detail by SHACKLETON (1977), the biostratigraphy by THIEDE (1977), and the accumulation rates were estimated by SUESS *et al.* (1978).

The sedimentation rates in core 12392 range from 3.5 to 23 cm each 1000 y and show a pronounced maximum during oxygen isotope stage 2 (Fig. 3a). In Fig. 3(b) the measured organic carbon distribution is compared to that calculated from equation (6), assuming that the primary production rate remained constant at the present rate (75 g C m^{-2} y^{-1}, SCHEMAINDA, NEHRING and SCHULZ, 1975) during the entire time interval cored and using the dry density and porosity values determined by SUESS *et al.* (1978) for each 10-cm depth interval. The nearly perfect agreement between measured and calculated organic carbon contents in the interglacial stages 1 and 5 suggests that productivity was similar during these periods. This approach ignores a possible diagenetic loss of organic carbon; however, as explained by HARTMANN *et al.* (1976), the major mineralization processes of sedimentary organic matter take place at the sediment surface (see also BALZER, 1978) whereas the diagenetic loss of organic matter in northwest African sediments does not exceed 2% of the amount still present.

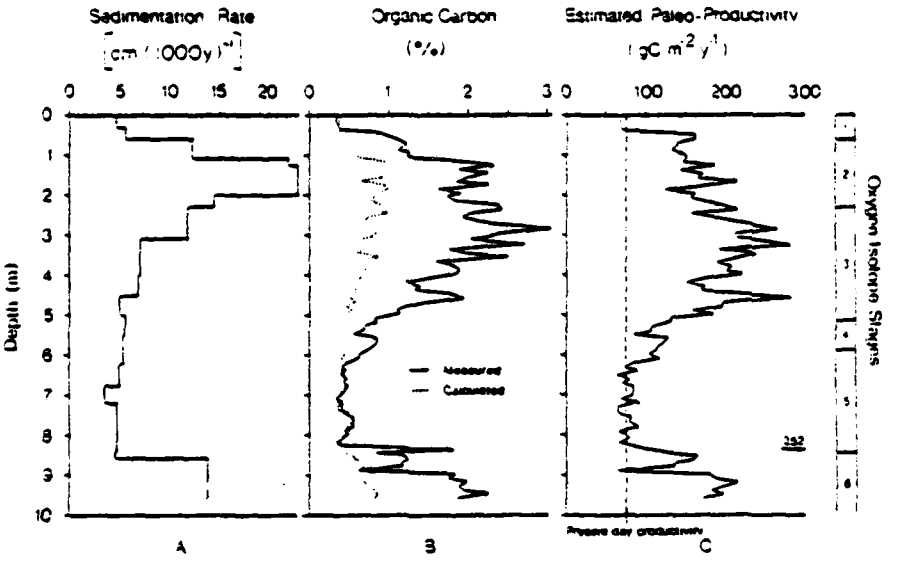

Fig. 3. Sedimentation rates (a), organic carbon distribution (b), and estimated paleo-production rates (c) for core 12392-1. The perfect agreement of calculated (equation 6) and measured organic carbon contents in stages 1 and 5 suggests that productivity was similar today and during *interglacial stages. During glacial stages* 2, 3, and 6, however, productivity must have been higher by a factor of 2 to 3 in order to explain the higher organic carbon contents for the prevailing sedimentation rates. Paleoproductivity was estimated using equation (7).

In contrast to stages 1 and 5, the two organic carbon curves in Fig. 3(b) deviate considerably in stages 2, 3, and 6, indicating that the increase of sedimentation rates during glacial periods was far from high enough to account for the higher organic carbon contents. Consequently, the organic carbon input must have been higher during glacial periods.

Provided that our assumption of negligible terrestrial organic matter input is correct (DEBYSER *et al.*, 1977), then the paleo-primary production rate can be estimated from equation (7), which is obtained from equation (6) by rearranging:

$$R = \frac{C \cdot p_s \cdot (1-\Phi)}{0.0030 \cdot S^{0.30}}. \qquad (7)$$

Substituting the measured organic carbon contents (C), sedimentation rates (S), dry densities of solids (p_s) and porosities (Φ) [for units see equation (2)], we obtain the paleo-primary production rates (R) plotted in Fig. 8(c). The rates thus calculated for stages 2, 3, and 6 are higher by a factor of 2 to 3 than the present productivity at Sta. 12392, with most values ranging between 150 and 250 g C m^{-2} y^{-1}, the highest occurring during stage 3, with almost 300 g C m^{-2} y^{-1}.

DISCUSSION

The primary production rates estimated for stages 2, 3, and 6 (Fig. 3c) are comparable to the rates presently prevailing on the shelf at this latitude (SCHEMAINDA *et al.*, 1975). This

may indicate either that upwelling centers shifted offshore during periods of low sea level, thus providing for a higher organic matter input to continental rise sediments during glacial periods, or that coastal upwelling was generally higher, perhaps as a result of stronger northeast trade winds (SARNTHEIN and WALGER, 1974; SARNTHEIN and DIESTER-HAASS, 1977; SARNTHEIN, 1978).

On the other hand, productivity in coastal regions may also be increased by river-derived nutrients. This has been shown by SCHEMAINDA *et al.* (1975) for the region between 10 and 25°N off northwest Africa where the annual average primary production rates on the shelf remain relatively constant (i.e., between 180 and 245 g C $m^{-2} y^{-1}$) although the annual duration of upwelling decreases from 12 months in the north to only 1 month in the south. According to the authors this is due to the nutrients supplied by rivers south of about 17°N where the present climate is increasingly more humid. Therefore the higher primary production rates during glacial stages could also be due to the nutrient supply by former rivers if the glacial climate was humid.

The discussion on climatic changes during the Late Quaternary off northwest Africa is, however, controversial. For example, DIESTER-HAASS *et al.* (1973), DIESTER-HAASS (1976), and CHAMLEY *et al.* (1977) deduced a humid climate for the last glacial period ("Würm", interrupted by a more arid phase during oxygen isotope stage 3) from their coarse grain and clay mineral studies off Spanish Sahara and Mauretania. However, SARNTHEIN (1978) concluded from the distribution of active sand dunes 18,000 years ago that the concept of a pluvially glacial maximum has to be reversed.

If the view of SARNTHEIN (1978) is correct, then we can exclude a significant river influence on productivity during the glacial maximum (stage 2) at the latitude of core 12392 and may thus conclude that the higher productivity during this period was primarily caused by an increased rate of upwelling. This conclusion is supported by the CLIMAP reconstruction of the glacial North Atlantic 18,000 years ago (MCINTYRE, KIPP, BE, CROWLEY, KELLOGG, GARDNER, PRELL and RUDDIMAN, 1976), which revealed a surface water temperature anomaly of 6°C off northwest Africa, signaling an increased rate of upwelling at that time. This is also in accordance with the conclusions reached by DIESTER-HAASS *et al.* (1973), MÜLLER (1975a), DIESTER-HAASS (1977, 1978) and BERGER, DIESTER-HAASS and KILLINGLEY (1978), although most parameters investigated in these studies were nonspecific for upwelling (DIESTER-HAASS and MÜLLER, 1979). Presently the most reliable indicators of upwelling seem to be cool water planktonic foraminiferal assemblages (SEIBOLD, 1978) and an endemic diatom species reported by SCHUETTE and SCHRADER (1979).

In view of the ongoing discussion on climatic changes during the Late Quaternary off northwest Africa we leave the question open whether the high productivities estimated for stages 3 and 6 reflect increased rates of upwelling or influence of increased sediment supply by rivers.

In the sediment cores from the Argentine Basin (STEVENSON and CHENG, 1972) and the Indian continental margin (MARCHIG, 1972), referred to in the introduction, changes in sedimentation rates and organic carbon contents between glacial and interglacial sections are similar in magnitude to those off Spanish Sahara (MÜLLER, 1975a; HARTMANN *et al.*, 1976; SEIBOLD, DIESTER-HAASS, FÜTTERER, HARTMANN, KÖGLER, LANGE, MÜLLER, PFLAUMANN, SCHRADER and SUESS, 1976) suggesting that the phenomenon of higher glacial productivity is not restricted to northwest Africa. This may indicate that the fertility of the oceans was generally higher during the Late Quaternary glacial periods than today and in other interglacial times.

CONCLUSIONS

The above results show that the evaluation of spatial and temporal fluctuations of sedimentary organic matter may be helpful in reconstructing past changes or cycles in oceanic fertility. The preservation effect by differing sedimentation rates has only to be taken into account if the rates are large relative to changes in sedimentary organic carbon contents. As a first approximation, one can expect a doubling of sedimentary organic carbon contents with each 10-fold increase in sedimentation rate, provided that other factors remain about constant. This means that the sedimentation rate has to be considered if organic carbon contents of sediments from such different environments as the deep sea, continental slopes, or shallow seas such as the Baltic, where sedimentation rates generally differ by several orders of magnitude, are to be compared. On the other hand, sedimentation rates within the stratigraphic record from one and the same location seldom differ by more than one order of magnitude so that organic carbon fluctuations by more than a factor of 2 can thus directly be interpreted in terms of paleo-productivity provided terrestrial sources are insignificant and the physical properties similar.

Acknowledgements—We are thankful for the technical assistance of I. DOLD, H. HENSCH (Kiel), and P. PRICE and G. DAVIS (Corvallis). Financial support was provided by the Deutsche Forschungsgemeinschaft, Bonn, and by the Office of Naval Research through contract N00014-76-C-0067 under project NR083-102 to Oregon State University, which we gratefully acknowledge.

REFERENCES

ANDERSON G. C. (1964) *The seasonal and geographic distribution of primary* productivity off the Washington and Oregon coasts. *Limnology and Oceanography* 9, 284–302.

BALZER W. (1978) Untersuchungen über Abbau organischer Materie und Nährstoff-Freisetzung im Boden der Kieler Bucht beim Übergang vom oxischen zum anoxischen Milieu. Reports Sonderforschungsbereich 95, No. 36. Universität Kiel, 126 pp.

BEIERSDORF H., H.-J. DÜRBAUM, G. FRIEDRICH, M. HARTMANN, F.-C. KÖGLER, P. J. MÜLLER, W. PLÜGER, H. U. SCHLÜTER and R. WOLFART (1974) Geophysikalische, geologische und geochemisch-lagerstättenkundliche Untersuchungen im Bereich von Manganknollenfeldern im zentralen P[illegible]nik. *Meerestechnik*, 5, 186–206.

BERGER W. H. (1976) Biogenous deep sea sediments: Production, preservation, and interpretation. In: *Chemical oceanography*, vol. 5. J. P. RILEY and R. CHESTER, editors. Academic Press, pp. 265–387.

BERGER W. H., L. DIESTER-HAASS and J. S. KILLINGLEY (1978) Upwelling off North-West Africa: The Holocene decrease as seen in carbon isotopes and sedimentological indicators. *Oceanologica*, 1, 3–7.

BERNER R. A. (1971) *Principles of chemical sedimentology*. McGraw-Hill Co., 245 pp.

BERNER R. A. (1978) Sulfate reduction and the rate of deposition of marine sediments. *Earth and Planetary Science Letters*, 37, 492–498.

BODUNGEN B., VON (1975) Der Jahresgang der Nährsalze und der Primärproduktion des Planktons in der Kieler Bucht unter Berücksichtigung der Hydrographie. Dissertation, Universität Kiel, 116 pp.

BRUYEVICH S. V. (1963) Rates of mineralization of suspended organic carbon in the low latitudes of the Pacific during the pre-depositional stage. *Geochemistry*, 3, 349–352.

CAUWET G. (1978) Organic chemistry of sea water particulates. Concepts and developments. *Oceanologica*, 1, 99–105.

CHAMLEY H., L. DIESTER-HAASS and H. LANGE (1977) Terrigenous material in east Atlantic sediment cores as an indicator of NW African climates. "*Meteor*" *Forschungsergebnisse*, C, No. 26, 44–59.

DEBYSER Y., R. PELET and M. DASTILLUNG (1977) Geochimie organique de sediments marins recents: Mer Noire, Baltique, Atlantique (Mauritanie). In: *Advances in organic geochemistry 1975*. R. CAMPOS and J. GONI, editors. Pergamon, pp. 289–320.

DEGENS E. T. (1974) Cellular processes in Black Sea sediments. In: *The Black Sea—geology, chemistry and biology*, vol. 20. E. T. DEGENS and D. A. ROSS, editors. AAPG Memoir, pp. 296–307.

DEMAISON G. J. and G. T. MOORE (1979) Anoxic environments and source bed genesis. In: *Organic Geochemistry*. In press.

DEMASTER D. J. (1979) The marine budgets of silica and ^{32}Si. Ph.D. Dissertation, Yale University, 308 pp.

DEUSER W. G. (1971) Organic carbon budget of the Black Sea. *Deep-Sea Research*, 18, 995–1004.

DIESTER-HAASS L. (1976) Late Quaternary climatic variations in northwest Africa deduced from east Atlantic sediment cores. *Quaternary Research*, 6, 299–314.

DIESTER-HAASS L. (1977) Radiolarian, planktonic foraminiferal ratios in a coastal upwelling region. *Journal of Foraminiferal Research*, 1, 25–33.

DIESTER-HAASS L. (1978) Sediments as an indicator of upwelling. In: *Upwelling ecosystems*. R. BOJE and M. TOMCZAK, editors. Springer, pp. 261–281.

DIESTER-HAASS L. and P. J. MÜLLER (1979) Processes influencing sand fraction composition and organic matter content in surface sediments off W. Africa (12–19°N). *"Meteor" Forschungsergebnisse, C*. In press.

DIESTER-HAASS L., H.-J. SCHRADER and J. THIEDE (1973) Sedimentological and paleoclimatological investigations of two pelagic ooze cores off Cape Barbas, North-West Africa. *"Meteor" Forschungsergebnisse, C*, 16, 19–66.

DOW W. G. (1978) Petroleum source beds on continental slopes and rises. *American Association of Petroleum Geologists, Bulletin*, 62, 1584–1606.

DUNCAN J. R., G. A. FOWLER and L. D. KULM (1970) Planktonic foraminiferan–radiolarian ratios and Holocene–Late Pleistocene deep-sea stratigraphy off Oregon. *Geological Society America Bulletin*, 81, 561–566.

ERLENKEUSER H., E. SUESS and W. WILLKOMM (1974) Industrialization affects heavy metal and carbon isotope concentrations in recent Baltic Sea sediments. *Geochimica Cosmochimica Acta*, 38, 823–842.

GUILLEN O., B. R. DE MENDIOLA and R. I. DE RONDAN (1973) Primary productivity and phytoplankton in the coastal Peruvian waters. Oceanography of the South Pacific. New Zealand National Commission for UNESCO, pp. 405–418.

HARTMANN M., F.-C. KÖGLER and P. J. MÜLLER (1978) Ergebnisse geochemischer und bodenmechanischer Untersuchungen an Tiefseesedimenten des Zentralen Pazifiks. Unpublished report, Kiel University, 56 pp.

HARTMANN M., P. J. MÜLLER, E. SUESS and C. H. VAN DER WEIJDEN (1976) Chemistry of Late Quaternary sediments and their interstitial waters from the NW African continental margin. *"Meteor" Forschungsergebnisse, C*, 24, 1–67.

HEATH G. R., T. C. MOORE and J. P. DAUPHIN (1977) Organic carbon in deep-sea sediments. In: *The fate of fossil fuel CO_2 in the oceans*. N. R. ANDERSEN and A. MALAHOFF, editors. Plenum Press, pp. 605–625.

HIRST D. M. (1974) Geochemistry of sediments from eleven Black Sea cores. In: *The Black Sea—geology, chemistry, and biology*. Vol. 20, E. T. DEGENS and D. A. ROSS, editors, American Association of Petroleum Geologists Memoir, pp. 430–455.

HONJO S. (1977) Biogenic carbonate particles in the ocean: do they dissolve in the water column? In: *The fate of fossil fuel CO_2 in the oceans*. N. R. ANDERSEN and A. MALAHOFF, editors. Plenum Press, pp. 269–299.

LERMAN A., D. LAL and M. F. DACEY (1975) Stokes' settling and chemical reactivity of suspended particles in natural waters. In: *Suspended solids in water*. R. J. GIBBS, editor. Plenum Press, pp. 17–47.

MANGINI A. and C. SONNTAG (1977) ^{231}Pa dating of deep-sea cores via ^{230}Th counting. *Earth and Planetary Science Letters*, 37, 251–256.

MARCHIG V. (1972) Zur Geochemie rezenter Sedimente des indischen Ozeans. *"Meteor" Forschungsergebnisse, C*, 11, 1–104.

MCCAVE I. N. (1975) Vertical flux of particles in the ocean. *Deep-Sea Research*, 22, 297–310.

MCINTYRE A., N. G. KIPP, A. W. H. BÉ, T. CROWLEY, T. KELLOGG, J. V. GARDNER, W. PRELL and W. F. RUDDIMAN (1976) Glacial North Atlantic 18,000 years ago: a CLIMAP reconstruction. *Geological Society of America Memoirs*, 145, 43–76.

MENZEL D. W. (1974) Primary productivity, dissolved and particulate organic matter, and the sites of oxidation of organic matter. In: *The sea*, vol. 5, E. D. GOLDBERG, editor, Wiley, pp. 659–678.

MÜLLER P. J. (1975a) Zur Diagenese stickstoffhaltiger Substanzen in marinen Sedimenten unter oxydierenden und reduzierenden Bedingungen. Dissertation, Universität Kiel, 179 pp.

MÜLLER P. J. (1975b) Diagenese stickstoffhaltiger organischer Substanzen in oxischen und anoxischen marinen Sedimenten. *"Meteor" Forschungsergebnisse, C*, 22, 1–60.

MÜLLER P. J. (1977) C/N ratios in Pacific deep-sea sediments: Effect of inorganic ammonium and organic nitrogen compounds sorbed by clays. *Geochimica et Cosmochimica Acta*, 41, 765–776.

MÜLLER P. J. and A. MANGINI (1979) Organic carbon decomposition rates in sediments of the Pacific manganese nodule belt dated by ^{230}Th and ^{231}Pa. *Earth and Planetary Science Letters*. In press.

MURRAY J. W., V. GRUNDMANIS and W. M. SMETHIE JR (1978) Interstitial water chemistry in the sediments of Saanich Inlet. *Geochimica et Cosmochimica Acta*, 42, 1011–1026.

PETERS K. E., R. E. SWEENEY and I. R. KAPLAN (1978) Correlation of carbon and nitrogen stable isotope ratios in sedimentary organic matter. *Limnology and Oceanography*, 23, 598–604.

PFLAUMANN U. (1975) Late Quaternary stratigraphy based on planktonic foraminifera off Senegal. *"Meteor" Forschungsergebnisse, C*, 23, 1–46.

ROSS D. A. and E. T. DEGENS (1974) Recent sediments of Black Sea. In: *The Black Sea—geology, chemistry, and biology*, vol. 20, E. T. DEGENS and D. A. ROSS, editors, American Association of Petroleum Geologists Memoir, pp. 183–199.

SARNTHEIN M. (1978) Sand deserts during glacial maximum and climatic optimum. *Nature*, 272, 43–46.

SARNTHEIN M. and L. DIESTER-HAASS (1977) Eolian-sand turbidites. *Journal of Sedimentary Petrology*, 47, 868–890.

SARNTHEIN M. and E. WALGER (1974) Der äolische Sandstrom aus der W-Sahara zur Atlantikküste. *Geologische Rundschau* 63, 1065–1087.

SCHEMAINDA R., D. NEHRING and S. SCHULZ (1975) Ozeanologische Untersuchungen zum Produktionspotential der nordwest-afrikanischen Wasseraufmeresregion 1970–1973. *Geodätische und Geophysikalische Veröffentlichungen*, IV, 35 pp.

SCHLUETTE G. and H. SCHRADER (1979) Diatom taphocoenoses in the coastal upwelling area of western South America. *Nova Hedwigia, Beiheft* 64, in press.

SCHULTZE-WESTRUM H. H. (1973) The station and cruise pattern of the R.V. *Valdivia* in relation to the variability of manganese nodule occurrence. In: *Papers on the origin and distribution of manganese nodules in the Pacific and prospects for exploration*, M. MORGENSTEIN, editor, Hawaii Institute of Geophysics, pp. 145–149.

SEIBOLD E. (1972) Cruise 25 1971 of R.V. "*Meteor*". Continental margin of West Africa. General report and preliminary results. "*Meteor*" *Forschungsergebnisse*, C, 10, 17–38.

SEIBOLD E. (1978) Sediments in upwelling areas, particularly off northwest Africa. *Rapports et Proces Verbaux Series, Conseil permanent pour l'exploration de la Mer Copenhagen*, in press.

SEIBOLD E., L. DIESTER-HAASS, D. FÜTTERER, M. HARTMANN, F. C. KÖGLER, H. LANGE, P. J. MÜLLER, U. PFLAUMANN, H. J. SCHRADER and E. SUESS (1976) Late Quaternary sedimentation off the Western Sahara. *Anales de la Academia Ciencias exactas, fisicas y naturales*, 48, 287–296.

SEIBOLD E. and K. HINZ (1976) German cruises to the continental margin of North West Africa in 1975. General reports and preliminary results from "*Valdivia*" 10 and "*Meteor*" 39. "*Meteor*" *Forschungsergebnisse*, C, 25, 47–80.

SHACKLETON N. J. (1977) Carbon-13 in Uvigerina: Tropical rainforest history and the equatorial Pacific carbonate dissolution cycles. In: *The fate of fossil fuel CO_2 in the oceans*, N. R. ANDERSEN and A. MALAHOFF, editors, Plenum Press, pp. 401–427.

SIMONEIT B. R. (1978) The Black Sea, a sink for terrigenous lipids. *Deep-Sea Research*, in press.

SMALL L. H., H. CURL, JR and W. A. GLOOSCHENKO (1972) Estimates of primary production off Oregon using an improved chlorophyll-light technique. *Journal of the Fisheries Research Board of Canada*, 29, 1261–1267.

STEVENSON F. J. and C. N. CHENG (1972) Organic geochemistry of Argentine Basin sediments: carbon-nitrogen relationships and Quaternary correlations. *Geochimica et Cosmochimica Acta*, 36, 653–671.

SUESS E., J. THIEDE and P. J. MÜLLER (1978) Accumulation patterns of biogenous and terrigenous sediment constituents off NW Africa (Abstr.). *Tenth International Congress of Sedimentology*, v. II, Jerusalem, July 9–14, 650–651.

THIEDE J. (1977) Aspects of the variability of the Glacial and Interglacial North Atlantic eastern boundary current (last 150,000 years). "*Meteor*" *Forschungsergebnisse*, C, 28, 1–36.

TOTH D. J. and A. LERMAN (1977) Organic matter reactivity and sedimentation rates in the ocean. *American Journal of Science*, 277, 465–485.

VAN ANDEL T. H., G. R. HEATH and T. C. MOORE JR (1975) Cenozoic history and paleoceanography of the central equatorial Pacific Ocean. *Geological Society of America Memoir* 143, 134 pp.

WHITICAR M. J. (1978) Relationships of interstitial gases and fluids during early diagenesis in some marine sediments. Dissertation, University of Kiel, 152 pp.

OCEANS 1979 Conference Proceedings.
Institute of Electrical and Electronic Engineers, Inc.
September 1979, San Diego, CA

AN XBT DIGITAL RECORDING AND DISPLAY SYSTEM

Dr. Roderick Mesecar & Dr. James Wagner

Oregon State University
School of Oceanography
Corvallis, Oregon 97331

Abstract

Thousands of expendable bathy-thermographs (XBTs) are used annually for ocean monitoring. This paper briefly describes the application of a microprocessor-based computer to encode signals directly from the XBTs, in a digital format for dissemination, and to prepare a bathy-message for radio transmission

Reference is also made to the development activity for other sensors to be used as expendable probes.

Introduction

The use of expendable probes, as temperature profilers, in the oceanographic research and operational data gathering community is well established. Directed and volunteer shipboard personnel participate in releasing thousands of probes in programs with a requirement to:

- provide a message format for (radio) transmission of synoptic bathy-thermograph (XBT) data for oceanographic forecasting.
- provide the National Oceanographic Data Center (NODC) with information for XBT analog and digital processing.

Associates and users of this data are participants in a broad suite of national research programs and the National Weather Service. The message, known as a bathy-message, is most commonly derived from encoding a strip chart after the expendable probe has been deployed. This message format follows specifications of the World Meteorological Organization (WMO)(1), and it is used internationally by interested agencies. In compliance with these specifications, four bathy-messages are transmitted daily at 6-hour intervals. The procedure to acquire, extract, and maintain the quality of data from these observations is noted to be labor-intensive, which thereby limits the effectiveness of how and when the data can be applied.

The procedure for developing the synoptic bathy-message requires the operator to visually select key data points from the temperature profile on the strip chart. The bathy-message is then sent by CW or teletype radio-message, by agreement, to the nearest shore-based data collecting receiver station for retransmission, often by other means, to a designated data center for integration into synoptic weather and ocean thermostructure maps. The data center may not be the final depot.

Any of the aforementioned steps in the preparation and delivery of data is a potential source of error. Up to 40 percent of the bathy-messages are estimated to contain operator and data transmission errors that nullify the data value.

To accomplish data dissemination specified by WMO, the original temperature profile strip charts are sent, after the vessels dock, by mail service, or a similar conveyance, to a data center for processing. Converting the strip charts to a digital-tape format is generally done on a manually operated electronic digitizer. The accuracy of this method for producing the digitized data is good; however, the operation is production-limited. The combined time of waiting for the vessel records and producing a digital-data set can be weeks.

Our goal has been to develop an instrumental system with the capability to automate some of the manual routines used in preparing bathy-messages, and formatting digital data for analysis, directly from the XBT sensor response. This effort is being done in cooperation with research personnel in the TRANSPAC program at Scripps Institution of Oceanography, where they have been developing a data set with XBTs deployed from 25 merchant vessels that shuttle between Japan and the West Coast of the United States.

System Description

In review the procedure for data handling and the operational requirement for the dissemination of digital data, an approach was selected to digitize the amplified electronic temperature signal from the XBT probe. This procedure completely bypasses the strip-chart recorder used in the more common XBT recording system. Once the decision was made to directly digitize the temperature signal, requirements for digital control of the digitizer and for direct data processing was defined. A number of small microprocessor-based computers (uCs) were evaluated for this task. It was decided that

µC technology was ideal for this application. The Commodore PET-2001 was chosen on the basis of cost, programming capability, simple electrical input and output busses, and mechanical integration of the keyboard, display, and cassette tape recorder in a single housing. A conceptualized XBT recording system is shown in Figure 1.

The decision to use a µC provided a number of benefits: instructions and messages are displayed, which allows better interaction between the operator and the machine; data can be presented in a variety of ways which includes graphing and listing; the instruction set for arithmetic operations on the data was adequate and simply modified from the keyboard when necessary.

Incorporating these capabilities, plus the design for interfacing circuits to directly digitize the XBT sensor output, resulted in a system that:

- self-tests prior to each XBT probe drop
- determines the presence of a probe canister in the launcher
- keeps time and date
- senses the time when the probe enters the water
- determines when samples are to be taken and stores the digital values
- graphs, on the CRT display, the XBT temperature profile for cast verification
- records the data digitally on a tape cassette
- determines when the cassette must be changed
- provides the computational capability for compressing the digitized cast data and formatting it into the bathy-message
- provides the capability for transferring the recorded digitized cast data through an RS-232 data buss to another computer system.

Reflected in this list are a number of automatic routines that significantly reduce the manual labor and personnel judgment needed to prepare XBT data for dissemination.

In addition to the preceding system capabilities, the simplicity of changing the operating mode by changing the program is a major asset. Changing sample rates, for example, can be a keyboard entry. Different sampling rates at different depths can easily be accommodated. This makes the system highly adaptable and operator-responsive for a variety of specialized tasks in addition to satisfying standard operational requirements.

Data compression for the bathy-message is the primary use of the computer processing capability. The data compression procedure was originally developed at White Sands Missile Proving Grounds [2] for compression of radiosonde data. It involves fitting straight lines to the data within a specified tolerance. In this situation, the tolerance is iteratively adjusted until 20 points are extracted. Processing typically requires 15 minutes--but may require up to 30 minutes. The results of the data compression routine are displayed on the LCD CRT in the bathy-message format.

For the more commonly used XBT (T-4), the system sampling and parameter specifications are:

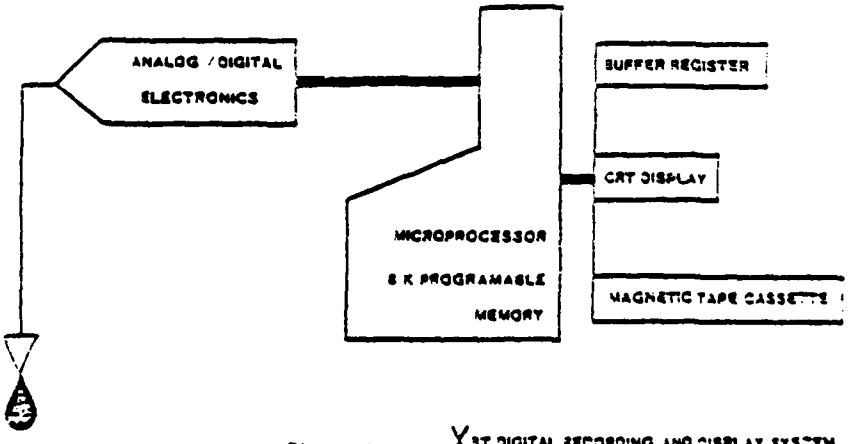

Figure 1. XBT DIGITAL RECORDING AND DISPLAY SYSTEM

- Sample rate: 2 per sec (~ 3.2 m- program adjustable)
- Drop length: 72 sec (460 m)
- Data word form digitizer: 12 bits
- Temperature range: -5°C to +30°C
- Temperature resolution: < .05°C
- Cassette capacity: approx. 20 drops on "60" size cassette
- Data compression: 150 points compressed to 20 points (software selectable) in 15 (bathy-message) minutes (typical)

Twenty XBT digital recording and display systems are currently committed to oceanographic research programs where they are demonstrating the flexibility and necessary time savings by expediently making XBT data available in a form for easy analysis and dissemination.

Future equipment development efforts will be divided between two goals: one goal to reduce data communications problems through direct coupled transmission of compressed data (i.e., bathy-message or equivalent) via CW, teletype radio-message, or, most preferable, a satellite data communications link. Satellite transmission will, in particular, be a major contribution toward the improvement of data reliability and reduced operator load. The second goal is to adapt similar AC technology to other types of expendable probes that are nearing their development phase and are now becoming available to the greater oceanographic research community.

Development Activities in Expendable Probes

The number of expendable probes being used, the variety, and the activity in evaluating the applicability of existing probes is on the increase. As a research tool, the XBT probe has provided some of the needed cost trade offs and expedient underway deployment features. It is now estimated that 55,000 of these probes are used annually by the science community. The majority of these probes are committed to vertical temperature profiles in the upper 460 meters of the ocean.

The incorporation of different parameter sensors and methods of deployment to the basic expendable body by experimentalists and manufacturers has resulted in widening its research applicability. Expendable probes have been developed to measure not only temperature but sound velocity with temperature (XSVT)*, seawater conductivity with temperature (XSTC)#, and current velocity as a function to predesigned probe-fall rate. Two other sensor parameter candidates contemplated for expendable probes are for measuring shear and oxygen. In a recently completed, but uncirculated, report, M. Miyake, et al., (3) detail the results of an evaluation of the XSVT and XSTD expendable probes for potential application in studies where the density of sea water is strongly influenced by the salinity distribution. With this capability, most sea-going vessels could be used to participate in a full-scale ocean survey.

Not all probes need to be deployed from ships. Deployments for research purposes have also been made from aircraft. For a program in the North Pacific, methods were developed for calibrating low precision Navy operational AXBTs so that they could be used in an experiment that required more precise measurements (4). The probes were dropped from a Navy P-3A aircraft to measure thermal structure to a depth of 300 meters. A typical track line in this experiment was 400 kilometers. In other instances, the ship-configured probes have been successfully released from helicopters.

In one program, the application of expendable probes was found to complement an already unique temperature recording instruments. Gregg and Cox (5), in 1971, described a free-fall probe designed to make high resolution measurements of vertical temperature gradients on a millimeter scale. Resolution of these measurements was achieved by virtue of a slow, uniform descent rate (1 m/s) of the instrument, a fast-response thermistor, and a self-contained, high-data rate, fm magnetic tape recorder. The extensive capability of the probe is acknowledged by the associated scientific papers resulting from data obtained with it. Personnel from this same research laboratory recently evaluated an XBT (T-7) modified to drop at 1.1 m/s (designated T-11) instead of 65. m/s, and which was coupled to a fast-sampling-rate deck recording unit (6). They found this modified probe allowed them to make rapid areal surveys of the fine scale temperature variability without having to jeopardize their high-precision probe and suffer the time penality of using it as a survey instrument. The verification that high resolution temperature measurements can be made with these probes exposes the opportunity for their inclusion into, or the development of, research programs requiring this class of measurement but which cannot afford the cost burden of the more refined free-fall probe.

Field tests are expected to be completed this year on another expendable probe for measuring current velocity. The measurement concept for this probe is based on earlier research and equipment development reported by Sanford, et al. (7). All of the expendable probes, thus fair, have the body style, wire-communications link to the surface, and deployment features of the XBTs.

* Manufactured by Sippican Corporation, Marion, Mass.

\# Manufactured by Bruncy Corporation, San Diego, Ca.

Acknowledgements

Much appreciation to Dr. Warren White and Mr. Michael Sucarek, both with SIO, for their helpful suggestions during the development of this equipment. Part of this effort was funded by the Office of Naval Research contract number N00014-79-C-0004.

References

(1) Instructions for preparing the bathythermogram log (February 1972) National Oceanic and Atmospheric Administration, Office of Meteorological Operations, Silver Spring, Maryland.

(2) Linearization for compacted storage of digitized analog data (1977) M. Don Hammitt and Don R. Heazley. IEEE Region 6 Conference Record, pp. 10-16.

(3) An evaluation of expendable salinity-temperature profilers in the Eastern North Pacific. M. Miyake, W. Emery and D. Lovett. Address for M. Miyake, Institute of Ocean Sciences, University of British Columbia, Vancouver, B.C. Canada.

(4) Aircraft expendable bathythermographs used in NORPAX experiment (1974) M. Sessions. Exposure, Vol. 2, No. 3: A newsletter published by Oregon State University, School of Oceanography, Corvallis, Oregon.

(5) Measurements of the oceanic microstructure of temperature and electrical conductivity (1977) M. C. Gregg and D. B. Cox. Deep-Sea Res., Vol. 18, p. 925.

(6) Rapid sampling of temperature and temperature gradient using XBTs (March 1979) B. P. Johnson and R. E. Lange. Scripps Institution of Oceanography, Reference Series #79-4.

(7) A velocity profiler based on the principles of geomagnetic induction (1978) T. B. Sanford, R. G. Drever and J. H. Dunlap. Deep-Sea Res., Vol. 25, p. 183.

Reprinted from SPIE Vol. 208—Ocean Optics VI

Introduction to ocean optics*

Howard R. Gordon
Department of Physics
University of Miami
Coral Gables, Florida 33124

Raymond C. Smith
Visibility Laboratory—S I O.
University of California, San Diego
La Jolla, California 92093

J. Ronald V. Zaneveld
Department of Oceanography
Oregon State University
Corvallis, Oregon 97331

*These investigations supported by National Aeronautics and Space Administration Contract No. NAS5-22963 (H.R.G.), by the National Oceanic and Atmospheric Administration Grant No. 04-6-158-44033 (R.C.S.), and by the Office of Naval Research Contract N000014-76-0067 under Project NR083-102 and the Department of Energy Contract No. EY-76-S-06-2227, Task Agreement No. 29 (JRVZ).

General Introduction

In this introductory survey of optical oceanography we first present the fundamental inherent and apparent optical properties of natural waters. Relationships between these inherent and apparent optical properties, as related through the radiative transfer equation, are then presented. Following the first three theoretical sections brief discussions describing the application of ocean optics to geophysics, biological oceanography, and ocean remote sensing are then presented. Authorship for each section is indicated by initials after the section heading.

1. Inherent Optical Properties (J.R.V.Z.)

Introduction

Electromagnetic radiation traversing the ocean can interact with the water and the materials dissolved and suspended in it. This interaction takes the form of absorption, scattering and fluorescence. Absorption is the change of radiation into other forms of energy. Scattering is the redirection of radiation by means of refraction, reflection and diffraction. Fluorescence is the absorption of radiation at one wavelength and emission at a longer wavelength. The polarization and wavelength of the radiation also affect the absorption and scattering.

If the absorption, scattering, and fluorescent characteristics of the medium are known, the behavior of light in the medium can be predicted by the means of the equation of radiative transfer. The absorption, scattering and their derived properties have been termed inherent optical properties by Preisendorfer as they do not depend directly on the external lighting conditions of the medium.

For monochromatic unpolarized light, the parameters that need to be known to describe the behavior of light in any medium are the absorption coefficient, the scattering coefficient, and the volume scattering function. These and some related functions are defined below. The definitions as well as the notation are those adopted by the International Association of the Physical Sciences of the Ocean. Jerlov[1], Ivanoff[2], and Preisendorfer[3] have excellent discussions of the principles of optical oceanography and should be consulted for more detailed descriptions.

Radiant Flux, Φ: The rate of transport of radiant energy.

$$\Phi = \frac{d(\text{energy transported})}{d(\text{time})} \quad (1\text{-}1)$$

Radiant Intensity, I: Radiated flux from an element of surface per unit solid angle.

$$I = d\Phi / d\omega \quad watts\ steradian^{-1} \quad (1\text{-}2)$$

Irradiance, E: Total radiant power falling on a detector of area dA divided by the area

$$E = d\Phi / dA, \quad watts\ m^{-2} \quad (1\text{-}3)$$

When speaking of the irradiance of a beam it is implicitly assumed that the detector surface is perpendicular to the beam. Φ, I, and E all depend on the spectral response of the detector, and in what follows, unless otherwise specified, it will be assumed that the detector is equipped with a filter which can accept only a narrow band of wavelengths between λ and $\lambda+\Delta\lambda$, and the associated $d\Phi$'s have been divided by $\Delta\lambda$. For example the spectral radiant power is $d\Phi/d\lambda$ with units $watts \cdot nanometer^{-1}$

Absorption Coefficient, a: The fraction of the energy absorbed from a collimated beam per unit distance traversed in the medium; see Fig. 1-1.

$$a = -d\Phi_{abs} / \Phi\ dx, \quad m^{-1} \quad (1\text{-}4)$$

Total Scattering Coefficient, b: The fraction of the energy scattered out of a collimated beam per unit distance traversed by the beam; see Fig. 1-1.

$$b = -d\Phi_{scatt} / \Phi\ dx, \quad m^{-1} \quad (1\text{-}5)$$

Attenuation Coefficient, c: The fraction of the energy in a beam removed by both scattering and absorption per unit distance traversed by the beam.

$$c = -(d\Phi_{abs} + d\Phi_{scatt})/\Phi\, dx, m^{-1} \quad (1\text{-}6)$$

Also,

$$c = a + b \quad (1\text{-}7)$$

Volume Scattering Function, $\beta(\theta)$. The scattered radiant intensity in a direction θ per unit scattering volume dV divided by the incident irradiance E, see Fig. 1-1.

$$\beta(\theta) = dI(\theta)/E\, dV, \; m^{-1}\, steradian^{-1} \quad (1\text{-}8)$$

The relationship between the volume scattering function and the total scattering coefficient is

$$b = 2\pi \int_0^{\pi} \beta(\theta) \sin\theta\, d\theta \quad (1\text{-}9)$$

When the medium is illuminated by radiation in a broad spectral band, for example sunlight, two other inherent optical properties must be considered.

Volume Fluorescence Function, $\beta_\phi(\theta, \lambda_E, \lambda_F)$. The radiant intensity emitted at a wavelength λ_F per unit volume in a direction θ with respect to an incident beam of irradiance $E(\lambda_E)$ in a narrow band of wavelengths $\Delta\lambda_E$

$$\beta_\phi(\theta, \lambda_E, \lambda_F) = \frac{dI(\theta, \lambda_F)}{dV \int_{\Delta\lambda_E} E(\lambda_E)\, d\lambda_E} \quad (1\text{-}10)$$

(β_ϕ is called the transpectral scattering function in Ref. 3)

Coefficient of Fluorescence, b_ϕ. The total radiant power emitted at a wavelength λ_F per unit volume with respect to an incident beam of irradiance $E(\lambda_E)$ in a narrow band of wavelengths $\Delta\lambda_E$

$$b_\phi(\lambda_E, \lambda_F) = 2\pi \int_0^{\pi} \beta(\theta, \lambda_E, \lambda_F)\, d\omega \quad (1\text{-}11)$$

Scattering and Absorbing Agents

The scattering and absorbing agents in natural waters can be divided into three categories: water itself, dissolved materials, and suspended materials.

Water. Table 1-1 shows the absorption, scattering and attenuation coefficients of pure water in the visible region. The absorption coefficient of pure water (a_w) can be obtained by subtracting the scattering coefficient (b_w) from the attenuation coefficient (c_w). It can be seen that the attenuation due to pure water is largely an absorption phenomena. In fact, the deep blue color of the ocean is due to the selective absorption of water, with a minimum near 475 nm.

The scattering of pure water is thought to be the result of scattering by fluctuations in density in small volume elements of the fluid[4]. If the depolarization of scattered light is also taken into account one obtains for pure water

$$\beta_w(\theta) = \frac{G}{\lambda^4}\left(1 + \frac{1-\delta}{1+\delta}\cos^2\theta\right), \quad (1\text{-}12)$$

where G is a constant which depends on the thermal compressibility, Boltzmann's constant, the refractive index, and temperature. δ is the depolarization constant. Alternatively, one may write

$$\beta_w(\theta) = \beta_w(90°)\left(1 + \frac{1-\delta}{1+\delta}\cos^2\theta\right) \quad (1\text{-}13)$$

Morel[6] has shown that $\delta = 0.09$ for pure water at 475 nm. The volume scattering function then becomes

$$\beta_w(\theta) = 1.73 \cdot 10^{-4}(1 + 0.835\cos^2\theta) \quad (1\text{-}14)$$

The volume scattering function for pure water may be calculated by substitution into Eq. (1-13) from Table 1-1.

Dissolved Materials. The dissolved materials that influence the absorption and scattering of light are the dissolved sea salts and dissolved humic acids, the so-called "yellow matter".

A. Morel[6] has reviewed the optical properties of pure water and pure sea water. In the visible region, the sea salts do not appear to contribute to the absorption. In the ultraviolet region, strong absorption by the various ions especially bromide occurs.

Scattering by pure sea water is about 30% higher than for pure water. Table 1-1 shows the scattering coefficient and the volume scattering function at 90° for various wavelengths for pure sea water. Equation (1-13) can be used to calculate the entire volume scattering function.

Dissolved humic acids, by-products of decay of organic matter (usually terrestrial but also oceanic) absorb strongly at the short wavelengths of light. The absorption increases nearly exponentially with decreasing wavelength. Yellow matter absorption can be ignored for $\lambda > 625$ nm, however. A discussion of the absorption of various types of humic acids may be found in Brown[7]. The absorption due to yellow matter (a_y) may be found by means of the following equation:

$$(c-c_w)_{380\ nm} - M(c-c_w)_{555\ nm} = a_y \quad (1\text{-}15)$$

where M is a constant for a given water mass. The equation assumes that the selective absorption by particles in the red is proportional to the particle scattering.

Suspended Materials. Usually the change of optical properties in natural waters relative to pure water is due to the presence of suspended particulate matter (SPM). The presence of SPM affects both the absorption and scattering properties of the water. The properties of SPM that affect the optics are the concentration, particle size distribution, index of refraction distribution and shape distribution.

Particulate matter in the ocean varies widely in terms of concentration, size and composition. Some approximations must be made if we wish to relate the particulate matter theoretically to the observed volume scattering function. Mie[8] has developed a theory giving the scattering and absorption characteristics for a spherical particle of uniform composition, and with a given index of refraction. It is this theory that is usually applied to oceanic suspensions. Typical oceanic particulate matter consists of live biological particles, detritus, and material of terrestrial origin. The shapes of these particles are usually not spherical. Hodkinson[9] has shown, however, that non-absorbing, non-spherical randomly oriented particles produce the same diffraction patterns to first order as spherical particles of the same cross-sectional area. Furthermore, opaque particles produce the same diffraction pattern as transparent ones. Volume scattering functions measured in sea water are dominant in the near-forward direction, in which diffraction predominates.

Particle shape and index of refraction play secondary roles compared to particle size in light scattering in the ocean. If the particles are separated by distances at least equal to three times their radii, which is usually the case in the oceans, one is justified in summing their individual contributions to obtain the volume scattering function for particulate matter.

If the particle size distribution is known, and an average index of refraction has been determined, Mie theory may be used to obtain the volume scattering function.

A size distribution of particulate matter, $f(D)dD$, gives the number of particles per unit volume between diameters D and $D - dD$. The cumulative particle size distribution $g(D)$ is the number of particles per unit volume with diameters larger than Dg(D) may be obtained from f(D) by integration:

$$g(D) = \int_D^\infty f(D')dD' . \quad (1\text{-}16)$$

where g(D) is the distribution usually measured in experimental work (the cumulative particle size distribution).

For a particle of diameter D and (complex) index of refraction relative to the surrounding medium m, Mie theory predicts a scattering function $\beta(\theta, D, m)$ ($ster^{-1}\ m^{-2}$). If this scattering function is integrated over all angles the scattering coefficient for the particle b(D,m) is obtained in a similar manner as in Eq. (1-9). When the scattering coefficient for a particle is divided by its cross-sectional area the effective area coefficient K_{sca} or scattering efficiency factor is obtained:

$$K_{sca}(D,m) = \frac{4b(D,m)}{\pi D^2} \quad (1\text{-}17)$$

The scattering efficiency is a function of both size and index of refraction, as can be seen from the diagram of Burt[10] in Fig. 1-2. Similar efficiencies exist for absorption, K_{abs}, and for attenuation, K_{att}. We now can write equations relating the observed optical quantities to the particle parameters.

$$\beta_p(\theta) = \int_0^\infty f(D)\beta(\theta, D, m)dD \quad (1\text{-}18)$$

is the volume scattering function (units of *steradian*$^{-1}$ m^{-1}) for a collection of particles with a size distribution $f(D)\,dD$ and with a relative index of refraction m. To this must be added the scattering function of water $\beta_w(\theta)$, and scattering due to other sources such as turbulence, bubbles, etc.

The total scattering coefficient for particles b_p is obtained by integration over the volume scattering function as in Eq. (1-4).

The cumulative particle size distribution in the ocean often takes the functional form

$$g(D) = ND^{-C} \tag{1-19}$$

(N is the number of particles per unit volume with diameters greater than 1 μm and C, the slope of the size distribution, is a constant).

If we assume the hyperbolic size distribution of Eq. (1-19), the scattering of a collection of particles may be related via Mie theory to the slope of the size distribution and the index of refraction (Figs. 1-3 and 1-4). The figures show that the scattering for a given volume of particulate matter may vary by as much as two orders of magnitude depending on the slope and index of refraction. Figures 1-3 and 1-4 were prepared using the tables of Morel[11]. In another paper, Morel[12] discusses in depth further interpretations of Mie theory calculations.

The concentration of SPM can change from a few micrograms per liter in the clearest ocean to tens of milligrams per liter in very turbid nearshore waters. When the nature of suspended matter does not change in a given region, but the concentration does, the particle attenuation in that region will be proportional to the total suspended mass (TSM) of particulate matter. Figure 1-5[13] shows examples of this observation. The slope of the beam attenuation vs. TSM curve depends on the nature of the suspended matter. It should also be observed that the linear correlation is much worse at the surface than at greater depth. This is due to phytoplankton patchiness in the surface zone. The nature of particulate matter is therefore not as constant as at greater depths.

The influence of the index of refraction on particulate scattering can be seen in Fig. 1-3. For a constant slope of the size distribution and constant particle volume, the total scattering coefficient increases with increasing relative index of refraction. If the index of refraction is held constant, the lower slopes tend to have larger scattering coefficients per unit volume SPM, but a maximum exists for the higher indices.

The influence of the index of refraction on the shape of the volume scattering function is shown in Fig. 1-6. The influence of slope is shown in Fig. 1-7. The curves are normalized so that the area under each one is the same. It is seen that lower slopes of the size distribution and lower indices of refraction result in steeper scattering functions in the forward direction.

Verification of this aspect of Mie theory in nature is difficult as it is impossible to control the variables one at a time. Particles, furthermore, do not have uniform indices of refraction. Several researchers[14,15,16,17] have attempted to determine a single index of refraction for a collection of SPM from observed optical properties. Results tend to indicate indices (relative to water) below 1.05 or above 1.15. Zaneveld *et al.*[18], have used a method whereby an index of refraction distribution can be calculated. This generally results in components with indices above 1.10 and below 1.05, possibly corresponding to skeletal and inorganic materials for the high index and organic matter for the low index.

The influence of particle shape on the volume scattering function is difficult to quantify. While Mie theory holds for spherical particles, it cannot be assumed that particles in the ocean are spherical. It has been shown by Penndorf[19] that Mie theory can be used for irregular particles of relative index of refraction less than 2.0 if the orientation of the particles is random. Hodkinson[20] and Holland and Gagne[21] have shown that the forward scattering of randomly oriented irregular particles is similar to that of a suspension of spheres having the same equivalent radius. In the backscattering region the influence of shape can be large. Gibbs[22] has recently demonstrated this for particles of extreme shapes. Since the influence of shape has not been quantified, fitting of observed scattering functions in the backward region ($90° \leqslant \theta \leqslant 180°$) by means of Mie theory is usually not very successful.

The spectral attenuation characteristics of particulate matter are relatively flat. Based on theoretical arguments, Morel[12] suggests that this dependence should be approximately λ^{-1}. Jerlov[23] shows that $(c - c_{w\,380nm}) = 1.8\,(c - c_{w\,555nm})$ based on many experimental observations. This relation is also nearly λ^{-1}. Figure 1-8[24] shows spectral beam attenuation measurements made in Monterey Bay. The spectra are shown for various particle concentrations as indicated by beam attenuation at 650 nm. The large fluctuation for small particle concentrations may be instrumental as two almost equal numbers (total attenuation and water attenuation) are subtracted. The decreasing attenuation with increasing wavelength is clearly visible, however.

The concentration of particulate matter has no influence on the spectral aspects of particulate scattering or absorption. The index of refraction on the other hand has a major influence on both the scattering and absorption. The real part of the index of refraction influences refraction and reflection at the surface of the particle. The imaginary part of the index of refraction governs the absorption in the interior of the particle. Mueller[25] has shown theoretically that for three layered absorbing spheres (modeled to resemble phytoplankton) both the absorption and non-0° scattering are strongly wavelength dependent, but in a complimentary fashion so that the attenuation is nearly flat spectrally. The absorption spectrum shows the chlorophyll absorption bands.

The percentage of absorption in particle attenuation varies depending on the nature of the particulate matter.

Nevertheless, Jerlov[23] has found a good correlation for the relationship $a_p = 0.43\ b_p$ using a large number of samples from turbid to clear ocean waters.

Variations In Natural Waters. The spatial distribution of optical properties in the ocean is most closely related to the concentration of suspended particles. River runoff and phytoplankton growth are sources of suspended matter near the surface, whereas resuspended sediments are a particle source near the bottom. Figure 1-9[26] shows the influence of a river plume on the horizontal distribution of light scattering. A scattering maximum is seen to coincide with a salinity minimum. Another scattering maximum is seen near shore. This maximum is due to phytoplankton growth in the near shore zone.

A transect taken perpendicular to the Oregon coast (Figure 1-10)[27] shows some typical features of the spatial distribution of the beam transmission (λ = 660 nm) which is equal to $100\ e^{-cz}$ where c is the beam attenuation coefficient. There is a near surface, near shore maximum due to phytoplankton growth. A bottom nepheloid layer, probably generated by bottom erosion as well as seaward transport of the near shore plankton material exists over the shelf bottom. This bottom nepheloid layer becomes an intermediate particle maximum at the shelf-slope break, as the suspended matter continues to be carried seaward rather than downslope. On the slope, a weak particle maximum continues to exist near the bottom, probably caused by local erosion.

The beam transmission in this section is seen to vary from less than 45% to 66%. This corresponds to beam attenuation coefficients of 0.80 to $0.41\ m^{-1}$. If we subtract c_w for pure water as indicated in Table 1-1 we get particulate attenuation coefficients from 0.48 to 0.10.

By means of Eq. (1-15) we can obtain a_p. If simultaneous volume scattering functions were measured, it is possible to obtain b_p by integration as in Eq. (1-9). Several investigators[28,29,30,31,32,33,34,35] have carried out such measurements, their results are summarized in Table 1-2. The table is a reasonable representation of the range of values for the various scattering and absorption components that can occur naturally.

The shape and absolute values of the volume scattering function vary a great deal in the oceans. $\beta(\theta)$ in the ocean is due to suspended particles and water. As we have already seen, $\beta(\theta)$ for water is nearly flat, whereas that for particles is peaked in the forward direction with the slope of $\beta(\theta)$ depending on the slope of the particle size distribution and the index of refraction.

Figure 1-11 shows several scattering functions measured by Petzold[36]. It is seen that the cleanest water has the lowest slope for low values of scattering angle. Similar results were obtained by Tucker[37] (Fig. 1-12). The deeper water is seen to be clearer and the slope of $\beta(\theta)$ is less steep. The relative contribution of pure water is larger for the deeper water, lowering the slope.

Temporal variations of optical properties in the ocean are usually due to variations in particle concentration. In the near surface zone, however, the nature of particles can change rapidly as phytoplankton patches can be advected past a given location. Near the bottom, erosion may cause a change in size distribution, but in either case most of the change in optical properties is still due to a concentration change. Figure 1-13[38] shows profiles of beam transmission at 500 nm taken on the Oregon shelf. Large variations in the shape of the profile occur in a few hours. Such large changes occur only when strong currents exist. Changes due to biological or chemical processes take days whereas those due to advection of particulate matter occur on very short time scales. Away from coasts, the water tends to be relatively free of particulate matter so that changes over periods of months are thought to be small. Long term observations of optical parameters have not been made in the deep ocean, however.

References (§ 1)

1. Jerlov, N. G., *Marine Optics.* Elsevier Scientific Publishing Company, Amsterdam 231pp., (1976).

2. Ivanoff, A., *Introduction à l'Océanographie:* Tome II, Librairie Vuibert, Paris 340pp., (1975).

3. Preisendorfer, R. W., *Hydrologic Optics Vol. I* U. S. Dept. of Commerce NOAA, Environmental Research Labs, Pacific Marine Environmental Laboratory 218pp., (1976).

4. Einstein, A., "Theorie der Opaleszenz von homogenen Flüssigkeiten and Flüssigkeitsgemischen in der Nähe des kritischen Zustandes", in der Nähe des kritischen Zustandes", Ann. Phys., 33: p. 1275 (1910).

5. Smoluchowski, M., "Molekular-kinetische Theorie der Opaleszenz von Gasen im kritischen Zustande, sowie einiger verwandter Erscheinungen", *Ann. Phys.*, 25: 205 (1908).

6. Morel, A., "Optical Properties of Pure Water and Pure Sea Water", in *Optical Aspects of Oceanography*, (ed) N. Jerlov and E. Steemann Nielsen (Academic Press, New Yorkk, 1974) pp. 1-24.

7. Brown, M. "Transmission Spectroscopy Investigations of Natural Waters", University of Copenhagen report #24 (1974).

8. Mie, G., "Beiträge zur Optik trüber Medien, speziel Kolloidalen Metallösungen, *Ann. Physik*, 25: 377-289 (1908).

9. Hodkinson, J. R., "Light Scattering and Extinction by Irregular Particles Larger Than the Wavelength", in *I.C.E.S. Electromagnetic Scattering.* M. Kerker (ed) (Potsdam Conference, 1962) MacMillan Co., New York, 587p. (1963).

10. Burt, W. V., "A Light-Scattering Diagram", *J. Mar. Res.*, 15: 76-80 (1956).

11. Morel, A., "Indicatrices de diffusion calculées par la theorie de Mie pour les systemes polydisperses, in vue de l'application aux particules marines", Rapport No. 10, Laboratoire d'Océanographie Physique (Université de Paris VI-CNRS), 75pp (1973a)

12. Morel, A., "Diffusion de la lumière par les eaux de mer", resultats expérimentaux et approche théoreque, in *AGARD Lecture Series, Optics of the Sea* No. 61 p. 3.1-1 - 3.1-76 (1973b)

13. Peterson, R. L., "A Study of Suspended Particulate Matter: Arctic Ocean and Northern Oregon Continental Shelf", Oregon State University, Ph.D. thesis, 122pp. (1977)

14. Kullenberg, G. and N. B. Olsen, "A Comparison Between Observed and Computed Light Scattering Functions II", University of Copenhagen Report Number 19, 15pp. (1972)

15. Brown, O. B. and H. R. Gordon, "Two Component Mie Scattering Models of Sargasso Sea Particles", Applied Optics 12: 2461-2465 (1973)

16. Gordon, H. R. and O. B. Brown, "A Theoretical Model of Light Scattering by Sargasso Sea Particulates", Limnol. and Oceanogr. 17: 826-832 (1972).

17. Zaneveld, J. R. V. and H. Pak, "Method for the Determination of the Index of Refraction of Particles Suspended in the Ocean", J. Opt. Soc. Am. 63: 321-324 (1972)

18. Zaneveld, J. R. V., D. Roach, and H. Pak, "The Determination of the Index of Refraction Distribution of Oceanic Particulates", J. Geophys. Res. 79(27): 4091-4095 (1974)

19. Penndorf, R., "On the Phenomenon of the Colored Sun", Air Force Cambridge Res. Center, Tech. Rept. No. 53-7, 41p. (1953)

20. Hodkinson, J. R., "Light Scattering and Extinction by Irregular Particles Larger than the Wavelength, in *I.C.E.S. Electromagnetic Scattering*, M. Kerker (ed), Pergamon, London, 5: 87-100 (1963).

21. Holland, A. C. and G. Gagne, "The Scattering of Polarized Light By Polydisperse Systems of Irregular Particles", Appl. Opt. 9: 1113-1121 (1970).

22. Gibbs, R. J., "Light Scattering from Particles of Different Shapes", J. Geophys. Res. 83(C1): 501-502 (1978)

23. Jerlov, N. G., "Significant Relationships Between Optical Properties of the Sea", in *Optical Aspects of Oceanography*, N. Jerlov and E. Steeman Nielsen (ed) (Academic Press, New York, 1974), pp. 77-94

24. Kitchen, J., "The Relationship Between Spectral Values of Optical Properties in a Region of Large Variability", SPIE Vol. 160, Ocean Optics V, 31-36 (1978)

25. Mueller, J. L., "The Influence of Phytoplankton on Ocean Color Spectra", Ph.D. thesis, Oregon State University, Corvallis, 239pp (1973)

26. Pak, H., G. F. Beardsley, Jr., and P. Kilho Park, "The Columbia River as a Source of Marine Light Scattering Particles", J. Geophys. Res. 75(24): 4570-4578 (1970)

27. Pak, H. and J. R. V. Zaneveld, "Intermediate Nepheloid Layers Observed Over the Continental Margins Off Oregon", SPIE Vol. 160, Ocean Optics V, 9-17 (1978).

28. Jerlov, N. G., "Optical Studies of Ocean Water", *Rep. Swedish Deep-Sea Exped.*, 3: 1-59 (1951)

29. Burt, W. V., "Selective Transmission of Light in Tropical Pacific Waters", *Deep-Sea Res.*, 5: 51-61 (1958)

30. Clarke, G. L. and James, H. R., "Laboratory Analysis of the Selective Absorption of Light by Sea Water", *J. Opt. Soc. Am.*, 29: 43-55 (1939).

31. Ivanoff, A., Jerlov, N. and Waterman, T. H., "A Comparative Study of Irradiance, Beam Transmittance and Scattering In the Sea Near Bermuda", *Limnol. Oceanogr.*, 6: 129-148 (1961).

32. Jerlov, N. G., "Factors Influencing the Transparency of the Baltic Waters", *Medd. Oceanogr. Inst. Goteborg*, 25: 19pp. (1955)

33. Kalle, K., "What Do We Know About The "Gelbstoff"?" *Union Geod. Geophys. Int. Monogr.*, 10: 59-62 (1961)

34. Kullenberg, G., Lundgren, B., Malmberg, Sv.A., Nygard, K. and Hojerslev, N. K., "Inherent Optical Properties of the Sargasso Sea", *Univ. Copenhagen, Inst. Phys. Oceanogr. Rep.*, 11: 18pp. (1970)

35. Hojerslev, N. K., "Inherent and Apparent Optical Properties of the Western Mediterranean and the Hardangerfjord", *Univ. Copenhagen, Inst. Phys. Oceanogr. Rep.*, 21: 70pp. (1973)

36. Petzold, T. J., "Volume Scattering Functions for Selected Ocean Waters", SIO Ref., 72-28: 79pp (1972)

37. Tucker, S. P., "Measurements of the Absolute Volume Scattering Function for Green Light in Southern California Coastal Waters", Ph.D. thesis, Oregon State University, Corvallis (1973)

38. Pak, H. and J. R. V. Zaneveld, "Bottom Nepheloid Layers and Bottom Mixed Layers Observed on the Continental Shelf Off Oregon", J. Geophys. Res., 82(27): 3921-3931 (1977)

39. Sullivan, S. A., "Experimental Study of the Absorption in Distilled Water", Artificial Sea Water, and Heavy Water in the Visible Region of the Spectrum", *J. Opt. Soc. Am.*, 53: 962-967 (1963)

Wavelength	350	375	400	425	450	475	500	525	550	575	600	625	650	675	700	725	750	775	800
Pure water transmittance in % after (3b) after (19)		95.6	95.8	96.8	98.1	98.2	98.3	96.0	93.3	91.3 89.7	83.3 75.2	79.6 73.7	75.0 70.6	69.3 64.5	60.7 52.3	29 17	9 7	9 7	10
Pure water attenuation coefficient in 10^{-3} m^{-1}, c after (4) after (5)		65	63	33	19	18	36	61	69	91 109	186 272	228 305	288 351	367 438	580 648	1,240 1,758	2,480 2,688	2,640 2,638	2,850
Pure water scattering coefficient in 10^{-3} m^{-1}, b after (6)	10.35	7.68	5.81	4.47	3.49	2.76	2.22	1.79	1.49	1.25	1.09								
Pure water volume scattering coefficient at 90° in m^{-1} sr^{-1}, $\beta_w(90°)$ after (6)	.047	.030	.023	.018	.014	.011	.009	.007	.006	.005	.004								
Pure seawater scattering coefficient in 10^{-3} m^{-1}, b after (6)	13.45	9.98	7.55	5.81	4.54	3.59	2.88	2.33	1.93	1.62	1.41								
Pure seawater volume scattering coefficient at 90° in m^{-1} sr^{-1}, $\beta(90°)$ after (6)	.041	.026	.022	.017	.013	.010	.008	.007	.005	.005	.004								

TABLE I. Scattering and attenuation parameters for pure water and pure seawater.

TABLE II
A comparison of inherent optical properties. Units of m^{-1}
$c_{observed} = c_w + a_p + b_p + a_y$

LOCATION	WAVELENGTH (nm)	$c-c_w$	a_p	b_p	c_p	a_y	reference
Sargasso Sea	440	0.05		0.04			
Carribean Sea	655	0.06	0	0.06	0.06		
	440	0.09		0.06			
Equator Central Pacific	440	0.09		0.05			(28)
Romanche Deep	440	0.12		0.07			
Galapagos	655	0.11	0.04	0.07	0.11		
	440	0.24		0.08			
Off Peru	700	0.39			0.39	0	
(64 miles)	400	0.73			0.64	0.09	
Galapagos	700	0.16			0.16	0	
	400	0.25			0.21	0.04	(29)
Northwestern	700	0.07			0.07	0	
Galapagos	400	0.11			0.08	0.03	
Continental	668	0.05				0	
slope	365	0.10			0.08	0.02	(30)
Bermuda	655	0.10			0.10	0	
	380	0.20			0.17	0.03	(31)
Kattegat	655	0.23	0.08	0.15	0.23	0	
	380	0.54	0.27	0.16	0.44	0.11	
South	655	0.27	0.07	0.20	0.27	0	(32)
Baltic Sea	380	1.15	0.28	0.21	0.49	0.68	
Bothnian	655	0.38	0.10	0.28	0.38	0	
Gulf	380	1.72	0.33	0.31	0.64	1.08	
North	665					0	
Atlantic	420					0.03	
North	665					0.01	(33)
Sea	420					0.10	
Baltic Sea	665					0.02	
	420					0.33	
Sargasso Sea	633	0.03	0.01	0.02	0.03		
	484	0.03	0.01				
	440	0.05	0.01	0.04			(34)
	375			0.02			
Western Mediterranean area	655	0.08	0.04	0.04	0.08	0	
	375	0.06		0.04			(35)

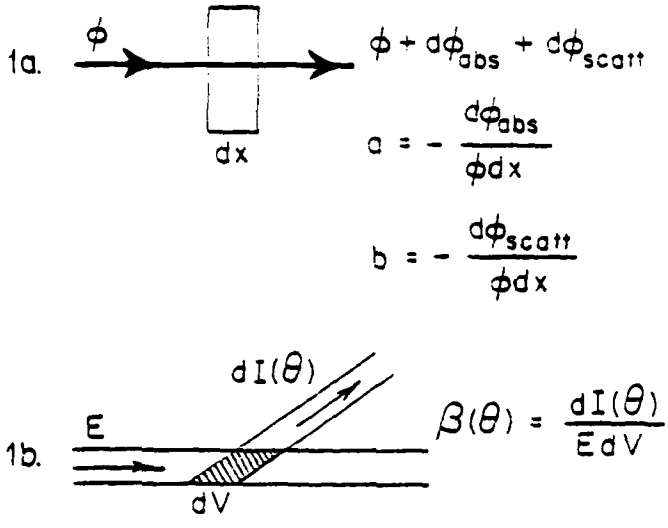

Figure 1-1. a) Absorption and scattering coefficients. b) The volume scattering function.

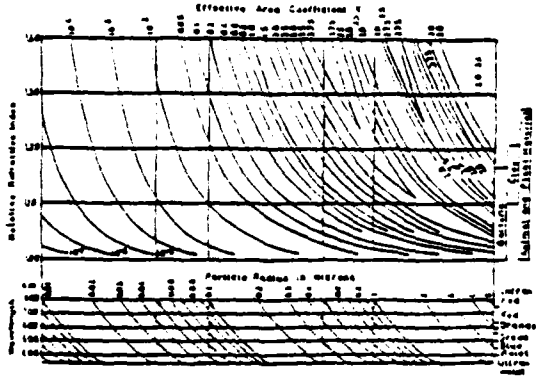

Figure 1-2. The effective area coefficient K_{aa} as a function of wavelength, index of refraction and particle radius. After (10).

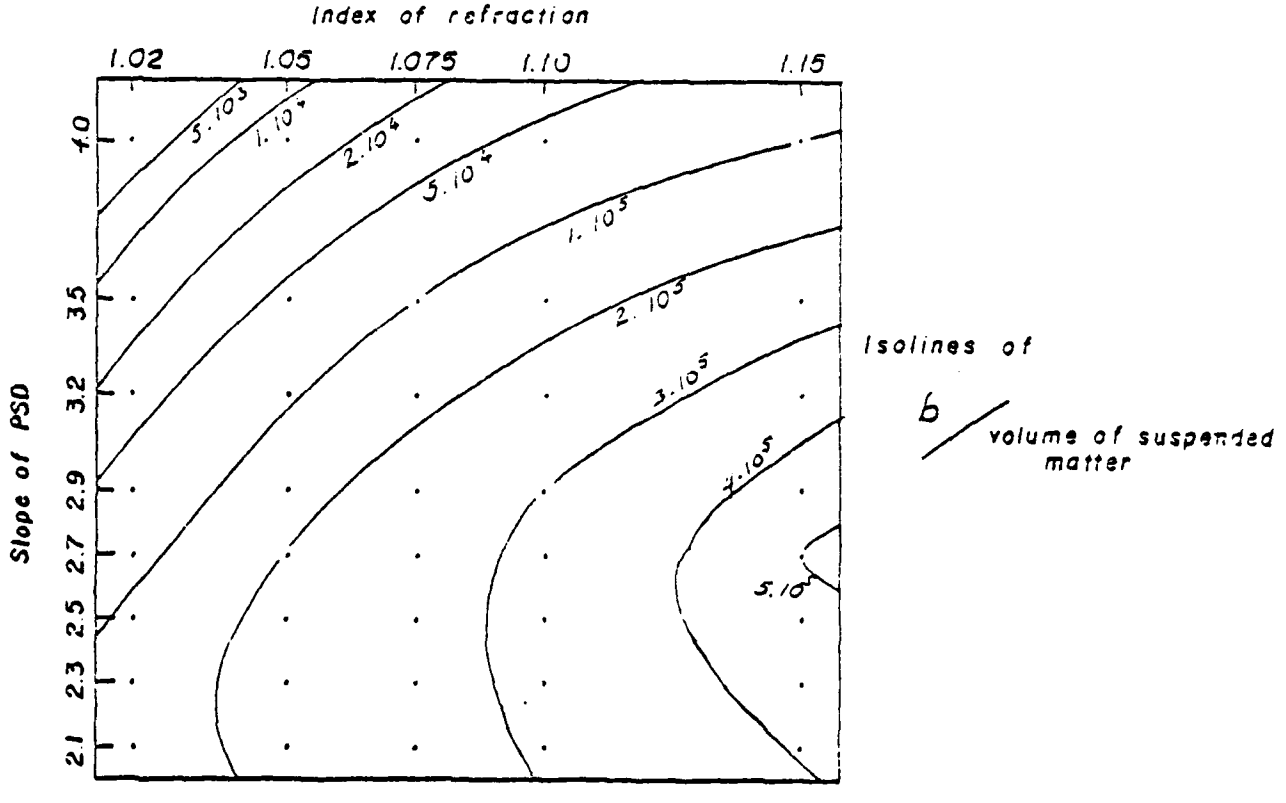

Figure 1-3. The total scattering coefficient per unit volume of particulate matter as a function of slope of the particle size and distribution and the index of refraction of the particles.

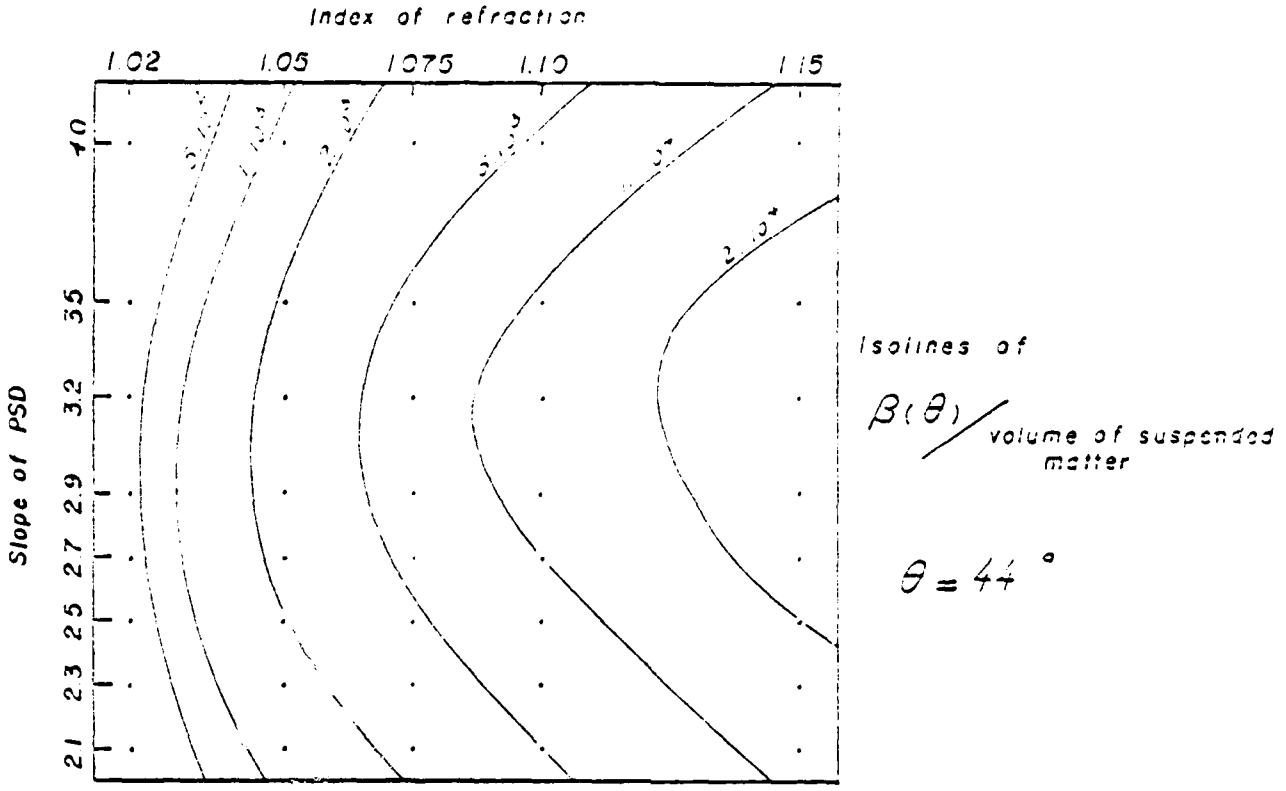

Figure 1-4. Light scattering at 44° per unit volume of particulate matter as a function of slope of the particle size distribution and the index of refraction of the particles.

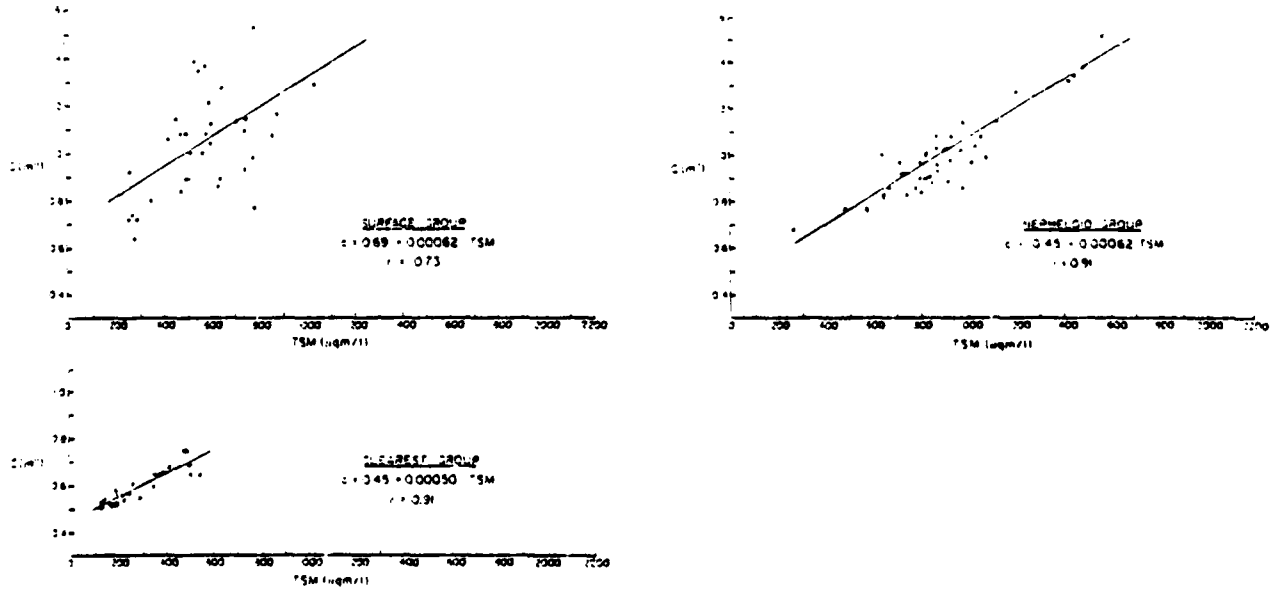

Figure 1-5. Scatter plots and regression lines for beam attenuation (c) as a function of total suspended matter. After (13).

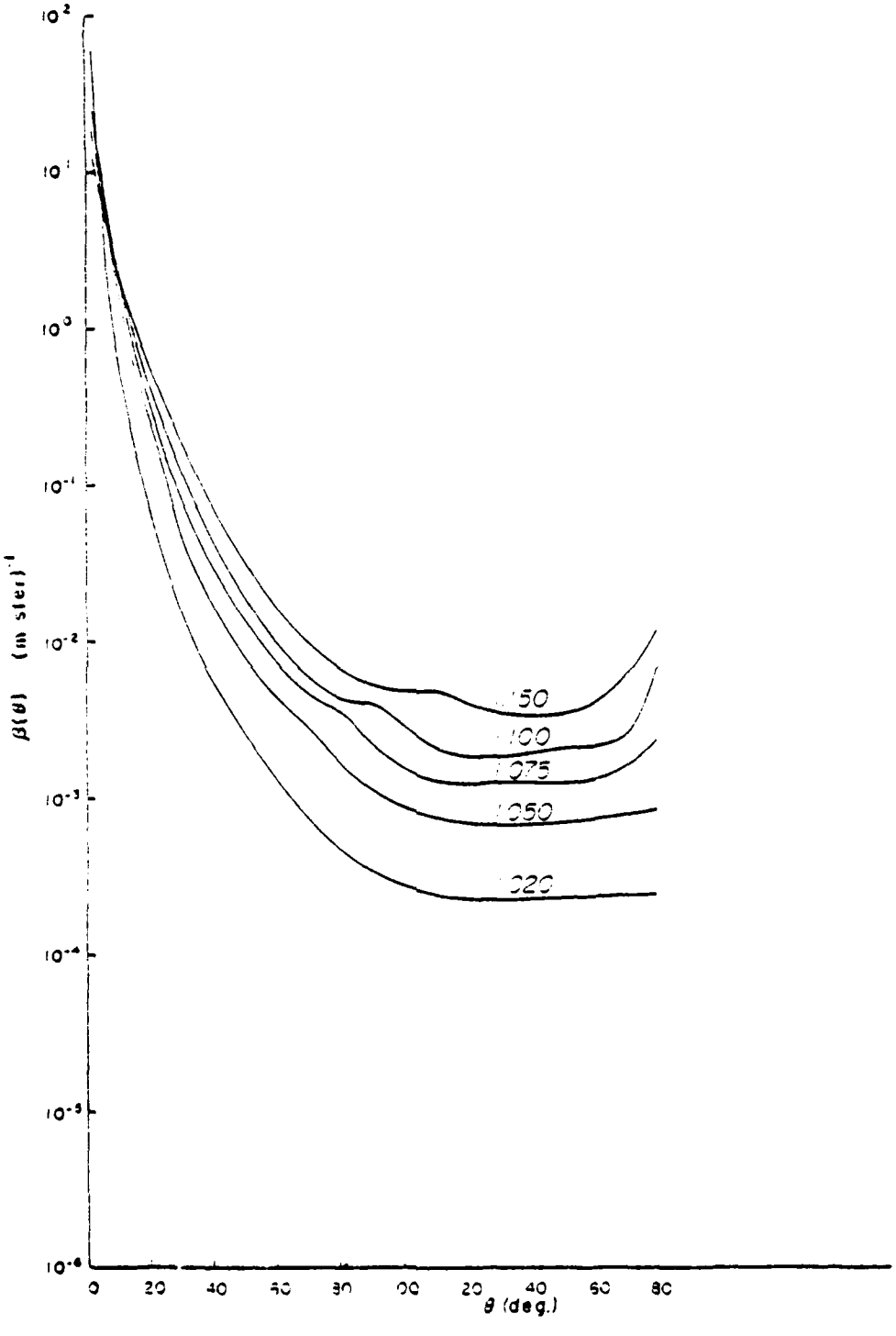

Figure 1-6. Normalized volume scattering functions for various refractive indices with Junge exponent C = 2.5. After (11).

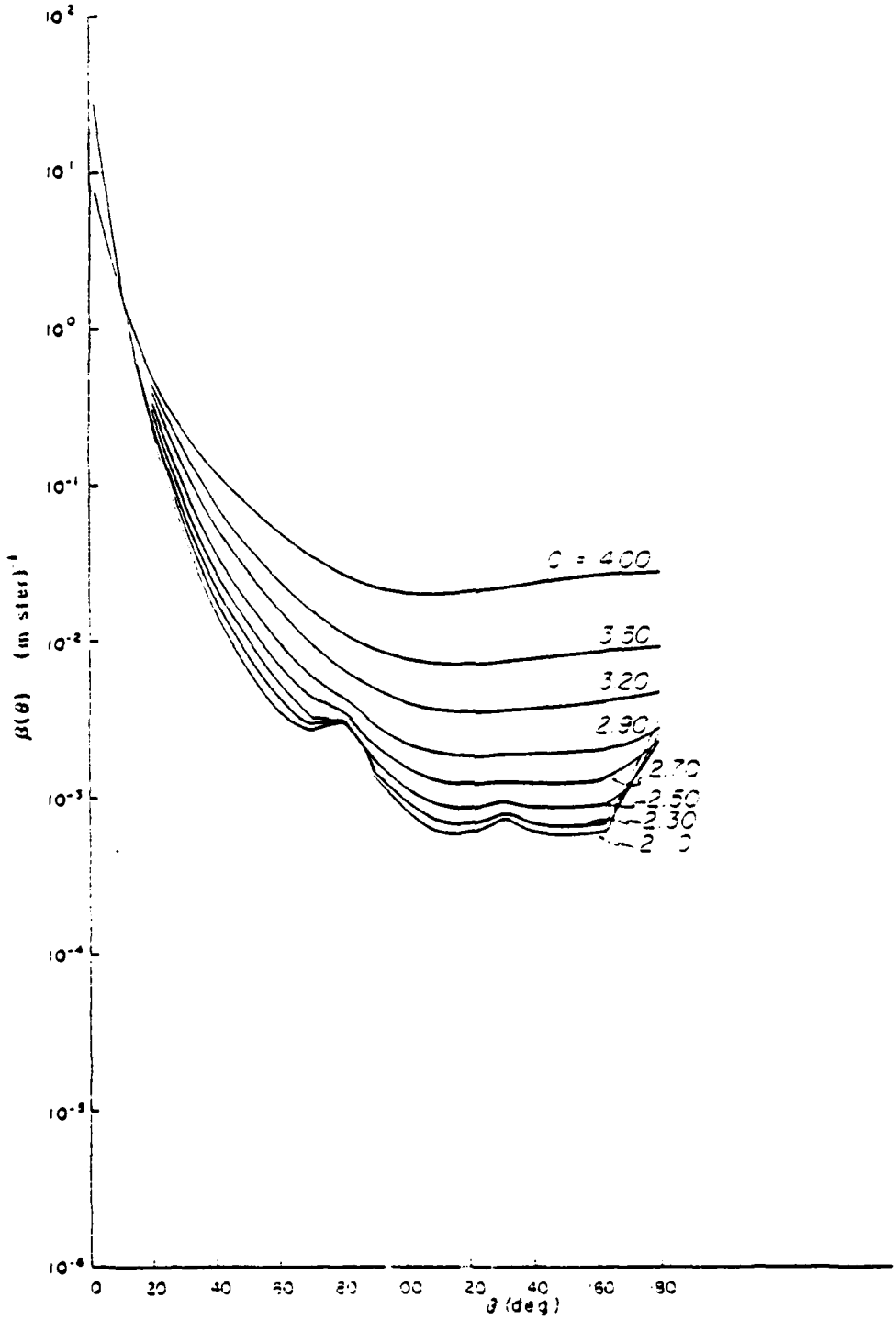

Figure 1-7. Normalized volume scattering functions for various particle size distributions characterized by the Junge exponent C with a refractive index 1.075. After (11).

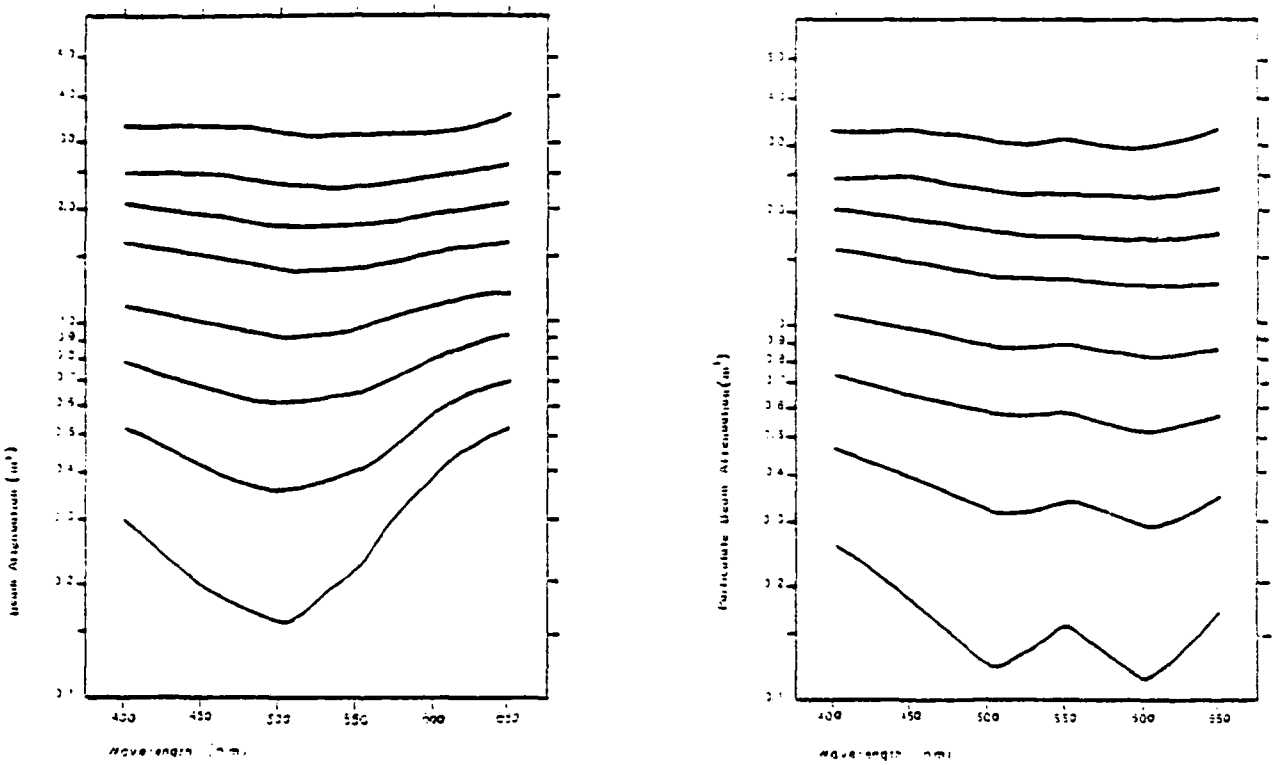

Figure 1-8. Average attenuation and particulate attenuation spectra for samples grouped according to their light transmission values at 650 nm wavelength (i.e. 1.5-5, 5-10, 10-15, 15-25, 25-35, 35-45, 45-55 and greater than 55% transmission). From (24).

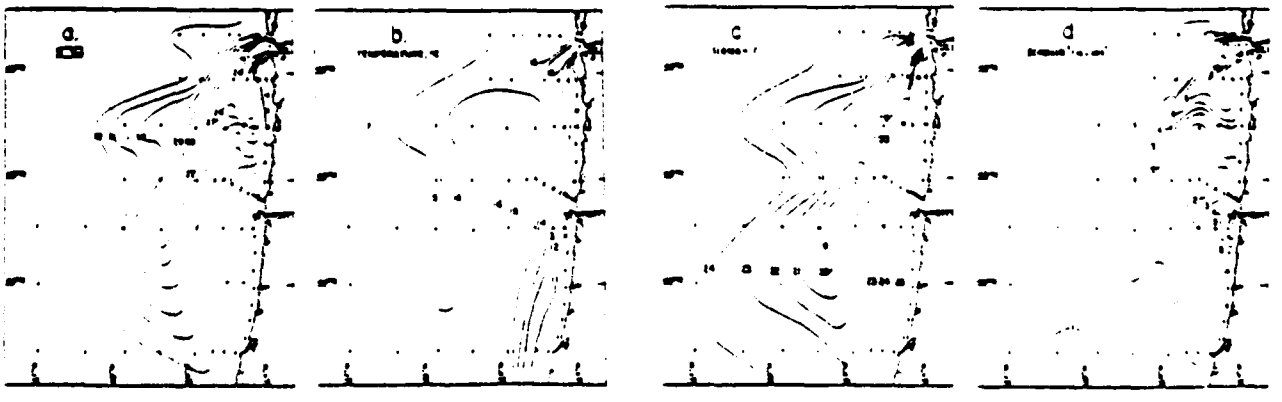

Figure 1-9 Horizontal distributions of salinity, temperature, density (σ_t) and light scattering at 45°, taken at the surface off the Oregon coast, during early summer, indicating the influence of the Columbia River plume. After (26)

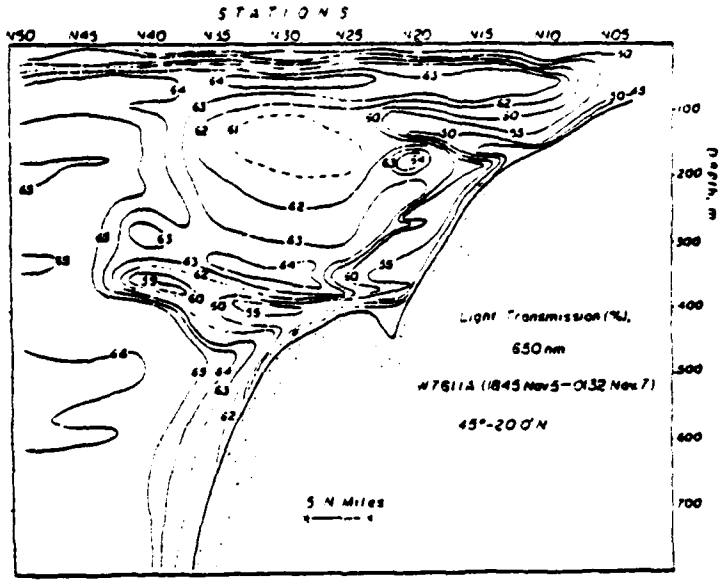

Figure 1-10. Distribution of light transmission (%) in the northern transect. From [27]

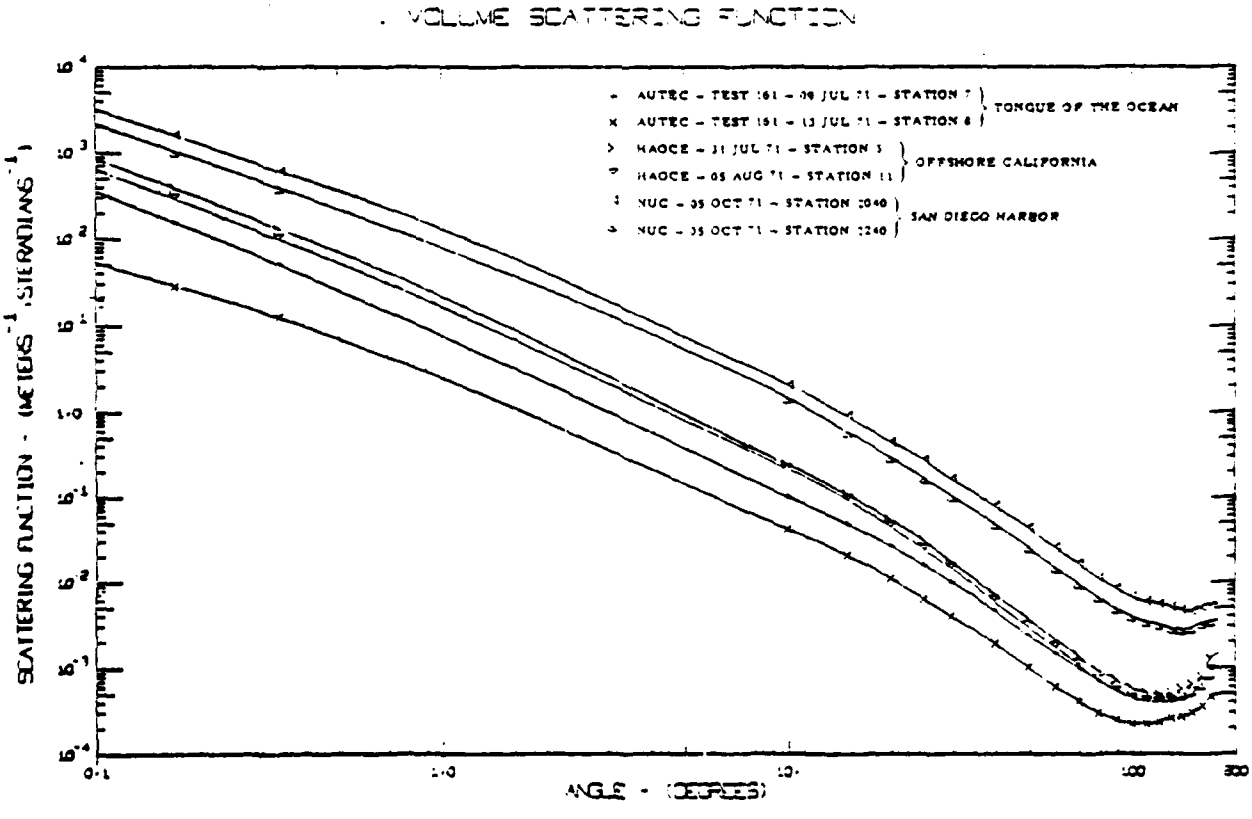

Figure 1-11. Volume scattering function of various water types. After Petzold, 1972.

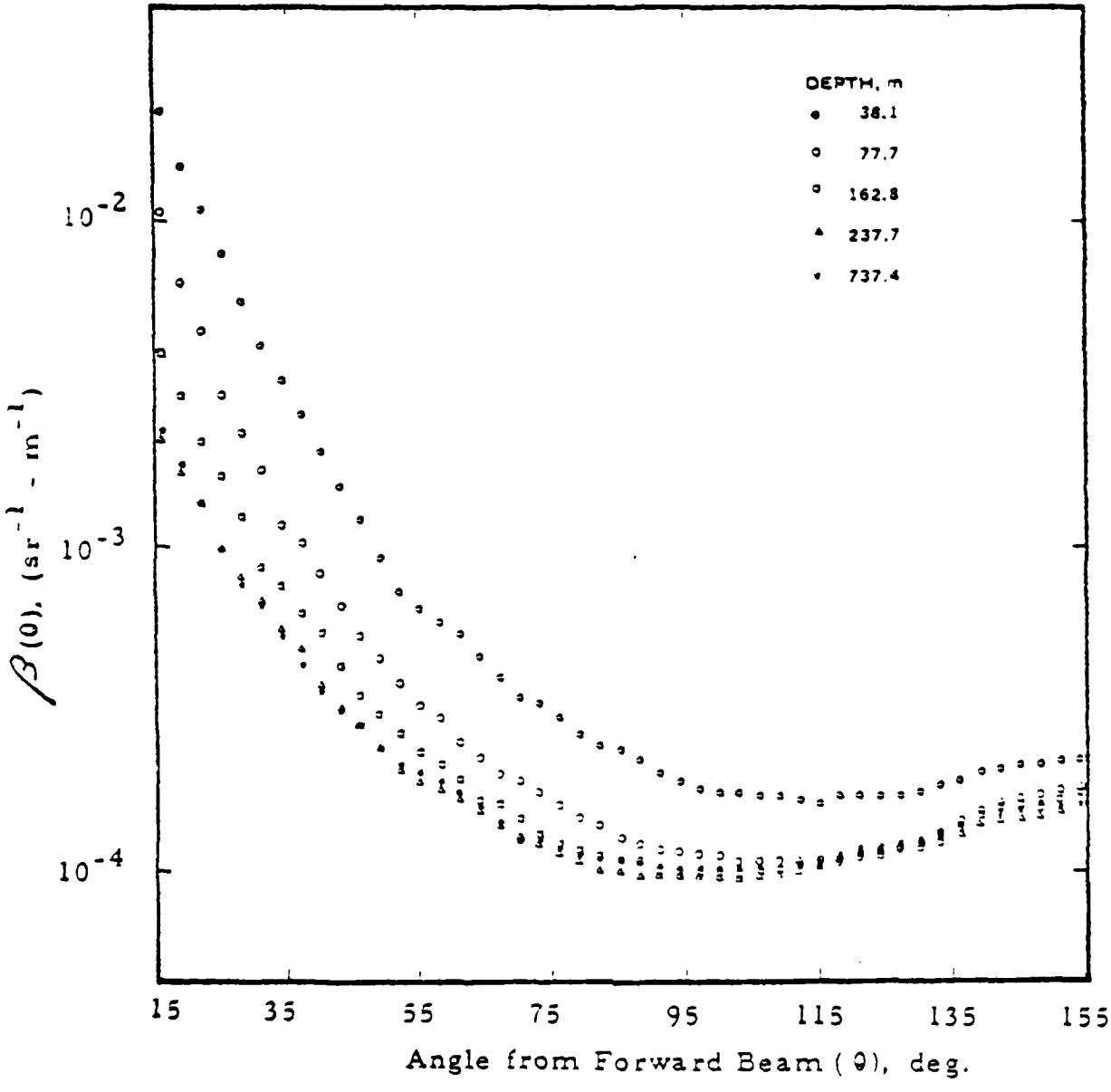

Figure 1-12. Volume scattering coefficient as a function of scattering angle and depth. USS REXBURG, 22-23 August 1967. From (37)

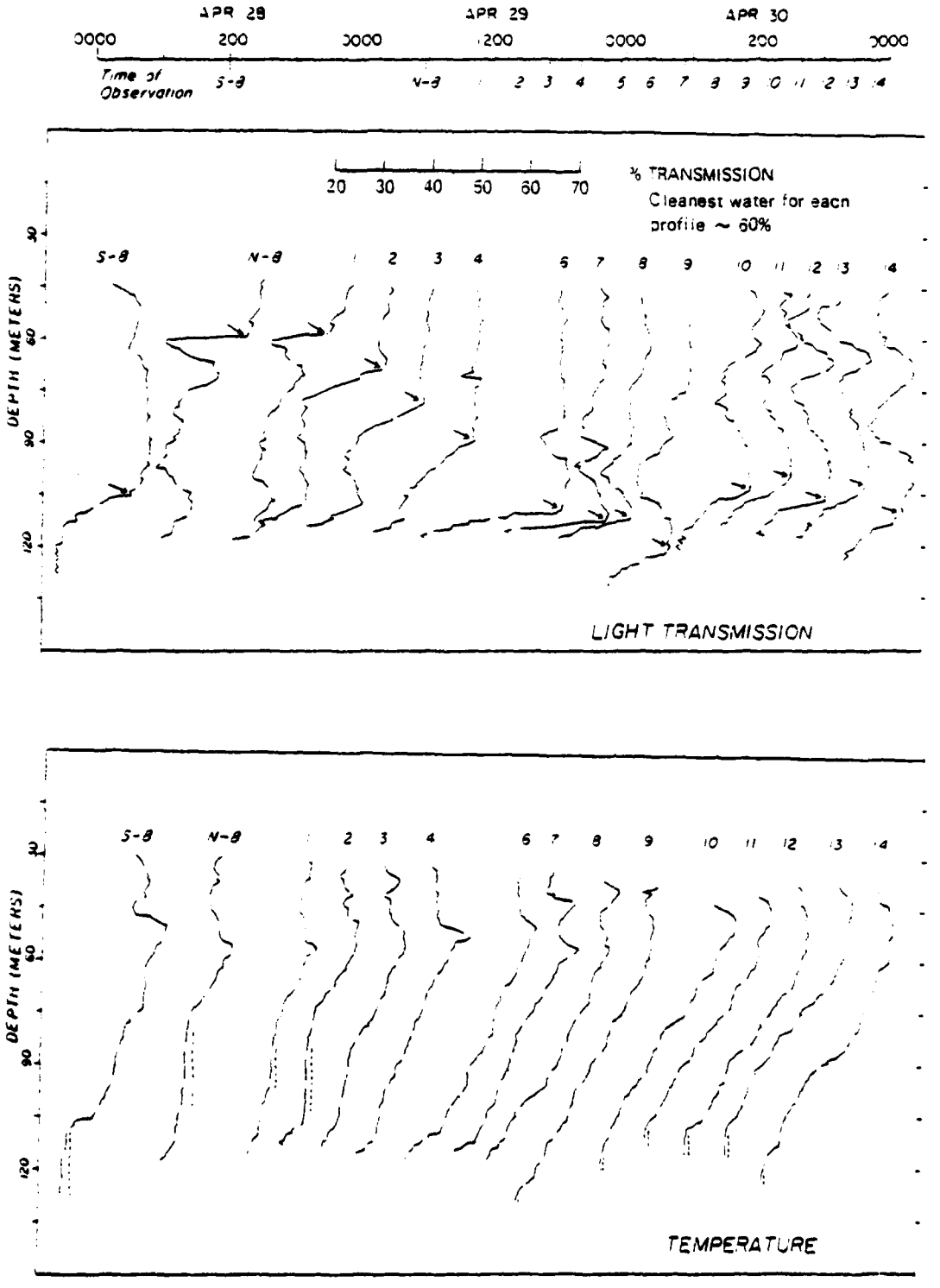

Figure 1-13. Profiles of light transmission, in percent, and temperature, in degrees Celsius, at anchor station A8. Arrows indicate the tops of BNL, and broken lines on the right side of the temperature profiles indicate the mixed layers. Time of each profile is indicated at the top of the figure. From (38).

2. Apparent Optical Properties (R.C.S.)

Introduction. Preisendorfer[1,2] and Tyler and Preisendorfer[3] have shown that the optical properties of the sea can be divided into two classes, the inherent and the apparent optical properties of the medium. An optical property is inherent if its operational value at a given point in a medium is invariant with changes of the radiance distribution at that point. An apparent optical property is one for which this is not the case.

Apparent optical properties depend jointly on the inherent optical properties of ocean waters and the geometrical structure of the radiant energy within these waters. In spite of the added complexity caused by their functional dependence on the geometrical structure of the light field, the apparent optical properties are so called because their gross behavior with depth exhibits reproducible regularities in a wide range of natural water types; it is possible to formulate exact mathematical interrelationships that hold, for all practical cases, between these apparent optical properties and the more fundamental inherent optical properties; and the use of apparent optical properties permits practical solutions to a wide range of ocean optical problems. Like the inherent optical properties, each of the apparent optical properties is implicitly a function of wavelength.

In this section we first discuss the angular radiance distribution of the sun's radiant energy in natural waters. It is from the radiance distribution, or the experimentally easier-to-measure irradiances that the apparent optical properties of natural waters can be derived. Two important apparent optical properties, reflectance and the diffuse attenuation coefficients, are then defined and their spectral characteristics discussed. Much of the material in this section is drawn from Chapter 3 of the Handbook of Underwater Optical Measurements by Austin, Petzold, Smith and Tyler[4]

The symbols used in this work are believed to be those currently accepted by most international standards organizations and frequently differ from symbols used in earlier references. Table 2-1 (from reference 4) presents a summary of the terms used in hydrologic optics and their recommended symbols along with the classic symbols used in much of the earlier work (especially Preisendorfer and others at the Visibility Laboratory)

Radiance, $L(Z,\theta,\phi)$ $[W \cdot m^{-2} \cdot sr^{-1}]$ is the energy per unit time and unit area and solid angle incident at a point at depth Z, from the direction (θ,ϕ). A radiance distribution, the totality of radiance values for every direction about the point, gives a complete description of the geometrical structure of the radiant energy field. The structure of radiance distribution in the upper layers of the sea is dependent upon factors which modify the solar radiation in the earth's atmosphere, conditions at the air-sea interface, and optical properties of the sea water. This geometrical structure of solar radiation in the upper layers of the sea has been discussed by several authors[4,5,6,7], who have also presented representative radiance data.

Figure 2-1 (after Tyler[5]) presents a chart illustrating optical properties which can be derived from the radiance distribution.

Irradiance. Downward irradiance, $E_d[W \cdot m^{-2}]$, is the flux per unit area measured by a horizontally oriented cosine collector (a collector with a $\cos\theta$ geometrical response) facing upward to accept downwelling flux. Upward irradiance, $E_u[W \cdot m^{-2}]$, is measured by a similar collector oriented to accept upwelling flux. Downward and upward irradiance are associated with a specific depth, Z, and are defined in terms of the radiance distribution by the following equations.

$$E_d(Z) = \int_{\phi=0}^{2\pi} \int_{\theta=0}^{\pi/2} L(Z,\theta,\phi)\cos\theta\, d\omega \tag{2-1}$$

$$E_u(Z) = -\int_{\phi=0}^{2\pi} \int_{\theta=\pi/2}^{\pi} L(Z,\theta,\phi)\cos\theta\, d\omega \tag{2-2}$$

where the solid angle

$$d\omega = \sin\theta\, d\theta\, d\phi \,. \tag{2-3}$$

Downward irradiance has been one of the most commonly measured quantities in optical oceanography. There are several reasons for this: irradiance is a well-defined and standardized physical quantity that can be quantitatively determined; it is a principal quantity used in physical theories[2,3,6,8] concerned with the behavior of radiant energy in natural waters thus allowing direct comparison of experimental data with physical theories; and it has been among the easiest radiometric quantities to measure underwater. In addition, irradiance serves as a useful measure of the radiant energy available for performing visual tasks, for underwater television or photography, or for photosynthesis. Actually, there are compelling reasons for choosing scalar irradiance for this latter purpose, as will be discussed in the following section.

Scalar irradiance. $E_0[W \cdot m^{-2}]$, (called energy fluence rate in photobiology[12]) is the integral of a radiance distribution at a point at depth Z over all directions about the point, *i.e.*,

$$E_o(Z) = \int_{4\pi} \int L(Z,\theta,\phi)\, d\omega \,. \tag{2-4}$$

The scalar irradiance, when divided by the velocity of light in the medium, c, yields the radiant density, w, the total amount of radiant energy per unit volume of space at the given point, i.e., the radiant energy density $w = E_o/c$ [J m^{-3}].

The scalar irradiances due to radiances received separately from the upper and lower hemispheres can be written:

$$E_{od}(Z) = \int_{\phi=0}^{2\pi} \int_{\theta=0}^{\pi/2} L(Z,\theta,\phi)\, d\omega \tag{2-5}$$

$$E_{ou}(Z) = \int_{\phi=0}^{2\pi} \int_{\theta=\pi/2}^{\pi} L(Z,\theta,\phi)\, d\omega \tag{2-6}$$

and

$$E_o(Z) = E_{od}(Z) + E_{ou}(Z) \,. \tag{2-7}$$

Several factors favor scalar irradiance as the parameter that serves as the optimum measure of the radiant energy available for aquatic photoprocesses[3]: it provides a measure of radiant energy incident upon a small sample volume weighing all directions of incidence equally; it is a scalar quantity, not defined with respect to some particular geometrical orientation (as are E_d and E_u), thus it allows all laboratory and field measurements to be directly compared on an absolute basis without regard for different lighting geometries; and, like E_d and E_u, it is a well-defined and standardized physical quantity that is amenable to theoretical description and mathematical manipulation, and possesses standardized units.

Reflectance, or the irradiance ratio, is the ratio of the upward to the downward irradiance at depth, Z.

$$R(Z) = \frac{E_u(Z)}{E_d(Z)} \,. \tag{2-8}$$

Experimentally R is usually determined by measuring E_u and E_d directly although it can also be determined from $L(Z,\theta,\phi)$ by means of Eqs. (2-1) and (2-2). R may be thought of as the reflectance at a hypothetical plane surface at depth Z in the medium. The irradiance ratio depends upon and exhibits information about the scattering properties of the entire medium above and below the level Z.

Distribution functions, D_d and D_u, are defined as:

$$D_d(Z) = \frac{E_{od}(Z)}{E_d(Z)} \tag{2-9}$$

$$D_u(Z) = \frac{E_{ou}(Z)}{E_u(Z)} \,. \tag{2-10}$$

These distribution factors are a simple means of characterizing the depth dependence of the shape of the radiance distribution. In addition, they play an important role in the equations of applied radiative transfer theory.

Reflectances, other than for irradiance, are frequently useful in particular applications. For example, a meaningful "reflectance" useful for remote sensing purposes, is the ratio of upward radiance (simulating the geometric acceptance of the remote collector) to downward irradiance.

$$R_{RS}(Z) = \frac{L_u(Z)}{E_d(Z)} \tag{2-11}$$

This "remote sensing reflectance" is related to the irradiance reflectance through a factor introduced by Austin[4]

$$R = \frac{E_u}{E_d} = \frac{L_u \cdot Q}{E_d} = R_{RS} \cdot Q \,. \tag{2-12}$$

where the "Q factor" would have the value π for a uniform upwelling radiance distribution. In practice this factor is found to be a function of wavelength and values between 3 and 12 have been reported.

Attenuation Coefficients for Irradiance. $K(Z)[m^{-1}]$, are defined as the logarithmic depth derivatives of the irradiance functions. Thus,

$$K_d(Z) = \frac{-1}{E_d(Z)} \left| \frac{dE_d(Z)}{dZ} \right| \tag{2-13}$$

or alternatively,

$$\frac{E_d(Z_1)}{E_d(Z_1)} = \exp[-K_d \cdot (Z_2 - Z_1)] . \tag{2-14}$$

where K_d has units of reciprocal length, and Z is the depth at which E_d is measured (Z increasing positively with depth). In practice, K_d is frequently determined from the slope of a plot of ln $E_d(Z)$ vs Z. Similar K-type functions can be defined for upward irradiance and for the scalar irradiances, *e.g.*,

$$K_u(Z) = \frac{-1}{E_u(Z)} \left| \frac{dE_u(Z)}{dZ} \right| . \tag{2-15}$$

In addition, a K-type radiance attenuation coefficient may be similarly defined as the logarithmic depth derivative of the radiance, $L(Z, \theta, \phi)$, for a fixed direction, θ, ϕ.

Physically, the K functions are the quantities that specify the individual depth dependence of irradiance functions. Historically, the K functions were derived from the experimental fact that, in general, radiant energy decreases exponentially with depth. Thus, given K and the radiant energy at any one depth, the radiant energy at any other depth can be calculated. In addition, K functions can be used to classify ocean water types[5,16].

Representative Data. Radiance distribution data are few[3,6,10,17], and to the best of our knowledge no one has obtained radiance data as a function of wavelength. Representative monochromatic data have been presented and discussed by several authors[4,5,6,10,17].

Spectral irradiance data are more numerous and have been obtained for a wide range of ocean water types[10,18–27]. Crater Lake (Fig. 2-2) and San Vicente Reservoir (Fig. 2-3) are examples of two extreme optical water types and span the full range of color one can normally expect in natural waters whose dissolved and suspended material is primarily of biogeneous origin. Crater Lake waters (1969) are among the clearest in the world, and have been referred to as a natural analogue to distilled water[27]. These waters, and those of oligotrophic open ocean areas such as the Sargasso Sea, have similar optical properties[19,27]. Natural radiant energy penetrates to hundreds of meters in these clearest waters and the wavelength of maximum transmittance is in the 450 to 475 nm region, imparting to them a characteristic deep blue appearance. These clear waters are relatively barren and generally have very low chlorophyll concentration in the range for 0.01 to 0.05 *mg Chl* $\cdot m^{-3}$.

In contrast, San Vicente waters contained a chlorophyll concentration two to three orders of magnitude higher (5 to 10 *mg Chl* $\cdot m^{-3}$) than that associated with clear waters. In these highly productive waters the penetration of ecologically significant radiation is only the order of meters, or even centimeters. The high concentration of pigments shifts the wavelength of maximum transmittance from the blue at least 100 nm into the green region of the spectrum (Fig. 2-3). Apparent optical properties, which can be derived from those spectral irradiance data, provide a quantitative description of these qualitative observations.

The diffuse attenuation coefficients for irradiance, $K(\lambda)$, derived from the data shown in Figs. 2-2 and 2-3 using Eq. (2-14), are shown in Fig. 2-4. Values of the minimum irradiance K (hence maximum transmission), for Crater Lake and San Vicente respectively, are $K(450) \approx 0.03 m^{-1}$ and $K(580) \approx 0.47 m^{-1}$. Thus, at their respective wavelengths of maximum transmittance, San Vicente waters attenuate irradiance with an exponential about fifteen times larger than that for Crater Lake. The respective maximum attenuation lengths (K^{-1}) are 30 to 40 meters and 2 meters. Finally, it should be noted that the "K value" for San Vicente, in the region from 670 to 690 nm is being influenced by chlorophyll-*a* fluorescence[28].

As demonstrated in Fig. 2-4, the shift in λ_{max}, with increasing chlorophyll concentration is a general feature of biogenous waters and has been observed and discussed by several authors[16,29,30]. This shift is more usually observed as a shift in water color, or spectral reflectance. The irradiance reflectances, for our two examples, derived from the data shown in Figs. 2-2 and 2-3 using Eq. (2-10), are shown in Fig. 2-5. These curves graphically demonstrate both the spectral shift (from blue to green) and the magnitude change in $R(\lambda)$ due to the addition of chlorophyll to otherwise clear ocean waters. It is this dramatic shift in ocean color due to chlorophyll that leads to the notion that ocean chlorophyll might be measureable by remotely sensing these changes in spectral reflectance (see sections 5 and 6 below).

These two extreme examples of optical water types demonstrate the wide range in optical properties that can be expected in natural waters. An important aspect of optical oceanography is an understanding of the physical and biological processes effecting these properties and their variability in time and space. Conversely, once these optical properties are measureable, or predictable based on an understanding of the processes influencing them, then a wide range of practical oceanographic problems are amenable to solution.

References (§ 2)

1. Preisendorfer, R. W., "Application of Radiative Transfer Theory to Light Measurement in the Sea", in *Radiant Energy in the Sea*, ed. N. G. Jerlov, Union Geod. Geophys. Inst. Mon. 10, 4-30 (1961).

2. Preisendorfer, R. W., "Hydrologic Optics", U. S. Department of Commerce, National Oceanic & Atmospheric Administration, Environmental Research Laboratories (1976).

3. Tyler, J. E. and R. W. Preisendorfer, "Transmission of Energy Within the Sea", in *The Sea* Vol. 2, ed. M. N. Hill (Interscience Pub., New York, 1962).

4. Austin, R. W., T. J. Petzold, R. C. Smith and J. E. Tyler, "Handbook of Underwater Optical Measurements", in preparation (1979).

5. Tyler, J. E., "Radiance Distribution as a Function of Depth in an Underwater Environment", Univ. of Calif. Bulletin of Scripps Inst. of Oceanog. Vol. 7 No. 5, pp. 363-411 (1960).

6. Smith, R. C., "Structure of Solar Radiation in the Upper Layers of the Sea", in *Optical Aspects of Oceanography*, ed. N. G. Jerlov, pp. 95-119 (1974).

7. Tyler, J. E., "A Survey of Experimental Hydrologic Optics", J. Quanta. Spectro. Radiat. Transfer Vol. 8, pp. 339-354 (1968).

8. Preisendorfer, R. W., "A Model for Radiant Distribution in Natural Hydrosols", in *Physical Aspects of Light in the Sea*", Univ. Hawaii Press, Honolulu, Hawaii, pp. 51-60 (1964).

9. Gordon, H. R., O. B. Brown and M. M. Jacobs, "Computed Relationships Between the Inherent and Apparent Optical Properties of a Flat Homogeneous Ocean", Appl. Opt. 14, 417-427 (1975).

10. Jerlov, N. G., "Marine Optics", Elsevier Scientific Pub. Co., New York, 231 (1976).

11. Duntley, S. Q., "Light in the Sea", J. Opt. Soc. Am. 53, 214-233 (1963).

12. Smith, R. C. and J. E. Tyler, "Transmission of Solar Radiation Into Natural Waters", Photochemical and Photobiological Reviews, Vol. 2, ed. K. C. Smith, Plenum Pub. Co. (1976).

13. Smith, R. C. and W. H. Wilson, "Photon Scalar Irradiance", Applied Optics 11, 934-938 (1972).

14. Austin, R. W., S. Q. Duntley, R. W. Austin, W. H. Wilson, C. F. Edgerton, and S. E. Moran, "In Ocean Color Analysis", SIO Ref. 74-10 (1974).

15. Smith, R. C. and K. S. Baker, "The Bio-Optical State of Ocean Waters and Remote Sensing", Limnol. Oceanogr. 23, 247-259 (1978).

16. Smith, R. C. and K. S. Baker, "Optical Classification of Natural Waters", Limnol. Oceanogr. 23, 260-267 (1978).

17. Anderson, R. D., "Underwater Radiance Scanner", Optical Engineering 17, 94-102 (1978).

18. Smith, R. C. and J. E. Tyler, "Optical Properties of Clear Natural Water", J.O.S.A. 57, 589-595 (1966).

19. Tyler, J. E. and R. C. Smith, "Spectroradiometric Characteristics of Natural Light Underwater", J.O.S.A. 57, 595-601 (1966).

20. Tyler, J. E. and R. C. Smith, "Measurement of Spectral Irradiance Underwater", Gordon & Breach Science Pub. New York, 103 pp., (1970).

21. Smith, R. C., "Spectral and Total Irradiance" in Data Report SCOR Discoverer Expedition, May 1970, J. E. Tyler ed., S.I.O. Ref. 73-16 (1973).

22. Morel, A., "Spectral and Total Irradiance", in Data Report SCOR Discoverer Expedition May 1970, J. E. Tyler ed., SIO Ref. 73-16 (1973).

23. Morel, A. and L. Caloumenos, "Measures d'eclairements sous marins flux de photons et analyse spectrale" (Campagnes Harmattan et Cencea II, 3e partie) Presentation des Rseultats. Rapport No. 11 Laboratoire d'Oceanographie Physique, Villefranche-sur-Mer, 180 pp. (1973).

24. Morel, A. and L. Prieur, "Analyse spectrale des coefficients d'absorption et de retrodiffusion pour diverses regions marines", Rapport No. 17, Laboratoire d'Oceanographie Physique Villefranche-sur-Mer, 157 pp. (1975).

25. Jerlov, N. G., "Optical Studies of Ocean Water", Rep. Swedish Deep-Sea Exped., 3, 1-59 (1951).

26. Sasaki, T. N. Okami, G. Oshiba and S. Watanabe, "Spectral Energy Distribution of Submarine Daylight off Kii Peninsula in Relation to the Investigation of Ocean Productivity", Reg. Oceanogr. Works. Jpr., Spec. No. 2, 119-128 (1958).

27. Smith, R. C., J. E. Tyler and C. R. Goldman, "Optical Properties and Color of Lake Tahoe and Crater Lake", Limnol. & Oceanogr. 18, 189-199, (1973).

28. Gordon, H. R., "Diffuse Reflectance of the Ocean: The Theory of its Augmentation by Chlorophyll-*a* Fluorescence at 685 nm", Applied Optics 18, 1161-1166 (1979).

29. Morel, A. and R. C. Smith, "Relation Between Total Quanta and Total Energy for Aquatic Photosynthesis", Limnol. Oceanogr. 19, 591-600 (1974).

30. Yentsch, C. S., "The Influence of Phytoplankton Pigments on the Color of Sea Water", Deep-Sea Research 7: 1-9 (1960).

TABLE 2-1.

QUANTITY [Units]		RECOMMENDED SYMBOL	CLASSIC SYMBOL
Quantity of Radiant Energy	[J]	Q	U
Radiant Flux	[W]	Φ	P
Radiant Intensity	[$W \cdot sr^{-1}$]	I	J
Radiance	[$W \cdot m^{-2} \cdot sr^{-1}$]	L	N
Irradiance	[$W \cdot m^{-2}$]	E	H
Radiant exitance	[$W \cdot m^{-2}$]	M	W
Downward irradiance	[$W \cdot m^{-2}$]	E_d	$H(-)$
Upward irradiance	[$W \cdot m^{-2}$]	E_u	$H(+)$
Net irradiance	[$W \cdot m^{-2}$]	$\bar{E}$	$\bar{H}$
Scalar irradiance	[$W \cdot m^{-2}$]	E_o	h
Downward scalar irradiance	[$W \cdot m^{-2}$]	E_{od}	$h(-)$
Upward scalar irradiance	[$W \cdot m^{-2}$]	E_{ou}	$h(+)$
Spherical irradiance	[$W \cdot m^{-2}$]	E_s	
Irradiance ratio		$R = E_u/E_d$	$R = H(+)/H(-)$
Distribution factor		$D_d = \frac{E_{od}}{E_d}$	$D- = h-/H-$
		$D_u = \frac{E_{ou}}{E_u}$	$D+ = h+/H+$
Absorption coefficient	[m^{-1}]	a	a
Volume scattering function	[$m^{-1} sr^{-1}$]	$\beta(\theta)$	$\beta(\theta)$
(Total Scattering coefficient	[m^{-1}]	b	s
(Beam) Attenuation coefficient	[m^{-1}]	c	α
Forward scattering coefficient	[m^{-1}]	b_f	f
Backward scattering coefficient	[m^{-1}]	b_b	b

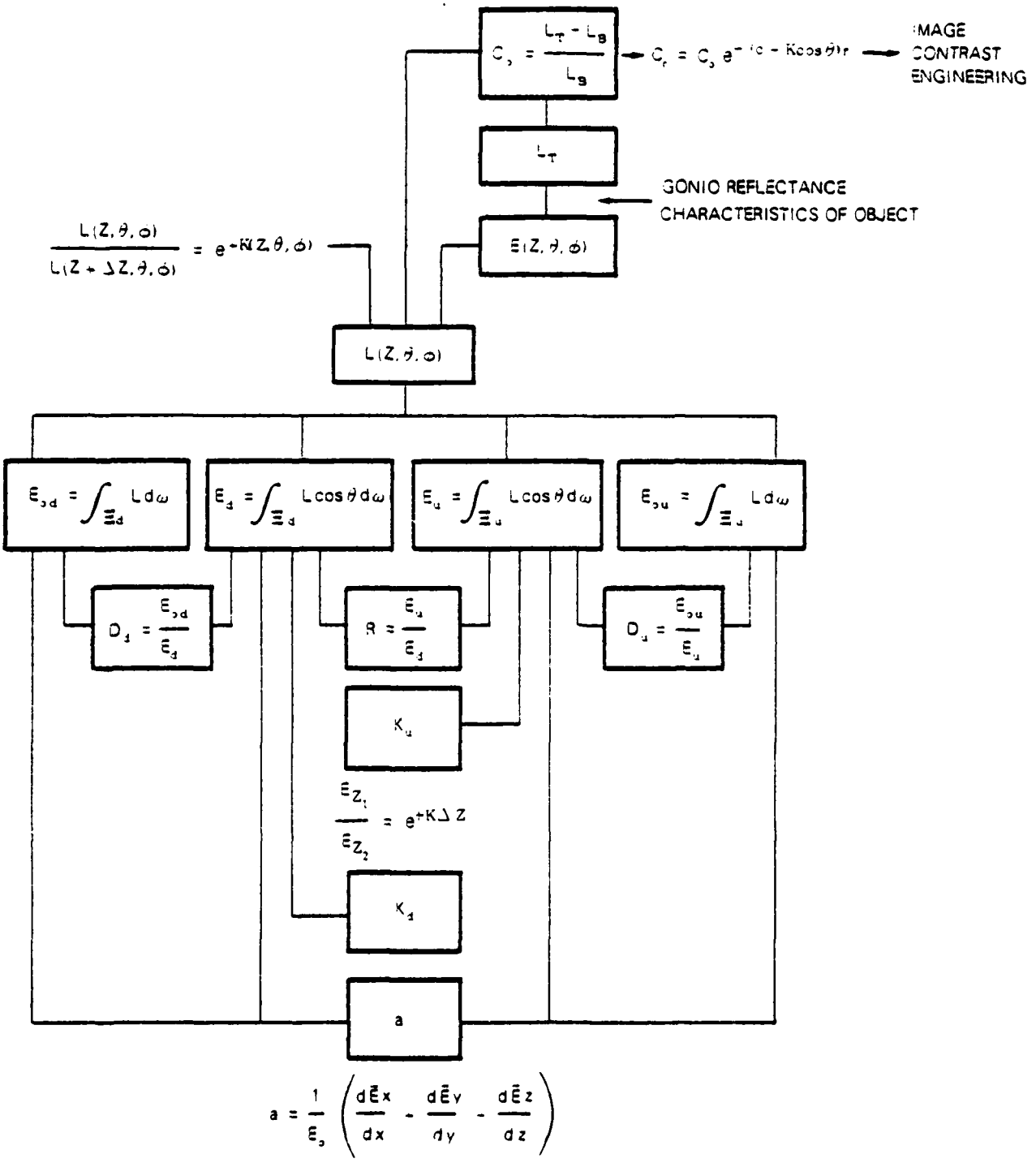

Figure 2-1. Chart illustrating optical properties which can be derived from the radiance distribution (after Tyler[7]). These properties are defined and discussed in the text.

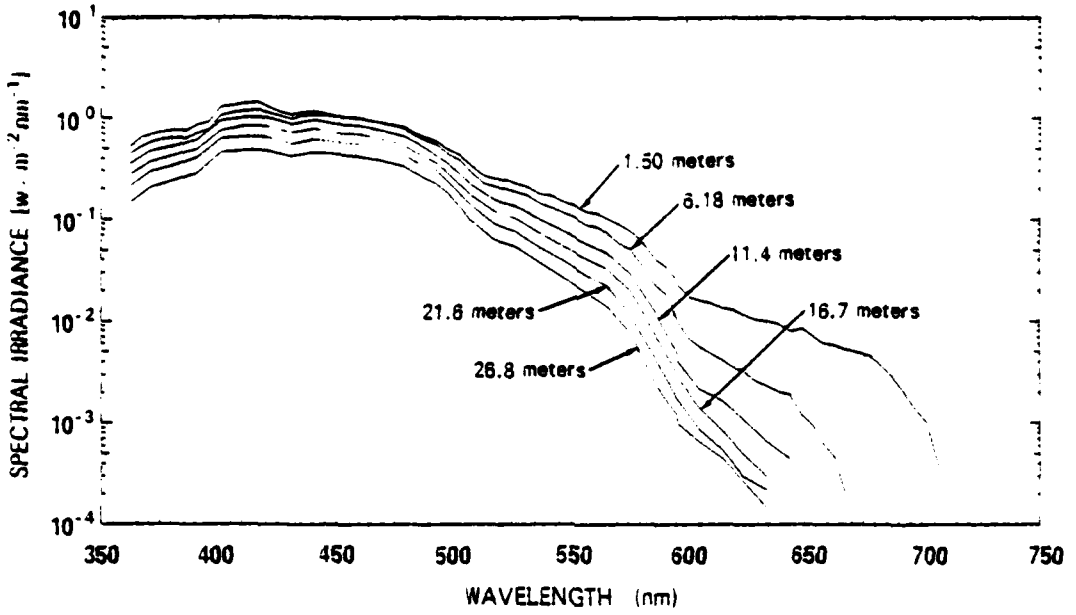

Figure 2-2. Downwelling spectral irradiance, $E_d(Z,\lambda)$, for Crater Lake (42°, 56'N, 122° 07'W)[27]

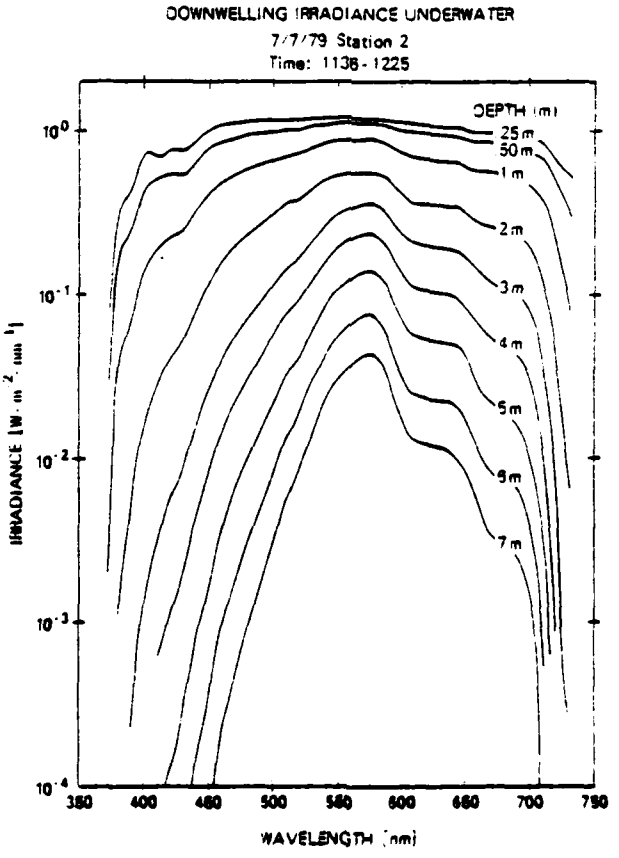

Figure 2-3. Downwelling spectral irradiance for San Vicente Reservoir (32° 50'N, 116° 55'W)

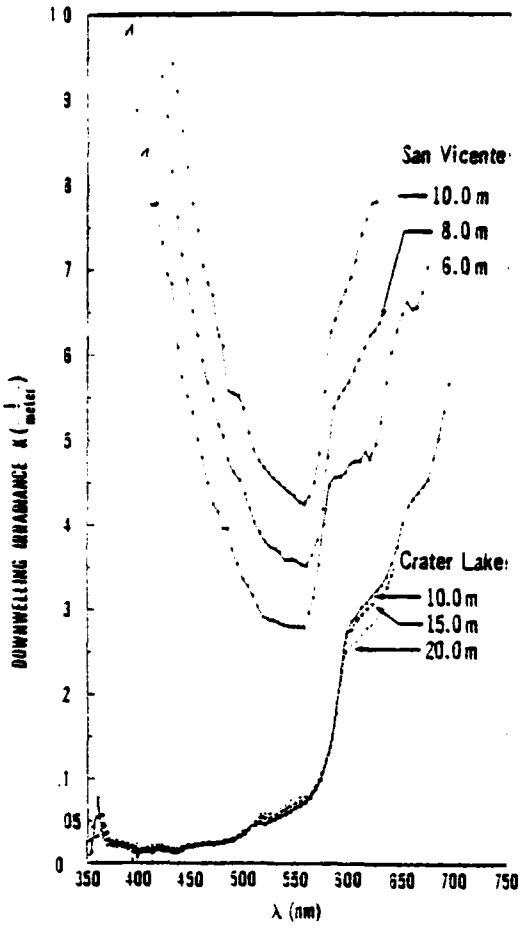

Figure 2-4. Diffuse attenuation coefficient, $K(\lambda)[m^{-1}]$, for Crater Lake[18] and San Vicente water[19].

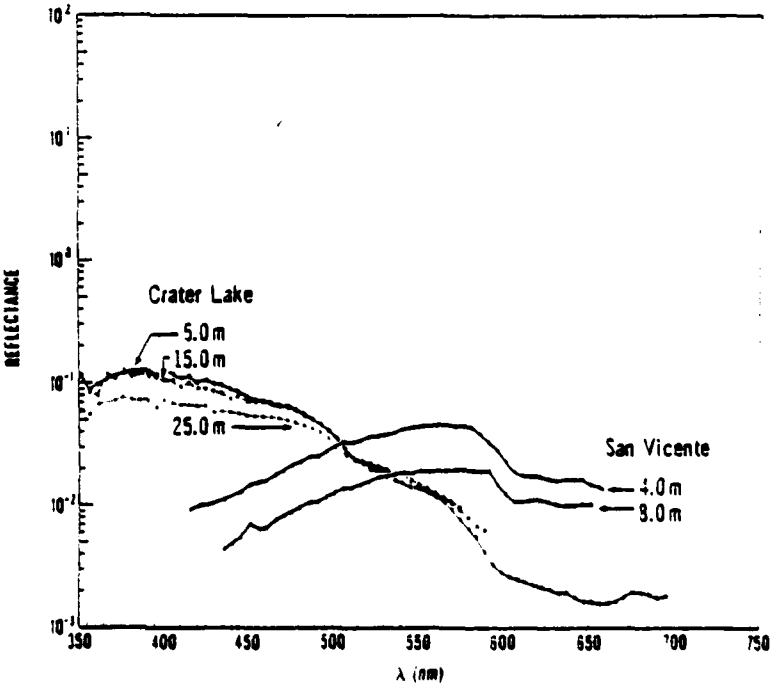

Figure 2-5. Irradiance reflectance function, $R(\lambda)$, for Crater Lake[18] and San Vicente waters[19].

3. Relationship Between Inherent and Apparent Optical Properties (H.R.G.)

A. The radiative transfer equation

The inherent and apparent optical properties of the ocean are related through the radiative transfer equation (RTE). For an exhaustive treatment of this equation and its application to optical oceanography, see Preisendorfer's *Hydrologic Optics*. The RTE governs the propagation of radiance through an absorbing, scattering, and fluorescent medium. It can be derived by keeping track of the gains and losses in power as a pencil of radiance of wavelength λ traveling in a direction $\hat{\xi}$ traverses a slab of thickness dl at $\vec{r}$ oriented normal to $\hat{\xi}$. The result for unpolarized light is

$$\frac{dL}{dl}(\vec{r},\hat{\xi},\lambda) = A_1 + A_2 + A_3 , \tag{3-1}$$

where

$$A_1 = -c(\vec{r},\lambda)L(\vec{r},\hat{\xi},\lambda)$$

accounts for the loss in radiance resulting from scattering and absorption from the pencil,

$$A_2 = \int_{\Omega'} \beta(\vec{r},\hat{\xi},\hat{\xi}',\lambda)L(\vec{r},\hat{\xi}',\lambda)\,d\Omega'$$

accounts for the increase in radiance resulting from the scattering of radiance traveling in a direction $\hat{\xi}'$ into the direction $\hat{\xi}$, and

$$A_3 = \int_{\lambda_E}\int_{\Omega'} \beta_\phi(\vec{r},\hat{\xi},\hat{\xi}',\lambda,\lambda_E)L(\vec{r},\hat{\xi}',\lambda_E)\,d\Omega'\,d\lambda_E$$

accounts for the increase in radiance produced by fluorescence excited by radiance of wavelength λ_E traveling in the direction $\hat{\xi}'$.

Given the inherent optical properties

$$c(\vec{r},\lambda),\ \beta(\vec{r},\hat{\xi},\hat{\xi}',\lambda) \text{ and } \beta_\phi(\vec{r},\hat{\xi},\hat{\xi}',\lambda,\lambda_E),$$

and the value of $L(\vec{r},\hat{\xi},\lambda)$ on the boundaries of the ocean, Eq. (3-1) can in principle be solved for the radiance $L(\vec{r},\hat{\xi},\lambda)$ throughout the medium allowing computation of other apparent optical properties. Some simplification can be introduced in the case of the ocean by observing that the length scale of horizontal variations in the attenuation coefficient is much larger than the attenuation length c^{-1}. Because of this the ocean can be treated as if it is inhomogeneous only in the *vertical*. Introducing a spherical coordinate system with origin at the sea surface and the z coordinate (depth) increasing *into* the ocean, the RTE becomes

$$\begin{aligned}\cos\theta\,\frac{dL(z,\hat{\xi},\lambda)}{dz} &= -c(z,\lambda)L(z,\hat{\xi},\lambda)\\ &+ \int_{\Omega'} \beta(z,\hat{\xi},\hat{\xi}',\lambda)L(z,\hat{\xi}',\lambda)\,d\Omega'\\ &+ \int_{\lambda_E}\int_{\Omega'} \beta_\phi(z,\hat{\xi},\hat{\xi}',\lambda,\lambda_E)L(z,\hat{\xi}',\lambda_E)\,d\Omega'\,d\lambda_E ,\end{aligned} \tag{3-2}$$

where θ is the angle between the direction $\hat{\xi}$ and the positive z axis. A famous integral[2] of this equation can be found by multiplying it by $d\Omega$ and integrating over Ω. This gives

$$\frac{dE(z,\lambda)}{dz} = -a(z,\lambda)E_0(z,\lambda) + \int_{\lambda_E} b_\phi(z,\lambda,\lambda_E)E_0(z,\lambda_E)\,d\lambda_E ,$$

where $E(z,\lambda) = E_d(z,\lambda) - E_u(z,\lambda)$. If there is no fluorescence generated at depth z, then

$$a(z,\lambda) = -\frac{1}{E_0(z,\lambda)}\frac{dE(z,\lambda)}{dz} .$$

This equation forms the basis for the so-called absorption meter described in detail by Hojerslev[3]. Clearly, the effects of fluorescence must be accounted for in detail in order to use this method for measuring absorption. The natural fluorescence observed in the ocean is due to chlorophyll-*a* *in-vivo* and phaeophytin-*a* *in-vitro*, which fluoresce near 685 nm and the yellow substances which fluoresce in the blue and near ultra-violet. The effects of chlorophyll-*a* fluorescence on radiative transfer in the ocean have been worked out[4]; however, the influence of yellow substance fluorescence has yet to be studied in detail. Since fluorescence is of minor interest in ocean optics, henceforth it will be assumed that $\beta_R=0$. A second solution of Eq. (3-2) which is of considerable value can be found in the case of a homogeneous ocean. Preisendorfer[5] and Hojerslev and Zaneveld[6] have shown that as $z\to\infty$,

$$L(z,\hat{\xi},\lambda) \to f(\hat{\xi})e^{-K(\lambda)z}.$$

Thus, at great depth, the radiance distribution is independent of the radiance distribution incident on the sea surface, which implies that in this limit both $f(\hat{\xi})$ and $K(\lambda)$ are inherent optical properties. Note that E_d, E_u, E_{od}, E_{ou}, E, and E_o all decay exponentially with the attenuation coefficient: $K(\lambda)$.

Near the surface the situation is far more complex; the various radiance and irradiance attenuation coefficients are not equal and depend on depth. The simplifications which arise in the solution of the RTE in the $z\to\infty$ case are absent and so the solution requires considerably more effort. There are several methods of attack now known which are capable of producing what are called exact solutions, *i.e.*, they provide numerical results as close to the true solution as desired. Among these are the Method of Discrete Ordinates[7], Invariant Imbedding[8,9] and Monte Carlo[10,11].

All of the above methods require at least moderate sized computers. There are several methods of finding approximate solutions to the RTE which yield analytical results. These include: the single scattering[12] method, in which photons are allowed to scatter only once in the medium; the two and four flow models[13], in which the upwelling and downwelling radiance distributions are assumed to consist of a totally diffuse radiance distribution plus a delta function to represent the unscattered solar beam; and the quasi-single scattering[14,15] approximation, in which the forward part of the volume scattering function is replaced by a delta function at $\alpha=0$ while the actual backward portion of $\beta(\alpha)$ is used. The validity of these approximate solutions depends on the ratio of the scattering coefficient to the total attenuation coefficient ($\omega_o \equiv b/c$). In estimating the up and downwelling irradiances, the single scattering model is applicable for only very small $\omega_o(\leqslant 0.05)$, while the quasi-single scattering approximation is useful over a much larger range in $\omega_o(\omega_o \leqslant 0.7)$. The two and four-flow approximations, on the other hand, provide the best results when ω_o is near unity. There are of course other exact and approximate methods of solving the RTE over and above those mentioned here; however, they have not been extensively used in ocean optics.

B. Semi-empirical relationships between inherent and apparent optical properties

The most commonly measured apparent optical properties are the up and downwelling irradiances and hence the associated irradiance attenuation coefficients $K_d(z)$ and $K_u(z)$ and the irradiance ratio $R(z)$. It is therefore of central importance to be able to relate these quantities to the inherent optical properties. Since an analytic solution to the RTE near the surface is difficult, such a relationship must be essentially empirical. The most comprehensive set of relationships published thus far are those given in Gordon, Brown, and Jacobs[11], as a result of analysis of a large number of Monte Carlo simulations of radiative transfer in the ocean. Briefly, in the quasi-single scattering approximation applied to a homogeneous ocean illuminated by a beam of *collimated* irradiance from the sun, K_d and R can be approximated by

$$\frac{K_d}{c}\cos\theta_o' = 1-\omega_o F = a+b_b,$$

$$R = \frac{1}{3}\,\frac{\omega_o B}{1-\omega_o F} = \frac{1}{3}\,\frac{b_b}{a+b_b},$$

where θ_o' is the solar zenith angle in the water. This expression for K_d is of course meaningless when the incident radiance distribution is diffuse (*e.g.*, skylight and/or cloud light) since θ_o' is undefined. The remedy for this is to note that in a non-scattering ocean, $\cos\theta_o' = 1/D_d$ and D_d is well defined even for diffuse illumination. Thus for any radiance distribution incident on the sea surface it is expected that K_d and R can be written,

$$\frac{K_d(z)}{cD_{do}(z)} = \sum_{n=0}^{N} k_n(z)(\omega_o F)^n, \tag{3-3}$$

$$R(z) = \sum_{n=0}^{N} r_n(z)[X]^n, \tag{3-4}$$

and

$$\omega_o F = \sum_{n=0}^{N} k_n'(z)\left[\frac{K_d(z)}{cD_{do}(z)}\right]^n. \tag{3-5}$$

$$Y = \sum_{n=0}^{N} a_n(z)\,[R(z)]^n \qquad (3\text{-}6)$$

where $Y = b_b/(a+b_b)$, and the subscript $_d$ has been added to D to indicate that it is the downwelling distribution function for a *totally absorbing ocean*. When K_d and R, computed from approximately 100 separate Monte Carlo simulations for collimated irradiance from the sun and a sky of totally diffuse irradiance, are fit to Eq. (3-3) and (3-5) it is found that the coefficients $k_n(z)$ can be chosen for $N=3$ so that the mean error in the equations is about 3% from the surface to an optical depth (cz) of four. Although the computations have been carried out only for a flat ocean, the results should be applicable to a rough ocean as well, since surface waves will only influence $D_{d0}(z)$, which can be computed once the form of the *incident* radiance distribution and the surface roughness is specified. Because of the fact that $K_d(z)/D_d(z)c$ depends only on the inherent optical properties and on constants which depend only on depth [$k_n(z)$] it has been termed a *quasi-inherent* optical property.

In contrast to this, when the irradiance ratios from the same simulations are fit to Eqs. (3-4) and (3-6) it is found that for a *given* radiance distribution, *i.e.*, a collimated solar beam incident at an angle θ_w (measured in water) from the zenith, or totally diffuse irradiance, the coefficients $r_n(z)$ and $r_n(z)$ for $N=3$ can be chosen so that the mean error is about 2%. For $0 \leqslant \theta_w \leqslant 20°$, these coefficients are essentially independent of θ_w, however, above 20° $R(z)$ begins to depend on θ_w. Even so, the total variation never exceeds about 15% as the solar position varies from zenith to horizon.

Simulations have also been carried out for a vertically stratified ocean[5]. The principal result of these simulations is the discovery that Eqs. (3-3) and (3-5) remain valid even in the presence of strong stratification as long as ω_0, F and c are evaluated at depth z, *i.e.*,

$$\frac{K_d(z)}{c(z)\,D_{d0}(z)} = \sum_{n=0}^{N} k_n(z)\,[\omega_0(z)\,F(z)]^n .$$

where the coefficients $k_n(z)$ are the same as those in Eq. (3-3). This indicates that $K_d(z)/c(z)D_{d0}(z)$ and therefore $K_d(z)/D_{d0}(z)$ is a *local* property of the medium; that is, its value at a given depth z depends, for the most part, only on the values of the inherent optical properties at the same depth z. This provides further justification for labeling K_d/D_{d0} a *quasi-inherent optical* property.

The irradiance *ratio* $R(z)$, however, does not possess this useful property. Clearly, at a given depth z because the upwelling irradiance was scattered from layers of the medium at depths greater than z while most of the downwelling irradiance at z was not, the irradiance ratio must depend on the inherent optical properties at depths greater than z. Hence the irradiance ratio is a *non-local* property of the medium in that even though it is, for the most part, expressible directly in terms in the inherent optical properties, it cannot be expressed in terms of these properties at a given depth.

Summarizing, Eqs. (3-3) to (3-6) can be used in the case of a homogeneous ocean to accurately relate the apparent optical properties K_d and R to the inherent optical properties a, b, and b_b. In a vertically stratified ocean, Eqs. (3-3) and (3-4) remain valid if the inherent optical properties in these equations are evaluated at the depth at which the apparent properties are desired or measured.

This section will be closed by presenting two examples of the possible use of these relationships in estimating the inherent optical properties a, b_b, and b from measurements of K_d, c, and R for a homogeneous ocean, and K_d, c, $\beta(45°)$, $\beta(90°)$, $\beta(135°)$ for a stratified ocean.

In a homogeneous ocean, once D_{d0} is computed, $\omega_0 F$ ($\equiv Y$) can be found from K_d/cD_{d0} and $Y = b_b/(a+b_b)$ from R. Then

$$b_b = c(1-Y)Y$$
$$b = c(X - Y - XY)$$
$$a = c - b .$$

If the ocean is inhomogeneous, a fact that can be easily ascertained by examination of K_d/cD_{d0} as a function of depth, Eq. (3-6) cannot be used and another technique must be found to replace the *information* supplied by this equation. One possibility which has been suggested[7] is to measure $\beta(45)$, $\beta(90)$, and $\beta(135)$ and fit these to the analytic formula

$$\beta_{esf}(\alpha) = \beta(90)/[(1-e_f\cos\alpha)(1-e_s\cos\alpha)]^2 .$$

Then $\beta_{esf}(\alpha)$ can be used to find b_b through

$$b_b = 2\pi \int_{\pi/2}^{\pi} \beta_{esf}(\alpha)\sin\alpha\, d\alpha .$$

This should provide an estimate to b_w accurate to within about 5 to 10%. Note, B_{90} cannot be used to find b_w. Again, $K_d \cdot D_{10}$ provides b and

$$b = \gamma b_w,$$

and

$$a = \zeta - b.$$

Thus, these empirical relationships can be used to determine the scattering and absorption coefficients without having to resort to the difficult small angle scattering measurements or the absorption meter.

References (§ 3)

1. Preisendorfer, R. W., *Hydrologic Optics*, Vol. I - VI, U.S. Government Printing Office, Boulder, Colorado (1976).

2. Gershun, A., "The Light Field", *J. Math. Phys.* **18**, 51-151 (1939).

3. Højerslev, N. K., "A Spectral Light Absorption Meter for Measurements in the Sea", *Limnol. Oceanogr.*, **20**, 1024-1034 (1975).

4. Gordon, H. R., "Diffuse Reflectance of the Ocean: The Theory of its Augmentation by Chlorophyll-a Fluorescence at 685 nm", *Appl. Opt.* **18**, 1161-1166 (1979).

5. Preisendorfer, R. W., "Theoretical Proof of the Existence of Characteristic Diffuse Light in Natural Waters", *J. Mar. Res.*, **18**, 1-9 (1959).

6. Højerslev, N. K. and Zaneveld, J. R. V., "A Theoretical Proof of the Existence of the Submarine Asymptotic Daylight Field", *J. Geophys. Res.* (in press).

7. Chandrasekhar, S., *Radiative Transfer*, Dover, New York (1960).

8. Preisendorfer, R. W., *Radiative Transfer on Discrete Spaces*, Pergamon, Oxford (1965).

9. Plass, G. N., Kattawar, G. W., and Catchings, F. E., "Matrix Operator Theory of Radiative Transfer". 1. Rayleigh Scattering, *Appl. Opt.*, **12**, 314-329, 1973.

10. Plass, G. N., and Kattawar, G. W., "Monte Carlo Calculations of Radiative Transfer in the Earth's Atmosphere-Ocean System: I. Flux in the Atmosphere and Ocean", *J. Phys. Ocean.* **2**, 139-145 (1972).

11. Gordon, H. R., Brown, O. B., and Jacobs, M. M., "Computed Relationships Between the Inherent and Apparent Optical Properties of a Flat Homogeneous Ocean", *Appl. Opt.* **14**, 417-427 (1975).

12. Jerlov, N. G., *Marine Optics*, Elsevier, Amsterdam (1976).

13. Duntley, S. Q., "Optical Properties of Diffusing Material", *J. Opt. Soc. Am.*, **32**, 61-69 (1942).

14. Hansen, J. E., "Multiple Scattering of Polarized Light in Planetary Atmospheres II Sunlight Reflected by Terrestrial Clouds", *J. Atmos. Sci.* **28**, 1400 (1971).

15. Gordon, H. R., "Simple Calculation of the Diffuse Reflectance of the Ocean", *Appl. Opt.* **12**, 2803-2804 (1973).

16. Gordon, H. R., "Irradiance Attenuation Coefficient in a Stratified Ocean: A Local Property of the Medium", *Appl. Opt.* (submitted).

17. Gordon, H. R., "Radiative Transfer in the Ocean: A Method for Determination of Absorption and Scattering Properties", *Appl. Opt.* **15**, 2611-2613 (1976).

4. Geophysical Applications (R. V. Z.)

It follows from elementary considerations that if the nature of the particulate matter does not change, the particle attenuation coefficient, particle scattering coefficient, or particle volume scattering coefficient at any angle must be proportional to the particle concentration.

Optical measurements are thus ideal for the determination of particle concentrations *in-situ*. For example, Fig. 1-5 in Section I showed the high correlation between total suspended mass and the beam attenuation coefficient. While it would be possible in principle to determine the correlation between c and particle concentration from Mie theory if the particle characteristics were precisely known, this is generally not possible. In order to calibrate an optical device it is thus necessary to take water samples and measure the particle weight or volume concentration directly after which a correlation curve for the optical and particle parameters can be obtained. This correlation is only valid for the limited region in which the particle nature is not expected to change.

The link between ocean circulation and optical parameters via particulate matter is often difficult as the particle source must be identified. Particles, furthermore, are nonconservative on time scales longer than several days. Biological and chemical processes can generate and destroy particles as well as modify existing size distributions. Vertical settling of particulate matter also affects the distribution of SPM in the ocean. On the other hand, on times scales short compared to settling, biological and chemical processes at a given location, particles behave in a conservative manner so that they can be used as tracers of currents. This fact has been used to advantage in studies of upwelling[1,2,3] (see Fig. 1-10) in which transport routes can be deduced from the distribution of optical properties. We have already shown (Fig. 1-9) that river water could be traced for 300 km in the ocean using light scattering. Small particles in the 1 to 2 μm range settle only about 10 m per year and can be used as tracers in the deep ocean over large distances[3]. Forward scattering profiles have been used to study microstructure in the ocean[9]. Pak, *et al.*[7] have used transmission minima at 400 m depth off Peru to demonstrate offshore transport over at least 1000 km. This offshore transport of particulates is of significance to the generation of the oxygen minimum in the Eastern tropical Pacific. Biscaye and Eittreim[8] used light scattering measurements to show that large scattering and hence high particle concentrations correlated well with the Western boundary undercurrent in the Atlantic. Optical measurements have been used by Kullenberg[4] and Zaneveld and Pak[10] to study diffusion at oceanic fronts. The latter authors point out that an optical amplification of the boundary between two water masses is often present (Fig. 4-1). This is a result of the front between two water masses being a unique environment in which phytoplankton growth can be more pronounced than on either side of the front. As these examples have shown, optical properties can be of considerable use in the study of ocean circulation, particularly in those cases where the usual hydrographic parameters show little variation.

When an optical devise is used in combination with a current meter it becomes possible to measure particle fluxes *in-situ*. Bartz, *et al.*[11] have recently developed a lightweight beam transmissometer with low power consumption that can be installed into the vane of a current meter. The signal is recorded on the current meter recorder. Figure 4-2 shows a resuspension event recorded in this manner. Optical devices can thus be used for the study of sediment transport.

References (§ 4)

1. Zaneveld, J. R. V., "Variation of Optical Sea Parameters With Depth", in *AGARD-NATO Lecture Series No. 61, Optics of the Sea: AGARD-LS-61* (1973).

2. Pak, H., G. F. Beardsley, Jr., and R. L. Smith, "An Optical and Hydrographic Study of a Temperature Inversion Off Oregon During", Upwelling J. Geophys. Res., 75(3): 629-636 (1970).

3. Kitchen, J., J. R. V. Zaneveld and H. Pak, "The Vertical Structure and Size Distributions of Suspended Particles Off Oregon During the Upwelling Season", Deep-Sea Res., 25: 453-468 (1978).

4. Kullenberg, G., "The Distribution of Particulate Matter in a Northwest African Coastal Upwelling Area", in *Suspended Solids in Water, Marine Science Series, 4*, R. J. Gibbs (ed) (Plenum Press, New York, 1974), pp. 195-202.

5. Jerlov, N. G., *Marine Optics*, Elsevier Scientific Publishing Company, Amsterdam 231pp. (1976).

6. Armi, L., "Mixing in the Deep Ocean - The Importance of Boundaries", Oceanics, 21(1): 14-19 (1978).

7. Pak, H., L. Codispoti, and J. R. V. Zaneveld, "An Intermediate Particle Maximum Associated with Low Oxygen Water Off Peru", submitted to J. Geophys. Res.

8. Biscaye, P. E., and S. L. Eittreim, "Suspended Particulate Loads and Transports in the Nepheloid Layer of the Abyssal Atlantic Ocean", Mar. Geol. 23: 155-172 (1977).

9. Kullenberg, G., "Light Scattering Observations in Frontal Zones", J. Geophys. Res. 83(C9) 4683-4690 (1978).

10. Zaneveld, J. R. V. and H. Pak, "Optical and Particulate Properties of Oceanic Fronts", J. Geophys. Res., in press (1979).

11. Bartz, R., J. R. V. Zaneveld and H. Pak, "A Transmissometer for Profiling and Moored Observations in Water", SPIE Vol. 160, Ocean Optics V, 102-108 (1978).

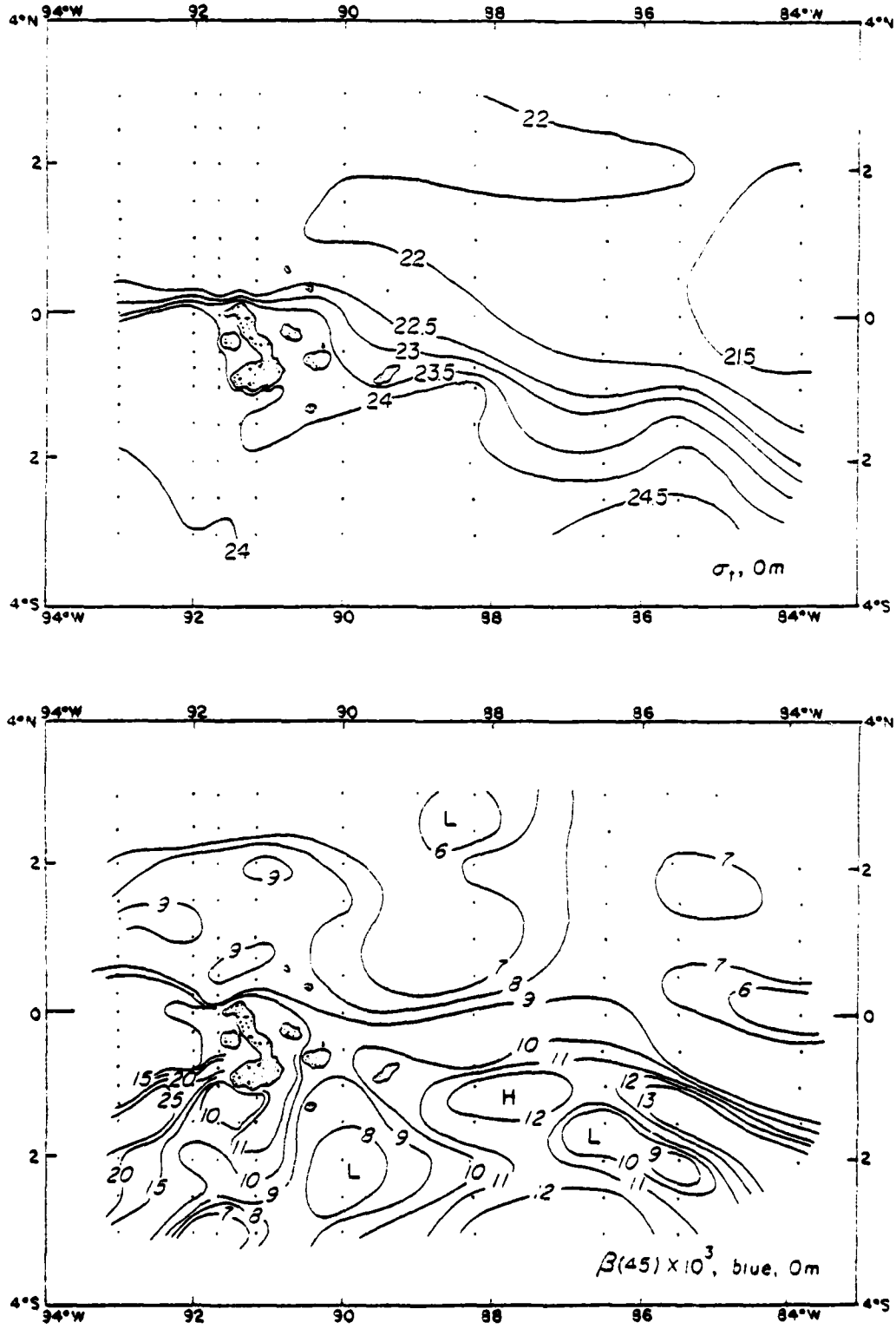

Figure 4-1. (a) Density (σ_t) in the sea surface near the Galapagos Islands. (b) Light scattering at 45° for the same region. Note scattering maximum at the front.

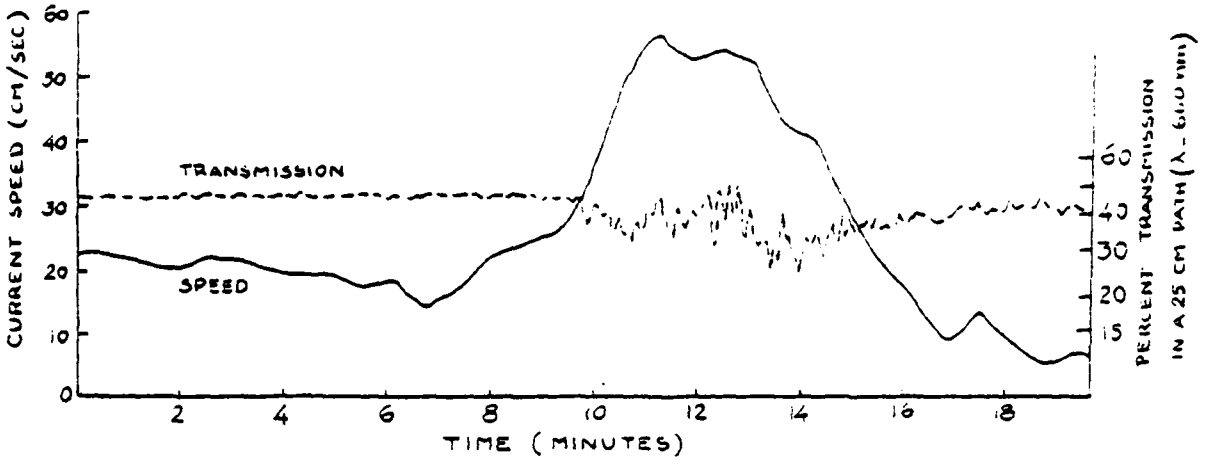

Figure 4-2. Transmission in a 25 cm path and current speed as measured off the Oregon coast in about 60 m water depth and 1 m above the bottom. From (11).

5. Bio-Optics (R.C.S.)

The production of organic matter in the ocean by phytoplankton is a fundamental process for life on earth. One of the basic requirements in understanding the processes of oceanic primary production is a knowledge of its relation to submarine irradiance. The penetration of radiant energy to depths is a function of the optical properties of ocean waters, which are in turn a function of dissolved and suspended organic material. The concept of "bio-optical state" has been introduced to represent a measure of the total effect of biological processes on the optical properties. This concept has proved useful to the extent that diverse constituents in natural waters can be described by a few optical parameters, which represent a meaningful average status of the biological material in the ocean water at a particular time and place. In this section we will: describe the relation of oceanic primary production to available photosynthetic irradiance; optically classify natural waters in terms of dissolved and suspended biogenous material; discuss how this classification is useful for the remote sensing of chlorophyll; and describe how these bio-optical data can be incorporated into existing models for the description of primary production.

Photosynthetic Irradiance. When considering oceanic primary productivity it is important to distinguish between available, useable and stored radiant energy. This has been discussed in detail by Morel[5] and the following is a brief synopsis of his development. It is preferable, when discussing photoprocesses, to convert spectral irradiance to quantum units.

$$E^q(\lambda)\,[\#quanta \cdot s^{-1} \cdot m^{-2} \cdot nm^{-1}] = \frac{\lambda}{hc} \cdot E_e(\lambda)\,[W \cdot m^{-2} \cdot nm^{-1}] \qquad (5\text{-}1)$$

where

$$c \approx 3\times10^{8}\ [m \cdot s^{-1}]\ ,$$

and

$$h \approx 6.6\times10^{-34}\ [J \cdot s]\ .$$

The instantaneous photosynthetically available radiation, PAR_i is defined as the amount of radiant energy at each depth within the spectral range from 350 to 700 nm[5], i.e.

$$PAR = \int_{350}^{700} E^q(\lambda)\ d\lambda \qquad (5\text{-}2)$$

This definition includes all photons within the spectral band, independent of their possible usefulness for carrying out photosynthesis. PAR is the easiest and most routinely measured of the energy quantities we shall discuss. Further, if K^q is the total diffuse attenuation coefficient for the downwelling quantum irradiance, then

$$PAR(Z) = PAR(0^-)\ e^{-K^q \cdot Z} \qquad (5\text{-}3a)$$

or

$$\ln\left\{\frac{PAR(Z)}{PAR(0^-)}\right\} = -K^q \cdot Z \qquad (5\text{-}3b)$$

In order to be used for photosynthesis these available photons must first be absorbed by algal pigments. Morel defined the photosynthetically useable (i.e. absorbed) radiation, PUR, as the fraction of radiant energy absorbed by the algae. PUR depends on the pigment composition of the algal population as well as on the spectral irradiance. [5]

$$PUR = \int_{350}^{700} E^q(\lambda)\ a(\lambda)\ d\lambda \qquad (5\text{-}4)$$

where $a(\lambda)$ is the fraction of energy, at each wavelength, absorbed by algae and is proportional to the [illegible] phytoplankton spectral absorption coefficient. PUR is not directly measureable, but can be computed using the above equation if the in-

...to absorption of living phytoplankton is known (or can be inferred).

Lastly, that portion of absorbed energy that is actually transferred into stored chemical energy in the form of organic matter through photosynthesis is called the photosynthetically stored radiation, PSR. As discussed below PSR can be calculated from measurements of primary productivity.

These three quantities are related by the inequalities,

$$PAR > PUR > PSR \tag{5-5}$$

In addition, these energy parameters, and their ratios, play a fundamental role in the description of marine photosynthesis. Primary production per unit biomass (expressed as the chlorophyll-*a* concentration), P_B, is the ratio of carbon fixed to the concentration of chlorophyll-*a*. Thus P_B has the units $(mg\ C \cdot m^{-3} \cdot day^{-1}) \cdot (mg\ Chl\text{-}a \cdot m^{-3})^{-1}$, and for the following discussion PAR, PUR and PSR are considered to be integrated over time to give their respective daily energy rates.

The photosynthetic yield (per unit chlorophyll concentration), Y, is defined as the ratio of P_B to PAR,

$$Y \equiv \frac{P_B}{PAR}\left[\frac{(mg\ C \cdot day^{-1}) \cdot (mg\ Chl\text{-}a)^{-1}}{\#quanta \cdot m^{-2} \cdot day^{-1}}\right] \tag{5-6}$$

In general, the photosynthetic yield increases with increasing depth as the available irradiance decreases. The radiation utilization coefficient, k_s, characterizes the photosynthetically stored radiation and is defined as the ratio of PSR (per unit chlorophyll concentration) to PAR,

$$k_s \equiv \frac{PSR}{PAR}\ [m^2 \cdot (mg\ Chl\text{-}a \cdot m^{-3})^{-1}] \tag{5-7}$$

This coefficient, k_s, is simply the photosynthetic yield, Y, after having converted the production to its equivalent in stored energy.

The quantum yield, which is the quantity most generally used by photobiologists in discussing photosynthesis, is defined as the number of molecules transformed (that is CO_2 molecules consumed or O_2 molecules liberated) per absorbed light quanta[4]. Thus, in our notation, the quantum yield (per unit chlorophyll concentration) Φ is given by

$$\Phi \equiv \frac{P_B}{PUR}\left[\frac{(mg\ C) \cdot (mg\ Chl\text{-}a \cdot m^{-3})^{-1}}{\#quanta\ absorbed}\right] \tag{5-8}$$

The quantum yield is independent of the optical properties of sea water and reflects the state of physiological adaption of the algae[5].

Finally, a dimensionless parameter is defined to express the efficiency of utilization of radiant energy by phytoplankton. Actually two such dimensionless ratios have been defined in the literature and it is important to distinguish between them. Morel[2], following the suggestion of Platt[6], introduces the ratio, ϵ_s, to express the ratio of energy chemically stored, to the energy removed from the submarine irradiance by all physically and chemical processes. Thus it follows that

$$\epsilon_s = \frac{k_s \cdot C}{K^d}, \tag{5-9a}$$

or alternatively

$$\epsilon_s = \frac{\frac{PSR}{PAR} \cdot C}{K^d}, \tag{5-9b}$$

where C is the chlorophyll-*a* concentration, K^d is defined in Eq. (5-3) and k_s in Eq. (5-7). The pure number ϵ_s is characteristic of both the water mass and its algal content, and its parameters are measureable so that it can be calculated at all depths.

A similar dimensionless ratio, which has occurred frequently in mathematical models of primary productivity[7,8,9], is the ratio ϵ_p, of energy absorbed by viable phytoplankton to the energy absorbed not only by water and its non-phytoplankton components, but also any pigments of dead and decaying algae; *i.e.*,

$$\epsilon_p = \frac{k_p \cdot C}{K^d}, \tag{5-10a}$$

or alternatively

$$\epsilon_u = \frac{\frac{PUR}{PSR} \cdot C}{K^*} \qquad (5\text{-}10b)$$

where k_c is the specific attenuation coefficient for viable phytoplankton. It has frequently been expedient to assume that k_c can be approximated by the specific attenuation coefficient of chlorophyll-like pigments[11], an assumption that neglects the contribution of accessory pigments to photosynthesis. This expedient then allows ϵ_u to be estimated from published values of $k_c(\lambda)$ for chlorophyll-like pigments[11]. Even if absorption by accessory pigments are accounted for in Eq. (5-10a), ϵ_c and ϵ_u will differ according to Eqs. (5-9b) and (5-10b) by the distinction between the absorbed (PUR) and actually stored (PSR) energy terms. To date, this distinction has not been explicit in most models of primary production.

Having described underwater radiant energy in terms of marine productivity we turn now to discuss the influence of biogenous material on the optical properties of water.

Bio-optical classification. In an attempt to bring about some order in experimental spectral irradiance data Jerlov[2] suggested a scheme of optical classification of ocean water that has recently been updated and broadened[13]. More recently Smith and Baker[11] have developed a bio-optical classification of natural waters in terms of the dissolved and suspended biogenous material present. This classification provides a good first approximation for spectrally characterizing the bio-optical state of ocean waters when dissolved and suspended material is primarily of biogenous origin and provides a point of departure for more detailed analysis. In the subsequent discussion we follow the development of Smith and Baker[11].

In this development the concentration of chlorophyll-like pigments is used as a key biological parameter for classifying ocean water types. By making use of Beer's law and taking into account non-linear biological effects which influence ocean optical properties, a general relationship between the total diffuse attenuation coefficient for irradiance and the average chlorophyll-like pigment concentration has been obtained for two regimes of concentration, viz.,

$$K_T(\lambda) - K_w(\lambda) = k_1(\lambda) \cdot C_K \qquad C_K < 1 \qquad (5\text{-}11)$$

$$K_T(\lambda) - K_w(\lambda) = k_2(\lambda) \cdot C_K + K_{x2}(\lambda) \cdot C_K > 1 \qquad (5\text{-}12)$$

Here, $K_T(\lambda)$ is the total downward diffuse attenuation coefficient for irradiance. $K_w(\lambda)$ is the diffuse attenuation coefficient for clear ocean waters, $k_1(\lambda)$ is the specific spectral attenuation coefficient due to plankton pigment, $k_2(\lambda)$ is the specific attenuation coefficient due to plankton and covarying detrital material, and C_K is the average concentration of chlorophyll-*a* plus phaeophytin to a depth of one diffuse attenuation length, K_T^{-1}. Thus,

$$C_K = \frac{1}{K_T^{-1}} \int_0^{K_T^{-1}} C(Z)\,dZ \qquad (5\text{-}13)$$

where $C(Z)$ is the chlorophyll-*a* + phaeopigment concentration of depth Z. The spectral parameters for Eqs. (5-11) and (5-12) are given in references 11 and 14. By using published data for these spectral parameters, a measure of C_K is sufficient to calculate $K_T(\lambda)$ for the water under consideration. Further, since

$$E_d(Z,\lambda) = E_d(0,\lambda)\, e^{-K_T(\lambda) \cdot Z} \qquad (5\text{-}14)$$

where $E_d(0,\lambda)$ is the downwelling spectral irradiance just beneath the ocean surface, it is then possible to calculate spectral irradiance at any depth, using this equation, provided $E_d(0,\lambda)$ is known.

As an example, Fig. 5-1, shows a comparison of experimentally measured (solid curves) and calculated values (dashed curves) of the diffuse attenuation coefficient for irradiance, $K_T(\lambda)$, for several ocean waters varying in chlorophyll-like pigment concentrations. The agreement between the calculated and experimental curves is satisfactory and indicates that Eqs. (5-11) and (5-12), along with the parameters published by Smith and Baker[11], provides a reliable method for estimating $K_T(\lambda)$, and hence the penetration of spectral irradiance into ocean waters, from a knowledge of the chlorophyll-like pigment concentration.

The spectral values for $K_T(\lambda)$ and $k_2(\lambda)$ can be related to K^* and k_c defined above by using $K_T(\lambda)$ and $k_2(\lambda)$ in Eqs. (5-11), (5-12) and (5-14) to obtain the downwelling spectral irradiance for various depths for the desired value of C_K, calculating the total quanta at each depth via Eq. (5-1); plotting total quanta vs depth, with C_K as a parameter, to obtain K^* and k_c. Smith and Baker carried out this procedure and found $K^* = k_2 = 0.14\ (m^2\ mg\ Chl\text{-}a)^{-1}$ in agreement with other workers[15,16,17,18].

Thus the ratio ϵ_u, giving the fraction of radiant energy attenuated (absorbed) by chlorophyll-like pigments (viable phytoplankton), can be estimated from a knowledge of the chlorophyll concentration by use of the above equations. In addition, since this model allows PUR to be estimated as a function of depth in natural waters, it also provides a technique

for estimating the *in-situ* quantum yield of photosynthesis via Eq. (5-8). Finally, this bio-optical classification provides an analytic framework for the development of algorithms designed to relate the upwelling spectral radiance from the ocean to the ocean chlorophyll concentration.

Remote sensing of ocean chlorophyll. Chlorophyll is a rough, albeit accepted, measure of phytoplankton biomass. Hence measurements of chlorophyll as a function of time in an oceanographic region can be used to estimate the primary productivity of a region. Also, it is known that chlorophyll (phytoplankton) is variable, or patchy, on a broad spectrum of spatial and temporal scales. This patchiness is so pervasive and general that there is little question of its ecological and evolutionary importance[19]. This variability also affects our ability to detect significant spatial and temporal changes in phytoplankton abundance. As a consequence it is of great importance that we understand the nature of this variability, its causes and effects.

It is also becoming increasingly clear that chlorophyll variability includes length scales up to hundreds of kilometers that seem to be related to various "large scale" physical phenomena including: upwelling, eddies, convergences, shear-zones, currents, underwater topography and island effects. The spatial scales of the chlorophyll variability associated with these phenomena make conventional shipboard sampling techniques inadequate and provides a strong incentive for complementary satellite sampling.

It has been demonstrated that the remote sensing from spacecraft of the upwelling spectral radiant energy from the ocean's surface makes it possible to synoptically determine ocean chlorophyll concentration. Equations (5-11) and (5-12) show how the near surface chlorophyll concentration is related to $K_T(\lambda)$. By relating the reflectance of ocean waters, $R(\lambda)$, to $K_T(\lambda)$ (or alternatively directly relating $R(\lambda)$ to the chlorophyll concentration) we can construct an algorithm linking the spectral upwelling signal from the ocean to the desired chlorophyll concentration.

There are several theoretical methods available for relating K_T to the irradiance reflectance, $R(\lambda)$, of ocean waters[21,22,23,24,25]. For the sake of simple illustration we adopt the expression[25],

$$R(\lambda) \approx \frac{1}{3} \frac{b_b(\lambda)}{a(\lambda)} \tag{5-15}$$

where the total backscattering coefficient, b_b, and the total absorption coefficient have been discussed in an earlier section. The spectral nature of the backscattering coefficient has been discussed[22,25], and *measured*[26] for various cultures of ocean phytoplankton. Again for simplicity, we can estimate $a(\lambda)$ by means of an approximation given by Preisendorfer[24],

$$a(\lambda) \approx \frac{3}{4} K_T(\lambda) . \tag{5-16}$$

More accurate approximations are also available[24]. This example demonstrates that by means of Eqs. (5-11), (5-12), (5-15) and (5-16) the ocean reflectance (color) can be related to the surface chlorophyll concentration. Figure 5-2 and 5-3 demonstrate how the reflectance, and ocean color, are effected by increasing concentrations of chlorophyll. This link demonstrates the basis for the remote sensing of chlorophyll concentration in ocean waters (and will be discussed in more detail in Section 6). Thus there exists the potential to measure primary productivity on a regional basis and to synoptically study chlorophyll patchiness and the phenomena giving rise to this variability.

Primary production equations. Bannister, in discussing primary production equations in terms of chlorophyll concentration, quantum yields and upper limits to production, has shown that the factor $k_1 C (K^{-1})^{-1}$ occurs in the production equations of a number of authors[5,7,10]. This factor, defined above by Eq. (5-10), is the fraction of total energy absorbed by viable phytoplankton. Bannister[5,7], reviewed these earlier equations and recast them into more fundamental and general forms. In particular, he showed that equation for daily primary production can be written

$$\Pi \left[g\ C\ m^{-2}\ d^{-1}\right] = \Psi \cdot \frac{k_1 C}{K^d} \tag{5-17a}$$

or

$$= \Psi \cdot \epsilon_a . \tag{5-17b}$$

where $\Psi\left[g\ C\ m^{-2}\ d^{-1}\right]$ is an unsurpassable upper limit to productivity corresponding to the absorption of all available radiant by viable phytoplankton. Ψ is not a function of chlorophyll concentration, but rather only of incident irradiance, day length, and photosynthetic parameters. Bannister[5] discussed the dependence of Ψ on algal parameters. Incident irradiance and day length are ancillary information that can be determined by, or in conjunction with, satellite data. Thus, to the extent that the physiological parameters of phytoplankton are measurable or predictable from surface data, Ψ can be estimated from satellite data. Further, these estimates can be made over spatial and temporal scales that are, at best, impractical to obtain from surface vessels.

Our understanding of the fundamental relationships between the environment, primary production and higher trophic levels is limited. This is in no small measure due to our inability, up to now, to obtain appropriate synoptic data. Satellite data will provide significant complementary information to that gathered at the ocean surface, that will allow the spatial and temporal variability inherent in the biological data to be more completely assessed.

We have shown how natural radiant energy, the optical properties of ocean water, primary productivity and models describing this productivity are inter related. Further, we have shown how these production equations provide a direct theoretical framework with which to connect remotely sensed data on the biological state of ocean waters to the gross daily production in the water column. Thus we have a theoretical framework, and are on the threshold of obtaining new extensive experimental data, with which to study plankton production in the world's oceans.

References (§ 5)

1. Smith, R. C. and K. S. Baker, "The Bio-Optical State of Ocean Waters and Remote Sensing", Limnol. Oceanogr. 23, 247-259 (1978).

2. Morel, A., "Available, Useable, and Stored Radiant Energy in Relation to Marine Photosynthesis", Deep Sea Research 25, 673-688 (1978).

3. Tyler, J. E. ed. Report on The Second Meeting of The Joint Group of Experts on Photosynthetic Radiant Energy, UNESCO Technical Papers on Marine Science, No. 2, 1-11 (1966).

4. Rabinowitch, E., and Govindjee, *Photosynthesis* (Wiley, New York, 1969).

5. Bannister, T. T., "Production Equations in Terms of Chlorophyll Concentration, Quantum Yield, and Upper Limit to Production", Limnol. Oceanogr. 19, 1-12 (1974a).

6. Platt, T., "The Concept of Energy Efficiency in Primary Production", Limnol. Oceanogr 14, 653-659 (1969)

7. Bannister, T. T., "A General Theory of Steady State Phytoplankton Growth in a Nutrient Saturated Mixed Layer" Limnol. Oceanogr. 19, 13-30 (1974b).

8. Vollenweider, R. A., "Calculation Models of Photosynthesis - Depth Curves and Some Implications Regarding Day Rate Estimates in Primary Production Measurements", p. 425-457, in C. R. Goldman (ed) Primary Productivity in Aquatic Environmenta. Mem. Ist. Ital. Idrobiol. 18 (suppl) (1965).

9. Steel, J. N., "Environmental Control of Photosynthesis in The Sea", Limnol Oceanogr. 7, 137-150 (1962).

10. Fee, E. J., "A Numerical Model for the Estimation of Photosynthetic Production, Integrated Over Time and Depth, in Natural Waters", Limnol. Oceanogr. 14, 906-911 (1969)

11. Smith, R. C. and K. S. Baker, "Optical Classification of Natural Waters", Limnol. Oceanogr. 23, 260-267 (1978)

12. Jerlov, N. G., "Optical Oceanography", Elsevier Scientific Pub. Co., New York (1972).

13. Jerlov, N. G., "Marine Optics", Elsevier Scientific Pub. Co., New York, 231 (1976)

14. Austin, R. W., T. J. Petzold, R. C. Smith and J. E. Tyler, Handbook of Underwater Optical Measurements, in preparation (1980)

15. Megard, R. O., "Phytoplankton, Photosynthesis, and Phosophorus in Lake Minnetonka, Minnesota", Limnol Oceanogr. 17, 68-87 (1972)

16. Tailing, J. F., "Generalized and Specialized Features of Phytoplankton as a Form of Photosynthetic Cover", p 431-435, in Prediction and Measurements of Photosynthetic Production. Centre Agr. Publ. Doc., Wageningen (1970)

17. Lorenzen, M., "The Role of Artificial Mixing in Eutrophication Control", Ph.D. thesis, Harvard Univ. (1972)

18. Lorenzen, C. J., "Extinction of Light in the Ocean by Phytoplankton", J. Cons., Cons. Int. Explor. Mer 34, 263-267 (1972).

19. Haury, L. R., J. A. McGowan and P. H. Wiebe, "Patterns and Processes in the Time-Space Scales of Plankton Distributions".

20. Duntley, S. Q., "Optical Properties of Diffusing Material", *J. Opt. Soc. Am.*, 32, 61-69 (1942)

21. Duntley, S. Q., Austin, R. W., Wilson, W. H., Edgerton, C. F., and Moran, S. E., "Ocean Color Analysis", Scripps Institution of Oceanography, Ref. 74-10 (1974)

22. Gordon, H. R., O. B. Brown and M. M. Jacobs, "Computed Relationships Between the Inherent and Apparent Optical Properties of a Flat Homogeneous Ocean", Appl. Opt. 14, 417-427 (1975)

23. Prieur, L., Ph.D. Thesis, Universite Pierre et Marie Curie (1976).

24. Preisendorfer, R. W., "Hydrologic Optics", U. S. Department of Commerce, National Oceanic & Atmospheric Administration, Environmental Research Laboratories, (1976).

25. Morel, A., and L. Prieur, "Analysis of Variations in Ocean Color", Limnol. Oceanogr. 22, 709-722 (1977)

27. Wilson, W. H., R. W. Austin, and R. C. Smith, "Optical Remote Sensing of Chlorophyll in Ocean Waters" Proceedings of the 12th International Symposium on Remote Sensing of the Environment, Manila, Philippines, 1103-1113 (1978).

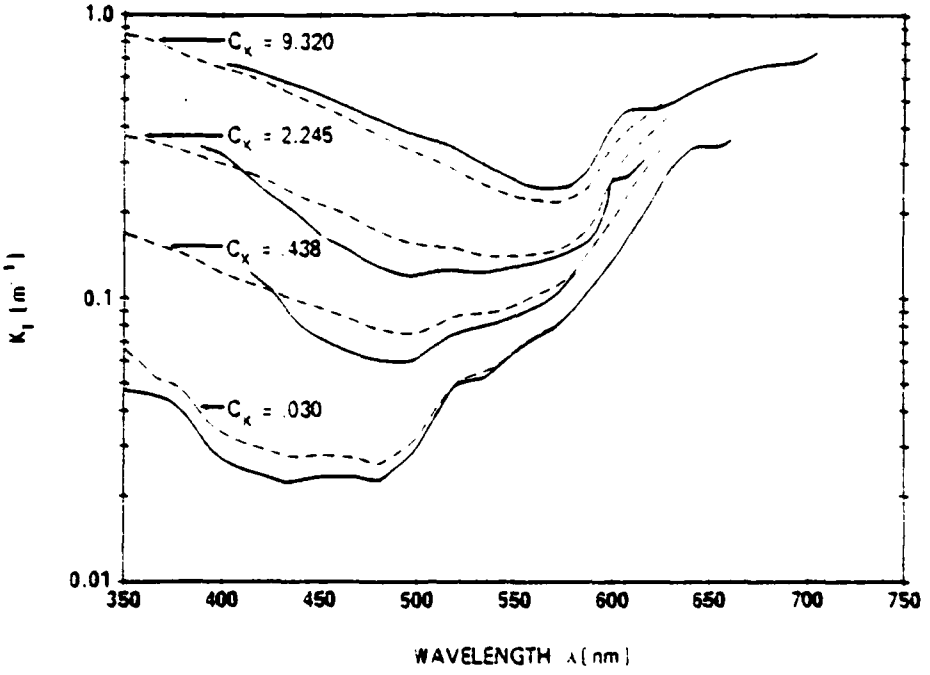

Figure 5-1. Experimentally measured (solid curves) and calculated values (dashed curves) of the diffuse attenuation coefficient for irradiance, $K_f(\lambda)$, for several ocean waters varying in chlorophyll-like pigment concentrations. After Smith and Baker[1]

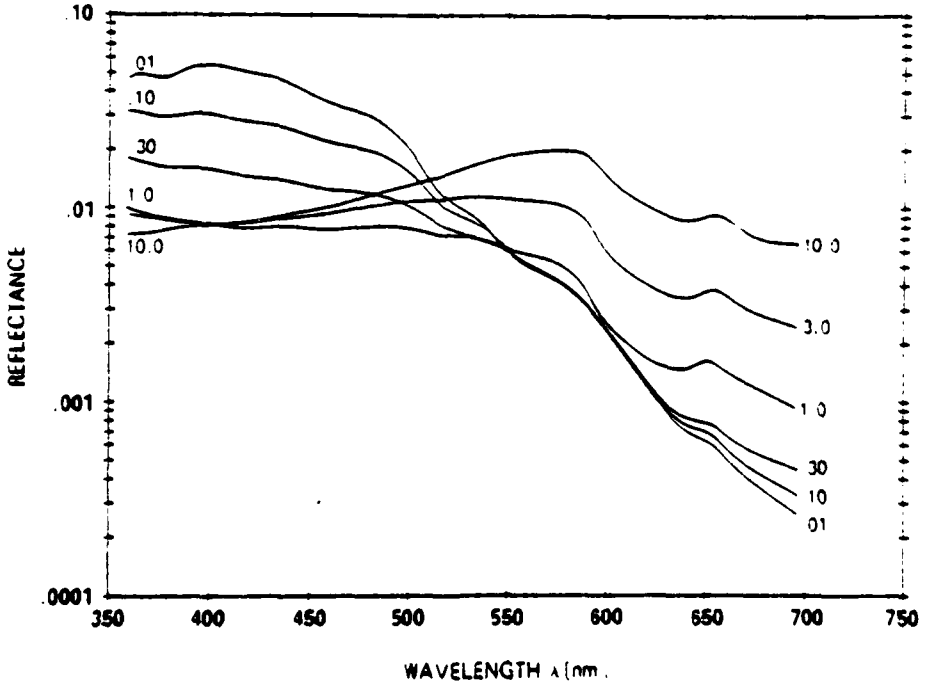

Figure 5-2. Irradiance reflectance, $R(\lambda)$, as a function of wavelength for various values of chlorophyll-like pigment concentration C_K[1]

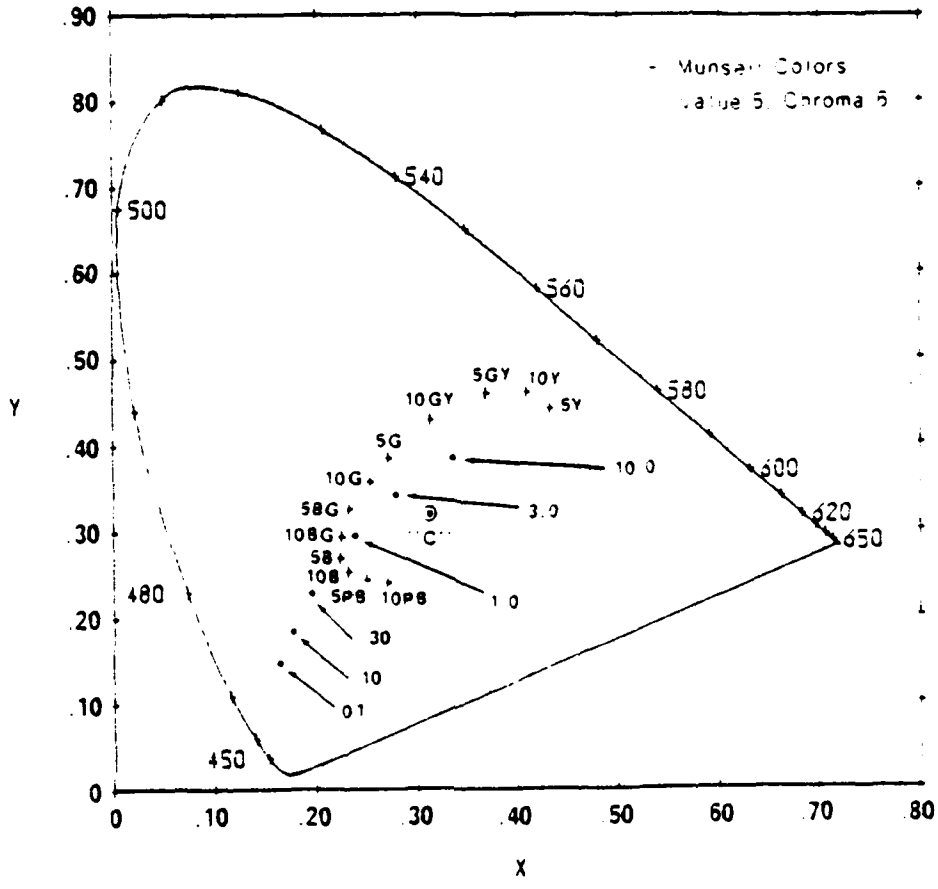

Figure 5-3. CIE chromaticity diagram with loci of spectrally pure wavelengths represented by curve labeled from 450 to 650 nm, based on standard source "C" as achromatic stimulus. Tristimulus values of reflectance for various values of C_Y are plotted and labeled. Munsell specifications for ocean color hue, as suggested by Austin (personal communication), also plotted and labeled[1].

6. Remote Sensing Applications (H.R.G.)

In this application, it is desired to relate the upwelled spectral radiance leaving the sea surface to the concentrations of the various constituents of the medium. For an observer just above the surface looking toward the water away from the direct sun-glint, the observed radiance will be:

$$L_u = \rho L_{sky} + \frac{t}{m^2} L_u \,. \tag{6-1}$$

where ρ is the surface specular reflection coefficient for the directions involved, L_{sky} is the radiance of that portion of the sky which is reflected from the sea surface, t is the transmittance of the air-sea interface, m is the refractive index of water, and L_u is the upwelled radiance just beneath the sea surface. Only L_u carries information about constituent concentrations. L_u is related to the $E_d(0)$ through $R(z)$ as defined in Eqs. (2-11) and (2-12). Combining these two equations, L_u can be written in terms of $R(0^-)$, *i.e.*,

$$L_u = Q\, E_d\, R(0^-) \,. \tag{6-2}$$

and if Q is constant, the variation in L_u with constituent concentration is totally contained in $R(0^-)$. R can easily be related to the constituent concentration using Eq. (3-4) since both a and b_b are additive over the constituent concentrations, that is,

$$a = a_w + \sum_i a_i$$

$$b_b = (b_b)_w + \sum_i (b_b)_i \,.$$

where a_i and $(b_b)_i$ are the absorption and backscattering coefficients of the ith constituent, C_i. If the specific absorption and backscattering coefficients are defined according to

$$a_i = a_i^* C_i \,,$$

and

$$(b_b)_i = (b_b)_i^* C_i \,,$$

then clearly $R(0^-)$ can be directly related to C_i. Given the optical properties of all of the constituents, the influence of variations in the concentration of any one of the constituents, on $R(0^-)$ can then be estimated. As an example of this, consider the addition of non-absorbing suspended particles to optically pure water.[2] Then

$$X = \frac{(b_b)_w + (b_b)^* C}{a_w + (b_b)_w + (b_b)^* C}$$

For small C,

$$X = X_w \left[1 + \frac{a_w}{(b_b)_w^2} (b_b)^* X_w C \right]$$

where X_w is the value of X for pure water. Note that in this regime, X varies linearly with C, so $R(0^-)$ will also depend nearly linearly on C. For large C, X becomes independent of C so variations in high concentrations of a non-absorbing suspended material will be nearly impossible to detect in $R(0^-)$.

A second example is the remote detection of chlorophyll-*a*. Clark, *et al.*[3] first provided evidence that it might be possible to use the color of the ocean, observed from aircraft or spacecraft, to estimate the chlorophyll concentration in surface waters. The first thorough discussion of the problems associated with such a venture was given by Duntley, *et al.*[4] (These studies led to the development of the Coastal Zone Color Scanner which was flown on Nimbus-7 launched in October 1978.) Several authors[5,6] have suggested relating the chlorophyll concentration to ratios of radiances at different wavelengths, *i.e.*, color ratios. Morel and Prieur[7] provide data suggesting that

$$C \approx [\, R(440nm) / R(560nm) \,]^{-2.5} \,. \tag{6-3}$$

where C is the concentration of chlorophyll-a plus phaeophytin-a. A very simple model of this can be constructed by assuming that the phytoplankton which contain the pigments either (1) do not scatter at all, in which case all of the scattering is due to water, or (2) scatter independently of concentration, and much more weakly than they absorb. In either case, using the large a approximation to Eq. (3-4),

$$R \approx \frac{1}{3} b_w / (a - b_w)$$

it is found that

$$\frac{R(440)}{R(560)} \approx \frac{a_w(560) - a^*(560)C}{a_w(440) - a^*(440)C}$$

Inserting the values of the absorption coefficients and plotting on log-log paper shows that for $0.3 \leqslant C \leqslant 10$ mg/m^3 this equation can be accurately represented by

$$C \approx [\, R(440)/R(560) \,]^{-2.3}$$

in excellent agreement with Eq. (6-3). This agreement is, of course, fortuitous since the scattering by phytoplankton and their associated detrital material cannot be ignored, especially at high concentrations. The calculation is presented merely to indicate that a power law relationship between ratios of radiances or reflectances and C can be explained on theoretical grounds.

Although the relationship in Eq. 6-3 can be said to be reasonably well understood, when radiance ratios rather than reflectance ratios are used, Gordon and Clark[3] found that

$$C \approx [\, L_u(440)/L_u(550) \,]^{-1.5} \qquad (6\text{-}4)$$

for the Gulf of Mexico, California waters, and the Chesapeake Bay. It is not known at present whether this difference between radiance and reflectance ratios is due to differences in the species distribution, growth rates, or nutrient stress[7] of the phytoplankton populations involved in Eqs. (6-3) and (6-4), or variations in Q in Eq. (6-1) which are known to exist.

Finally, it has been shown[9-11] that the depth to which ocean constituents can be remotely sensed is approximately $1/K_d$, and hence depends on the constituents' concentration and optical properties. Equation (3-3) can be used to estimate this "penetration depth" when the optical properties of all of the constituents are known. In the case of chlorophyll-a remote sensing, the K_d chlorophyll-a relationship given in Section 5 can be used to estimate the penetration depth.

References (§ 6)

1. Austin, R. W., "Remote Sensing of Spectral Radiance", in *Optical Aspects of Oceanography*, N. G. Jerlov and E. Steeman Nielsen, ed (Academic Press, 1974).

2. Maul, G. A., and Gordon, H. R., "On the Use of the Earth Resources Technology Satellite in Optical Oceanography", *Rem. Sensing Environ.*, 4, 95-128 (1975).

3. Clark, G. L., Ewing, G. C., and Lorenzen, C. J., "Spectra of Backscattering Light from the Sea obtained from Aircraft as a Measure of Chlorophyll Concentration", *Science* **167** 1119-1121 (1970).

4. Duntley, S. Q., Austin, R. W., Wilson, W. H., Edgerton, C. F., and Moran, S. E., "Ocean Color Analysis", Scripps Institution of Oceanography, Ref. 74-10, (1974).

5. Clark, G. L. and Ewing, G. C., "Remote Spectroscopy of the Sea for Biological Production studies", in *Optical Aspects of Oceanography*, N. G. Jerlov, and E. Steeman Nielsen, Ed., (Academic Press (1974).

6. Arvesen, J. C., Millard, J. P., and Weaver, E. C., "Remote Sensing of Chlorophyll and Temperature in Marine and Fresh Waters", *Astronaut Acta*, 18, 229-239 (1973).

7. Morel, A. and Prieur, L., "Analysis of Variations in Ocean Color", *Limnol. Oceanogr.*, 22, 709-722 (1977).

8. Gordon, H. R. and Clark, D. C., "Atmospheric Effects in the Remote Sensing of Phytoplankton Pigments", *Boundary Layer Meteorology*, in press.

9. Kiefer, D. A., Olsen, R., and Wilson, W. H., "Reflectance Spectroscopy of Marine Phytoplankton. Part I. Optical Properties as Related to Age and Growth Rate", *Limnol. Oceanogr.*, 24, 664-672 (1979).

10. Gordon, H. R. and McCluney, R. W., "Estimation of the Depth of Sunlight Penetration in the Sea for Remote Sensing, *Appl. Opt.*, 14, 413-416 (1975).

11. Gordon, H. R., "Remote Sensing of Optical Properties in Continuously Stratified Waters", *Appl. Opt.*, 17, 1893-1897 (1978).

9791

END

DATE

FILMED

-81

DTIC